Special Issue Reprint

Natural and Synthetic Compounds for Management, Prevention and Treatment of Obesity, 2nd Edition

Edited by
Marianna Lauricella and Antonella D'Anneo

MDPI

Natural and Synthetic Compounds for Management, Prevention and Treatment of Obesity, 2nd Edition

Natural and Synthetic Compounds for Management, Prevention and Treatment of Obesity, 2nd Edition

Editors

Marianna Lauricella
Antonella D'Anneo

MDPI

Editors

Marianna Lauricella   Antonella D'Anneo
University of Palermo   University of Palermo
Palermo, Italy   Palermo, Italy

This is a reprint of articles from the Special Issue published online in the open access journal *International Journal of Molecular Sciences* (ISSN 1422-0067) (available at: https://www.mdpi.com/journal/ijms/special_issues/Prevention_Treatment_Obesity_2).

For citation purposes, cite each article independently as indicated on the article page online and as indicated below:

LastName, A.A.; LastName, B.B.; LastName, C.C. Article Title. *Journal Name* **Year**, *Volume Number*, Page Range.

Contents

About the Editors

Marianna Lauricella

Associate Professor in Biochemistry at the Department of Biomedicine, Neuroscience and Advanced Diagnostics, School of Medicine, University of Palermo. Lecturer in "Biochemistry" at master's degree Course in Medicine, University of Palermo. Member of the Italian Society of Biochemistry and Molecular Biology (SIB). Associate Editor of BMC Cancer and Editorial Board Member of International Journal of Molecular Sciences. The research activity mainly concerns the study of the mechanisms governing the control of survival and death in cultured tumor cells. In particular, the aim of the research is to identify natural and synthetic compounds which can selectively induce cell death processes (apoptosis, autophagy, necroptosis). She has also expertise in the study of role exerted by oxidative stress in inducing obesity and the anti-obesity effects of natural compounds in in vitro models of obesity. She is author of over 70 peer-reviewed articles. (https://orcid.org/0000-0002-0157-3834).

Antonella D'Anneo

Associate Professor in Biochemistry at the Department of Biological, Chemical and Pharmaceutical Sciences and Technologies (STEBICEF), University of Palermo. Lecturer in "Biochemistry" at Bachelor degree in Biological Sciences, University of Palermo. Member of the Italian Society of Biochemistry and Molecular Biology (SIB). Associate Editor in Chief of Cancer Management and Research and Associate Editor for Frontiers in Pharmacology. She began her studies on the field of tumor biology, cell death mechanisms (apoptosis, necrosis, necroptosis, autophagy and anoikis) activated by natural and synthetic compounds and biochemical pathways which can be activated in tumor cells. To complement the graduate training in biochemistry, she obtained, as visiting scholar, a training at Rangos Research Center (University of Pittsburgh, USA) taking part in projects concerning gene therapy approaches to determine tolerization of diabetic patients against the cells of islet donor. More recently, her studies were focused on the identification nutraceutical properties (anti-tumor, anti-inflammatory, anti-obesity and antioxidant) of phytochemicals to disclose their biological activity and potential medicinal use. She is the author of over 60 scientific publications in ISI-indexed journals (https://orcid.org/0000-0002-1785-8236).

Editorial

Multimodal Strategies to Fight Obesity: Research on Tailored Therapies Based on Natural and Synthetic Compounds for Prevention, Management and Treatment

Antonella D'Anneo [1],* and Marianna Lauricella [2],*

1   Laboratory of Biochemistry, Department of Biological, Chemical and Pharmaceutical Sciences and Technologies (STEBICEF), University of Palermo, 90127 Palermo, Italy
2   Department of Biomedicine, Neurosciences and Advanced Diagnostics (BIND), Institute of Biochemistry, University of Palermo, 90127 Palermo, Italy
*   Correspondence: antonella.danneo@unipa.it (A.D.); marianna.lauricella@unipa.it (M.L.)

In the past 50 years, the global prevalence of obesity and overweight has tripled, reaching pandemic proportions and blatantly representing an urgent problem for public health [1,2]. Many different factors have actively fed the spread of this chronic condition, from the rising global intake of calorie-dense food to widespread bad behaviors such as living a sedentary lifestyle [3,4]. The most worrying aspect of this condition is its correlation with other comorbidities. Indeed, obesity has been proven to be associated with an increased risk of developing dyslipidemia, hypertension, type 2 diabetes, coronary heart disease, non-alcoholic fatty liver disease (NAFLD), arthritis and even many types of cancers [1,5,6], all of which severely impact the quality and life expectancy of affected subjects.

Thus far, the urgent need for intervention strategies focused on tailored targets, as well as the development of personalized medicine, has been a crucial aim in obesity research [7].

Some of these approaches have been focused on inflammation as a possible target in the development of effective therapeutic strategies [8,9]. Indeed, inflammation in adipose tissues represents a primary force that can contribute to the onset of obesity-associated pathologies [10]. White adipose tissue (WAT) represents an endocrine organ assigned to store lipid deposits and monitor both metabolism and inflammation through the production of adipokines (leptin and adiponectin) and cytokines [11,12]. Indeed, in WAT, many different cell types, such as adipocyte precursors (AP), adipocytes and immune cell subsets (i.e., dendritic cells, T and B cells and macrophages) coexist [13], creating a complicated network for the maintenance of the correct metabolic functionality and integrity of adipocytes. However, substantial evidence has proven that hypoxic conditions fulfill the expansion of adipose tissue and the upregulation of inflammatory response-related adipokines. As a consequence, hypoxia of fat cells increases glucose consumption, promoting the development of adipocyte insulin resistance and adipose tissue fibrosis [14].

In this scenario, a consistent amount of extracellular matrix (ECM) proteins (i.e., fibronectin and many different types of collagen) released by adipocytes, adipocyte progenitors and fibroblasts accumulate in ECM, modifying WAT plasticity and its functionality [15,16], two characteristic events which occur in adipose tissue fibrosis. A pro-fibrotic action in this process is carried out by cytokine secretion by immune system cells as adipose tissue macrophages and mast cells [17]. In a recent study, Arndt et al., using an ex vivo WAT organotypic culture system, identified IL-13 and IL-4 as critical pathogenic mediators of WAT fibrosis. The authors demonstrated that this effect is dependent on WAT-associated macrophages, since their removal by clodronate liposome treatment decreased the fibrotic deposition in WAT in mice intraperitoneally injected with IL-4. A strong positive correlation between fibrosis markers and IL-13/IL-4 receptors was found, but the data seem to indicate

that both IL-13 and IL-4 can play a role in ex vivo WAT systems, though only partly in in vivo models [18].

The state of chronic inflammation which characterizes obese subjects contributes to the development of several chronic diseases [11]. Regarding this connection, it has been reported that obesity represents a risk factor for myofascial disease, one of the leading causes of physical disability. Ugwoke et al. highlighted how several pathological processes in obesity, including changes in adipose tissue metabolism, chronic inflammatory state and oxidative stress, may alter the mechanical and biological properties of fascial hyaluronan [19]. Hyaluronan is the main polysaccharide of the ECM of connective tissues; it provides mechanical stability and acts as a water reservoir and lubricant. Moreover, hyaluronan, by binding to cell-surface receptors in adipose tissue, is able to modulate adipogenesis and adipose tissue metabolism. Alterations in the physical and chemical properties of hyaluronan alter the viscoelasticity of the matrix and deregulate molecular signaling, contributing to the development of myofascial disease in obesity.

Some investigations have focused on the identification of pro-inflammatory biomarkers in the saliva of obese subjects. A higher level of some matrix metalloproteinases (i.e., gelatinases MMP-2 and MMP-9), as well as of IL-1β, were found in the saliva of obese women compared to the control group, while in obese men, higher contents of MMP-9, IL-6 and resistin were observed compared to individuals of normal body weight [20].

Zazula et al. demonstrated that an early and sustained inflammatory state favors the acquisition of persistent muscle changes and typical obesogenic features [21]. Such a study was performed via subcutaneous injection of monosodium glutamate (MNG) in Wistar rats. When administered in the perinatal phase, MNG provokes lesions of hypothalamic nuclei in animal models, leading, in adult life, to hyperphagia and unbalanced consumption of nutrients, two typical features of obesity [22–24]. In line with this evidence, Zazula's data demonstrated that MSG exposure promoted adiposity in Wistar rats, favoring a hyperinsulinemic and pro-inflammatory state that were accompanied with fibrosis, oxidative injury and muscle mass reduction in adult rats. The plasmatic profiles of the animals showed remarkable increases in glucose content, total cholesterol, LDL and VLDL, as well as in the amount of triacylglycerols. The analysis of muscle markers in MSG-treated rats provided evidence of an increase in lactate content and a decrease in creatine kinase with respect to the control group [21].

The main cause leading to the accumulation of fat in adipose tissue is an excessive food intake. Several reports have suggested that high sugar consumption is contributing to the global rise in obesity and type 2 diabetes. To reduce sugar intake and its dangerous consequences, the ingestion of polyols, natural sweeteners with low caloric content and a low glycemic index, can be useful [25]. Erythriol and xylitol are two polyols which are partly adsorbed in the small intestine. Bordier et al. evaluated the enteral adsorption of erythriol and xylitol and their potential metabolization into the oxidate form erytronate, whose implications for human health remain to be determined, in healthy volunteers [26]. Based on the results, the authors demonstrated that erythriol is dose-dependently adsorbed and metabolized in small amounts to erytronate, whereas xylitol absorption is low, and no metabolization to erytronate takes place.

Other studies have demonstrated that a high-fat diet (HFD) can contribute to adiposity and obesity status [27]. In particular, the presence of high levels of long-chain saturated fatty acids (FAs), such as palmitate, in the diet has been associated with hypertrophic and dysfunctional adipocytes, as well as with a state of low-grade inflammation in white adipose tissue (WAT) [28]. Thus, reducing the hypertrophy adipose tissue represents a strategy to counteract the detrimental effects of obesity.

Nowadays, numerous foods rich in antioxidants, phytochemicals and essential oils have been found to be helpful in maintaining body weight, and can be considered protective and/or therapeutic against obesity [29,30]. Mango (*Mangifera indica* L.) is a food appreciated for its nutritive and nutraceutical properties. Different parts of the mango plant and fruit have been reported to exert anti-tumoral, antioxidant and anti-inflammatory effects due

to the high content of polyphenols [31–33]. Pratelli et al. demonstrated that extracts of Sicilian mango peels and seeds, the main bio-wastes of mango processing, are capable of counteracting in 3T3-L1 adipocyte lipotoxicity induced by high doses of palmitate, the main long-chain FA present in the diet. In particular, mango extracts counteracted palmitate-induced hypertrophy by reducing lipid droplets and triglyceride content, as well as reducing endoplasmic reticulum stress induced by palmitate. The lipolytic and antioxidant effects exerted by mango peel and seed extracts seem to be mediated by the activation of the AMPK and Nrf2 antioxidant pathway [34].

A beneficial effect against HFD-induced lipotoxicity also seems to be also exerted by 4-methylesculetin (6,7-dihydroxy-4-methylcoumarin, 4-ME), a coumarin derivative isolated from Artemisia annua [35]. Li et al. showed that 4-ME treatment attenuated adipocyte hypertrophy, macrophage infiltration, hypoxia and fibrosis in epididymal adipose tissue in HFD-fed mice, thus improving the adipose tissue microenvironment. In addition, 4-ME reduced liver fibrosis by lowering FAs uptake and de novo lipogenesis. These effects are correlated with the ability of 4-ME to down-regulate CD36; the free FA cell-surface receptor; as well as SREBP-1, PPAR-γ and FASN protein, transcription factors and enzymes that are involved in lipogenesis. Furthermore, 4-ME activated Nrf2, an important antioxidant transcriptional factor that can also indirectly suppress the expression of SREBP-1 and its lipogenic target genes [35].

A natural compound that has attracted the interest of researchers is curcumin, a polyphenol extracted from the rhizome of *Curcuma longa* L. A consistent piece of evidence has demonstrated that it has different pharmacological properties, including anti-inflammatory, antioxidant, neuroprotective and anti-tumoral effects [36], and it is also able to improve glucose and lipid metabolism [37]. However, the potential therapeutic application of this molecule is strongly limited by its scarce bioavailability as a consequence of its low solubility in water and rapid clearance [38]. Combinatorial treatments aimed at improving both curcumin bioavailability and its half-life have identified piperine, an alkaloid extracted by *Piper nigrum* L. and *Piper longum*, as a possible candidate to be co-administered with curcumin. However, in a recent case study, Servida et al. demonstrated that this combination treatment should be better explored. Indeed, in a patient exposed to a low-altitude condition, curcumin/piperine co-administration induced severe hypoglycemia followed by a transient loss of consciousness [38].

Several studies support the conclusion that obesity represents a risk factor for the development of neurodegenerative diseases, including dementia and Alzheimer's disease [39]. Indeed, obesity is associated with chronic low-grade inflammation and oxidative stress, which contribute to the onset and progression of neurodegeneration. There is an assumption that foods rich in antioxidants may exert protective effects on neurodegeneration. To this end, Terzo et al. evaluated the effect of combined administration of Sicilian black bee chestnut honey and D-limonene, which are known to mitigate inflammation and oxidative stress, in HFD-fed mice. After 10 weeks of consuming an HFD, the mice developed neuronal apoptosis, increased pro-inflammatory cytokines and oxidative stress markers. Interestingly, all of these alterations were counteracted by the combined administration of honey and limonene [40]. Notably, they also reduced amyloid plaque processing and improved synaptic function, thus suggesting that a honey and limonene combination can represent a potential dietary supplement to counteract HFD-induced brain damage.

In addition to natural compounds, some synthetic molecules with targeted action showed promising effects for reducing obesity and related diseases. Adenosine receptor subtypes A2A and A2B represent important therapeutic targets for the treatment of obesity [41]. Theophylline is a non-selective adenosine receptor antagonist that has been shown to reduce body weight in obese animals [42]. However, its side effects, such as hyperactivity and heart rhythm disturbances, represent a problem. Kotańska et al. [43] compared the effect of theophylline with that of PSB-603, a specific adenosine A2B receptor antagonist, on high-fat/high-sugar diet-fed mice and demonstrated that both the A2B receptor antagonists significantly lowered the body weights of the mice. However, only

PSB-603 was also capable of reducing triglycerides and total cholesterol blood levels in mice, thus suggesting that blocking A2A with a specific antagonist has stronger effects on lipid reduction than non-selective inhibition.

In addition, several studies supported the existence of an anti-obesity effect of compounds stimulating histamine release [44]. The histaminergic system is involved in the regulation of food intake and body weight control [44]. Stimulation of the H3 receptor activates a negative feedback due to histamine release, while H3 receptor inhibition by specific antagonists shows efficacy in inhibiting weight gain [45]. In a recent publication, Mika et al. demonstrated that KSK-74, a new specific H3R antagonist, reduced weight gain in overfeeding rats. It also improved their glucose tolerance and adipocyte hypertrophy, suggesting its potential use as an anti-obesity compound [46].

Beyond these emerging data, new insights for the development of therapeutic strategies against obesity come from the identification of epigenetic molecular targets. During adipogenesis, a highly orchestrated gene expression program occurs [47]. It favors the cell commitment of pluripotent stem cells (first stage) into pre-adipocytes, and then the terminal differentiation of pre-adipocytes into mature adipocytes (second stage) [48]. A complex system of epigenetic changes and chromatin remodeling processes alternates during the differentiation flux, causing the silencing of stemness-associated genes [49]. In recent years, such an aspect has been a hot topic in the scientific community, pushing the search for natural and synthetic compounds able to modulate that intricate network of proteins and transcription factors that are directly involved in stem cell differentiation or in uncontrolled adipocyte tissue hyperproliferation [50,51]. In this context, metformin and vitamin D have been revealed as very promising therapeutic agents, since their administration to adipose-derived stem cells upregulates HDAC1 expression, affected the stem cell phenotype and modulated the expression of those miRNAs playing a key role in stem cell adipogenesis [47,52].

Author Contributions: Conceptualization, A.D. and M.L.; writing—original draft preparation, A.D. and M.L.; writing—review and editing A.D and M.L. All authors have read and agreed to the published version of the manuscript.

Conflicts of Interest: The authors declare no conflict of interest.

References

1. Blüher, M. Obesity: Global Epidemiology and Pathogenesis. *Nat. Rev. Endocrinol.* **2019**, *15*, 288–298. [CrossRef]
2. Caballero, B. Humans against Obesity: Who Will Win? *Adv. Nutr.* **2019**, *10*, S4–S9. [CrossRef]
3. Conway, B.; Rene, A. Obesity as a Disease: No Lightweight Matter. *Obes. Rev.* **2004**, *5*, 145–151. [CrossRef]
4. Allom, V.; Mullan, B.; Smith, E.; Hay, P.; Raman, J. Breaking Bad Habits by Improving Executive Function in Individuals with Obesity. *BMC Public Health* **2018**, *18*, 505. [CrossRef]
5. Khaodhiar, L.; McCowen, K.C.; Blackburn, G.L. Obesity and Its Comorbid Conditions. *Clin. Cornerstone* **1999**, *2*, 17–31. [CrossRef] [PubMed]
6. Morales Camacho, W.J.; Molina Díaz, J.M.; Plata Ortiz, S.; Plata Ortiz, J.E.; Morales Camacho, M.A.; Calderón, B.P. Childhood Obesity: Aetiology, Comorbidities, and Treatment. *Diabetes Metab. Res. Rev.* **2019**, *35*, e3203. [CrossRef] [PubMed]
7. D'Anneo, A.; Lauricella, M. Natural and Synthetic Compounds for Management, Prevention and Treatment of Obesity. *Int. J. Mol. Sci.* **2022**, *23*, 2890. [CrossRef]
8. Karczewski, J.; Śledzińska, E.; Baturo, A.; Jończyk, I.; Maleszko, A.; Maleszko, A.; Samborski, P.; Begier-Krasińska, B.; Dobrowolska, A. Obesity and Inflammation. *Eur. Cytokine Netw.* **2018**, *29*, 83–94. [CrossRef] [PubMed]
9. Kawai, T.; Autieri, M.V.; Scalia, R. Adipose Tissue Inflammation and Metabolic Dysfunction in Obesity. *Am. J. Physiol.-Cell Physiol.* **2021**, *320*, C375–C391. [CrossRef]
10. Hildebrandt, X.; Ibrahim, M.; Peltzer, N. Cell Death and Inflammation during Obesity: "Know My Methods, WAT(Son)". *Cell Death Differ.* **2023**, *30*, 279–292. [CrossRef]
11. Longo, M.; Zatterale, F.; Naderi, J.; Parrillo, L.; Formisano, P.; Raciti, G.A.; Beguinot, F.; Miele, C. Adipose Tissue Dysfunction as Determinant of Obesity-Associated Metabolic Complications. *Int. J. Mol. Sci.* **2019**, *20*, 2358. [CrossRef] [PubMed]
12. Ghaben, A.L.; Scherer, P.E. Adipogenesis and Metabolic Health. *Nat. Rev. Mol. Cell Biol.* **2019**, *20*, 242–258. [CrossRef] [PubMed]

13. Liu, R.; Nikolajczyk, B.S. Tissue Immune Cells Fuel Obesity-Associated Inflammation in Adipose Tissue and Beyond. *Front. Immunol.* **2019**, *10*, 1587. [CrossRef] [PubMed]
14. Trayhurn, P. Hypoxia and Adipose Tissue Function and Dysfunction in Obesity. *Physiol. Rev.* **2013**, *93*, 1–21. [CrossRef] [PubMed]
15. Sakers, A.; De Siqueira, M.K.; Seale, P.; Villanueva, C.J. Adipose-Tissue Plasticity in Health and Disease. *Cell* **2022**, *185*, 419–446. [CrossRef] [PubMed]
16. Marcelin, G.; Gautier, E.L.; Clément, K. Adipose Tissue Fibrosis in Obesity: Etiology and Challenges. *Annu. Rev. Physiol.* **2022**, *84*, 135–155. [CrossRef]
17. Keophiphath, M.; Achard, V.; Henegar, C.; Rouault, C.; Clément, K.; Lacasa, D. Macrophage-Secreted Factors Promote a Profibrotic Phenotype in Human Preadipocytes. *Mol. Endocrinol.* **2009**, *23*, 11–24. [CrossRef]
18. Arndt, L.; Lindhorst, A.; Neugebauer, J.; Hoffmann, A.; Hobusch, C.; Alexaki, V.-I.; Ghosh, A.; Blüher, M.; Wolfrum, C.; Glaß, M.; et al. The Role of IL-13 and IL-4 in Adipose Tissue Fibrosis. *Int. J. Mol. Sci.* **2023**, *24*, 5672. [CrossRef]
19. Ugwoke, C.K.; Cvetko, E.; Umek, N. Pathophysiological and Therapeutic Roles of Fascial Hyaluronan in Obesity-Related Myofascial Disease. *Int. J. Mol. Sci.* **2022**, *23*, 11843. [CrossRef]
20. Ostrowska, L.; Smarkusz-Zarzecka, J.; Gornowicz, A.; Lendzion, K.; Zyśk, B.; Pogodziński, D. Analysis of Selected Salivary Adipokines and Cytokines in Patients with Obesity—A Pilot Study. *Int. J. Mol. Sci.* **2023**, *24*, 4145. [CrossRef]
21. Zazula, M.F.; Saraiva, D.F.; Theodoro, J.L.; Maciel, M.; Sepulveda, E.V.d.S.; de Andrade, B.Z.; Boaretto, M.L.; Maciel, J.I.H.N.; Bronczek, G.A.; Soares, G.M.; et al. An Early and Sustained Inflammatory State Induces Muscle Changes and Establishes Obesogenic Characteristics in Wistar Rats Exposed to the MSG-Induced Obesity Model. *Int. J. Mol. Sci.* **2023**, *24*, 4730. [CrossRef]
22. Hernández Bautista, R.J.; Mahmoud, A.M.; Königsberg, M.; López Díaz Guerrero, N.E. Obesity: Pathophysiology, Monosodium Glutamate-Induced Model and Anti-Obesity Medicinal Plants. *Biomed. Pharmacother.* **2019**, *111*, 503–516. [CrossRef] [PubMed]
23. Olney, J.W. Brain Lesions, Obesity, and Other Disturbances in Mice Treated with Monosodium Glutamate. *Science* **1969**, *164*, 719–721. [CrossRef] [PubMed]
24. Quines, C.B.; Rosa, S.G.; Velasquez, D.; Prado, V.C.; Neto, J.S.S.; Nogueira, C.W. (P-ClPhSe)2 Stabilizes Metabolic Function in a Rat Model of Neuroendocrine Obesity Induced by Monosodium Glutamate. *Food Chem. Toxicol.* **2018**, *118*, 168–180. [CrossRef] [PubMed]
25. Livesey, G. Health Potential of Polyols as Sugar Replacers, with Emphasis on Low Glycaemic Properties. *Nutr. Res. Rev.* **2003**, *16*, 163–191. [CrossRef]
26. Bordier, V.; Teysseire, F.; Senner, F.; Schlotterbeck, G.; Drewe, J.; Beglinger, C.; Wölnerhanssen, B.K.; Meyer-Gerspach, A.C. Absorption and Metabolism of the Natural Sweeteners Erythritol and Xylitol in Humans: A Dose-Ranging Study. *Int. J. Mol. Sci.* **2022**, *23*, 9867. [CrossRef]
27. DiNicolantonio, J.J.; O'Keefe, J.H. Good Fats versus Bad Fats: A Comparison of Fatty Acids in the Promotion of Insulin Resistance, Inflammation, and Obesity. *Mo. Med.* **2017**, *114*, 303–307. [PubMed]
28. Ishaq, A.; Tchkonia, T.; Kirkland, J.L.; Siervo, M.; Saretzki, G. Palmitate Induces DNA Damage and Senescence in Human Adipocytes in Vitro That Can Be Alleviated by Oleic Acid but Not Inorganic Nitrate. *Exp. Gerontol.* **2022**, *163*, 111798. [CrossRef]
29. De Blasio, A.; D'Anneo, A.; Lauricella, M.; Emanuele, S.; Giuliano, M.; Pratelli, G.; Calvaruso, G.; Carlisi, D. The Beneficial Effects of Essential Oils in Anti-Obesity Treatment. *Int. J. Mol. Sci.* **2021**, *22*, 11832. [CrossRef]
30. Pratelli, G.; Carlisi, D.; D'Anneo, A.; Maggio, A.; Emanuele, S.; Palumbo Piccionello, A.; Giuliano, M.; De Blasio, A.; Calvaruso, G.; Lauricella, M. Bio-Waste Products of *Mangifera indica* L. Reduce Adipogenesis and Exert Antioxidant Effects on 3T3-L1 Cells. *Antioxidants* **2022**, *11*, 363. [CrossRef]
31. Lo Galbo, V.; Lauricella, M.; Giuliano, M.; Emanuele, S.; Carlisi, D.; Calvaruso, G.; De Blasio, A.; Di Liberto, D.; D'Anneo, A. Redox Imbalance and Mitochondrial Release of Apoptogenic Factors at the Forefront of the Antitumor Action of Mango Peel Extract. *Molecules* **2021**, *26*, 4328. [CrossRef] [PubMed]
32. Lauricella, M.; Lo Galbo, V.; Cernigliaro, C.; Maggio, A.; Palumbo Piccionello, A.; Calvaruso, G.; Carlisi, D.; Emanuele, S.; Giuliano, M.; D'Anneo, A. The Anti-Cancer Effect of *Mangifera indica* L. Peel Extract Is Associated to ΓH2AX-Mediated Apoptosis in Colon Cancer Cells. *Antioxidants* **2019**, *8*, 422. [CrossRef] [PubMed]
33. Sferrazzo, G.; Palmeri, R.; Restuccia, C.; Parafati, L.; Siracusa, L.; Spampinato, M.; Carota, G.; Distefano, A.; Di Rosa, M.; Tomasello, B.; et al. *Mangifera indica* L. Leaves as a Potential Food Source of Phenolic Compounds with Biological Activity. *Antioxidants* **2022**, *11*, 1313. [CrossRef] [PubMed]
34. Pratelli, G.; Di Liberto, D.; Carlisi, D.; Emanuele, S.; Giuliano, M.; Notaro, A.; De Blasio, A.; Calvaruso, G.; D'Anneo, A.; Lauricella, M. Hypertrophy and ER Stress Induced by Palmitate Are Counteracted by Mango Peel and Seed Extracts in 3T3-L1 Adipocytes. *Int. J. Mol. Sci.* **2023**, *24*, 5419. [CrossRef] [PubMed]
35. Li, L.; Zhu, G.; Fu, G.; Zha, W.; Li, H. Metabolic Syndrome Ameliorated by 4-Methylesculetin by Reducing Hepatic Lipid Accumulation. *Int. J. Mol. Sci.* **2022**, *23*, 10465. [CrossRef] [PubMed]
36. Scazzocchio, B.; Minghetti, L.; D'Archivio, M. Interaction between Gut Microbiota and Curcumin: A New Key of Understanding for the Health Effects of Curcumin. *Nutrients* **2020**, *12*, 2499. [CrossRef]
37. Panahi, Y.; Khalili, N.; Sahebi, E.; Namazi, S.; Simental-Mendía, L.; Majeed, M.; Sahebkar, A. Effects of Curcuminoids Plus Piperine on Glycemic, Hepatic and Inflammatory Biomarkers in Patients with Type 2 Diabetes Mellitus: A Randomized Double-Blind Placebo-Controlled Trial. *Drug Res.* **2018**, *68*, 403–409. [CrossRef]

38. Servida, S.; Panzeri, E.; Tomaino, L.; Marfia, G.; Garzia, E.; Appiani, G.C.; Moroncini, G.; Colonna, V.D.G.; Vecchia, C.L.; Vigna, L. Overview of Curcumin and Piperine Effects on Glucose Metabolism: The Case of an Insulinoma Patient's Loss of Consciousness. *Int. J. Mol. Sci.* **2023**, *24*, 6621. [CrossRef]

39. Terzo, S.; Amato, A.; Mulè, F. From Obesity to Alzheimer's Disease through Insulin Resistance. *J. Diabetes Complicat.* **2021**, *35*, 108026. [CrossRef]

40. Terzo, S.; Calvi, P.; Nuzzo, D.; Picone, P.; Allegra, M.; Mulè, F.; Amato, A. Long-Term Ingestion of Sicilian Black Bee Chestnut Honey and/or D-Limonene Counteracts Brain Damage Induced by High Fat-Diet in Obese Mice. *Int. J. Mol. Sci.* **2023**, *24*, 3467. [CrossRef]

41. D'Antongiovanni, V.; Fornai, M.; Pellegrini, C.; Blandizzi, C.; Antonioli, L. Managing Obesity and Related Comorbidities: A Potential Pharmacological Target in the Adenosine System? *Front. Pharmacol.* **2021**, *11*, 621955. [CrossRef] [PubMed]

42. Carrageta, D.F.; Dias, T.R.; Alves, M.G.; Oliveira, P.F.; Monteiro, M.P.; Silva, B.M. Anti-Obesity Potential of Natural Methylxan-thines. *J. Funct. Foods* **2018**, *43*, 84–94. [CrossRef]

43. Kotańska, M.; Dziubina, A.; Szafarz, M.; Mika, K.; Bednarski, M.; Nicosia, N.; Temirak, A.; Müller, C.E.; Kieć-Kononowicz, K. Preliminary Evidence of the Potent and Selective Adenosine A2B Receptor Antagonist PSB-603 in Reducing Obesity and Some of Its Associated Metabolic Disorders in Mice. *Int. J. Mol. Sci.* **2022**, *23*, 13439. [CrossRef] [PubMed]

44. Malmlöf, K.; Golozoubova, V.; Peschke, B.; Wulff, B.S.; Refsgaard, H.H.F.; Johansen, P.B.; Cremers, T.; Rimvall, K. Increase of Neuronal Histamine in Obese Rats Is Associated with Decreases in Body Weight and Plasma Triglycerides. *Obesity* **2006**, *14*, 2154–2162. [CrossRef] [PubMed]

45. Malmlöf, K.; Zaragoza, F.; Golozoubova, V.; Refsgaard, H.H.F.; Cremers, T.; Raun, K.; Wulff, B.S.; Johansen, P.B.; Westerink, B.; Rimvall, K. Influence of a Selective Histamine H3 Receptor Antagonist on Hypothalamic Neural Activity, Food Intake and Body Weight. *Int. J. Obes.* **2005**, *29*, 1402–1412. [CrossRef]

46. Mika, K.; Szafarz, M.; Zadrożna, M.; Nowak, B.; Bednarski, M.; Szczepańska, K.; Pociecha, K.; Kubacka, M.; Nicosia, N.; Juda, I.; et al. KSK-74: Dual Histamine H3 and Sigma-2 Receptor Ligand with Anti-Obesity Potential. *Int. J. Mol. Sci.* **2022**, *23*, 7011. [CrossRef]

47. Cruciani, S.; Delitala, A.P.; Cossu, M.L.; Ventura, C.; Maioli, M. Management of Obesity and Obesity-Related Disorders: From Stem Cells and Epigenetics to Its Treatment. *Int. J. Mol. Sci.* **2023**, *24*, 2310. [CrossRef]

48. Cawthorn, W.P.; Scheller, E.L.; MacDougald, O.A. Adipose Tissue Stem Cells Meet Preadipocyte Commitment: Going Back to the Future. *J. Lipid Res.* **2012**, *53*, 227–246. [CrossRef]

49. Szymczak-Pajor, I.; Miazek, K.; Selmi, A.; Balcerczyk, A.; Śliwińska, A. The Action of Vitamin D in Adipose Tissue: Is There the Link between Vitamin D Deficiency and Adipose Tissue-Related Metabolic Disorders? *Int. J. Mol. Sci.* **2022**, *23*, 956. [CrossRef]

50. Ammendola, S.; Scotto d'Abusco, A. Nutraceuticals and the Network of Obesity Modulators. *Nutrients* **2022**, *14*, 5099. [CrossRef]

51. Santaniello, S.; Cruciani, S.; Basoli, V.; Balzano, F.; Bellu, E.; Garroni, G.; Ginesu, G.; Cossu, M.L.; Facchin, F.; Delitala, A.P.; et al. Melatonin and Vitamin D Orchestrate Adipose Derived Stem Cell Fate by Modulating Epigenetic Regulatory Genes. *Int. J. Med. Sci.* **2018**, *15*, 1631–1639. [CrossRef] [PubMed]

52. Cruciani, S.; Garroni, G.; Balzano, F.; Pala, R.; Bellu, E.; Cossu, M.L.; Ginesu, G.C.; Ventura, C.; Maioli, M. Tuning Adipogenic Differentiation in ADSCs by Metformin and Vitamin D: Involvement of MiRNAs. *Int. J. Mol. Sci.* **2020**, *21*, 6181. [CrossRef] [PubMed]

Article

The Role of IL-13 and IL-4 in Adipose Tissue Fibrosis

Lilli Arndt [1,2], Andreas Lindhorst [1], Julia Neugebauer [1], Anne Hoffmann [3], Constance Hobusch [1], Vasileia-Ismini Alexaki [4], Adhideb Ghosh [5,6], Matthias Blüher [3], Christian Wolfrum [5], Markus Glaß [7] and Martin Gericke [1,2,*]

1   Institute of Anatomy, Leipzig University, 04103 Leipzig, Germany
2   Institute of Anatomy and Cell Biology, Martin-Luther-University Halle-Wittenberg,
    06108 Halle (Saale), Germany
3   Helmholtz Institute for Metabolic, Obesity and Vascular Research, 04103 Leipzig, Germany
4   Institute of Clinical Chemistry and Laboratory Medicine, University Hospital Dresden,
    01307 Dresden, Germany
5   Institute of Food, Nutrition and Health, ETH Zurich, 8603 Schwerzenbach, Switzerland
6   Functional Genomics Center Zurich, ETH Zurich and University of Zurich, 8057 Zurich, Switzerland
7   Institute of Molecular Medicine, Martin-Luther-University Halle-Wittenberg, 06120 Halle (Saale), Germany
*   Correspondence: martin.gericke@medizin.uni-leipzig.de; Tel.: +49-3431-22055

Abstract: White adipose tissue (WAT) fibrosis, characterized by an excess of extracellular (ECM) matrix components, is strongly associated with WAT inflammation and dysfunction due to obesity. Interleukin (IL)-13 and IL-4 were recently identified as critical mediators in the pathogenesis of fibrotic diseases. However, their role in WAT fibrosis is still ill-defined. We therefore established an ex vivo WAT organotypic culture system and demonstrated an upregulation of fibrosis-related genes and an increase of α-smooth muscle actin (αSMA) and fibronectin abundance upon dose-dependent stimulation with IL-13/IL-4. These fibrotic effects were lost in WAT lacking *il4ra*, which encodes for the underlying receptor controlling this process. Adipose tissue macrophages were found to play a key role in mediating IL-13/IL-4 effects in WAT fibrosis as their depletion through clodronate dramatically decreased the fibrotic phenotype. IL-4-induced WAT fibrosis was partly confirmed in mice injected intraperitoneally with IL-4. Furthermore, gene correlation analyses of human WAT samples revealed a strong positive correlation of fibrosis markers with IL-13/IL-4 receptors, whereas *IL13* and *IL4* correlations failed to confirm this association. In conclusion, IL-13 and IL-4 can induce WAT fibrosis ex vivo and partly in vivo, but their role in human WAT remains to be further elucidated.

Keywords: adipose tissue; fibrosis; IL-13; IL-4; macrophages; obesity

1. Introduction

Obesity is one of the gravest global health problems in western societies, leading to an increasing risk for cardiovascular and metabolic diseases including dyslipidemia, insulin resistance, and type 2 diabetes [1]. Obesity-related chronic nutrient overload promotes white adipose tissue (WAT) expansion through both increased lipid storage in adipocytes (hypertrophy) and formation of new adipocytes (hyperplasia); these are accompanied by extracellular matrix (ECM) remodeling to accommodate adipose tissue modifications. Further obesity-associated dysregulations in WAT, such as hypoxia and inflammation characterized by accumulation of macrophages and other immune cells, can advance WAT fibrosis [2]. Fibrosis of adipose tissue is considered both a feature of obesity and a contributing factor to loss of WAT function and plasticity [3] and is closely correlated to more metabolic complications [4]. As with other fibrotic diseases, WAT fibrosis arises due to the excessive accumulation of ECM proteins; this can either result from increased production or impaired degradation of ECM components such as collagens I, III, VI, and fibronectin [5], which are primarily produced by adipocyte progenitors, adipocytes, fibroblasts, and myofibroblasts [4]. Immune cells, such as mast cells and

adipose tissue macrophages (ATMs), appear to have the greatest regulatory role in ECM production through their effects on other cell types via cytokine secretion [6,7]. It is widely accepted that transforming growth factor β-1 (TGF-β1), interleukin (IL)-4, and IL-13 are the most prominent cytokines driving fibrosis in liver, lung, kidney, and skin [8].

IL-4 and IL-13 are the key cytokines in the type 2 immune responses, sharing structural and functional similarities. Both cytokines are primarily produced by T-helper type 2 (Th2) cells, as well as by some innate immune cells, including basophils, mast cells, eosinophils, and macrophages. Both cytokines also share several biological functions. These include the promotion of Th2 cell differentiation, inducing the immunoglobulin switch from IgM to IgE in B cells, and recruiting and activating immune cells such as macrophages [9,10]. Consistent with these functional similarities, IL-4 and IL-13 exhibit approximately 30% amino acid sequence homology and share a common receptor, the type 2 IL-4 receptor [11]. Although IL-4 and IL-13 receptors share a common alpha chain (IL 4Rα), IL-4Rα also interacts with the gamma common (γc) chain to form the type 1 IL-4 receptor, while the type 2 IL-4/IL-13 receptor, IL-4Rα, binds to the IL-13Rα1 chain. Both receptor complexes can be activated by IL-4, resulting in JAK/STAT6-dependent signaling; this is also triggered by IL-13 binding but exclusively via the type 2 receptor complex. In contrast, IL-13 exhibits a higher binding affinity to the α2 chain of the IL-13 receptor (IL-13Rα2), which was previously specified as a decoy receptor for the internalization of excessive IL-13 [12,13]. Recently, a new signaling pathway for the IL-13Rα2 has been described in which activator protein 1 (AP1) acts as the signaling molecule to induce the production of TGF-β1 in macrophages and, therefore, mediates fibrosis [12]. It is widely accepted that, upon TGF-β1 stimulation, fibroblasts are activated and undergo a phenotypic transition into myofibroblasts accompanied by increased alpha-smooth muscle actin (α-SMA) production [14]. Recently, Marcelin et al. identified adipocyte progenitors (defined as PDGFRa+ and Cd9high) capable of adopting a myofibroblast-like phenotype leading to ECM deposition and fibrosis under a high-fed diet (HFD) [15]. Obesity and fibrotic WAT are also closely associated with increased pro-inflammatory ATMs, that primarily accumulate around dead adipocytes, forming crown-like structures (CLS) [16–18]. Here, most CLS-associated ATMs are lipid-associated macrophages (LAMs), a novel macrophage subset that are closely related to lipid metabolism and phagocytosis [19]. Interestingly, dying adipocytes induced the activation of macrophage-inducible C-type lectin (Mincle) exclusively in pro-inflammatory ATMs localized in CLS, thereby leading to myofibroblasts formation and ECM production [20].

On the other hand, fibrosis is closely linked with Th2 immune responses. The effects of IL-13 and IL-4 on fibrosis pathogenesis have been extensively studied, but their role in WAT fibrosis has not yet been elucidated. This study demonstrates, for the first time, that IL-13 and IL-4 stimulation results in a fibrotic phenotype in mouse WAT ex vivo and partly in vivo. Furthermore, we identify ATMs as the key driver mediating the IL 13/IL-4 signal. In contrast, data concerning human WAT cannot entirely support this conclusion. Indeed, visceral WAT expression revealed a positive correlation of IL-13/IL-4 receptors with fibrosis markers, but there was no positive correlation for IL-13 and IL-4, thereby suggesting a controversial role for IL-13 and IL-4 in human WAT fibrosis.

2. Results

2.1. IL-13 and IL-4 Induced WAT Fibrosis

Several studies have demonstrated that IL-13 and IL-4 act as important inducers of fibrosis in several diseases. To study the impact of IL-13 and IL-4 on WAT fibrosis, we established an ex vivo culture system of WAT explants. Because varying susceptibility to WAT fibrosis has been reported in different mouse strains [21], we compared the commonly used fibrosis-prone C3H/HeOuj (C3H) mice with more fibrosis-resistant C57BL6/J (B6J) mice, as it has been shown that C3H mice possess more advanced WAT fibrosis after HFD feeding compared to B6J mice with similar body weight [15]. Studying the effect of cytokines solely on fibrosis development, we used WAT explants from lean chow-fed mice. After 4 days of IL-13 or IL-4 stimulation, the mRNA expression of their respective receptors

Il13ra1 and *Il13ra2* was significantly increased in both mouse strains, with C3H mice displaying higher upregulation in stimulated WAT explants (Figures 1A and S1A). *Il4ra* expression was upregulated only after IL-4 treatment in C3H mice (Figure 1A). Interestingly, the IL-13-receptor *Il13ra2*, known as a decoy receptor, showed an upregulation up to 64-fold after stimulation with both cytokines, suggesting binding of excess cytokines, as previously described [13]. Importantly, IL-13 and IL-4 treatment upregulated the mRNA expression of many fibrosis-related and cross-linking enzyme genes (*Col1a1, Col3a1, Col6a1, Fn1, Lox, Loxl2, Timp1*) in both strains, whereby the expression levels were slightly higher in C3H mice (Figures 1B,C and S1A). Counterintuitively, the expression level of *Tgfb1*, which is described to be upregulated in many fibrotic diseases [14], was not altered. Additionally, a concentration range from 1 to 250 ng/mL was used to test the dose dependency of IL-13 and IL-4 to induce fibrosis phenotype. We observed that only high concentrations (50 ng/mL and above) could induce expression of fibrosis-related genes (Figure S3A) and increase the amount of secreted fibronectin (Figure S3B).
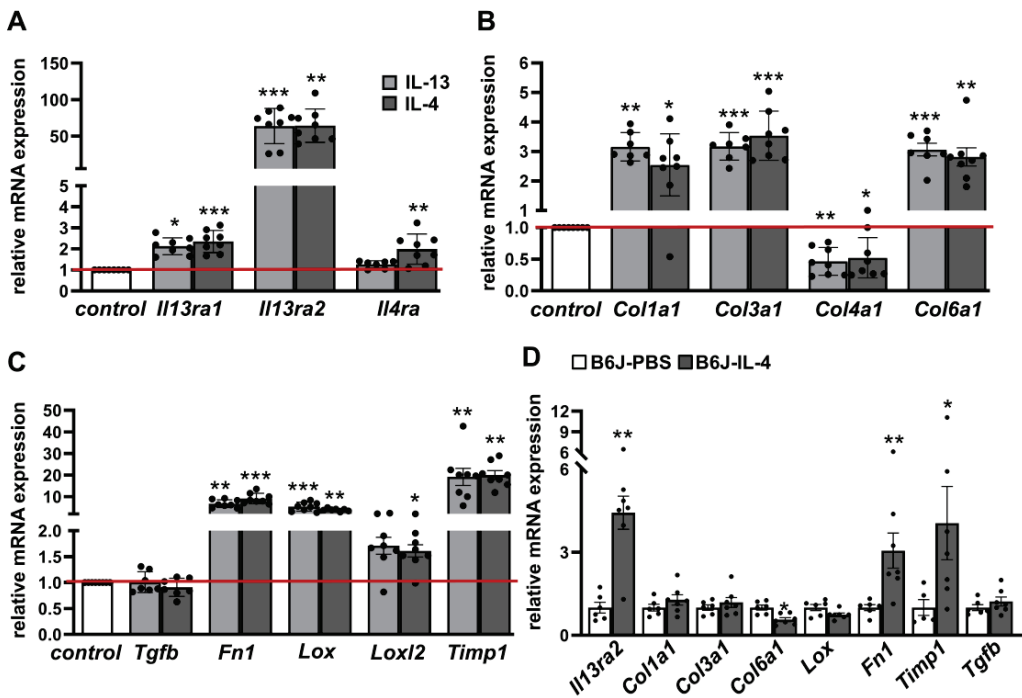
Figure 1. IL-13 and IL-4 induce fibrosis-related genes in adipose tissue of C3H mice and partial in WAT from B6J mice injected with IL-4. White adipose tissue (WAT) explants from C3H mice (n = 7–8) were stimulated either with IL-13 (50 ng/mL) or IL-4 (50 ng/mL) or non-stimulated (control) for four days. mRNA expression of cytokine receptors (**A**), collagens (**B**) and other fibrosis markers (**C**) are given as fold change compared to control condition. B6J mice were fed HFD over 6 weeks and were injected every two days with recombinant mouse IL-4 (66 µg/kg body weight) complexed with anti-IL-4 (333 µg/kg body weight) or PBS intraperitoneally (i.p.) for the final 2 weeks of feeding (n = 5–7). mRNA expression of Il13ra2 and fibrosis markers are given as fold change compared to PBS condition (**D**). Data represented as mean ± SEM. * p-value < 0.05; ** p-value < 0.01; *** p-value < 0.001. The red line indicates the level of the control group.

Next, we investigated our recent findings in an in vivo model. We used B6J mice receiving HFD for 6 weeks and recombinant mouse IL-4 complexed with IL-4 antibodies to stabilize IL-4 in vivo for the final two weeks of the feeding period. IL-4 treatment led

to a significant increase of mRNA levels of the *Il13ra2* receptor (4.4-fold) as well as *Fn1* (3.1-fold) and *Timp1* (4.1-fold); expression levels other genes associated with fibrosis were unaltered (*Col1a1, Col3a1, Lox, Tgfb1*) or even decreased (*Col6a1*) (Figure 1D). This result partially reflects the findings from the ex vivo WAT explants.

Activation of type 1 and type 2 IL-4 receptors results in downstream phosphorylation of STAT6. To investigate STAT6-signaling under IL-13 and IL-4 stimulation in WAT explants, explants from C3H mice were stimulated in an ex vivo culture system for 4 days. We detected a distinct elevation of phosphorylated STAT6 in IL-13 and IL-4 treated AT explants when compared to control conditions (Figure 2A). In addition, total STAT6 levels were higher in the IL-13 and IL-4 treated AT explants.
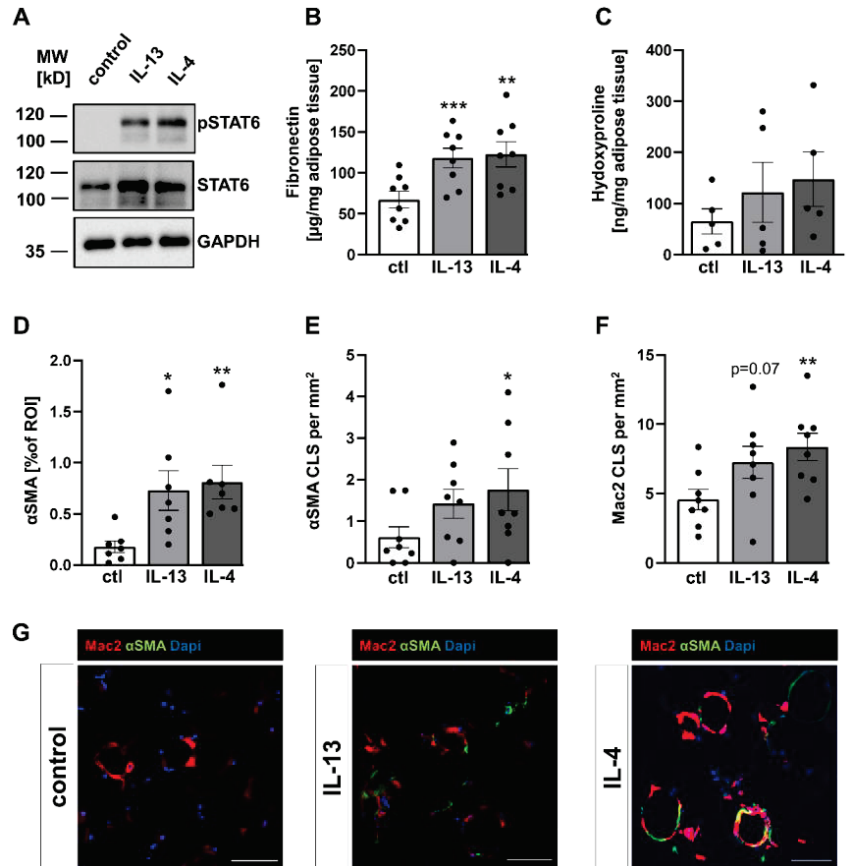
Figure 2. Increased STAT6 phosphorylation and fibrosis-associated proteins were induced by IL-13 and IL-4. WAT explants from C3H mice were stimulated with either IL-13 (50 ng/mL) or IL-4 (50 ng/mL) or non-stimulated (control) for four days. (**A**) A representative immunoblot from WAT explant lysates using antibodies against phosphorylated STAT6, total STAT6 and GAPDH to assess equal protein loading, from four independent experiments. (**B**) Levels of fibronectin were determined in supernatants of the explants (n = 8) by ELISA. (**C**) Collagen content in WAT explants was measured by hydroxyproline colorimetric assay (n = 5). (**D**) The area of α-SMA positive cells (n = 7), (**E**) the number of α-SMA positive crown-like structures (CLS, n = 8) and (**F**) the number of Mac-2 positive CLS (n = 8) in WAT explants were assessed by α-SMA (green) and Mac-2 (red) immunofluorescence staining. (**G**) Representative images of α-SMA and Mac-2 immunofluorescence staining. DAPI was used for nuclei counterstaining (blue). Data represented as mean ± SEM. * *p*-value < 0.05; ** *p*-value < 0.01; *** *p*-value < 0.001; scale bars = 50 μm.

Referring to the increase of fibrosis-related genes, we wanted to ensure that changes in expression patterns were also reflected at the protein level. Therefore, we measured levels of fibronectin, one of the highest expressed genes after IL-13/IL-4 stimulation, in the supernatant of stimulated and non-stimulated explants. In agreement with expression data, the levels of secreted fibronectin in WAT explants of C3H mice were significantly increased by ~75% or 80% after IL-13 or IL-4 treatment, respectively (Figure 2B). Quantification of fibronectin levels in the supernatant of AT explants from B6J mice confirmed these data (Figure S1B). Furthermore, we also measured levels of the amino acid hydroxyproline, a broadly employed method used for quantifying collagen. In contrast to upregulated collagen expression, we only detected a non-significant increase of hydroxyproline in explants from C3H mice (Figures 2C and S1C).

In many tissues affected by fibrotic diseases, αSMA expression levels were used to identify myofibroblasts, the major collagen-producing cell type in fibrotic tissues [22,23]. Immunofluorescence analysis revealed that αSMA-positive cells were increased 3 to 4-fold after IL-13 or IL-4 stimulation in C3H mice (Figure 2D). In addition to single αSMA-positive cells, presumably myofibroblasts, we also observed an αSMA-positive circular staining pattern, resembling crown-like structures (CLS; an accumulation of ATMs surrounding dying adipocytes). The presence of ATMs within these circular structures was confirmed by the macrophage marker Mac-2. Hence, we defined these structures as αSMA-positive CLS (αSMA-CLS). We found significantly higher numbers of αSMA-CLS in AT explants stimulated with IL-4, whereas the increase of αSMA-CLS after IL-13 treatment did not reach significance (Figure 2E). Most interestingly, a few CLS-associated ATMs showed co-expression of αSMA (Figure 2G), while interstitial ATMs (outside of CLS) revealed no obvious αSMA expression, suggesting a correlation between ATMs in CLS and αSMA expression. In addition, the numbers of Mac-2 positive CLS were also elevated after IL-13 and IL-4 stimulation, raising the question of a positive correlation between number of CLS, as marker for inflammation, and αSMA-positive areas (Figures 2F and S1D–F). In line with this, we observed a significant positive correlation for IL-4 induced Mac-2-CLS with αSMA-CLS in C3H mice (Figure S2).

Overall, WAT explants stimulated with 50 ng/mL of IL-13 and IL-4 from C3H mice and B6J mice are characterized by an increased propensity for WAT fibrosis, whereas WAT fibrosis is more pronounced in C3H animals. Furthermore, in vivo data from B6J mice injected with IL-4 partially confirmed its effects on fibrosis marker expression.

2.2. IL-4Rα-Chain Is Required for IL-13 and IL-4 Induced Fibrosis

Given the significant induction of fibrosis in response to IL-13 and IL-4, we next investigated which receptor was mediating this effect in WAT. There are three potential receptors: the type 1 and type 2 IL-4 receptor, which share the common receptor IL-4Rα-chain and can be activated by IL-4 (type 1, type 2) or IL-13 (type 2), and IL-13Rα2, which is activated by IL-13 only [24]. Since both cytokines can induce fibrosis, we hypothesized that the IL4Rα-chain could be the major receptor chain for IL-13 and IL-4 signaling. Hence, we used WAT explants from mice lacking the IL4rα-chain (*Il4ra−/−*) and age-matched B6J control mice. WAT explants were stimulated in an ex vivo model with IL-13 and IL-4 for 4 days as described above. In B6J control mice, we determined similar levels of mRNA expression for receptor genes (*Il13ra1, Il13ra2, Il4ra*) and fibrosis as well as cross-linking enzyme genes (*Col1a1, Col3a1, Col6a1, Fn1, Lox, Timp1*) (Figure 3A) as observed in B6J mice described in Figure S1A.

However, WAT explants from *Il4ra−/−* mice showed no response to IL-13 and IL-4 when compared to explants from age-matched wild-type B6J mice (Figure 3A). Moreover, the abundance of secreted fibronectin was quantified. In line with mRNA expression, the level of fibronectin did not increase upon IL-13 and IL-4 treatment in *Il4ra* deficient WAT explants (Figure 3B); this confirms that the IL4rα-chain is absolutely required for IL-13 and IL-4 induced fibrosis.
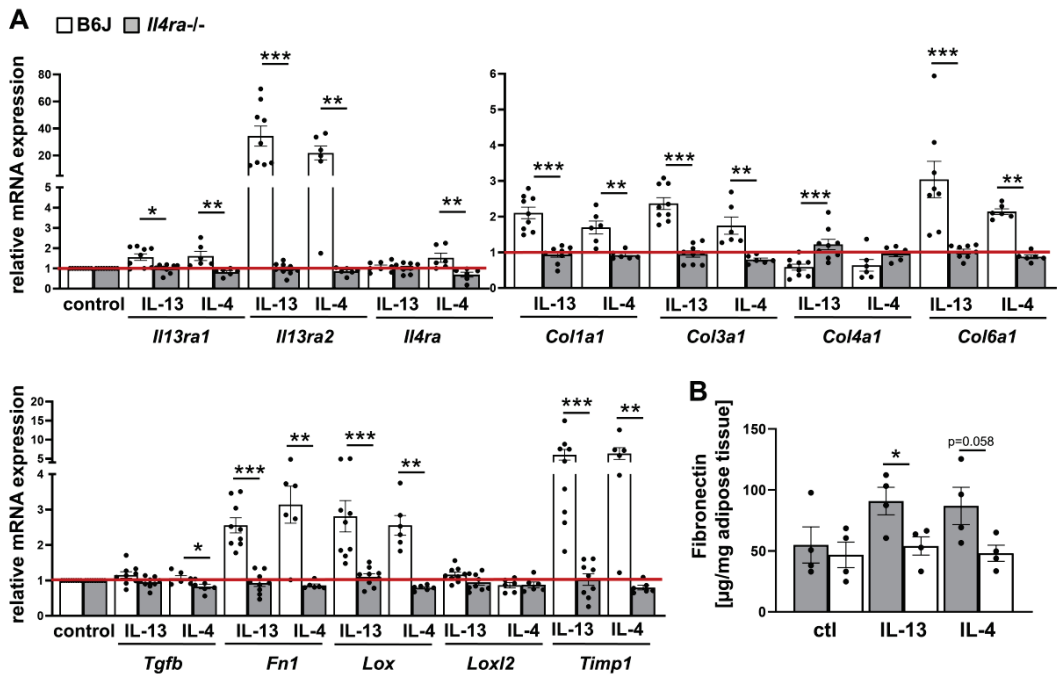
Figure 3. WAT explants from *Il4ra−/−* mice show no response to IL-13 and IL-4 stimulation. WAT explants from *Il4ra−/−* mice (n = 6–9) and control B6J mice (n = 6–9) were stimulated with either IL-13 (50 ng/mL) or IL-4 (50 ng/mL) or not (control) for four days. (**A**) mRNA expression of cytokine receptors and fibrosis-related genes were determined in stimulated explants and represented as relative changes to the control group (B6J). (**B**) Fibronectin content was measured in the supernatant of cultured explants by ELISA. All data were represented as mean ± SEM. * *p*-value < 0.05; ** *p*-value < 0.01; *** *p*-value < 0.001. The red line indicates the level of the control group.

2.3. IL-13 and IL-4 Induced Fibrosis Phenotype Depends on ATMs

Next, we set out to examine the mediator cells of IL-13 and IL-4 induced fibrosis in WAT. We characterized cultured adipocytes and macrophages by analyzing their gene expression profile. Differentiated 3T3-L1 adipocytes were stimulated with 50 ng/mL IL–13 or IL-4 over 48 h, respectively and with 5 ng/mL TGF-β1 as a positive control. Analysis of mRNA expression revealed no induction of fibrosis-related genes under IL-13 and IL-4 stimulation. TGF-β1, as a well-known stimulus for fibrosis, increased mRNA expression of some genes, including *Col1a1, Fn1, Lox,* and *Timp1* (Figure S4A).

To examine the impact of macrophages, we stimulated bone marrow derived macrophages (BMDMs) from *Il4ra−/−* deficient mice and littermate wild-type (WT) control mice with IL-13 (20 ng/mL) over 48 h and analyzed them using RNA sequencing (Figure 4A). Interestingly, we only observed an increased mRNA expression of *Fn1* in response to IL-13 in WT BMDMs; other fibrosis-related genes were not altered. In *Il4ra−/−* deficient BMDMs, fibrosis-related genes were not upregulated in response to IL-13. In contrast, comparing only BMDMs from WT and *Il4ra−/−* deficient mice without stimulation, we determined an increase in some fibrosis-related genes such as *Col1a1, Col1a2, Col3a1, Col5a1, Col6a3, Fn1, Timp1, Acta2* and *Lox* in *Il4ra−/−* deficient BMDMs, suggesting a basal difference between WT und *Il4ra−/−* deficient BMDMs; this was not altered even after IL-13 stimulation. Hence, basal gene expression of fibrosis genes in cultured macrophages depend on *Il4r* expression. However, to mimic fibrosis induction due to IL-13 stimulation, more complex culture systems (such as WAT explants) are needed, presumably due to the lack of myofibroblasts or adipocyte progenitors as additional mediators.
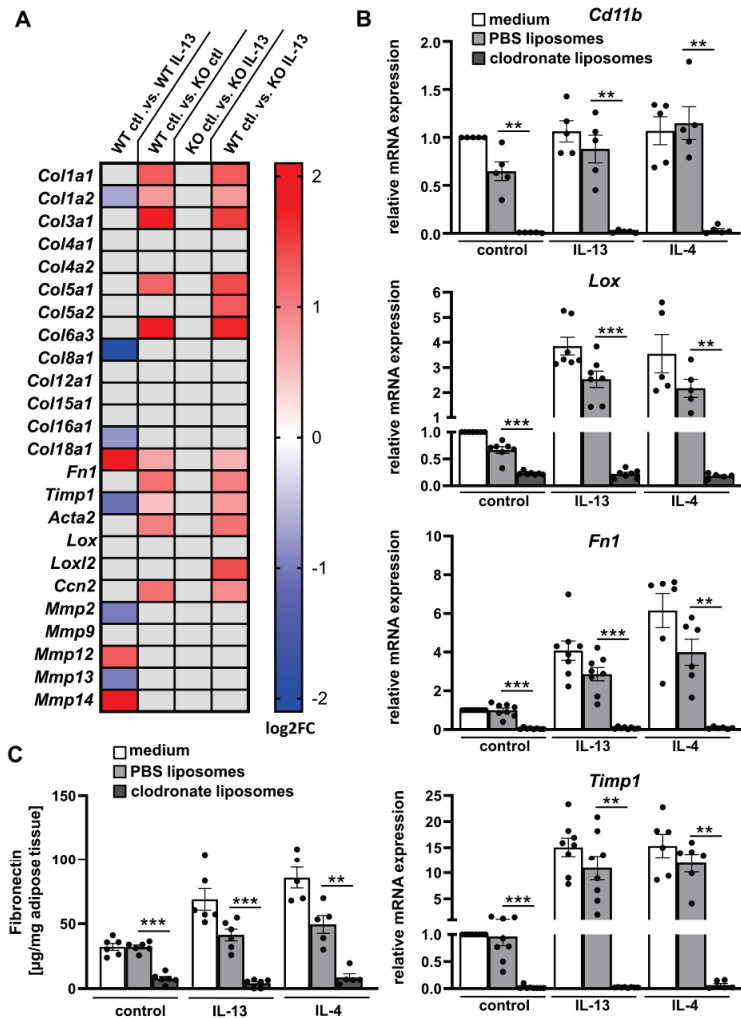
Figure 4. Adipose tissue fibrosis is dependent on adipose tissue macrophages (ATMs). (**A**) BMDMs were isolated from *Il4ra−/−* mice (KO, n = 4) and *Il4ra+/+* littermate controls (WT, n = 4) and stimulated with IL-13 (20 ng/mL) for 48 h. Differential gene expressions (DEGs) were determined from RNA bulk sequencing data and Log2FC of fibrosis-related genes were represented in a heat map; gray boxes illustrate non-significant data (FDR > 0.05) (**B**) Explants from B6J mice (n = 5–8) treated with clodronate or PBS liposomes or non-treated (medium) were stimulated for four days with 50 ng/mL IL-13 or IL-4, respectively. mRNA expression of the macrophage marker (*Cd11b*) and fibrosis markers are shown as fold change compared to control conditions (medium, non-stimulated). (**C**) Levels of fibronectin were determined in supernatants of WAT explants (n = 6) by ELISA. All data were represented as mean ± SEM. ** *p*-value < 0.01; *** *p*-value < 0.001.

Therefore, we further examined the role of ATMs in IL-4/IL-13-induced WAT fibrosis using WAT explants. A suitable mechanism to eliminate macrophages in vivo is treatment with clodronate liposomes [25]. First, we confirmed ATMs depletion by mRNA expression of the macrophage marker Cd11b (*Itgam*). *Cd11b* expression was only slightly decreased in WAT explants treated with PBS liposomes or IL-13 and unaltered after IL-4 stimulation, while clodronate liposomes dramatically reduced the expression of *Cd11b* in all conditions (Figure 4B). This finding demonstrates that clodronate liposomes can efficiently deplete

ATMs in our ex vivo model. We further characterized ATMs depleted WAT explants regarding the expression of fibrosis-related genes upon IL-13 or IL-4 treatment. Interestingly, *Lox*, *Fn1*, and *Timp1* mRNA levels were decreased by > 90% when compared to PBS control liposomes (Figure 4B). In line with the expression data, secreted fibronectin abundance was also reduced by ~90% and 80% in IL-13 or IL-4 stimulated WAT explants treated with clodronate liposomes (Figure 4C), respectively. These data clearly support the important role of ATMs in WAT fibrosis.

2.4. IL-13 and IL-4 Do Not Positively Correlate with Fibrosis Markers and Parameters Associated with Obesity in Human WAT

Finally, we performed a gene correlation analysis of *IL13* and *IL4* expression with cytokine receptors, fibrosis markers, IL-13/IL-4 signaling components, and metabolic parameters in human WAT to address the clinical relevance of our data and potential association with parameters of obesity. We analyzed the mRNA expression of visceral and subcutaneous WAT samples from 1553 adult patients from the Leipzig Obesity BioBank and adjusted for sex, BMI, and age. Most of the patients in this cohort were obese (BMI $\geq$ 30, N = 1470), which increases the occurrence of WAT fibrosis.

IL13 and *IL4* expression positively correlated with *IL13RA2*, *JAK3*, *TGFB1* and several matrix metalloproteinases (MMP) in visceral and subcutaneous WAT (Figures 5A and S5). In contrast, other fibrosis markers (*TIMP1*, *FN1*, *LOX*, *LOXL2*, *CCN2*, *COL1A1*, *COL3A1*, and *COL6A1*), showed an inverse correlation in both WAT tissues with *IL4* and *IL13* expression. However, *IL13RA1* revealed a positive correlation to all fibrosis markers (except *TGFB1*) and *IL4RA* only for a few (*TIMP1*, *TGFB1*, *COL1A1*, and *COL6A1*) in visceral WAT, consistent with the results in mouse WAT explants. We further correlated *IL13* and *IL4* expression with metabolic parameters in visceral and subcutaneous WAT. For *IL13*, we found a significant inverse correlation to body weight, body fat, and waist circumference, whereas *IL4* expression inversely correlated with waist circumference, fasting plasma glucose (FPI), and homeostatic model assessment for insulin resistance (HOMA-IR) in visceral WAT (Figure 5B, Table S1). We observed no significant correlations for *IL13* and *IL4* in subcutaneous WAT (Table S2). It is worth nothing that several fibrosis markers, including *TIMP1*, *FN1*, *LOX*, *CCN1*, *COL1A1*, *COL3A1*, and *COL6A1*, positively correlated with either body fat or/and waist circumference (Tables S1 and S2).

Figure 5. *Cont.*

B
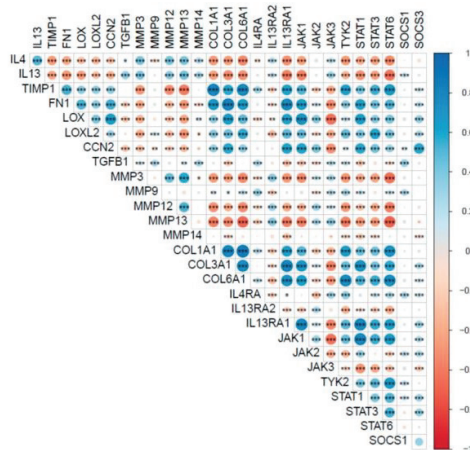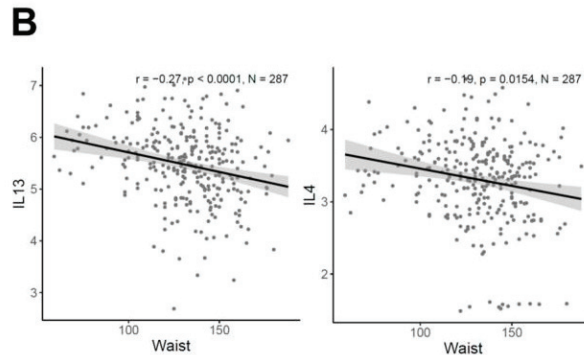
Figure 5. Human gene correlation analysis of visceral adipose tissues. The presented data are RNA-Seq data from human visceral adipose tissue samples (n = 1553). (**A**) Correlation analysis of fibrotic-related genes as well as *IL13* and *IL4* in visceral WAT. (**B**) Significant negative correlation of IL13 and IL4 with waist circumference (N = 287). Positive correlations are shown in blue while negative correlations are represented in red. The size of the dot refers to the degree of correlation; * *p*-value < 0.05; ** *p*-value < 0.01; *** *p*-value < 0.001.

Overall, the correlation data from a large human WAT Obesity BioBank offered conflicting results, as discussed below.

3. Discussion

Numerous studies have focused on WAT fibrosis, a consequence of a chronic inflamed and progressive metabolic imbalance during obesity. WAT fibrosis is characterized by excessive accumulation of ECM to counterbalance the arising WAT dysfunction [18,26]. However, the underlying cellular and molecular mechanisms are still ill-defined.

In this study, we aimed to clarify whether IL-13 and/or IL-4, well-known fibrosis inducers in various tissues, can also promote fibrosis in WAT. Therefore, we used an organotypic culture model that preserves the physiological function of WAT and the in vivo crosstalk between various types of cells [27]. Expression of several fibrosis markers, as well as levels of fibronectin and αSMA protein levels, were increased upon IL-13 and IL-4 stimulation, but this phenotype was entirely absent in WAT lacking *Il4ra*. This suggests that IL-13 and IL-4 are also involved in fibrotic remodeling in WAT depending on the IL-4 receptor α-chain. Notably, only concentrations above 50 ng/mL could induce the fibrotic phenotype, which does not reflect physiological cytokine concentrations [28,29]. An in vivo mouse model with repeated IL-4 injections partly confirmed our results from the ex vivo WAT explants. Here, we only observed an increase of two fibrosis markers (*Timp1* and *Fn1*), while other key markers, such as collagens, were not altered, suggesting that the in vivo effect of IL-4 on WAT fibrosis is not very pronounced or only occurs after chronic stimulation over longer time periods. Even though the injected IL-4 concentration was very high (66 μg/kg body weight), the expression levels of *Timp1* and *Fn1* were not comparable with those of ex vivo results. There are very few studies regarding fibrosis in IL-4- or IL-13-injected mice but, in contrast to our results, Kaviratne et al. provided evidence that intraperitoneal injections of IL-13 can lead to liver fibrosis by upregulating hepatic *Col1*, *Col3*, and *Timp1* expression [30]. However, we assume that physiological concentrations of IL-13 and IL-4 may not induce WAT fibrosis within a short time frame, but maybe over longer periods. Interestingly, we found that *Il13ra2*, an exclusive IL-13 decoy receptor, was induced even upon IL-4 stimulation, both ex vivo and in vivo. We hypothesize that a negative feedback mechanism may exist, by which IL-4 reduces an overactive Th2 response via the expression of *Il13ra2*. This feedback mechanism appears to be regulated by the α-chain of the IL-4 receptor, as *Il4ra* deficient mice do not show an increase of *Il13ra2* upon IL-4/IL-13 stimulation.

Th2 inflammation is considered to be one of the primary mediators in the pathogenesis of several fibrotic disorders. Surprisingly, the mechanism by which Th2 cytokines mediate fibrosis has not been consistently addressed. Several studies have found that IL-13 and IL-4 can activate fibroblasts and stimulate collagen deposition, as has already been shown for the prominent fibrosis inducer TGF-β1 [29,31,32]. Depending on tissues and cell types, fibrogenic effects of IL-13 and IL-4 are mediated by TGF-β1 induction [32,33] or conveyed independently [30], suggesting a broad spectrum of Th2-effective pathways. Previously published articles have already demonstrated that macrophages stimulated with IL-4 and/or IL-13 can produce different ECM components, affecting the biomechanical properties of a tissue; this is clearly seen in fibrotic diseases [34–38]. Here, we showed that WAT explants stimulated with IL-13 or IL-4 increased the expression of fibrosis genes as well as fibronectin secretion. Importantly, *Tgfb1* expression was not altered, indicating a TGF-β1-independent activation of WAT fibrosis through IL-13 and IL-4. However, the peak of *Tgfb1* induction might be earlier than our observation point at 48 h. As shown in macrophages and fibroblasts, IL-13 and IL-4 are also potent inducers of arginase expression, which converts L-arginine into L-ornithine and urea. Of note, L-ornithine is a precursor of proline, which promotes collagen synthesis and cell proliferation [39,40]. While we demonstrated an increase of collagen expression upon IL-13 and IL-4 stimulation in WAT explants, we could also observe an increased number of CLS containing Mac-2-positive ATMs. This observation is in line with our previous finding that M2-like ATMs possess the ability to proliferate within CLS [41]. Moreover, the αSMA positive area that increased upon IL-13 or IL-4 stimulation also appears to be localized in CLS; this could be evidence for cellular crosstalk within CLS. The recently found Mincle expression, localized only in pro-inflammatory ATMs within CLS, supports this assumption. As endogenous ligands (e.g., free fatty acids), released from dying adipocytes, Mincle is activated in ATMs, which in turn leads to expression of fibrosis-related genes and myofibroblasts activation [20,42]. Moreover, Mincle KO mice are protected from obesity-induced CLS formation and WAT fibrosis, indicating that Mincle plays a role in the crosstalk between adipocytes and macrophages within CLS [20]. A newly found subset of macrophages, called LAMs, were also localized within CLS, thereby expressing high levels of Cd9 and Trem2. Of note, TREM2 deficiency exacerbates WAT hypertrophy and insulin resistance by preventing LAM formation in response to a HFD [19]. This suggests an important role for LAMs in attenuating metabolic remodeling in obese WAT. It is worth noting that this subpopulation is also classified as pro-fibrotic, as TREM2$^+$CD9$^+$ macrophages expand in liver fibrosis [43]. Further investigations are needed to clarify if IL-13 or IL-4 have an impact on the fibrotic effects associated with LAMs within CLS.

Interestingly, Itoh et al. found that αSMA-positive myofibroblasts and collagen depositions are localized in proximity to hepatic CLS in a NASH mouse model [44]. This raises the question of the origin of αSMA-positive myofibroblasts within CLS. The origin of myofibroblasts in fibrotic WAT has been the subject of intensive investigation but remains controversial. For a long time, tissue-resident fibroblasts were thought to be the main precursor of myofibroblasts in WAT. However, recent studies have implicated an unexpected role of mature adipocytes, which can acquire a myofibroblast phenotype under fibrotic stimuli [45,46]. This process has been described as adipocyte mesenchymal transition [47]. In addition, Marcelin et al. have shown a phenotypical switch of adipose progenitors, classified as Cd9highPDGFRα+ progenitors, to myofibroblasts, which promote ECM deposition and WAT fibrosis [15]. However, we detected αSMA-positive myofibroblasts within CLS formed by ATMs as well as CLS formed only by myofibroblasts. It should be mentioned that only IL-4 stimulation significantly increased the number of αSMA-positive CLS, whereas the increase with IL-13 stimulation did not reach significance. This lower efficacy of IL-13 may be due to the higher binding affinity of IL-13 to IL-13Rα2 compared with IL-13Rα1, which suppresses the impact of IL-13 at the IL-4 receptor type II. Regardless, the cellular origin of IL-13 and IL-4 induced myofibroblasts remains unclear to date and warrants further investigation. There are multiple theories regarding the phenotypical switch of

adipocytes within fibrosis progression. One theory states that adipocytes dedifferentiate into mesenchymal progenitor cells upon systemic metabolic stress or hypoxia and then differentiate into myofibroblasts under fibrotic stimuli such as TGF-β1 [48]. On the other hand, these conditions could also cause ATM localization around dying adipocytes and thereby initiate the differentiation of adipose progenitors into myofibroblasts [47]. However, we studied the impact of ATMs on IL-13 and IL-4 induced fibrosis. Interestingly, the treatment with clodronate liposomes decreased the expression of fibrotic markers up to 99% and fibronectin abundance up to 90%. Thus, we postulate a direct crosstalk of ATMs to other cells, promoting the phenotypical switch towards myofibroblasts. Our finding that isolated macrophages and mature adipocytes do not respond upon IL-13 and IL-4 stimulation emphasizes this assumption. It is worth mentioning that mature adipocytes reduce *Il4ra* expression during the early phase of differentiation [49]; thus, using preadipocytes would be more physiological. In line with this, primary human adipocytes and preadipocytes co-cultured with THP-1 macrophages strongly increased collagen VI expression, most notably through M2-polarized macrophages [50]. Direct effects on the differentiation of SGBS preadipocytes by macrophages were reported by Sarsenbayeva et al., whereby the presence of macrophages induced αSMA expression in SGBS preadipocytes [51].

Interestingly, IL-4 can inhibit adipogenesis at the early phase of adipocyte differentiation through the STAT6 pathway [49]. This could be a possible mechanism by which IL-4 (and IL-13) increases the number of preadipocytes and, thereafter, myofibroblasts.

In human subjects, there are numerous studies indicating the significance of IL-13 and IL-4 for fibrotic diseases in different tissues. A study on 611 patients with *Schistosoma japonicum* infection confirmed the association of Th2 cytokines, including IL-4 and IL-13, with liver fibrosis [52]. Moreover, lung biopsies from patients suffering from idiopathic pulmonary fibrosis also exhibited elevated levels of IL-13 and IL-4 [53]. In this study, we investigated visceral and subcutaneous WAT expression from 1553 patients with a wide range of metabolic data. Regarding the expression of *IL13* and *IL4*, we found no evidence of a positive correlation with any fibrosis markers or metabolic parameters suggesting a controversial role of IL-13 and IL-4 in human WAT fibrosis. Although most of the patients were obese (N = 1470), indicating a higher risk for WAT fibrosis, the histological evidence for confirmed fibrosis was not available and needs to be provided in future studies. Of note, Kwon et al. found an increase of *IL13* expression in WAT of obese patients and HFD-fed mice compared to lean conditions; this was mediated by adipocytes, presumably to counterbalance tissue inflammation [54]. Moreover, IL-4 was also elevated in obese patients [55], suggesting the participation of IL-4 in the process of diet-induced obesity and metabolism. Controversially, we observed an inverse correlation for *IL13* with body weight, body fat, and waist circumference. In line with this finding, *IL4* correlated inversely with FPI and HOMA-IR as well as waist circumference. Supporting this data, Chang et al. reported an improved glucose tolerance and insulin sensitivity in mice injected with recombinant IL-4 during HFD feeding [56]. In contrast to our finding of the inverse correlations of *IL13* and *IL4*, we observed positive correlations of several collagens and other fibrotic marker genes with receptors of IL-13 and IL-4 as well as body fat and waist circumference in visceral and partly subcutaneous WAT. This result is in line with previous findings, showing that *COL6a3* expression increases with obesity and correlates positively with visceral fat mass and BMI [57,58].

While our analyses seem to suggest a controversial role for *IL13* and *IL4*, we acknowledge that no firm conclusions can be drawn from these correlations regarding the functional significance of IL-13 and IL-4 in WAT fibrosis. Therefore, further investigations are required to clarify pathophysiological mechanisms behind WAT fibrosis and concomitantly the role of IL-13 and IL-4 in this context.

4. Materials and Methods

4.1. Animals

All mice were maintained in temperature-controlled, pathogen-free facilities with a 12 h light/dark cycle and given free access to food and water. Male C57BL/6J mice (named B6J), Il4ra−/− mice, and Il4ra+/+ littermate controls were housed at the Universities of Halle and Leipzig. Fibrosis sensitive mouse strain C3H/HeOuJ (hereafter named C3H) were purchased from Jackson Laboratories (2498063-66). Male animals were fed a normal chow diet (9% kcal fat, Ssniff Spezialdiäten; Germany) and euthanized at the age of 18 to 22 weeks. Male C57BL/6J mice were fed an HFD (60% kcal deriving from fat, Research Diets, Inc.) over 6 weeks at the University of Dresden. Mice were injected with recombinant mouse IL-4 (66 μg/kg body weight) complexed with anti-IL-4 (333 μg/kg body weight) or PBS i.p. every other day for the final two weeks of the HFD feeding. Experiments were performed in accordance with the rules of animal care issued by the local government authorities and were approved by the animal care committee of the Universities of Halle, Leipzig, and Dresden, as well as by the state of Saxony and Saxony-Anhalt (Bezirksregierung Leipzig, Bezirksregierung Halle, Germany, T11/21, I11M25, Landesdirektion Sachsen, Germany, TVV57/2018).

4.2. Adipose Tissue Explant Culture

Epididymal WAT of male mice was used to generate ex vivo WAT organotypic cultures (WAT explants) [59]. Therefore, under sterile conditions, the dissected WAT was cut into small pieces (<1 mm^3) at 37 °C in PBS. 30–50 mg of these explants were transferred to six-well plates, overcasted with cell culture inserts (Merck Millipore, Darmstadt, Germany) and cultured in RPMI cell culture medium supplemented with 10% fetal bovine serum (FBS), 1% insulin-transferrin-selenium mixture, and 1% penicillin/streptomycin (all from Thermo Fisher Scientific, Waltham, MA, USA) for 7 days at 37 °C with 5% CO$_2$. After 3 days, AT explants were stimulated with 50 ng/mL of IL-13 or IL-4. On day 7, WAT explants were snap frozen in liquid nitrogen for RNA isolation or hydroxyproline assays and the supernatant was collected to quantify the volume. Testing the effect of different cytokine concentrations, WAT explants were stimulated in a range from 1 ng/mL up to 250 ng/mL of IL-13 or IL-4.

4.3. Clodronate Liposomes Treatment

A suitable mechanism to deplete macrophages in vivo is treatment with clodronate liposomes [25]. A high intracellular concentration of clodronate initiates programmed cell death and subsequently leads to the elimination of the macrophages [60]. Free clodronate does not easily cross cell membranes, so we used lipid vesicles encapsulating clodronate or an aqueous PBS solution (control) which were ingested by macrophages (Liposoma, The Netherlands). For macrophage depletion in AT explants, we used RPMI cell culture medium supplemented with 10% FBS, 1% insulin-transferrin-selenium mixture, 1% penicillin/streptomycin with 1 mg/mL clodronate, or PBS liposomes. First, the explants were transferred to tubes containing clodronate or PBS liposomes media followed by a rotation time at 37 °C for 60 min. Then, explants were cultivated as described above.

4.4. Culture of Bone Marrow-Derived Macrophages (BMDMs)

BMDMs were generated from bone marrow cells of *Il4ra*−/− mice and littermate controls (*Il4ra+/+*). Bone marrow cells were collected by flushing tibias and femurs with PBS and centrifuged for 10 min at 300 g [61]. Subsequently, the cells were differentiated into macrophages in BMDM medium (RPMI1640 medium supplemented with 10% FBS, 1 mM GlutaMax, 1% penicillin/streptomycin, all from Thermo Fisher Scientific, Waltham, MA, USA) and 20 ng/mL M-CSF (PeproTech, Hamburg, Germany) at 37 °C with 5% CO$_2$. After 7 days, BMDMs were harvested with an ice-cold 1 mM EDTA/PBS solution and 5×10^5 cell/mL were seeded in 1 mL BMDM medium. For cytokine stimulation, BMDMs were treated 24 h after seeding with 20 ng/mL IL-13 (PeproTech, Hamburg, Germany) for 48 h.

4.5. Culture of 3T3-L1 Cells

Murine 3T3-L1 cells were cultivated in DMEM high glucose supplement with 10% FBS and 1% penicillin/streptomycin (all from Thermo Fisher Scientific, Waltham, MA, USA) at 37 °C and 5% CO2 [62]. After 5 days, 3T3-L1 cells were seeded into 6-well plates at a density of 1×105 cells per well. 3T3-L1 cells were differentiated into adipocytes by treating confluent cells with DMEM, 10% FBS, 1% penicillin/streptomycin, 0.5 mM 3-isobutyl-1-methylxanthine (IBMX), 0.25 µM Dexamethasone, 0.2 µM Insulin, and 2 µM Rosiglitazone. On day 3, the media was switched to DMEM, 10% FBS, 1% penicillin/streptomycin, and 0.2 µM Insulin. From day 6 on, cells were further cultured under standard conditions. Cytokine stimulation on day 9 was performed with 50 ng/mL IL-13 or IL-4 or 5 ng/mL Tgf-β1 (PeproTech, Hamburg, Germany) for 48 h.

4.6. RNA Isolation and Quantitative RT-PCR

Total RNA was extracted from epididymal WAT and AT explants using the RNeasy Lipid Tissue Mini Kit (Qiagen, Hilden, Germany) followed by cDNA synthesis from 1 µg of total RNA with the First Strand cDNA Synthetis Kit (New England Biolabs) [61]. Quantitative real-time PCR was performed by using a SYBR green qPCR Master Mix (Thermo) and a ViiA™ 7 Real-Time PCR System (Thermo Fisher Scientific, Waltham, MA, USA). Primer sequences are listed in Table S3 in the supplementary materials. Gene expression levels were calculated through the ΔCt method by using Ipo8 as a housekeeping gene. For a better visualization, the values of the control group were set to 1 and mRNA expression was given as fold change compared to the control group.

4.7. Western Blotting

Western blotting was performed as recently described [51]. Total protein from WAT explants was extracted using an extraction buffer (Thermo Fisher Scientific, Waltham, MA, USA) supplemented with a protease and phosphatase inhibitor cocktail (Roche, Basel, Switzerland). Protein concentration was measured with the DC protein assay (Bio-Rad, Hercules, USA) according to the manufacturer's instructions. Equal amounts of protein (25 µg) were loaded to SDS-PAGE and transferred to a PVDF membrane. After blocking with 5% bovine serum albumin (BSA) in TBS/T, blots were incubated with primary antibodies against pSTAT6 (1:1000, #56554; Cell Signaling Technology, Boston, MA, USA), STAT6 (1:1000, #5397; Cell Signaling Technology, Boston, MA, USA), and GAPDH (1:1000, #3686; Cell Signaling Technology, Boston, MA, USA) for 16 h. After an incubation with a HRP-conjugated secondary antibody, immunoreactions were detected by visualizing the peroxidase activity with an ECL Kit (Pierce™ ECL Western Blotting Substrate, Thermo Fisher Scientific, Waltham, MA, USA). For reloading the membrane with primary antibody, blots were stripped with western blot stripping buffer (Thermo Fisher Scientific, Waltham, MA, USA) according to the manufacturer's instruction.

4.8. Collagen Content

Hydroxyproline measurement was performed using a hydroxyproline colorimetric assay (BioVision, Waltham, MA, USA) [15]. Snap frozen WAT explants were weighted and homogenized in water (100 mL water/10 mg WAT explants) using tissue homogenization (Precellys 24 Tissue Homogenizer, Bertin technologies, Montigny-le-Bretonneux, France). Homogenates (100 µL) were heated with 100 µL 12 M HCl for 3 h at 120 °C; then, 10 µL of the supernatant and a hydroxyproline standard were evaporated before being incubated with chloramine-T and p-dimethyl amino-benzaldehyde (DMAB) reagent at 60 °C for 90 min. The absorbance was read at 560 nm and the concentration was calculated using the standard curve and weights from WAT explants.

4.9. Fibronectin Content

The measurement of fibronectin levels was performed using a specific fibronectin ELISA kit (Fibronectin mouse ELISA kit 108849, Abcam, Cambridge, UK) [63]. Cell culture

media from WAT explants were centrifuged to remove debris, and supernatants were collected and diluted 1:50 in the diluent buffer provided with the kit. The fibronectin ELISA was performed according to the manufacturer's protocol.

4.10. Immunofluorescence

For immunofluorescence staining, AT explants were fixed in zinc formalin for 2 h and embedded in paraffin [64]. Paraffin sections were deparaffinized, unmasked in a pressure cooker at 120 °C in Tris/EDTA buffer (pH 9.5), and washed in PBS with 0.3% Triton. Unspecific binding sites were blocked using 1% BSA in PBS with 0.3% Triton for 1 h at room temperature. Sections were incubated overnight at 4 °C with primary antibodies against the macrophage marker Mac-2 (1:1000; Cedarlane CL8942AP, Canada) and the myofibroblast marker αSMA (1:200; Cell Signaling 19245, USA), followed by appropriate fluorochrome-conjugated secondary antibodies (1:200; Invitrogen; Waltham, MA, USA) and Hoechst for nuclear staining (1:10,000 in PBS, Life Technologies, Carlsbad, CA, USA). Control stainings were performed following the same routines without primary antibodies. Images were taken using an Olympus BX40 epifluorescence microscope. For αSMA quantification, a region of interest (ROI) was defined around the intact WAT explant and the αSMA positive area, above a determined threshold, within this ROI was then measured using ImageJ software 1.53 k. The threshold was determined in ROI sections of the control staining to exclude unspecific background noise. αSMA and Mac-2 positive CLS were quantified by counting in 10 randomly chosen fields in one section per animal, whereby CLS were defined as adipocytes surrounded by Mac-2 or αSMA positive cells.

4.11. RNA Bulk Sequencing from BMDMs and Differential Gene Expression Analysis

BMDMs were snap frozen in TRIzol (Quiagen, Hilden, Germany) and RNA bulk sequencing was performed by Single Cell Discoveries (Utrecht, The Netherlands). RNA extraction and library preparation followed the CELseq2 protocol [65] with a sequencing depth of 10 million reads/sample. For RNA-sequencing data analyses, low quality read ends were clipped off using Cutadapt (v 1.14) [66]. Subsequently, the processed sequencing reads were aligned to the murine reference genome (UCSC mm39) using HiSat2 (v 2.1.0) [67]. Samtools (v 1.10) was used to extract primary alignments and to index the resulting bam-files [68]. FeatureCounts (v 2.0.0) was used for summarizing gene-mapped reads [69]. ENSEMBL (GRCm39 v105) was used as annotation basis [70]. Differential gene expression (DGE) was determined using the R package edgeR (v 3.38.4) utilizing trimmed mean of M-values (TMM) normalization [71,72]. In order to account for biases in the expression values introduced by different batches, blocking was used to reduce these effects. A false discovery rate (FDR) value below 0.05 was considered as threshold for the determination of differential gene expression.

4.12. RNA Bulk Sequencing from Human Data

The human cross-sectional cohort from the Leipzig Obesity BioBank comprises 1553 individuals. Omental visceral and abdominal subcutaneous WAT samples were collected from each individual; these individuals were either non-obese (N = 83; 50.6% female; age: 64.2 ± 13.4 years old; BMI: 25.4 ± 2.7 kg/m^2) or obese (N = 1470; 70.8% female; age: 47.2 ± 11.9 years old; BMI: 48.9 ± 8.5 kg/m^2). Tissue samples were collected during elective laparoscopic abdominal surgery, as previously described [73]. Measurements of metabolic parameters and body composition were performed as described in detail before [74]. Bulk RNA-seq data were conducted with a SMARTseq protocol [75]. All libraries were sequenced on a Novaseq 6000 instrument at the Functional Genomics Center Zurich (FGCZ). Adapter and quality trimming of the raw reads were performed using fastp v0.20.0 [76] (minimum read length of 18 nts, quality cut-off of 20). Sequence pseudo alignment of the resulting high-quality reads to the human reference genome (build GRCh38.p13) and gene level expression quantification (gene model definition from GENCODE release 32) was computed using Kallisto v0.46 [77]. Samples with more than 20 million mapped

read counts were downsampled to 20 million read counts using the subsampleCountMatrix function of the R package ezRun v3.14.1 (https://github.com/uzh/ezRun, accessed on 23 March 2022). Count data were homoscedastic normalized with respect to library size using the variance stabilizing transformation from DESeq2 v1.32.084 [78] and adjusted for age, BMI, and sex.

4.13. Statistical Analysis

Statistical analyses were performed using GraphPad Prism9 (GraphPad Software, Inc., New York, NY, USA). At first, data were checked for statistical outliers using the ROUT test (Q = 1%). Normality and homogeneity of variance were assessed using the Shapiro–Wilk test and F-test, respectively. For two-group analyses with normally distributed data, an unpaired Student's *t*-test (data with equal variances) or Welch *t*-test (data with unequal variances) were used. For non-normally distributed data, a Mann–Whitney U test was used for two-group analyses. To compare more than two groups, a one-way ANOVA followed by Dunnett's multiple comparison test was assessed for normally distributed data. For non-normally distributed data of more than two groups, a Kruskal–Wallis test followed by Dunn's multiple comparison test was performed. Fibronectin and collagen content was analyzed by pairing one-way ANOVA with (data with unequal variances) or without (data with equal variances) followed by Geisser–Greenhouse correction or Dunnett's multiple comparison test. A Friedman test was used for non-normally distributed and repeated-measured data followed by Dunn's multiple comparison test. The data are expressed as means ± SEM and sample size is given in the respective figure legends. A Pearson correlation analysis was performed between the number of αSMA-positive CLS and Mac2-positive CLS. Correlation analysis between genes, body composition, and metabolic parameter of the human cohort were calculated using the R package ggstatsplot v0.9.185 [79] with the Spearman correlation coefficient and a confidence interval of 0.95. *p*-values were corrected for multiple inferences using the Holm method. Analyses were performed under R version 4.2.2 [80].

References

1. Blüher, M. Obesity: Global epidemiology and pathogenesis. *Nat. Rev. Endocrinol.* **2019**, *15*, 288–298. [CrossRef] [PubMed]
2. Johnston, E.K.; Abbott, R.D. Adipose Tissue Paracrine-, Autocrine-, and Matrix-Dependent Signaling during the Development and Progression of Obesity. *Cells* **2023**, *12*, 407. [CrossRef] [PubMed]
3. Sakers, A.; de Siqueira, M.K.; Seale, P.; Villanueva, C.J. Adipose-tissue plasticity in health and disease. *Cell* **2022**, *185*, 419–446. [CrossRef] [PubMed]
4. Datta, R.; Podolsky, M.J.; Atabai, K. Fat fibrosis: Friend or foe? *JCI Insight* **2018**, *3*, e122289. [CrossRef]
5. DeBari, M.K.; Abbott, R.D. Adipose Tissue Fibrosis: Mechanisms, Models, and Importance. *Int. J. Mol. Sci.* **2020**, *21*, 6030. [CrossRef]
6. Hirai, S.; Ohyane, C.; Kim, Y.-I.; Lin, S.; Goto, T.; Takahashi, N.; Kim, C.-S.; Kang, J.; Yu, R.; Kawada, T. Involvement of mast cells in adipose tissue fibrosis. *Am. J. Physiol. Endocrinol. Metab.* **2014**, *306*, E247–E255. [CrossRef]
7. Keophiphath, M.; Achard, V.; Henegar, C.; Rouault, C.; Clément, K.; Lacasa, D. Macrophage-secreted factors promote a profibrotic phenotype in human preadipocytes. *Mol. Endocrinol.* **2009**, *23*, 11–24. [CrossRef]
8. Borthwick, L.A.; Wynn, T.A.; Fisher, A.J. Cytokine mediated tissue fibrosis. *Biochim. Biophys. Acta* **2013**, *1832*, 1049–1060. [CrossRef]
9. Junttila, I.S. Tuning the Cytokine Responses: An Update on Interleukin (IL)-4 and IL-13 Receptor Complexes. *Front. Immunol.* **2018**, *9*, 888. [CrossRef]
10. Zhu, J. T helper 2 (Th2) cell differentiation, type 2 innate lymphoid cell (ILC2) development and regulation of interleukin-4 (IL-4) and IL-13 production. *Cytokine* **2015**, *75*, 14–24. [CrossRef]
11. Zurawski, S.M.; Vega, F.; Huyghe, B.; Zurawski, G. Receptors for interleukin-13 and interleukin-4 are complex and share a novel component that functions in signal transduction. *EMBO J.* **1993**, *12*, 2663–2670. [CrossRef]
12. Fichtner-Feigl, S.; Strober, W.; Kawakami, K.; Puri, R.K.; Kitani, A. IL-13 signaling through the IL-13alpha2 receptor is involved in induction of TGF-beta1 production and fibrosis. *Nat. Med.* **2006**, *12*, 99–106. [CrossRef]
13. Wood, N.; Whitters, M.J.; Jacobson, B.A.; Witek, J.; Sypek, J.P.; Kasaian, M.; Eppihimer, M.J.; Unger, M.; Tanaka, T.; Goldman, S.J.; et al. Enhanced interleukin (IL)-13 responses in mice lacking IL-13 receptor alpha 2. *J. Exp. Med.* **2003**, *197*, 703–709. [CrossRef]
14. Biernacka, A.; Dobaczewski, M.; Frangogiannis, N.G. TGF-β signaling in fibrosis. *Growth Factors* **2011**, *29*, 196–202. [CrossRef]
15. Marcelin, G.; Ferreira, A.; Liu, Y.; Atlan, M.; Aron-Wisnewsky, J.; Pelloux, V.; Botbol, Y.; Ambrosini, M.; Fradet, M.; Rouault, C.; et al. A PDGFRα-Mediated Switch toward CD9high Adipocyte Progenitors Controls Obesity-Induced Adipose Tissue Fibrosis. *Cell. Metab.* **2017**, *25*, 673–685. [CrossRef] [PubMed]
16. Cinti, S.; Mitchell, G.; Barbatelli, G.; Murano, I.; Ceresi, E.; Faloia, E.; Wang, S.; Fortier, M.; Greenberg, A.S.; Obin, M.S. Adipocyte death defines macrophage localization and function in adipose tissue of obese mice and humans. *J. Lipid Res.* **2005**, *46*, 2347–2355. [CrossRef] [PubMed]
17. Lindhorst, A.; Raulien, N.; Wieghofer, P.; Eilers, J.; Rossi, F.M.V.; Bechmann, I.; Gericke, M. Adipocyte death triggers a pro-inflammatory response and induces metabolic activation of resident macrophages. *Cell. Death Dis.* **2021**, *12*, 579. [CrossRef] [PubMed]
18. Marcelin, G.; Gautier, E.L.; Clément, K. Adipose Tissue Fibrosis in Obesity: Etiology and Challenges. *Annu. Rev. Physiol.* **2022**, *84*, 135–155. [CrossRef] [PubMed]
19. Jaitin, D.A.; Adlung, L.; Thaiss, C.A.; Weiner, A.; Li, B.; Descamps, H.; Lundgren, P.; Bleriot, C.; Liu, Z.; Deczkowska, A.; et al. Lipid-Associated Macrophages Control Metabolic Homeostasis in a Trem2-Dependent Manner. *Cell* **2019**, *178*, 686–698.e14. [CrossRef]
20. Tanaka, M.; Ikeda, K.; Suganami, T.; Komiya, C.; Ochi, K.; Shirakawa, I.; Hamaguchi, M.; Nishimura, S.; Manabe, I.; Matsuda, T.; et al. Macrophage-inducible C-type lectin underlies obesity-induced adipose tissue fibrosis. *Nat. Commun.* **2014**, *5*, 4982. [CrossRef]
21. Vila, I.K.; Badin, P.-M.; Marques, M.-A.; Monbrun, L.; Lefort, C.; Mir, L.; Louche, K.; Bourlier, V.; Roussel, B.; Gui, P.; et al. Immune cell Toll-like receptor 4 mediates the development of obesity- and endotoxemia-associated adipose tissue fibrosis. *Cell. Rep.* **2014**, *7*, 1116–1129. [CrossRef] [PubMed]
22. Klingberg, F.; Hinz, B.; White, E.S. The myofibroblast matrix: Implications for tissue repair and fibrosis. *J. Pathol.* **2013**, *229*, 298–309. [CrossRef] [PubMed]
23. Antar, S.A.; Ashour, N.A.; Marawan, M.E.; Al-Karmalawy, A.A. Fibrosis: Types, Effects, Markers, Mechanisms for Disease Progression, and Its Relation with Oxidative Stress, Immunity, and Inflammation. *Int. J. Mol. Sci.* **2023**, *24*, 4004. [CrossRef]
24. Chomarat, P.; Banchereau, J. Interleukin-4 and interleukin-13: Their similarities and discrepancies. *Int. Rev. Immunol.* **1998**, *17*, 1–52. [CrossRef] [PubMed]
25. Van Rooijen, N.; van Nieuwmegen, R. Elimination of phagocytic cells in the spleen after intravenous injection of liposome-encapsulated dichloromethylene diphosphonate. An enzyme-histochemical study. *Cell. Tissue Res.* **1984**, *238*, 355–358. [CrossRef] [PubMed]
26. Sun, K.; Tordjman, J.; Clément, K.; Scherer, P.E. Fibrosis and adipose tissue dysfunction. *Cell. Metab.* **2013**, *18*, 470–477. [CrossRef] [PubMed]
27. Gericke, M.; Weyer, U.; Braune, J.; Bechmann, I.; Eilers, J. A method for long-term live imaging of tissue macrophages in adipose tissue explants. *Am. J. Physiol. Endocrinol. Metab.* **2015**, *308*, E1023–E1033. [CrossRef]

28. D'Arcy, Q.; Gharaee-Kermani, M.; Zhilin-Roth, A.; Macoska, J.A. The IL-4/IL-13 signaling axis promotes prostatic fibrosis. *PLoS ONE* **2022**, *17*, e0275064. [CrossRef]

29. Jinnin, M.; Ihn, H.; Yamane, K.; Tamaki, K. Interleukin-13 stimulates the transcription of the human alpha2(I) collagen gene in human dermal fibroblasts. *J. Biol. Chem.* **2004**, *279*, 41783–41791. [CrossRef]

30. Kaviratne, M.; Hesse, M.; Leusink, M.; Cheever, A.W.; Davies, S.J.; McKerrow, J.H.; Wakefield, L.M.; Letterio, J.J.; Wynn, T.A. IL-13 activates a mechanism of tissue fibrosis that is completely TGF-beta independent. *J. Immunol.* **2004**, *173*, 4020–4029. [CrossRef]

31. Aoudjehane, L.; Pissaia, A., Jr.; Scatton, O.; Podevin, P.; Massault, P.-P.; Chouzenoux, S.; Soubrane, O.; Calmus, Y.; Conti, F. Interleukin-4 induces the activation and collagen production of cultured human intrahepatic fibroblasts via the STAT-6 pathway. *Lab. Investig.* **2008**, *88*, 973–985. [CrossRef] [PubMed]

32. Nguyen, J.K.; Austin, E.; Huang, A.; Mamalis, A.; Jagdeo, J. The IL-4/IL-13 axis in skin fibrosis and scarring: Mechanistic concepts and therapeutic targets. *Arch. Dermatol. Res.* **2020**, *312*, 81–92. [CrossRef] [PubMed]

33. Lee, C.G.; Homer, R.J.; Zhu, Z.; Lanone, S.; Wang, X.; Koteliansky, V.; Shipley, J.M.; Gotwals, P.; Noble, P.; Chen, Q.; et al. Interleukin-13 induces tissue fibrosis by selectively stimulating and activating transforming growth factor beta(1). *J. Exp. Med.* **2001**, *194*, 809–821. [CrossRef] [PubMed]

34. O'Brien, J.; Lyons, T.; Monks, J.; Lucia, M.S.; Wilson, R.S.; Hines, L.; Man, Y.-g.; Borges, V.; Schedin, P. Alternatively activated macrophages and collagen remodeling characterize the postpartum involuting mammary gland across species. *Am. J. Pathol.* **2010**, *176*, 1241–1255. [CrossRef]

35. Takemoto, R.; Kamiya, T.; Atobe, T.; Hara, H.; Adachi, T. Regulation of lysyl oxidase expression in THP-1 cell-derived M2-like macrophages. *J. Cell. Biochem.* **2021**, *122*, 777–786. [CrossRef]

36. Da Costa Santos, M.A.R.; Dos Reis, J.S.; do Nascimento Santos, C.A.; da Costa, K.M.; Barcelos, P.M.; de Oliveira Francisco, K.Q.; Barbosa, P.A.G.N.; da Silva, E.D.S.; Freire-de-Lima, C.G.; Morrot, A.; et al. Expression of O-glycosylated oncofetal fibronectin in alternatively activated human macrophages. *Immunol. Res.* **2023**, *71*, 92–104. [CrossRef] [PubMed]

37. Nakamura, R.; Bing, R.; Gartling, G.J.; Branski, R.C. Macrophages alter inflammatory and fibrotic gene expression in human vocal fold fibroblasts. *Exp. Cell. Res.* **2022**, *419*, 113301. [CrossRef]

38. Rudnik, M.; Hukara, A.; Kocherova, I.; Jordan, S.; Schniering, J.; Milleret, V.; Ehrbar, M.; Klingel, K.; Feghali-Bostwick, C.; Distler, O.; et al. Elevated Fibronectin Levels in Profibrotic CD14+ Monocytes and CD14+ Macrophages in Systemic Sclerosis. *Front. Immunol.* **2021**, *12*, 642891. [CrossRef]

39. Munder, M.; Eichmann, K.; Morán, J.M.; Centeno, F.; Soler, G.; Modolell, M. Th1/Th2-regulated expression of arginase isoforms in murine macrophages and dendritic cells. *J. Immunol.* **1999**, *163*, 3771–3777. [CrossRef]

40. Lindemann, D.; Racké, K. Glucocorticoid inhibition of interleukin-4 (IL-4) and interleukin-13 (IL-13) induced up-regulation of arginase in rat airway fibroblasts. *Naunyn Schmiedebergs Arch. Pharmacol.* **2003**, *368*, 546–550. [CrossRef]

41. Haase, J.; Weyer, U.; Immig, K.; Klöting, N.; Blüher, M.; Eilers, J.; Bechmann, I. Local proliferation of macrophages in adipose tissue during obesity-induced inflammation. *Diabetologia* **2014**, *57*, 562–571. [CrossRef]

42. Ichioka, M.; Suganami, T.; Tsuda, N.; Shirakawa, I.; Hirata, Y.; Satoh-Asahara, N.; Shimoda, Y.; Tanaka, M.; Kim-Saijo, M.; Miyamoto, Y.; et al. Increased expression of macrophage-inducible C-type lectin in adipose tissue of obese mice and humans. *Diabetes* **2011**, *60*, 819–826. [CrossRef]

43. Ramachandran, P.; Dobie, R.; Wilson-Kanamori, J.R.; Dora, E.F.; Henderson, B.E.P.; Luu, N.T.; Portman, J.R.; Matchett, K.P.; Brice, M.; Marwick, J.A.; et al. Resolving the fibrotic niche of human liver cirrhosis at single-cell level. *Nature* **2019**, *575*, 512–518. [CrossRef]

44. Itoh, M.; Kato, H.; Suganami, T.; Konuma, K.; Marumoto, Y.; Terai, S.; Sakugawa, H.; Kanai, S.; Hamaguchi, M.; Fukaishi, T.; et al. Hepatic crown-like structure: A unique histological feature in non-alcoholic steatohepatitis in mice and humans. *PLoS ONE* **2013**, *8*, e82163. [CrossRef]

45. Marangoni, R.G.; Korman, B.D.; Wei, J.; Wood, T.A.; Graham, L.V.; Whitfield, M.L.; Scherer, P.E.; Tourtellotte, W.G.; Varga, J. Myofibroblasts in murine cutaneous fibrosis originate from adiponectin-positive intradermal progenitors. *Arthritis Rheumatol.* **2015**, *67*, 1062–1073. [CrossRef]

46. Jones, J.E.C.; Rabhi, N.; Orofino, J.; Gamini, R.; Perissi, V.; Vernochet, C.; Farmer, S.R. The Adipocyte Acquires a Fibroblast-Like Transcriptional Signature in Response to a High Fat Diet. *Sci. Rep.* **2020**, *10*, 2380. [CrossRef] [PubMed]

47. Marangoni, R.G.; Korman, B.; Varga, J. Adipocytic Progenitor Cells Give Rise to Pathogenic Myofibroblasts: Adipocyte-to-Mesenchymal Transition and Its Emerging Role in Fibrosis in Multiple Organs. *Curr. Rheumatol. Rep.* **2020**, *22*, 79. [CrossRef] [PubMed]

48. Côté, J.A.; Lessard, J.; Pelletier, M.; Marceau, S.; Lescelleur, O.; Fradette, J.; Tchernof, A. Role of the TGF-β pathway in dedifferentiation of human mature adipocytes. *FEBS Open Bio* **2017**, *7*, 1092–1101. [CrossRef] [PubMed]

49. Tsao, C.-H.; Shiau, M.-Y.; Chuang, P.-H.; Chang, Y.-H.; Hwang, J. Interleukin-4 regulates lipid metabolism by inhibiting adipogenesis and promoting lipolysis. *J. Lipid Res.* **2014**, *55*, 385–397. [CrossRef] [PubMed]

50. Spencer, M.; Yao-Borengasser, A.; Unal, R.; Rasouli, N.; Gurley, C.M.; Zhu, B.; Peterson, C.A.; Kern, P.A. Adipose tissue macrophages in insulin-resistant subjects are associated with collagen VI and fibrosis and demonstrate alternative activation. *Am. J. Physiol. Endocrinol. Metab.* **2010**, *299*, E1016–E1027. [CrossRef] [PubMed]

51. Sarsenbayeva, A.; Pereira, M.J.; Nandi Jui, B.; Ahmed, F.; Dipta, P.; Fanni, G.; Almby, K.; Kristófi, R.; Hetty, S.; Eriksson, J.W. Excess glucocorticoid exposure contributes to adipose tissue fibrosis which involves macrophage interaction with adipose precursor cells. *Biochem. Pharmacol.* **2022**, *198*, 114976. [CrossRef]

52. Coutinho, H.M.; Acosta, L.P.; Wu, H.W.; McGarvey, S.T.; Su, L.; Langdon, G.C.; Jiz, M.A.; Jarilla, B.; Olveda, R.M.; Friedman, J.F.; et al. Th2 cytokines are associated with persistent hepatic fibrosis in human *Schistosoma japonicum* infection. *J. Infect. Dis.* **2007**, *195*, 288–295. [CrossRef]

53. Chandriani, S.; DePianto, D.J.; N'Diaye, E.N.; Abbas, A.R.; Jackman, J.; Bevers, J., III; Ramirez-Carrozzi, V.; Pappu, R.; Kauder, S.E.; Toy, K.; et al. Endogenously expressed IL-13Rα2 attenuates IL-13-mediated responses but does not activate signaling in human lung fibroblasts. *J. Immunol.* **2014**, *193*, 111–119. [CrossRef]

54. Kwon, H.; Laurent, S.; Tang, Y.; Zong, H.; Vemulapalli, P.; Pessin, J.E. Adipocyte-specific IKKβ signaling suppresses adipose tissue inflammation through an IL-13-dependent paracrine feedback pathway. *Cell Rep.* **2014**, *9*, 1574–1583. [CrossRef]

55. El-Wakkad, A.; Hassan, N.E.-M.; Sibaii, H.; El-Zayat, S.R. Proinflammatory, anti-inflammatory cytokines and adiponkins in students with central obesity. *Cytokine* **2013**, *61*, 682–687. [CrossRef]

56. Chang, Y.-H.; Ho, K.-T.; Lu, S.-H.; Huang, C.-N.; Shiau, M.-Y. Regulation of glucose/lipid metabolism and insulin sensitivity by interleukin-4. *Int. J. Obes. (Lond.)* **2012**, *36*, 993–998. [CrossRef]

57. Pasarica, M.; Gowronska-Kozak, B.; Burk, D.; Remedios, I.; Hymel, D.; Gimble, J.; Ravussin, E.; Bray, G.A.; Smith, S.R. Adipose tissue collagen VI in obesity. *J. Clin. Endocrinol. Metab.* **2009**, *94*, 5155–5162. [CrossRef] [PubMed]

58. Khan, T.; Muise, E.S.; Iyengar, P.; Wang, Z.V.; Chandalia, M.; Abate, N.; Zhang, B.B.; Bonaldo, P.; Chua, S.; Scherer, P.E. Metabolic dysregulation and adipose tissue fibrosis: Role of collagen VI. *Mol. Cell. Biol.* **2009**, *29*, 1575–1591. [CrossRef]

59. Braune, J.; Weyer, U.; Hobusch, C.; Mauer, J.; Brüning, J.C.; Bechmann, I.; Gericke, M. IL-6 Regulates M2 Polarization and Local Proliferation of Adipose Tissue Macrophages in Obesity. *J. Immunol.* **2017**, *198*, 2927–2934. [CrossRef] [PubMed]

60. Van Rooijen, N.; Sanders, A.; van den Berg, T.K. Apoptosis of macrophages induced by liposome-mediated intracellular delivery of clodronate and propamidine. *J. Immunol. Methods* **1996**, *193*, 93–99. [CrossRef] [PubMed]

61. Ackermann, J.; Arndt, L.; Kirstein, M.; Hobusch, C.; Brinker, G.; Klöting, N.; Braune, J.; Gericke, M. Myeloid Cell-Specific IL-4 Receptor Knockout Partially Protects from Adipose Tissue Inflammation. *J. Immunol.* **2021**, *207*, 3081–3089. [CrossRef] [PubMed]

62. Braune, J.; Lindhorst, A.; Fröba, J.; Hobusch, C.; Kovacs, P.; Blüher, M.; Eilers, J.; Bechmann, I.; Gericke, M. Multinucleated Giant Cells in Adipose Tissue Are Specialized in Adipocyte Degradation. *Diabetes* **2021**, *70*, 538–548. [CrossRef] [PubMed]

63. Brentnall, M.; Weir, D.B.; Rongvaux, A.; Marcus, A.I.; Boise, L.H. Procaspase-3 regulates fibronectin secretion and influences adhesion, migration and survival independently of catalytic function. *J. Cell. Sci.* **2014**, *127*, 2217–2226.

64. Brinker, G.; Froeba, J.; Arndt, L.; Braune, J.; Hobusch, C.; Lindhorst, A.; Bechmann, I.; Gericke, M. CD4^{+} T cells regulate glucose homeostasis independent of adipose tissue dysfunction in mice. *Eur. J. Immunol.* **2021**, *51*, 1399–1411. [CrossRef] [PubMed]

65. Hashimshony, T.; Senderovich, N.; Avital, G.; Klochendler, A.; de Leeuw, Y.; Anavy, L.; Gennert, D.; Li, S.; Livak, K.J.; Rozenblatt-Rosen, O.; et al. CEL-Seq2: Sensitive highly-multiplexed single-cell RNA-Seq. *Genome Biol.* **2016**, *17*, 77. [CrossRef]

66. Martin, M. Cutadapt removes adapter sequences from high-throughput sequencing reads. *EMBnet J.* **2011**, *17*, 10. [CrossRef]

67. Kim, D.; Langmead, B.; Salzberg, S.L. HISAT: A fast spliced aligner with low memory requirements. *Nat. Methods* **2015**, *12*, 357–360. [CrossRef] [PubMed]

68. Li, H.; Handsaker, B.; Wysoker, A.; Fennell, T.; Ruan, J.; Homer, N.; Marth, G.; Abecasis, G.; Durbin, R. The Sequence Alignment/Map format and SAMtools. *Bioinformatics* **2009**, *25*, 2078–2079. [CrossRef]

69. Liao, Y.; Smyth, G.K.; Shi, W. featureCounts: An efficient general purpose program for assigning sequence reads to genomic features. *Bioinformatics* **2014**, *30*, 923–930. [CrossRef]

70. Aken, B.L.; Achuthan, P.; Akanni, W.; Amode, M.R.; Bernsdorff, F.; Bhai, J.; Billis, K.; Carvalho-Silva, D.; Cummins, C.; Clapham, P.; et al. Ensembl 2017. *Nucleic Acids Res.* **2017**, *45*, D635–D642. [CrossRef]

71. Robinson, M.D.; McCarthy, D.J.; Smyth, G.K. edgeR: A Bioconductor package for differential expression analysis of digital gene expression data. *Bioinformatics* **2010**, *26*, 139–140. [CrossRef] [PubMed]

72. Robinson, M.D.; Oshlack, A. A scaling normalization method for differential expression analysis of RNA-seq data. *Genome Biol.* **2010**, *11*, R25. [CrossRef] [PubMed]

73. Langhardt, J.; Flehmig, G.; Klöting, N.; Lehmann, S.; Ebert, T.; Kern, M.; Schön, M.R.; Gärtner, D.; Lohmann, T.; Dressler, M.; et al. Effects of Weight Loss on Glutathione Peroxidase 3 Serum Concentrations and Adipose Tissue Expression in Human Obesity. *Obes. Facts* **2018**, *11*, 475–490. [CrossRef] [PubMed]

74. Klöting, N.; Blüher, M. Insulin-sensitive obesity. *Am. J. Physiol. Endocrinol. Metab.* **2010**, *299*, E506–E515. [CrossRef]

75. Picelli, S.; Faridani, O.R.; Björklund, A.K.; Winberg, G.; Sagasser, S.; Sandberg, R. Full-length RNA-seq from single cells using Smart-seq2. *Nat. Protoc.* **2014**, *9*, 171–181. [CrossRef]

76. Chen, S.; Zhou, Y.; Chen, Y.; Gu, J. fastp: An ultra-fast all-in-one FASTQ preprocessor. *Bioinformatics* **2018**, *34*, i884–i890. [CrossRef]

77. Bray, N.L.; Pimentel, H.; Melsted, P.; Pachter, L. Near-optimal probabilistic RNA-seq quantification. *Nat. Biotechnol.* **2016**, *34*, 525–527. [CrossRef]

78. Love, M.I.; Huber, W.; Anders, S. Moderated estimation of fold change and dispersion for RNA-seq data with DESeq2. *Genome Biol.* **2014**, *15*, 550. [CrossRef]

79. Patil, I. Visualizations with statistical details: The 'ggstatsplot' approach. *JOSS* **2021**, *6*, 3167. [CrossRef]
80. R Foundation for Statistical Computing. R Core Team R: A Language and Environment for Statistical Computing. 2022. Available online: http://www.r-project.org (accessed on 18 February 2022).

Review

Pathophysiological and Therapeutic Roles of Fascial Hyaluronan in Obesity-Related Myofascial Disease

Chiedozie Kenneth Ugwoke, Erika Cvetko and Nejc Umek *

Institute of Anatomy, Faculty of Medicine, University of Ljubljana, 1000 Ljubljana, Slovenia
* Correspondence: nejc.umek@mf.uni-lj.si

Abstract: Myofascial disease is an important complication associated with obesity and one of the leading causes of physical disability globally. In the face of limited treatment options, the burden of myofascial disorders is predicted to increase along with the escalating prevalence of obesity. Several pathological processes in obesity contribute to modifications in fascial extracellular matrix mechanical and biological properties and functions. Changes in adipose tissue metabolism, chronic inflammatory phenotype, oxidative stress, and other mechanisms in obesity may alter the physiochemical and biomechanical properties of fascial hyaluronan. Understanding the pathophysiological importance of hyaluronan and other components of the fascial connective tissue matrix in obesity may shed light on the etiology of associated myofascial disorders and inform treatment strategies. Given its unique and favorable pharmacological properties, hyaluronan has found a broad range of clinical applications, notably in orthopedic conditions such as osteoarthritis and tendinopathies, which share important pathophysiological mechanisms implicated in myofascial diseases. However, while existing clinical studies uniformly affirm the therapeutic value of hyaluronan in myofascial disorders, more extensive studies in broader pharmacological and clinical contexts are needed to firmly validate its therapeutic adaptation.

Keywords: Fascia; obesity; hyaluronan; fasciopathy; myofascial disease; pathophysiology; therapeutics

1. Introduction

The Fascia Research Society, through its Fascia Nomenclature Committee, has proposed both anatomical and functional definitions of the fascia. Morphologically, a fascia was defined as "a sheath, a sheet, or any other dissectible aggregations of connective tissue that forms beneath the skin to attach, enclose, and separate muscles and other internal organs". Functionally, the fascial system was defined as "the three-dimensional continuum of soft, collagen-containing, loose and dense fibrous connective tissues that permeate the body, providing an environment that enables all body systems to operate in an integrated manner" [1–3]. Based on histological properties and anatomical relationships, fascia may be classified into four types: superficial (subcutaneous) fascia, deep/muscular fasciae (aponeurotic and epimysial fasciae), visceral fasciae, and neural fasciae (meningeal layers and connective tissue sheath of peripheral nerves) [4,5]. Structurally, the fascia tissue consists of various cell types (fibroblasts, myofibroblasts, fasciacytes, and telocytes), an extracellular matrix consisting of fibrous (types I and III collagen fibers, elastin, and fibrillin), and aqueous (water and complex mixture of glycosaminoglycans) components, and nerve elements (free nerve endings and mechanoreceptors) [4,6].

While the biomechanical properties of the clinically important fascia, such as the plantar fascia, have been well-studied [7–10], the microscopic anatomy and pathology of the fascia have received limited attention. Little is known about the elastic fiber composition, extracellular matrix characteristics, vascularity, innervation extent of the fascia tissue, and their role in disease and therapeutics [11]. Deepening our understanding of the microanatomical and biochemical basis of fascial disease in obesity may provide novel

therapeutic insights for the medical and surgical treatment of obesity-related myofascial complications. A significant body of evidence has highlighted the critical role of fascial cells, extracellular matrix, and nerve elements in the pathogenesis of myofascial disease [4,6]. In this regard, a therapeutically relevant consideration is the role of hyaluronan (hyaluronic acid) in clinical fasciopathy. The present review aims to examine the current evidence on the pathological role and therapeutic potential of fascial hyaluronan in obesity-related myofascial disorders.

2. Hyaluronan Biochemistry, Cellular Synthesis, and Homeostasis

Despite being first described nearly 90 years ago, the role of hyaluronan in fascia physiology and pathology has only received focal attention in recent decades [12,13]. Hyaluronan is the dominant polysaccharide of the extracellular matrix of connective tissues with high cross-species structural homology, being structurally identical in bacteria and vertebrates [14]. It can be found in connective, epithelial, and neural tissues, where it provides mechanical stability and acts as a water reservoir, lubricant, and extracellular matrix homeostatic regulator [15]. Besides fascial hyaluronan, other body tissues such as the skin, tendon sheaths, pleura, pericardium, synovial fluid, the vitreous body, and the umbilical cord are also rich in hyaluronan. A 70-kg body has 15 g of hyaluronan, and about 50% of total body hyaluronan is located in the dermis [14,16].

Hyaluronan is a linear non-sulfated glycosaminoglycan composed of a single polysaccharide chain built by repeated disaccharide units of N-acetyl-D-glucosamine and D-glucuronic acid, respectively linked by β1–3 and β1–4 glycosidic bonds [12]. It is synthesized by three plasma membrane-bound hyaluronan synthases (HAS1, HAS2, and HAS3). As hyaluronan is synthesized in the plasma membrane rather than the Golgi, it lacks peptides in its fundamental structure, unlike other glycosaminoglycans [17]. Hyaluronan may be found in tissues in three forms: attached to plasma membranes, aggregated with other organic molecules, or as unbound polysaccharides [17]. Hyaluronan can interact with several extracellular matrix-binding proteins, such as aggrecans, but when not coupled to other molecules, it forms a viscous environment by self-associating and binding to water molecules [18]. In vivo, hyaluronan polymers range in size from 5000 to 20,000,000 Da and are divided into high and low molecular weight hyaluronan, each having different functional properties [19]. While high-molecular-weight hyaluronan contributes to tissue homeostasis by inhibiting cell proliferation, migration, angiogenesis, inflammation, and immunogenicity, hyaluronan oligomers have been shown to stimulate endothelial proliferation and migration, including tumor cell motility via their interaction with cluster determinant 44 (CD44) receptors, which is currently thought to be the major hyaluronan receptor on most cell types [20–22]. The membrane-bound CD44 regulates adhesion, motility, and intracellular signaling, while the receptor for hyaluronan-mediated motility (RHAMM) modulates intracellular signaling [23]. RHAMM is a centrosome- and microtubule-associated protein that is highly expressed before and during mitosis and hence prominent in neoplastic and other hyperproliferative tissues [24]. Besides the widely distributed CD44, hyaluronan fragments may also activate RHAMM, LYVE-1 (lymphatic vessel endothelial hyaluronan receptor), HARE (hyaluronan-receptor for endocytosis), ICAM-1 (intercellular adhesion molecule 1), layilin, Toll-like receptor 4, and other cell surface receptors which modulate gene expression via signaling pathways [23,25]. Accordingly, hyaluronan binding is critical for morphogenesis, matrix organization, wound repair/regeneration, inflammation, and metastasis [23].

While the predominant cell type in the fascia is the fibroblast which plays critical roles in mechanotransduction and synthesis of extracellular matrix precursors, a new class of previously undescribed cells termed "fasciacytes", which are modified fibroblast-like cells located at the border of the different fascial layers, have been proposed as the site of fascial hyaluronan synthesis and secretion [4,26]. These cells are termed synoviocytes in the joints and hyalocytes in the eye, where they respectively secrete the hyaluronan of the synovial and vitreous fluids. Fasciacytes stain prominently with Alcian blue and are visualized as

small clusters of rounded cells with circular nuclei, perinuclear cytoplasm, and small, less-elongated cellular processes [26]. They have been shown to express hyaluronan synthase 2 mRNA and are positive for the fibroblast marker vimentin, and negative for anti-CD68 indicating they are non-derivatives of the monocyte/macrophage lineage [26,27]. The deep muscular fascia expresses high levels of hyaluronan in the interface between the fascia and the epimysium [28]. This layer of hyaluronan-rich loose connective tissue between the deep fascia and the underlying skeletal muscle was also demonstrated by Stecco and colleagues using a combination of histological and sonographic analysis [29]. Hyaluronan has been shown to facilitate the gliding between different fascial sublayers and between fascia and muscle [28,30]. Given the evidence on its endomysial histolocalisation, it has also been suggested that hyaluronan not only lubricates but promotes muscle fiber motility [31].

Proteoglycans/glycosaminoglycans, elastin, fibronectin, laminin, and numerous other glycoproteins make up the thick dynamic extracellular matrix surrounding all fascia cells [4]. Fascia homeostasis is the outcome of dynamic interactions between cellular components and the extracellular matrix, and reciprocally, small extracellular matrix functional and structural changes contribute to complex cellular adaption mechanisms [32]. Additionally, the extracellular matrix functions as a molecular storage system, capturing and releasing physiologically active chemicals that govern cellular and tissue function, development, regeneration, and repair [33]. The mechanical properties of hyaluronan are determined by its molecular weight, tissue concentration, pH, covalent modifications, alterations in binding interactions with other molecules, and fluid dynamics [30,34]. The tissue half-life of hyaluronan ranges from a few hours to several days, and removal occurs by receptor-mediated endocytosis and lysosomal breakdown with subsequent elimination via lymph nodes, liver, and kidney [17,18]. Tissue hyaluronan equilibrium is maintained by both hyaluronan synthases and the cleavage enzymes, hyaluronidases (HYAL 1, 2, and 3), as well as non-enzymatic degradation via thermal or shear stress, acidic/alkaline hydrolysis, and reactive oxygen species [14,34]. Tissue volume, viscosity, and elasticity are all affected when hyaluronan mass or molecular weight decreases due to degradation or a decline in synthesis [18].

Healthy fascia requires a specific level of the lubricating layer of hyaluronan, which allows sliding between fascial sublayers and between fasciae and adjacent structures [35,36]. The hyaluronan composition of human fascial samples obtained from different anatomic regions was first quantified by Fede and colleagues in 2018 [36]. They demonstrated that hyaluronan concentration varies in accordance with the degree of fascial plane sliding and gliding functions in different anatomic regions. For example, the average hyaluronan concentration in the retinacula of the ankle (fascia associated with a mobile joint) was 90 µg/g of fascial tissue, in contrast to the fascia adherent to a muscle (epimysial fascia), with limited lubrication requirement, such as fascia overlying the trapezius and deltoid, which had an average hyaluronan content of 6 µg/g of fascial tissue [36].

3. Obesity and Myofascial Disease

The global prevalence of obesity has escalated to pandemic proportions over the past half-century [37–39], with recent data from the World Health Organization revealing that the condition affects 13% of the world's population [40]. A recent estimate of the economic impact of obesity in eight countries reported that the condition costs between 0.8% and 2.4% of gross domestic product (GDP) and that the magnitude of economic impact was similarly substantial in both low-, middle-, and high-income countries, and projected to increase if current trends persist [41]. The rising global trend of obesity is associated with the increasing prevalence of cardiometabolic disorders such as type 2 diabetes mellitus and hypertension, as well as a broad spectrum of orthopedic morbidities [42,43]. A growing body of evidence suggests that the histological and biomolecular changes of the human fascia contribute to several myofascial and other connective tissue disorders associated with obesity and metabolic syndrome, including adhesive capsulitis, Dupuytren's contracture,

crystal-induced arthritis, plantar fasciitis, plantar fascia rupture, plantar fibromatosis, plantar xanthoma, and enthesopathy [12,29,43,44].

Myofascial pain syndromes are musculoskeletal pain disorders with a commonly associated neuropathic component and represent a leading cause of physical disability globally. They are thought to originate from myofascial trigger points, which are palpable hyperirritable painful spots involving a select number of muscle fibers, and may be acute or chronic, primary, or secondary to another comorbidity [45]. It was long assumed that the syndrome exclusively involved muscles, but current research suggests that the fascia plays a critical role, although the exact mechanisms and therapeutic significance of fascial pathophysiological roles remain an open subject for further investigation [46]. Pathological degenerative changes in the fascia, or fasciitis, are among the leading causes of functionally limiting musculoskeletal pain syndromes. For example, plantar fasciitis affects one in ten people in their lifetime and accounts for 1% of all orthopedic consultations [47]. A high prevalence of myofascial pain (high proportion of latent and active myofascial trigger points) is similarly reported in patients presenting with chronic back pain, non-specific neck pain, and chronic non-traumatic shoulder pain [48–51]. The prevalence of myofascial pain ranges from 21–93% in general orthopedic practice and specialist pain clinic patients, respectively, and up to 85% of people in the general population will experience myofascial pain in their lifetime [52]. In the United States alone, the national economic burden of plantar fasciitis was estimated at 284 million US dollars, with medication costs accounting for about 80% of total costs [53]. Several risk factors have been identified, including obesity, traumatic musculoskeletal injuries, spine disease, cumulative and repeated strain, postural dysfunction, and physical deconditioning [45].

Obesity is a key epidemiological risk factor for myofascial disease [54–60]. A systematic review of 51 studies found that the only significant predictor related to plantar fasciitis was a body mass index (BMI) >27 kg/m^2 [61]. Even in an active population such as recreational and competitive runners, of eleven analyzed risk factors, increased BMI and body mass were found to be primary risk factors for fasciopathy [55]. In recent-onset type 2 diabetic subjects without complications, plantar fascia thickness was increased compared to the controls and significantly associated with adiposity and BMI values, suggesting important clinical implications in obese diabetic patients [62]. Plantar fascia thickness has also been shown to be a reliable alternative index of tissue glycation and a significant predictor of microvasculopathy, an essential denominator in several obesity-related complications [63–67]. Cytokines and other inflammatory molecules that have been demonstrated in the environment of myofascial trigger points are also typically overexpressed in the skeletal muscle of obese patients [68,69]. High-fat diet-induced obese mice were shown to express elevated spontaneous neurotransmission, which facilitates the development of myofascial trigger points [60].

4. Pathophysiological Importance and Associated Alterations of Hyaluronan in Obesity

Hyaluronan dysregulation has been implicated in the pathophysiology of several clinical conditions, including cancer, diabetes, autoimmune disease, and vascular disease [70–76]. Similarly, hyaluronan-mediated signaling is disrupted in various tissues in obesity. In metabolic comorbidities associated with obesity, such as nonalcoholic hepatic steatosis and insulin resistance, elevated circulatory levels of hyaluronan have been demonstrated and suggested to have diagnostic value [77–80].

Hyaluronan binds to cell-surface proteins, including receptors, to exert a broad range of biological effects on adipose tissue. Increasing evidence points to the involvement of hyaluronan and its receptors in obesity-related adipocyte hyperplasia and hypertrophy and adipose tissue metabolism [81]. An enhanced expression of hyaluronan synthase-1 was demonstrated in adipose tissue from obese patients [82]. It has been suggested that adipocyte hypertrophy contributes to adipose tissue inflammation [83]. Adipose tissue hypertrophy during obesity-related weight gain severely destabilizes extracellular matrix

homeostasis by modifying the local oxygen supply, which in turn triggers cellular stress events and inflammation [82]. A potential role of hyaluronan in adipogenesis in vivo has been demonstrated in mouse models of high-fat diet-induced obesity [79,84–87]. Hyaluronan levels were noted to be increased in these mice, mediating insulin resistance via CD44-dependent mechanisms. Treatment with exogenous hyaluronidase was found to dose-dependently decrease fat mass and adipocyte size and inhibit abdominal, muscular, and hepatic lipid accumulation, consequently increasing insulin sensitivity [84–86].

The accumulation and turnover of hyaluronan polymers in many cell types have been linked to inflammation. The role of hyaluronan in regulating inflammatory responses, including the expression of inflammatory genes, the recruitment of inflammatory cells, and the production of inflammatory cytokines, is now firmly established [88]. Hyaluronan modulates the cellular proliferative phase of tissue repair following inflammatory damage by facilitating fibroblast detachment from the extracellular matrix, mitosis, and cell migration via CD44 and RHAMM interactions [89–91]. Human and animal inflammatory disorders such as sarcoidosis, idiopathic pulmonary fibrosis, farmer's lung, graft rejection, experimental myocarditis, myocardial infarction, and inflammatory bowel disease are associated with increased hyaluronan levels in tissues [92]. As previously noted, high-molecular-weight hyaluronan is anti-inflammatory and immunosuppressive, while low-molecular-weight hyaluronan is pro-inflammatory [21,22].

It was shown that while total plasma hyaluronan molecules remain unaltered, the circulating level of low-molecular-weight hyaluronan fragments is elevated in obesity and may play a key role via Toll-like receptor (TLR)-mediated activation of innate immune cells in activating low-grade inflammatory phenotypes and other metabolic complications [82,93]. The expression of hyaluronan receptors in leukocytes is altered in obesity, with consequent alterations in the inflammatory response of leucocytes to low-molecular-weight hyaluronan. It was shown that low-molecular-weight hyaluronan induces nuclear factor kappa B (NF-κB)-dependent activation in peripheral blood monocytes and THP-1 monocytes, leading to an increase in pro-inflammatory markers [82]. Hyaluronan increases tumor necrosis factor-α (TNF-α), insulin-like growth factor-1 (IGF-1) mRNA transcript expression and protein synthesis, interleukin 1 beta (IL-1β), and interleukin 8 (IL-8) via a CD44-mediated mechanism and modulates cytokine-activated lymphocyte adhesion to the endothelium [94,95]. TNF-α may also trigger the release of the hyaluronan-binding protein, TSG-6 (TNFα-stimulated gene-6 protein), which propagates the inflammatory response [96], while IL-1β up-regulates hyaluronan synthase-1 gene expression in adipose tissue [82].

The inflammatory milieu in obesity underlies the pathophysiology of several associated complications, including the development of fasciopathies and tendinopathies [97–101]. The array of proinflammatory mediators, such as cytokines, adipokines (e.g., leptins), lipocalin-1, serum amyloid A-3, and adiponectin released during the development of obesity-related chronic inflammatory phenotypes promote insulin resistance by altering the extracellular matrix, the capillary network architecture, and the glucose uptake mechanisms [102]. The resulting hyperglycemia causes changes in the stiffness, gliding, and distribution of force transmission in the fasciae due to collagen thickening, elastic fiber fragmentation, and changes in glycosaminoglycans, particularly hyaluronan, with cascading ramifications at the cellular and molecular levels, including alterations in cellular proliferation, differentiation, growth, and migration [4]. In addition, inflammation increases reactive oxygen species, which degrade collagen, laminin, and hyaluronan, and hyaluronan fragments generated by this process sustain an inflammatory cycle (recruitment of leukocytes and release of various inflammatory mediators such as reactive oxygen species, cytokines, chemokines, and destructive enzymes) [14,88]. Conversely, high molecular weight hyaluronan works as an effective barrier to the inflammatory process and protects against oxidative damage by free radicals (superoxide anions, hydroxyl radicals, and hypochlorite) [103].

5. The Etiological Significance of Changes in Hyaluronan Properties in Myofascial Disease

The fibrous and glycosaminoglycan components of the fascial extracellular matrix can be affected by various physical, mechanical, hormonal, and pharmacological factors [4]. Alterations in the physiological levels of hyaluronan have been demonstrated to be etiologically important in myofascial pain syndromes [29,36]. Changes in the physical and chemical properties of hyaluronan are associated with modifications in extracellular matrix viscoelasticity, mechanical plasticity, and nonlinear elasticity [104,105], all of which may contribute to myofascial disease (Figure 1). Although the evidence is conflicting, it has been suggested that a strong association exists between body temperature and obesity markers [106]. With increasing temperature, both stiffening and weakening of hyaluronan-based hydrogels were observed [107,108]. Given that pH is directly related to viscosity [109], the biomechanical properties of hyaluronan may be altered by tissue acidity from increased lactic acid accumulation seen in obesity [110]. It was shown that hyaluronan degradation occurs at pH < 4 and pH > 11 [111]. Alterations in hyaluronan function may result from the effects of van der Waals and hydrophobic forces on its concentration, polyelectrolyte properties, and aggregation characteristics [25,108]. Hyaluronan takes on non-Newtonian characteristics and becomes more viscous at higher concentrations [112]. Myofascial disorders may originate from altered hydrodynamic characteristics and atypical viscoelastic properties of fascia [46]. Obesity is associated with diminished physical mobility [113,114], which has been shown to raise the concentration of hyaluronan without adequate hyaluronan recycling, increase hyaluronan viscosity, and limit the lubrication and gliding of the layers of connective tissue and muscle, with a consequent increase in overall fascial thickness, stiffness, and pain perception [30]. Any loading condition reduces hyaluronan viscosity; however, resting conditions allow hyaluronan to recover to a more viscous state.

The distribution of lines of force inside the fascia alters when hyaluronan changes from lubricating to adhesive function, a process referred to as densification of fascia [115,116]. As the connective tissue and its extracellular matrix thicken and become denser, the capacity of fascial tissue to slide is reduced or eliminated [116,117]. Chronic densification modifies the gliding of the fibrous layers, influencing collagen fiber deposition locally and remotely [116]. While fascial densification and fibrosis describe alterations in the fascia resulting in myofascial pain syndromes, it is important to differentiate both processes as they have distinct pathological and therapeutic implications. Densification indicates a potentially easily reversible modification in the loose connective tissue due to hyaluronan super-aggregation with a decreased water-binding capacity resulting in altered mechanical characteristics of the fascia but not its overall structure, whereas fibrosis refers to a difficult-to-reverse modification of the general tissue structure and mechanical properties from the excessive deposition of fibrous connective tissue as part of a reparative or reactive response [25,116]. The loose connective tissue found within the deep fascia can be altered by diet, exercise, and overuse syndromes, resulting in fascial densification, whereas trauma, surgery, and diabetes can modify the fibrous layers of the deep fasciae, resulting in fibrosis of the fascia [116]. Chronic, nonspecific neck pain may be reflective of fascial densification, whereas Dupuytren's disease and eosinophil fasciitis are typical fibrotic disorders, and therapeutic approaches are distinct in both pathologies [46,118]. Studies have demonstrated that mechanosensitive signaling underlies obesity-induced connective tissue fibrosis [119]. Fascial tissues contain various types of mechanoreceptors, in addition to the vast network of free nerve endings that play important roles in pain perception and regulation [120,121]. Myofibroblasts in the fascia, which are specialized fibroblasts with contractile properties that regulate the tissue basal tone, are also etiologically important in some pathological fibrotic contractures such as Dupuytren disease that affects the palmar and digital fascia of the hand [4].
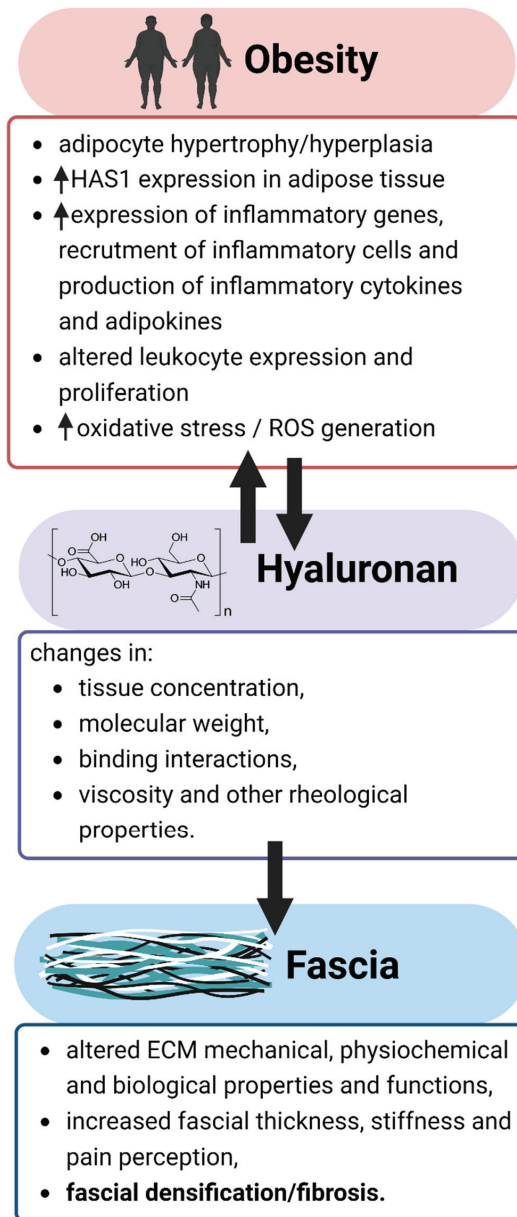
Figure 1. Relationships of pathophysiological mechanisms in obesity with changes in hyaluronan properties and the development of myofascial disease. ECM: extracellular matrix; HAS1: hyaluronan synthase 1; ROS: reactive oxygen species.

6. Therapeutic Considerations of Hyaluronan in Myofascial Disease

The complicated peripheral and central pathophysiological mechanisms in myofascial pain syndromes present unique challenges for effective treatment. Current pharmacological therapies include nonsteroidal anti-inflammatory drugs (NSAIDs), opioid analgesics (e.g., tramadol), muscle relaxants (e.g., tizanidine, cyclobenzaprine), anticonvulsants (e.g., gabapentin and pregabalin), antidepressants (e.g., tricyclic antidepressants such as

amitriptyline and serotonin-norepinephrine reuptake inhibitors such as duloxetine), benzodiazepines, tropisetron (5-HT$_3$ receptor antagonist and alpha-7-nicotinic receptor agonist), sumatriptan (peripheral 5-HT receptor agonist), lidocaine transdermal patch, intramuscular ketamine, steroid injections, and botulinum type A toxin (BoNT-A) injections. Several non-pharmacological treatment modalities have also been proposed, including manual therapy, dry needling, ultrasound therapy, ischemic compression, phonophoresis, pressure release, transcutaneous electric nerve stimulation (TENS), electrical twitch obtaining intramuscular stimulation (ETOIMS), magnetic stimulation, and laser therapy [52,122–126]. Unfortunately, the current pharmacological and non-pharmacological treatment modalities are not backed by high-quality evidence regarding efficacy and safety, and the search for evidence-based effective treatment options continues.

Unraveling novel therapeutic approaches to alleviate chronic pain syndromes may be facilitated by an enhanced understanding of the pathophysiological importance of hyaluronan and other components of the connective tissue matrix of fascia, as well as the mechanical forces that are both permitted and restricted by fascial planes [116]. Hyaluronan's ubiquitous availability, complete resorbability, biocompatibility, hydrophilicity, unique viscoelasticity, and minimal immunogenicity and adverse effects account for its wide biomedical and clinical applications in different fields of medicine (e.g., viscosupplementation for osteoarthritis treatment, vitreous substitution/replacement in ophthalmic surgery, as dermatological fillers, as scaffolds in nerve-, vessel-, and adipose tissue- engineering, as drug conjugation and delivery agent, and as an immunomodulatory agent in cancer therapeutics) [14,18,127–129]. Cosmetic injection of hyaluronan as a dermal filler (an FDA-approved clinical use) was ranked as the second and third most common non-surgical procedure for women and males, respectively [130,131]. Intra-synovial injection of crosslinked and non-crosslinked hyaluronan as viscosupplements is also a favored and FDA-approved treatment for osteoarthritic pain [132–134].

Several preclinical and clinical studies have reported on the therapeutic applications of hyaluronan in managing fasciopathies, tendinopathies, and osteoarthritis, all of which share important pathophysiological mechanisms [18,135–146]. In an animal model of osteoarthritis, administration of hyaluronan to isolated medial articular nerves dramatically lowered both ongoing and movement-evoked nerve activities, indicating a therapeutically important antinociceptive activity in inflamed joints through an elastoviscous, rheological effect on nociceptive afferent fibers [147]. In vitro experiments have demonstrated therapeutically important effects of hyaluronan on the extracellular matrix in osteoarthritis, including increased synthesis of chondroitin sulfate and proteoglycans, suppressed proteoglycan release from chondrocyte, and cartilage cell-matrix, and inhibited proteoglycan breakdown from cartilage. Several effects of hyaluronan on inflammatory mediators and immune cells have been described, notably decreased levels of IL-1-induced prostaglandin E$_2$, TNF-α, plasminogen activator activity, increased tissue inhibitor of metalloproteinases-1, enhanced antioxidant effects, reduced lymphocyte stimulation, motility, and proliferation, suppressed neutrophil aggregation and adhesion, inhibited macrophage and neutrophil phagocytosis, and enhanced polymorphonuclear leukocyte phagocytosis, adherence, and migration [148]. These effects of hyaluronan on the extracellular matrix, inflammatory mediators, and immune cells are therapeutically important in fascial disease and support the adaptability of hyaluronan for the treatment of myofascial disorders. As in osteoarthritis, functionally limited patients with myofascial disease who have not responded adequately to conventional pharmacological and nonpharmacological treatment options, those who have gastrointestinal or renal intolerance to NSAIDs and other therapies, and those who wish to postpone or are ineligible for surgery are good candidates for hyaluronan treatment [132]. On the other hand, it has been suggested that obesity may be an independent risk factor for viscosupplementation failure in patients with osteoarthritis [149], although further investigation demonstrated that benefits were similar in normal-weight and obese patients with mild or moderate knee osteoarthritis who responded to treatment [150].

Indeed, a potential therapeutic role of hyaluronan injections in treating fasciopathies has been demonstrated [151]. A recent randomized controlled trial found that the administration of five injections of high-molecular-weight hyaluronan is a safe and effective treatment option for patients with persistent pain for more than 12 weeks from plantar fasciopathy [152]. In patients with various enthesopathies (lateral epicondylitis, patellar tendinopathy, insertional Achilles tendinopathy, and plantar fasciitis), a single injection of up to 2.5 mL hyaluronan uniformly reduced pain as assessed by the visual analog scale (VAS) for pain and local pain symptoms 1 week after injection [145]. Tendinopathies and fasciopathies share similar pathophysiological mechanisms, mindful that tendons are technically part of the fascial system. Recall that the broader functional definition of the fascial system incorporates elements such as adipose tissue, adventitiae and neurovascular sheaths, aponeuroses, deep and superficial fasciae, epineurium, joint capsules, ligaments, membranes, meninges, myofascial expansions, periostea, retinacula, septa, tendons, and visceral fasciae [1].

A few studies have compared hyaluronan and other conventional therapies, as well as different pharmacological preparations and modifications of hyaluronan. Raeissadat et al. found that while corticosteroid injection appeared to have a faster trend of improvement in the short term, hyaluronan injection was comparably effective in reducing the symptoms of plantar fasciitis [144]. Additionally, hyaluronan may also be considered a physiologically more favorable option than corticosteroids which are notorious for a broad spectrum of short- and long-term adverse effects. At three months post-treatment, pain ratings indicated that two peritendinous hyaluronan injections were more effective than conventional extracorporeal shock wave therapy in treating patients with Achilles' midportion tendinopathy for ≥6 weeks [153]. In patients with lateral elbow, Achilles, and patellar tendinopathy, ultrasound-guided peritendinous injections of lower-molecular-weight hyaluronan (500–730 kDa) were safe, well-tolerated, and associated with significant pain improvement and reduction in ultrasound-assessed tendon thickness and neovascularization [141]. In a recent study comparing ultrasound-guided injections with low molecular weight (500–730 KDa) and high molecular weight (>2000 KDa) hyaluronan, Mohebbi et al. found that while both hyaluronan types had similar efficacy in the treatment of rotator cuff tendinopathy, patients tolerated low-molecular-weight injections better [154]. In patients with knee osteoarthritis, Bahrami et al. showed that a single high-molecular-weight hyaluronan injection is as effective as multiple injections of low-molecular-weight hyaluronan at 2- and 6-months follow-up [155]. In contrast to the native form of hyaluronan (>1000 kDa), lower-molecular-weight forms of the molecule (<500 kDa, especially preparations in 100–250 kDa) are pathophysiologically important as proinflammatory mediators [156,157]. Thus, further studies will be needed to clarify the impact of molecular weight on the therapeutic effects of hyaluronan. Furthermore, mindful that most of the current pharmacologic adaptations of hyaluronan in myofascial disease primarily aim to address the pathological consequences of the changes in its tissue concentration or molecular weight, it would be useful to explore the therapeutic endogenous or exogenous modifications of hyaluronan to target other pathophysiological mechanisms such as covalent modifications, binding interactions, rheological alterations, pH changes, and alterations in adipose tissue metabolism and inflammatory phenotype. Focal studies in obese patients with myofascial disease are also warranted to clarify the impact of obesity on the therapeutic potential of hyaluronan in myofascial disease.

Some investigators have explored molecular alterations to exogenously administered hyaluronan to change the extracellular matrix's mechanics. Low-load elastic mechanical features, such as lower toe modulus and a tendency toward lower toe stiffness and a larger transition strain, are seen in the fascial extracellular matrix treated with tyramine-substituted high-molecular-weight hyaluronan [158]. Given its relatively short half-life in biological fluids, a number of modifications of hyaluronan molecules to extend the duration of its biological actions have been explored. The most common of these is crosslinking to form a hydrogel; however, this could lead to higher viscosity and toxicity [159]. On

the other hand, stimulating endogenous hyaluronan production has been explored as another therapeutic strategy. The endocannabinoid receptors 1 and 2 (CB1 and CB2) are expressed in various deep fasciae, and it is known that the endocannabinoid system is crucially involved in the modulation of pain, inflammation, and fibrosis [160]. For example, a synthetic cannabinoid induced a rapid production of hyaluronan and hyaluronan-rich vesicles in an in vitro culture of fascial fibroblasts, confirming a peripheral effect of the endocannabinoid system on fascial cell regulation and remodeling of the formation of the extracellular matrix [143].

A potential therapeutic role of exogenous hyaluronidases has also been suggested. Trigger point injection of hyaluronidase was reported to substantially decrease clinically assessed pain in patients with myofascial pain disorders [161]. Similarly, in patients with spastic disorders partly related to hyaluronan accumulation in muscles, hyaluronidase injections improved both passive and active mobility [162]. It is thought that the beneficial effects may be related to modifications in hyaluronan viscosity. In addition, recombinant hyaluronidase PH20 (PEGPH20) was found to significantly reduce adipose tissue mass and adipocyte size and improve insulin sensitivity in a mouse model of diet-induced obesity [79]. These effects may ameliorate the pathological ramifications of adipose tissue inflammation in myofascial disease. Finally, an understanding of the rheological properties of hyaluronan provides a physiochemical explanation of the therapeutic effects of massage, manipulation, laser therapy, and other physical therapy procedures in myofascial disease, namely the disaggregation of the pathologic chain–chain interactions of hyaluronan molecule under controlled physical conditions such as high temperature [46].

7. Conclusions

Obesity is a primary risk factor for myofascial disease, which is a leading cause of physical disability globally. With the escalating prevalence of obesity, it is expected that the burden of myofascial disease will worsen. Unfortunately, current treatment options are limited in terms of safety and efficacy, and thus new therapeutic strategies are needed. Clarifying the etiological significance of various components of the connective tissue matrix of the fascia in obesity may aid in developing novel therapeutic methods for obesity-related myofascial disorders. In particular, understanding the pathophysiological importance of fascial hyaluronan may provide valuable therapeutic insights. Hyaluronan is the dominant polysaccharide of the extracellular matrix of connective tissues, which provides mechanical stability and acts as a water reservoir and lubricant, allowing sliding between fascial sublayers and between fasciae and adjacent structures. It also acts as an extracellular matrix homeostatic regulator via various cellular mechanisms and interactions.

Alterations in the physical and chemical properties of hyaluronan are associated with modifications in extracellular matrix viscoelasticity and other mechanical properties and biological functions and have been demonstrated as critical factors in the development of myofascial disease in obesity. Understanding this pathophysiological connection paves the way for the potential therapeutic exploitation of hyaluronan. Given its ubiquitous availability and unique pharmacological properties, hyaluronan has found a broad range of clinical applications, including in orthopedic disorders such as osteoarthritis, tendinopathies, and fasciopathies. While the relatively few results of therapeutic adaptation in myofascial disease are promising and supported by the current understanding of the pathophysiological importance of hyaluronan in fasciopathy, larger and more rigorous clinical trials utilizing a broader spectrum of myofascial disorders or different modifications of hyaluronan molecule are warranted to validate its therapeutic potential.

Author Contributions: Conceptualization, C.K.U., E.C. and N.U.; writing—original draft preparation, C.K.U.; writing—review and editing, C.K.U., E.C. and N.U.; visualization, C.K.U. and N.U.; supervision, N.U. and E.C. All authors have read and agreed to the published version of the manuscript.

References

1. Adstrum, S.; Hedley, G.; Schleip, R.; Stecco, C.; Yucesoy, C.A. Defining the Fascial System. *J. Bodyw. Mov. Ther.* **2017**, *21*, 173–177. [CrossRef]
2. Bordoni, B.; Escher, A.R.; Tobbi, F.; Pianese, L.; Ciardo, A.; Yamahata, J.; Hernandez, S.; Sanchez, O. Fascial Nomenclature: Update 2022. *Cureus* **2022**, *14*, e25904. [CrossRef]
3. Schleip, R.; Hedley, G.; Yucesoy, C.A. Fascial Nomenclature: Update on Related Consensus Process. *Clin. Anat.* **2019**, *32*, 929–933. [CrossRef]
4. Fede, C.; Pirri, C.; Fan, C.; Petrelli, L.; Guidolin, D.; de Caro, R.; Stecco, C. A Closer Look at the Cellular and Molecular Components of the Deep/Muscular Fasciae. *Int. J. Mol. Sci.* **2021**, *22*, 1411. [CrossRef]
5. Bordoni, B.; Varacallo, M. Anatomy, Fascia. In *StatPearls*; StatPearls Publishing: Tampa, FL, USA, 2018.
6. Pirri, C.; Fede, C.; Pirri, N.; Petrelli, L.; Fan, C.; de Caro, R.; Stecco, C. Diabetic Foot: The Role of Fasciae, a Narrative Review. *Biology* **2021**, *10*, 759. [CrossRef]
7. Wang, M.; Li, S.; Teo, E.C.; Fekete, G.; Gu, Y. The Influence of Heel Height on Strain Variation of Plantar Fascia During High Heel Shoes Walking-Combined Musculoskeletal Modeling and Finite Element Analysis. *Front. Bioeng. Biotechnol.* **2021**, *9*, 791238. [CrossRef] [PubMed]
8. Schleip, R.; Klingler, W. Active Contractile Properties of Fascia. *Clin. Anat.* **2019**, *32*, 891–895. [CrossRef]
9. White, A.; Abbott, H.; Masi, A.T.; Henderson, J.; Nair, K. Biomechanical Properties of Low Back Myofascial Tissue in Younger Adult Ankylosing Spondylitis Patients and Matched Healthy Control Subjects. *Clin. Biomech.* **2018**, *57*, 67–73. [CrossRef]
10. Schleip, R.; Gabbiani, G.; Wilke, J.; Naylor, I.; Hinz, B.; Zorn, A.; Jäger, H.; Breul, R.; Schreiner, S.; Klingler, W. Fascia Is Able to Actively Contract and May Thereby Influence Musculoskeletal Dynamics: A Histochemical and Mechanographic Investigation. *Front. Physiol.* **2019**, *10*, 336. [CrossRef] [PubMed]
11. Stecco, C.; Corradin, M.; Macchi, V.; Morra, A.; Porzionato, A.; Biz, C.; de Caro, R. Plantar Fascia Anatomy and Its Relationship with Achilles Tendon and Paratenon. *J. Anat.* **2013**, *223*, 665–676. [CrossRef] [PubMed]
12. Pratt, R.L. Hyaluronan and the Fascial Frontier. *Int. J. Mol. Sci.* **2021**, *22*, 6845. [CrossRef]
13. Meyer, K.; Palmer, J.W. The Polysaccharide of the Vitreous Humor. *J. Biol. Chem.* **1934**, *107*, 629–634. [CrossRef]
14. Salwowska, N.M.; Bebenek, K.A.; Żądło, D.A.; Wcisło-Dziadecka, D.L. Physiochemical Properties and Application of Hyaluronic Acid: A Systematic Review. *J. Cosmet. Dermatol.* **2016**, *15*, 520–526. [CrossRef]
15. Balazs, E.A.; Laurent, T.C.; Jeanloz, R.W. Nomenclature of Hyaluronic Acid. *Biochem. J.* **1986**, *235*, 903. [CrossRef]
16. Keen, M.A. Hyaluronic Acid in Dermatology. *Skinmed* **2017**, *15*, 441–448. [PubMed]
17. Fraser, J.R.E.; Laurent, T.C.; Laurent, U.B.G. Hyaluronan: Its Nature, Distribution, Functions and Turnover. *J. Intern. Med.* **1997**, *242*, 27–33. [CrossRef]
18. Fakhari, A.; Berkland, C. Applications and Emerging Trends of Hyaluronic Acid in Tissue Engineering, as a Dermal Filler and in Osteoarthritis Treatment. *Acta Biomater.* **2013**, *9*, 7081–7092. [CrossRef] [PubMed]
19. Ruckmani, K.; Shaikh, S.Z.; Khalil, P.; Muneera, M.S.; Thusleem, O.A. Determination of Sodium Hyaluronate in Pharmaceutical Formulations by HPLC–UV. *J. Pharm. Anal.* **2013**, *3*, 324–329. [CrossRef] [PubMed]
20. Jacobetz, M.A.; Chan, D.S.; Neesse, A.; Bapiro, T.E.; Cook, N.; Frese, K.K.; Feig, C.; Nakagawa, T.; Caldwell, M.E.; Zecchini, H.I.; et al. Hyaluronan Impairs Vascular Function and Drug Delivery in a Mouse Model of Pancreatic Cancer. *Gut* **2013**, *62*, 112–120. [CrossRef] [PubMed]
21. Lee, B.M.; Park, S.J.; Noh, I.; Kim, C.H. The Effects of the Molecular Weights of Hyaluronic Acid on the Immune Responses. *Biomater. Res.* **2021**, *25*, 27. [CrossRef]
22. Tavianatou, A.G.; Caon, I.; Franchi, M.; Piperigkou, Z.; Galesso, D.; Karamanos, N.K. Hyaluronan: Molecular Size-Dependent Signaling and Biological Functions in Inflammation and Cancer. *FEBS J.* **2019**, *286*, 2883–2908. [CrossRef] [PubMed]
23. Entwistle, J.; Hall, C.L.; Turley, E.A. HA Receptors: Regulators of Signalling to the Cytoskeleton. *J. Cell Biochem.* **1996**, *61*, 569–577. [CrossRef]
24. Jiang, X.; Tang, L.; Yuan, Y.; Wang, J.; Zhang, D.; Qian, K.; Cho, W.C.; Duan, L. NcRNA-Mediated High Expression of HMMR as a Prognostic Biomarker Correlated with Cell Proliferation and Cell Migration in Lung Adenocarcinoma. *Front. Oncol.* **2022**, *12*, 362. [CrossRef] [PubMed]
25. Stecco, A.; Cowman, M.; Pirri, N.; Raghavan, P.; Pirri, C. Densification: Hyaluronan Aggregation in Different Human Organs. *Bioengineering* **2022**, *9*, 159. [CrossRef] [PubMed]
26. Stecco, C.; Fede, C.; Macchi, V.; Porzionato, A.; Petrelli, L.; Biz, C.; Stern, R.; de Caro, R. The Fasciacytes: A New Cell Devoted to Fascial Gliding Regulation. *Clin. Anat.* **2018**, *31*, 667–676. [CrossRef] [PubMed]

27. Bartok, B.; Firestein, G.S. Fibroblast-like Synoviocytes: Key Effector Cells in Rheumatoid Arthritis. *Immunol. Rev.* **2010**, *233*, 233–255. [CrossRef] [PubMed]

28. McCombe, D.; Brown, T.; Slavin, J.; Morrison, W.A. The Histochemical Structure of the Deep Fascia and Its Structural Response to Surgery. *J. Hand Surg. Br.* **2001**, *26*, 89–97. [CrossRef] [PubMed]

29. Stecco, C.; Stern, R.; Porzionato, A.; MacChi, V.; Masiero, S.; Stecco, A.; de Caro, R. Hyaluronan within Fascia in the Etiology of Myofascial Pain. *Surg. Radiol. Anat.* **2011**, *33*, 891–896. [CrossRef] [PubMed]

30. Cowman, M.K.; Schmidt, T.A.; Raghavan, P.; Stecco, A. Viscoelastic Properties of Hyaluronan in Physiological Conditions. *F1000Research* **2015**, *4*, 622. [CrossRef]

31. Piehl-Aulin, K.; Laurent, C.; Engstrom-Laurent, A.; Hellstrom, S.; Henriksson, J. Hyaluronan in Human Skeletal Muscle of Lower Extremity: Concentration, Distribution, and Effect of Exercise. *J. Appl. Physiol.* **1991**, *71*, 2493–2498. [CrossRef]

32. Chen, B.; Ji, B.; Gao, H. Modeling Active Mechanosensing in Cell-Matrix Interactions. *Annu. Rev. Biophys.* **2015**, *44*, 1–32. [CrossRef] [PubMed]

33. Zügel, M.; Maganaris, C.N.; Wilke, J.; Jurkat-Rott, K.; Klingler, W.; Wearing, S.C.; Findley, T.; Barbe, M.F.; Steinacker, J.M.; Vleeming, A.; et al. Fascial Tissue Research in Sports Medicine: From Molecules to Tissue Adaptation, Injury and Diagnostics: Consensus Statement. *Br. J. Sports Med.* **2018**, *52*, 1497. [CrossRef] [PubMed]

34. Wolf, K.J.; Kumar, S. Hyaluronic Acid: Incorporating the Bio into the Material. *ACS Biomater. Sci. Eng.* **2019**, *5*, 3753–3765. [CrossRef] [PubMed]

35. Csoka, A.B.; Stern, R. Hypotheses on the Evolution of Hyaluronan: A Highly Ironic Acid. *Glycobiology* **2013**, *23*, 398–411. [CrossRef] [PubMed]

36. Fede, C.; Angelini, A.; Stern, R.; Macchi, V.; Porzionato, A.; Ruggieri, P.; de Caro, R.; Stecco, C. Quantification of Hyaluronan in Human Fasciae: Variations with Function and Anatomical Site. *J. Anat.* **2018**, *233*, 552–556. [CrossRef]

37. Bentham, J.; di Cesare, M.; Bilano, V.; Bixby, H.; Zhou, B.; Stevens, G.A.; Riley, L.M.; Taddei, C.; Hajifathalian, K.; Lu, Y.; et al. Worldwide Trends in Body-Mass Index, Underweight, Overweight, and Obesity from 1975 to 2016: A Pooled Analysis of 2416 Population-Based Measurement Studies in 128·9 Million Children, Adolescents, and Adults. *Lancet* **2017**, *390*, 2627–2642. [CrossRef]

38. Reilly, J.J.; El-Hamdouchi, A.; Diouf, A.; Monyeki, A.; Somda, S.A. Determining the Worldwide Prevalence of Obesity. *Lancet* **2018**, *391*, 1773–1774. [CrossRef]

39. Yanovski, J.A. Obesity: Trends in Underweight and Obesity—Scale of the Problem. *Nat. Rev. Endocrinol.* **2018**, *14*, 5–6. [CrossRef]

40. World Health Organization. Obesity and Overweight. Available online: https://www.who.int/news-room/fact-sheets/detail/obesity-and-overweight (accessed on 25 September 2022).

41. Okunogbe, A.; Nugent, R.; Spencer, G.; Ralston, J.; Wilding, J. Economic Impacts of Overweight and Obesity: Current and Future Estimates for Eight Countries. *BMJ Glob. Health* **2021**, *6*, e006351. [CrossRef]

42. GBD 2015 Obesity Collaborators; Afshin, A.; Forouzanfar, M.H.; Reitsma, M.B.; Sur, P.; Estep, K.; Lee, A.; Marczak, L.; Mokdad, A.H.; Moradi-Lakeh, M.; et al. Health Effects of Overweight and Obesity in 195 Countries over 25 Years. *N. Engl. J. Med.* **2017**, *377*, 13–27. [CrossRef]

43. Paulis, W.D.; Silva, S.; Koes, B.W.; van Middelkoop, M. Overweight and Obesity Are Associated with Musculoskeletal Complaints as Early as Childhood: A Systematic Review. *Obes. Rev.* **2014**, *15*, 52–67. [CrossRef] [PubMed]

44. Jannini, S.N.; Doŕia-Filho, U.; Damiani, D.; Silva, C.A.A. Musculoskeletal Pain in Obese Adolescents. *J. Pediatr.* **2011**, *87*, 329–335. [CrossRef] [PubMed]

45. Weller, J.L.; Comeau, D.; Otis, J.A.D. Myofascial Pain. *Semin. Neurol.* **2018**, *38*, 640–643. [CrossRef] [PubMed]

46. Stecco, A.; Gesi, M.; Stecco, C.; Stern, R. Fascial Components of the Myofascial Pain Syndrome. *Curr. Pain Headache Rep.* **2013**, *17*, 352. [CrossRef] [PubMed]

47. Riddle, D.L.; Schappert, S.M. Volume of Ambulatory Care Visits and Patterns of Care for Patients Diagnosed with Plantar Fasciitis: A National Study of Medical Doctors. *Foot Ankle Int.* **2004**, *25*, 303–310. [CrossRef]

48. Ezzati, K.; Ravarian, B.; Saberi, A.; Salari, A.; Reyhanian, Z.; Khakpour, M.; Chabok, S.Y. Prevalence of Cervical Myofascial Pain Syndrome and Its Correlation with the Severity of Pain and Disability in Patients with Chronic Non-Specific Neck Pain. *Arch. Bone Jt. Surg.* **2021**, *9*, 230. [CrossRef]

49. Cerezo-Téllez, E.; Torres-Lacomba, M.; Mayoral-del Moral, O.; Sánchez-Sánchez, B.; Dommerholt, J.; Gutiérrez-Ortega, C. Prevalence of Myofascial Pain Syndrome in Chronic Non-Specific Neck Pain: A Population-Based Cross-Sectional Descriptive Study. *Pain Med.* **2016**, *17*, 2369–2377. [CrossRef]

50. Bron, C.; Dommerholt, J.; Stegenga, B.; Wensing, M.; Oostendorp, R.A. High Prevalence of Shoulder Girdle Muscles with Myofascial Trigger Points in Patients with Shoulder Pain. *BMC Musculoskelet. Disord.* **2011**, *12*, 139. [CrossRef]

51. Chen, C.K.; Nizar, A.J. Myofascial Pain Syndrome in Chronic Back Pain Patients. *Korean J. Pain* **2011**, *24*, 100–104. [CrossRef]

52. Desai, M.J.; Saini, V.; Saini, S. Myofascial Pain Syndrome: A Treatment Review. *Pain Ther.* **2013**, *2*, 21–36. [CrossRef]

53. Tong, K.B.; Furia, J. Economic Burden of Plantar Fasciitis Treatment in the United States. *Am. J. Orthop.* **2010**, *39*, 227–231. [PubMed]

54. Rogers, J.A.; Jones, G.; Cook, J.; Squibb, K.; Wills, K.; Lahham, A.; Winzenberg, T. Chronic Plantar Heel Pain Modifies Associations of Ankle Plantarflexor Strength and Body Mass Index with Calcaneal Bone Density and Microarchitecture. *PLoS ONE* **2021**, *16*, e0260925. [CrossRef]

55. Hamstra-Wright, K.L.; Huxel Bliven, K.C.; Bay, R.C.; Aydemir, B. Risk Factors for Plantar Fasciitis in Physically Active Individuals: A Systematic Review and Meta-Analysis. *Sports Health* **2021**, *13*, 296–303. [CrossRef] [PubMed]

56. Choudhary, R.; Kunal, K. Modifiable Risk Factors of Plantar Fasciitis in Non-Athletic Patients and Proposal of a New Objective Assessment System—RKISP. *Rev. Bras. Ortop.* **2021**, *56*, 368–371. [CrossRef]

57. Riddle, D.L.; Pulisic, M.; Pidcoe, P.; Johnson, R.E. Risk Factors for Plantar Fasciitis: A Matched Case-Control Study. *J. Bone Jt. Surg. Ser. A* **2003**, *85*, 872–877. [CrossRef]

58. Irving, D.B.; Cook, J.L.; Young, M.A.; Menz, H.B. Obesity and Pronated Foot Type May Increase the Risk of Chronic Plantar Heel Pain: A Matched Case-Control Study. *BMC Musculoskelet. Disord.* **2007**, *8*, 41. [CrossRef] [PubMed]

59. Mickle, K.J.; Steele, J.R. Obese Older Adults Suffer Foot Pain and Foot-Related Functional Limitation. *Gait Posture* **2015**, *42*, 442–447. [CrossRef] [PubMed]

60. Gimenez-Donoso, C.; Bosque, M.; Vila, A.; Vilalta, G.; Santafe, M.M. Effects of a Fat-Rich Diet on the Spontaneous Release of Acetylcholine in the Neuromuscular Junction of Mice. *Nutrients* **2020**, *12*, 3216. [CrossRef]

61. van Leeuwen, K.D.B.; Rogers, J.; Winzenberg, T.; van Middelkoop, M. Higher Body Mass Index Is Associated with Plantar Fasciopathy/'plantar Fasciitis': Systematic Review and Meta-Analysis of Various Clinical and Imaging Risk Factors. *Br. J. Sports Med.* **2016**, *50*, 972–981. [CrossRef]

62. Abate, M.; Schiavone, C.; di Carlo, L.; Salini, V. Achilles Tendon and Plantar Fascia in Recently Diagnosed Type II Diabetes: Role of Body Mass Index. *Clin. Rheumatol.* **2012**, *31*, 1109–1113. [CrossRef]

63. Craig, M.E.; Cusumano, J.; Duffin, A.C.; Hing, S.; Gallego, P.H.; Donaghue, K.C.; Lam, A. Plantar Fascia Thickness, a Measure of Tissue Glycation, Predicts the Development of Complications in Adolescents with Type 1 Diabetes. *Diabetes Care* **2008**, *31*, 1201–1206. [CrossRef] [PubMed]

64. Benitez-Aguirre, P.Z.; Craig, M.E.; Jenkins, A.J.; Gallego, P.H.; Cusumano, J.; Dufin, A.C.; Hing, S.; Donaghue, K.C. Plantar Fascia Thickness Is Longitudinally Associated with Retinopathy and Renal Dysfunction: A Prospective Study from Adolescence to Adulthood. *J. Diabetes Sci. Technol.* **2012**, *6*, 348–355. [CrossRef] [PubMed]

65. Ursini, F.; Arturi, F.; Nicolosi, K.; Ammendolia, A.; D'Angelo, S.; Russo, E.; Naty, S.; Bruno, C.; de Sarro, G.; Olivieri, I.; et al. Plantar Fascia Enthesopathy Is Highly Prevalent in Diabetic Patients without Peripheral Neuropathy and Correlates with Retinopathy and Impaired Kidney Function. *PLoS ONE* **2017**, *12*, e0174529. [CrossRef] [PubMed]

66. Khor, B.Y.C.; Woodburn, J.; Newcombe, L.; Barn, R. Plantar Soft Tissues and Achilles Tendon Thickness and Stiffness in People with Diabetes: A Systematic Review. *J. Foot Ankle Res.* **2021**, *14*, 35. [CrossRef]

67. Ugwoke, C.K.; Cvetko, E.; Umek, N. Skeletal Muscle Microvascular Dysfunction in Obesity-Related Insulin Resistance: Pathophysiological Mechanisms and Therapeutic Perspectives. *Int. J. Mol. Sci.* **2022**, *23*, 847. [CrossRef] [PubMed]

68. Wu, H.; Ballantyne, C.M. Skeletal Muscle Inflammation and Insulin Resistance in Obesity. *J. Clin. Investig.* **2017**, *127*, 43–54. [CrossRef]

69. Money, S. Pathophysiology of Trigger Points in Myofascial Pain Syndrome. *J. Pain Palliat. Care Pharmacother.* **2017**, *31*, 158–159. [CrossRef]

70. Kratochvil, M.J.; Kaber, G.; Demirdjian, S.; Cai, P.C.; Burgener, E.B.; Nagy, N.; Barlow, G.L.; Popescu, M.; Nicolls, M.R.; Ozawa, M.G.; et al. Biochemical, Biophysical, and Immunological Characterization of Respiratory Secretions in Severe SARS-CoV-2 Infections. *JCI Insight* **2022**, *7*, e152629. [CrossRef] [PubMed]

71. Kaul, A.; Short, W.D.; Wang, X.; Keswani, S.G. Hyaluronidases in Human Diseases. *Int. J. Mol. Sci.* **2021**, *22*, 3204. [CrossRef] [PubMed]

72. Nagy, N.; Kuipers, H.F.; Marshall, P.L.; Wang, E.; Kaber, G.; Bollyky, P.L. Hyaluronan in Immune Dysregulation and Autoimmune Diseases. *Matrix Biol.* **2019**, *78–79*, 292–313. [CrossRef] [PubMed]

73. Karousou, E.; Misra, S.; Ghatak, S.; Dobra, K.; Götte, M.; Vigetti, D.; Passi, A.; Karamanos, N.K.; Skandalis, S.S. Roles and Targeting of the HAS/Hyaluronan/CD44 Molecular System in Cancer. *Matrix Biol.* **2017**, *59*, 3–22. [CrossRef]

74. Heldin, P.; Kolliopoulos, C.; Lin, C.Y.; Heldin, C.H. Involvement of Hyaluronan and CD44 in Cancer and Viral Infections. *Cell. Signal.* **2020**, *65*, 109427. [CrossRef] [PubMed]

75. Homann, S.; Grandoch, M.; Kiene, L.S.; Podsvyadek, Y.; Feldmann, K.; Rabausch, B.; Nagy, N.; Lehr, S.; Kretschmer, I.; Oberhuber, A.; et al. Hyaluronan Synthase 3 Promotes Plaque Inflammation and Atheroprogression. *Matrix Biol.* **2018**, *66*, 67–80. [CrossRef]

76. Nagy, N.; Sunkari, V.G.; Kaber, G.; Hasbun, S.; Lam, D.N.; Speake, C.; Sanda, S.; McLaughlin, T.L.; Wight, T.N.; Long, S.R.; et al. Hyaluronan Levels Are Increased Systemically in Human Type 2 but Not Type 1 Diabetes Independently of Glycemic Control. *Matrix Biol.* **2019**, *80*, 46–58. [CrossRef]

77. Suzuki, A.; Angulo, P.; Lymp, J.; Li, D.; Satomura, S.; Lindor, K. Hyaluronic Acid, an Accurate Serum Marker for Severe Hepatic Fibrosis in Patients with Non-Alcoholic Fatty Liver Disease. *Liver Int.* **2005**, *25*, 779–786. [CrossRef]

78. Kaneda, H.; Hashimoto, E.; Yatsuji, S.; Tokushige, K.; Shiratori, K. Hyaluronic Acid Levels Can Predict Severe Fibrosis and Platelet Counts Can Predict Cirrhosis in Patients with Nonalcoholic Fatty Liver Disease. *J. Gastroenterol. Hepatol.* **2006**, *21*, 1459–1465. [CrossRef] [PubMed]

79. Kang, L.; Lantier, L.; Kennedy, A.; Bonner, J.S.; Mayes, W.H.; Bracy, D.P.; Bookbinder, L.H.; Hasty, A.H.; Thompson, C.B.; Wasserman, D.H. Hyaluronan Accumulates with High-Fat Feeding and Contributes to Insulin Resistance. *Diabetes* **2013**, *62*, 1888–1896. [CrossRef] [PubMed]

80. Morita, M.; Yano, S.; Ishibashi, Y.; Nakata, N.; Kurioka, S.; Sugimoto, T. Close Relationship between Serum Hyaluronan Levels and Vascular Function in Patients with Type 2 Diabetes. *Biomarkers* **2014**, *19*, 493–497. [CrossRef]

81. Zhu, Y.; Kruglikov, I.L.; Akgul, Y.; Scherer, P.E. Hyaluronan in Adipogenesis, Adipose Tissue Physiology and Systemic Metabolism. *Matrix Biol.* **2019**, *78–79*, 284–291. [CrossRef]

82. Romo, M.; López-Vicario, C.; Pérez-Romero, N.; Casulleras, M.; Martínez-Puchol, A.I.; Sánchez, B.; Flores-Costa, R.; Alcaraz-Quiles, J.; Duran-Güell, M.; Ibarzábal, A.; et al. Small Fragments of Hyaluronan Are Increased in Individuals with Obesity and Contribute to Low-Grade Inflammation through TLR-Mediated Activation of Innate Immune Cells. *Int. J. Obes.* **2022**. [CrossRef] [PubMed]

83. Zatterale, F.; Longo, M.; Naderi, J.; Raciti, G.A.; Desiderio, A.; Miele, C.; Beguinot, F. Chronic Adipose Tissue Inflammation Linking Obesity to Insulin Resistance and Type 2 Diabetes. *Front. Physiol.* **2020**, *10*, 1607. [CrossRef] [PubMed]

84. Fogelstrand, P.; Borén, J. Treatment of Hyaluronan Accumulation Ameliorates High-Fat Diet-Induced Insulin Resistance in Mice. *Diabetes* **2013**, *62*, 1816–1817. [CrossRef] [PubMed]

85. Hasib, A.; Hennayake, C.K.; Bracy, D.P.; Bugler-Lamb, A.R.; Lantier, L.; Khan, F.; Ashford, M.L.J.; McCrimmon, R.J.; Wasserman, D.H.; Kang, L. CD44 Contributes to Hyaluronan-Mediated Insulin Resistance in Skeletal Muscle of High-Fat-Fed C57BL/6 Mice. *Am. J. Physiol. Endocrinol. Metab.* **2019**, *317*, E973–E983. [CrossRef]

86. Ji, E.; Jung, M.Y.; Park, J.H.; Kim, S.; Seo, C.R.; Park, K.W.; Lee, E.K.; Yeom, C.H.; Lee, S. Inhibition of Adipogenesis in 3T3-L1 Cells and Suppression of Abdominal Fat Accumulation in High-Fat Diet-Feeding C57BL/6J Mice after Downregulation of Hyaluronic Acid. *Int. J. Obes.* **2014**, *38*, 1035–1043. [CrossRef]

87. Kodama, K.; Horikoshi, M.; Toda, K.; Yamada, S.; Hara, K.; Irie, J.; Sirota, M.; Morgan, A.A.; Chen, R.; Ohtsu, H.; et al. Expression-Based Genome-Wide Association Study Links the Receptor CD44 in Adipose Tissue with Type 2 Diabetes. *Proc. Natl. Acad. Sci. USA* **2012**, *109*, 7049–7054. [CrossRef] [PubMed]

88. Avenoso, A.; Bruschetta, G.; D'Ascola, A.; Scuruchi, M.; Mandraffino, G.; Saitta, A.; Campo, S.; Campo, G.M. Hyaluronan Fragmentation During Inflammatory Pathologies: A Signal That Empowers Tissue Damage. *Mini Rev. Med. Chem.* **2020**, *20*, 54–65. [CrossRef] [PubMed]

89. Brecht, M.; Mayer, U.; Schlosser, E.; Prehm, P. Increased Hyaluronate Synthesis Is Required for Fibroblast Detachment and Mitosis. *Biochem. J.* **1986**, *239*, 445–450. [CrossRef]

90. Thomas, L.; Byers, H.R.; Vink, J.; Stamenkovic, I. CD44H Regulates Tumor Cell Migration on Hyaluronate-Coated Substrate. *J. Cell Biol.* **1992**, *118*, 971–977. [CrossRef]

91. Hall, C.L.; Turley, E.A. Hyaluronan: RHAMM Mediated Cell Locomotion and Signaling in Tumorigenesis. *J. Neurooncol.* **1995**, *26*, 221–229. [CrossRef] [PubMed]

92. Gerdin, B.; Hällgren, R. Dynamic Role of Hyaluronan (HYA) in Connective Tissue Activation and Inflammation. *J. Intern. Med.* **1997**, *242*, 49–55. [CrossRef]

93. Garantziotis, S.; Savani, R.C. Proteoglycans in Toll-like Receptor Responses and Innate Immunity. *Am. J. Physiol. Cell Physiol.* **2022**, *323*, C202–C214. [CrossRef] [PubMed]

94. Mohamadzadeh, M.; DeGrendele, H.; Arizpe, H.; Estess, P.; Siegelman, M. Proinflammatory Stimuli Regulate Endothelial Hyaluronan Expression and CD44/HA-Dependent Primary Adhesion. *J. Clin. Investig.* **1998**, *101*, 97–108. [CrossRef] [PubMed]

95. Kobayashi, H.; Terao, T. Hyaluronic Acid-Specific Regulation of Cytokines by Human Uterine Fibroblasts. *Am. J. Physiol.* **1997**, *273*, C1151–C1159. [CrossRef] [PubMed]

96. Baranova, N.S.; Nilebäck, E.; Haller, F.M.; Briggs, D.C.; Svedhem, S.; Day, A.J.; Richter, R.P. The Inflammation-Associated Protein TSG-6 Cross-Links Hyaluronan via Hyaluronan-Induced TSG-6 Oligomers. *J. Biol. Chem.* **2011**, *286*, 25675–25686. [CrossRef]

97. Lui, P.P.Y.; Yung, P.S.H. Inflammatory Mechanisms Linking Obesity and Tendinopathy. *J. Orthop. Translat.* **2021**, *31*, 80–90. [CrossRef]

98. MacChi, M.; Spezia, M.; Elli, S.; Schiaffini, G.; Chisari, E. Obesity Increases the Risk of Tendinopathy, Tendon Tear and Rupture, and Postoperative Complications: A Systematic Review of Clinical Studies. *Clin. Orthop. Relat. Res.* **2020**, *478*, 1839–1847. [CrossRef] [PubMed]

99. He, L.; Yu, T.; Zhang, W.; Wang, B.; Ma, Y.; Li, S. Causal Associations of Obesity with Achilles Tendinopathy: A Two-Sample Mendelian Randomization Study. *Front. Endocrinol.* **2022**, *13*, 902142. [CrossRef]

100. Jomaa, G.; Kwan, C.K.; Fu, S.C.; Ling, S.K.K.; Chan, K.M.; Yung, P.S.H.; Rolf, C. A Systematic Review of Inflammatory Cells and Markers in Human Tendinopathy. *BMC Musculoskelet. Disord.* **2020**, *21*, 78. [CrossRef]

101. Chisari, E.; Rehak, L.; Khan, W.S.; Maffulli, N. Tendon Healing in Presence of Chronic Low-Level Inflammation: A Systematic Review. *Br. Med. Bull.* **2019**, *132*, 97–116. [CrossRef] [PubMed]

102. Wu, H.; Ballantyne, C.M. Metabolic Inflammation and Insulin Resistance in Obesity. *Circ. Res.* **2020**, *126*, 1549–1564. [CrossRef] [PubMed]

103. Albano, G.D.; Bonanno, A.; Cavalieri, L.; Ingrassia, E.; di Sano, C.; Siena, L.; Riccobono, L.; Gagliardo, R.; Profita, M. Effect of High, Medium, and Low Molecular Weight Hyaluronan on Inflammation and Oxidative Stress in an In Vitro Model of Human Nasal Epithelial Cells. *Mediat. Inflamm.* **2016**, *2016*, 8727289. [CrossRef] [PubMed]

104. Chaudhuri, O.; Cooper-White, J.; Janmey, P.A.; Mooney, D.J.; Shenoy, V.B. Effects of Extracellular Matrix Viscoelasticity on Cellular Behaviour. *Nature* **2020**, *584*, 535–546. [CrossRef] [PubMed]

105. Grolma, J.M.; Weinand, P.; Moone, D.J. Extracellular Matrix Plasticity as a Driver of Cell Spreading. *Proc. Natl. Acad. Sci. USA* **2020**, *117*, 25999–26007. [CrossRef] [PubMed]

106. Bastardot, F.; Marques-Vidal, P.; Vollenweider, P. Association of Body Temperature with Obesity. The CoLaus Study. *Int. J. Obes.* **2018**, *43*, 1026–1033. [CrossRef]

107. Smilek, J.; Jarábková, S.; Velcer, T.; Pekař, M. Compositional and Temperature Effects on the Rheological Properties of Polyelectrolyte–Surfactant Hydrogels. *Polymers* **2019**, *11*, 927. [CrossRef]

108. Matteini, P.; Dei, L.; Carretti, E.; Volpi, N.; Goti, A.; Pini, R. Structural Behavior of Highly Concentrated Hyaluronan. *Biomacromolecules* **2009**, *10*, 1516–1522. [CrossRef]

109. Gatej, I.; Popa, M.; Rinaudo, M. Role of the PH on Hyaluronan Behavior in Aqueous Solution. *Biomacromolecules* **2005**, *6*, 61–67. [CrossRef]

110. Chen, C.N.J.; Liao, Y.H.; Lin, S.Y.; Yu, J.X.; Li, Z.J.; Lin, Y.C.; Chang, G.J.; Lin, C.H.; Wong, A.M.K. Diet-Induced Obesity Accelerates Blood Lactate Accumulation of Rats in Response to Incremental Exercise to Maximum. *Am. J. Physiol. Regul. Integr. Comp. Physiol.* **2017**, *313*, R601–R607. [CrossRef]

111. Maleki, A.; Kjøniksen, A.L.; Nyström, B. Effect of PH on the Behavior of Hyaluronic Acid in Dilute and Semidilute Aqueous Solutions. *Macromol. Symp.* **2008**, *274*, 131–140. [CrossRef]

112. Pisárčik, M.; Bakoš, D.; Čeppan, M. Non-Newtonian Properties of Hyaluronic Acid Aqueous Solution. *Colloids Surf. A Physicochem. Eng. Asp.* **1995**, *97*, 197–202. [CrossRef]

113. Lang, I.A.; Llewellyn, D.J.; Alexander, K.; Melzer, D. Obesity, Physical Function, and Mortality in Older Adults. *J. Am. Geriatr. Soc.* **2008**, *56*, 1474–1478. [CrossRef] [PubMed]

114. Vincent, H.K.; Vincent, K.R.; Lamb, K.M. Obesity and Mobility Disability in the Older Adult. *Obes. Rev.* **2010**, *11*, 568–579. [CrossRef] [PubMed]

115. Hughes, E.J.; McDermott, K.; Funk, M.F. Evaluation of Hyaluronan Content in Areas of Densification Compared to Adjacent Areas of Fascia. *J. Bodyw. Mov. Ther.* **2019**, *23*, 324–328. [CrossRef] [PubMed]

116. Pavan, P.G.; Stecco, A.; Stern, R.; Stecco, C. Painful Connections: Densification versus Fibrosis of Fascia. *Curr. Pain Headache Rep.* **2014**, *18*, 441. [CrossRef] [PubMed]

117. Wilke, J.; Macchi, V.; de Caro, R.; Stecco, C. Fascia Thickness, Aging and Flexibility: Is There an Association? *J. Anat.* **2019**, *234*, 43–49. [CrossRef]

118. Stecco, A.; Meneghini, A.; Stern, R.; Stecco, C.; Imamura, M. Ultrasonography in Myofascial Neck Pain: Randomized Clinical Trial for Diagnosis and Follow-Up. *Surg. Radiol. Anat.* **2014**, *36*, 243–253. [CrossRef]

119. Marcelin, G.; Silveira, A.L.M.; Martins, L.B.; Ferreira, A.V.M.; Clément, K. Deciphering the Cellular Interplays Underlying Obesity-Induced Adipose Tissue Fibrosis. *J. Clin. Investig.* **2019**, *129*, 4032–4040. [CrossRef]

120. Fede, C.; Petrelli, L.; Guidolin, D.; Porzionato, A.; Pirri, C.; Fan, C.; de Caro, R.; Stecco, C. Evidence of a New Hidden Neural Network into Deep Fasciae. *Sci. Rep.* **2021**, *11*, 12623. [CrossRef]

121. Suarez-Rodriguez, V.; Fede, C.; Pirri, C.; Petrelli, L.; Loro-Ferrer, J.F.; Rodriguez-Ruiz, D.; de Caro, R.; Stecco, C. Fascial Innervation: A Systematic Review of the Literature. *Int. J. Mol. Sci.* **2022**, *23*, 5674. [CrossRef]

122. Charles, D.; Hudgins, T.; MacNaughton, J.; Newman, E.; Tan, J.; Wigger, M. A Systematic Review of Manual Therapy Techniques, Dry Cupping and Dry Needling in the Reduction of Myofascial Pain and Myofascial Trigger Points. *J. Bodyw. Mov. Ther.* **2019**, *23*, 539–546. [CrossRef]

123. Barbero, M.; Schneebeli, A.; Koetsier, E.; Maino, P. Myofascial Pain Syndrome and Trigger Points: Evaluation and Treatment in Patients with Musculoskeletal Pain. *Curr. Opin. Support Palliat. Care* **2019**, *13*, 270–276. [CrossRef] [PubMed]

124. Galasso, A.; Urits, I.; An, D.; Nguyen, D.; Borchart, M.; Yazdi, C.; Manchikanti, L.; Kaye, R.J.; Kaye, A.D.; Mancuso, K.F.; et al. A Comprehensive Review of the Treatment and Management of Myofascial Pain Syndrome. *Curr. Pain Headache Rep.* **2020**, *24*, 43. [CrossRef] [PubMed]

125. Thottungal, A.; Kumar, P.; Bhaskar, A. Interventions for Myofascial Pain Syndrome in Cancer Pain: Recent Advances: Why, When, Where and How. *Curr. Opin. Support Palliat. Care.* **2019**, *13*, 262–269. [CrossRef]

126. Urits, I.; Charipova, K.; Gress, K.; Schaaf, A.L.; Gupta, S.; Kiernan, H.C.; Choi, P.E.; Jung, J.W.; Cornett, E.; Kaye, A.D.; et al. Treatment and Management of Myofascial Pain Syndrome. *Best Pract. Res. Clin. Anaesthesiol.* **2020**, *34*, 427–448. [CrossRef]

127. Abatangelo, G.; Vindigni, V.; Avruscio, G.; Pandis, L.; Brun, P. Hyaluronic Acid: Redefining Its Role. *Cells* **2020**, *9*, 1743. [CrossRef] [PubMed]

128. Hamidi, M.; Azadi, A.; Rafiei, P. Hydrogel Nanoparticles in Drug Delivery. *Adv. Drug Deliv. Rev.* **2008**, *60*, 1638–1649. [CrossRef] [PubMed]

129. Serban, M.A.; Skardal, A. Hyaluronan Chemistries for Three-Dimensional Matrix Applications. *Matrix Biol.* **2019**, *78–79*, 337–345. [CrossRef]

130. Buck, D.W.; Alam, M.; Kim, J.Y.S. Injectable Fillers for Facial Rejuvenation: A Review. *J. Plast. Reconstr. Aesthet. Surg.* **2009**, *62*, 11–18. [CrossRef] [PubMed]

131. Gold, M.H. Use of Hyaluronic Acid Fillers for the Treatment of the Aging Face. *Clin. Interv. Aging* **2007**, *2*, 369–376. [CrossRef] [PubMed]

132. Sun, S.F.; Chou, Y.J.; Hsu, C.W.; Chen, W.L. Hyaluronic Acid as a Treatment for Ankle Osteoarthritis. *Curr. Rev. Musculoskelet. Med.* **2009**, *2*, 78–82. [CrossRef] [PubMed]

133. Urits, I.; Hasegawa, M.; Orhurhu, V.; Peck, J.; Kelly, A.C.; Kaye, R.J.; Orhurhu, M.S.; Brinkman, J.; Giacomazzi, S.; Foster, L.; et al. Minimally Invasive Treatment of Chronic Ankle Instability: A Comprehensive Review. *Curr. Pain Headache Rep.* **2020**, *24*, 8. [CrossRef]

134. Papalia, R.; Albo, E.; Russo, F.; Tecame, A.; Torre, G.; Sterzi, S.; Bressi, F.; Denaro, V. The Use of Hyaluronic Acid in the Treatment of Ankle Osteoarthritis: A Review of the Evidence. *J. Biol. Regul. Homeost. Agents* **2017**, *31*, 91–102.

135. Honda, H.; Gotoh, M.; Kanazawa, T.; Ohzono, H.; Nakamura, H.; Ohta, K.; Nakamura, K.I.; Fukuda, K.; Teramura, T.; Hashimoto, T.; et al. Hyaluronic Acid Accelerates Tendon-to-Bone Healing After Rotator Cuff Repair. *Am. J. Sports Med.* **2017**, *45*, 3322–3330. [CrossRef]

136. Osti, L.; Berardocco, M.; di Giacomo, V.; di Bernardo, G.; Oliva, F.; Berardi, A.C. Hyaluronic Acid Increases Tendon Derived Cell Viability and Collagen Type i Expression in Vitro: Comparative Study of Four Different Hyaluronic Acid Preparations by Molecular Weight. *BMC Musculoskelet. Disord.* **2015**, *16*, 284. [CrossRef] [PubMed]

137. Crimaldi, S.; Liguori, S.; Tamburrino, P.; Moretti, A.; Paoletta, M.; Toro, G.; Iolascon, G. The Role of Hyaluronic Acid in Sport-Related Tendinopathies: A Narrative Review. *Medicina* **2021**, *57*, 1088. [CrossRef] [PubMed]

138. Kogan, G.; Šoltés, L.; Stern, R.; Gemeiner, P. Hyaluronic Acid: A Natural Biopolymer with a Broad Range of Biomedical and Industrial Applications. *Biotechnol. Lett.* **2007**, *29*, 17–25. [CrossRef]

139. Abate, M.; Schiavone, C.; Salini, V. The Use of Hyaluronic Acid after Tendon Surgery and in Tendinopathies. *Biomed. Res. Int.* **2014**, *2014*, 783632. [CrossRef]

140. Kaux, J.-F.; Samson, A.; Crielaard, J.-M. Hyaluronic Acid and Tendon Lesions. *Muscles Ligaments Tendons J.* **2015**, *5*, 264–269. [CrossRef]

141. Giordan, N.; Giordan, N.; Mazzoni, G. Efficacy and Safety of Hyaluronic Acid (500-730kDa) Ultrasound-Guided Injections on Painful Tendinopathies: A Prospective, Open Label, Clinical Study. *Muscles Ligaments Tendons J.* **2017**, *7*, 388. [CrossRef]

142. Oliva, F.; Marsilio, E.; Asparago, G.; Frizziero, A.; Berardi, A.C.; Maffulli, N. The Impact of Hyaluronic Acid on Tendon Physiology and Its Clinical Application in Tendinopathies. *Cells* **2021**, *10*, 3081. [CrossRef]

143. Fede, C.; Pirri, C.; Petrelli, L.; Guidolin, D.; Fan, C.; de Caro, R.; Stecco, C. Sensitivity of the Fasciae to the Endocannabinoid System: Production of Hyaluronan-Rich Vesicles and Potential Peripheral Effects of Cannabinoids in Fascial Tissue. *Int. J. Mol. Sci.* **2020**, *21*, 2936. [CrossRef] [PubMed]

144. Raeissadat, S.A.; Nouri, F.; Darvish, M.; Esmaily, H.; Ghazihosseini, P. Ultrasound-Guided Injection of High Molecular Weight Hyaluronic Acid versus Corticosteroid in Management of Plantar Fasciitis: A 24-Week Randomized Clinical Trial. *J. Pain Res.* **2020**, *13*, 109–121. [CrossRef] [PubMed]

145. Kumai, T.; Muneta, T.; Tsuchiya, A.; Shiraishi, M.; Ishizaki, Y.; Sugimoto, K.; Samoto, N.; Isomoto, S.; Tanaka, Y.; Takakura, Y. The Short-Term Effect after a Single Injection of High-Molecular-Weight Hyaluronic Acid in Patients with Enthesopathies (Lateral Epicondylitis, Patellar Tendinopathy, Insertional Achilles Tendinopathy, and Plantar Fasciitis): A Preliminary Study. *J. Orthop. Sci.* **2014**, *19*, 603–611. [CrossRef] [PubMed]

146. Ferreira, G.F.; Sevilla, D.; Oliveira, C.N.; Junior, L.C.N.; Arliani, G.G.; Oliveira, V.O.; Filho, M.V.P. Comparison of the Effect of Hyaluronic Acid Injection versus Extracorporeal Shockwave Therapy on Chronic Plantar Fasciitis: Protocol for a Randomized Controlled Trial. *PLoS ONE* **2021**, *16*, e0250768. [CrossRef] [PubMed]

147. Pozo, M.A.; Balazs, E.A.; Belmonte, C. Reduction of Sensory Responses to Passive Movements of Inflamed Knee Joints by Hylan, a Hyaluronan Derivative. *Exp. Brain Res.* **1997**, *116*, 3–9. [CrossRef]

148. Moreland, L.W. Intra-Articular Hyaluronan (Hyaluronic Acid) and Hylans for the Treatment of Osteoarthritis: Mechanisms of Action. *Arthritis Res. Ther.* **2003**, *5*, 54. [CrossRef]

149. Eymard, F.; Chevalier, X.; Conrozier, T. Obesity and Radiological Severity Are Associated with Viscosupplementation Failure in Patients with Knee Osteoarthritis. *J. Orthop. Res.* **2017**, *35*, 2269–2274. [CrossRef]

150. Conrozier, T.; Eymard, F.; Chouk, M.; Chevalier, X. Impact of Obesity, Structural Severity and Their Combination on the Efficacy of Viscosupplementation in Patients with Knee Osteoarthritis. *BMC Musculoskelet. Disord.* **2019**, *20*, 376. [CrossRef]

151. Coombes, B.K.; Bisset, L.; Vicenzino, B. Efficacy and Safety of Corticosteroid Injections and Other Injections for Management of Tendinopathy: A Systematic Review of Randomised Controlled Trials. *Lancet* **2010**, *376*, 1751–1767. [CrossRef]

152. Kumai, T.; Samoto, N.; Hasegawa, A.; Noguchi, H.; Shiranita, A.; Shiraishi, M.; Ikeda, S.; Sugimoto, K.; Tanaka, Y.; Takakura, Y. Short-Term Efficacy and Safety of Hyaluronic Acid Injection for Plantar Fasciopathy. *Knee Surg. Sports Traumatol. Arthrosc.* **2018**, *26*, 903–911. [CrossRef]

153. Lynen, N.; de Vroey, T.; Spiegel, I.; van Ongeval, F.; Hendrickx, N.J.; Stassijns, G. Comparison of Peritendinous Hyaluronan Injections Versus Extracorporeal Shock Wave Therapy in the Treatment of Painful Achilles' Tendinopathy: A Randomized Clinical Efficacy and Safety Study. *Arch. Phys. Med. Rehabil.* **2017**, *98*, 64–71. [CrossRef] [PubMed]

154. Mohebbi, R.; Rezasoltani, Z.; Mir, M.; Mohebbi, M.; Vatandoost, S.; Esmaily, H. High- Versus Low-Molecular-Weight Hyaluronic Acid for the Treatment of Rotator Cuff Tendinopathy: A Triple-Blind Randomized Comparative Trial. *Ann. Pharmacother.* **2021**, *55*, 1203–1214. [CrossRef]

155. Bahrami, M.H.; Raeissadat, S.A.; Cheraghi, M.; Rahimi-Dehgolan, S.; Ebrahimpour, A. Efficacy of Single High-Molecular-Weight versus Triple Low-Molecular-Weight Hyaluronic Acid Intra-Articular Injection among Knee Osteoarthritis Patients. *BMC Musculoskelet. Disord.* **2020**, *21*, 550. [CrossRef] [PubMed]

156. Petrey, A.C.; de la Motte, C.A. Hyaluronan, a Crucial Regulator of Inflammation. *Front. Immunol.* **2014**, *5*, 101. [CrossRef] [PubMed]
157. Jiang, D.; Liang, J.; Noble, P.W. Hyaluronan as an Immune Regulator in Human Diseases. *Physiol. Rev.* **2011**, *91*, 221–264. [CrossRef] [PubMed]
158. Chin, L.; Calabro, A.; Walker, E.; Derwin, K.A. Mechanical Properties of Tyramine Substituted-Hyaluronan Enriched Fascia Extracellular Matrix. *J. Biomed. Mater. Res. A* **2012**, *100*, 786–793. [CrossRef]
159. Marinho, A.; Nunes, C.; Reis, S. Hyaluronic Acid: A Key Ingredient in the Therapy of Inflammation. *Biomolecules* **2021**, *11*, 1518. [CrossRef]
160. Fede, C.; Albertin, G.; Petrelli, L.; Sfriso, M.M.; Biz, C.; de Caro, R.; Stecco, C. Expression of the Endocannabinoid Receptors in Human Fascial Tissue. *Eur. J. Histochem.* **2016**, *60*, 130–134. [CrossRef]
161. Ghasemi, M.; Mosaffa, F.; Hoseini, B.; Behnaz, F. Comparison of the Effect of Bicarbonate, Hyaluronidase, and Lidocaine Injection on Myofascial Pain Syndrome. *Anesth. Pain Med.* **2020**, *10*, e101037. [CrossRef]
162. Raghavan, P.; Lu, Y.; Mirchandani, M.; Stecco, A. Human Recombinant Hyaluronidase Injections for Upper Limb Muscle Stiffness in Individuals with Cerebral Injury: A Case Series. *eBioMedicine* **2016**, *9*, 306–313. [CrossRef] [PubMed]

Article

Analysis of Selected Salivary Adipokines and Cytokines in Patients with Obesity—A Pilot Study

Lucyna Ostrowska [1], **Joanna Smarkusz-Zarzecka** [1,*], **Agnieszka Gornowicz** [2], **Karolina Lendzion** [2], **Beata Zyśk** [1] **and Damian Pogodziński** [1]

[1] Department of Dietetics and Clinical Nutrition, Medical University of Bialystok, 15-054 Bialystok, Poland
[2] Department of Biotechnology, Medical University of Bialystok, 15-089 Bialystok, Poland
* Correspondence: joanna.smarkusz-zarzecka@umb.edu.pl; Tel.: +48-857-328-244

Abstract: Obesity is a chronic, progressive and relapsing disease that produces many adverse health, social and economic effects. The aim of the study was to analyse the concentrations of selected proinflammatory parameters in the saliva of obese and normal body weight individuals. The study included 116 people divided into two groups: the study group ($n = 75$, subjects with obesity) and the control group ($n = 41$, individuals with normal body weight). Bioelectrical impedance analysis was performed, and saliva samples were collected from all study participants to determine the concentrations of selected proinflammatory adipokines and cytokines. Statistically significantly higher concentrations of MMP-2, MMP-9 and IL-1β were found in the saliva of obese women compared to women with normal body weight. Furthermore, statistically significantly higher concentrations of MMP-9, IL-6 and resistin were observed in the saliva of obese men compared to men with normal body weight. Higher concentrations of selected proinflammatory cytokines and adipokines were found in the saliva of obese individuals compared to individuals with normal body weight. It is likely that higher concentrations of MMP-2, MMP-9 and IL-1β can be detected in the saliva of obese women compared to non-obese women, while higher concentrations of MMP-9, IL-6 and resistin can be found in the saliva of obese men compared to non-obese men, which suggests that further research to confirm our observations and determine the mechanisms of development of metabolic complications associated with obesity depending on gender is needed.

Keywords: obesity; saliva; body composition; proinflammatory cytokines; proinflammatory adipokines; IL-6; IL-1β; resistin; MMP-9; MMP-2

1. Introduction

Obesity is a chronic, progressive, relapsing disease that produces many adverse health, psychological, social and economic effects. In 2013, the Member States of the World Health Assembly agreed to a set targets which include halting the rise in obesity at 2010 levels by 2025 [1]. However, the World Obesity Federation Annual Report 2020 indicates that the probability of most countries achieving this target is less than 10%. Furthermore, it is forecast that the prevalence of obesity will increase from 11.4% to 17.5% in the years 2010–2030, with over 1 billion people living with obesity globally by 2030. One in five women and one in seven men will be obese [2]. According to the Organization for Economic Cooperation and Development (OECD) data from 2019, obesity and its complications will contribute to approximately 92 million premature deaths in OECD, Group 20 (G20) and European Union (EU28) member countries in the next 30 years. Furthermore, life expectancy will decrease by 0.9–4.2 years in the above countries within the same period of time [3]. Therefore, routine monitoring of obese individuals aimed at early identification of those at risk for developing metabolic complications should be introduced.

It is crucial that the mechanisms underlying metabolic disturbances in the obese in relation to inflammatory processes involving white adipose tissue are fully understood.

Adipose tissue cells secrete adipokines and cytokines that induce immune cell infiltration, thus promoting the proinflammatory phenotype. Furthermore, they produce not only paracrine and autocrine but also endocrine effects, and consequently affect both inflammation in adipose tissue and systemic inflammation. They can cause metabolic diseases, including hypertension, atherogenic dyslipidemia, insulin resistance, non-alcoholic fatty liver disease, type 2 diabetes, and may be an indirect cause of many chronic diseases, i.e., cancer or cardiovascular diseases [4].

The use of saliva for early detection of inflammation in the oral cavity and diagnosis of periodontal diseases is well established [5]. However, changes in the concentration of many salivary parameters may also be useful as biomarkers for other diseases, including caries [6]. Systematic reviews and meta-analyses conducted in recent years indicate that saliva can be used for the diagnosis and surveillance of a number of systemic diseases, including inflammatory bowel diseases [7], oral cancer and systemic oncological diseases [8]. Saliva could be a valuable diagnostic tool in everyday clinical practice and in screening large populations due to the non-invasiveness of the test and a lower risk of infection compared to serum [5].

In one of our previous studies, we investigated proinflammatory adipokines and cytokines which may play a role in metabolic disturbances in the obese. A review of the available literature suggests that research on resistin and interleukin 6 (IL-6) should be continued since the results of previous studies are inconclusive [9]. IL-6 is a multidirectional cytokine, the activity of which depends on the source of its expression. When secreted by adipose tissue cells in response to the development of obesity, it causes increased accumulation of macrophages in the tissue [10]. On the other hand, elevated resistin concentration is involved in the pathogenesis of inflammation and the development of insulin resistance, type 2 diabetes, hypertension, atherogenic dyslipidemia and atherosclerosis [11].

Matrix metalloproteinase-2 (MMP-2) and MMP-9 as well as interleukin 1-beta (IL-1β) may be potential salivary biomarkers for risk prediction of metabolic disturbances in the obese. To date, few studies have been conducted on the subject. However, they should be continued as promising results have been obtained [9]. Matrix metalloproteinases (MMPs), and more specifically MMP-2 and MMP-9 gelatinases, have been implicated in the development of atherosclerosis [12]. IL-1β contributes to the development of insulin resistance that accompanies obesity [13].

Many previous studies that investigated obesity markers were based mainly on body mass index (BMI) as a diagnostic criterion for this disease. Future research should also assess the content and distribution of adipose tissue which correlates, to a greater extent, with the risk of metabolic disturbances [4,9].

The aim of the study was to analyse the concentrations of selected proinflammatory parameters in the saliva of obese and normal body weight individuals.

2. Results

The characteristics of selected anthropometric and body composition parameters of women ($n = 77$) from the study group ($n = 46$) and women from the control group ($n = 31$), and men ($n = 39$) from the study group ($n = 29$) and men from the control group ($n = 10$) are presented in Table 1.

Comparison of women from the study and control groups revealed statistically significant differences for age, body weight, BMI (body mass index), waist circumference, hip circumference, WHR (waist-to-hip ratio), total body fat (kg and %), VAT (visceral adipose tissue, cm^2 and %), SAT (subcutaneous adipose tissue, cm^2 and %) and the VAT/SAT ratio. Similar results were obtained for men, but no statistically significant differences were found for body height, percentage of visceral and subcutaneous fat and the VAT/SAT ratio.

Table 1. Comparison of anthropometric and body composition parameters of women and men from the study and control groups.

| Parameter | Women (*n* = 77) | | | | | Men (*n* = 39) | | | | |
| | Study Group (*n* = 46) | | Control Group (*n* = 31) | | *p* * | Study Group (*n* = 29) | | Control Group (*n* = 10) | | *p* ** |
	Median	Q1–Q3	Median	Q1–Q3		Median	Q1–Q3	Median	Q1–Q3	
Age (years)	46.00	39.00–52.00	36.00	30.00–45.00	<0.001 *	44.00	37.00–50.00	37.00	29.00–40.00	0.039 **
Height (cm)	164.25	159.00–169.00	163.00	160.00–170.00	0.897	181.00	175.00–186.00	181.50	174.00–184.00	0.646
Weight (kg)	93.50	88.00–100.40	63.00	58.00–66.00	<0.001 *	110.50	101.00–118.50	80.50	76.00–83.00	<0.001 **
BMI (kg/m^2)	32.85	32.60–36.60	23.00	21.90–24.50	<0.001 *	33.70	31.80–35.70	24.73	24.30–24.92	<0.001 **
Waist circumference (cm)	107.00	104.00–112.00	81.00	78.00–85.00	<0.001 *	113.00	109.00–117.00	87.00	85.00–94.00	<0.001 **
Hip circumference (cm)	120.00	116.00–124.00	97.00	94.00–101.00	<0.001 *	116.00	113.50–118.00	103.00	101.00–107.00	<0.001 **
WHR	0.92	0.88–0.95	0.84	0.79–0.88	<0.001 *	0.97	0.96–0.99	0.86	0.83–0.88	<0.001 **
Body fat (kg)	42.31	36.99–45.73	16.97	13.85–20.41	<0.001 *	36.77	32.12–41.14	15.46	13.62–18.02	<0.001 **
Body fat (%)	45.42	41.09–47.38	28.37	24.45–30.39	<0.001 *	33.43	30.49–36.14	19.38	16.91–21.24	<0.001 **
VAT (cm^2)	261.00	179.00–350.00	93.00	65.00–124.00	<0.001 *	296.00	238.50–350.00	120.00	83.00–214.00	<0.001 **
SAT (cm^2)	127.00	105.00–145.00	72.00	54.00–93.00	<0.001 *	128.50	109.50–149.00	69.50	63.00–74.00	<0.001 **
VAT (%)	68.22	60.36–74.12	56.02	48.33–62.32	<0.001 *	69.43	67.49–74.86	60.71	58.15–76.77	0.1514
SAT (%)	31.77	25.88–39.64	43.98	37.68–51.67	<0.001 *	30.57	25.13–32.51	39.29	23.23–41.85	0.1514
VAT/SAT ratio	2.14	1.52–2.86	1.27	0.94–1.65	<0.001 *	2.27	2.07–2.98	1.54	1.39–3.31	0.1514

Q1–Q3: 1st–3rd quartile, BMI—body mass index, WHR—waist-to-hip ratio, VAT—visceral adipose tissue, SAT—subcutaneous adipose tissue. Statistical significance ($p < 0.05$), *p* *—statistical differences between women from study and control groups, *p* **—statistical differences between men from study and control groups.

Next, concentrations of selected proinflammatory cytokines and adipokines in the saliva of participants from the study and control groups were assessed and the results are presented in Table 2.

Table 2. Comparison of the concentration of selected proinflammatory cytokines and adipokines between women and men from the study and control groups.

| Parameter | Women (*n* = 77) | | | | | Men (*n* = 39) | | | | |
| | Study Group (*n* = 46) | | Control Group (*n* = 31) | | *p* * | Study Group (*n* = 29) | | Control Group (*n* = 10) | | *p* ** |
	Median	Q1–Q3	Median	Q1–Q3		Median	Q1–Q3	Median	Q1–Q3	
MMP-2 (ng/mL)	0.97	0.75–1.35	0.64	0.50–1.00	0.0012 *	1.16	0.72–1.78	0.74	0.55–1.26	0.1744
MMP-9 (ng/mL)	439.90	274.80–760.50	301.20	171.90–498.40	0.0451 *	519.10	295.20–995.20	178.15	84.60–333.20	0.0028 **
IL-6 (pg/mL)	9.88	4.04–15.23	8.25	3.13–31.70	0.9547	12.88	6.53–22.23	5.85	3.13–9.33	0.0430 **
Resistin (ng/mL)	3.58	1.41–5.03	1.97	0.59–4.56	0.0875	4.76	2.03–6.71	0.94	0.48–4.85	0.0397 **
IL-1β (pg/mL)	390.68	272.43–869.06	239.02	135.35–538.50	0.0035 *	494.70	262.39–1443.07	313.57	109.65–1631.30	0.3484

MMP-2—metalloproteinase-2, MMP-9—metalloproteinase-9, IL-6—interleukin-6, IL-1β—interleukin 1β. Statistical significance ($p < 0.05$), *p* *—statistical differences between women from study and control group, *p* **—statistical differences between men from study and control group.

Statistically significantly higher concentrations of MMP-2, MMP-9 and IL-1β were found in the saliva of obese women compared to women with normal body weight. Furthermore, statistically significantly higher concentrations of MMP-9, IL-6 and resistin were observed in the saliva of obese men compared to men with normal body weight.

Next, correlations between selected anthropometric/body composition parameters and cytokines/adipokines in the saliva of women from the study and control groups (*n* = 77) were analysed, and the results are presented in Table 3 and Supplementary Tables S1 and S2.

Table 3. Correlations between selected anthropometric/body composition parameters and the concentrations of cytokines/adipokines in the saliva of women from the study and control groups.

Parameter	Women (n = 77)				
	MMP-2 (ng/mL)	MMP-9 (ng/mL)	IL-6 (pg/mL)	Resistin (ng/mL)	IL-1β (pg/mL)
BMI (kg/m^2)	r = 0.460	r = 0.343	r = 0.144	r = 0.258	r = 0.396
	p = 0.000 *	p = 0.002 *	p = 0.208	p = 0.023 *	p = 0.000 *
Waist circumference (cm)	r = 0.330	r = 0.264	r = 0.069	r = 0.200	r = 0.284
	p = 0.003 *	p = 0.019 *	p = 0.549	p = 0.080	p = 0.012 *
Hip circumference (cm)	r = 0.355	r = 0.330	r = 0.120	r = 0.247	r = 0.309
	p = 0.001 *	p = 0.003 *	p = 0.296	p = 0.029 *	p = 0.006 *
WHR	r = 0.171	r = 0.106	r = −0.005	r = 0.049	r = 0.148
	p = 0.136	p = 0.356	p = 0.963	p = 0.667	p = 0.198
Body fat (kg)	r = 0.387	r = 0.359	r = 0.126	r = 0.224	r = 0.347
	p = 0.000 *	p = 0.001 *	p = 0.273	p = 0.049 *	p = 0.001 *
Body fat (%)	r = 0.421	r = 0.345	r = 0.136	r = 0.200	r = 0.396
	p = 0.000 *	p = 0.002 *	p = 0.234	p = 0.079	p = 0.000 *
VAT (cm^2)	r = 0.373	r= 0.209	r = 0.066	r = 0.305	r = 0.327
	p = 0.000 *	p = 0.066	p = 0.563	p = 0.006 *	p = 0.003 *
SAT (cm^2)	r = 0.258	r = 0.287	r = 0.165	r = 0.182	r = 0.275
	p = 0.023 *	p = 0.011 *	p = 0.150	p = 0.112	p = 0.015 *
VAT (%)	r = 0.305	r = 0.073	r = −0.021	r = 0.216	r = 0.214
	p = 0.006 *	p = 0.522	p = 0.849	p = 0.058	p = 0.061
SAT (%)	r = −0.073	r = −0.305	r = 0.021	r = −0.216	r = −0.214
	p = 0.522	p = 0.006 *	p = 0.849	p = 0.058	p = 0.061
VAT/SAT ratio	r = 0.304	r = 0.077	r = −0.019	r = 0.217	r = 0.218
	p = 0.007 *	p = 0.502	p = 0.864	p = 0.057	p = 0.056

BMI—body mass index, WHR—waist hip ratio, VAT—visceral adipose tissue, SAT—subcutaneous adipose tissue. MMP-2—metalloproteinase-2, MMP-9—metalloproteinase-9, IL-6—interleukin-6, IL-1β—interleukin 1β. p *—statistical significance (p < 0.05).

Statistically significant positive correlations were found between BMI and the salivary concentrations of MMP-2, MMP-9, resistin and IL-1β. A similar relationship was also observed for hip circumference and total body fat (kg). Statistically significant positive correlations were also found between waist circumference and serum concentrations of MMP-2, MMP-9 and IL-1β. A similar relationship was also observed for the percentage of total body fat and subcutaneous fat (SAT (cm^2)). No statistically significant correlations were found between the WHR index and the salivary concentrations of cytokines/adipokines. Statistically significant positive correlations were found between VAT (cm^2) and the salivary concentrations of MMP-2, resistin and IL-1β, whereas the percentage of VAT showed a statistically significant positive correlation only with the concentration of MMP-2 in saliva. A similar relationship was observed for the VAT/SAT ratio. A statistically significant negative correlation was found only between SAT (%) and the concentration of MMP-9 in saliva. There were no statistically significant correlations between IL-6 and selected anthropometric and body composition parameters in women from the study and control groups.

Next, correlations between selected anthropometric/body composition parameters and the concentrations of cytokines/adipokines in the saliva of men from the study and control groups (n = 39) were analysed. The results are presented in Table 4 and Supplementary Tables S3 and S4.

Table 4. Correlations between selected anthropometric/body composition parameters and the concentrations of cytokines/adipokines in the saliva of men from the study and control groups.

Parameter	Men (*n* = 39)				
	MMP-2 (ng/mL)	MMP-9 (ng/mL)	IL-6 (pg/mL)	Resistin (ng/mL)	IL-1β (pg/mL)
BMI (kg/m²)	r = 0.289	r = 0.416	r = 0.282	r = 0.318	r = 0.309
	p = 0.073	p = 0.008 *	p = 0.081	p = 0.047 *	p = 0.055
Waist circumference (cm)	r = 0.303	r = 0.362	r = 0.360	r = 0.325	r = 0.251
	p = 0.060	p = 0.023 *	p = 0.024 *	p = 0.043 *	p = 0.122
Hip circumference (cm)	r = 0.179	r = 0.353	r = 0.329	r = 0.310	r = 0.217
	p = 0.275	p = 0.027 *	p = 0.040 *	p = 0.054	p = 0.183
WHR	r = 0.362	r = 0.297	r = 0.360	r = 0.321	r = 0.239
	p = 0.023 *	p = 0.066	p = 0.024 *	p = 0.046 *	p = 0.141
Body fat (kg)	r = 0.118	r = 0.300	r = 0.143	r = 0.226	r = 0.104
	p = 0.477	p = 0.066	p = 0.390	p = 0.170	p = 0.533
Body fat (%)	r = 0.168	r = 0.314	r = 0.120	r = 0.176	r = 0.124
	p = 0.312	p = 0.054	p = 0.470	p = 0.290	p = 0.456
VAT (cm²)	r = 0.147	r = −0.027	r = 0.106	r = −0.174	r = −0.144
	p = 0.378	p = 0.869	p = 0.525	p = 0.293	p = 0.388
SAT (cm²)	r = 0.204	r = 0.353	r = 0.437	r = 0.326	r = 0.263
	p = 0.218	p = 0.029 *	p = 0.005 *	p = 0.045 *	p = 0.109
VAT (%)	r = 0.138	r = 0.063	r = 0.261	r = −0.002	r = −0.007
	p = 0.407	p = 0.702	p = 0.113	p = 0.987	p = 0.963
SAT (%)	r = −0.147	r = 0.027	r = −0.106	r = 0.174	r = 0.144
	p = 0.378	p = 0.869	p = 0.525	p = 0.293	p = 0.388
VAT/SAT ratio	r = 0.151	r = −0.024	r = 0.110	r = −0.178	r = −0.130
	p = 0.362	p = 0.882	p = 0.507	p = 0.284	p = 0.434

BMI—body mass index, WHR—waist–hip ratio, VAT—visceral adipose tissue, SAT—subcutaneous adipose tissue. MMP-2—metalloproteinase-2, MMP-9—metalloproteinase-9, IL-6—interleukin-6, IL-1β—interleukin 1β. p *—statistical significance ($p < 0.05$).

Statistically significant positive correlations were found between BMI and the concentrations of MMP-9 and resistin in saliva. Statistically significant positive correlations were also shown for waist circumference and the concentrations of MMP-9, IL-6 and resistin in saliva. Furthermore, statistically significant positive correlations were demonstrated between hip circumference and the salivary concentrations of MMP-9 and IL-6. However, a statistically significant positive correlation was demonstrated between the WHR index and the concentrations of MMP-2, IL-6 and resistin. Statistically significant positive correlations were found between subcutaneous fat content (cm²) and the salivary concentrations of MMP-9, IL-6 and resistin. However, no statistically significant correlations were found between total body fat content in percentages and kilograms, the content of visceral (cm² and %) and subcutaneous (%) fat, as well as the VAT/SAT ratio and the salivary concentrations of selected cytokines/adipokines.

3. Discussion

Chronic low-grade inflammation is one of the mediators of metabolic disturbances associated with obesity. Recent reports have investigated the mechanisms and assessed the impact of proinflammatory cytokines/adipokines on the development of metabolic derangements in obesity [14]. Particular attention has been paid to saliva testing, mainly

because of the non-invasive method of its collection and the diagnostic possibilities it offers in routine medical practice.

MMPs play an important role in the pathological remodelling of blood vessel walls, including vascular endothelial dysfunction, smooth muscle hyperplasia and the formation of unstable atherosclerotic plaques [12]. The present study demonstrated higher concentrations of MMP-2 in the saliva of subjects with obesity compared to individuals with normal body weight. Furthermore, statistically significant differences in the concentrations of MMP-2 in the saliva of obese women compared to women with normal body weight were found ($p = 0.0012$). Similar results were obtained in a study by Mota et al. from 2019, in which salivary concentrations of MMP-2 were statistically significantly ($p < 0.05$) higher in obese subjects compared to individuals with normal body weight [15]. The present study as well as one of our previous investigations [16] revealed similar, positive correlations regarding MMP-2 concentrations in the saliva of obese individuals. We previously demonstrated strong, positive correlations between salivary MMP-2 concentrations and BMI (r = 0.806, $p < 0.001$), total body fat content (TBFkg r = 0.804, $p < 0.001$, TBF% r = 0.794, $p < 0.001$), waist circumference (r = 0.796, $p < 0.001$), visceral fat (VAT cm^2, r = 0.646, $p < 0.005$) and the VAT/SAT ratio (r = 0.701, $p < 0.002$). The fact that we again obtained statistically significant positive correlations between salivary MMP-2 concentrations, BMI and total body fat content indicates that the concentration of this cytokine may depend on body fat content, but further research exploring the mechanisms of metabolic disturbances that may influence salivary MMP-2 concentrations is needed [16].

Our study also showed statistically significantly higher concentrations of MMP-9 in the saliva of subjects with obesity compared to those with normal body weight, both in women ($p = 0.0451$) and men ($p = 0.0028$). Due to a limited number of studies on the concentration of MMP-9 in the saliva of individuals with excessive body weight, we decided to compare the obtained results with blood serum concentrations of MMP-9 reported in the available literature. Andrade et al. revealed statistically significantly ($p < 0.001$) higher concentrations of MMP-9 in the serum of women with primary obesity ($n = 36$) in comparison to women with normal body weight ($n = 30$) [17]. Similar findings were reported by Kosmal et al., who demonstrated a statistically significantly ($p < 0.001$) higher concentration of MMP-9 in the serum of obese women compared to women with normal weight [18]. To the best of our knowledge, the present study is the first to examine MMP-9 concentrations in the saliva of obese individuals, and therefore further studies evaluating the concentration of this cytokine in saliva are recommended.

Interleukin 6 (IL-6) is a proinflammatory cytokine that modulates the body's immune response, affecting the function of the nervous, hematopoietic and endocrine systems. IL-6 plays an important role in the pathogenesis of coronary artery disease as well as type 1 and type 2 diabetes. Moreover, IL-6 may increase the risk of cancer in people with excessive body weight [19]. Our study showed higher concentrations of IL-6 in the saliva of obese subjects compared to individuals with normal body weight. Moreover, statistically significant differences were found in the salivary concentrations of this cytokine between men from the study group and men from the control group ($p = 0.0430$). To date, a limited number of reports on the concentration of IL-6 in the saliva of obese people have been published. Furthermore, the reports mainly examined children. A study by Pîrsean et al. demonstrated that the concentrations of IL-6 in the saliva of overweight/obese children were significantly higher than the concentrations of this cytokine in the saliva of children with normal body weight [20]. The study, in contrast to our study, revealed a positive correlation between the salivary IL-6 concentration and BMI. However, in a study by Selvaraju et al., the concentrations of IL-6 in the saliva of obese children were 3.4 times higher compared to children with normal body weight [21]. The above results were confirmed by Roytblat et al. who showed statistically significantly ($p < 0.05$) higher concentrations of IL-6 in the serum of patients with excessive body weight compared to individuals with normal weight [22]. Due to a limited number of studies in adults and inconsistent data regarding children, it is suggested that further research on salivary IL-6

concentrations is conducted in order to elucidate the potential impact of IL-6 levels on metabolic derangements in obesity.

Resistin is an adipokine that may contribute to the development of insulin resistance, type 2 diabetes, hypertension, dyslipidemia and atherosclerosis [23]. Our study demonstrated higher resistin concentrations in the saliva of obese subjects compared to people with normal body weight and a statistically significant difference was found for men from both groups ($p = 0.0397$). Similar results were obtained by Lehmann-Kalata et al., who revealed statistically significantly ($p = 0.013$) higher concentrations of resistin in the saliva of obese patients compared to individuals with normal body weight [24]. Similar results were reported by Al.-Ravi et al., who found statistically significantly higher concentrations of resistin in obese subjects compared to individuals with normal body weight [25]. The difference between the above study and our present investigation is that Al.-Ravi et al. compared obese individuals with patients with diabetes. The latter showed the highest salivary concentrations of resistin [25]. The authors of the study concluded that high levels of resistin in saliva, which are associated with obesity, may be one of the factors predisposing obese individuals to type 2 diabetes. Therefore, it is suggested that further studies exploring the potential impact of high concentrations of resistin on the development of type 2 diabetes are conducted.

The salivary concentrations of IL-1β were also assessed in the present study. The cytokine, produced by macrophages, impairs insulin signalling and increases lipolysis [26]. To the best of our knowledge, our study is the first to assess the concentrations of this cytokine in the saliva of obese patients. We demonstrated higher concentrations of IL-1β in the saliva of obese patients in comparison to individuals with normal body weight. Furthermore, statistically significantly ($p = 0.0035$) higher concentrations of IL-1β were demonstrated in the saliva of obese men in comparison to men with normal body weight. Similar results were reported by Tvarijonaviciute et al., who revealed that IL-1β concentrations in the saliva of children with excessive body weight were 2.6 times higher compared to children with normal body weight [27]. Therefore, further studies are needed to confirm the benefits of evaluating salivary IL-1β concentrations in obese adults as risk factors for metabolic disturbances associated with obesity.

The limitation of our study is a small sample size. The main reason for this limitation is the high cost of reagents for the analysis of selected proinflammatory cytokines/adipokines. Furthermore, the authors of the study focused on uncomplicated obesity, which limited the number of people eligible for the study. On the other hand, careful selection of the small sample allowed us to produce accurate results that were not cofounded by other factors. Another limitation of the study is the use of electrical bioimpedance only. The gold standard for assessing body composition is the DEXA (dual-energy X-ray absorptiometry) test. We believe that further studies on larger populations may enable researchers to learn the mechanisms of the development of metabolic disorders related to the concentration of proinflammatory cytokines in the saliva of obese patients and translate the findings into everyday clinical practice.

4. Materials and Methods

This study followed an observational design. It included 116 individuals (77 women and 39 men). The study protocol was approved by the Bioethics Committee of the Medical University of Bialystok, Poland (No. R-I-002/647/2019 and APK.002.39.2021). All participants gave written informed consent to participate in the study prior to its commencement.

Men and women aged 20–55 years with primary obesity were enrolled in the study. An additional inclusion criterion was the absence of periodontal disease and inflammation in the oral cavity. The exclusion criteria were secondary obesity, type 1 and type 2 diabetes, acute coronary artery disease, endocrine disorders, appetite disorders, pregnancy and lactation, use of hormonal contraception or hormone replacement therapy, steroid therapy, antiretroviral therapy, previous surgical or pharmacological treatment for obesity, chronic inflammatory diseases, malignancies, a pacemaker. Women were also asked about the

phase of the menstrual cycle and the regularity of menstruation. The analyses in women were performed in the follicular phase (i.e., between the 8th and 11th day of the cycle).

Basic anthropometric measurements (body weight and height) of the study participants were taken, their BMIs were calculated and bioelectrical impedance analysis (BIA) was performed. Based on the obtained results, the participants were divided into two groups: the study group and the control group. The study group consisted of 75 people (46 women and 29 men) with obesity (BMI = 30.0–39.9 kg/m^2; >30% total body fat content for women and >25% for men). The control group comprised 41 people (31 women and 10 men) with normal body weight (BMI = 18.5–24.9 kg/m^2, 20–30% total body fat content for women and 15–20% for men). Saliva samples were collected from all study participants to determine the concentrations of selected proinflammatory cytokines and adipokines.

4.1. Body Composition Analysis

In order to measure body composition, BIA was performed on all participants using the BioScan 920-2 Analyzer (Essex, UK). It enabled the assessment of the following parameters: total body fat percentage (%), total fat-free mass percentage (%), total body fat mass (kg), total skeletal muscle mass (kg), total body water (L), extracellular (L) and intracellular water (L). The area of adipose tissue in the transverse section of the abdomen was also determined: VAT (in cm^2 and %) and SAT (in cm^2 and %), and the VAT/SAT ratio was also determined. Body composition analysis was performed in the morning, following an overnight fast, with no strenuous physical activity prior to the test.

4.2. Saliva Sample Collection

Saliva was collected using a standard method. Samples were collected between 9:00 and 11:00 a.m. All subjects abstained from eating and drinking for 2 h prior to sample collection. The subjects rinsed their mouths with deionised water and were sitting in a comfortable position with their eyes open and head titled slightly forward. Unstimulated whole saliva was collected for 10 min by spitting, as described by Navazesh [28]. Saliva samples were homogenised and clarified by centrifugation at 1200 RPMI for 15 min at 4 °C. The aliquots of clarified supernatants were stored at −70 °C for ELISA measurements.

4.3. Determination of IL-6, IL-1β, Resistin, MMP-9 and MMP-2

Highly sensitive assay kits (R&D Systems) were used to determine protein concentrations in saliva samples. The tests were performed according to the manufacturer's recommended protocols. The microtiter plate provided in the kits was pre-coated with a monoclonal antibody specific to the analysed protein. Standards and samples were added to the appropriate microtiter plate wells. Following incubation at room temperature, an enzyme-linked polyclonal antibody was added. Then, the microplate wells were aspirated and washed four times. Next, a substrate solution was added to each well. The enzyme–substrate reaction was terminated by addition of a stop solution and the colour change was measured spectrophotometrically at 450 ± 2 nm. The antigen concentration in the samples was determined by comparing the O.D. to the standard curve.

4.4. Statistical Analysis

Statistical analysis of the obtained results was performed using STATISTICA 13.3 software by StatSoft (version 13.3, Warsaw, Poland). Descriptive statistics were prepared by determining the value of the median and the upper and lower quartiles for quantitative features. A significance level of $p < 0.05$ was assumed. Non-parametric methods were used due to a lack of normal distribution. Two independent samples were compared using the Mann–Whitney U test (analysis of the concentrations of adipokines and cytokines in saliva for differences between the study and control groups). Spearman's rank correlations were used to assess the relationships between the concentrations of proinflammatory parameters and body composition parameters.

5. Conclusions

1. Higher concentrations of selected proinflammatory cytokines and adipokines are found in the saliva of obese individuals in comparison to individuals with normal body weight.
2. It is likely that higher concentrations of MMP-2, MMP-9 and IL-1β can be detected in the saliva of obese women compared to non-obese women, while higher concentrations of MMP-9, IL-6 and resistin can be found in the saliva of obese men compared to non-obese men, which suggests that further research to confirm our observations and determine the mechanisms of development of metabolic complications associated with obesity depending on gender is needed.

References

1. World Health Assembly. Follow-up to the Political Declaration of the High-level Meeting of the General Assembly on the Prevention and Control of Non-communicable Diseases. *Pap. WHA66.10* **2013**, 1–55.
2. World Obesity Federation. Global trends in obesity. In *Obesity: Missing the 2025 Global Targets*; Trends, Costs and Country Reports; World Obesity Federation: London, UK, 2020; pp. 16–33.
3. OECD. *OECD Health Policy Studies. The Heavy Burden of Obesity: The Economics of Prevention*; OECD: Paris, France, 2019; p. 256.
4. Hill, J.H.; Solt, C.; Foster, M.T. Obesity associated disease risk: The role of inherent differences and location of adipose depots. *Horm. Mol. Biol. Clin. Investig.* **2018**, *33*. [CrossRef] [PubMed]
5. Zhang, C.-Z.; Cheng, X.-Q.; Li, J.-Y.; Zhang, P.; Yi, P.; Xu, X.; Zhou, X.-D. Saliva in the diagnosis of diseases. *Int. J. Oral Sci.* **2016**, *8*, 133–137. [CrossRef]
6. Gornowicz, A.; Bielawska, A.; Bielawski, K.; Grabowska, S.Z.; Wójcicka, A.; Zalewska, M.; Maciorkowska, E. Pro-inflammatory cytokines in saliva of adolescents with dental caries disease. *Ann. Agric. Environ. Med.* **2012**, *19*, 711–716.
7. Nijakowski, K.; Surdacka, A. Salivary Biomarkers for Diagnosis of Inflammatory Bowel Diseases: A Systematic Review. *Int. J. Mol. Sci.* **2020**, *21*, 7477. [CrossRef] [PubMed]
8. Diesch, T.; Filippi, C.; Fritschi, N.; Filippi, A.; Ritz, N. Cytokines in saliva as biomarkers of oral and systemic oncological or infectious diseases: A systematic review. *Cytokine* **2021**, *143*, 155506. [CrossRef]
9. Zyśk, B.; Ostrowska, L.; Smarkusz-Zarzecka, J. Salivary Adipokine and Cytokine Levels as Potential Markers for the Devel-opment of Obesity and Metabolic Disorders. *Int. J. Mol. Sci.* **2021**, *22*, 11703. [CrossRef] [PubMed]
10. Han, M.S.; White, A.; Perry, R.J.; Camporez, J.P.; Hidalgo, J.; Shulman, G.I.; Davis, R.J. Regulation of adipose tissue inflam-mation by interleukin 6. *Proc. Natl. Acad. Sci. USA* **2020**, *117*, 2751–2760. [CrossRef] [PubMed]
11. Park, H.K.; Kwak, M.K.; Kim, H.J.; Ahima, R.S. Linking resistin, inflammation, and cardiometabolic diseases. *Korean J. Int. Med.* **2017**, *32*, 239–247. [CrossRef]

12. Baszczuk, A.; Kopczyński, Z.; Thielemann, A.; Musialik, K.; Kopczyński, J.; Bielawska, L.; Banaszewska, A.; Skrypnik, D. Evaluation of concentrations of metalloproteinase 2 (MMP-2) and metalloproteinase 9 (MMP-9) in serum of patients with primary hypertension. *Forum. Zab. Metabol.* **2015**, *6*, 2.

13. Bing, C. Is interleukin-1β a culprit in macrophage-adipocyte crosstalk in obesity? *Adipocyte* **2015**, *4*, 149–152. [CrossRef]

14. Kunz, H.E.; Hart, C.R.; Gries, K.J.; Parvizi, M.; Laurenti, M.; Dalla Man, C.; Moore, N.; Zhang, X.; Ryan, Z.; Polley, E.C.; et al. Adipose tissue macrophage populations and inflammation are associated with systemic inflam-mation and insulin resistance in obesity. *Am. J. Physiol. Endocrinol. Metab.* **2021**, *321*, E105–E121. [CrossRef] [PubMed]

15. Mota, F.; Silva, A.F.; Almeida, D.; Oliveira, C.; Luís, T.; Tavares, C.; Figueiredo, J.P.; Gonçalves, R.; Caseiro, A. Salivary and Serum Matrix Metalloproteinase (MMP)-2, MMP-9 and Their Tissue In-hibitors (TIMP)-1 and TIMP-2 in Young Obesity. *IJBLS* **2019**, *2*, 10–21.

16. Ostrowska, L.; Gornowicz, A.; Pietraszewska, B.; Bielawski, K.; Bielawska, A. Which salivary components can differentiate metabolic obesity? *PLoS ONE* **2020**, *15*, e0235358. [CrossRef] [PubMed]

17. Andrade, V.L.; Petruceli, E.; Belo, V.A.; Andrade-Fernandes, C.M.; Caetano Russi, C.V.; Bosco, A.A.; Tanus-Santos, J.E.; Sandrim, V.C. Evaluation of plasmatic MMP-8, MMP-9, TIMP-1 and MPO levels in obese and lean women. *Clin. Biochem.* **2012**, *45*, 412–415. [CrossRef]

18. Kosmala, W.; Plaksej, R.; Przewlocka-Kosmala, M.; Kuliczkowska-Plaksej, J.; Bednarek-Tupikowska, G.; Mazurek, W. Matrix metalloproteinases 2 and 9 and their tissue inhibitors 1 and 2 in premenopausal obese women: Relationship to cardiac function. *Int. J. Obes. (Lond.)* **2008**, *32*, 763–771. [CrossRef] [PubMed]

19. Ghosh, S.; Ashcraft, K. An IL-6 link between obesity and cancer. *Front. Biosci. (Elite Ed.)* **2013**, *5*, 461–478. [CrossRef]

20. Pîrsean, C.; Neguţ, C.; Stefan-Van Staden, R.-I.; Dinu-Pirvu, C.E.; Armean, P.; Udeanu, D.I. The salivary levels of leptin and interleukin-6 as potential inflammatory markers in children obesity. *PLoS ONE* **2019**, *14*, e0210288. [CrossRef] [PubMed]

21. Selvaraju, V.; Babu, J.R.; Geetha, T. Association of salivary C-reactive protein with the obesity measures and markers in children. *Diabetes Metab. Syndr. Obes. Targets Ther.* **2019**, *12*, 1239–1247. [CrossRef]

22. Roytblat, L.; Rachinsky, M.; Fisher, A.; Greemberg, L.; Shapira, Y.; Douvdevani, A.; Gelman, S. Raised Interleukin-6 Levels in Obese Patients. *Obes. Res.* **2000**, *8*, 673–675. [CrossRef]

23. Acquarone, E.; Monacelli, F.; Borghi, R.; Nencioni, A.; Odetti, P. Resistin: A reappraisal. *Mech. Ageing Dev.* **2019**, *178*, 46–63. [CrossRef] [PubMed]

24. Lehmann-Kalata, A.; Miechowicz, I.; Korybalska, K.; Swora-Cwynar, E.; Czepulis, N.; Łuczak, J.; Orzechowska, Z.; Grzymisławski, M.; Surdacka, A.; Witowski, J. Salivary fingerprint of simple obesity. *Cytokine* **2018**, *110*, 174–180. [CrossRef] [PubMed]

25. Al-Rawi, N.; Al-Marzooq, F. The Relation between Periodontopathogenic Bacterial Levels and Resistin in the Saliva of Obese Type 2 Diabetic Patients. *J. Diabetes Res.* **2017**, *2017*, 1–7. [CrossRef] [PubMed]

26. Pereira, S.S.; Alvarez-Leite, J.I. Low-Grade Inflammation, Obesity, and Diabetes. *Curr. Obes. Rep.* **2014**, *3*, 422–431. [CrossRef] [PubMed]

27. Tvarijonaviciute, A.; Martinez-Lozano, N.; Rios, R.; Marcilla de Teruel, M.C.; Garaulet, M.; Cerón, J.J. Saliva as a non-invasive tool for assessment of metabolic and inflammatory biomarkers in children. *Clin. Nutr.* **2020**, *39*, 2471–2478. [CrossRef]

28. Navazesh, M. Methods for collecting saliva. *Ann. N. Y. Acad. Sci.* **1993**, *694*, 72–77. [CrossRef]

Article

An Early and Sustained Inflammatory State Induces Muscle Changes and Establishes Obesogenic Characteristics in Wistar Rats Exposed to the MSG-Induced Obesity Model

Matheus Felipe Zazula [1,*], Diego Francis Saraiva [1], João Lucas Theodoro [1], Mônica Maciel [1], Eliel Vieira dos Santos Sepulveda [1], Bárbara Zanardini de Andrade [2], Mariana Laís Boaretto [3], Jhyslayne Ignácia Hoff Nunes Maciel [3], Gabriela Alves Bronczek [4], Gabriela Moreira Soares [4], Sara Cristina Sagae Schneider [5], Gladson Ricardo Flor Bertolini [3], Márcia Miranda Torrejais [6], Lucinéia Fátima Chasko Ribeiro [2], Luiz Claudio Fernandes [7] and Katya Naliwaiko [1,*]

[1] Laboratório de Plasticidade Morfofuncional, Departamento de Biologia Celular, Setor de Ciências Biológicas, Universidade Federal do Paraná, Curitiba 81530-000, Paraná, Brazil
[2] Laboratório de Biologia Estrutural e Funcional, Centro de Ciências Biológicas e da Saúde, Universidade Estadual do Oeste do Paraná, Cascavel 85819-110, Paraná, Brazil
[3] Laboratório de Estudo de Lesões e Recursos Fisioterapêuticos, Centro de Ciências Biológicas e da Saúde, Universidade Estadual do Oeste do Paraná, Cascavel 85819-110, Paraná, Brazil
[4] Centro de Pesquisa em Obesidade e Comorbidades, Departamento de Biologia Estrutural e Funcional, Universidade Estadual de Campinas, Campinas 13083-970, São Paulo, Brazil
[5] Laboratório de Fisiologia Endócrina e Metabolismo, Centro de Ciências Biológicas e da Saúde, Universidade Estadual do Oeste do Paraná, Cascavel 85819-110, Paraná, Brazil
[6] Laboratório Experimental de Morfologia, Centro de Ciências Médicas e Farmacêuticas, Universidade Estadual do Oeste do Paraná, Cascavel 85819-110, Paraná, Brazil
[7] Laboratório de Metabolismo Celular, Departamento de Fisiologia, Setor de Ciências Biológicas, Universidade Federal do Paraná, Curitiba 81530-000, Paraná, Brazil
* Correspondence: matheuszazula@gmail.com (M.F.Z.); naliwaiko@gmail.com (K.N.); Tel.: +55-41-3360-1544 (M.F.Z. & K.N.)

Abstract: The model of obesity induced by monosodium glutamate cytotoxicity on the hypothalamic nuclei is widely used in the literature. However, MSG promotes persistent muscle changes and there is a significant lack of studies that seek to elucidate the mechanisms by which damage refractory to reversal is established. This study aimed to investigate the early and chronic effects of MSG induction of obesity upon systemic and muscular parameters of Wistar rats. The animals were exposed to MSG subcutaneously (4 mg·g^{-1} b.w.) or saline (1.25 mg·g^{-1} b.w.) daily from PND01 to PND05 ($n = 24$). Afterwards, in PND15, 12 animals were euthanized to determine the plasma and inflammatory profile and to assess muscle damage. In PND142, the remaining animals were euthanized, and samples for histological and biochemical analyses were obtained. Our results suggest that early exposure to MSG reduced growth, increased adiposity, and inducted hyperinsulinemia and a pro-inflammatory scenario. In adulthood, the following were observed: peripheral insulin resistance, increased fibrosis, oxidative distress, and a reduction in muscle mass, oxidative capacity, and neuromuscular junctions, increased fibrosis, and oxidative distress. Thus, we can conclude that the condition found in adult life and the difficulty restoring in the muscle profile is related to the metabolic damage established early on.

Keywords: hyperinsulinemia; monosodium glutamate; metabolic syndrome; distress oxidative; pro-inflammatory profile; skeletal muscle fiber types

1. Introduction

The model of obesity induced by perinatal injections of monosodium glutamate is widely studied and known in the literature [1–3]. The main alteration determined in this model is the damage and cell death of neurons in the hypothalamic nuclei, mainly in the

arcuate nucleus (ARC), where this neuronal loss impairs the signaling mediated by insulin and affects the energy balance of the organism [3–6].

Due to the hyperphagic characteristic of the MSG model [7], the excessive consumption of nutrients is associated with the energy imbalance promoted by the hypothalamic lesion. In this model, obesity is associated with the secretion of pro-inflammatory cytokines by adipose tissue, which leads to insulin resistance, stimulating cell damage and impairing metabolic homeostasis in the adipose tissue, liver, pancreas, brain, and muscles [1,2,8–13].

It is recognized in the literature that insulin sensitivity and resistance depend on AMPK-mediated signaling pathways, where the main effect of this pathway is the increased GLUT4 translocation in the membranes of insulin-dependent tissues [8,14,15]. As a consequence of this activation, there is a reduction in the phosphorylation rate of the mTOR protein [16,17]. As insulin sensitivity is reduced, especially in skeletal muscle, mTOR signaling which has been implicated in insulin resistance and obesity pathogenesis contributes to the development of the inflammatory process by stimulating the activation of the Nf_KB pathway [1,17–20].

The reduction in the body growth of animals exposed to the MSG model has been evidenced by several authors [1,9,21–23]. This reduction can be identified immediately after the induction period, depending on the concentration and frequency of injections, and is also confirmed in adulthood [22,24]. In addition, the changes in growth caused by this model are not reversible when considering muscle tissue, which suggests that metabolic impairment may be established earlier than has been described in the literature and may resemble models of metabolic programming that affect muscle development and maturation [25–27].

Although the endocrine, metabolic, and autonomic aspects of obesity induced by MSG have been extensively studied and described for adult animals, the early effects of MSG exposure and the establishment of muscle changes are less understood and have been little explored. Thus, the present study aimed to identify whether the changes found in adulthood were established early by exposure to MSG.

2. Results

2.1. Murinometric Profile

2.1.1. Lactation Period

To access the effect of MSG injections on the animals' developmental delay, the pups were weighed and measured every 2 days. Evaluating the body weight of these offspring, we could observe that from PND07 onwards, MSG animals showed reduced weight gain when compared to CTL ($p < 0.0001$; Figure 1A), and this difference persisted until euthanasia (PND15). Likewise, MSG animals showed less gain in nasoanal length from PND07 when compared to the CTL group ($p < 0.0001$; Figure 1B). However, when evaluating the Lee index, it was only possible to observe lower values in MSG animals in PND09 ($p = 0.002$; Figure 1C). However, when we observed the total gain during the period, through the calculation of the area under the curve, we could observe that in terms of body weight ($p < 0.0001$; Figure 1A'), nasoanal length ($p < 0.0001$; Figure 1B'), and in the Lee index ($p = 0.0223$; Figure 1C'), MSG animals showed reduced development.

2.1.2. Post-Weaning Period

To assess whether the effect of MSG injections would persist into adulthood and whether it participates in the onset of metabolic syndrome and obesity, the animals were weighed, and their food intake was measured once a week from weaning until euthanasia (day 142 of age). The percentage of body weight gain ($p < 0.0001$; Figure 2A) in MSG animals was minor when compared to CTL from week 8 ($p = 0.0134$). Interestingly, this difference was accentuated from week 10, the period where puberty started ($p < 0.001$) and worsened from week 14 with the onset of adulthood ($p < 0.0001$). As expected, the MSG effect on general food consumption was higher in MSG animals when compared to CTL animals ($p = 0.0019$; Figure 2B). Furthermore, to confirm those findings, the area under

the curve of total body weight gain and total food consumption was calculated. In both situations, differences between the groups were found. Thus, the total weight gain was lower in MSG animals when compared to CTL ($p = 0.0026$; Figure 2A'), while the total food intake was higher in MSG animals when compared to CTL ($p = 0.0018$; Figure 2B').
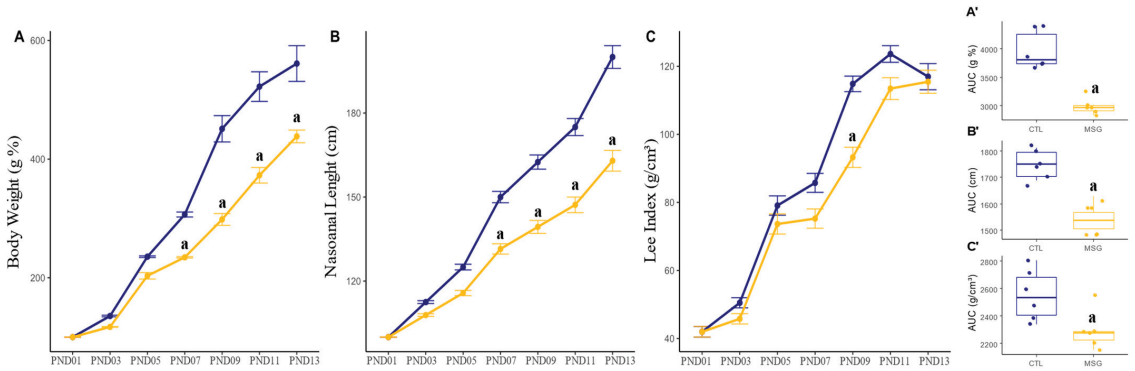

Figure 1. Graphs related to the development of CTL and the MSG animals during the perinatal period (PND01 to PND13). (**A**): Line plot of per cent weight gain (g%); (**B**): line plot of nasoanal length gain (cm); (**C**): Lee's index gain line plot (g/cm³); (**A'**): AUC of body weight gain; (**B'**): AUC of nasoanal length gain (cm); (**C'**): AUC of the Lee index gain (g/cm³). The CTL is represented in blue and the MSG group is represented in yellow. The letter a represents the difference between the MSG group when compared to the CTL. (**A–C**): repeated measurements ANOVA. (**A'–C'**): Student's *t*-test.
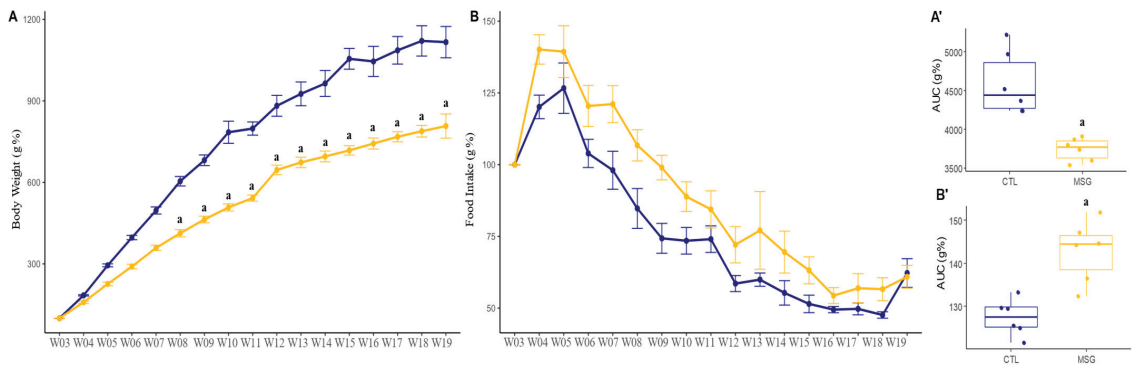
Figure 2. Graphs related to weight gain and feed consumption of CTL and the MSG animals after weaning (PND21, or W03, to PND142, or W19). (**A**): Percent weight gain line graph (g%); (**B**): line plot of food consumption (g%); (**A'**): AUC of body weight gain; (**B'**): AUC of food consumption (g%). The CTL is represented in blue and the MSG group is represented in yellow. The letter a represents the difference between the MSG group when compared to the CTL. (**A,B**): repeated measurements ANOVA. (**A',B'**): Student's *t*-test.

2.2. Intraperitoneal Glucose Tolerance Test (ipGTT) and Insulin Measurement

A glucose tolerance test was performed to assess whether alteration of glucose sensibility and metabolism had been established at 135 days of life, followed by a measurement of plasma insulin levels. In this sense, when we evaluated the response in the ipGTT test ($p < 0.0001$; Figure 3A), we could observe that even with no difference in baseline blood glucose levels between the groups, the MSG animals had higher blood glucose levels at T15 ($p = 0.0167$) and a smaller decrease in blood glucose at T30 ($p = 0.0492$) when compared

to CTL. When assessing insulin levels ($p < 0.0001$; Figure 3B), it was identified that MSG animals had elevated basal insulin concentrations when compared to CTL animals. Furthermore, this elevation of insulin concentrations was maintained throughout the test when compared to CTL, suggesting a picture of persistent hyperinsulinemia. When calculating the area under the curve for the total concentration of glucose and insulin throughout the experiment, it was observed that the MSG animals had higher glycemia ($p = 0.0317$; Figure 3A') and this was accompanied by higher plasma insulin ($p < 0.0001$; Figure 3B').
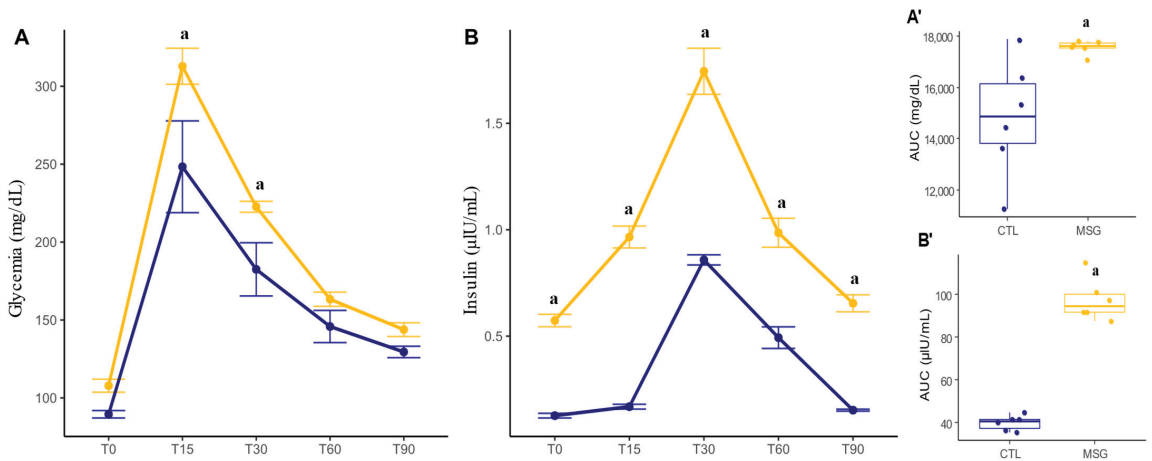
Figure 3. Graphs related to ipGTT and insulin dosage of CTL and MSG animals at 135 days of life. (**A**): Graph of blood glucose during the test (mg/dL); (**B**): insulin level graph (μIU/mL); (**A'**): AUC of blood glucose during the test (mg/dL); (**B'**): AUC of insulin level (μIU/mL). The CTL is represented in blue and the MSG group is represented in yellow. The letter a represents the difference between the MSG group when compared to the CTL. (**A,B**): repeated measurements ANOVA. (**A',B'**): Student's *t*-test.

2.3. Inflammatory and Obesogenic Scenario at 15 Days

2.3.1. Corporal Characterization

On day PND15, MSG animals presented lower weight ($p < 0.0001$) and nasoanal length ($p = 0.0002$) when compared to CTL. However, when calculating the Lee index, there was no difference between the groups ($p = 0.6851$) Figure 4.
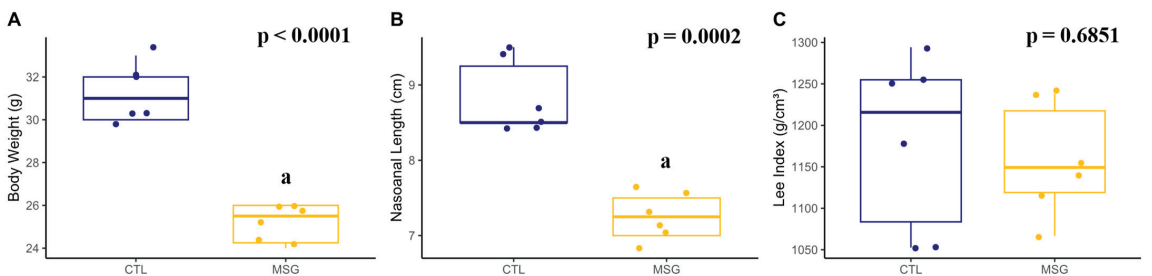
Figure 4. Graphs related to corporal characterization in PND15: (**A**): body weight (g); (**B**): nasoanal length (cm); (**C**): Lee index (g/cm^3). The CTL is represented in blue and the MSG group is represented in yellow. The letter a represents the difference between the MSG group when compared to the CTL. All data: Student's *t*-test.

2.3.2. Plasmatic Profile

When we evaluated the plasma of MSG and CTL animals, no differences were identified for glucose ($p = 0.312$), total cholesterol ($p = 0.9248$), LDL ($p = 0.6471$), VLDL ($p = 0.9951$), triacylglycerols ($p = 0.9951$), and HDL ($p = 0.3501$). When calculating the dyslipidemia predictors, no change was identified in the lipid ratio ($p = 0.4318$), in the Castelli index 1 ($p = 0.9485$), and in the Castelli index 2 ($p = 0.9485$). Similar results were identified for muscle damage markers, where lactate ($p = 0.7789$) and creatine kinase ($p = 0.8872$) levels were not different in MSG animals when compared to CTL, Figure 5.
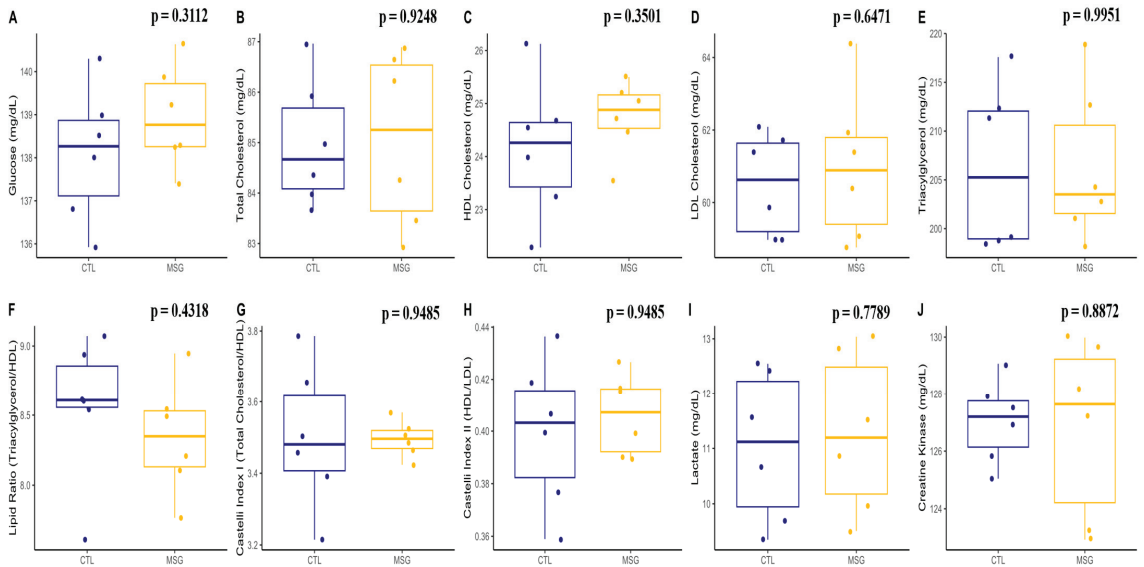
Figure 5. Graphs related to plasmatic profile in PND15: (**A**): glucose (mg/dL); (**B**): total cholesterol (mg/dL); (**C**): HDL cholesterol (mg/dL); (**D**): LDL cholesterol (mg/dL); (**E**): total triacylglycerols (mg/dL); (**F**): lipid ratio (total triacylglycerols/HDL); (**G**): Castelli index I (Total Cholesterol/HDL); (**H**): Castelli index II (HDL/LDL); (**I**): lactate (mg/dL); (**J**): creatine kinase (mg/dL). The CTL is represented in blue and the MSG group is represented in yellow.

Interestingly, when measuring insulin levels and calculating HOMA-IR, it was observed that MSG animals showed an increase when compared to CTL ($p < 0.0001$, in both). Meanwhile, the calculation of QUICKI ($p < 0.0001$) showed a reduction in MSG animals when compared to CTL. However, MSG animals showed increased concentrations of TNFα ($p = 0.0284$), IL-06 ($p < 0.0001$), and IL-10 ($p = 0.0053$), Figure 6.

2.3.3. Skeletal Muscle Antioxidant System and Oxidative Damage

When evaluating the antioxidant system and oxidative damage of the skeletal muscle pool, it was again identified that there were no differences between the MSG and CTL groups in the activity of the enzymes superoxide dismutase ($p = 0.5249$), catalase ($p = 0.5198$), and total cholinesterase ($p = 0.3159$), as well as in the levels of soluble proteins ($p = 0.8843$), lipid peroxides ($p = 0.5253$), and non-protein thiols ($p = 0.9972$), Figure 7.
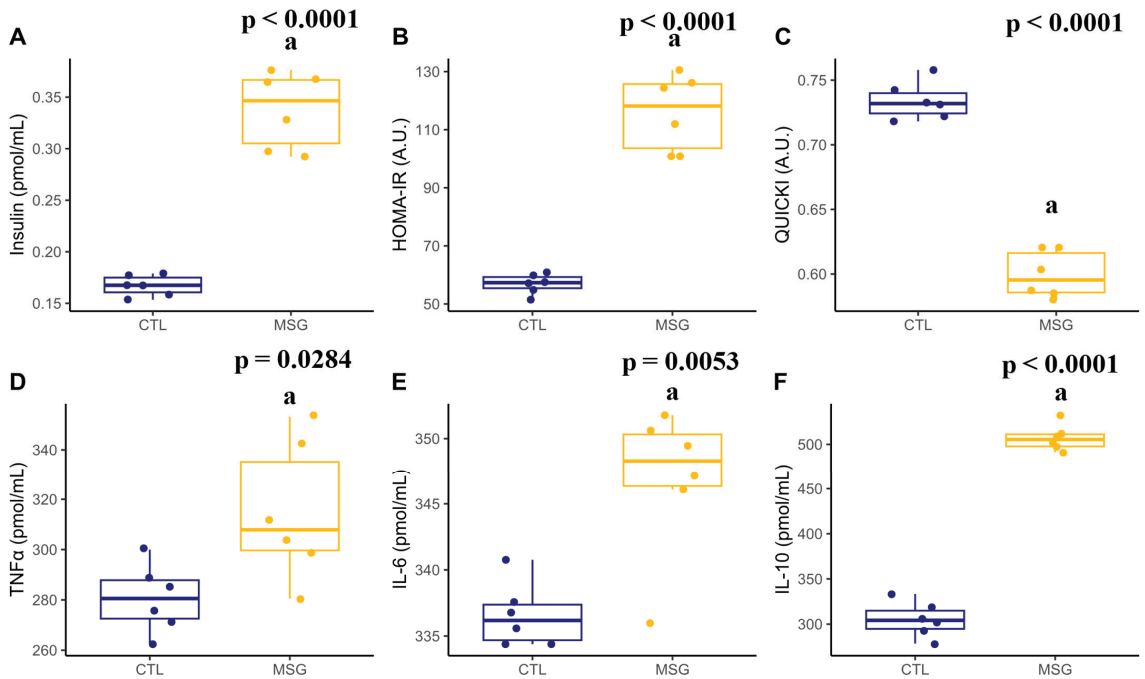
Figure 6. Graphs related to insulin and inflammatory plasmatic profile in PND15: (**A**): insulin (μIU/mL); (**B**): HOMA-R (A.U); (**C**): QUICKI (A.U); (**D**): TNFα (pmol/mL); (**E**): IL-6 (pmol/mL); (**F**): IL-10 (pmol/mL). The CTL is represented in blue and the MSG group is represented in yellow. The letter a represents the difference between the MSG group when compared to the CTL group. All data: Student's *t*-test.

2.4. Obesity and Muscle Damage at 142 Days

2.4.1. Corporal Characterization

The analysis of the animals in the PND142 showed that the MSG animals had a lower weight ($p < 0.0001$) and nasoanal length ($p = 0.0002$) when compared to the CTL animals. However, when compared to the CTL animals, the MSG animals had a higher Lee index ($p = 0.0153$) and higher adiposity ($p < 0.0001$), Figure 8.

2.4.2. Plasmatic Profile

When the plasma profile of the animals was evaluated, the MSG animals showed an increase in glucose ($p = 0.0011$), total cholesterol ($p < 0.0001$), LDL ($p < 0.00,01$), and VLDL ($p = 0.0052$) cholesterol fractions, as well as in total triacylglycerols levels ($p = 0.0052$). There was no difference in HDL between the groups ($p = 0.0657$). When performing the calculation of dyslipidemia predictors, an increase in the lipid ratio was identified ($p = 0.0115$), in the Castelli index 1 ($p = 0.0001$), and the Castelli index 2 ($p = 0.0061$). Likewise, when evaluating some muscle damage markers, an increase in lactate levels ($p = 0.0008$) and a decrease in creatine kinase concentrations ($p < 0.0001$) were identified in the MSG animals when compared with the CTL animals, Figure 9.
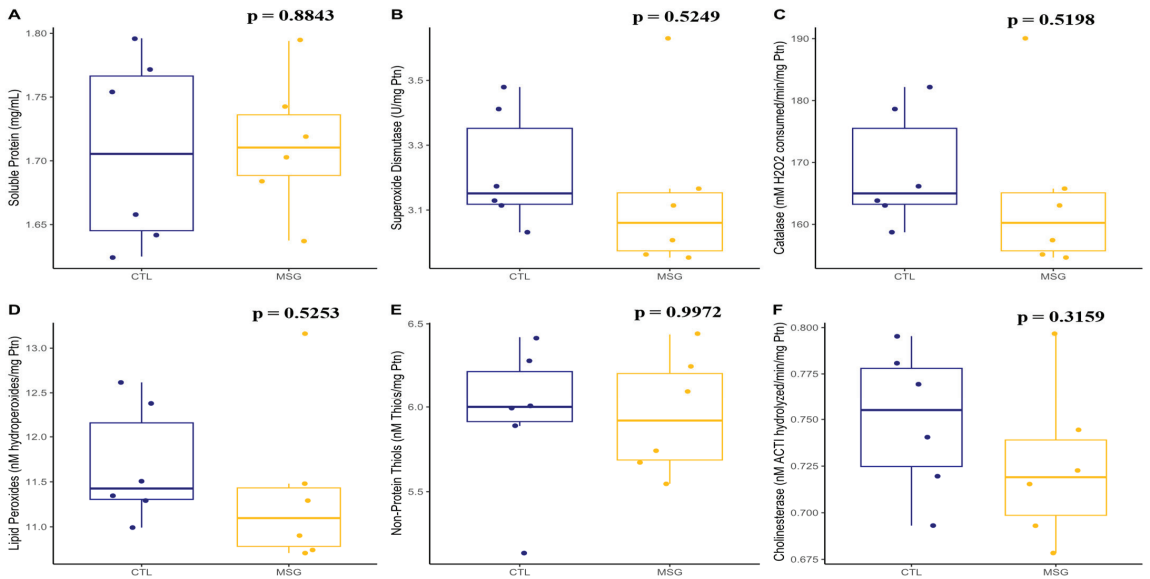
Figure 7. Graphs related to skeletal muscle antioxidant system in PND15: (**A**): soluble proteins (mg/mL); (**B**): superoxide dismutase activity (U/mg protein); (**C**): catalase activity (mM H_2O_2 consumed/min/mg protein); (**D**): lipid peroxides (nM hydroperoxides/mg protein); (**E**): non-protein thiols concentration (nM thiols/mg protein); (**F**): cholinesterase activity (nM acetylthiocholine hydrolyzed/min/mg protein). The CTL group is represented in blue and the MSG group is represented in yellow. All data: Student's *t*-test.
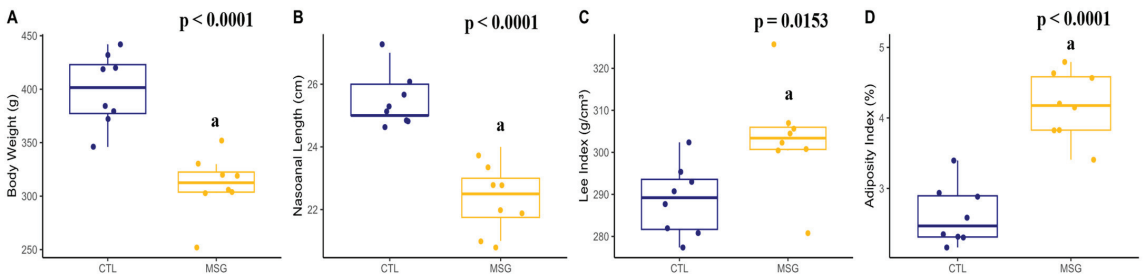
Figure 8. Graphs related to corporal characterization in PND142: (**A**): body weight (g); (**B**): nasoanal length (cm); (**C**): Lee index (g/cm^3); (**D**): adiposity index (%). The CTL is represented in blue and the MSG group is represented in yellow. The letter a represents the difference between the MSG group when compared to the CTL group. All data: Student's *t*-test.

Interestingly, when measuring the insulin levels and calculating HOMA-IR, it was observed that the MSG animals showed an increase when compared to the CTL animals ($p < 0.0001$, in both). Meanwhile, the calculation of QUICKI ($p < 0.0001$) showed a reduction in MSG animals when compared to the CTL animals, Figure 10.
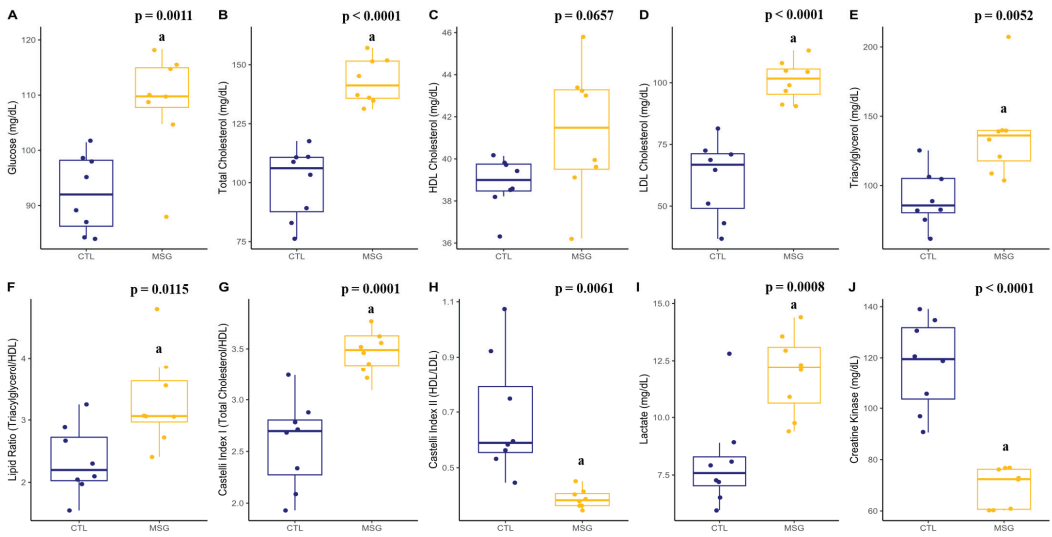
Figure 9. Graphs related to plasmatic profile in PND142: (**A**): glucose (mg/dL); (**B**): total cholesterol (mg/dL); (**C**): HDL cholesterol (mg/dL); (**D**): LDL cholesterol (mg/dL); (**E**): total triacylglycerols (mg/dL); (**F**): lipid ratio (total triacylglycerols/HDL); (**G**): Castelli index I (total cholesterol/HDL); (**H**): Castelli index II (HDL/LDL); (**I**): lactate (mg/dL); (**J**): creatine kinase (mg/dL). The CTL is represented in blue and the MSG group is represented in yellow. The letter a represents the difference between the MSG group when compared to the CTL group. All data: Student's *t*-test.
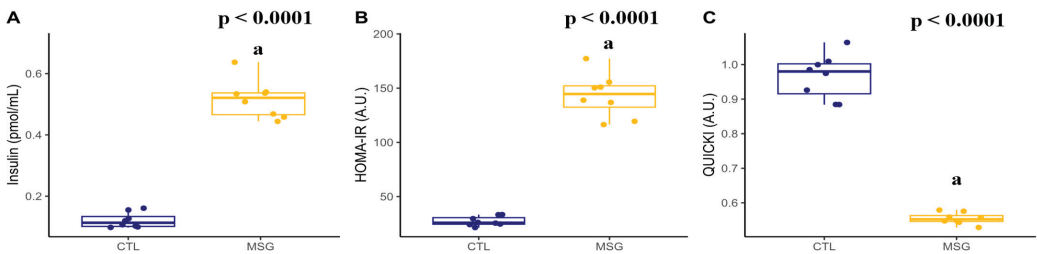
Figure 10. Graphs related to insulin plasmatic profile in PND142: (**A**): insulin (µIU/mL); (**B**): HOMA-R (A.U); (**C**): QUICKI (A.U). The CTL group is represented in blue and the MSG group is represented in yellow. The letter a represents the difference between the MSG group when compared to the CTL group. All data: Student's *t*-test.

2.4.3. Skeletal Muscle Structure

When we evaluated the macroscopic characteristics of the muscle, the MSG animals had lower EDL muscle weight ($p < 0.0001$) and shorter SOL ($p = 0.0011$) and EDL muscle length ($p < 0.0001$) when compared to the CTL animals. When evaluating the muscular structure of the EDL and SOL, it was identified that the MSG animals had a higher density of fibers per mm^2 in both muscles ($p = 0.0022$; $p < 0.0001$, respectively), when compared to the CTL animals, accompanied by a reduction in the cross-sectional area of muscle fibers, observed in both muscles of the MSG animals ($p = 0.0020$; $p < 0.0001$, respectively). In addition, we found a reduction in the largest ($p = 0.0003$; $p < 0.0001$, respectively) and smallest ($p = 0.0006$; $p < 0.0001$, respectively) diameters in both muscles of the MSG animals when compared to the CTL animals. It was also possible to identify that the SOL of the MSG animals showed a reduction in the diameter ratio, an important predictor of muscle fiber rounding ($p = 0.0178$), Table 1.

Table 1. Skeletal muscle structure, fiber types profile, and neuromuscular junctions structure from CTL and MSG animals to PND142.

Grouping Category	Variable	EDL			SOL		
		CTL	MSG	*p*-Value	CTL	MSG	*p*-Value
Macroscopical Structure	Muscle Weight	0.16 ± 0.01	0.12 ± 0.01 [a]	<0.0001	0.11 ± 0.01	0.12 ± 0.01	0.1382
	Muscle Length	31.60 ± 1.18	27.55 ± 0.92 [a]	<0.0001	23.64 ± 1.80	20.38 ± 0.64 [a]	0.0011
Skeletal Muscle Structure	Fiber Density	574.82 ± 24.01	629.13 ± 32.43 [a]	0.0022	318.60 ± 27.67	466.44 ± 15.27 [a]	<0.0001
	Cross-Sectional Area	1743.2 ± 73.4	1595.3 ± 82.2 [a]	0.0020	3165.9 ± 284.4	2146.2 ± 70.7 [a]	<0.0001
	Larger Diameter	58.86 ± 7.14	43.37 ± 2.22 [a]	0.0003	78.51 ± 5.68	57.00 ± 5.59 [a]	<0.0001
	Smaller Diameter	42.37 ± 5.76	31.31 ± 2.60 [a]	0.0006	46.77 ± 2.98	36.99 ± 3.83 [a]	<0.0001
	Diameter Ratio	1.39 ± 0.03	1.39 ± 0.05	0.9332	1.68 ± 0.12	1.54 ± 0.05 [a]	0.0178
	Capillaries/Fibers	1.50 ± 0.14	3.03 ± 0.41 [a]	<0.0001	3.28 ± 0.24	2.05 ± 0.02 [a]	<0.0001
	Nuclei/Fibers	2.12 ± 0.37	1.88 ± 0.19	0.1891	2.72 ± 0.09	1.85 ± 0.08 [a]	<0.0001
	Central Nuclei	1.63 ± 0.41	4.87 ± 1.17 [a]	<0.0001	1.63 ± 0.24	2.96 ± 0.49 [a]	<0.0001
	Myonuclear Domain	1195.1 ± 208.3	909.6 ± 152.3 [a]	0.0081	1160.6 ± 97.1	1019.1 ± 198.5	0.0998
	Nuclei/Sarcoplasm Area	0.010 ± 0.001	0.017 ± 0.001 [a]	<0.0001	0.013 ± 0.001	0.012 ± 0.000	0.1082
	Total Connective Tissue	3.58 ± 0.56	6.83 ± 1.10 [a]	<0.0001	4.31 ± 0.41	6.91 ± 1.38 [a]	0.0008
	Epimysium	1.92 ± 0.30	3.35 ± 0.54 [a]	<0.0001	2.32 ± 0.21	3.39 ± 0.68 [a]	<0.0001
	Perimysium	0.64 ± 0.10	1.96 ± 0.31 [a]	<0.0001	0.77 ± 0.07	1.98 ± 0.39 [a]	<0.0001
	Endomysium	1.01 ± 0.15	1.51 ± 0.24 [a]	0.0004	1.22 ± 0.11	1.52 ± 0.31	0.2689
	Collagen Type I	75.27 ± 3.49	66.32 ± 5.44 [a]	0.0014	75.27 ± 6.36	78.52 ± 8.56	0.4048
	Collagen Type III	24.23 ± 3.49	33.67 ± 5.44 [a]	0.0014	33.09 ± 5.86	21.47 ± 8.56 [a]	0.0078
Fiber Types Profile	Proportion Fiber Type I	9.31 ± 1.49	5.40 ± 1.18 [a]	<0.0001	86.05 ± 1.89	79.29 ± 1.35 [a]	<0.0001
	Proportion Fiber Type IIA	41.68 ± 2.59	43.61 ± 3.08	0.1968	13.94 ± 1.89	20.71 ± 1.35 [a]	<0.0001
	Proportion Fiber Type IIB	49.00 ± 2.28	50.98 ± 2.16	0.0973	NA	NA	NA
	Cross-Sectional Area Type I	833.87 ± 26.92	779.70 ± 22.64 [a]	0.0007	2923.4 ± 843.8	1669.2 ± 273.5 [a]	<0.0001
	Cross-Sectional Area Type IIA	1158.1 ± 87.3	985.7 ± 131.6 [a]	0.0093	4233.6 ± 685.6	3867.7 ± 463.9 [a]	<0.0001
	Cross-Sectional Area Type IIB	2514.3 ± 149.2	2357.4 ± 292.4	0.2048	NA	NA	NA
Neuromuscular Junctions Structure	NMJ Cross-Sectional Area	151.38 ± 15.10	134.31 ± 7.75 [a]	0.0167	161.64 ± 10.84	96.03 ± 6.55 [a]	<0.0001
	NMJ Larger Diameter	25.71 ± 4.19	22.90 ± 1.53	0.1089	23.69 ± 0.94	16.17 ± 1.21 [a]	<0.0001
	NMJ Smaller Diameter	10.03 ± 0.88	10.10 ± 1.23	0.8939	7.11 ± 0.40	5.58 ± 0.42 [a]	<0.0001
	NMJ Diameter Ratio	2.56 ± 0.29	2.29 ± 0.22	0.0621	3.34 ± 0.30	2.90 ± 0.28 [a]	0.0102
Antioxidant System	Superoxide Dismutase	6.61 ± 0.69	6.95 ± 0.70	0.3439	5.65 ± 0.25	5.64 ± 0.43	0.9409
	Catalase	403.37 ± 107.70	258.43 ± 84.11 [a]	0.0101	204.45 ± 37.45	435.22 ± 28.13 [a]	<0.0001
	Soluble Proteins	1.74 ± 0.06	1.81 ± 0.03 [a]	0.0268	1.83 ± 0.07	1.91 ± 0.03 [a]	0.0268
	Lipid Peroxides	27.60 ± 3.85	21.51 ± 2.95 [a]	0.0405	13.44 ± 1.50	17.58 ± 1.37 [a]	<0.0001
	Non-Protein Thiols	6.73 ± 0.44	5.42 ± 0.04 [a]	<0.0001	7.37 ± 0.70	5.89 ± 0.45 [a]	0.0003
	Total Cholinesterase's	0.99 ± 0.06	0.85 ± 0.04 [a]	0.0001	1.10 ± 0.12	0.84 ± 0.03 [a]	0.0003

Legend: muscle weight (g/100 g), muscle length (mm), fiber density (number of fibers/mm^2), cross-sectional area (μm^2), larger and smaller diameters (μm), diameter ratio (larger diameter/smaller diameter), capillaries and nuclei (total number/total number fibers), central nuclei and proportion of fiber types (%), mionuclear domain (fiber cross-sectional area/total nuclei), nuclei/sarcoplasm area (nuclei cross-sectional area/fiber cross-sectional area). All analysis of connective tissue and collagen types (% pixels). Superoxide dismutase activity (U/mg protein); catalase activity (mM H_2O_2 consumed/min/mg protein); soluble proteins (mg/mL); lipid peroxides (nM hydroperoxides/mg protein); non-protein thiols concentration (nM thiols/mg protein); cholinesterase activity (nM acetylthiocholine hydrolyzed/min/mg protein). The letter a represents the difference between the MSG group when compared to the CTL group. All data: Student's *t*-test.

Another feature evaluated was the distribution of capillaries and nuclei in the cells of both muscles. MSG animals showed a greater distribution of capillaries in EDL when compared to CTL (*p* < 0.0001), while the distribution of capillaries was reduced in SOL (*p* < 0.0001). In the distribution of nuclei, the MSG animals showed lower values in SOL (*p* < 0.0001) when compared to the CTL animals. However, when we evaluated the presence of nuclei in a central position in the muscle fibers, we could observe that for both the EDL and SOL muscles, the MSG animals showed an increase comparable to the CTL animals (*p* < 0.0001, in both). In the case of the myonuclear domain, there was a reduction in MSG animals compared to the CTL animals for EDL only (*p* = 0.0081), Table 1.

When evaluating the distribution of connective tissue in the EDL and SOL muscles, it was found that in MSG animals there was an increase in total connective tissue in both muscles when compared to the CTL animals (*p* < 0.0001; *p* = 0.0008, respectively). In addition, in the MSG animals higher values of connective tissue in the epimysium (*p* < 0.0001, in both) and perimysium (*p* < 0.0001, in both) in both muscles were shown. However,

endomysium thickening was identified only in the EDL of MSG animals ($p = 0.0004$). The evaluation of the type of collagen in each of the muscles revealed that in the EDL, the MSG animals showed a reduction in type I collagen ($p = 0.0014$) and an increase in type III collagen ($p = 0.00014$), while in the SOL, only type III collagen reduction ($p = 0.0078$) could be identified in MSG animals when compared to the CTL animals, Table 1.

2.4.4. Fiber Types Profile and Neuromuscular Junction Structure

When analyzing the prevalence of each type of f, the MSG animals showed a reduction in the proportion of type I fibers in EDL and SOL ($p < 0.0001$, in both) and a reduction in the cross-sectional area of type I fibers in EDL and SOL ($p < 0.0001$, in both) when compared to the CTL animals. In SOL, MSG animals showed an increase in the proportion of IIA-type fibers ($p < 0.0001$), and in both muscles, EDL and SOL, there was a reduction in the cross-sectional area of IIA-type fibers ($p = 0.0093$; $p < 0.0001$, respectively) of the MSG animals when compared to the CTL. Furthermore, it was identified that the MSG animals showed a reduction in the cross-sectional area of the neuromuscular junctions both in the EDL ($p = 0.0167$) and in the SOL ($p < 0.0001$) when compared to the CTL animals. The MSG animals showed a reduction in the major ($p < 0.0001$) and minor ($p < 0.0001$) diameters in the SOL muscle junctions when compared to the CTL animals. Therefore, when evaluating the ratio between the largest and smallest diameters, a predictor of damage to the structure, it was observed that the MSG animals had a lower ratio ($p = 0.0102$) when compared to the CTL animals. Finally, when analyzing the antioxidant system and oxidative damage in EDL and SOL, it was identified that catalase activity was reduced in EDL ($p = 0.0101$) and increased in SOL ($p < 0.0001$) in MSG animals compared to the CTL animals. However, in both muscles, the MSG animals showed an increase in the concentration of proteins ($p = 0.0268$, in both), of lipid peroxides ($p = 0.0405$; $p < 0.0001$, respectively), and a reduction in the concentration of non-protein thiols ($p < 0.0001$; $p = 0.0003$, respectively), when compared to the CTL animals. Finally, when we evaluated the total cholinesterase activity in both muscles, the MSG animals showed a decrease in activity when compared to the CTL animals ($p = 0.0001$; $p = 0.0003$, respectively), Table 1.

2.5. Multivariate Analysis

When the interaction between the variables was evaluated, it was observed that the MSG animals already had body impairment characteristics of the model in the PDN15 ($F_{1,10} = 2.7748$, $R^2 = 0.2172$, $p = 0.0021$, Figure 11A). These characteristics are due to the delay in body development ($F_{1,10} = 13.4489$, $R^2 = 0.5735$, $p = 0.0027$, Figure 11B) and the inflammatory profile established in the animals, associated with the state of hyperinsulinemia ($F_{1,10} = 28.0549$, $R^2 = 0.7372$, $p = 0.0025$, Figure 11E). Despite these findings, changes in plasma ($F_{1,10} = 0.2948$, $R^2 = 0.0286$, $p = 0.9722$, Figure 11C) or in the muscle antioxidant system ($F_{1,10} = 0.3958$, $R^2 = 0.0381$, $p = 0.2875$, Figure 11D), which are commonly described as fundamental factors for establishing of the condition in adult animals, were not identified at this age. We also observed that the alterations observed in the young animals intensified in adulthood, producing the body impairment characteristic of MSG induction ($F_{1,14} = 18.3229$, $R^2 = 0.5668$, $p = 0.0002$, Figure 12A). These model characteristics are due to delayed body development, reduced muscle mass, and fat accumulation ($F_{1,14} = 24.7399$, $R^2 = 0.6386$, $p = 0.0002$, Figure 12B). In this sense, it is possible to identify the establishment of the metabolic syndrome in these animals ($F_{1,14} = 21.0869$, $R^2 = 0.6009$, $p = 0.0002$, Figure 12C). These factors are fundamental for the impairment identified in the muscle structure, such as the reduction in fiber size, alteration in the distribution of nuclei and capillaries, and thickening of the connective envelopes ($F_{1,14} = 20.9169$, $R^2 = 0.5991$, $p < 0.0001$, Figure 12D). It was also possible to observe a reduction in the oxidative capacity of muscle fibers ($F_{1,14} = 19.5689$, $R^2 = 0.5629$, $p = 0.0001$, Figure 12E) and a reduction in neuromuscular junctions ($F_{1,14} = 12.8698$, $R^2 = 0.4789$, $p = 0.0002$, Figure 12F), in addition to the accumulation of oxidative damage markers accompanied by impairment of the muscular antioxidant system ($F_{1,14} = 12.8419$, $R^2 = 0.4784$, $p = 0.0002$, Figure 12G).
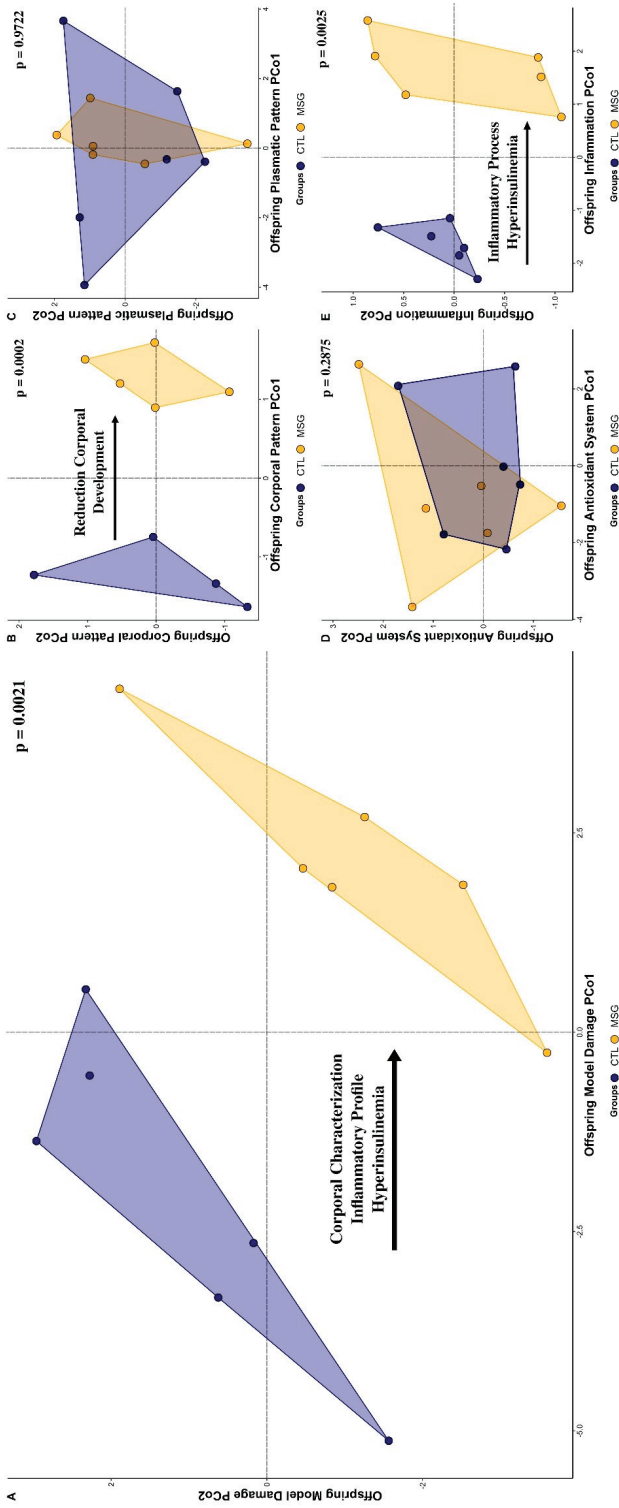
Figure 11. Graphical representation in scatterplot form of the multivariate relationships of the principal coordinates analysis (PCoA) of the animals to the PND15. (**A**): General Model Damage (all data); (**B**): corporal pattern; (**C**): plasmatic pattern; (**D**): antioxidant system; (**E**): inflammation. The CTL group is represented in blue and MSG group is represented in yellow. All data: principal coordinates analysis.
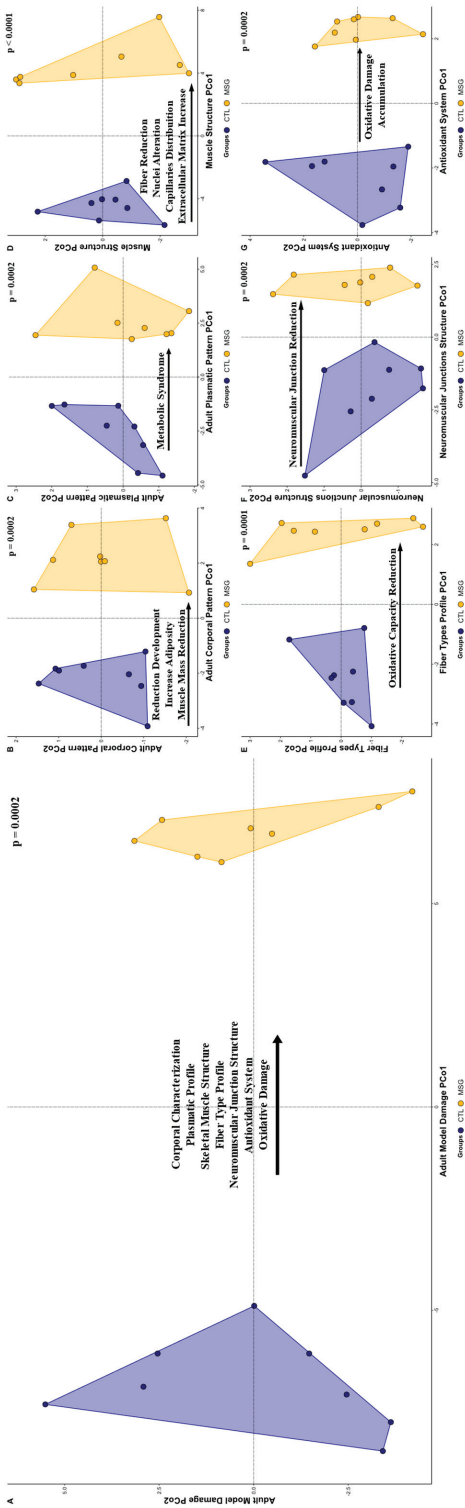
Figure 12. Graphical representation in scatterplot form of the multivariate relationships of the principal coordinates analysis (PCoA) of the animals to the PND142. (**A**): General Model Damage (all data); (**B**): corporal pattern; (**C**): plasmatic pattern; (**D**): skeletal muscle structure; (**E**): fiber types profile; (**F**): neuromuscular junctions structure; (**G**): antioxidant system. The CTL group is represented in blue and MSG group is represented in yellow All data: principal coordinates analysis.

3. Discussion

The literature has reported the effects of MSG as an inducer of obesity, where the main object of study is adult animals with obesity already installed. Here, we present a new study proposal, where the main objective was to investigate whether exposure to MSG in the first days of postnatal life could produce early metabolic changes. In this study, instead of evaluating only the conditions of the animals in the adult phase, we sought to identify the characteristics of the animals 10 days after the end of the monosodium glutamate injections. The main results obtained agree with the results established in the literature for the MSG-obesity model; however, significant alterations in the inflammatory and insulin profile were identified, early in the installation of obesity parameters. These results suggest a slightly different scenario from that classically found for this model, in which damage to the hypothalamic nuclei may be associated with early identified pro-inflammatory disorders and hyperinsulinemia. Thus, it is likely that the muscle changes induced by the model are due not only to the chronicity of the metabolic condition in adulthood but also to this metabolic pattern established early on.

The induction of obesity by MSG causes cytotoxic damage to the hypothalamic nuclei, which induces significant changes in the development of animals, mainly due to cell loss in the GH-secreting hypothalamic nuclei [28], as has been well described in the literature [7] and previously identified in works by our research group [9,21,29,30]. The relationship between reduced body growth and reduced muscle growth has also been extensively explored [1,22,28], with a consensus in the literature that MSG cytotoxicity also results in a model of short stature due to hormonal insufficiency that leads to low growth [22,31]. In this sense, the reduction in body weight gain accompanied by a lower nasoanal length in the MSG animals suggests that from the second day after the end of the injections (PND07) such changes are being established, corroborating that the effects of MSG reach different tissues, since the start of the exhibition.

It is known that GH participates in the close relationship between factors that repress the development and differentiation of muscle fibers, such as myostatin, and that in the MSG-induced obesity model, GH-secreting hypothalamic nuclei are affected, altering GH secretion. Thus, it is possible that in this model this injury results in the attenuation of the feedback mechanisms that repress myostatin activity, producing a reduction in the size of muscle fibers and altering the proportion of fiber types during the final process of development [32,33]. Here, the data obtained demonstrate that in the presence of MSG, muscle fibers are smaller, suggesting the participation of regulation mediated by GH-myostatin, in the reduction of muscle fiber size. Furthermore, such results may be due to an imbalance in the secretion of growth factors, due to muscle damage induced by the obesity model. The model may promote the reduction of growth factors, such as the fibroblast growth factor, required by the muscle for proliferation, as well as for the growth and differentiation of mesenchymal cells during development [8,34,35].

It has also been reported that the metabolic changes associated with the model may originate from lesions that occur in several central structures of the paraventricular region of the hypothalamus, where the arcuate and ventromedial nuclei are the most affected. It is believed that about 80 to 90% of the control of food consumption, energy expenditure, and glucose homeostasis is due to the neuronal activity of these nuclei [12,14,36]. Dysfunction of these structures promotes an imbalance i metabolic pathways, causing the increase in plasma lipid concentrations and their incorporation into adipose tissue, as found in the adult animals of this work [1,12]. Dysfunction of these structures promotes an imbalance of metabolic pathways, causing an increase in plasma lipid concentrations and their incorporation into adipose tissue, as found in the adult animals of this work [37].

By evaluating the levels of insulin and plasmatic cytokines, we could see that through a reduction in glucose sensibility, it is first possible that signaling of peripheral insulin resistance, accompanied by a pro-inflammatory profile, evidenced by increased concentrations of IL-6 and TNFα, is already identifiable in PND15. The increase in IL-6 associated with the MSG model has an important effect on muscle development, as it reduces IGF-1 secretion

and muscle sensitivity to insulin, negatively modulating the differentiation, and growth of muscle fibers [38–40]. In models of dietary obesity, increased IL-6 secretion has also been associated with reduced muscle mass [41,42]; however, in models that use MSG exposure, there is a recurrent reduction in the secretion of this cytokine in animals. The effect of MSG was also evaluated in adulthood, which supports the idea that there may be early metabolic programming in the active phase of obesity [43,44]. Finally, we found an increase in plasma TNFα secretion associated with this scenario, which may be related to the lower availability of MyoD for the paracrine effect, causing a reduction in the differentiation of myoblasts into myocytes, in addition to a reduction in the fusion of myotubes, which is implicated in the muscular alterations identified in the study. In addition, the increase in TNFα is related to reduced insulin sensitivity, increased muscle catabolism, sarcomere ubiquitination, and NADPH oxidation, which together may negatively modulate muscle development and differentiation [38–41].

The characteristics related to the number, position, and structure of the myonuclei of MSG-obese animals in the present study, have been associated with the response mediated by the chronic stress resulting from the established metabolic syndrome [45,46], which may be indicative of damage caused by the incomplete state of differentiation muscle, resulting from the early inflammatory process. Furthermore, this set of changes found in the proposed obesity model is essential to induce the phenotypic transition of muscle fibers [47–49]. The condition of insulin resistance promoted by the inflammatory process, which becomes chronic due to the dyslipidemic profile, is a determining factor for the reduction of muscle oxidative capacity, especially when associated with the characteristics of reduced size and the number of types I and IIA fibers and the increase in type I fibers and IIB fibers [49–51].

The establishment of the early hyperinsulinemic condition, found in the PND15 of MSG-obese animals, may indicate the anticipation of the dynamic phase of obesity, where the induction of increased glucose uptake by insulin-responsive tissues seems to occur. However, maintenance of this condition in PND142, where obesity was chronic due to persistent damage, reinforces the establishment of peripheral reduction in glucose sensibility, as observed in MSG animals [52–54]. During the worsening of obesity, damage resulting from MSG-induced hepatotoxicity is common, which causes an increase in the generation of reactive oxygen species and feeds back the inflammatory process [15,55,56]. In addition, the inflammatory process, mainly mediated by the increase in TNFα, negatively and significantly modulates the rate of lipolysis, favouring adipose tissue hypertrophy and an increase in fat panicles [12,31,57].

Something intriguing in the MSG cytotoxicity model of obesity induction is the difficulty in applying treatment protocols that restore the physiological state of these animals, after the establishment of obesity. In a resistance exercise model, obese MSG animals submitted to the training protocol showed partial reversal of the obesogenic parameters, but even though they were significant, the reduction in lipemia and adipose panicles did not return to the values found in the control animals [15]. Likewise, after applying a swimming model, the reduction in adiposity and insulin secretion did not return to physiological patterns, and changes in intestinal structure were still persistent [58]. Previous data from our research group show that whole-body vibration training was not able to completely repair the soleus [29,59], extensor digitorum longus [30], tibialis anterior [21], and diaphragm [60] muscles despite promoting anti-obesogenic effects. Furthermore, it did not restore the physiological levels, biochemical, and structural parameters of the liver, adipose tissue, and plasma [9]. Finally, models with leucine [61] and taurine [62] supplementation, as well as herbal treatment [63], showed a partial reduction in body adiposity and food intake, accompanied by improvement in glucose metabolism and insulin sensitivity and cardiovascular effects.

Considering all the initial characteristics of the neurotoxic effect of MSG, associated with the hyperinsulinemic and pro-inflammatory condition in the dynamic phase of obesity induction, we can correlate these developmental alterations with the muscular charac-

teristics found. Thus, as obesity becomes chronic and metabolic syndrome sets in, it is reasonable that most studies find similar results in obese adult animals under the influence of MSG. Although there were several forms of administration, the doses and periods proposed and evaluated, the analyses have the observation of animals at a certain moment in common, when obesity is already well established. Despite this limitation, it is common to find studies that manage to partially repair the damage caused, a fact that reinforces our hypothesis that early damage is established and prevents the correct development of animals, suggesting that exposure to MSG, in the perinatal phase, is capable of inducing some metabolic programming that becomes worse over time. Thus, although the MSG model is remarkably effective in inducing obesity, limitations arising from the proposed study setting may underestimate the systemic effects of MSG and the possible effects of treatment protocols. Finally, considering the role of muscle tissue in metabolic regulation, obtaining results that support muscle restructuring may represent an important strategy for improving metabolic conditions, even in the absence of the reversal of body parameters of obesity.

4. Materials and Methods

4.1. Ethical Approval

All trials in this study were conducted following national and international recommendations and legislation [64] and with the approval of the University Animal Care Committee (protocol # 08/18).

4.2. Animals and Experimental Design

From postnatal day (PND) 01 to PND05, male Wistar rats (n = 24) received daily subcutaneous injections of MSG solution in the dorsocervical region (4 mg·g^{-1} body weight, MSG group) or equimolar saline solution (1.25 mg g^{-1} body weight, control group—CTL) [3,9]. Every two days, the animals were weighed and their nasoanal length was measured, until the 14th day of life. In PND15, 12 animals were euthanized (n = 6 per group) to assess the establishment of molecular damage. After weaning (PND21), food consumption and the evolution of body weight were monitored weekly. All of the animals were housed in standard cages at a constant temperature (22 ± 1 °C), on a 12 h light-dark cycle, and had ad libitum access to water and standard laboratory chow (BioBase$^®$, Santa Catarina, Brazil).

4.3. Intraperitoneal Glucose Tolerance Test (ipGTT) and Insulin Dosage

The ipGTT was performed after eight hours of fasting and consisted of a small cut in the tail of the animals followed by the collection of blood samples to measure glucose with the aid of an Accu Chek glucometer (Roche Diabetes Care Brasil LTDA, São Paulo, Brazil). Blood was collected in the fasted state (time 0) and 15, 30, 60, and 90 min after IP injection of a glucose overload (2 g·kg^{-1} of body weight). Additional blood samples were collected with heparinized glass capillaries and then centrifuged at 4 °C and 12,000× g for 10 min. The supernatant was stored in a freezer at −80 °C for later measurement of insulin by radioimmunoassay.

4.4. Euthanasia and Material Collection

In PND15, the Lee index ($\sqrt[3]{}$bodyweight / nasalanal length × 1000) was calculated. The animals were then desensitized in a carbon dioxide chamber and then euthanized by decapitation [7]. Blood was collected in heparinized tubes and centrifuged at 4 °C, at 12,000× g for 10 min to measure the plasma biochemical and inflammatory profile. The abdominal wall and pelvic limb muscles were collected (approximately 0.2 g) and intended for the analysis of oxidative damage markers.

In PND142, the Lee index ($\sqrt[3]{}$bodyweight/nasalanal length × 1000) was calculated. The animals were then desensitized in a carbon dioxide chamber and then euthanized by decapitation [7]. Retroperitoneal, perigonadal, and brown fats were removed, weighed,

normalized to g·100 g^{-1} of body weight, and used to calculate body adiposity [2]. Blood was collected in heparinized tubes and centrifuged at 4 °C, at 12,000× g for 10 min to measure the plasma biochemical profile. The extensor digitorum longus (EDL) and soleus muscle (SOL) were dissected, collected, weighed, measured, and destined for biochemical and morphological analysis.

4.5. Skeletal Muscle Structure Analysis

The muscle was sectioned in the middle region of the muscle belly, and the proximal fragments of the right antimere were fixed in metacarn and stored in 70% alcohol. Subsequently, they were submitted to the histological procedure with dehydration in an increasing series of alcohol, diaphanization in N-butyl alcohol, and inclusion and embedding in histological paraffin, after which they were cut transversely at 5 μm with the aid of a microtome. For the study of muscle fibers, the sections were stained with hematoxylin–eosin (HE), morphologically analyzed under a light microscope, and 10 visual fields of interest were photographed at 400× magnification. In the images obtained, the cross-sectional area of the fiber and cores, fiber density, number, and position of nuclei were analyzed.

The distal fragments of the right antimere were used for histoenzymological analysis, which analyzes the oxidative and glycolytic metabolism of muscle fibers. For this, immediately after collection, they were covered with neutral talc for tissue preservation and subsequently frozen in liquid nitrogen, conditioned in cryotubes, and stored in a Biofreezer at −80 °C, up to a 7 μm section in a cryostat chamber (LUPETEC CM 2850 Cryostat Microtome) at −20 °C. The sections were submitted to the enzymatic reaction of NADH–TR (nicotinamide adenine dinucleotide—tetrazolium reductase). This analysis quantifies the different types of muscle fibers (I, IIa, and IIb) according to the tone presented in the fibers after the reaction. For each animal, five microscopic fields were randomly chosen at 200× magnification to count and analyze the area size of the different types of fibers.

The proximal fragments of the left antimere were used for the study of JNM, and they were immersed in Karnovisky's fixative. The muscles were cut longitudinally into small portions with stainless steel blades, and the selected cuts were found in the nonspecific esterase reaction. Subsequently, a morphological analysis of the slides was performed with a light microscope, photomicrographing the visual fields of interest at 200× magnification. The size of the area, the largest diameter, and the smallest diameter of 150 JNM per animal were measured.

The morphological analyzes were performed in the Image ProPlus 6.0 (Media Cybernetics, Inc., Rockeville, MD, USA) program, and in each image the muscle fasciculus was scanned to randomly select ten fibers, thus totaling 120 fibers per animal.

4.6. Antioxidant System and Oxidative Damages Analysis

For the evaluation of the antioxidant system, the distal portion of the left antimer of EDL muscle was homogenized with Tris-HCl buffer (0.4 M, pH 7.4) and centrifugated for 20 min at 4 °C and 12,000× g. Tissue protein quantification was determined by the Bradford method, using bovine serum albumin as a standard. All of the samples were normalized to 1 mg protein × mL^{-1}.

The enzymatic activity of the superoxide dismutase (SOD—EC 1.15.1.1) of the muscles was determined by inhibiting the formation of formazan blue by reducing nitrotetrazolium blue (NBT); increasing absorbance by reducing NBT by the superoxide anion was monitored at 560 nm (RS: 182 mM sodium carbonate buffer pH 10.2; 50 μM EDTA; 100 μM NBT; 36.86 mM hydroxylamine sulfate). The values were expressed in U × mg protein^{-1} [65].

The enzyme activity of the catalase (CAT—EC 1.11.1.6) of the muscles was determined through the formation of H_2O and O_2 from the consumption of H_2O_2, the reduction in absorbance by the consumption of H_2O_2 was monitored at 240 nm (RS: 50 mM of potassium phosphate buffer pH 7.0; 10 mM H_2O_2). The values were expressed in mM of H_2O_2 consumed × min^{-1} × mg protein^{-1} [66].

The lipid peroxidation index (LPO) of the muscles was determined by the generation of complexes between Fe^{+2} and xylenol orange and the formation of a chromophore stabilized by butylated hydroxytoluene. The absorbance by the generation of the chromophore was measured at 560 nm. The values were expressed in nM hydroperoxides $\times$ mg protein^{-1} [67].

The enzymatic activity of total cholinesterase (ChE—EC 3.1.1.8) was determined by the generation of 2-nitrobenzoate-5-mercaptothiocholine from the interaction of thiocholine and DTNB; the increase in absorbance by the formation of the chromophore was monitored at 405 nm (RS: 487 μM DTNB; 2.25 mM acetylthiocholine iodide). The values were expressed in nM acetylthiocholine hydrolyzed $\times$ min^{-1} $\times$ mg protein^{-1} [68].

4.7. Statistical Analysis

Data were expressed as mean $\pm$ standard deviation and analyzed using descriptive and inferential statistics in the R program version 4.0.3 (45). Data were evaluated for normality (Shapiro–Wilk test). Parametric data were evaluated by the Student's *t*-test. In the case of non-parametric data, the test used was the Mann–Whitney U test. In the case of data analyzed over time, the ANOVA test of repeated measures with the post-Tukey's HSD test was used. In all cases, the significance level adopted was 5%.

The data were ordered in response matrices, and in the PND15 the groupings were: general model damage (all data); body pattern; plasma standard; antioxidant system; inflammation. As for PND142, the groups were: general model damage (all data); body pattern; plasma standard; skeletal muscular structure; fiber type profile; structure of neuromuscular junctions; antioxidant system.

this present work, who, despite the anti-scientific, denialist and demoralizing policy of the federal government (2018–2022), in the figure of President Bolsonaro and his Ministers of Health, Education and Science and Technology, which frequently attacked researchers, scrapped and suffocated universities. All Brazilian researchers remained firm and active in the development of their work in the hope of the end of this gloomy government and a prosperous future for national science.

Conflicts of Interest: The authors declare no conflict of interest. The funders had no role in the design of the study; in the collection, analysis, or interpretation of data; in the writing of the manuscript; or in the decision to publish the results.

References

1. Hernández Bautista, R.J.; Mahmoud, A.M.; Königsberg, M.; López Díaz Guerrero, N.E. Obesity: Pathophysiology, Monosodium Glutamate-Induced Model and Anti-Obesity Medicinal Plants. *Biomed. Pharmacother.* **2019**, *111*, 503–516. [CrossRef] [PubMed]
2. Borck, P.C.; de C Leite, N.; Valcanaia, A.C.; Rickli, S.; de L Alípio, J.C.; Machado, M.; Vellosa, J.C.; de F Mathias, P.C.; Boschero, A.C.; Grassiolli, S. Swimming Training Reduces Glucose-amplifying Pathway and Cholinergic Responses in Islets from Lean- and MSG-obese Rats. *Clin. Exp. Pharmacol. Physiol.* **2020**, *47*, 286–293. [CrossRef] [PubMed]
3. Olney, J.W. Brain Lesions, Obesity, and Other Disturbances in Mice Treated with Monosodium Glutamate. *Science* **1969**, *164*, 719–721. [CrossRef]
4. Torii, K.; Takasaki, Y.; Iwata, S.; Wurtman, R.J. Changes in Blood Osmolarity, Electrolytes, and Metabolites among Adult Rats Treated with a Neurotoxic Dose of MSG1. *Life Sci.* **1981**, *28*, 2855–2864. [CrossRef] [PubMed]
5. Lemkey-Johnston, N.; Butler, V.; Reynolds, W.A. Brain Damage in Neonatal Mice Following Monosodium Glutamate Administration: Possible Involvement of Hypernatremia and Hyperosmolality. *Exp. Neurol.* **1975**, *48*, 292–309. [CrossRef] [PubMed]
6. Ibrahim, M.N.; Mostafa, E.M.; Toama, F.N. Histological Effects of Monosodium Glutamate on Brain of Infant Albino Swiss Mice Mus Musculus. *J. Med. Chem. Sci.* **2021**, *4*, 564–570. [CrossRef]
7. de Souza, T.A.; de Souza, D.W.; Siqueira, B.S.; Rentz, T.; de Oliveria Emílio, H.R.; Grassiolli, S. Splenic Participation in Glycemic Homeostasis in Obese and Non-Obese Male Rats. *Obes. Res. Clin. Pract.* **2020**, *14*, 479–486. [CrossRef]
8. Quines, C.B.; Rosa, S.G.; Velasquez, D.; Prado, V.C.; Neto, J.S.S.; Nogueira, C.W. (P-ClPhSe)2 Stabilizes Metabolic Function in a Rat Model of Neuroendocrine Obesity Induced by Monosodium Glutamate. *Food Chem. Toxicol.* **2018**, *118*, 168–180. [CrossRef]
9. de Andrade, B.Z.; Zazula, M.F.; Bittencourt Guimarães, A.T.; Sagae, S.C.; Boaretto, M.L.; Felicio Poncio, A.C.; Hoff Nunes Maciel, J.I.; de Oliveira, C.M.T.; Costa, R.M.; Flor Bertolini, G.R.; et al. Whole-Body Vibration Promotes Lipid Mobilization in Hypothalamic Obesity Rat. *Tissue Cell* **2021**, *68*, 101456. [CrossRef]
10. Hazzaa, S.M.; Abdelaziz, S.A.M.; Eldaim, M.A.A.; Abdel-Daim, M.M.; Elgarawany, G.E. Neuroprotective Potential of Allium Sativum against Monosodium Glutamate-Induced Excitotoxicity: Impact on Short-Term Memory, Gliosis, and Oxidative Stress. *Nutrients* **2020**, *12*, 1028. [CrossRef]
11. Guareschi, Z.M.; Valcanaia, A.C.; Ceglarek, V.M.; Hotz, P.; Amaral, B.K.; De Souza, D.W.; De Souza, T.A.; Nardelli, T.; Ferreira, T.R.; Leite, N.C.; et al. The Effect of Chronic Oral Vitamin D Supplementation on Adiposity and Insulin Secretion in Hypothalamic Obese Rats. *Br. J. Nutr.* **2019**, *121*, 1334–1344. [CrossRef] [PubMed]
12. Hernández-Bautista, R.; Alarcón-Aguilar, F.; Escobar-Villanueva, M.D.C.; Almanza-Pérez, J.; Merino-Aguilar, H.; Fainstein, M.; López-Diazguerrero, N. Biochemical Alterations during the Obese-Aging Process in Female and Male Monosodium Glutamate (MSG)-Treated Mice. *Int. J. Mol. Sci.* **2014**, *15*, 11473–11494. [CrossRef] [PubMed]
13. Dludla, P.V.; Nkambule, B.B.; Jack, B.; Mkandla, Z.; Mutize, T.; Silvestri, S.; Orlando, P.; Tiano, L.; Louw, J.; Mazibuko-Mbeje, S.E. Inflammation and Oxidative Stress in an Obese State and the Protective Effects of Gallic Acid. *Nutrients* **2019**, *11*, 23. [CrossRef] [PubMed]
14. Araujo, T.R.; Freitas, I.N.; Vettorazzi, J.F.; Batista, T.M.; Santos-Silva, J.C.; Bonfleur, M.L.; Balbo, S.L.; Boschero, A.C.; Carneiro, E.M.; Ribeiro, R.A. Benefits of L-Alanine or l-Arginine Supplementation against Adiposity and Glucose Intolerance in Monosodium Glutamate-Induced Obesity. *Eur. J. Nutr.* **2017**, *56*, 2069–2080. [CrossRef] [PubMed]
15. Quines, C.B.; Jardim, N.S.; Araujo, P.C.O.; Cechella, J.L.; Prado, V.C.; Nogueira, C.W. Resistance Training Restores Metabolic Alterations Induced by Monosodium Glutamate in a Sex-Dependent Manner in Male and Female Rats. *J. Cell. Biochem.* **2019**, *120*, 13426–13440. [CrossRef] [PubMed]
16. Hoppeler, H. Molecular Networks in Skeletal Muscle Plasticity. *J. Exp. Biol.* **2016**, *219*, 205–213. [CrossRef] [PubMed]
17. Kido, K.; Sase, K.; Yokokawa, T.; Fujita, S. Enhanced Skeletal Muscle Insulin Sensitivity after Acute Resistance-Type Exercise Is Upregulated by Rapamycin-Sensitive MTOR Complex 1 Inhibition. *Sci. Rep.* **2020**, *10*, 8509. [CrossRef] [PubMed]
18. Pomytkin, I.; Krasil'nikova, I.; Bakaeva, Z.; Surin, A.; Pinelis, V. Excitotoxic Glutamate Causes Neuronal Insulin Resistance by Inhibiting Insulin Receptor/Akt/MTOR Pathway. *Mol. Brain* **2019**, *12*, 112. [CrossRef]
19. Hung IKKβ Suppression of TSC1 Function Links the MTOR Pathway with Insulin Resistance. *Int. J. Mol. Med.* **1998**, *22*, 633–638. [CrossRef]
20. Shan, T.; Zhang, P.; Jiang, Q.; Xiong, Y.; Wang, Y.; Kuang, S. Adipocyte-Specific Deletion of MTOR Inhibits Adipose Tissue Development and Causes Insulin Resistance in Mice. *Diabetologia* **2016**, *59*, 1995–2004. [CrossRef]

21. Zazula, M.F.; Bergmann Kirsch, C.; Theodoro, J.L.; de Toni Boaro, C.; Saraiva, D.F.; de Oliveira Gonçalves, S.; Zanardini de Andrade, B.; Peretti, A.L.; Naliwaiko, K.; Flor Bertolini, G.R.; et al. Whole-Body Vibration Promotes Beneficial Changes on the Anterior Tibial Muscle Histomorphometry of Hypothalamic Obese Rats. *Muscles. Ligaments Tendons J.* **2021**, *11*, 657. [CrossRef]

22. de Paula, D.G.; Bohlen, T.M.; Zampieri, T.T.; Mansano, N.S.; Vieira, H.R.; Gusmao, D.O.; Wasinski, F.; Donato, J.; Frazao, R. Distinct Effects of Growth Hormone Deficiency and Disruption of Hypothalamic Kisspeptin System on Reproduction of Male Mice. *Life Sci.* **2021**, *285*, 119970. [CrossRef] [PubMed]

23. Wakabayashi, I.; Hatano, H.; Minami, S.; Tonegawa, Y.; Akira, S.; Sugihara, H.; Ling, N.C. Effects of Neonatal Administration of Monosodium Glutamate on Plasma Growth Hormone (GH) Response to GH-Releasing Factor in Adult Male and Female Rats. *Brain Res.* **1986**, *372*, 361–365. [CrossRef] [PubMed]

24. Maiter, D.; Underwood, L.E.; Martin, J.B.; Koenig, J.I. Neonatal Treatment with Monosodium Glutamate: Effects of Prolonged Growth Hormone (GH)-Releasing Hormone Deficiency on Pulsatile GH Secretion and Growth in Female Rats. *Endocrinology* **1991**, *128*, 1100–1106. [CrossRef]

25. Yan, X.; Zhu, M.; Dodson, M.V.; Du, M. Developmental Programming of Fetal Skeletal Muscle and Adipose Tissue Development. *J. Genomics* **2013**, *1*, 29–38. [CrossRef]

26. Tarry-adkins, J.L.; Fernandez-twinn, D.S.; Chen, J.H.; Hargreaves, I.P.; Neergheen, V.; Aiken, C.E.; Ozanne, S.E. Poor Maternal Nutrition and Accelerated Postnatal Growth Induces an Accelerated Aging Phenotype and Oxidative Stress in Skeletal Muscle of Male Rats. *Dis. Model. Mech.* **2016**, *9*, 1221–1229. [CrossRef]

27. Shrestha, N.; Sleep, S.L.; Cuffe, J.S.M.; Holland, O.J.; Perkins, A.V.; Yau, S.Y.; McAinch, A.J.; Hryciw, D.H. Role of Omega-6 and Omega-3 Fatty Acids in Fetal Programming. *Clin. Exp. Pharmacol. Physiol.* **2020**, *47*, 907–915. [CrossRef]

28. Davies, J.S.; Gevers, E.F.; Stevenson, A.E.; Coschigano, K.T.; El-Kasti, M.M.; Bull, M.J.; Elford, C.; Evans, B.A.J.; Kopchick, J.J.; Wells, T. Adiposity Profile in the Dwarf Rat: An Unusually Lean Model of Profound Growth Hormone Deficiency. *Am. J. Physiol. Endocrinol. Metab.* **2007**, *292*, E1483–E1494. [CrossRef]

29. Boaretto, M.L.; de Andrade, B.Z.; Maciel, J.I.H.N.; Moha, I.; Schneider, S.C.S.; Torrejais, M.M.; de Fátima Chasko Ribeiro, L.; Bertolini, G.R.F. Effects of Vibratory Platform Training on the Histomorphometric Parameters of the Soleus Muscle in Obese Wistar Rats. *Sport Sci. Health* **2020**, *16*, 501–510. [CrossRef]

30. Maciel, J.I.H.N.; Zazula, M.F.; Rodrigues, D.F.S.; De Toni Boaro, C.; Boaretto, M.L.; de Andrade, B.Z.; Schneider, S.C.S.; Naliwaiko, K.; Torrejais, M.M.; Costa, R.M.; et al. Whole-Body Vibration Promotes Skeletal Muscle Restructuring and Reduced Obesogenic Effect of MSG in Wistar Rats. *Appl. Biochem. Biotechnol.* **2022**, *194*, 3594–3608. [CrossRef]

31. Hirata, A.E.; Andrade, I.S.; Vaskevicius, P.; Dolnikoff, M.S. Monosodium Glutamate (MSG)-Obese Rats Develop Glucose Intolerance and Insulin Resistance to Peripheral Glucose Uptake. *Brazilian J. Med. Biol. Res.* **1997**, *30*, 671–674. [CrossRef] [PubMed]

32. Marcell, T.J.; Harman, S.M.; Urban, R.J.; Metz, D.D.; Rodgers, B.D.; Blackman, M.R. Comparison of GH, IGF-I, and Testosterone with MRNA of Receptors and Myostatin in Skeletal Muscle in Older Men. *Am. J. Physiol. Metab.* **2001**, *281*, 1159–1164. [CrossRef] [PubMed]

33. Grade, C.V.C.; Mantovani, C.S.; Alvares, L.E. Myostatin Gene Promoter: Structure, Conservation and Importance as a Target for Muscle Modulation. *J. Anim. Sci. Biotechnol.* **2019**, *10*, 32. [CrossRef] [PubMed]

34. Du, M.; Yan, X.; Tong, J.F.; Zhao, J.; Zhu, M.J. Maternal Obesity, Inflammation, and Fetal Skeletal Muscle Development. *Biol. Reprod.* **2010**, *82*, 4–12. [CrossRef] [PubMed]

35. Mann, C.J.; Perdiguero, E.; Kharraz, Y.; Aguilar, S.; Pessina, P.; Serrano, A.L.; Muñoz-Cánoves, P. Aberrant Repair, and Fibrosis Development in Skeletal Muscle. *Skelet. Muscle* **2011**, *1*, 21. [CrossRef]

36. Lima, C.B.; de Sousa Ferreira Soares, G.; Vitor, S.M.; Andrade-da-Costa, B.L.d.S.; Castellano, B.; Guedes, R.C.A. Spreading Depression Features and Iba1 Immunoreactivity in the Cerebral Cortex of Developing Rats Submitted to Treadmill Exercise after Treatment with Monosodium Glutamate. *Int. J. Dev. Neurosci.* **2014**, *33*, 98–105. [CrossRef]

37. Jung, U.; Choi, M.-S. Obesity and Its Metabolic Complications: The Role of Adipokines and the Relationship between Obesity, Inflammation, Insulin Resistance, Dyslipidemia and Nonalcoholic Fatty Liver Disease. *Int. J. Mol. Sci.* **2014**, *15*, 6184–6223. [CrossRef]

38. Stenvinkel, P.; Ketteler, M.; Johnson, R.J.; Lindholm, B.; Pecoits-Filho, R.; Riella, M.; Heimbürger, O.; Cederholm, T.; Girndt, M. IL-10, IL-6, and TNF-α: Central Factors in the Altered Cytokine Network of Uremia—The Good, the Bad, and the Ugly. *Kidney Int.* **2005**, *67*, 1216–1233. [CrossRef]

39. Sharma, B.; Dabur, R. Role of Pro-Inflammatory Cytokines in Regulation of Skeletal Muscle Metabolism: A Systematic Review. *Curr. Med. Chem.* **2018**, *27*, 2161–2188. [CrossRef]

40. Bian, A.L.; Hu, H.Y.; Rong, Y.D.; Wang, J.; Wang, J.X.; Zhou, X.Z. A Study on Relationship between Elderly Sarcopenia and Inflammatory Factors IL-6 and TNF-α. *Eur. J. Med. Res.* **2017**, *22*, 25. [CrossRef]

41. Kim, H.J.; Higashimori, T.; Park, S.Y.; Choi, H.; Dong, J.; Kim, Y.J.; Noh, H.L.; Cho, Y.R.; Cline, G.; Kim, Y.B.; et al. Differential Effects of Interleukin-6 and -10 on Skeletal Muscle and Liver Insulin Action In Vivo. *Diabetes* **2004**, *53*, 1060–1067. [CrossRef]

42. Von Dentz, K.E.; Silva, B.S.; Queiroz, E.A.I.F.; Bomfim, G.F.; Nascimento, A.F.; Sugizaki, M.M.; Luvizotto, R.A.M. Hibiscus Sabdariffa Ethanolic Extract Modulates Adipokine Levels, Decreases Visceral Fat and Improves Glycemic Profile in High-Fat/Sugar Diet-Induced Obese Rats. *Nutr. Food Sci.* **2020**, *51*, 222–233. [CrossRef]

43. Yonamine, C.Y.; Pinheiro-Machado, E.I.; Michalani, M.L.; Alves-Wagner, A.B.; Esteves ID, J.V.; Freitas, H.S.; Machado, U.F. Molecules Resveratrol Improves Glycemic Control in Type 2 Diabetic Obese Mice by Regulating Glucose Transporter Expression in Skeletal Muscle and Liver. *Molecules* **2017**, *22*, 1180. [CrossRef] [PubMed]

44. Alarcon-Aguilar, F.J.; Almanza-Perez, J.; Blancas, G.; Angeles, S.; Garcia-Macedo, R.; Roman, R.; Cruz, M. Glycine Regulates the Production of Pro-Inflammatory Cytokines in Lean and Monosodium Glutamate-Obese Mice. *Eur. J. Pharmacol.* **2008**, *599*, 152–158. [CrossRef] [PubMed]

45. Cutler, A.A.; Jackson, J.B.; Corbett, A.H.; Pavlath, G.K. Non-Equivalence of Nuclear Import among Nuclei in Multinucleated Skeletal Muscle Cells. *J. Cell Sci.* **2018**, *131*, jcs207670. [CrossRef]

46. Dungan, C.M.; Peck, B.D.; Walton, R.G.; Huang, Z.; Bamman, M.M.; Kern, P.A.; Peterson, C.A. In Vivo Analysis of ΓH2AX+ Cells in Skeletal Muscle from Aged and Obese Humans. *FASEB J.* **2020**, *34*, 7018–7035. [CrossRef] [PubMed]

47. Blaauw, B.; Schiaffino, S.; Reggiani, C. Mechanisms Modulating Skeletal Muscle Phenotype. *Compr. Physiol.* **2013**, *3*, 1645–1687. [CrossRef]

48. Hoppeler, H.; Flück, M. Normal Mammalian Skeletal Muscle and Its Phenotypic Plasticity. *J. Exp. Biol.* **2002**, *205*, 2143–2152. [CrossRef]

49. Hu, C.; Yang, Y.; Chen, M.; Hao, X.; Wang, S.; Yang, L.; Yin, Y.; Tan, C. A Maternal High-Fat/Low-Fiber Diet Impairs Glucose Tolerance and Induces the Formation of Glycolytic Muscle Fibers in Neonatal Offspring. *Eur. J. Nutr.* **2021**, *60*, 2709–2718. [CrossRef]

50. Kong, X.F.; Zhou, X.L.; Feng, Z.M.; Li, F.N.; Ji, Y.J.; Tan, B.E.; Liu, Y.Y.; Geng, M.M.; Wu, G.Y.; Blachier, F.; et al. Dietary Supplementation with Monosodium L-Glutamate Modifies Lipid Composition and Gene Expression Related to Lipid Metabolism in Growing Pigs Fed a Normal- or High-Fat Diet. *Livest. Sci.* **2015**, *180*, 247–252. [CrossRef]

51. Jana, B.A.; Chintamaneni, P.K.; Krishnamurthy, P.T.; Wadhwani, A.; Mohankumar, S.K. Cytosolic Lipid Excess-Induced Mitochondrial Dysfunction Is the Cause or Effect of High Fat Diet-Induced Skeletal Muscle Insulin Resistance: A Molecular Insight. *Mol. Biol. Rep.* **2019**, *46*, 957–963. [CrossRef] [PubMed]

52. De Carvalho Papa, P.; Vargas, A.M.; Tavares Da Silva, J.L.; Nunes, M.T.; Machado, U.F. GLUT4 Protein Is Differently Modulated during Development of Obesity in Monosodium Glutamate-Treated Mice. *Life Sci.* **2002**, *71*, 1917–1928. [CrossRef] [PubMed]

53. Bahadoran, Z.; Mirmiran, P.; Ghasemi, A. Monosodium Glutamate (MSG)-Induced Animal Model of Type 2 Diabetes. *Methods Mol. Biol.* **2019**, *1916*, 49–65. [PubMed]

54. Reijrink, M.; De Boer, S.A.; Antunes, I.F.; Spoor, D.S.; Heerspink, H.J.L.; Lodewijk, M.E.; Mastik, M.F.; Boellaard, R.; Greuter, M.J.W.; Benjamens, S.; et al. [18 F]FDG Uptake in Adipose Tissue Is Not Related to Inflammation in Type 2 Diabetes Mellitus. *Mol. Imaging Biol.* **2021**, *23*, 117–126. [CrossRef]

55. Kazmi, Z.; Fatima, I.; Perveen, S.; Malik, S.S. Monosodium Glutamate: Review on Clinical Reports. *Int. J. Food Prop.* **2017**, *20*, 1807–1815. [CrossRef]

56. Zanfirescu, A.; Ungurianu, A.; Tsatsakis, A.M.; Nițulescu, G.M.; Kouretas, D.; Veskoukis, A.; Tsoukalas, D.; Engin, A.B.; Aschner, M.; Margină, D. A Review of the Alleged Health Hazards of Monosodium Glutamate. *Compr. Rev. Food Sci. Food Saf.* **2019**, *18*, 1111–1134. [CrossRef]

57. Dolnikoff, M.; Martín-Hidalgo, A.; Machado, U.F.; Lima, F.B.; Herrera, E. Decreased Lipolysis and Enhanced Glycerol and Glucose Utilization by Adipose Tissue Prior to Development of Obesity in Monosodium Glutamate (MSG) Treated-Rats. *Int. J. Obes.* **2001**, *25*, 426–433. [CrossRef]

58. Svidnicki, P.V.; de Carvalho Leite, N.; Venturelli, A.C.; Camargo, R.L.; Vicari, M.R.; de Almeida, M.C.; Artoni, R.F.; Nogaroto, V.; Grassiolli, S. Swim Training Restores Glucagon-like Peptide-1 Insulinotropic Action in Pancreatic Islets from Monosodium Glutamate-Obese Rats. *Acta Physiol.* **2013**, *209*, 34–44. [CrossRef]

59. Boaretto, M.; de Andrade, B.Z.; Maciel, J.I.H.N.; de Campos Oliveira, M.; de Oliveira, C.M.T.; Guimarães, A.T.B.; Torrejais, M.M.; Schneider, S.C.S.; Ribeiro, L.d.F.C.; Bertolini, G.R.F. Alterations in Neuromuscular Junctions and Oxidative Stress of the Soleus Muscle of Obese Wistar Rats Caused by Vibratory Platform Training. *J. Musculoskelet. Neuronal Interact.* **2020**, *20*, 570–578.

60. de Campos Oliveira, M.; Laís Boaretto, M.; Barbosa, A.; Bittencourt Guimarães, A.T.; Flor Bertolini, G.R.; Torrejais, M.M.; Costa, R.M. Whole-Body Vibration, Morphological and Antioxidant Effects on the Diaphragm Muscle of Obese Rats. *Muscles. Ligaments Tendons J.* **2021**, *11*, 648. [CrossRef]

61. Ceglarek, V.M.; Coelho, M.L.; Coelho, R.L.; Almeida, D.L.; de Souza Rodrigues, W.; Camargo, R.L.; Barella, L.F.; de Freitas Mathias, P.C.; Grassiolli, S. Chronic Leucine Supplementation Does Not Prevent the Obesity and Metabolic Abnormalities Induced by Monosodium Glutamate. *Clin. Nutr. Exp.* **2020**, *29*, 62–75. [CrossRef]

62. Wen, C.; Li, F.; Zhang, L.; Duan, Y.; Guo, Q.; Wang, W.; He, S.; Li, J.; Yin, Y. Taurine Is Involved in Energy Metabolism in Muscles, Adipose Tissue, and the Liver. *Mol. Nutr. Food Res.* **2019**, *63*, e1800536. [CrossRef] [PubMed]

63. Fouda, Y.B.; Ngo Lemba Tom, E.; Atsamo, A.D.; Bonabe, C.; Dimo, T. Effects of Stem Bark Aqueous Extract of Fagara Tessmannii Engl (Rutaceae) on Cardiovascular Risks Related to Monosodium Glutamate-Induced Obesity in Rat: In Vivo and in Vitro Assessments. *J. Ethnopharmacol.* **2020**, *260*, 112972. [CrossRef] [PubMed]

64. du Sert, N.P.; Hurst, V.; Ahluwalia, A.; Alam, S.; Avey, M.T.; Baker, M.; Browne, W.J.; Clark, A.; Cuthill, I.C.; Dirnagl, U.; et al. The Arrive Guidelines 2.0: Updated Guidelines for Reporting Animal Research. *PLoS Biol.* **2020**, *18*, e3000410. [CrossRef]

65. Crouch, R.K.; Gandy, S.E.; Kimsey, G.; Galbraith, R.A.; Galbraith, G.M.; Buse, M.G. The Inhibition of Islet Superoxide Dismutase by Diabetogenic Drugs. *Diabetes* **1981**, *30*, 235–241. [CrossRef]

66. Aebi, H. Catalase in Vitro. *Methods Enzimol.* **1985**, *105*, 121–126.
67. Jiang, Z.-Y.; Woollard, A.C.S.; Wolff, S.P. Lipid Hydroperoxides Measurement by Oxidation of Fe^{2+} in the Presence of Xylenol Orange. Comparison with the TBA Assay and an Iodometric Method. *Lipids* **1991**, *26*, 853–856. [CrossRef]
68. Ellman, G.L.; Courtney, K.D.; Andres, V.; Featherstone, R.M. A New and Rapid Colorimetric Determination of Acetylcholinesterase Activity. *Biochem. Pharmacol.* **1961**, *7*, 88–95. [CrossRef]

Article

Absorption and Metabolism of the Natural Sweeteners Erythritol and Xylitol in Humans: A Dose-Ranging Study

Valentine Bordier [1,2], Fabienne Teysseire [1,2], Frank Senner [3], Götz Schlotterbeck [3], Jürgen Drewe [4], Christoph Beglinger [1,2], Bettina K. Wölnerhanssen [1,2,*,†] and Anne Christin Meyer-Gerspach [1,2,*,†]

[1] St. Clara Research Ltd., St. Claraspital, 4002 Basel, Switzerland
[2] Faculty of Medicine, University of Basel, 4001 Basel, Switzerland
[3] Institute for Chemistry and Bioanalytics, School of Life Science, FHNW University of Applied Sciences and Arts Northwestern Switzerland, 4132 Muttenz, Switzerland
[4] Department of Clinical Pharmacology and Toxicology, University Hospital Basel, 4001 Basel, Switzerland
* Correspondence: bettina.woelnerhanssen@unibas.ch (B.K.W.); annechristin.meyergerspach@unibas.ch (A.C.M.-G.); Tel.: +41-61-685-8585 (B.K.W. & A.C.M.-G.)
† These authors contributed equally to this work.

Abstract: The natural sweeteners erythritol and xylitol might be helpful to reduce sugar consumption and therefore prevent obesity and diabetes. The aim of the present study was to determine the absorption and metabolization into erythronate of different concentrations of erythritol and xylitol. Seventeen healthy lean participants received intragastric solutions of 10, 25, or 50 g erythritol or 7, 17, or 35 g xylitol on three study days in a randomized order. The study was double blinded with respect to the doses administered. We assessed plasma concentrations of erythritol, xylitol, and erythronate at fixed time intervals after administration with gas chromatography-mass spectrometry. We found: (i) a dose-dependent and saturable absorption of erythritol, (ii) a very low absorption of xylitol, (iii) a dose-dependent metabolization of erythritol into erythronate, and (iv) no metabolization of xylitol into erythronate. The implications of the metabolization of erythritol into erythronate for human health remain to be determined and more research in this area is needed.

Keywords: erythritol; xylitol; erythronate; natural sweeteners; absorption; metabolism; obesity; diabetes

1. Introduction

The still-steady rise in sugar consumption is a key contributor to the dramatic global rise in obesity and associated metabolic disorders, especially type 2 diabetes mellitus. The WHO has proposed a reduction in sugar intake as a preventive and therapeutic strategy to curb these disorders [1]. A possible solution to achieve a reduction in sugar intake is the partial substitution of table sugar and added sugars with low-caloric, naturally occurring bulk sweeteners, also called polyols. Polyols are mono- and polysaccharides in which a carbonyl group is replaced by an alcohol (hydroxyl) group. Polysaccharide polyols are difficult to digest and metabolize due to their hydroxyl groups and their glycosidic linkages other than α1-4 and α1-6 [2]. Monosaccharide polyols, such as erythritol and xylitol, are partly absorbed by passive diffusion along a concentration gradient in the small intestine [3]. These monosaccharide polyols are gaining popularity among patients with overweight and diabetes thanks to their low glycemic indexes [2], which gives them anti-hyperglycemic and anti-diabetic properties [4]. In addition, erythritol and xylitol induce the secretion of gastrointestinal satiation hormones (such as cholecystokinin (CCK) and glucagon-like peptide-1 (GLP-1)) and promote satiety and slow gastric emptying [5–7]. Furthermore, the two polyols actively benefit oral health [5].

Erythritol is a four-carbon sugar alcohol ($C_4H_{10}O_4$, see Figure 1) with a molar mass of 122.12 g/mol and a glycemic index of 0 (in comparison, sucrose and glucose have glycemic

indexes of 65 and 100, respectively). In 1996, Bornet et al. [8] found that plasma and urine levels increased within two hours proportionally to the amount of erythritol ingested. They found that the total urinary excretion reached 78% of ingested erythritol after 24 h [9]. A chronic intake of erythritol over seven days showed that 78% of ingested erythritol was excreted in the urine [10]. Munro et al. [11] summarized that erythritol is rapidly absorbed up to 90% by the gastrointestinal tract and quantitatively excreted unchanged with the urine. Whether the remaining 10% of the erythritol dose is fermented in the colon or excreted unchanged via the stool is unknown in humans. However, in an in vitro setting, erythritol was shown to be completely resistant to bacterial fermentation within 24 h [12]. In conclusion, available data suggest that erythritol is mainly absorbed in the intestine, not metabolized by the body, and excreted unchanged via the kidney. However, in a side experiment of their study on metabolic markers of adiposity gain, Hootman et al. [13] recently shed light on an unknown pathway of erythritol metabolism. In their study, three healthy males ingested a single dose of 50 g erythritol and gave finger-prick blood samples at regular intervals after ingestion. The authors observed an immediate increase in blood erythritol concentrations, followed by an increase in erythronate concentrations. They suggest that ingested erythritol is oxidized into the sugar erythrose ($C_4H_8O_4$), which is in turn oxidized to erythronate ($C_4H_7O_5^-$). The authors suggest that 5–10% of the ingested amount of erythritol is metabolized into erythronate [13]. These results lead to new questions about the metabolization of erythritol and the role of erythritol and its metabolites, especially erythronate, for human health in relation to obesity and diabetes.
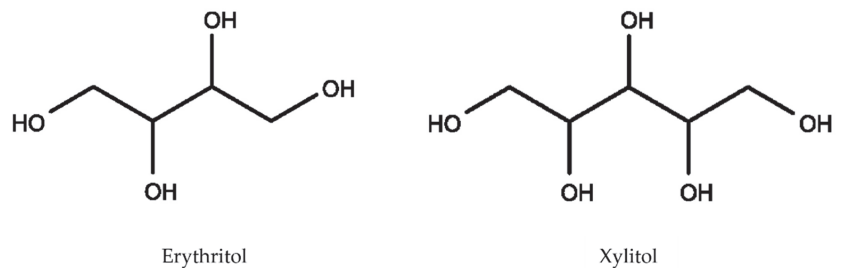
Figure 1. Chemical structures of erythritol and xylitol.

Xylitol is a five-carbon sugar alcohol ($C_5H_{12}O_5$, see Figure 1) with a molar mass of 152.15 g/mol and a glycemic index of 13. Due to its higher molar mass, xylitol is absorbed in smaller proportions than erythritol. There are only a few studies investigating the absorption and metabolism of xylitol. In 1973, Asano et al. [14] studied the intestinal absorption of oral xylitol by aspiration and analysis of ileal content in five healthy subjects. They found that xylitol absorption ranged from 49–95%. However, they did not find any xylitol in plasma samples one and two hours after ingestion, nor did they notice significant amounts in urine up to 24 h after ingestion. After being absorbed, monosaccharide polyols can be excreted unchanged via the kidneys, oxidized directly, or metabolized in the liver to glycogen or glucose [15]. The latter is what Asano et al. [14] suggested as a hypothesis for the absence of xylitol in the blood, while at least half of the ingested quantity was absorbed. Other estimates of xylitol intestinal absorption range from 48% [15] over 53% [16] up to 75% [17]. Xylitol is fermentable by colonic microorganisms and is considered a prebiotic, as it promotes the proliferation and metabolic activity of beneficial bacteria and the production of short-chain fatty acids such as butyrate [18,19]. Livesey summarized the evidence and suggested a consensus of around 49% for absorptive capacity, less than 2% for urinary excretion, and approximately 50% for fermentation [2]. However, like for erythritol, the metabolism of absorbed xylitol still needs further investigation to understand its effect on the human body better and evaluate its potential as a sugar substitute for patients with obesity and diabetes.

We administered different doses of each substance to healthy volunteers to investigate the enteral absorption of erythritol and xylitol and their potential metabolization into erythronate. We showed that the absorption of erythritol and its metabolization into erythronate occur in a dose-dependent manner. The absorption of xylitol was low, and no metabolization into erythronate took place.

2. Results

All participants tolerated the study treatments well, and there were no adverse events that led to study discontinuation. Therefore, complete data from 2×12 participants were available for analysis. There was no abdominal pain, nausea, flatulence, or vomiting reported after any dose of erythritol or xylitol. One participant had diarrhea after 10 g erythritol. Four participants reported feelings of bloating (after 25 g and 50 g erythritol and after 17 g and 35 g xylitol) and two participants reported increased eructation (after 10 g erythritol and after 7 g xylitol). A subjective increase in bowel sounds was reported by nine participants after 10 g erythritol, seven after 25 g erythritol, and eight after 50 g erythritol; and nine participants after 7 g xylitol, eight after 17 g xylitol, and nine after 35 g xylitol.

2.1. Absorption of Erythritol and Xylitol

The absorption of erythritol occurred in a dose-dependent manner. The area under the curve from 0 to 180 min (AUC_{180}) and the maximum erythritol plasma concentrations (C_{max}) increased in response to the three intragastric loads (AUC_{180}: 10 g vs. 25 g, $p < 0.001$; 10 g vs. 50 g, $p < 0.001$; 25 g vs. 50 g, $p < 0.001$; C_{max}: 10 g vs. 25 g, $p < 0.001$; 10 g vs. 50 g, $p < 0.001$; 25 g vs. 50 g, $p = 0.001$, see Table 1).

Table 1. Absorption of erythritol.

	A: 10 g Erythritol (n = 11)	B: 25 g Erythritol (n = 12)	C: 50 g Erythritol (n = 12)	*p*-Values
AUC_{180} (mM·min)	201.0 ± 12.7	450.6 ± 29.3	707.1 ± 53.9	A vs. B: $p < 0.001$ A vs. C: $p < 0.001$ B vs. C: $p < 0.001$
C_{max} (µM)	1810.6 ± 124.6	3676.9 ± 251.2	5404.3 ± 450.6	A vs. B: $p < 0.001$ A vs. C: $p < 0.001$ B vs. C: $p = 0.001$
Absorption rate k_a (min^{-1})	0.126 ± 0.183	0.374 ± 0.257	0.036 ± 0.031	All n.s.
Absorption half-life $t_{ka,1/2}$ (min)	5.40 ± 1.16	4.88 ± 0.86	14.23 ± 2.66	A vs. B: n.s. A vs. C: $p = 0.004$ B vs. C: $p = 0.002$
Elimination rate k10 (min^{-1})	0.008 ± 0.002	0.008 ± 0.001	0.002 ± 0.001	All n.s.
Elimination half-life $t_{ka,1/2}$ (min)	46.09 ± 5.68	51.41 ± 3.62	42.69 ± 5.24	All n.s.
Volume of distribution V1 (L)	38.50 ± 4.27	37.74 ± 2.43	50.95 ± 5.62	All n.s.

Data are expressed as mean $\pm$ SEM and reported from baseline. Linear mixed effect model analysis with Šidak correction for multiple testing. AUC_{180}: area under the curve from 0 to 180 min, C_{max}: maximum plasma concentration, n.s.: not significant.

The absorption of erythritol was significantly slower with the 50 g load compared to the lower doses (absorption half-life $t_{ka,1/2}$: 10 g vs. 50 g, $p = 0.004$, 25 g vs. 50 g, $p = 0.002$, see Table 1), suggesting a saturable process. Neither the elimination rate constant k_{10} of erythritol and its half-life $t_{k10,1/2}$ nor the volume of erythritol distribution (V1) were significantly different between the treatment doses (Table 1).

Figure 2 shows the concentration-time curves and the dose-response diagram for AUC_{180} (dose-response: $R^2 = 0.996$, $p = 0.02$) and C_{max} (dose-response: $R^2 = 0.999$, $p = 0.01$) of erythritol after administration of the three loads.
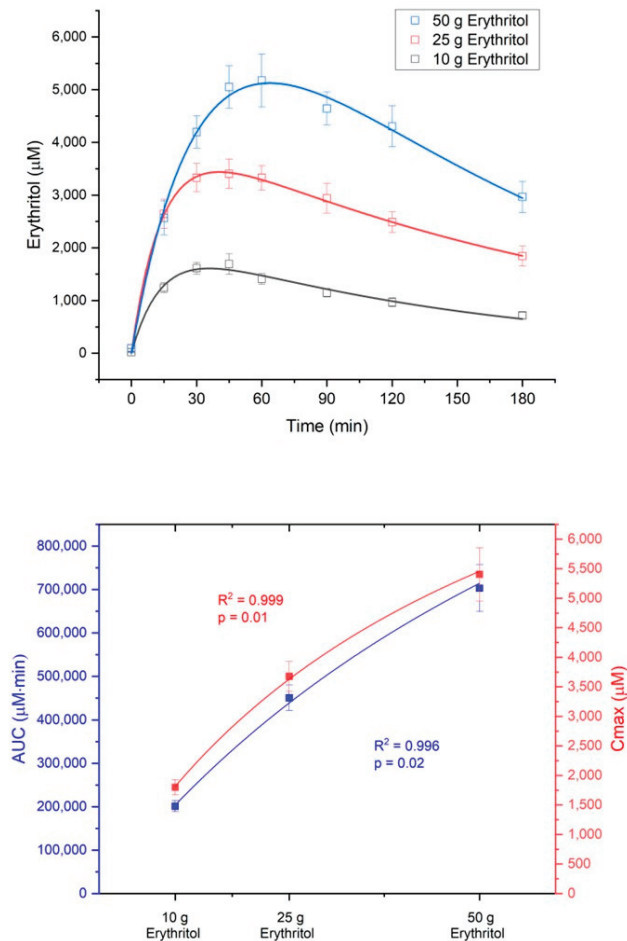
Figure 2. Dose-dependent absorption of erythritol. Upper part: concentration–time curves after administration of the three loads; lower part: dose-response for the area under the curve from 0 to 180 min (AUC180) and the maximum deviations from baseline (Cmax). Data are expressed as mean ± SEM. Data were best fit with a non-linear dose-response model.

Xylitol absorption was low and could not be detected in any of the participants after the 7 g dose, only in some of the participants after the 17 g dose and in all participants after the 35 g dose (data not shown).

2.2. Metabolization of Erythritol and Xylitol into Erythronate

The metabolization of erythritol into erythronate occurred in a dose-dependent manner. The AUC_{180} and C_{max} for erythronate plasma concentrations increased in response to the three intragastric loads of erythritol (AUC_{180}: 10 g vs. 25 g, $p = 0.069$; 10 g vs. 50 g, $p = 0.001$; 25 g vs. 50 g, $p = 0.002$; C_{max}: 10 g vs. 25 g, n.s.; 10 g vs. 50 g, $p < 0.001$; 25 g vs. 50 g, $p = 0.01$, see Table 2). Figure 3 shows the concentration–time curves of erythronate and the dose–response diagram for AUC_{180} (dose–response: $R^2 = 0.999$, $p = 0.018$) and C_{max} (dose–response: $R^2 = 0.989$, $p = 0.045$) of erythronate after administration of the three loads of erythritol. Neither the formation rate (k_{12}), nor the elimination rate k_{20} of erythronate and its half-life $t_{k20,1/2}$, nor the volume of erythronate distribution (V2) were significantly different between the treatment doses (Table 2).
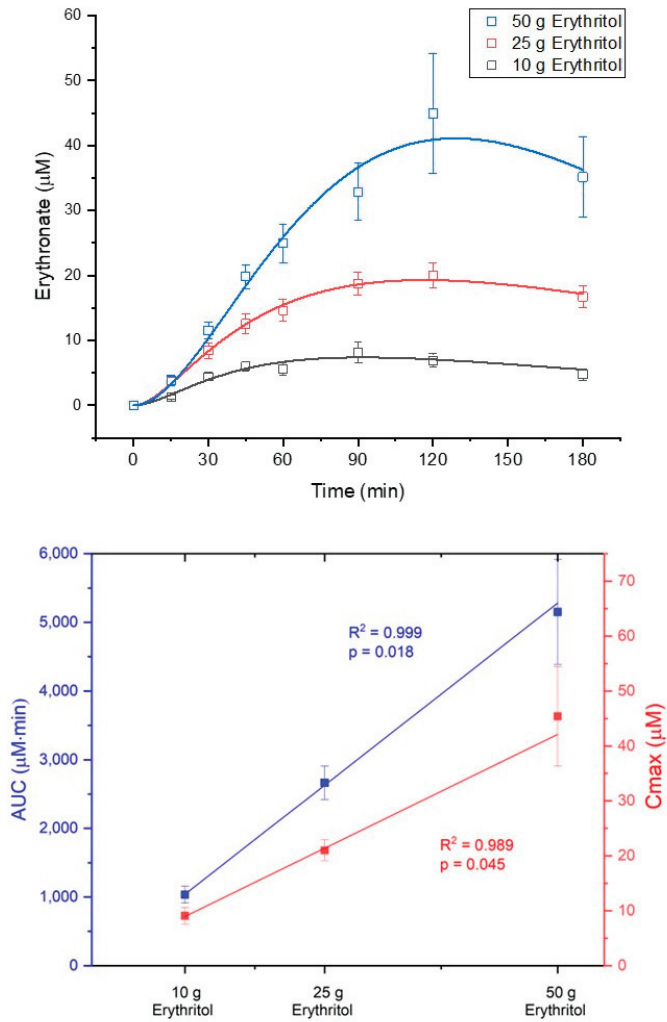
Figure 3. Dose-dependent metabolization of erythritol into erythronate. Upper part: concentration–time curves after administration of the three erythritol loads; lower part: dose–response for area under the curve from 0 to 180 min (AUC180) and maximum deviations from baseline (Cmax). Data are expressed as mean ± SEM.

Table 2. Metabolization of erythritol into erythronate.

	A: 10 g Erythritol (n = 11)	B: 25 g Erythritol (n = 12)	C: 50 g Erythritol (n = 12)	*p*-Values
AUC$_{180}$ erythronate (µM·min)	1034.4 ± 122.8	2664.8 ± 241.6	5151.9 ± 763.2	A vs. B: $p = 0.069$ A vs. C: $p = 0.001$ B vs. C: $p = 0.002$
C$_{max}$ erythronate (µM)	9.1 ± 1.5	21.0 ± 1.9	45.4 ± 9.1	A vs. B: n.s. A vs. C: $p < 0.001$ B vs. C: $p = 0.01$

Table 2. *Cont.*

	A: 10 g Erythritol (n = 11)	B: 25 g Erythritol (n = 12)	C: 50 g Erythritol (n = 12)	*p*-Values
Formation rate k_{12} (min^{-1})	0.0003 ± 0.00009	0.0002 ± 0.00030	0.0002 ± 0.00002	All n.s.
Elimination rate k_{20} (min^{-1})	0.0229 ± 0.0019	0.0188 ± 0.0012	0.0210 ± 0.0018	All n.s.
Elimination half-life $t_{k20,1/2}$ (min)	14.34 ± 1.54	16.89 ± 1.23	15.59 ± 1.46	All n.s.
Volume of distribution V2 (L)	54.39 ± 14.61	49.33 ± 7.69	39.21 ± 5.34	All n.s.

Data are expressed as mean $\pm$ SEM and reported from baseline. Linear mixed effect model analysis with Šidak correction for multiple testing. AUC180: area under the curve from 0 to 180 min, Cmax: maximum plasma concentration, n.s.: not significant.

The metabolic ratio $AUC_{erythritol}/AUC_{erythronate}$ was highest with the 10 g erythritol load and decreased with higher doses (ratio AUC_{180} for 10 g: 236.2 ± 46.3 vs. 25 g: 187.6 ± 22.4 vs. 50 g: 162.3 ± 20.1, differences not significant). The $C_{max, erythritol}/C_{max, erythronate}$ ratio was also highest with the 10 g erythritol load compared to the higher doses (ratio C_{max} for 10 g: 229.0 ± 26.5 vs. 25 g: 193.1 ± 23.3 vs. 50 g: 153.8 ± 20.4, differences not significant). These decreasing metabolic ratios with higher doses of erythritol indicate that an increasing fraction of erythritol is metabolized into erythronate. Figure 4 shows the metabolic ratios depending on the different doses of erythritol. This phenomenon is also reflected by the non-linear dose-response for AUC_{180} and C_{max}, as shown in the lower part of Figure 2.
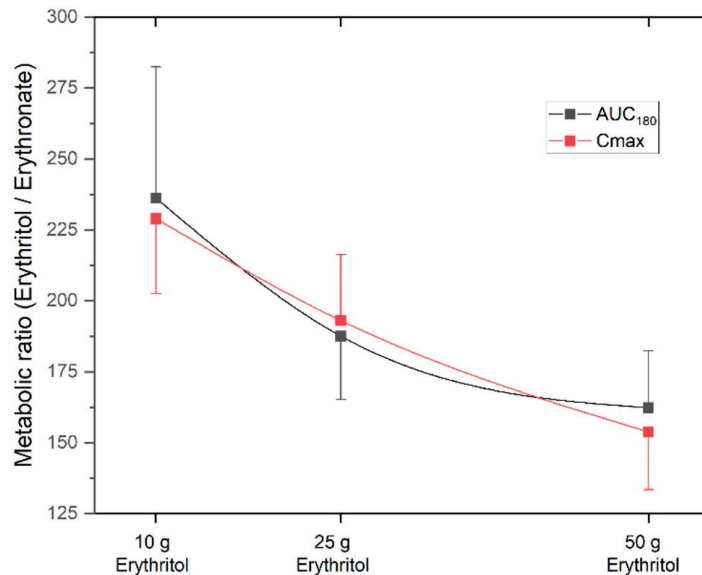
Figure 4. Metabolic ratios erythritol/erythronate for the three doses of erythritol. AUC_{180}: area under the curve from 0 to 180 min, C_{max}: maximum deviation from baseline. Data are expressed as mean $\pm$ SEM.

The concentrations of erythronate in response to the intragastric loads of xylitol were under the detection limit of the analytical assay, indicating no metabolization of xylitol into erythronate at the doses applied in this study.

3. Discussion

This study aimed to determine the absorption of different intragastric doses of erythritol and xylitol and their potential metabolization into erythronate in healthy volunteers. The results show that: (i) the absorption of erythritol is dose-dependent and saturable; (ii) the absorption of xylitol is low; (iii) erythritol is metabolized into erythronate, the metabolization is dose-dependent and higher with high doses of erythritol; and (iv) there is no metabolization of xylitol into erythronate. The implications for human health remain to be determined.

The absorption results for erythritol are in line with other human studies showing that erythritol is rapidly absorbed [8–10]. However, the extent can only be estimated in comparison to an intravenous control. The dose-dependent absorption of erythritol found here confirms the results of Bornet et al. [8], who showed increasing plasma erythritol concentrations as a function of ingested doses (0.4 or 0.8 g/kg body weight). More importantly, we observed that the absorption of erythritol was slower with the highest dose (50 g) suggesting a saturable process. The slower absorption might explain gastrointestinal symptoms such as nausea, borborygmi, bloating, and diarrhea observed at high doses [5,20]. The hypothesis of a saturable absorption of erythritol at high doses is compatible with these observations.

Xylitol, on the other hand, was poorly absorbed in the present study. This contrasts with results showing absorption of at least 50% in healthy subjects [14]. In contrast, the previous study used a test solution consisting of xylitol with an equal amount of glucose, which is different from the current design. The addition of glucose might have affected the absorption of xylitol. Moreover, the authors estimated absorption by aspiration and analysis of ileal content (i.e., disappearance); of note, they did not find any xylitol in plasma samples one and two hours after ingestion [14].

Erythritol is metabolized into erythronate, confirming the findings of Hootman et al. [13]. In addition, we extend these findings by showing that this metabolization is dose-dependent and increases with high doses of erythritol. The metabolization process occurred, however, in minimal amounts: less than 1% of erythritol was converted into erythronate—which is less than Hootman et al. who reported a conversion rate of 5–10%. In their study, only three men were included and they received 50 g of oral erythritol 43 min after having consumed 2 g of labeled glucose. Although the dose is similar, the limited sample size, the route, and the timing of administration are important differences in the study design. Both studies agree that only on a small amount of erythritol is metabolized (<10%). We think that erythritol is converted by an alcohol dehydrogenase to threose, which is in turn probably further biochemically oxidized to erythronate (Figure 5).
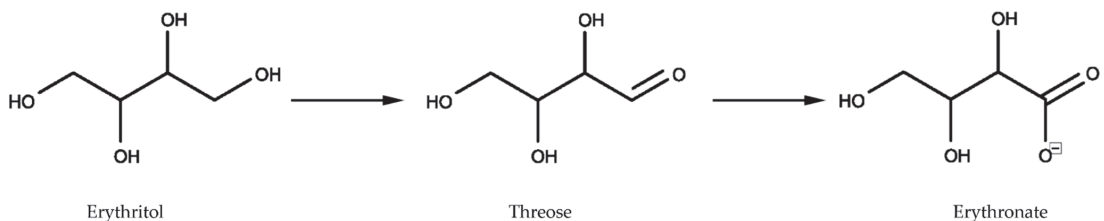
Figure 5. Oxidation reactions of erythritol into threose and erythronate.

The formation rate of erythronate did not significantly differ between the different doses of erythritol, although numerically, the metabolic ratio decreased with higher doses indicating that the metabolization increased. It is interesting to note that erythronate is eliminated faster than erythritol. The elimination rate of erythronate is about 0.02 min^{-1}, while the elimination rate of erythritol is only 0.008 min^{-1} for the two lower doses and even lower (0.002 min^{-1}) for the 50 g dose of erythritol. The reasons for these differences are unclear: the higher polarity of erythronate compared to erythritol could be an explanation,

although both substances are quite hydrophilic. It is not known if erythronate is further metabolized or directly excreted in the urine.

We did not detect any metabolization of xylitol into erythronate. The metabolization of erythritol into erythronate might follow an oxidation reaction including the sugar erythrose. Therefore, xylitol has to be metabolized into erythrose before being further oxidized into erythronate. This reaction is possible requiring multiple steps: xylitol can be transformed into xylulose and then into xylulose-5-phosphate through enzymatic reactions. Xylulose-5-phosphate is an entry point into the pentose phosphate cycle [21]. Within this cycle, xylulose-5-phosphate can be metabolized into erythrose-4-phosphate, which, in turn, can be transformed into erythrose and further oxidized into erythronate. This process involves several steps; the resulting concentrations were not detectable within the dose range investigated here. Therefore, we conclude that xylitol is not metabolized into erythronate at the concentrations administered in this study.

Little is known about the role of erythronate in the human body. It seems that erythronate is an oxidative stress product [22,23]. It has been shown in feces of colorectal cancer patients, that erythronate correlated with the presence of Enterobacteriaceae, a potentially pathogenic group of bacteria [24]. In patients with liver cirrhosis, erythronate was associated with the severity of hepatorenal dysfunction and it was a significant predictor of mortality [25,26]. A stepwise increase in erythronate plasma concentration in patients with renal disease was observed with decreasing renal function [27]. In addition, erythronate was associated with the estimated glomerular filtration rate in the general European population, and the authors suggest that it may be an early marker of reduced kidney function [28]. However, before using erythronate as a marker of different conditions, more research is necessary and it must be taken into account that increasing amounts of erythritol is consumed, and that this consumption influences the circulating levels of erythronate.

Hootman et al. [13] found a positive association between circulating levels of erythritol and the incidence of central adiposity gain in nonobese young adults studied over nine months. They also showed that glucose can be metabolized into erythritol, and erythritol can be metabolized into erythronate. We and others hypothesize that the presence of erythritol and erythronate in the plasma of subjects who are not regularly consuming erythritol might serve as a marker of elevated blood sugar levels and oxidative stress, which are associated with central adiposity [29]. More research is needed to validate the role of erythronate metabolized from erythritol ingestion in the human body.

The present study has some limitations: first, it is an a posteriori analysis, and therefore, no pre-study sample size calculation was made. However, as the results of the main trial (dose-response effect on satiation hormones secretion) were significant [6,7], we can assume that the sample size was robust to detect a dose-dependent effect in the absorption of erythritol and xylitol and their conversion into erythronate. Second, the doses chosen might have been too low to observe the conversion of xylitol into erythronate. However, as mentioned before, the doses in this study were chosen to represent real life conditions and to limit gastrointestinal symptoms. Finally, we only assessed erythritol, xylitol, and erythronate concentrations in the plasma. It would be interesting to measure their concentration in urine and feces, too, to understand whether erythronate is further metabolized or directly eliminated.

In conclusion, erythritol is absorbed in a dose-dependent and saturable manner. It is metabolized in a small amount into erythronate, and this process is dose-dependent. The absorption of xylitol is low, and no metabolization into erythronate takes place at the doses used in this study. The implications for human health remain to be determined.

4. Materials and Methods

4.1. Study Approval

The trial was approved by the local ethical committee of Basel, Switzerland (Ethikkommission Nordwest- und Zentralschweiz; EKNZ 2016-01928) and was performed in compli-

ance with the current version of the Declaration of Helsinki, the ICH-GCP, and national legal and regulatory requirements. Each participant gave written informed consent for the trial. The trial was registered at ClinicalTrial.gov under NCT03039478.

4.2. Participants

A total of 17 healthy normal-weight participants took part in the trial. The participants' baseline characteristics are shown in Table 3. Participants were excluded if they suffered from acute infections, chronic diseases, or diseases of the gastrointestinal tract, if they took medications regularly, if they were pregnant, or if they consumed substances in abuse. In addition, none of the participants had a history of food allergies, dietary restrictions, or pre-existing consumption of erythritol or xylitol on a regular basis.

Table 3. Participants' baseline characteristics (mean $\pm$ SD (range)).

Parameter	Xylitol Group	Erythritol Group	*p*-Values
Gender	n = 12 (7♀, 5♂)	n = 12 (5♀, 7♂)	0.683 [†]
Age (yrs)	25.6 $\pm$ 5.1 (23; 41)	26.2 $\pm$ 6.6 (18; 40)	0.810 [§]
Weight (kg)	64.5 $\pm$ 9.5 (51.0; 82.9)	66.4 $\pm$ 8.3 (54.7; 82.9)	0.607 [§]
Height (m)	1.74 $\pm$ 0.11 (1.61; 1.90)	1.75 $\pm$ 0.09 (1.65; 1.90)	0.836 [§]
BMI (kg/m^2)	21.2 $\pm$ 1.3 (19.4; 23.0)	21.7 $\pm$ 1.4 (19.4; 24.0)	0.422 [§]

[†] Chi-square test, [§] Analysis of variance, ♀ stands for women, ♂ stands for men, BMI: body mass index, SD: standard deviation.

4.3. Study Design

This acute study was conducted as a parallel trial. The first twelve included participants were given erythritol; the following twelve participants were included in the xylitol arm. Within the arms, the doses were given in a randomized order. The trial was conducted double blind, meaning that the study participant, the person carrying out all tests, and the personnel performing the analyses of blood samples were blinded concerning the dosage assigned to the participant. Some participants (n = 7) participated in the xylitol arm after enrolling in the erythritol arm. That is why the total number of participants was only 17. For participants included in both arms, a wash-out phase of at least four days between the two interventions was respected.

4.4. Experimental Procedure

Participants were admitted to St. Clara Research Ltd. in the morning after a 10 h overnight fast. A feeding tube was placed to administer the substances intragastrically. This route of administration was chosen to bypass exteroceptive cues (e.g., taste and smell) and their associated hedonic responses and cognitions that may influence subjective ratings or even physiological/endocrine responses [30]. An antecubital catheter was inserted into a forearm vein for blood sampling. After taking fasting blood samples, participants received one of the following solutions (*t* = 0 min) directly into the stomach, over two minutes, in a randomized order, depending on the intervention arm:

For the erythritol arm:

- 10 g of erythritol dissolved in 300 mL tap water
- 25 g of erythritol dissolved in 300 mL tap water
- 50 g of erythritol dissolved in 300 mL tap water

For the xylitol arm:

- 7 g of xylitol dissolved in 300 mL tap water
- 17 g of xylitol dissolved in 300 mL tap water
- 35 g of xylitol dissolved in 300 mL tap water

The doses of erythritol were chosen to represent everyday life conditions. For example, 50 g erythritol dissolved in 300 mL corresponds to 30 g sucrose in 330 mL, the concentration

found in common sweet beverages. Moreover, the gastrointestinal tolerance of 50 g of erythritol seems acceptable, as this dose only causes nausea and borborygmi, while 50 g of xylitol can cause bloating, colic, and watery feces in some subjects. Lower doses of erythritol do not cause any symptoms [20]. The doses of xylitol were chosen to be equisweet to erythritol.

After administration of the test solutions, blood samples were taken at regular time intervals (t = 15, 30, 45, 60, 90, 120, and 180 min). Participants were asked to rate GI symptoms at 30, 60, 90, 120, 150, 180, and 240 min after administration of the test solutions. The experimental procedure is depicted in Figure 6.
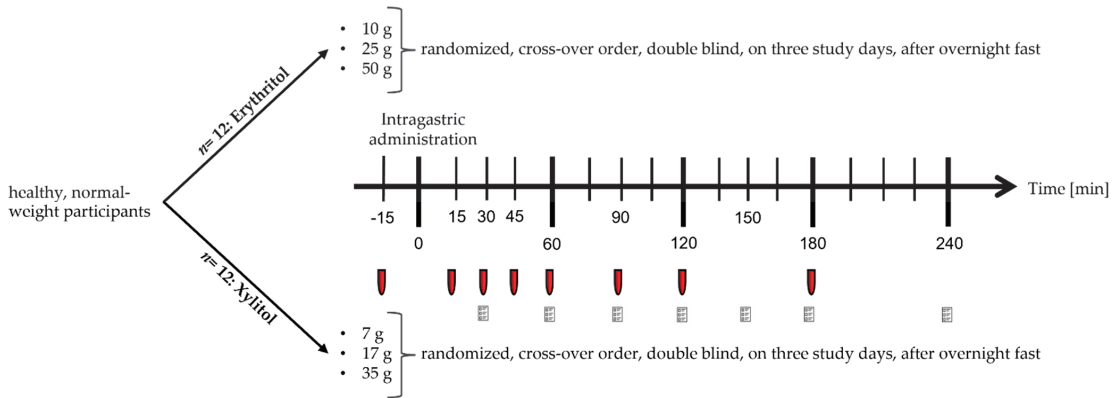

Figure 6. Diagram of the experimental procedure. The red tubes stand for blood sampling, the paper forms stand for gastrointestinal symptoms questionnaires.

4.5. Blood Sample Collection and Processing

Blood samples were collected on ice into tubes containing EDTA (6 µmol/L blood) and a protease-inhibitor cocktail (Complete, EDTA-free, one tablet/50 mL blood, Roche, Mannheim, Germany). After centrifugation (4 °C at 3000 rpm for 10 min), plasma samples were processed into aliquots. The samples were then stored at −80 °C until analysis.

4.6. Materials

Erythritol and xylitol were purchased from Mithana GmbH (Zimmerwald, Switzerland).

4.7. Assessments of Erythritol, Xylitol, and Erythronate Concentrations

To analyze erythritol, xylitol, and erythronate, the plasma samples were first extracted with a solution of water/methanol (1/8) *v/v* containing the internal standard and dried at 55 °C on a vacuum centrifuge for one hour. The dried sample spots were then reconstituted in pyridine containing methoxyamine and derivated at 70 °C for 30 min. Before analysis, the samples were derivated a second time by adding N-Methyl-N-(trimethylsilyl)-trifluoracetamid at 40 °C for another 30 min. Finally, the concentration of erythritol, xylitol, and erythronate was assessed using gas chromatography-mass spectrometry with helium as carrier gas. In samples from the erythritol arm, xylitol was used as an internal standard; in samples from the xylitol arm, erythritol was used as the internal standard.

4.8. Statistical Analysis

This study is an a posteriori sample analysis. Therefore, no sample size calculation was made, and 12 participants per group was chosen for comparability and practicability. However, as the results of the main trial (dose-response of satiation hormones secretion) were significant [6,7], we can assume that the sample size is enough to detect a dose-dependent effect in the absorption of erythritol and xylitol and their conversion into erythronate.

Molar concentrations of erythritol, xylitol, and erythronate were analyzed kinetically using the following system of coupled differential Equation (1), based on the three-compartment model depicted in Figure 7.

$$dX_0/dt = -k_a \cdot X_0$$
$$dX_1/dt = k_a \cdot X_0 - k_{10} \cdot X_1 - k_{12} \cdot X_1 \qquad (1)$$
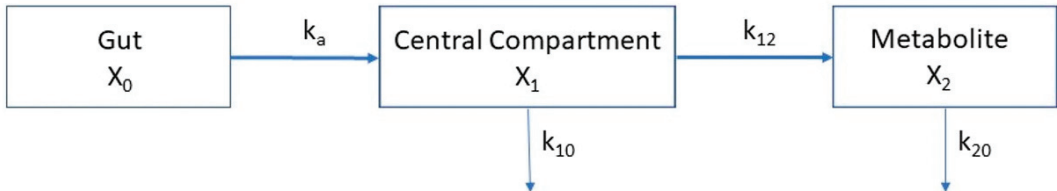$$dX_2/dt = k_{12} \cdot X_1 - k_{20} \cdot X_2$$

Figure 7. Three-compartment model for the absorption of erythritol/xylitol and the conversion into erythronate.

This linear three-compartment model describes the mass transfer between the first compartment (X_0, gut), from which the absorbable fraction of the erythritol/xylitol dose (F × dose, where F = bioavailability) is absorbed into the central compartment (X_1, blood) by a linear process with a rate constant k_a. Erythritol/xylitol in compartment X_1 is either eliminated from the compartment (elimination rate constant k_{10}) or metabolized into erythronate in the compartment X_2. Although the formation of erythronate from erythritol/xylitol is done by enzymatic reaction, it could best be modeled by a linear process and was denoted by the formation rate constant k_{12}. The elimination of erythronate from the metabolite compartment (X_2, blood) is described by the elimination rate constant k_{20}. The volumes of distribution of compartments X_1 and X_2, called V_1 and V_2, respectively, relate the masses to plasma concentration (y_1 and y_2), as shown in the following Equation (2):

$$y_1(t) = X_1(t)/V_1 \text{ and } y_2(t) = X_2(t)/V_2. \qquad (2)$$

The initial conditions at t = 0 were set to $X_0(0)$ = molar doses, $X_1(0)$ = 0, and $X_2(0)$ = 0.

Data were modeled using Python programming language (version 3.8.5), and the Limfit module version 1.0.2 (Newville, M. et al., LMFIT: Non-Linear Least-Square Minimization and Curve-Fitting for Python (2021), https://zenodo.org/record/11813#.Yex0ZerMJZc) to numerically solve the Equations (1) and (2) and fit them to the observed concentrations of xylitol, erythritol, and erythronate.

The half-life of the respective rate constant k for absorption and elimination was calculated as shown in the following Equation (3):

$$t_{k,1/2} = \ln(2)/k, \ln = \text{natural logarithm.} \qquad (3)$$

The concentrations of erythritol, xylitol, and erythronate were baseline-corrected before analysis.

All statistical analysis was done using the statistical software package IBM SPSS Statistics for Windows, Version 27.0 (Armonk, NY, USA: IBM Corp.). Values were reported and displayed as means ± standard error of the mean (SEM) if not otherwise specified.

Data were compared between doses by linear mixed model analysis with Šidak correction for multiplicity of testing. Differences were considered to be statistically significant when $p < 0.05$.

References

1. WHO. *Guideline: Sugars Intake for Adutls and Children*; World Health Organization: Geneva, Switzerland, 2015.
2. Livesey, G. Health potential of polyols as sugar replacers, with emphasis on low glycaemic properties. *Nutr. Res. Rev.* **2003**, *16*, 163–191. [CrossRef] [PubMed]
3. Herman, R.H. Hydrolysis and absorption of carbohydrates, and adaptive responses of the jejunum. In *Sugars in Nutrition*; Sipple, H.L., McNutt, K.W., Eds.; Academic Press Inc.: New York, NY, USA, 1974; pp. 145–172.
4. Wölnerhanssen, B.K.; Meyer-Gerspach, A.C.; Beglinger, C.; Islam, S. Metabolic effects of the natural sweeteners xylitol and erythritol: A comprehensive review. *Crit. Rev. Food Sci. Nutr.* **2020**, *60*, 1986–1998. [CrossRef] [PubMed]
5. Wölnerhanssen, B.K.; Cajacob, L.; Keller, N.; Doody, A.; Rehfeld, J.F.; Drewe, J.; Peterli, R.; Beglinger, C.; Meyer-Gerspach, A.C. Gut hormone secretion, gastric emptying, and glycemic responses to erythritol and xylitol in lean and obese subjects. *Am. J. Physiol. Endocrinol. Metab.* **2016**, *310*, E1053–E1061. [CrossRef] [PubMed]
6. Wölnerhanssen, B.K.; Drewe, J.; Verbeure, W.; le Roux, C.W.; Dellatorre-Teixeira, L.; Rehfeld, J.F.; Holst, J.J.; Hartmann, B.; Tack, J.; Peterli, R.; et al. Gastric emptying of solutions containing the natural sweetener erythritol and effects on gut hormone secretion in humans: A pilot dose-ranging study. *Diabetes Obes. Metab.* **2021**, *23*, 1311–1321. [CrossRef] [PubMed]
7. Meyer-Gerspach, A.C.; Drewe, J.; Verbeure, W.; le Roux, C.W.; Dellatorre-Teixeira, L.; Rehfeld, J.F.; Holst, J.J.; Hartmann, B.; Tack, J.; Peterli, R.; et al. Effect of the Natural Sweetener Xylitol on Gut Hormone Secretion and Gastric Emptying in Humans: A Pilot Dose-Ranging Study. *Nutrients* **2021**, *13*, 174. [CrossRef]
8. Bornet, F.R.J.; Blayo, A.; Dauchy, F.; Slama, G. Gastrointestinal Response and Plasma and Urine Determinations in Human Subjects Given Erythritol. *Regul. Toxicol. Pharmacol.* **1996**, *24*, S296–S302. [CrossRef]
9. Bornet, F.R.J.; Blayo, A.; Dauchy, F.; Slama, G. Plasma and Urine Kinetics of Erythritol after Oral Ingestion by Healthy Humans. *Regul. Toxicol. Pharmacol.* **1996**, *24*, 280–285. [CrossRef]
10. Tetzloff, W.; Dauchy, F.; Medimagh, S.; Carr, D.; Bar, A. Tolerance to Subchronic, High-Dose Ingestion of Erythritol in Human Volunteers. *Regul. Toxicol. Pharmacol.* **1996**, *24*, S286–S295. [CrossRef]
11. Munro, I.C.; Bernt, W.O.; Borzelleca, J.F.; Flamm, G.; Lynch, B.S.; Kennepohl, E.; Bar, E.A.; Modderman, J. Erythritol: An Interpretive Summary of Biochemical, Metabolic, Toxicological and Clinical Data. *Food Chem. Toxicol.* **1998**, *36*, 1139–1174. [CrossRef]
12. Arrigoni, E.; Brouns, F.; Amado, R. Human gut microbiota does not ferment erythritol. *Br. J. Nutr.* **2005**, *94*, 643–646. [CrossRef]
13. Hootman, K.C.; Trezzi, J.-P.; Kraemer, L.; Burwell, L.S.; Dong, X.; Guertin, K.A.; Jaeger, C.; Stover, P.J.; Hiller, K.; Cassano, P.A. Erythritol is a pentose-phosphate pathway metabolite and associated with adiposity gain in young adults. *Proc. Natl. Acad. Sci. USA* **2017**, *114*, E4233–E4240. [CrossRef] [PubMed]
14. Asano, T.; Levitt, M.D.; Goetz, F.C. Xylitol Absorption in Healthy Men. *Diabetes* **1973**, *22*, 279–281. [CrossRef] [PubMed]
15. Livesey, G. The energy values of dietary fibre and sugar alcohols for man. *Nutr. Res. Rev.* **1992**, *5*, 61–84. [CrossRef] [PubMed]
16. Bär, A. Factorial calculation model for the estimation of the physiological caloric value of polyols. In *Caloric Evaluation of Carbohydrates*; Hosoya, N., Ed.; Research Foundation for Sugar Metabolism: Tokyo, Japan, 1990; pp. 209–257.
17. Office, L.S.R. *The Evaluation of the Energy of Certain Sugar Alcohols Used as Food Ingredients*; Federation of American Societies for Experimental Biology: Bethesda, MD, USA, 1994.
18. Xiang, S.; Ye, K.; Li, M.; Ying, J.; Wang, H.; Han, J.; Shi, L.; Xiao, J.; Shen, Y.; Feng, X.; et al. Xylitol enhances synthesis of propionate in the colon via cross-feeding of gut microbiota. *Microbiome* **2021**, *9*, 62. [CrossRef]

19. Sato, T.; Kusuhura, S.; Yokoi, W.; Ito, M.; Miyazaki, K. Prebiotic potential of L-sorbose and xylitol in promoting the growth and metabolic activity of specific butyrate-producing bacteria in human fecal culture. *FEMS Microbiol. Ecol.* **2017**, *93*, fiw227. [CrossRef]
20. Storey, D.; Lee, A.; Bornet, F.; Brouns, F. Gastrointestinal tolerance of erythritol and xylitol ingested in a liquid. *Eur. J. Clin. Nutr.* **2007**, *61*, 349–354. [CrossRef]
21. Makinen, K.K. Can the pentitol-hexitol theory explain the clinical observations made with xylitol? *Med. Hypotheses* **2000**, *54*, 603–613. [CrossRef]
22. Ellis, J.K.; Athersuch, T.J.; Thomas, L.D.K.; Teichert, F.; Perez-Trujillo, M.; Svendsen, C.; Spurgeon, D.J.; Singh, R.; Jarup, L.; Bundy, J.G.; et al. Metabolic profiling detects early effects of environmental and lifestyle exposure to cadmium in a human population. *BMC Med.* **2012**, *10*, 61. [CrossRef]
23. Jahn, M.; Baynes, J.W.; Spiteller, G. The reaction of hyaluronic acid and its monomers, glucuronic acid and N-acetylglucosamine, with reactive oxygen species. *Carbohydr. Res.* **1999**, *321*, 228–234. [CrossRef]
24. Sinha, R.; Ahn, J.; Sampson, J.N.; Shi, J.; Yu, G.; Xiong, X.; Hayes, R.B.; Goedert, J.J. Fecal Microbiota, Fecal Metabolome, and Colorectal Cancer Interrelations. *PLoS ONE* **2016**, *11*, e0152126. [CrossRef]
25. Mindikoglu, A.L.; Opekun, A.R.; Putluri, N.; Devaraj, S.; Sheikh-Hamad, D.; Vierling, J.M.; Goss, J.A.; Rana, A.; Sood, G.K.; Jalal, P.K.; et al. Unique metabolomic signature associated with hepatorenal dysfunction and mortality in cirrhosis. *Transl. Res.* **2018**, *195*, 25–47. [CrossRef] [PubMed]
26. Mindikoglu, A.L.; Coarfa, C.; Opekun, A.R.; Shah, V.H.; Arab, J.P.; Lazaridis, K.N.; Putluri, N.; Ambati, C.R.; Robertson, M.J.; Devaraj, S.; et al. Metabolomic biomarkers are associated with mortality in patients with cirrhosis caused by primary biliary cholangitis or primary sclerosing cholangitis. *Future Sci.* **2019**, *6*, FSO441. [CrossRef] [PubMed]
27. Tsalik, E.L.; Willig, L.K.; Rice, B.J.; van Velkinburgh, J.C.; Mohney, R.P.; McDunn, J.E.; Dinwiddie, D.L.; Miller, N.A.; Mayer, E.S.; Glickman, S.W.; et al. Renal systems biology of patients with systemic inflammatory response syndrome. *Kidney Int.* **2015**, *88*, 804–814. [CrossRef] [PubMed]
28. Sekula, P.; Goek, O.-N.; Quaye, L.; Barrios, C.; Levey, A.S.; Romisch-Margl, W.; Menni, C.; Yet, I.; Gieger, C.; Inker, L.A.; et al. A Metabolome-Wide Association Study of Kidney Function and Disease in the General Population. *J. Am. Soc. Nephrol.* **2016**, *27*, 1175–1188. [CrossRef] [PubMed]
29. Ortiz, S.R.; Field, M.S. Mammalian metabolism of erythritol: A predictive biomarker of metabolic dysfunction. *Curr. Opin. Clin. Nutr. Metab. Care* **2020**, *23*, 296–301. [CrossRef]
30. Crum, A.J.; Corbin, W.R.; Brownell, K.D.; Salovey, P. Mind over milkshakes: Mindsets, not just nutrients, determine ghrelin response. *Health Psychol.* **2011**, *30*, 424–429; discussion 430–431. [CrossRef]

Hypertrophy and ER Stress Induced by Palmitate Are Counteracted by Mango Peel and Seed Extracts in 3T3-L1 Adipocytes

Giovanni Pratelli [1,†], Diana Di Liberto [1,†], Daniela Carlisi [1], Sonia Emanuele [1], Michela Giuliano [2], Antonietta Notaro [2], Anna De Blasio [2], Giuseppe Calvaruso [2], Antonella D'Anneo [2,‡] and Marianna Lauricella [1,*,‡]

[1] Section of Biochemistry, Department of Biomedicine, Neurosciences and Advanced Diagnostics (BIND), University of Palermo, 90127 Palermo, Italy
[2] Laboratory of Biochemistry, Department of Biological, Chemical and Pharmaceutical Sciences and Technologies (STEBICEF), University of Palermo, 90127 Palermo, Italy
[*] Correspondence: marianna.lauricella@unipa.it; Tel.: +39-09123865854
[†] These authors equally contributed to the paper.
[‡] These authors equally contributed to the paper.

Abstract: A diet rich in saturated fatty acids (FAs) has been correlated with metabolic dysfunction and ROS increase in the adipose tissue of obese subjects. Thus, reducing hypertrophy and oxidative stress in adipose tissue can represent a strategy to counteract obesity and obesity-related diseases. In this context, the present study showed how the peel and seed extracts of mango (*Mangifera indica L.*) reduced lipotoxicity induced by high doses of sodium palmitate (PA) in differentiated 3T3-L1 adipocytes. Mango peel (MPE) and mango seed (MSE) extracts significantly lowered PA-induced fat accumulation by reducing lipid droplet (LDs) and triacylglycerol (TAGs) content in adipocytes. We showed that MPE and MSE activated hormone-sensitive lipase, the key enzyme of TAG degradation. In addition, mango extracts down-regulated the adipogenic transcription factor PPARγ as well as activated AMPK with the consequent inhibition of acetyl-CoA-carboxylase (ACC). Notably, PA increased endoplasmic reticulum (ER) stress markers GRP78, PERK and CHOP, as well as enhanced the reactive oxygen species (ROS) content in adipocytes. These effects were accompanied by a reduction in cell viability and the induction of apoptosis. Interestingly, MPE and MSE counteracted PA-induced lipotoxicity by reducing ER stress markers and ROS production. In addition, MPE and MSE increased the level of the anti-oxidant transcription factor Nrf2 and its targets MnSOD and HO-1. Collectively, these results suggest that the intake of mango extract-enriched foods in association with a correct lifestyle could exert beneficial effects to counteract obesity.

Keywords: mango peel extracts; mango seed extracts; saturated fatty acids; 3T3-L1 adipocytes; ER stress; AMPK; Nrf2

1. Introduction

Obesity is a multifactorial disease characterized by the accumulation of body fat resulting from excessive food intake, reduced physical activity, environmental factors and genetic susceptibility [1,2]. For decades now, the incidence of obesity has increased in developing countries, representing a public health problem [1]. Hypertrophic expansion of white adipose tissue (WAT) represents an important risk factor for the development of several chronic diseases, including insulin resistance, type II diabetes, non-alcoholic fatty liver disease (NAFLD), cardiovascular diseases and some forms of cancers, such as pancreatic, colorectal, ovarian, thyroid and breast cancers [3–6].

Excess dietary fat intake has been associated with overweight and fat deposition in mice and humans and represents a serious health risk [7–9]. However, the quality of dietary

fats has been shown to induce differential lipid storage. In fact, evidence shows that a high intake of saturated long-chain fatty acids (SLFAs), such as palmitic acid (PA), is associated with obesity [10], while a diet containing monounsaturated (MUFAs) and polyunsaturated fatty acids (PUFA), such as oleic or linoleic acid, or medium-chain fatty acids (MFAs), including caprylic acid, capric acid and lauric acid, may have beneficial effects on body weight and obesity [11]. This can be explained considering that certain fatty acids (FAs) are more likely to be stored in adipose tissue versus being oxidized for energy. In particular, SLFAs have lower oxidation rates than MUFAs, PUFAs and MFAs, leading to increased fat storage in white adipose tissue (WAT) [12].

Fat accumulation into adipose tissue due to high consumption of LSFAs produces hypertrophic and dysfunctional adipocytes, leading to a state of chronic low-grade inflammation [13] that contributes to the development of obesity-related diseases [14]. PA induces hypertrophy by increasing lipids droplet (LDs) content, and causes DNA damage in adipocytes in vitro [15]. Moreover, high consumption of PA increases the expression of pro-inflammatory cytokines (TNFα, IL-6, IL-1β) in adipose tissue [16]. The mechanisms through which high levels of LSFAs induce adipocyte disfunction and inflammation in WAT are different. When a large amount of PA is present, adipocytes metabolize it into lysophosphatidylcholine, diacylglycerol (DAG) and ceramides [17]. These compounds have been shown to induce PKC activation, endoplasmic reticulum (ER) stress induction and NF-kB activation [18–20].

Several studies suggest that increased oxidative stress is positively correlated with obesity [21]. Obese patients exhibit an abnormal oxidant/antioxidant status with higher levels of oxidative stress markers such as hydroperoxides and carbonyl proteins, while their antioxidant defenses are lower than those of their normal-weight counterparts [22]. The increased presence of reactive oxygen species (ROS) causes extensive oxidative damage to proteins, lipids and DNA, promoting metabolic dysfunction and lipotoxicity in adipocytes [23]. High-fat diets promote oxidative stress in adipose tissue [24]. It has been shown that PA increases ROS production in adipocytes by increasing NADPH oxidase 4 (NOX4) activity [23–25]. Moreover, it has been suggested that the elevated bioavailability of FAs can overwhelm the mitochondrial respiratory chain and oxygen consumption, leading to mitochondrial dysfunction and ROS production [26]. Interestingly, oxidative stress and inflammation appear to be closely interlinked in obesity. ROS may activate redox-sensitive transcription factors, such as NF-κB, that transactivate pro-inflammatory cytokines, such as IL-6 and TNF-α [27]. These, in turn, may further induce ROS production, generating a vicious circle between inflammation and oxidative stress [27].

Several studies showed that caloric restriction or increased physical activity lowered fat mass with a consequent reduction of oxidative stress and inflammation-associated obesity [28,29]. In addition, there is an increasing interest in natural antioxidant compounds, such as polyphenols contained in plants, due to their effectiveness against obesity and the related chronic diseases [30,31].

Mango (*Mangifera indica* L.) is a tropical plant belonging to the *Anacardiaceae* family whose cultivation has recently spread to the coastal areas of Sicily (Italy), where the favorable climatic conditions stimulate the growth of the plant and the ripening of the fruit [32]. Mango fruit is appreciated for its nutritive and nutraceutical properties [32,33]. It has been shown that different parts of the plant and of the fruit exert anti-inflammatory, anti-oxidant and anti-tumor effects in in vitro as well as in vivo models because of the presence of a wide range of polyphenols [34–36].

In addition, several studies demonstrated that mango also exerts anti-obesity and antidiabetic effects. *Mangifera indica* L. leaf extracts have been shown to reduce adipogenesis in 3T3-L1 adipocytes by decreasing the expression of genes involved in lipid metabolism [37]. In addition, mango juice intake decreases adiposity and inflammation in high-fat-diet-fed obese rats [38], while mango fruit powder reduces insulin resistance and steatosis [39]. Furthermore, it has been shown that fresh mango consumption improves postprandial glucose and insulin responses in obese adults [40]. Arshad et al. demonstrated that the

consumption of mango peel powder reduced oxidative stress and dyslipidemia in obese subjects [41]. These studies highlighted the potential of mango as a functional food for the treatment of obesity and related diseases.

The edible part of mango is only the pulp. However, it has been reported that mango peel and seed, which are the main bio-wastes of mango processing, contain high levels of bioactive compounds [42,43]. We previously demonstrated that extracts of mango peel and seed cultivated in Sicily exert anti-adipogenic effects by reducing the differentiation of 3T3-L1 fibroblasts into adipocytes. These effects results from the down-regulation of adipogenic factors such as PPARγ and SREBP as well as the activation of AMPK [43].

Keeping in view the potent health benefits of these mango extracts, the present study was designed to evaluate the ability of mango peel extracts (MPE) and mango seed extracts (MSE) to counteract lipotoxicity induced in adipocytes by SLFAs. To this end, we used an in vitro model in which mature 3T3-L1 adipocytes were treated with high doses of PA, resulting in artificially hypertrophied mature adipocytes. In our model, we examined the effect of mango extracts on PA-induced hypertrophy and oxidative stress. Our data provide evidence that MPE and MSE reduced lipid accumulation and exerted anti-oxidant effects by reducing lipogenesis, inducing lipolysis and counteracting ER stress and ROS increase. The activation of the AMPK and Nrf2 pathways seems to suggest that MPE and MSE reduced lipotoxicity induced by PA in adipocytes.

2. Results

2.1. MPE and MSE Reduce PA-Induced Toxicity in 3T3-L1 Adipocytes

The present study aimed at investigating whether peel and seed extracts of mango were capable of reducing lipotoxicity exerted by high doses of PA on differentiated 3T3-L1 adipocytes. The compositions of both MPE and MSE have been previously characterized by HPLC-ESI-MS analysis [35,43]. Data showed that both the extracts are rich in polyphenols with antioxidant properties [35,43]. In particular, methyl digallate, methyl gallate, gallic acid and glucosyl gallate were the main phenolic compounds. A representative picture of the main phenolic compounds of MPE and MSE is shown in Figure 1. Moreover, our previous studies demonstrated that 100 µg/mL of MPE or MSE counteracted the adipocyte differentiation of 3T3-L1 cells [43].

Figure 1. The main phenolic compounds in mango peel and seed extracts. The compositions of MPE and MSE were characterized by HPLC-ESI-MS analysis. Methyl-digallate ester isomer, methyl gallate, gallic acid and glucosyl gallate are the most representative polyphenols in both the extracts.

In this study, we used an in vitro model in which differentiated 3T3-L1 adipocytes were treated with high doses of PA to generate artificially hypertrophied mature adipocytes [44]. Firstly, 3T3-L1 pre-adipocyte cells were differentiated into adipocytes as reported in Section 4

and then treated for 48 h with different doses of PA (100–750 µM) to evaluate their effect on cell viability, in accordance with other authors [45]. Data obtained by MTT assay demonstrated that PA inhibited cell survival in a dose-dependent manner with a reduction of cell viability of 50% with 500 µM PA (Figure 2A). Notably, the addition of 100 µg/mL MPE or MSE increased cell viability by 46% and 77%, respectively, in comparison with PA-treated adipocytes (Figure 2B). Microscope images highlighted that the number of cells was reduced in PA-treated adipocyte cells with respect to adipocytes co-treated with PA and MPE or MSE (Figure 2C). In addition, signs of toxicity were observed after PA treatment alone that disappeared after the addition of mango extracts (Figure 2C). Thus, in the following experiments, 100 µg/mL MPE or MSE was used to investigate the mechanism underlying the protective effects of mango extracts on lipotoxicity induced by 500 µM PA.
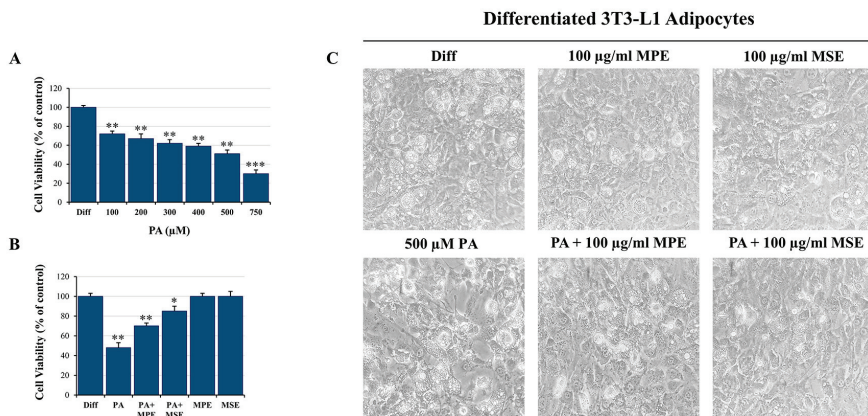
Figure 2. MPE and MSE counteract PA-induced toxicity in 3T3-L1 adipocytes. Differentiated 3T3-L1 adipocytes were exposed for 48 h to different doses of PA alone or in the presence of 100 µg/mL MPE and MSE. (**A**) MTT assays showing the reduction of cell viability induced in differentiated 3T3-L1 adipocytes by different doses of PA. (**B**) MTT assays showing the ability of 100 µg/mL of MPE or MSE to counteract the cytotoxic effect of 500 µM PA in differentiated 3T3-L1 adipocytes. (**C**) Representative phase contrast microscopy images showing the morphological changes induced by 500 µM PA alone or in the presence of 100 µg/mL MPE or MSE in differentiated 3T3-L1 adipocytes. (**A**,**B**) The values reported are the mean ± SD of three independent experiments. The statistical differences between groups were evaluated using a one-way ANOVA test. * $p < 0.05$, ** $p < 0.01$ and *** $p < 0.001$ were significant with respect to differentiated 3T3-L1 adipocytes treated with only vehicle BSA.

2.2. MPE and MSE Reduce Lipid Accumulation in Adipocytes Exposed to High Doses of PA

Excessive lipid availability has been related to adipose tissue hypertrophy [46]. To examine the anti-lipogenic effect of MPE and MSE, differentiated 3T3-L1 adipocytes were treated for 48 h with 500 µM PA in the absence or presence of 100 µg/mL MPE or MSE. Microscope images highlighted that the treatment of mature 3T3-L1 adipocytes with PA increased the content of lipids, as demonstrated by the presence of larger lipid vacuoles with respect to differentiated control 3T3-L1 adipocytes (Figure 2C). Notably, the content of these vacuoles was markedly reduced by MPE and MSE (Figure 2C). These observations were confirmed by staining the cells with Oil Red O (Figure 3A). In comparison with differentiated control adipocytes, 48 h treatment with 500 µM PA resulted in an increase in lipid droplets (LDs) in adipocytes. The addition of 100 µg/mL MPE or MSE to PA-treated adipocytes lowered lipid accumulation in comparison with PA-treated adipocytes. A modest reduction of LDs was also observed in adipocytes not exposed to PA and treated with the extracts alone (Figure 3A). These data were confirmed by microscopic quantification of the Oil Red O staining area (Figure 3B) as well as by measuring the absorbance of the solubi-

lized Oil Red O at 490 nm (Figure 3C). As shown in Figure 3B,C, the addition of 100 µg/mL MPE or MSE to PA-treated adipocytes reduced both the staining area and the absorbance of the stained cells by about 30% and 47%, respectively in comparison with PA-treated adipocytes alone. Such a reduction in lipid accumulation was also sustained by measuring the TAG content (Figure 3D). The results showed that the intracellular TAG accumulation increased in PA-treated cells by 80% with respect to untreated differentiated adipocytes. Interestingly, the addition of MPE or MSE to PA-treated cells significantly decreased the TAG content by 23% and 34%, respectively compared with PA-treated adipocytes (Figure 3D).
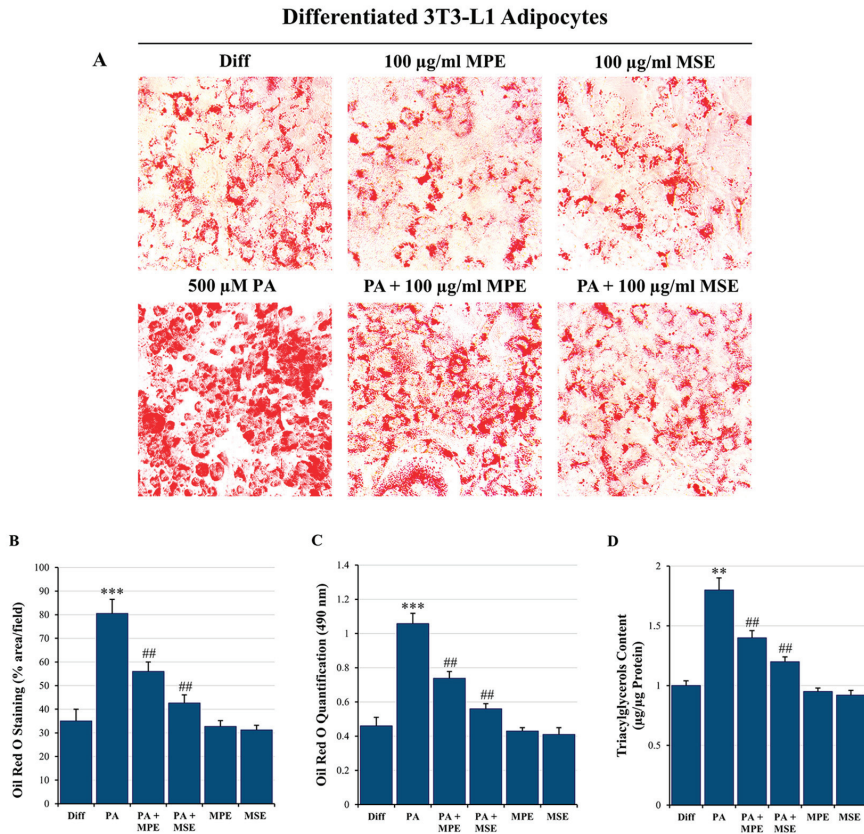
Figure 3. MPE and MSE reduce 3T3-L1 adipocyte hypertrophy induced by high concentrations of PA. 3T3-L1 differentiated adipocytes were treated for 48 h with 500 µM PA alone or in the presence of 100 µg/mL MPE or MSE. (**A**) Representative Oil red O staining microscopy images showing the increase in LDs after treatment with 500 µM PA alone and their reduction when 100 µg/mL MPE or MSE was added (200× original magnification). (**B**) LD content was ascertained by analyzing the percentage area of Oil Red O stained by ImageJ. (**C**) Quantitative Oil red O staining was measured by a spectrophotometer at 490 nm. (**D**) Cellular TAG content was quantified by spectrophotometer at 546 nm. The results are the mean of three independent experiments ± SD. The statistical differences between groups were evaluated using a one-way ANOVA test. ** $p < 0.01$ and *** $p < 0.001$ were significant with respect to differentiated 3T3-L1 adipocytes and ## $p < 0.01$ with respect to PA-treated 3T3-L1 adipocytes.

2.3. MPE and MSE Inhibit PPARγ and Activate AMPK

To investigate the molecular basis for the anti-obesity effect of MPE and MSE, we first evaluated whether mango extracts are capable of reducing the level of PPARγ, the

master regulator of adipogenesis [47]. Our data supported the conclusion that PPARγ signaling sustained PA-induced hypertrophy in adipocytes. In fact, we observed an increase of 50% of PPARγ levels in adipocytes treated for 48 h with 500 μM PA, with respect to untreated adipocytes (Figure 4). A concomitant increase in the perilipin-2 levels (80%), a lipid droplet coating protein [48], was observed in PA-treated adipocytes (Figure 4). Notably, the addition of MPE or MSE to PA-treated adipocytes reduced the increase in PPARγ to only 18% and 23%, respectively as well as that in perilipin-2 to only 15% and 30%, respectively, in comparison with PA-treated adipocytes (Figure 4).
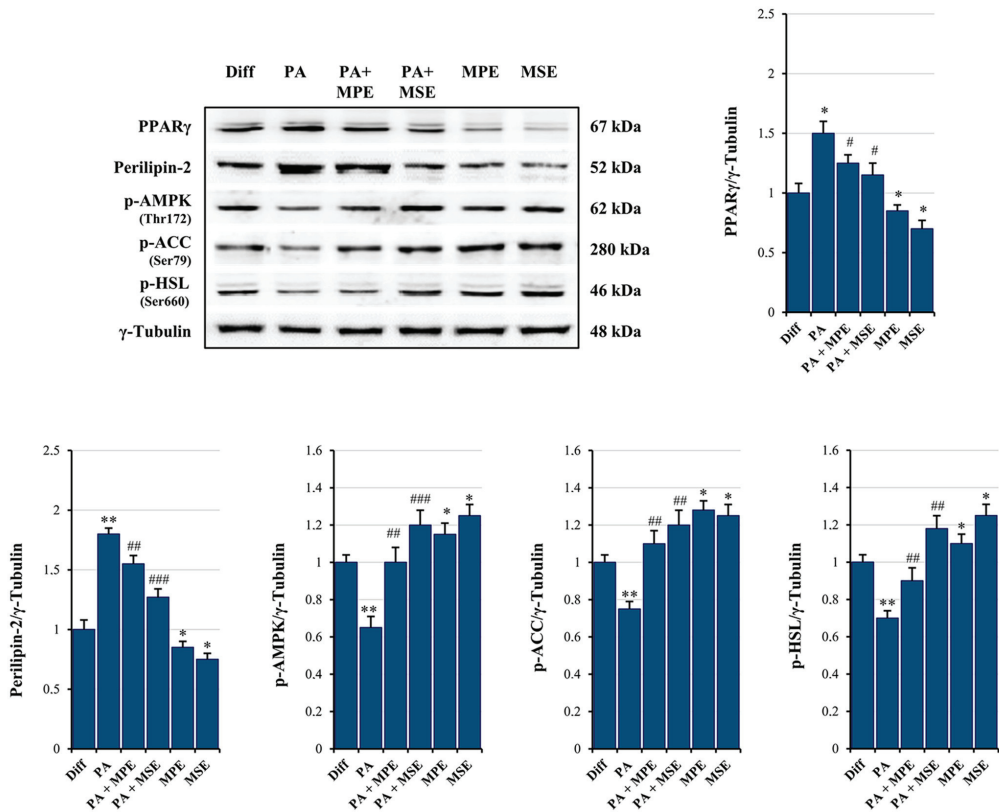
Figure 4. MPE and MSE reduce lipid accumulation, preventing lipogenesis and promoting lipolysis. Differentiated 3T3-L1 adipocytes were treated with 500 μM PA for 48 h in the presence or absence of 100 μg/mL MPE or MSE, as reported in Section 4. Then, cell lysates were analyzed by Western blotting using specific primary antibodies directed against PPARγ, Perilipin-2, phosphorylated AMPK (p-AMPK), phosphorylated ACC (p-ACC) and phosphorylated HSL (p-HSL). Equal amounts of proteins were loaded in each lane (30 μg) as normalized by γ-Tubulin detection. The bar graphs represent the means of three independent experiments ±SD. The statistical differences between groups were evaluated using a one-way ANOVA test. * $p < 0.05$, ** $p < 0.01$ were significant with respect to differentiated 3T3-L1 adipocytes. # $p < 0.05$, ## $p < 0.01$, ### $p < 0.001$ were significant with respect to PA-treated differentiated 3T3-L1 adipocytes.

Next, we examined whether MPE and MSE affects AMPK activation, a kinase promoting catabolic pathways in adipocytes [49]. As shown in Figure 4, the expression of the phosphorylated and active form of AMPK lowered in PA-treated differentiated 3T3-L1 adipocytes compared with control adipocytes. Interestingly, MPE or MSE alone and in

the presence of PA significantly enhanced the phosphorylated form of AMPK (p-AMPK) (Figure 4). This is in line with our previous study demonstrating that MPE and MSE activate AMPK during adipocyte differentiation [43]. Moreover, the addition of MPE or MSE in control adipocytes as well as in PA-treated adipocytes increased the levels of the phosphorylated and inactive form of acetyl-CoA-carboxylase (p-ACC) (Figure 4), the key enzyme of fatty acid synthesis, which is inactivated by phosphorylation by AMPK [49].

Finally, our data also demonstrated that MPE and MSE markedly increased the phosphorylated and active form of hormone sensitive lipase (p-HSL), the enzyme activating lipolysis in adipocytes [50], by 30% and 65%, respectively (Figure 4).

2.4. MPE and MSE Reduce PA-Induced ER Stress in 3T3-L1 Adipocytes

Elevated levels of FAs, in particular saturated fatty acids (SFAs) such as PA, have been shown to produce ER stress in a number of cell types, including adipocytes [51]. The activation of ER stress, in turn, represents a potential molecular mechanism of lipotoxicity [52]. We thus examined whether high doses of PA induce ER stress in mature adipocytes and the ability of MPE and MSE to counteract it. Interestingly, we observed an increase in ER stress protein markers, evidenced by an up-regulation in the expression of PERK, GRP78 and CHOP, as well as in JNK phosphorylation following the treatment of mature 3T3-L1 adipocytes with 500 μM PA for 48 h (Figure 5). These results suggest that the ER-associated unfolded protein response (UPR) pathway is activated by PA [53]. Notably, the addition of 100 μg/mL MPE or MSE to PA-treated differentiated adipocytes reduced the levels of all ER stress protein markers (Figure 5), thus suggesting the ability of mango extracts to counteract ER stress.
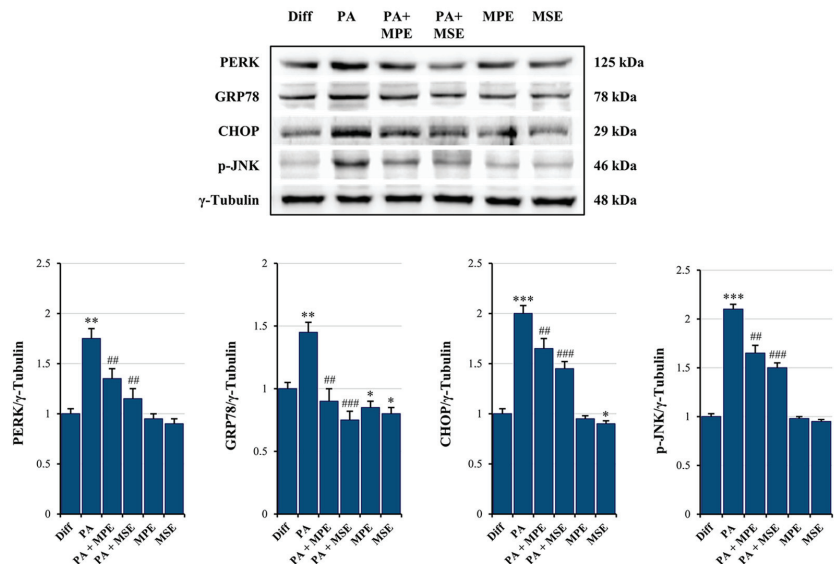
Figure 5. MPE and MSE reduce PA-induced ER stress in 3T3-L1 adipocytes. Differentiated 3T3-L1 adipocytes were treated with 500 μM PA for 48 h in the presence or absence of 100 μg/mL MPE or MSE. Cell lysates underwent Western blotting analysis for ER stress protein markers PERK, GRP78 and CHOP, as well as for phosphorylated JNK (p-JNK). Equal loading of protein (30 μg) was verified by immunoblotting for γ-Tubulin. The bar graphs represent the means of three independent experiments ± SD. The statistical differences between groups were evaluated using a one-way ANOVA test. * $p < 0.05$, ** $p < 0.01$ and *** $p < 0.001$ were significant with respect to differentiated 3T3-L1 adipocytes. ## $p < 0.01$, ### $p < 0.001$ were significant with respect to PA-treated differentiated 3T3-L1 adipocytes.

2.5. MPE and MSE Prevent PA-Induced ROS Production

It has been reported that free FAs generate ROS in different cell types, including adipocytes [19,54]. Thus, to evaluate whether PA increased intracellular ROS production, differentiated 3T3-L1 adipocytes were incubated with H_2DCFDA, a specific fluorescent probe that visualizes intracellular ROS [55]. H_2DCFDA-associated fluorescence was elevated by 65% after incubation with 500 μM PA for 48 h compared with untreated differentiated 3T3-L1 adipocytes (Figure 6A,B). Interestingly, the addition of 100 μg/mL MPE or MSE markedly reduced ROS content to 35% and 23% compared with adipocytes only treated with PA (Figure 6A,B), thus highlighting that mango extracts counteract ROS production and oxidative stress induced in adipocytes after PA treatment.

Differentiated 3T3-L1 Adipocytes
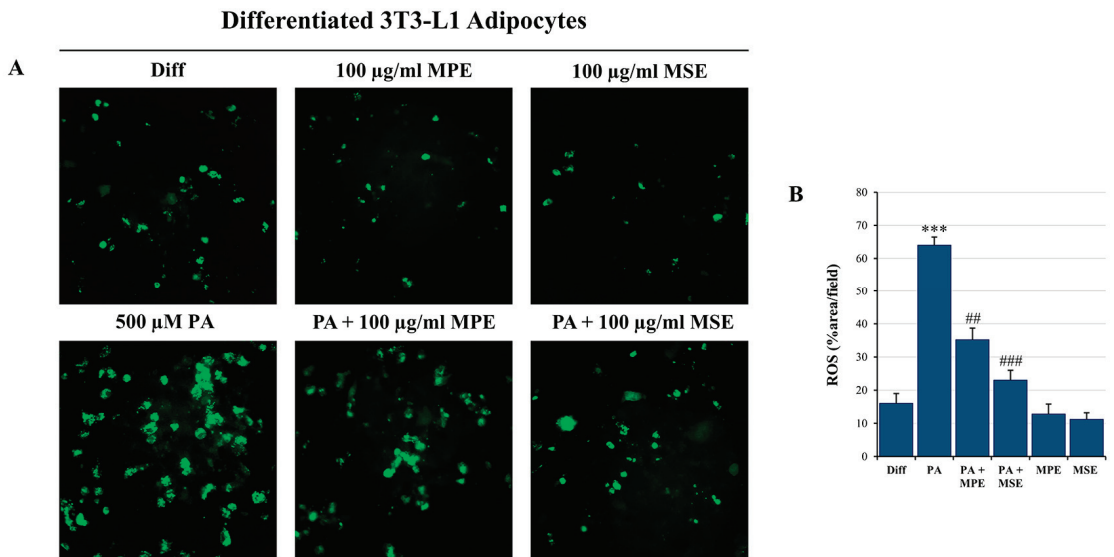
Figure 6. MPE and MSE reduce PA-induced oxidative stress in 3T3-L1 adipocytes, reducing ROS production. Intracellular ROS detection was performed by redox-sensitive fluorochrome H_2DCFDA. Differentiated 3T3-L1 adipocytes were treated with 500 μM PA for 48 h in the presence or absence of 100 μg/mL MPE or MSE, as reported in Section 4. Then, cells were incubated with 10 μM H_2DCFDA solution for 30 min at 37 °C. The oxidation of the fluorochrome-generated green fluorescence was visualized by a Leica microscope equipped with a DC300F camera using a FITC filter. (**A**) Representative images of fluorescence microscopy were taken at 200× magnification. (**B**) ROS content was ascertained by analyzing the percentage area with Image J. *** $p < 0.001$ was significant with respect to differentiated 3T3-L1 adipocytes, and ## $p < 0.01$, ### $p < 0.001$ were significant with respect to PA-treated 3T3-L1 adipocytes.

In addition, propidium iodide (PI) staining of cells confirmed the induction of cytotoxic effects in PA-treated differentiated adipocytes. PA treatment increased cell death by about 35% compared with control adipocyte cells (Figure 7A,B). These effects were counteracted by the addition of 100 μg/mL MPE or MSE that markedly reduced cell death by about 57% and 65%, respectively, with respect to PA-treated adipocytes.
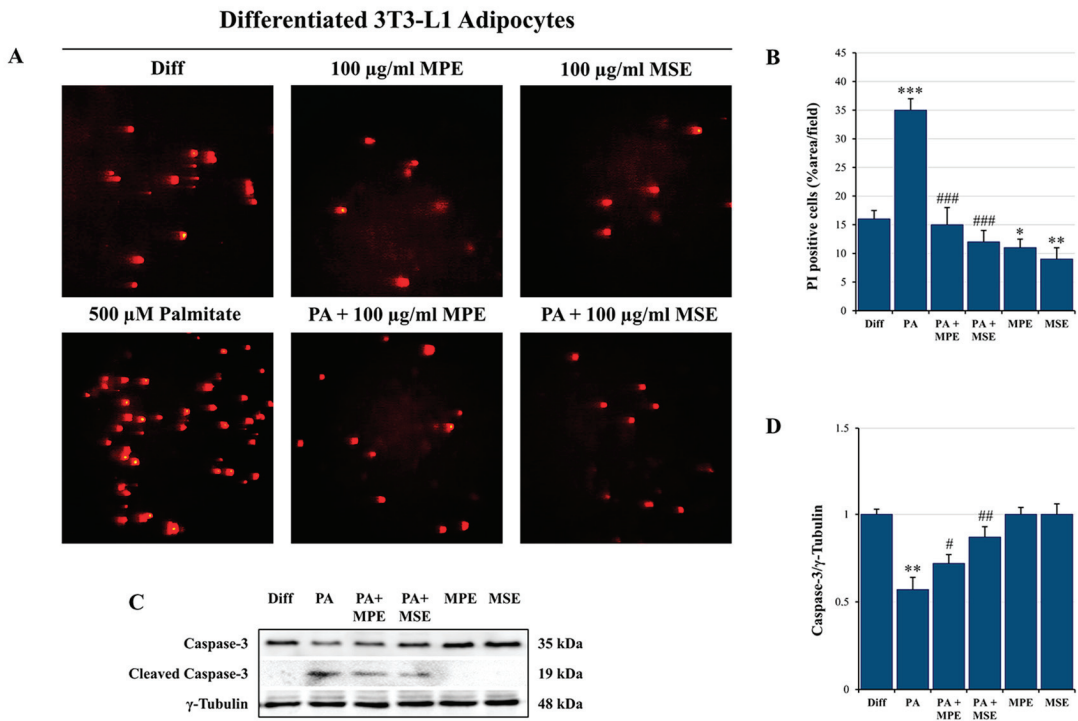
Figure 7. MPE and MSE reduce the cytotoxic effects of PA in 3T3-L1 adipocytes. Propidium iodide (PI) staining of differentiated 3T3-L1 adipocytes treated with 500 μM PA for 48 h in the presence or absence of 100 μg/mL MPE or MSE. (**A**) Representative fluorescence microscopy images were taken at 200× magnification by a Leica microscope equipped with a DC300F camera using a PE filter. (**B**) PI content was ascertained by analyzing the percentage area with Image J. (**C**) Western blotting analysis of the procaspase-3 levels. An equal loading of protein (30 μg) was verified by immunoblotting for γ-Tubulin (**D**). The bar graphs represent the means of three independent experiments ± SD. * $p < 0.05$, ** $p < 0.01$ and *** $p < 0.001$ with respect to differentiated 3T3-L1 adipocytes. # $p < 0.05$, ## $p < 0.01$, ### $p < 0.001$ were significant with respect to PA-treated 3T3-L1 adipocytes.

The cytotoxic effects induced by PA in adipocytes seem to be related to apoptosis induction. Pro-caspase-3 is a master apoptosis protein marker cleaved in active form during this process [56]. PA treatment decreased the level of pro-caspase-3 by 43% (Figure 7C,D) and promoted the appearance of the cleaved active form of caspase-3. Notably, caspase activation was counteracted by the addition of MPE or MSE (Figure 7C,D). Our previous studies provided evidence that MPE and MSE contain factors capable of exerting ROS scavenger effects during 3T3-L1 adipocyte differentiation [43]. These effects have been correlated with the ability of mango extracts to increase Nrf2, the main antioxidant transcription factor [57], during adipocyte differentiation [43]. In accordance with our previous data, we demonstrated that in PA-treated adipocytes, MPE or MSE increased the level of Nrf2 by about 40% and 60%, respectively (Figure 8). Our data also showed that the levels of MnSOD and HO-1, two scavenger enzymes transcriptionally regulated by Nrf2 [57,58], markedly increased after treatment with MPE or MSE. In particular, the increase in MnSOD in the presence of MPE or MSE was estimated to be 46% and 50%, while that of HO-1 was estimated to be 12% and 28%, respectively.
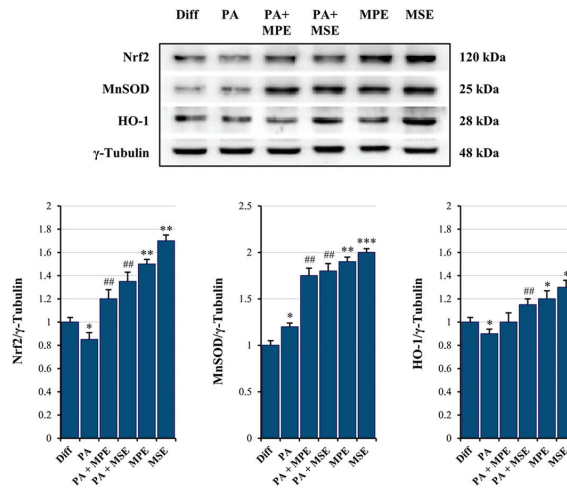
Figure 8. MPE and MSE increase the expression levels of the anti-oxidant molecules. Differentiated 3T3-L1 adipocytes were treated with 500 μM PA for 48 h in the presence or absence of 100 μg/mL MPE or MSE. Cell lysates underwent Western blotting analysis for Nrf2, MnSOD and HO-1. An equal loading (30 μg) of proteins was verified by immunoblotting for γ-Tubulin. The bar graphs represent the means of three independent experiments ±SD. The statistical differences between groups were evaluated using a one-way ANOVA test. * $p < 0.05$, ** $p < 0.01$ and *** $p < 0.001$ were significant with respect to differentiated 3T3-L1 adipocytes. ## $p < 0.01$ was significant with respect to PA-treated differentiated 3T3-L1 adipocytes.

3. Discussion

The current study was designed to investigate whether extracts of mango peel (MPE) and seed (MSE) could ameliorate PA-induced lipotoxicity in adipocytes. Peel and seed are the main bio-waste products of mango processing. In an earlier study, we demonstrated that MPE and MSE have the ability to reduce the number of adipocytes by preventing adipocyte differentiation of 3T3-L1 pre-adipocyte cells [43]. In the present study, we provided evidence that MPE and MSE are also capable of lowering adipocyte hypertrophy induced by high doses of PA, the main saturated long fatty acid present in the diet [59]. Notably, we demonstrated that MPE and MSE reduced PA-induced fat accumulation, as evidenced by the decrease in LD and TAG content in differentiated 3T3-L1 adipocytes co-treated with PA and MPE or MSE.

The ability of MPE and MSE to reduce lipid content in PA-treated adipocytes results from both stimulation of lipolysis and inhibition of lipogenesis. PPARγ is a transcription factor that has been reported to play a critical role in adipocyte hypertrophy under high fat diets [60]. We provided evidence that the PPARγ level increased under PA-treatment in differentiated 3T3-L1 adipocytes. Notably, this effect was markedly counteracted by the addition of MPE or MSE to PA-treated adipocytes. These results are in line with our previous data demonstrating that MPE and MSE counteract 3T3-L1 adipocyte differentiation by reducing the level of PPARγ and its target FABP4 [43].

Furthermore, our data showed that MPE and MSE significantly enhanced the phosphorylation of AMPK and its substrate acetil-CoA carboxylase (ACC) in both controls and PA-treated adipocytes, thus suggesting a role of AMPK activation in reducing lipogenesis induced by MPE and MSE. AMPK is an important regulator of lipid metabolism [61]. Activation of AMPK by phosphorylation increases lipolysis and fatty acid oxidation, while inhibiting lipogenesis [62]. AMPK inactivates by phosphorylation ACC, the key enzyme of fatty acid synthesis [63], leading to the reduction of fatty acid synthesis [64]. Different phenolic compounds contained in plants and fruits, such as quercetin, curcumin, resveratrol

and gallic acid, exert anti-obesity effects by activating AMPK [61]. We previously character-ized the composition of peel and seed extracts of Sicilian mango fruits by HPLC/MS and demonstrated the presence of different polyphenols, among which methyl digallate and methyl gallate are the most represented components [34,43]. These compounds could be responsible for the anti-lipogenic effects of the mango extracts. In line with this conclusion, Fang et al. [65] demonstrated that gallotannin derivatives from mango counteract adipogen-esis by activating AMPK. In addition, Lu, et al. showed that gallic acid reduced lipogenesis and improved liver steatosis by activating AMPK [66]. This effect could result by a direct interaction of gallic acid with AMPKα/β subunits, as evidenced by computational docking analysis [66]. Finally, mangiferin, a polyphenol derived from *Mangifera indica* promotes browning of adipocytes by activating AMPK [67].

In this study, we also provided evidence that MPE and MSE increased the level of the phosphorylated and active forms of hormone-sensitive lipase (HSL), the key lipase activating lipolysis of TAGs in adipocytes, in PA-treated adipocytes [68]. Different lipolytic agents activate HSL by increasing cAMP levels, with the consequent activation of cAMP-dependent protein kinase (protein kinase A; PKA). This enzyme in turn phosphorylates and activates HSL [69]. MSE and MPE could activate HSL because of their content of polyphenols. In line of this conclusion, it has been shown that different polyphenols are able to increase cAMP by inhibiting phosphodiesterase, the enzyme that degrades cAMP [70,71].

A high content of SLFAs has been associated with lipotoxicity in adipocytes as a consequence of ER stress induction [72]. Notably, when present at a high level, PA is metab-olized into saturated DAG and saturated lysophosphatidylcholine [19]. These PA-derived metabolites accumulate in the ER, causing destructive changes in its structure and the activation of ER stress sensors [19]. In line with these observations, we demonstrated that PA treatment enhanced the ER stress markers GRP78, PERK and CHOP as well as activated JNK by increasing its phosphorylated form in differentiated 3T3-L1 adipocytes. ER stress is a protective cellular mechanism that initiates the unfolded protein response (UPR) to restore cellular homeostasis [73]; however, in severe ER stress, the adaptive response fails and apoptotic cell death is induced [73]. In obese animals, elevated ER stress is present in different organs [74,75]. In this condition, ER stress-induced UPR activates JNK, which in turn promotes apoptosis by inhibiting the mitochondrial respiratory chain and activating caspases [76]. Our data confirmed that PA causes lipotoxicity in differentiated adipocytes, as evidenced by cell viability reduction, increased PI-positive cells and caspase-3 activation. Interestingly, MPE and MSE counteracted PA-induced ER stress by lowering all ER stress markers, GRP78, PERK and CHOP, as well as p-JNK. Concomitantly, mango extracts re-stored cell viability, reduced PI-positive cells and the activation of caspase-3 induced by PA treatment, thus suggesting their protective effects against lipotoxicity induced by high levels of SFAs in adipocytes. Furthermore, we demonstrated that PA treatment increased in 3T3-L1 adipocytes the level of ROS, as evidenced by staining adipocytes with H$_2$DCFDA. This finding is in line with previous reports demonstrating that high levels of fatty acid increase oxidative stress in adipocytes [77]. It has been reported that ceramide and DAG, which are fatty acid-derived lipid metabolites, activate NADPH oxidase (NOX), enhancing the ROS level in adipocytes [78]. In addition, dysfunction of the mitochondrial respiratory chain in obesity can amplify oxidative stress and inflammation [79]. ROS production has been shown to activate JNK, which mediates activation of NF-κB and AP-1 [80] with the consequent enhanced expression of pro-inflammatory cytokines, such as IL-6 and TNFα. Notably, we showed that the production of ROS in PA-treated adipocytes was markedly reduced by the addition of MPE and MSE. This effect could be a consequence of the high content of polyphenols in mango extracts. This is in line with the observation that methyl-gallate, the main component of MPE and MSE, protects the cells against oxidative damage through its ROS scavenger ability [81]. Furthermore, the lowering in ROS content induced by MPE and MSE could be a consequence of the up-regulation of Nrf2 and its transcriptional targets MnSOD and HO-1, two important antioxidant enzymes [34,43]. The

activation of Nrf2, the main transcriptional factor against exogenous and endogenous oxidative stress injury [82,83], has been reported in different dietary polyphenols, including resveratrol, gallic acid and caffeic acid [84]. The mechanisms underlying Nrf2 activation include increased Nrf2 nuclear translocation, inhibition of Keap1-Nrf2 interaction and enhanced Keap1 ubiquitination [84]. Finally, MPE and MSE could reduce ROS levels and oxidative stress in adipocytes by activating AMPK. In line with this hypothesis, the deregulated activity of AMPK has been associated with an inflammatory state in in vivo models of obesity and obese patients [85]. Indeed, the activation of AMPK signaling has been shown to protect against oxidative stress by suppressing NOX [86] and mitochondrial dysfunction [87].

4. Materials and Methods

4.1. MPE and MSE Preparation

Peel and seed extracts were obtained from mango fruits (*Mangifera Indica* L.) cultivated in Sicily (Italy), as reported before [43]. In particular, after washing with distilled water, the peels and seeds of mango fruits were cut and lyophilized (Hetosicc Lyophilizer Heto CD 52-1). Then, an ethanol:PBS 1:1 solution was used in order to solubilize the lyophilized products by keeping them overnight at 37 °C under constant shaking. The final concentration of both the extracts was 75 mg/mL. Then, we centrifuged both the extracts of MPE and MSE at $120 \times g$ for 10 min. The obtained supernatants of MPE and MSE were centrifuged again at $15,500 \times g$ for 10 min and then the extracts (supernatants) were frozen at -20 °C until use. MPE and MSE working solutions were prepared by diluting them to the final concentration in culture medium. The final concentration of ethanol in the extracts showed no toxicity on differentiated 3T3-L1 adipocytes.

4.2. PA Solution Preparation

PA was solubilized in an EtOH 10% solution (25mM) in a heated and stirred water bath at 65 °C for 15 min. Once completely solubilized, a 500 μM working dilution was appropriately prepared in culture medium containing 5% BSA and incubated at 37 °C for 1 h under constant shaking to ensure their conjugation before adding it to differentiated 3T3-L1 adipocytes. Vehicle containing 5% BSA was used as control (differentiated 3T3-L1 adipocytes, Diff).

4.3. Cell Cultures

A mouse 3T3-L1 pre-adipocyte cell line from the American Type Culture Collection (ATCC) was maintained in culture as monolayer in flasks of 75 cm^2, at 37 °C and in a 5% CO_2 humidified incubator in DMEM (Euroclone, Pero, Italy), supplemented with 10% (v/v) heat-inactivated fetal bovine serum (FBS; Euroclone, Pero, Italy), 2 mM L-glutamine (BioWest SAS, Nuaillé, France), 100 U/mL penicillin and 50 μg/mL streptomycin (Euroclone, Pero, Italy). Once 80% of confluence was reached, 3T3-L1 pre-adipocytes were detached from the flasks using trypsin-EDTA (0.5 mg/mL trypsin and 0.2 mg/mL EDTA) and seeded according to the experimental conditions. All compounds and reagents used for our experiments, unless otherwise stated, were purchased from Sigma-Aldrich (Milan, Italy).

4.4. Adipocyte Differentiation, Reagents and Treatments

Differentiated 3T3-L1 adipocytes were obtained from 3T3-L1 pre-adipocyte cells (undifferentiated cells) as previously reported [43]. In particular, 3T3-L1 cells were seeded at 0.2×10^5/well in 24-well plates or 0.8×10^5/well in 6-well plates and kept until the confluence was reached. Then, after two days post-confluence, undifferentiated cells were incubated with a differentiation culture medium constituted by DMEM supplemented with 10% (v/v) heat-inactivated FBS, 2 mM L-glutamine, 1% Non-Essential Amino Acids, 100 U/mL penicillin and 50 μg/mL streptomycin, containing the pro-differentiative agents 0.5 mM 3-isobutyl-1-methylxanthine (IBMX), 1 μM dexamethasone and 10 μg/mL insulin. After another three days, the differentiation medium was removed and maintenance cul-

ture medium (DMEM supplemented with 10% (*v/v*) heat-inactivated fetal bovine serum, 2 mM L-glutamine, 1% Non-Essential Amino Acids 100 U/mL penicillin and 50 µg/mL streptomycin containing 10 µg/mL insulin) was added and left for 5 days. Complete differentiation was reached at day 8 when the cells showed typical features of mature adipocytes, such as LD formation and TAG accumulation. PA alone or in the presence of 100 µg/mL MPE or MSE was added to differentiated 3T3-L1 adipocytes and kept for 48 h.

4.5. Cell Viability Assessment

Cell viability was evaluated by measuring mitochondrial dehydrogenase activity using 3-(4,5-dimethylthiazol-2-yl)-2,5-diphenyltetrazolium bromide (MTT), as reported before [88]. For the cell viability assay, undifferentiated 3T3-L1 cells were seeded in 96-well plates (8×10^3 cells/well) until complete differentiation. Then, differentiated 3T3-L1 adipocyte cells were exposed to different concentrations of PA alone or in the presence of 100 µg/mL MPE or MSE for 48 h. Then, 20 µL of MTT reagent (11 mg/mL diluted in PBS) was added to each well and incubated for another 2 hours at 37 °C. The colored crystals of the formazan produced by viable cells were dissolved by adding 100 µL of lysis buffer containing 20% sodium dodecyl sulphate in 50% N,N-dimethylformamide, pH 4.0 and the absorbance was measured by a microplate reader (OPSYS MR, Dynex Technologies, Chantilly, VA, USA) at 540 nm with a reference wavelength of 630 nm. Cell viability was measured as the percentage of the optical density (OD) values found in treated cells compared with those found in untreated cells as control.

The cytotoxic effects of PA on differentiated 3T3-L1 adipocyte cells were also evaluated by propidium iodide (PI) staining. Differentiated cells were treated with 500 µM PA alone or together with 100 µg/mL MSE or MPE. After 48 h of treatment, cells were washed and stained with PI. After a short incubation at the dark, the fluorochrome in excess was removed and the cells were analyzed by fluorescence microscopy using excitation and emission wavelengths appropriate for PI fluorescence (λex = 488 nm and λem = 610/620nm).

4.6. Oil Red O Staining of Treated Mature 3T3-L1 Adipocytes

Oil Red O staining (Sigma-Aldrich, St. Luois, MO, USA) was performed for evaluating LD accumulation. Oil Red O stock solution was prepared by solubilizing 0.35 gr in 100 mL isopropanol 100%. Once differentiated in a 24-well plate, differentiated 3T3-L1 adipocytes were fixed by incubation in 10% formaldehyde for 30 min, washed with PBS and rinsed with 60% isopropanol for 5 min until they were completely dry. Fixed cells were then stained with Oil Red O working solution (3:2, stock solution—dH$_2$O) for 10 min and then washed with dH$_2$O several times. Red pixel areas, stained by Oil Red O, detecting LDs, were divided by the total area scanned. The whole bottom surface of a single well from a 24-well plate was analyzed for the establishment of LD production. A Leica DM-IRB microscope was used and pictures were taken by a Leica DC300F digital camera with a Leica IM50 software, as representative images of the experimental conditions. The pictures were analyzed in ImageJ, converted into high-contrast black and white images to visualize LDs and scored as the percentage area per field. Finally, Oil Red O quantification was performed by measuring its absorbance at 490 nm after extraction of the dye by 100% isopropanol for 10 min. The percentages of the OD values found in treated cells were compared with those found in untreated differentiated 3T3-L1 cells as control.

4.7. ROS Detection

ROS production was detected through the oxidation of the cell-permeant 2′,7′-dichloro dihydrofluorescein diacetate (H$_2$DCFDA) (Molecular Probe, Life Technologies, Eugene, OR, USA) dye, as reported before [89]. Differentiated 3T3-L1 adipocytes were treated with 500 µM PA in absence or presence of 100 µg/mL MPE or MSE for 48 h. Then, the cells were washed in PBS and incubated with 10 µM H$_2$DCFDA dye for 30 min in the dark and in the presence of 5% CO$_2$ at 37 °C. At the end of incubation, the fluorochrome in excess was

removed washing in PBS and the fluorescent 2′,7′-dichlorofluorescein (DCF), produced by intracellular oxidation, was analyzed by fluorescence microscopy using excitation and emission wavelengths appropriate for green fluorescence (FITC filter with λex = 485 nm and λem = 530 nm).

4.8. TAGs Evaluation

Differentiated 3T3-L1 adipocytes were treated with 500 μM PA in absence or presence of 100 μg/mL MPE or MSE for 48 h. Then, the cells were lysed with 5% NP-40 and the number of TAGs in the supernatants was quantified by a spectrophotometric commercial kit for triglyceride determination (SENTINEL C H. SpA, Milan, Italy) [43]. A standard curve with different TAG concentrations, normalized to total cellular protein content measured by Bradford assay, was used for quantifying the samples' TGA concentrations.

4.9. Western Blot Procedures

Protein levels were detected by western blotting analysis. Differentiated and treated cells were lysed as reported before [90]. Bradford Protein Assay was used to quantify protein concentration (Bio-Rad Laboratories S.r.l., Segrate, Milan, Italy). Afterwards, the same number of proteins (30 μg/sample) was loaded and underwent sodium dodecyl sulfate (SDS)-polyacrylamide gel electrophoresis (PAGE). Finally, gels were blotted onto a nitrocellulose membrane (Bio-Rad).

Immunodetection was then performed, incubating the filters with specific primary antibodies against PERK (ab65142) purchased from Abcam (Cambridge, UK), namely, GRP78 (sc-166490), phosphorylated-JNK (sc-6254), CHOP (sc-793), PPARγ (sc-7273), MnSOD (sc-133254) and caspase-3 (sc-65487), all purchased from Santa Cruz Biotechnology (Santa Cruz, CA, USA). Phosphorylated-ACC (#07-303) was purchased from EMD Millipore Corporation (Temecula, 40 CA, USA), phosphorylated-AMPKα (#2535) and phosphorylated-HSL (#4126) were purchased from Cell Signaling (Danvers, MA, USA); Nrf2 (NBP1-32822) and Perilipin-2 (NB110-40877SS) was purchased from Novus Biologicals (Bio-Techne SRL, Milan, Italy); additionally, HO-1, Heme Oxygenase 1 (orb5455) was purchased from Biorbyt Ltd. (Cambridge, UKi). Immunoreactive signals, developed through HPR-conjugated secondary antibodies (Amersham, GE Healthcare Life Science, Milan, Italy), were detected using enhanced chemiluminescence (ECL) reagents (Cyanagen, Bologna, Italy) and obtained with ChemiDoc XRS (Bio-Rad, Hercules, CA, USA).

A quantification of the signal was performed by Quantity One 1-D Analysis software (Bio-Rad) and γ-Tubulin (T3559; Sigma-Aldrich) was used for loading normalization.

4.10. Statistical Analysis

All the experiments and their determinations were performed in triplicate. Data were represented as mean ± S.D and the statistical significance was provided. Data analysis was performed using the GraphPadPrismTM 4.0 software (Graph PadPrismTM Software Inc., San Diego, CA, USA). The differences between groups were evaluated using Tukey's test following one-way ANOVA test. A p-value < 0.05 was considered the threshold for statistical significance. When not specified, the data were not significant with respect to the related control.

5. Conclusions

In conclusion, the present study demonstrated that MPE and MSE protect against PA-induced lipotoxicity in differentiated 3T3-L1 adipocytes by reducing lipid content and oxidative stress. These anti-obesity effects of MPE and MSE might partly involve the inhibition of lipogenesis, the activation of lipolysis and the induction of antioxidant effects. A representative picture of the anti-lipolytic and anti-oxidative effects of MPE and MSE is reported in Figure 9. In light of the chemical data providing evidence of MSE and MPE composition, we wondered about the putative phytochemicals responsible for the effect observed in 3T3-L1 adipocytes exposed to MPE or MSE treatment. A possible

candidate seems to be methyl gallate. This is a phenolic compound that is the most represented phytochemical in our tested mango extracts. Our hypothesis is also sustained by experimental evidence reported by Roh et al. [91] demonstrating that methyl gallate is able to counteract the lipid accumulation in 3T3-L1 cells and could represent a good candidate as an anti-obesity agent. However, we cannot exclude that the ability of MPE and MSE to counteract PA lipotoxicity, and as hypertrophy and ER stress induced by PA exposure could be ascribed to a combined or synergistic effect among the different phytochemicals identified in mango. To better elucidate this aspect, in our future studies we will test mango phytochemicals as compounds alone and their combinations on 3T3-L1 cells.
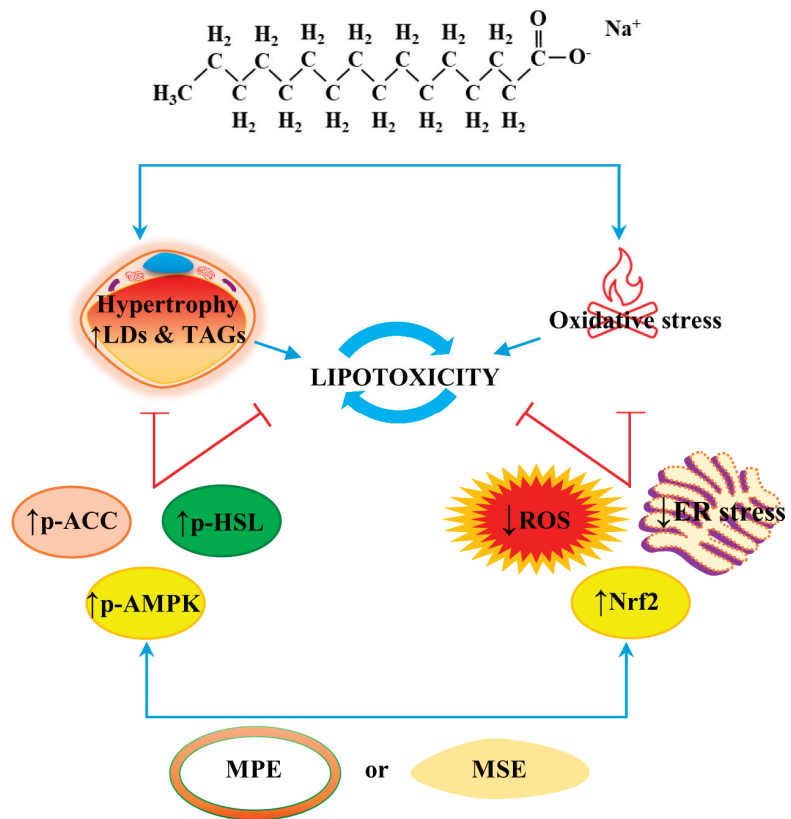
Figure 9. MPE and MSE counteracted lipotoxicity induced by PA in differentiated adipocytes. MPE and MSE lowered fat accumulation induced by high doses of PA in differentiated 3T3-L1 adipocytes, as demonstrated by the reduction of LD and TAG contents. These MPE and MSE anti-lipogenic effects seem to be mediated by the activation of HSL and inhibition of ACC as a result of AMPK activation. MPE and MSE also counteracted PA-induced ER stress and ROS increase in adipocytes. The anti-oxidative effects of MPE and MSE could be ascribed to the activation of the Nrf2/OH-1/MnSOD pathway. Reduced fat content and oxidative stress production could protect the cells from PA-induced cytotoxicity.

Our data offer novel perspectives suggesting that MPE and MSE may be associated with the reduced metabolic dysfunction of adipose tissue induced by high levels of SLFAs. Thus, the development of mango extract-rich foods could be useful to counteract obesity and its consequences.

References

1. Lin, X.; Li, H. Obesity: Epidemiology, Pathophysiology, and Therapeutics. *Front Endocrinol. (Lausanne)* **2021**, *12*, 706978. [CrossRef]
2. Singh, R.K.; Kumar, P.; Mahalingam, K. Molecular genetics of human obesity: A comprehensive review. *C. R. Biol.* **2017**, *340*, 87–108. [CrossRef] [PubMed]
3. Liu, Y.; Douglas, P.S.; Lip, G.Y.H.; Thabane, L.; Li, L.; Ye, Z.; Li, G. Relationship between obesity severity, metabolic status and cardiovascular disease in obese adults. *Eur. J. Clin. Investig.* **2022**, *53*, e13912. [CrossRef] [PubMed]
4. Barnes, A.S. The epidemic of obesity and diabetes: Trends and treatments. *Tex. Heart Inst. J.* **2011**, *38*, 142–144.
5. Sarwar, R.; Pierce, N.; Koppe, S. Obesity and nonalcoholic fatty liver disease: Current perspectives. *Diabetes Metab. Syndr. Obes.* **2018**, *11*, 533–542. [CrossRef]
6. Avgerinos, K.I.; Spyrou, N.; Mantzoros, C.S.; Dalamaga, M. Obesity and cancer risk: Emerging biological mechanisms and perspectives. *Metabolism* **2019**, *92*, 121–135. [CrossRef] [PubMed]
7. Raatz, S.K.; Conrad, Z.; Johnson, L.K.; Picklo, M.J.; Jahns, L. Relationship of the Reported Intakes of Fat and Fatty Acids to Body Weight in US Adults. *Nutrients* **2017**, *9*, 438. [CrossRef]
8. Hu, S.; Wang, L.; Yang, D.; Li, L.; Togo, J.; Wu, Y.; Liu, Q.; Li, B.; Li, M.; Wang, G.; et al. Dietary Fat, but Not Protein or Carbohydrate, Regulates Energy Intake and Causes Adiposity in Mice. *Cell Metab.* **2018**, *28*, 415–431.e4. [CrossRef]
9. Hill, J.O.; Melanson, E.L.; Wyatt, H.T. Dietary fat intake and regulation of energy balance: Implications for obesity. *J. Nutr.* **2000**, *130* (Suppl. S2), 284S–288S. [CrossRef]
10. Palomer, X.; Pizarro-Delgado, J.; Barroso, E.; Vazquez-Carrera, M. Palmitic and Oleic Acid: The Yin and Yang of Fatty Acids in Type 2 Diabetes Mellitus. *Trends Endocrinol. Metab.* **2018**, *29*, 178–190. [CrossRef]
11. Ibrahim, K.S.; El-Sayed, E.M. Dietary conjugated linoleic acid and medium-chain triglycerides for obesity management. *J. Biosci.* **2021**, *46*, 12. [CrossRef]
12. DiNicolantonio, J.J.; O'Keefe, J.H. Good Fats versus Bad Fats: A Comparison of Fatty Acids in the Promotion of Insulin Resistance, Inflammation, and Obesity. *Mo Med.* **2017**, *114*, 303–307.
13. Calder, P.C. Fatty acids and inflammation: The cutting edge between food and pharma. *Eur. J. Pharmacol.* **2011**, *668* (Suppl. S1), S50–S58. [CrossRef]
14. Russo, S.; Kwiatkowski, M.; Govorukhina, N.; Bischoff, R.; Melgert, B.N. Meta-Inflammation and Metabolic Reprogramming of Macrophages in Diabetes and Obesity: The Importance of Metabolites. *Front Immunol.* **2021**, *12*, 746151. [CrossRef] [PubMed]
15. Ishaq, A.; Tchkonia, T.; Kirkland, J.L.; Siervo, M.; Saretzki, G. Palmitate induces DNA damage and senescence in human adipocytes in vitro that can be alleviated by oleic acid but not inorganic nitrate. *Exp. Gerontol.* **2022**, *163*, 111798. [CrossRef] [PubMed]
16. Fritsche, K.L. The science of fatty acids and inflammation. *Adv. Nutr.* **2015**, *6*, 293S–301S. [CrossRef] [PubMed]
17. Engin, A.B. What Is Lipotoxicity? *Adv. Exp. Med. Biol.* **2017**, *960*, 197–220.
18. Ajuwon, K.M.; Spurlock, M.E. Palmitate activates the NF-kappaB transcription factor and induces IL-6 and TNFalpha expression in 3T3-L1 adipocytes. *J. Nutr.* **2005**, *135*, 1841–1846. [CrossRef]
19. Korbecki, J.; Bajdak-Rusinek, K. The effect of palmitic acid on inflammatory response in macrophages: An overview of molecular mechanisms. *Inflamm. Res.* **2019**, *68*, 915–932. [CrossRef]
20. Solinas, G.; Karin, M. JNK1 and IKKbeta: Molecular links between obesity and metabolic dysfunction. *FASEB J.* **2010**, *24*, 2596–2611. [CrossRef] [PubMed]
21. Rani, V.; Deep, G.; Singh, R.K.; Palle, K.; Yadav, U.C. Oxidative stress and metabolic disorders: Pathogenesis and therapeutic strategies. *Life Sci.* **2016**, *148*, 183–193. [CrossRef] [PubMed]

22. Hauck, A.K.; Huang, Y.; Hertzel, A.V.; Bernlohr, D.A. Adipose oxidative stress and protein carbonylation. *J. Biol. Chem.* **2019**, *294*, 1083–1088. [CrossRef]

23. Furukawa, S.; Fujita, T.; Shimabukuro, M.; Iwaki, M.; Yamada, Y.; Nakajima, Y.; Nakayama, O.; Makishima, M.; Matsuda, M.; Shimomura, I. Increased oxidative stress in obesity and its impact on metabolic syndrome. *J. Clin. Investig.* **2004**, *114*, 1752–1761. [CrossRef]

24. Patel, C.; Ghanim, H.; Ravishankar, S.; Sia, C.L.; Viswanathan, P.; Mohanty, P.; Dandona, P. Prolonged reactive oxygen species generation and nuclear factor-kappaB activation after a high-fat, high-carbohydrate meal in the obese. *J. Clin. Endocrinol. Metab.* **2007**, *92*, 4476–4479. [CrossRef] [PubMed]

25. Han, C.Y.; Umemoto, T.; Omer, M.; Den Hartigh, L.J.; Chiba, T.; LeBoeuf, R.; Buller, C.L.; Sweet, I.R.; Pennathur, S.; Abel, E.D.; et al. NADPH oxidase-derived reactive oxygen species increases expression of monocyte chemotactic factor genes in cultured adipocytes. *J. Biol. Chem.* **2012**, *287*, 10379–10393. [CrossRef]

26. Gao, C.L.; Zhu, C.; Zhao, Y.P.; Chen, X.H.; Ji, C.B.; Zhang, C.M.; Zhu, J.G.; Xia, Z.K.; Tong, M.L.; Guo, X.R. Mitochondrial dysfunction is induced by high levels of glucose and free fatty acids in 3T3-L1 adipocytes. *Mol. Cell. Endocrinol.* **2010**, *320*, 25–33. [CrossRef]

27. Bryan, S.; Baregzay, B.; Spicer, D.; Singal, P.K.; Khaper, N. Redox-inflammatory synergy in the metabolic syndrome. *Can. J. Physiol. Pharmacol.* **2013**, *91*, 22–30. [CrossRef] [PubMed]

28. La Russa, D.; Marrone, A.; Mandala, M.; Macirella, R.; Pellegrino, D. Antioxidant/Anti-Inflammatory Effects of Caloric Restriction in an Aged and Obese Rat Model: The Role of Adiponectin. *Biomedicines* **2020**, *8*, 532. [CrossRef]

29. Monda, V.; Polito, R.; Lovino, A.; Finaldi, A.; Valenzano, A.; Nigro, E.; Corso, G.; Sessa, F.; Asmundo, A.; Nunno, N.D.; et al. Short-Term Physiological Effects of a Very Low-Calorie Ketogenic Diet: Effects on Adiponectin Levels and Inflammatory States. *Int. J. Mol. Sci.* **2020**, *21*, 3228. [CrossRef] [PubMed]

30. D'Anneo, A.; Lauricella, M. Natural and Synthetic Compounds for Management, Prevention and Treatment of Obesity. *Int. J. Mol. Sci.* **2022**, *23*, 2890. [CrossRef]

31. De Blasio, A.; D'Anneo, A.; Lauricella, M.; Emanuele, S.; Giuliano, M.; Pratelli, G.; Calvaruso, G.; Carlisi, D. The Beneficial Effects of Essential Oils in Anti-Obesity Treatment. *Int. J. Mol. Sci.* **2021**, *22*, 11832. [CrossRef]

32. Lauricella, M.; Emanuele, S.; Calvaruso, G.; Giuliano, M.; D'Anneo, A. Multifaceted Health Benefits of Mangifera indica L. (Mango): The Inestimable Value of Orchards Recently Planted in Sicilian Rural Areas. *Nutrients* **2017**, *9*, 525. [CrossRef] [PubMed]

33. Lebaka, V.R.; Wee, Y.J.; Ye, W.; Korivi, M. Nutritional Composition and Bioactive Compounds in Three Different Parts of Mango Fruit. *Int. J. Environ. Res. Public Health* **2021**, *18*, 741. [CrossRef] [PubMed]

34. Lo Galbo, V.; Lauricella, M.; Giuliano, M.; Emanuele, S.; Carlisi, D.; Calvaruso, G.; De Blasio, A.; Di Liberto, D.; D'Anneo, A. Redox Imbalance and Mitochondrial Release of Apoptogenic Factors at the Forefront of the Antitumor Action of Mango Peel Extract. *Molecules* **2021**, *26*, 4328. [CrossRef]

35. Lauricella, M.; Lo Galbo, V.; Cernigliaro, C.; Maggio, A.; Palumbo Piccionello, A.; Calvaruso, G.; Carlisi, D.; Emanuele, S.; Giuliano, M.; D'Anneo, A. The Anti-Cancer Effect of Mangifera indica L. Peel Extract is Associated to gammaH2AX-mediated Apoptosis in Colon Cancer Cells. *Antioxidants (Basel)* **2019**, *8*, 422. [CrossRef]

36. Sferrazzo, G.; Palmeri, R.; Restuccia, C.; Parafati, L.; Siracusa, L.; Spampinato, M.; Carota, G.; Distefano, A.; Di Rosa, M.; Tomasello, B.; et al. Mangifera indica L. Leaves as a Potential Food Source of Phenolic Compounds with Biological Activity. *Antioxidants* **2022**, *11*, 1313. [CrossRef]

37. Sferrazzo, G.; Palmeri, R.; Vanella, L.; Parafati, L.; Ronsisvalle, S.; Biondi, A.; Basile, F.; Li Volti, G.; Barbagallo, I. Mangifera indica L. Leaf Extract Induces Adiponectin and Regulates Adipogenesis. *Int. J. Mol. Sci.* **2019**, *20*, 3211. [CrossRef]

38. Gomes Natal, D.I.; de Castro Moreira, M.E.; Soares Miliao, M.; Dos Anjos Benjamin, L.; de Souza Dantas, M.I.; Machado Rocha Ribeiro, S.; Stampini Duarte Martino, H. Uba mango juices intake decreases adiposity and inflammation in high-fat diet-induced obese Wistar rats. *Nutrition* **2016**, *32*, 1011–1018. [CrossRef] [PubMed]

39. Sabater, A.G.; Ribot, J.; Priego, T.; Vazquez, I.; Frank, S.; Palou, A.; Buchwald-Werner, S. Consumption of a Mango Fruit Powder Protects Mice from High-Fat Induced Insulin Resistance and Hepatic Fat Accumulation. *Cell Physiol. Biochem.* **2017**, *42*, 564–578. [CrossRef]

40. Pinneo, S.; O'Mealy, C.; Rosas, M., Jr.; Tsang, M.; Liu, C.; Kern, M.; Hooshmand, S.; Hong, M.Y. Fresh Mango Consumption Promotes Greater Satiety and Improves Postprandial Glucose and Insulin Responses in Healthy Overweight and Obese Adults. *J. Med. Food* **2022**, *25*, 381–388. [CrossRef]

41. Arshad, F.; Umbreen, H.; Aslam, I.; Hameed, A.; Aftab, K.; Al-Qahtani, W.H.; Aslam, N.; Noreen, R. Therapeutic Role of Mango Peels in Management of Dyslipidemia and Oxidative Stress in Obese Females. *Biomed. Res. Int.* **2021**, *2021*, 3094571. [CrossRef] [PubMed]

42. Kim, H.; Castellon-Chicas, M.J.; Arbizu, S.; Talcott, S.T.; Drury, N.L.; Smith, S.; Mertens-Talcott, S.U. Mango (Mangifera indica L.) Polyphenols: Anti-Inflammatory Intestinal Microbial Health Benefits, and Associated Mechanisms of Actions. *Molecules* **2021**, *26*, 2732. [CrossRef] [PubMed]

43. Pratelli, G.; Carlisi, D.; D'Anneo, A.; Maggio, A.; Emanuele, S.; Palumbo Piccionello, A.; Giuliano, M.; De Blasio, A.; Calvaruso, G.; Lauricella, M. Bio-Waste Products of Mangifera indica L. Reduce Adipogenesis and Exert Antioxidant Effects on 3T3-L1 Cells. *Antioxidants* **2022**, *11*, 363. [CrossRef]

44. Baldini, F.; Fabbri, R.; Eberhagen, C.; Voci, A.; Portincasa, P.; Zischka, H.; Vergani, L. Adipocyte hypertrophy parallels alterations of mitochondrial status in a cell model for adipose tissue dysfunction in obesity. *Life Sci.* **2021**, *265*, 118812. [CrossRef]
45. Leroy, C.; Tricot, S.; Lacour, B.; Grynberg, A. Protective effect of eicosapentaenoic acid on palmitate-induced apoptosis in neonatal cardiomyocytes. *Biochim. Biophys. Acta* **2008**, *1781*, 685–693. [CrossRef]
46. Moseti, D.; Regassa, A.; Kim, W.K. Molecular Regulation of Adipogenesis and Potential Anti-Adipogenic Bioactive Molecules. *Int. J. Mol. Sci.* **2016**, *17*, 124. [CrossRef] [PubMed]
47. Ambele, M.A.; Dhanraj, P.; Giles, R.; Pepper, M.S. Adipogenesis: A Complex Interplay of Multiple Molecular Determinants and Pathways. *Int. J. Mol. Sci.* **2020**, *21*, 4283. [CrossRef] [PubMed]
48. Sztalryd, C.; Brasaemle, D.L. The perilipin family of lipid droplet proteins: Gatekeepers of intracellular lipolysis. *Biochim Biophys. Acta Mol. Cell Biol. Lipids* **2017**, *1862 Pt 10*, 1221–1232. [CrossRef] [PubMed]
49. Fullerton, M.D.; Galic, S.; Marcinko, K.; Sikkema, S.; Pulinilkunnil, T.; Chen, Z.P.; O'Neill, H.M.; Ford, R.J.; Palanivel, R.; O'Brien, M.; et al. Single phosphorylation sites in Acc1 and Acc2 regulate lipid homeostasis and the insulin-sensitizing effects of metformin. *Nat. Med.* **2013**, *19*, 1649–1654. [CrossRef] [PubMed]
50. Holm, C. Molecular mechanisms regulating hormone-sensitive lipase and lipolysis. *Biochem. Soc. Trans.* **2003**, *31 Pt 6*, 1120–1124. [CrossRef] [PubMed]
51. Wei, Y.; Wang, D.; Topczewski, F.; Pagliassotti, M.J. Saturated fatty acids induce endoplasmic reticulum stress and apoptosis independently of ceramide in liver cells. *Am. J. Physiol. Endocrinol. Metab.* **2006**, *291*, E275–E281. [CrossRef] [PubMed]
52. Han, J.; Kaufman, R.J. The role of ER stress in lipid metabolism and lipotoxicity. *J. Lipid Res.* **2016**, *57*, 1329–1338. [CrossRef]
53. Ben-Dror, K.; Birk, R. Oleic acid ameliorates palmitic acid-induced ER stress and inflammation markers in naive and cerulein-treated exocrine pancreas cells. *Biosci. Rep.* **2019**, *39*, BSR20190054. [CrossRef]
54. Masschelin, P.M.; Cox, A.R.; Chernis, N.; Hartig, S.M. The Impact of Oxidative Stress on Adipose Tissue Energy Balance. *Front Physiol* **2019**, *10*, 1638. [CrossRef] [PubMed]
55. Kaliuzhka, V.; Tkachenko, A.; Myasoedov, V.; Markevych, M.; Onishchenko, A.; Babalyan, I.; Piatykop, V. The Prognostic Value of Eryptosis Parameters in the Cerebrospinal Fluid for Cerebralvasospasm and Delayed Cerebral Ischemia Formation. *World Neurosurg.* **2023**. [CrossRef]
56. Kivinen, K.; Kallajoki, M.; Taimen, P. Caspase-3 is required in the apoptotic disintegration of the nuclear matrix. *Exp. Cell Res.* **2005**, *311*, 62–73. [CrossRef] [PubMed]
57. Emanuele, S.; Celesia, A.; D'Anneo, A.; Lauricella, M.; Carlisi, D.; De Blasio, A.; Giuliano, M. The Good and Bad of Nrf2: An Update in Cancer and New Perspectives in COVID-19. *Int. J. Mol. Sci.* **2021**, *22*, 7963. [CrossRef]
58. Li, H.; Zhang, Q.; Li, W.; Li, H.; Bao, J.; Yang, C.; Wang, A.; Wei, J.; Chen, S.; Jin, H. Role of Nrf2 in the antioxidation and oxidative stress induced developmental toxicity of honokiol in zebrafish. *Toxicol. Appl. Pharmacol.* **2019**, *373*, 48–61. [CrossRef] [PubMed]
59. Murru, E.; Manca, C.; Carta, G.; Banni, S. Impact of Dietary Palmitic Acid on Lipid Metabolism. *Front Nutr.* **2022**, *9*, 861664. [CrossRef] [PubMed]
60. Guo, F.; Xu, S.; Zhu, Y.; Zheng, X.; Lu, Y.; Tu, J.; He, Y.; Jin, L.; Li, Y. PPARgamma Transcription Deficiency Exacerbates High-Fat Diet-Induced Adipocyte Hypertrophy and Insulin Resistance in Mice. *Front Pharmacol.* **2020**, *11*, 1285. [CrossRef] [PubMed]
61. Marin, T.L.; Gongol, B.; Zhang, F.; Martin, M.; Johnson, D.A.; Xiao, H.; Wang, Y.; Subramaniam, S.; Chien, S.; Shyy, J.Y. AMPK promotes mitochondrial biogenesis and function by phosphorylating the epigenetic factors DNMT1, RBBP7, and HAT1. *Sci. Signal* **2017**, *10*, eaaf7478. [CrossRef]
62. Ahmad, B.; Serpell, C.J.; Fong, I.L.; Wong, E.H. Molecular Mechanisms of Adipogenesis: The Anti-adipogenic Role of AMP-Activated Protein Kinase. *Front Mol. Biosci.* **2020**, *7*, 76. [CrossRef]
63. Cho, Y.S.; Lee, J.I.; Shin, D.; Kim, H.T.; Jung, H.Y.; Lee, T.G.; Kang, L.W.; Ahn, Y.J.; Cho, H.S.; Heo, Y.S. Molecular mechanism for the regulation of human ACC2 through phosphorylation by AMPK. *Biochem. Biophys. Res. Commun.* **2010**, *391*, 187–192. [CrossRef] [PubMed]
64. Galic, S.; Loh, K.; Murray-Segal, L.; Steinberg, G.R.; Andrews, Z.B.; Kemp, B.E. AMPK signaling to acetyl-CoA carboxylase is required for fasting- and cold-induced appetite but not thermogenesis. *eLife* **2018**, *7*, e32656. [CrossRef]
65. Fang, C.; Kim, H.; Noratto, G.; Sun, H.; Talcott, S.T.; Mertens-Talcott, S.U. Gallotannin derivatives from mango (Mangifera indica L.) suppress adipogenesis and increase thermogenesis in 3T3-L1 adipocytes in part through the AMPK pathway. *J. Funct. Foods* **2018**, *46*, 101–109. [CrossRef]
66. Lu, Y.; Zhang, C.; Song, Y.; Chen, L.; Chen, X.; Zheng, G.; Yang, Y.; Cao, P.; Qiu, Z. Gallic acid impairs fructose-driven de novo lipogenesis and ameliorates hepatic steatosis via AMPK-dependent suppression of SREBP-1/ACC/FASN cascade. *Eur. J. Pharmacol.* **2022**, *940*, 175457. [CrossRef]
67. Rahman, M.S.; Kim, Y.S. Mangiferin induces the expression of a thermogenic signature via AMPK signaling during brown-adipocyte differentiation. *Food Chem. Toxicol.* **2020**, *141*, 111415. [CrossRef] [PubMed]
68. Grabner, G.F.; Xie, H.; Schweiger, M.; Zechner, R. Lipolysis: Cellular mechanisms for lipid mobilization from fat stores. *Nat. Metab.* **2021**, *3*, 1445–1465. [CrossRef]
69. Braun, K.; Oeckl, J.; Westermeier, J.; Li, Y.; Klingenspor, M. Non-adrenergic control of lipolysis and thermogenesis in adipose tissues. *J. Exp. Biol.* **2018**, *221* (Suppl. S1), jeb165381. [CrossRef] [PubMed]

70. Rauf, A.; Orhan, I.E.; Ertas, A.; Temel, H.; Hadda, T.B.; Saleem, M.; Raza, M.; Khan, H. Elucidation of Phosphodiesterase-1 Inhibitory Effect of Some Selected Natural Polyphenolics Using In Vitro and In Silico Methods. *Curr. Top. Med. Chem.* **2017**, *17*, 412–417. [CrossRef]

71. Rouse, M.; Younes, A.; Egan, J.M. Resveratrol and curcumin enhance pancreatic beta-cell function by inhibiting phosphodiesterase activity. *J. Endocrinol.* **2014**, *223*, 107–117. [CrossRef]

72. Fernandes-da-Silva, A.; Miranda, C.S.; Santana-Oliveira, D.A.; Oliveira-Cordeiro, B.; Rangel-Azevedo, C.; Silva-Veiga, F.M.; Martins, F.F.; Souza-Mello, V. Endoplasmic reticulum stress as the basis of obesity and metabolic diseases: Focus on adipose tissue, liver, and pancreas. *Eur. J. Nutr.* **2021**, *60*, 2949–2960. [CrossRef]

73. Tabas, I.; Ron, D. Integrating the mechanisms of apoptosis induced by endoplasmic reticulum stress. *Nat. Cell. Biol.* **2011**, *13*, 184–190. [CrossRef]

74. Yilmaz, E. Endoplasmic Reticulum Stress and Obesity. *Adv. Exp. Med. Biol.* **2017**, *960*, 261–276. [PubMed]

75. Kawasaki, N.; Asada, R.; Saito, A.; Kanemoto, S.; Imaizumi, K. Obesity-induced endoplasmic reticulum stress causes chronic inflammation in adipose tissue. *Sci. Rep.* **2012**, *2*, 799. [CrossRef] [PubMed]

76. Win, S.; Than, T.A.; Fernandez-Checa, J.C.; Kaplowitz, N. JNK interaction with Sab mediates ER stress induced inhibition of mitochondrial respiration and cell death. *Cell Death Dis.* **2014**, *5*, e989. [CrossRef] [PubMed]

77. Wang, M.; Chen, Y.; Xiong, Z.; Yu, S.; Zhou, B.; Ling, Y.; Zheng, Z.; Shi, G.; Wu, Y.; Qian, X. Ginsenoside Rb1 inhibits free fatty acids-induced oxidative stress and inflammation in 3T3-L1 adipocytes. *Mol. Med. Rep.* **2017**, *16*, 9165–9172. [CrossRef] [PubMed]

78. Brookheart, R.T.; Michel, C.I.; Schaffer, J.E. As a matter of fat. *Cell Metab.* **2009**, *10*, 9–12. [CrossRef] [PubMed]

79. de Mello, A.H.; Costa, A.B.; Engel, J.D.G.; Rezin, G.T. Mitochondrial dysfunction in obesity. *Life Sci.* **2018**, *192*, 26–32. [CrossRef] [PubMed]

80. Nakano, H.; Nakajima, A.; Sakon-Komazawa, S.; Piao, J.H.; Xue, X.; Okumura, K. Reactive oxygen species mediate crosstalk between NF-kappaB and JNK. *Cell Death Differ.* **2006**, *13*, 730–737. [CrossRef] [PubMed]

81. Crispo, J.A.; Piche, M.; Ansell, D.R.; Eibl, J.K.; Tai, I.T.; Kumar, A.; Ross, G.M.; Tai, T.C. Protective effects of methyl gallate on H2O2-induced apoptosis in PC12 cells. *Biochem. Biophys. Res. Commun.* **2010**, *393*, 773–778. [CrossRef] [PubMed]

82. Ngo, V.; Duennwald, M.L. Nrf2 and Oxidative Stress: A General Overview of Mechanisms and Implications in Human Disease. *Antioxidants* **2022**, *11*, 2345. [CrossRef]

83. Dovinova, I.; Kvandova, M.; Balis, P.; Gresova, L.; Majzunova, M.; Horakova, L.; Chan, J.Y.; Barancik, M. The role of Nrf2 and PPARgamma in the improvement of oxidative stress in hypertension and cardiovascular diseases. *Physiol. Res.* **2020**, *69* (Suppl. S4), S541–S553. [CrossRef]

84. Zhou, Y.; Jiang, Z.; Lu, H.; Xu, Z.; Tong, R.; Shi, J.; Jia, G. Recent Advances of Natural Polyphenols Activators for Keap1-Nrf2 Signaling Pathway. *Chem. Biodivers.* **2019**, *16*, e1900400. [CrossRef]

85. Gauthier, M.S.; O'Brien, E.L.; Bigornia, S.; Mott, M.; Cacicedo, J.M.; Xu, X.J.; Gokce, N.; Apovian, C.; Ruderman, N. Decreased AMP-activated protein kinase activity is associated with increased inflammation in visceral adipose tissue and with whole-body insulin resistance in morbidly obese humans. *Biochem. Biophys. Res. Commun.* **2011**, *404*, 382–387. [CrossRef]

86. Huang, Y.; Zhu, X.; Chen, K.; Lang, H.; Zhang, Y.; Hou, P.; Ran, L.; Zhou, M.; Zheng, J.; Yi, L.; et al. Resveratrol prevents sarcopenic obesity by reversing mitochondrial dysfunction and oxidative stress via the PKA/LKB1/AMPK pathway. *Aging* **2019**, *11*, 2217–2240. [CrossRef]

87. Wang, S.; Zhang, M.; Liang, B.; Xu, J.; Xie, Z.; Liu, C.; Viollet, B.; Yan, D.; Zou, M.H. AMPKalpha2 deletion causes aberrant expression and activation of NAD(P)H oxidase and consequent endothelial dysfunction in vivo: Role of 26S proteasomes. *Circ. Res.* **2010**, *106*, 1117–1128. [CrossRef] [PubMed]

88. Lauricella, M.; D'Anneo, A.; Giuliano, M.; Calvaruso, G.; Emanuele, S.; Vento, R.; Tesoriere, G. Induction of apoptosis in human osteosarcoma Saos-2 cells by the proteasome inhibitor MG132 and the protective effect of pRb. *Cell Death Differ.* **2003**, *10*, 930–932. [CrossRef] [PubMed]

89. Carlisi, D.; D'Anneo, A.; Martinez, R.; Emanuele, S.; Buttitta, G.; Di Fiore, R.; Vento, R.; Tesoriere, G.; Lauricella, M. The oxygen radicals involved in the toxicity induced by parthenolide in MDA-MB-231 cells. *Oncol. Rep.* **2014**, *32*, 167–172. [CrossRef]

90. Lauricella, M.; Carlisi, D.; Giuliano, M.; Calvaruso, G.; Cernigliaro, C.; Vento, R.; D'Anneo, A. The analysis of estrogen receptor-alpha positive breast cancer stem-like cells unveils a high expression of the serpin proteinase inhibitor PI-9: Possible regulatory mechanisms. *Int. J. Oncol.* **2016**, *49*, 352–360. [CrossRef] [PubMed]

91. Roh, C.; Jung, U.; Jo, S.K. Screening of anti-obesity agent from herbal mixtures. *Molecules* **2012**, *17*, 3630–3638. [CrossRef] [PubMed]

Article

Metabolic Syndrome Ameliorated by 4-Methylesculetin by Reducing Hepatic Lipid Accumulation

Linghuan Li [1], Guangyao Zhu [1], Gaohang Fu [1], Weiwei Zha [1] and Hanbing Li [1,2,*]

[1] Institute of Pharmacology, Zhejiang University of Technology, Hangzhou 310014, China
[2] Section of Endocrinology, School of Medicine, Yale University, New Haven, CT 06520, USA
* Correspondence: hanniballee@zjut.edu.cn; Tel.: +86-571-88320535

Abstract: Obesity is a chronic metabolic disease caused by an imbalance between energy intake and expenditure during a long period and is characterized by adipose tissue disfunction and hepatic steatosis. The aim of this study was to investigate the effect of 4-methylesculetin (4-ME), a coumarin derivative, upon adipose microenvironment and hepatic steatosis in mice induced by a high-fat diet (HFD), and to explore potential mechanisms of its beneficial effect on metabolic disorders. HFD-fed mice displayed visceral obesity, insulin resistance, and hepatic lipid accumulation, which was remarkably ameliorated by 4-ME treatment. Meanwhile, 4-ME ameliorated adipocyte hypertrophy, macrophage infiltration, hypoxia, and fibrosis in epididymal adipose tissue, thus improving the adipose tissue microenvironment. Furthermore, 4-ME reversed the increase in CD36, PPAR-γ, SREBP-1, and FASN, and the decrease in CPT-1A, PPAR-α, and Nrf2 translocation into the nucleus in livers of HFD mice and in FFA-incubated hepatocytes. Moreover, the beneficial effects of 4-ME upon lipid deposition and the expression of proteins related to lipid metabolism in FFA-induced LO2 cells were abolished by ML385, a specific Nrf2 inhibitor, indicating that Nrf2 is necessary for 4-ME to reduce hepatic lipid deposition. These findings suggested that 4-ME might be a potential lead compound candidate for preventing obesity and MAFLD.

Keywords: visceral obesity; hepatic steatosis; 4-methylesculetin; adipose microenvironment; metabolic syndrome

1. Introduction

Obesity refers to excessive fat accumulation and ectopic body mass increase, which is a multi-factor chronic metabolic disease [1]. It is not only the proliferation and hypertrophy of adipocytes, but also the apoptosis and necrosis of adipocytes and preadipocytes. Obesity can cause many metabolic diseases, such as diabetes, cardiovascular diseases, fatty liver, and cancer, and a common characteristic of insulin resistance. According to World Health Organization reports, worldwide obesity has nearly tripled since 1975. In 2016, more than 1.9 billion adults 18 years and older were overweight. Of these, over 650 million were obese. Therefore, obesity is a critical public health problem worldwide [2,3].

With deeper knowledge of adipose tissue, it is no longer regarded as an inert energy storage organ. The discovery of leptin and other important adipose-derived hormones makes the new definition of adipose tissue as an endocrine organ, which has been extensively accepted [4]. The abnormality of adipose tissue and its microenvironment is of great significance to the metabolism of other tissues and organs as well as the whole body [5]. Commonly, the fat microenvironment in obese patients changes, causing macrophage infiltration [6]. At the same time, excessive accumulation of fat can lead to inflammation and disorder of adipokine secretion, chronic inflammation, and a hypoxic microenvironment, and ultimately leads to the production of adipose fibrosis [7]. In addition, hypoxia can increase the expression of hypoxia-inducible factor 1α (HIF1α) in adipose tissue, activate the signal pathway related to Transforming Growth Factor β (TGF-β), and promote the

infiltration of immune cells, leading to adipose fibrosis [8]. The interaction of hypoxia, inflammation, and fibrosis in the adipose tissue microenvironment plunges the microenvironment into a vicious circle [9]. When obesity is induced by internal and external factors such as high fat, the microenvironment of adipose tissue deteriorates, which usually causes or aggravates the accumulation of fat in other tissues (such as liver, muscle, etc.), leading to diabetes, fatty liver, and so forth. In obese patients, plasma non-esterified fatty acid (NEFA) levels are usually elevated because of the enhancement of adipose tissue lipolysis. Roughly 60% of triglyceride (TG) arises from the plasma NEFA pool, 30% from de novo lipogenesis, and 10% from the diet in the liver of obese individuals [10]. Furthermore, adipose tissue failure or dysfunction may signal progression of hepatic steatosis toward NASH [11]. Thus, the adipose tissue microenvironment could be targeted for the treatment of obesity and metabolic-associated fatty liver disease (MAFLD).

The coumarin derivative 4-methylesculetin (6,7-dihydroxy-4-methylcoumarin, 4-ME) is isolated from *Artemisia annua* [12]. Coumarins and their derivatives have drawn much attention due to a wide range of bioactivities such as antioxidant [13], antiarthritic, anti-inflammatory properties [14–17], and beneficial effects upon obesity and its related comorbidities as well [18–22]. However, whether 4-ME ameliorates adipose tissue dysfunction and obesity-related insulin resistance remains to be elucidated. The aim of this study was to investigate the effect of 4-ME on the adipose tissue microenvironment and hepatic steatosis induced by a high-fat diet, and to explore potential mechanisms of its beneficial effect upon metabolic disorders, so as to lay a foundation for further research and development.

2. Results

2.1. Effects of 4-ME upon Visceral Obesity and Insulin Resistance in HFD-Fed Mice

To investigate the effects of 4-ME upon obesity and its related metabolic disorders, mice were fed an HFD for 8 weeks and then treated with 15 mg/kg 4-ME, 50 mg/kg 4-ME, or 250 mg/kg metformin. As shown in Table 1, the average body weight was significantly lower in the 50 mg/kg 4-ME group and the metformin group compared with the Model group after the 8-week treatment, as well as epididymal adipose tissue weight manifested by the ratio of epididymal fat/body weight and the Lee Index defined by Lee in 1929 as the cube root of body weight (g) divided by the naso-anal length (cm) [23]. In addition, 4-ME and metformin did not cause changes in food intake (Figure S1).

Table 1. Effects of 4-ME upon physiological parameters in HFD-fed mice.

Groups (n = 8)	Body Weight (g)					Epididymal Fat/Body Weight (mg/g)	The Lee Index
	0 Week	2 Week	4 Week	6 Week	8 Week		
Control	37.1 ± 0.4	36.4 ± 0.3	35.2 ± 0.8	35.5 ± 0.5	34.6 ± 0.97	15.6 ± 1.2	0.301 ± 0.001
Model	48.8 ± 2.0 [###]	49.3 ± 2.3 [###]	49.8 ± 2.9 [###]	51.8 ± 3.1 [###]	52.6 ± 3.1 [###]	46.0 ± 6.8 [###]	0.338 ± 0.003 [###]
15 mg/kg 4-ME	48.8 ± 2.3	48.1 ± 2.0	48.9 ± 2.1	50.3 ± 2.2	49.5 ± 2.5	37.3 ± 2.8	0.331 ± 0.004
50 mg/kg 4-ME	48.6 ± 2.9	48.4 ± 2.6	48.0 ± 2.8	47.0 ± 1.1	45.8 ± 2.3 *	30.7 ± 2.8 *	0.320 ± 0.002 ***
Metformin	49.0 ± 2.0	48.1 ± 1.6	47.9 ± 1.4	46.7 ± 2.2	45.5 ± 1.1 *	29.3 ± 3.1 *	0.326 ± 0.003 *

[###] $p < 0.001$ compared with the Control group; * $p < 0.05$, *** $p < 0.001$ compared with the Model group.

Meanwhile, serum biochemical parameters in mice were determined to assess the effects of 4-ME upon obesity and its related disorders induced by HFD. Mice fed an HFD had increases in serum levels of FBG, insulin, and leptin compared with the Control group, which were reversed by 4-ME, especially 50 mg/kg 4-ME, and metformin (Table 2). Insulin resistance shown as HOMA-IR induced by HFD was significantly ameliorated by 4-ME and metformin. The results are consistent with those of the intraperitoneal glucose tolerance test (IPGTT), which show that the impaired glucose tolerance induced by HFD was improved by 4-ME and metformin (Figure 1A,B).
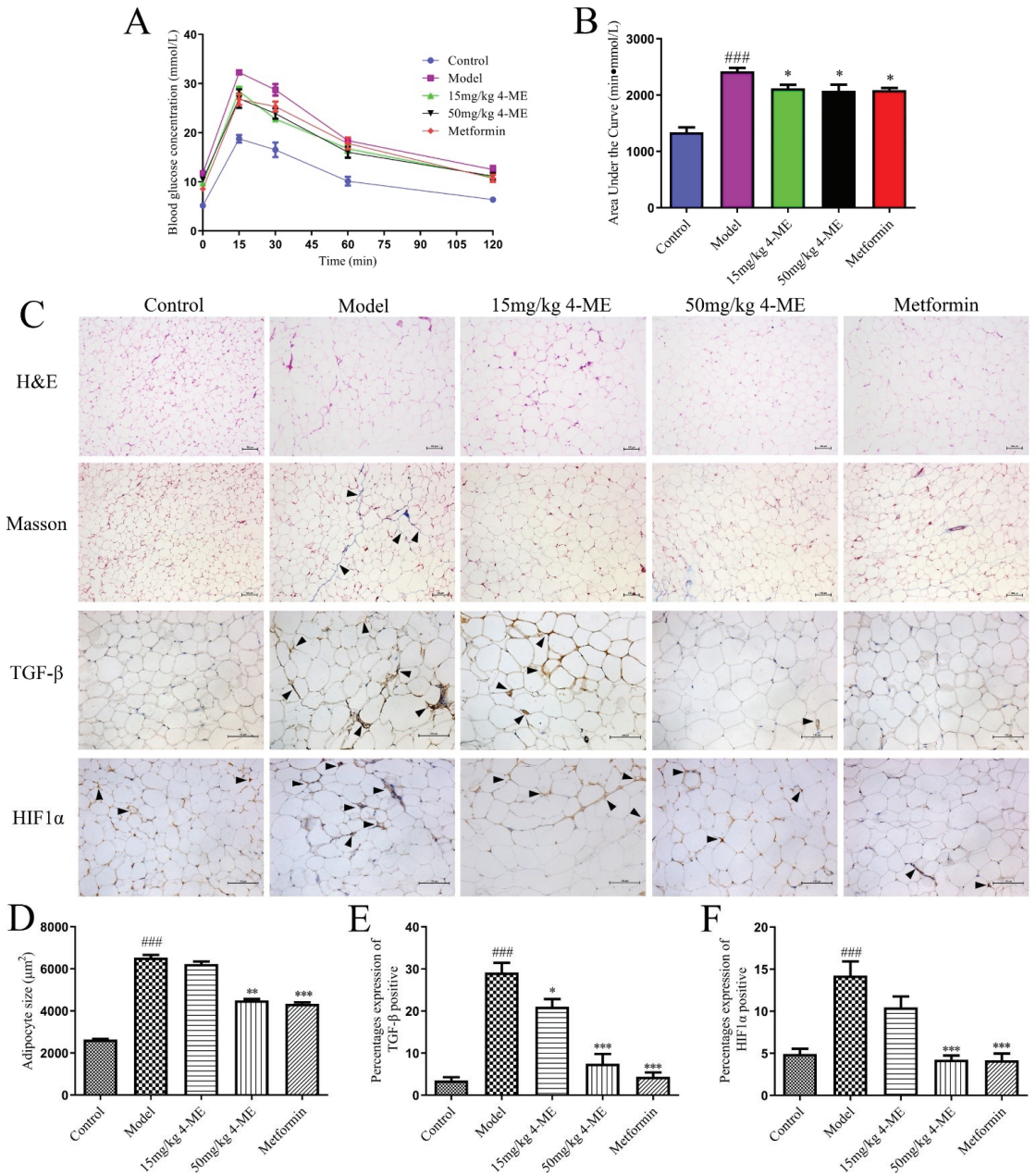
Figure 1. Effects of 4-ME upon intraperitoneal glucose tolerance test (IPGTT) and adipose tissue microenvironment in HFD-fed mice. (**A**) IPGTT (*n* = 5). (**B**) The area under the curve of IPGTT (*n* = 5). (**C**) The rows from the top to the bottom represent H&E staining (original magnification, 100×), Masson staining (100×), and immunostaining of TGF-β antibody (200×) and HIF1α (200×) in adipose tissue sections, respectively. (**D**) The size of adipocytes (*n* = 300). (**E**,**F**) Quantification for the percentage expression of TGF-β and HIF1α protein in panel (*n* = 4). Arrowheads indicate pathological changes. Values were given as mean ± SEM; ### *p* < 0.001 compared with the Control group, * *p* < 0.05, ** *p* < 0.01, *** *p* < 0.001 compared with the Model group.

Table 2. Effects of 4-ME on serum biochemical parameters in HFD-fed mice.

Groups (n = 8)	FBG (mmol/L)	Insulin (mIU/L)	HOMA-IR	Leptin (pg/mL)	HDL-C (mmol/L)	LDL-C (mmol/L)	T-CHO (mmol/L)	TG (mmol/L)	NEFA (μmol/L)
Control	4.9 ± 0.3	4.3 ± 0.3	0.91 ± 0.04	499.4 ± 31.2	1.2 ± 0.1	0.9 ± 0.1	3.7 ± 0.2	0.88 ± 0.03	441.1 ± 23.8
Model	11.7 ± 0.8 ###	6.1 ± 0.3 ###	3.17 ± 0.16 ###	634.5 ± 29.3 ##	0.9 ± 0.1	2.1 ± 0.2 ###	7.0 ± 0.6 ###	1.27 ± 0.12 ##	1023.0 ± 88.6 ###
15 mg/kg 4-ME	9.5 ± 0.5 *	5.8 ± 0.3	2.82 ± 0.34	610.2 ± 29.0	1.0 ± 0.1	2.1 ± 0.1	6.6 ± 0.4	1.25 ± 0.07	797.3 ± 121.1 *
50 mg/kg 4-ME	9.9 ± 0.6 *	5.3 ± 0.2 *	2.35 ± 0.12 **	548.8 ± 25.0 *	1.1 ± 0.2	1.7 ± 0.1	6.4 ± 0.5	1.13 ± 0.08	521.2 ± 18.9 ***
Metformin	8.7 ± 0.5 **	6.8 ± 0.2	2.53 ± 0.13 **	571.7 ± 16.2	1.4 ± 0.2 *	1.2 ± 0.1 **	6.4 ± 0.3	1.18 ± 0.11	655.4 ± 48.8 **

p < 0.01, ### p < 0.001 compared with the Control group; * p < 0.05, ** p < 0.01, *** p < 0.001 compared with the Model group.

2.2. Effects of 4-ME upon Adipose Tissue Microenvironment in HFD-Fed Mice

The adipose tissue hypertrophy and inflammation in HFD-fed mice were investigated by examining adipocyte size and macrophage infiltration in epididymal adipose tissue sections stained with hematoxylin and eosin. Masson's trichrome staining was introduced to measure collagen levels. The hypoxia and fibrosis in epididymal adipose tissue were detected via immunohistochemistry using HIF1α and TGF-β antibodies. As shown in Figure 1C–F, the increased adipocyte size, macrophage infiltration, upregulated collagen level, and HIF1α and TGF-β expression in the epididymal adipose tissue in HFD-fed mice were ameliorated by 4-ME and metformin, indicating the improvement of the adipose tissue hypertrophy, inflammation, hypoxia, and fibrosis.

2.3. Effects of 4-ME upon Lipid Metabolism and Hepatic Steatosis in HFD-Fed Mice

To examine whether 4-ME regulates lipid metabolism, the serum levels of TG, NEFA, T-CHO, LDL-C, and HDL-C were measured in mice fed an HFD for 16 weeks. The HFD increased serum levels of TG, NEFA, T-CHO, and LDL-C compared with the Control group, while 4-ME and metformin decreased all these serum parameters, but only NEFA with statistical significance. In contrast, the HFD downregulated the serum level of HDL-C, while 4-ME and metformin upregulated it, but only metformin had a significant difference (Table 2). These results indicate that 4-ME can alleviate obesity-associated serum lipid metabolic disorders.

Then, the liver tissue sections were stained with H&E and Oil red O, respectively (Figure 2A). Histological observations in both H&E and Oil red O staining show that visible hepatic lipid accumulation in HFD-fed mice was remarkably reduced by 4-ME and metformin. In addition, the HFD-induced increase in hepatic TG accumulation was significantly decreased by high-dose 4-ME treatment (Figure 2B), suggesting that 4-ME prevents hepatic steatosis induced by an HFD.

2.4. Effects of 4-ME on the Expression of Proteins Involved in NEFA Uptake, Lipogenesis, and Fatty Acid β-Oxidation in Livers of HFD-Fed Mice

Furthermore, the expression of proteins related to NEFA uptake, lipogenesis, and fatty acid β-oxidation was analyzed in liver samples of HFD-fed mice. We found that the HFD increased the protein expression of cluster of differentiation 36 (CD36), peroxisome proliferator-activated receptor γ (PPAR-γ), sterol regulatory element-binding protein 1c (SREBP-1c), and fatty acid synthase (FASN), and decreased the expression of peroxisome proliferator-activated receptor α (PPAR-α) and carnitine palmitoyltransferase 1A (CPT-1A) compared with the Control group. Treatment with 4-ME counteracted the expression changes of these proteins, indicating the beneficial effects of 4-ME on lipid metabolism in the livers of HFD-fed mice (Figure 2C–H).
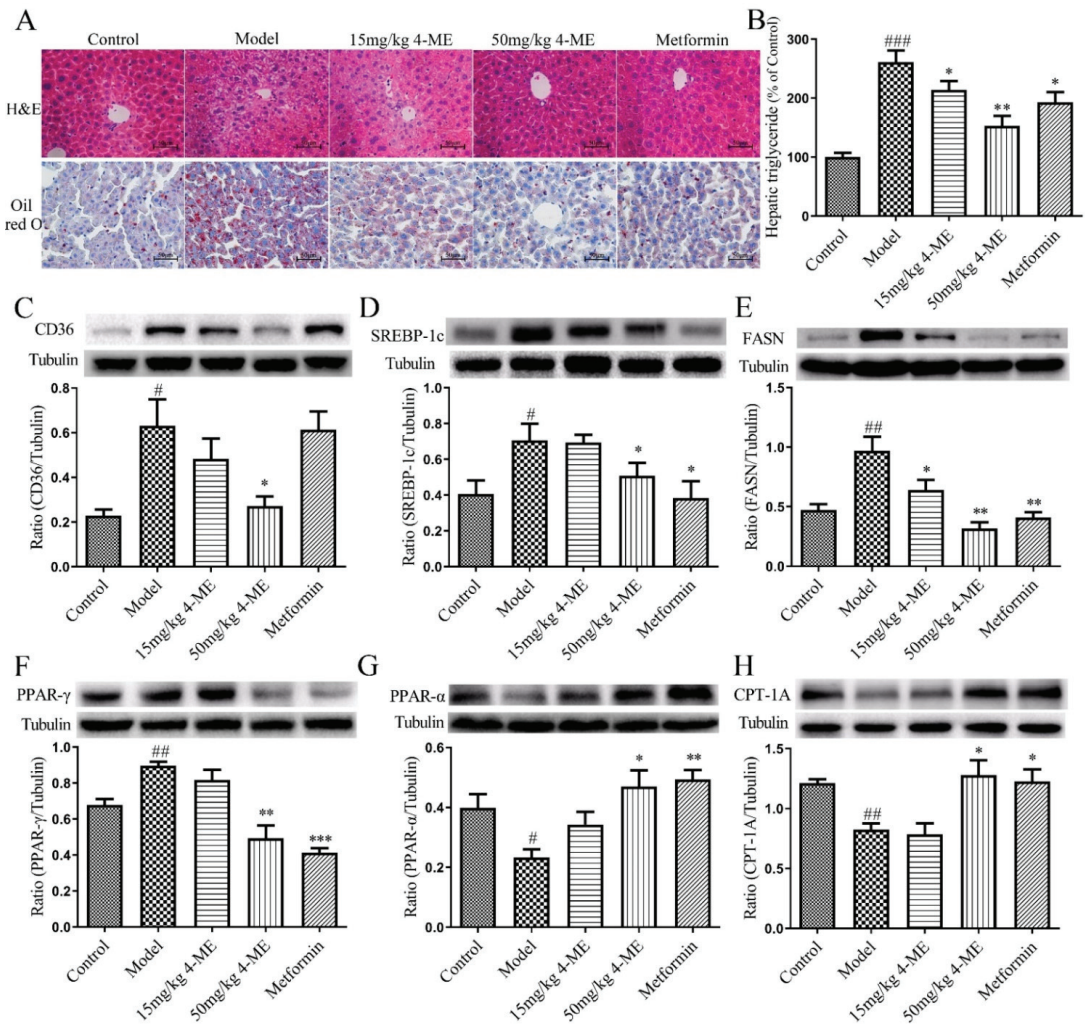
Figure 2. Effects of 4-ME on hepatic steatosis in HFD-fed mice. (**A**) Histological observation of the liver in experimental mice with H&E staining (original magnification, 400×) and Oil red O staining (400×). (**B**) Hepatic TG content (*n* = 8). (**C–H**) Shown are representative immunoblots and densitometric quantification of CD36, SREBP-1c, FASN, PPAR-γ, PPAR-α, and CPT-1A protein expressions (*n* = 3–4). The results were expressed as mean ± SEM; # *p* < 0.05, ## *p* < 0.01, ### *p* < 0.001 compared with the Control group, * *p* < 0.05, ** *p* < 0.01, *** *p* < 0.001 compared with the Model group.

2.5. Effects of 4-ME upon Lipid Deposition in FFA-Incubated LO2 Cells

As shown in Figure 3A, treatment of LO2 cells with different concentrations (1, 3, 10, 30, and 100 μM) of 4-ME had no significant influence on cell viability. Then, the effects of 4-ME upon lipid metabolism in free fatty acid (FFA)-incubated LO2 cells were evaluated using Oil red O staining. In Oil red O staining (Figure 3B), the intracellular lipid droplets were stained red. After the 4-ME treatment, the intracellular lipid droplets decreased in a dose-dependent manner (1, 3, 10, 30, and 100 μM). In addition, metformin inhibited lipid accumulation compared with the FFA group. In addition, 4-ME treatment reduced the content of intracellular TG (Figure 3C). Taken together, these findings uncover that 4-ME

treatment can ameliorate the accumulation of intracellular lipid droplets in FFA-incubated LO2 cells.
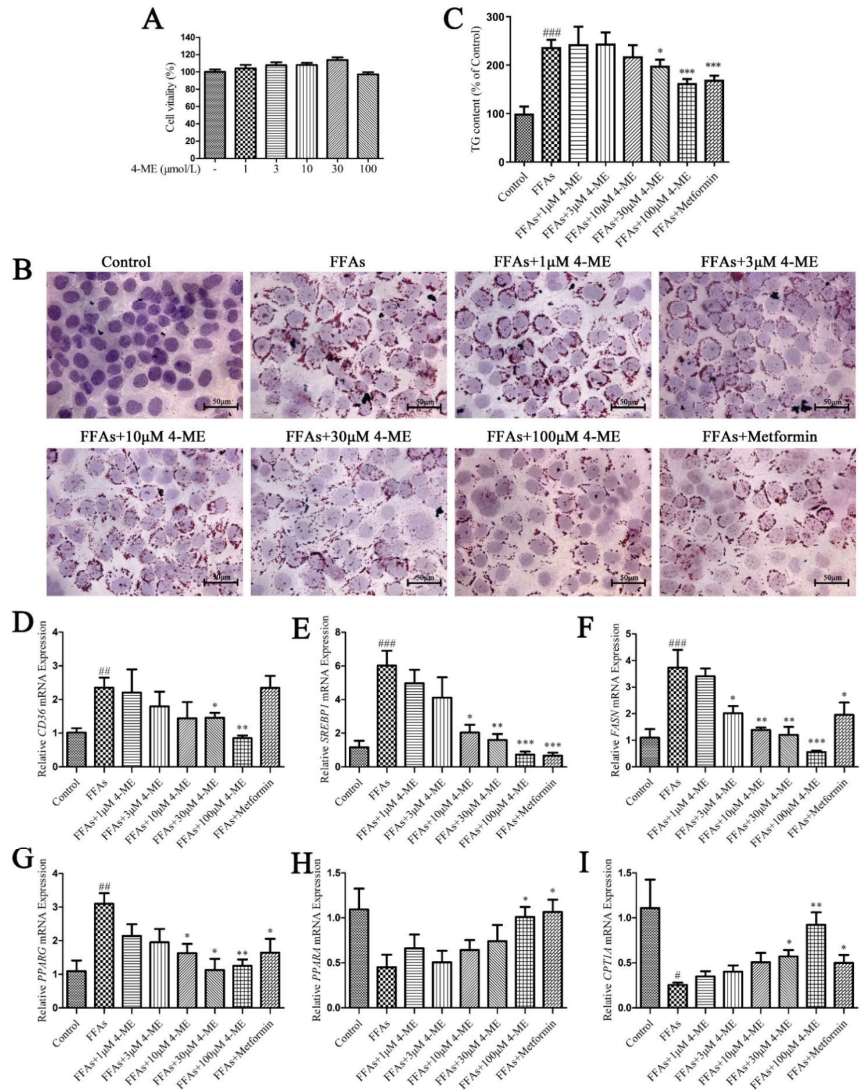
Figure 3. The 4-ME reduced lipid accumulation in FFA-induced LO2 cells. (**A**) Effects of different concentrations of 4-ME on cell viability (*n* = 8). (**B**) Effect of 4-ME on lipid accumulation was visualized using Oil red O staining. (**C**) Quantitative analysis of intracellular TG content (*n* = 6). (**D–I**) Effect of 4-ME on the expression of genes related to lipid metabolism in FFA-incubated LO2 cells (*n* = 3–4). The results were expressed as mean ± SEM; # $p < 0.05$, ## $p < 0.01$, ### $p < 0.001$ compared with the Control group, * $p < 0.05$, ** $p < 0.01$, *** $p < 0.001$ compared with the FFA group.

We next explored the effects of 4-ME on the expression of genes and proteins related to lipid metabolism. We found that the FFA challenge significantly increased the mRNA levels of CD36, FASN, SREBP1, and PPARG in LO2 cells compared with the Control group, whereas these alternations were dramatically abrogated when supplemented with different concentrations of 4-ME (Figure 3D–G). In addition, FFA incubation displayed the downregulation of the mRNA expression levels of PPARA and CPT1A, but 4-ME prevented

the reduction in the mRNA expression of these genes (Figure 3H,I). Consistently, the results of Western blotting presented that an enhancement in protein expression of CD36, SREBP-1c, FASN, and PPAR-γ was reversed by 4-ME administration, and a reduction in protein expression of PPAR-α and CPT-1A was rescued by 4-ME treatment in FFA-incubated LO2 cells (Figure 4). Collectively, these data reveal that 4-ME can ameliorate lipid accumulation through regulating fatty acid uptake, β-oxidation, and lipogenesis in FFA-induced hepatocytes.
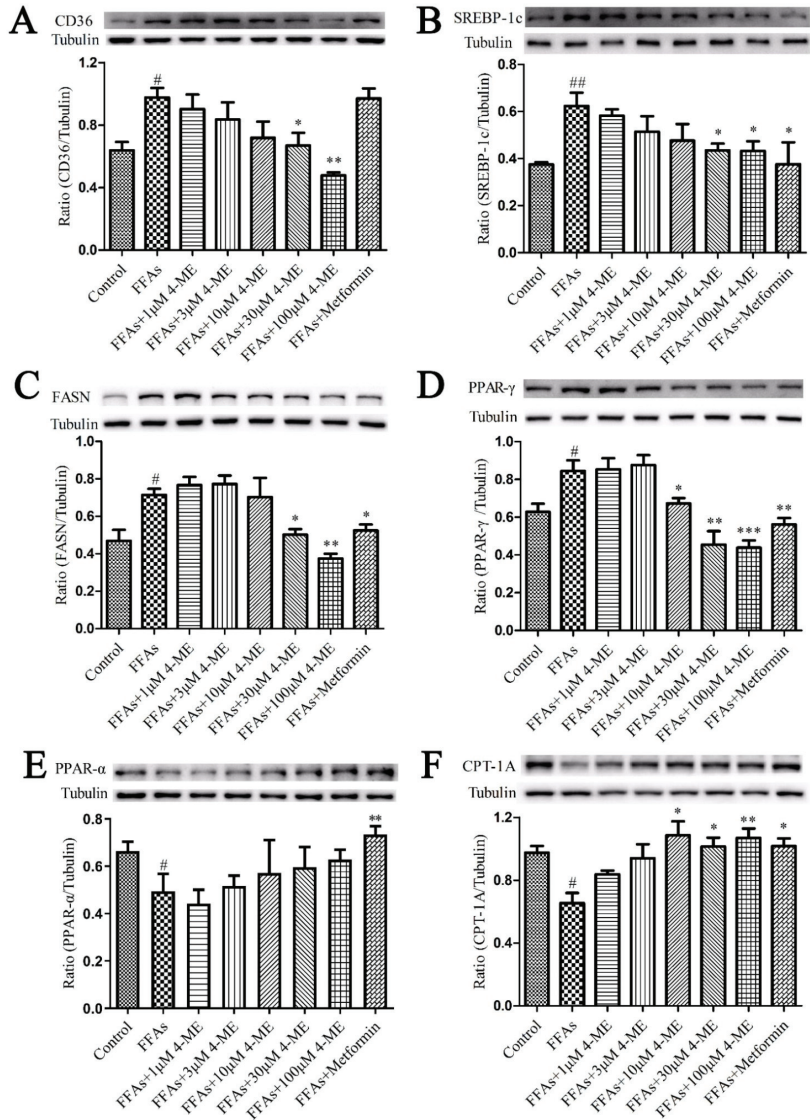
Figure 4. Effects of 4-ME on the expression of proteins involved in lipid metabolism in FFA-induced LO2 cells. Quantification data of CD36 (**A**), SREBP-1c (**B**), FASN (**C**), PPAR-γ (**D**), PPAR-α (**E**), and CPT-1A (**F**) protein expression levels are presented. The results were expressed as mean ± SEM (n = 3–4); [#] $p < 0.05$, [##] $p < 0.01$ compared with the Control group, * $p < 0.05$, ** $p < 0.01$, *** $p < 0.001$ compared with the Model group.

2.6. Nrf2 Is Necessary for 4-ME Reducing Lipid Deposition

Nuclear factor erythroid 2-related factor 2 (Nrf2) is a transcriptional factor that not only regulates a battery of cellular defense elements against oxidative stresses, but also acts as a regulator of cellular lipid configuration in the liver [24]. Western blotting results showed that in the liver of HFD-fed mice, Nrf2 translocation into the nucleus was decreased, while it was enhanced by 4-ME treatment. Meanwhile, in FFA-induced LO2 cells, the protein levels of nuclear Nrf2 were reduced, whereas they were significantly increased by 4-ME in a dose-dependent manner (Figure 5A–D).
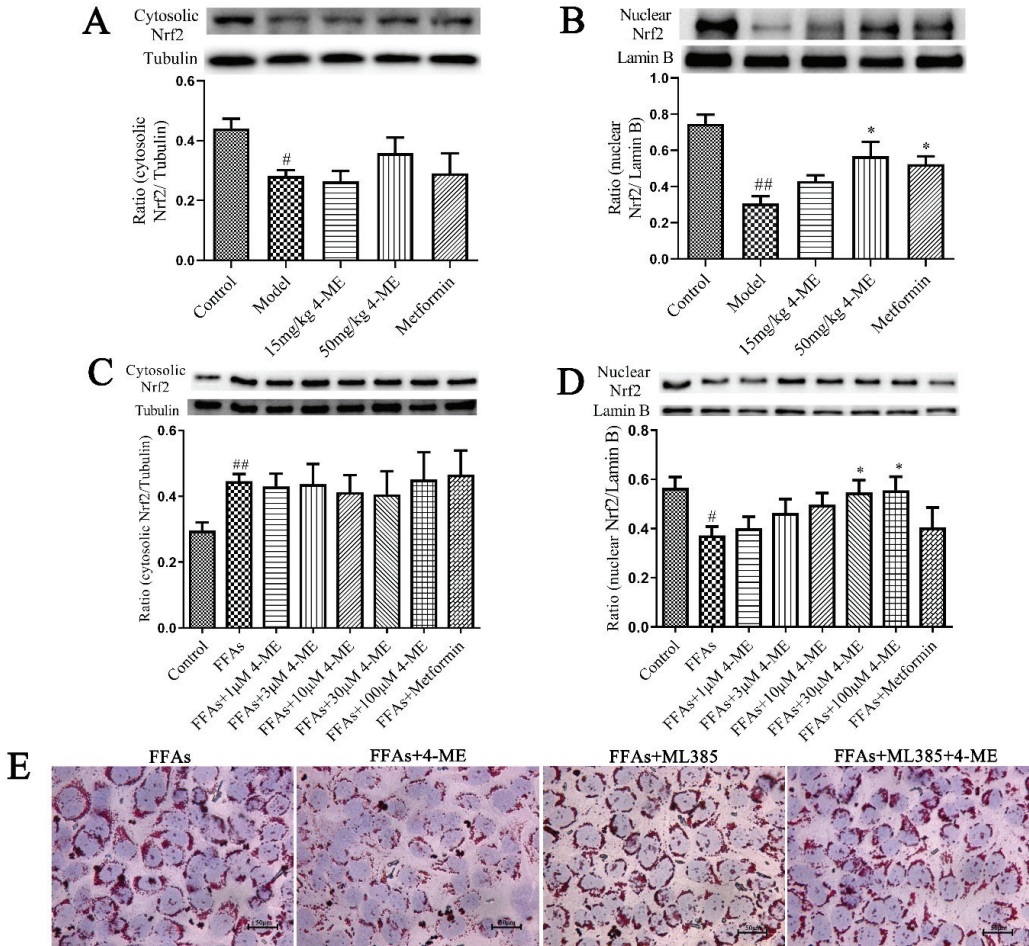
Figure 5. *Cont.*
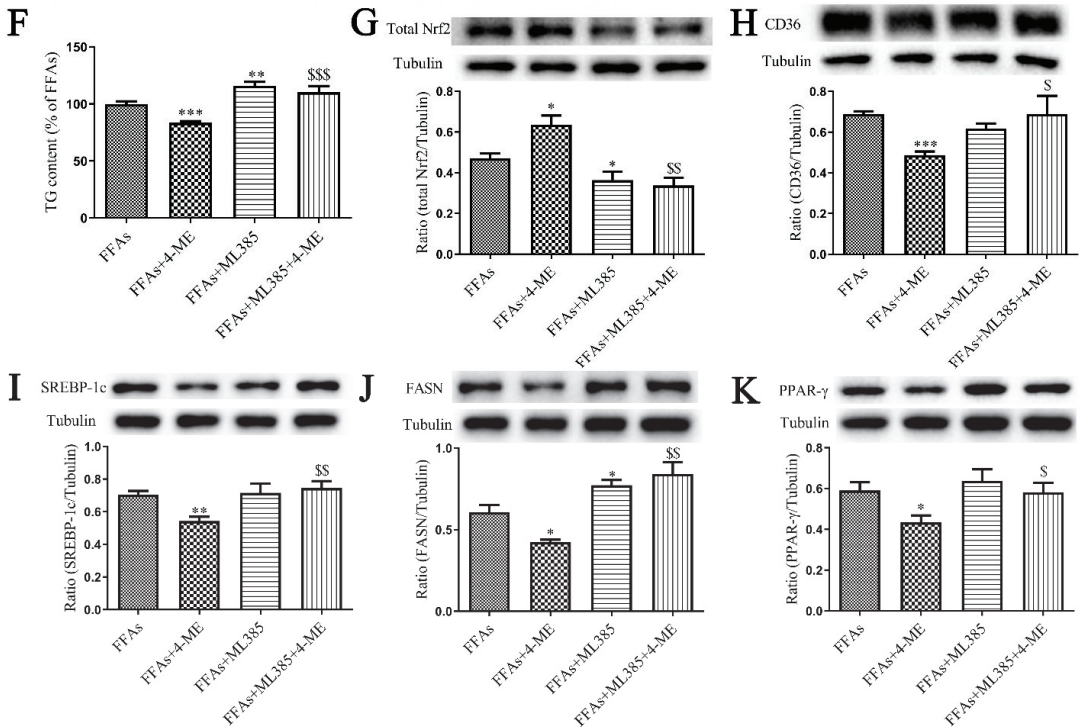
Figure 5. The 4-ME attenuated lipid metabolism by activating Nrf2. (**A–D**) The protein levels of cytosolic and nuclear Nfr2 in the liver or LO2 cells ($n = 3$–4). (**E**) Oil red O staining. (**F**) Intracellular TG content ($n = 8$). (**G–K**) Quantification data of Nfr2, CD36, SREBP-1c, FASN, and PPAR-γ protein expression levels in LO2 cells ($n = 3$–4). The results were expressed as mean ± SEM; [#] $p < 0.05$, [##] $p < 0.01$ compared with the Control group, * $p < 0.05$, ** $p < 0.01$, *** $p < 0.001$ compared with the Model group or FFA group, [$] $p < 0.05$, [$$] $p < 0.01$, [$$$] $p < 0.001$ compared with the FFAs+4-ME group.

To further elucidate the role of Nrf2 in lipid metabolism, a specific Nrf2 inhibitor, ML385, was used to treat FFA-induced LO2 cells prior to 4-ME incubation. The beneficial effects of 4-ME upon lipid deposition and the expression of proteins related to lipid metabolism in FFA-induced LO2 cells were abolished by ML385 (Figure 5E–K), indicating that Nrf2 acts as a negative regulator participating in hepatic lipid metabolism, which is consistent with previous reports [25].

3. Discussion

Obesity is characterized by lipid metabolic disorder. In this study, mice fed an HFD for 16 weeks displayed an increase in body weight, epididymal fat mass, epididymal adipocyte size, and the Lee Index, indicating visceral obesity that is a marker of ectopic fat accumulation in several key organs [26] and a critical mediator of steatohepatitis in metabolic liver disease [11]. Among these, intrahepatic fat accumulation is the hallmark profile of MAFLD [27]. The HFD-fed mice showed visible lipid droplets in the liver and elevated intrahepatic triglyceride accumulation, which was remarkably reduced by treatment with 4-ME and metformin.

Adipose tissue plays an important role in lipid metabolism. Adipose tissue dysfunction is characterized by disorders of the adipose tissue microenvironment including adipose hypertrophy, macrophage infiltration, hypoxia, fibrosis, and insulin resistance. It is extensively known to play a critical role in the pathogenesis of metabolic disorders such as MAFLD [28]. Adipocyte hypertrophy leads to adipocyte dysfunction and insulin

resistance and induces local adipose tissue hypoxia manifested by activation of a critical transcriptional factor HIF1α that can accelerate adipose tissue fibrosis [29,30]. Adipose tissue fibrosis is characterized by the deposition of excessive extracellular matrix (ECM), mainly collagens, which can be promoted by a potent profibrotic factor TGF-β and lead to adipose tissue dysfunction and ultimately metabolic complications [9]. Furthermore, in hypertrophic adipocytes, elevated lipolysis leads to the release of large amounts of NEFAs, which can be taken by other tissues. Excessive NEFA uptake by the liver can induce increased lipid synthesis and gluconeogenesis. Increased serum levels of NEFAs can lead to peripheral insulin resistance [31]. In our study, the phenomena of adipocyte hypertrophy, macrophage infiltration, hypoxia, and fibrosis in obese mice were observed by means of histopathology and immunohistochemistry. Metformin and 4-ME could significantly ameliorate the macrophage infiltration, collagen level, and HIF1α and TGF-β expression in the epididymal adipose tissue in HFD-fed mice, indicating the improvement of the epididymal adipose tissue microenvironment, thus counteracting the disorder of lipid metabolism in the liver caused by obesity.

Additionally, hepatic lipid accumulation results either from increased NEFA uptake and de novo lipogenesis in the liver and/or decreased fatty acid β-oxidation [32]. NEFA uptake is facilitated by cell-surface receptor CD36 whose expression is normally low, while much higher in response to an HFD [33]. FASN is a key enzyme in the de novo lipogenesis pathway that is responsible for the synthesis of excess fat in the liver of patients with MAFLD and is regulated by SREBP-1 and PPAR-γ [34]. Furthermore, Nrf2 is considered as a negative regulator of hepatic lipid metabolism, which not only participates in antioxidant pathways, but also can indirectly suppress the expressions of SREBP-1 and its lipogenic target genes [25,35,36]. CPT-1A is essential for fatty acid oxidation, a process that metabolizes fats and converts them into energy, which is regulated by transcriptional factor PPAR-α [37]. In our study, the HFD-treated mice or FFA-incubated hepatocytes displayed increased protein expression of CD36, SREBP-1, PPAR-γ, and FASN, decreased protein expression of PPAR-α and CPT-1A, and reduced nuclear translocation of Nrf2 as well, leading to increased FFA uptake, elevated de novo lipogenesis, and suppressed fatty acid oxidation, while 4-ME dose-dependently reversed these changes, contributing to the beneficial effects of 4-ME upon lipid metabolism both in vivo and in vitro. Further experiment results show that Nrf2 is required for 4-ME to ameliorate lipid deposition in livers of HFD mice and in FFAs-incubated hepatocytes. In addition, we found that 4-ME alleviated lipid accumulation by Nrf2 activation in hepatocytes, but the mechanism for the 4-ME effect in the adipose tissue is yet to be elucidated. Several studies reported controversial roles of Nrf2 in the adipogenesis in adipose tissue depending on the different approaches and animal models [38,39]. Therefore, more research concerning the tissue-specific effects of Nrf2 KO and Nrf2 overexpression and thereafter the mechanism of 4-ME in improving the adipose tissue microenvironment requires further investigation.

Taken together, 4-ME attenuated adipose tissue dysfunction and hepatic steatosis, and thus improved metabolic syndrome (Figure 6), providing a potential lead compound candidate against obesity and MAFLD. Meanwhile, esculetin has been reported to exert beneficial effects upon liver fat accumulation [40,41]. Given the structural similarity of these two coumarin compounds, it is worthy of further investigation in the future, especially with head-to-head comparative experiments, in order to elucidate the structure–activity relationship and provide clues for drug development. From the pharmacokinetic aspect, Li et al. [42] investigated the bioavailability and corresponding mechanisms of these two compounds and reported that the average absolute bioavailability of esculetin and 4-ME was 10.07% and 22.28%, respectively, indicating that 4-ME has a higher bioavailability than esculetin. However, the systematic investigation of in vivo biotransformation of coumarins is warranted to see if the interconversion between esculetin and 4-ME exists. In further studies, we will conduct in-depth research on the pharmacokinetics of 4-ME and the mechanisms and the precise target of 4-ME.
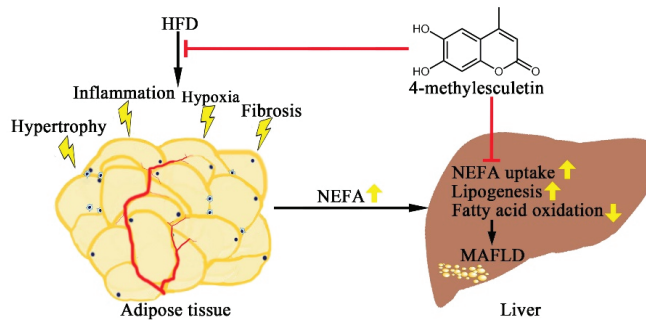
Figure 6. A depiction of effects of 4-ME upon obesity and MAFLD.

4. Materials and Methods

4.1. Materials

The high-fat diet (HFD) consists of 15% lard (*w/w*) and 15% sucrose (*w/w*), 70% basic diet which was obtained from Zhejiang Academy of Medical Sciences (Hangzhou, China). The ingredients of the high-fat diet and standard chow diet are shown in Supplementary Table S1. The 4-ME was obtained from Chengdu Biopurify Phytochemicals Ltd. (Chengdu, China) with a purity of 99.95% in Supplementary Figure S2. Insulin and leptin Elisa kits were provided by Shanghai Hengyuan Biological Technology Co., Ltd. (Shanghai, China); ML385 was purchased from Glpbio (Montclair, NJ, USA); metformin (purity more than 98%) and fatty free-bovine serum albumin (BSA) were obtained from Sangon Biotech (Shanghai, China). The following items were purchased from the cited commercial sources: CD36, CPT-1A, FASN, PPAR-α, PPAR-γ, TGF-β, Tubulin, and Lamin B antibodies (Proteintech, Chicago, IL, USA); HIF1α antibody (Invitrogen, Carlsbad, CA, USA); SREBP-1c antibody (Novus Biologicals, Littleton, CO, USA); Nrf2 antibody (Affinity Biologicals, Shanghai, China).

4.2. Animals Studies

Eight-week-old male wild-type ICR mice were purchased from Zhejiang Academy of Medical Sciences (Hangzhou, China) (License Number: SCXK (Zhe) 2014-0001) and housed under a temperature-controlled (23 $\pm$ 2 °C) and humidity-controlled (50–60%) environment with a light–dark cycle (12 h, respectively). After one week of acclimatization, model mice were fed with an HFD ad libitum while Control mice were fed with a low-fat diet, also ad libitum. Eight weeks later, model mice were divided into four groups, namely Model, 15 mg/kg 4-ME, 50 mg/kg 4-ME, and metformin, each group consisting of 8 mice. The Control and Model animals were gavaged with an equivalent volume of 0.5% sodium carboxymethyl cellulose (CMCNa$_2$) solution; 15 mg/kg 4-ME group: 4-methylesculetin (15 mg/kg/day, p.o.); 50 mg/kg 4-ME group: 4-methylesculetin (50 mg/kg/day, p.o.); and metformin group: metformin (250 mg/kg/day, p.o.), respectively, for 8 weeks. According to the EPA TSCA Section 8(b) chemical inventory data, the lethal dose of 4-ME when administered orally is above 3000 mg/kg body weight for rodents (RTECS No.: GN6384500), and the high dose of 4-ME was selected according to the study of Hemshekhar et al. [15] Body weights were measured bi-weekly. After fasting on the last day of the study, all animals were euthanized humanely for serum and tissue analysis. The serum was separated and stored at −80 °C. Tissues were harvested, weighed, snap-frozen in liquid nitrogen, and stored at −80 °C. All animal operations were conducted in compliance with the guidelines for animal care and use of the Zhejiang University of Technology Laboratory Animal Center.

4.3. Cell Culture and Treatment

LO2 (HL-7702) cells, a human normal liver cell line, were provided by Procell Life Science & Technology Co., Ltd. (Wuhan, China). Cell culture and FFAs-BSA mixture (containing 0.33 mM oleic acid and 0.17 mM palmitic acid) were the same as described

previously [43]. LO2 cells were divided into 8 groups, the Control group, FFAs group, FFAs+1 μM 4-ME group, FFAs+3 μM 4-ME group, FFAs+10 μM 4-ME group, FFAs+30 μM 4-ME group, FFAs+100 μM 4-ME group, and metformin group; each group was given the corresponding treatments. ML385 (10 μM), a specific Nrf2 inhibitor, was used to treat LO2 cells. The cells were incubated with freshly prepared medium supplemented with FFAs-BSA mixture for 24 h to induce hepatocyte steatosis and concurrently added with different concentrations of 4-ME or ML385.

4.4. Cell Viability Assay

The MTT method was adopted to assess cell viability. Briefly, LO2 cells were treated with different concentrations of 4-ME (1, 3, 10, 30, and 100 μM) in a 96-well plate. After 24 h of incubation, 20 μL of MTT solution (5 mg/mL) was added into each well. Following incubation for 4 h, the solution was replaced by 150 μL dimethyl sulfoxide to dissolve the formazan crystal. Finally, the optical densities were measured at 490 nm on a microplate reader (BioTek Synergy H1, Winooski, VT, USA).

4.5. Hepatic and Intracellular Triglyceride Determination

Evaluation of triglyceride content was achieved using a kit (Jiancheng Bioengineering Institute, Nanjing, China), according to the manufacturer's instructions. Briefly, 100 mg of liver tissue was homogenized in 1 mL ethanol and then centrifuged at $2500 \times g$ for 10 min. Hepatic TG levels were measured with TG Quantification Kits. The cell samples were collected from 6 cm dishes to determine intracellular TG levels by TG Quantification Kits. The protein concentration of lysates was determined by Bicinchoninic Acid protein assay kit with BSA as a standard (Beyotime, Haimen, China).

4.6. Oil Red O Staining

After fixation, liver specimens were embedded in OCT and stored at −80 °C. Then, frozen liver sections (6 μm thick) were stained with Oil red O solution for 15 min at room temperature and stained with hematoxylin. Eventually, all sections were observed by microscopy. The cell samples were fixed with paraformaldehyde for 20 min, then stained with Oil red O for 15 min at room temperature and stained with hematoxylin. Images were obtained by microscopy.

4.7. Intraperitoneal Glucose Tolerance Test

All animals strictly fasted overnight. The mice were injected intraperitoneally with glucose (2 g/kg body weight). Blood samples were collected from the tail tips of mice at 0, 15, 30, 60, and 120 min, and blood glucose was measured using a glucometer.

4.8. Serum Analysis

Serum levels of T-CHO, LDL-C, HDL-C, NEFA and TG, and insulin were measured with kits from Nanjing Jiancheng Bioengineering Institute (Nanjing, China). Fasting serum insulin and leptin were analyzed by Elisa kits.

4.9. Histological and Immunohistochemistry Studies

Tissue specimens were fixed in 4% paraformaldehyde solution, embedded in paraffin, stained with hematoxylin and eosin (H&E), and Masson's trichrome, respectively, after tissue dehydration with gradient ethanol, and assessed for histopathological changes using image analysis system. Adipocyte size was determined in hematoxylin/eosin-stained sections as the mean cell area (in μm^2) of 300 random adipocytes on digital images acquired at $100 \times$ magnification by light microscope (Nikon) using IPP software (Image-Pro Plus 6.0). Adipose hypoxia and fibrosis were also detected using HIF1α and TGF-β antibodies. Adipose tissue sections were incubated with HIF1α (1:100) and TGF-β (1:100) primary antibodies, respectively, and a secondary antibody and then diaminobenzidine as a color

substrate. At 200× magnification, the area of the staining signal (HIF1α and TGF-β) was measured using the IPP software.

4.10. Western Blotting

Tissue specimens were homogenized in ice-cold lysis buffer to extract the protein. Lysates were centrifuged at 14,000× *g* for 5 min at 4 °C and supernatants were collected. The protein concentration was determined by Bicinchoninic Acid protein assay kit with BSA as a standard (Beyotime, Haimen, China). Protein samples were mixed with loading buffer and boiled for 5 min, then resolved by SDS-PAGE and transferred onto 0.22 μm PVDF membranes (Bio-Rad, Hercules, CA, USA) in a semidry transfer system (Bio-Rad, Hercules, CA, USA). PVDF membranes were blocked with freshly prepared 5% BSA or non-fat milk in Tris-buffered saline containing 0.05% Tween-20 surfactant for 60 min at room temperature, immunoblotted with the primary antibodies for 4 h at room temperature or overnight at 4 °C, washed with TBST 3 times and incubated with secondary antibodies for 2 h at room temperature, and finally visualized with enhanced chemiluminescence method.

4.11. Total RNA Extraction and Quantitative RT-PCR

Total RNA was extracted from LO2 cells using TRIzol reagent (Invitrogen, Carlsbad, CA, USA). A 1 μg aliquot of RNA was converted to cDNA. The sequences of primers used for PCR amplification are listed in Table 3. qRT-PCR was performed using SYBR Green PCR master mix (Beyotime, Haimen, China) on stepone™ quantitative RT-PCR system (Applied Biosystems, Waltham, MA, USA). A 20 μL reaction mixture was amplified using the following thermal parameters: denaturation at 95 °C for 2 min, 40 cycles of the amplification step (95 °C for 15 s and 60 °C for 15 s), and a final extension at 95 °C for 15 s and 60 °C for 15 s. Glyceraldehyde 3-phosphate dehydrogenase (GAPDH) was served as the endogenous control. Relative mRNA expression levels were analyzed by the $2^{-\Delta\Delta Ct}$ method.

Table 3. Primer sequences for qRT-PCR.

Gene Name	Forward Primer (5′→3′)	Reverse Primer (5′→3′)
CD36	GAG AAC TGT TAT GGG GCT AT	TTC AAC TGG AGA GGC AAA GG
SREBP1	ACG GGA TGG ACT GAC TT	AGG CTT CTT TGC TGT GAG ATG
FASN	AAG GAC CTG TCT AGG TTT GAT GC	TGG CTT CAT AGG TGA CTT CCA
PPARG	ACT CCA CAT TAC GAA GAC AT	CTC CAC AGA CAC GAC ATT
PPARA	GCG AAC GAT TCG ACT CAA GC	TAC CGT TGT GTG ACA TCC CG
CPT1A	TGT CCA GCC AGA CGA AGA AC	ATC TTG CCG TGC TCA GTG AA
GAPDH	GTC TCC TCT GAC TTC AAC AGC G	ACC ACC CTG TTG CTG TAG CCA A

4.12. Statistical Analysis

All values were expressed as mean ± standard error of the mean (SEM). The difference between two groups was assessed using Student's *t*-test, and multiple comparisons were performed by analysis of variance (ANOVA) followed by Tukey's post hoc tests using GraphPad Prism 5 (GraphPad Prism Software Inc., San Diego, CA, USA). A value of $p < 0.05$ was considered to be statistically significant.

Institutional Review Board Statement: All animal experiments were performed in accordance with the guidelines of the Institutional Review Board of Zhejiang University of Technology. The animal study protocol was approved by the Zhejiang University of Technology Laboratory Animal Center (protocol code 22-008284 and date of approval 27 January 2017).

Informed Consent Statement: Not applicable.

Data Availability Statement: Data will be made available by the corresponding author upon request.

Conflicts of Interest: The authors declare no conflict of interest.

References

1. Bluher, M. Obesity: Global epidemiology and pathogenesis. *Nat. Rev. Endocrinol.* **2019**, *15*, 288–298. [CrossRef] [PubMed]
2. Jaacks, L.M.; Vandevijvere, S.; Pan, A.; McGowan, C.J.; Wallace, C.; Imamura, F.; Mozaffarian, D.; Swinburn, B.; Ezzati, M. The obesity transition: Stages of the global epidemic. *Lancet Diabetes Endocrinol.* **2019**, *7*, 231–240. [CrossRef]
3. NCD Risk Factor Collaboration (NCD-RisC). Worldwide trends in body-mass index, underweight, overweight, and obesity from 1975 to 2016: A pooled analysis of 2416 population-based measurement studies in 128.9 million children, adolescents, and adults. *Lancet* **2017**, *390*, 2627–2642. [CrossRef]
4. Cao, H. Adipocytokines in obesity and metabolic disease. *J. Endocrinol.* **2014**, *220*, T47–T59. [CrossRef]
5. Luo, L.; Liu, M. Adipose tissue in control of metabolism. *J. Endocrinol.* **2016**, *231*, R77–R99. [CrossRef] [PubMed]
6. Guzik, T.J.; Skiba, D.S.; Touyz, R.M.; Harrison, D.G. The role of infiltrating immune cells in dysfunctional adipose tissue. *Cardiovasc. Res.* **2017**, *113*, 1009–1023. [CrossRef]
7. Muir, L.A.; Neeley, C.K.; Meyer, K.A.; Baker, N.A.; Brosius, A.M.; Washabaugh, A.R.; Varban, O.A.; Finks, J.F.; Zamarron, B.F.; Flesher, C.G.; et al. Adipose tissue fibrosis, hypertrophy, and hyperplasia: Correlations with diabetes in human obesity. *Obesity* **2016**, *24*, 597–605. [CrossRef]
8. Lee, Y.S.; Kim, J.W.; Osborne, O.; Oh, D.Y.; Sasik, R.; Schenk, S.; Chen, A.; Chung, H.; Murphy, A.; Watkins, S.M.; et al. Increased adipocyte O2 consumption triggers HIF-1alpha, causing inflammation and insulin resistance in obesity. *Cell* **2014**, *157*, 1339–1352. [CrossRef]
9. Sun, K.; Tordjman, J.; Clement, K.; Scherer, P.E. Fibrosis and Adipose Tissue Dysfunction. *Cell Metab.* **2013**, *18*, 470–477. [CrossRef]
10. Donnelly, K.L.; Smith, C.I.; Schwarzenberg, S.J.; Jessurun, J.; Boldt, M.D.; Parks, E.J. Sources of fatty acids stored in liver and secreted via lipoproteins in patients with nonalcoholic fatty liver disease. *J. Clin. Investig.* **2005**, *115*, 1343–1351. [CrossRef]
11. van der Poorten, D.; Milner, K.L.; Hui, J.; Hodge, A.; Trenell, M.I.; Kench, J.G.; London, R.; Peduto, T.; Chisholm, D.J.; George, J. Visceral fat: A key mediator of steatohepatitis in metabolic liver disease. *Hepatology* **2008**, *48*, 449–457. [CrossRef]
12. Zhu, X.X.; Yang, L.; Li, Y.J.; Zhang, D.; Chen, Y.; Kostecká, P.; Kmoníčková, E.; Zídek, Z. Effects of sesquiterpene, flavonoid and coumarin types of compounds from Artemisia annua L. on production of mediators of angiogenesis. *Pharm. Rep.* **2013**, *65*, 410–420. [CrossRef]
13. Paya, M.; Halliwell, B.; Hoult, J.R.S. Interactions of a series of coumarins with reactive oxygen species. Scavenging of superoxide, hypochlorous acid and hydroxyl radicals. *Biochem. Pharmacol.* **1992**, *44*, 205–214. [CrossRef]
14. Gao, X.; Wang, C.; Ning, C.; Liu, K.; Wang, X.; Liu, Z.; Sun, H.; Ma, X.; Sun, P.; Meng, Q. Hepatoprotection of auraptene from peels of citrus fruits against thioacetamide-induced hepatic fibrosis in mice by activating farnesoid X receptor. *Food Funct.* **2018**, *9*, 2684–2694. [CrossRef] [PubMed]
15. Hemshekhar, M.; Sunitha, K.; Thushara, R.M.; Sebastin Santhosh, M.; Shanmuga Sundaram, M.; Kemparaju, K.; Girish, K.S. Antiarthritic and antiinflammatory propensity of 4-methylesculetin, a coumarin derivative. *Biochimie* **2013**, *95*, 1326–1335. [CrossRef] [PubMed]
16. Witaicenis, A.; de Oliveira, E.C.S.; Tanimoto, A.; Zorzella-Pezavento, S.F.G.; de Oliveira, S.L.; Sartori, A.; Di Stasi, L.C. 4-methylesculetin, a coumarin derivative, ameliorates dextran sulfate sodium-induced intestinal inflammation. *Chem. Biol. Interact.* **2018**, *280*, 59–63. [CrossRef]
17. Witaicenis, A.; Seito, L.N.; Di Stasi, L.C. Intestinal anti-inflammatory activity of esculetin and 4-methylesculetin in the trinitrobenzenesulphonic acid model of rat colitis. *Chem. Biol. Interact.* **2010**, *186*, 211–218. [CrossRef]
18. Li, H.; Yao, Y.; Li, L. Coumarins as potential antidiabetic agents. *J. Pharm. Pharmacol.* **2017**, *69*, 1253–1264. [CrossRef]
19. Li, J.; Li, X.; Li, Z.; Zhang, L.; Liu, Y.; Ding, H.; Yin, S. Isofraxidin, a coumarin component improves high-fat diet induced hepatic lipid homeostasis disorder and macrophage inflammation in mice. *Food Funct.* **2017**, *8*, 2886–2896. [CrossRef]
20. Nugara, R.N.; Inafuku, M.; Takara, K.; Iwasaki, H.; Oku, H. Pteryxin: A coumarin in Peucedanum japonicum Thunb leaves exerts antiobesity activity through modulation of adipogenic gene network. *Nutrition* **2014**, *30*, 1177–1184. [CrossRef]
21. Singh, L.R.; Kumar, A.; Upadhyay, A.; Gupta, S.; Palanati, G.R.; Sikka, K.; Siddiqi, M.I.; Yadav, P.N.; Sashidhara, K.V. Discovery of coumarin-dihydroquinazolinone analogs as niacin receptor 1 agonist with in-vivo anti-obesity efficacy. *Eur. J. Med. Chem.* **2018**, *152*, 208–222. [CrossRef]
22. Watanabe, A.; Kato, T.; Ito, Y.; Yoshida, I.; Harada, T.; Mishima, T.; Fujita, K.; Watai, M.; Nakagawa, K.; Miyazawa, T. Aculeatin, a coumarin derived from Toddalia asiatica (L.) Lam., enhances differentiation and lipolysis of 3T3-L1 adipocytes. *Biochem. Biophys. Res. Commun.* **2014**, *453*, 787–792. [CrossRef]

23. Lee, M.O. Determination of the surface area of the white rat with its application to the expression of metabolic results. *Am. J. Physiol. Leg. Content* **1929**, *89*, 24–33. [CrossRef]

24. Kitteringham, N.R.; Abdullah, A.; Walsh, J.; Randle, L.; Jenkins, R.E.; Sison, R.; Goldring, C.E.; Powell, H.; Sanderson, C.; Williams, S.; et al. Proteomic analysis of Nrf2 deficient transgenic mice reveals cellular defence and lipid metabolism as primary Nrf2-dependent pathways in the liver. *J. Proteom.* **2010**, *73*, 1612–1631. [CrossRef] [PubMed]

25. Chambel, S.S.; Santos-Gonçalves, A.; Duarte, T.L. The Dual Role of Nrf2 in Nonalcoholic Fatty Liver Disease: Regulation of Antioxidant Defenses and Hepatic Lipid Metabolism. *BioMed Res. Int.* **2015**, *2015*, 597134. [CrossRef]

26. Smith, U. Abdominal obesity: A marker of ectopic fat accumulation. *J. Clin. Investig.* **2015**, *125*, 1790–1792. [CrossRef]

27. Seebacher, F.; Zeigerer, A.; Kory, N.; Krahmer, N. Hepatic lipid droplet homeostasis and fatty liver disease. *Semin. Cell Dev. Biol.* **2020**, *108*, 72–81. [CrossRef] [PubMed]

28. Azzu, V.; Vacca, M.; Virtue, S.; Allison, M.; Vidal-Puig, A. Adipose Tissue-Liver Cross Talk in the Control of Whole-Body Metabolism: Implications in Nonalcoholic Fatty Liver Disease. *Gastroenterology* **2020**, *158*, 1899–1912. [CrossRef]

29. Halberg, N.; Khan, T.; Trujillo, M.E.; Wernstedt-Asterholm, I.; Attie, A.D.; Sherwani, S.; Wang, Z.V.; Landskroner-Eiger, S.; Dineen, S.; Magalang, U.J.; et al. Hypoxia-inducible factor 1alpha induces fibrosis and insulin resistance in white adipose tissue. *Mol. Cell. Biol.* **2009**, *29*, 4467–4483. [CrossRef] [PubMed]

30. Kim, J.I.; Huh, J.Y.; Sohn, J.H.; Choe, S.S.; Lee, Y.S.; Lim, C.Y.; Jo, A.; Park, S.B.; Han, W.; Kim, J.B. Lipid-overloaded enlarged adipocytes provoke insulin resistance independent of inflammation. *Mol. Cell. Biol.* **2015**, *35*, 1686–1699. [CrossRef] [PubMed]

31. Stinkens, R.; Goossens, G.H.; Jocken, J.W.; Blaak, E.E. Targeting fatty acid metabolism to improve glucose metabolism. *Obes. Rev.* **2015**, *16*, 715–757. [CrossRef]

32. Manne, V.; Handa, P.; Kowdley, K.V. Pathophysiology of Nonalcoholic Fatty Liver Disease/Nonalcoholic Steatohepatitis. *Clin. Liver Dis.* **2018**, *22*, 23–37. [CrossRef] [PubMed]

33. Koonen, D.P.; Jacobs, R.L.; Febbraio, M.; Young, M.E.; Soltys, C.L.; Ong, H.; Vance, D.E.; Dyck, J.R. Increased hepatic CD36 expression contributes to dyslipidemia associated with diet-induced obesity. *Diabetes* **2007**, *56*, 2863–2871. [CrossRef] [PubMed]

34. Sanders, F.W.; Griffin, J.L. De novo lipogenesis in the liver in health and disease: More than just a shunting yard for glucose. *Biol. Rev. Camb. Philos. Soc.* **2016**, *91*, 452–468. [CrossRef] [PubMed]

35. Kay, H.Y.; Kim, W.D.; Hwang, S.J.; Choi, H.S.; Gilroy, R.K.; Wan, Y.J.; Kim, S.G. Nrf2 inhibits LXRalpha-dependent hepatic lipogenesis by competing with FXR for acetylase binding. *Antioxid. Redox Signal.* **2011**, *15*, 2135–2146. [CrossRef] [PubMed]

36. Tanaka, Y.; Aleksunes, L.M.; Yeager, R.L.; Gyamfi, M.A.; Esterly, N.; Guo, G.L.; Klaassen, C.D. NF-E2-related factor 2 inhibits lipid accumulation and oxidative stress in mice fed a high-fat diet. *J. Pharmacol. Exp. Ther.* **2008**, *325*, 655–664. [CrossRef] [PubMed]

37. Pawlak, M.; Lefebvre, P.; Staels, B. Molecular mechanism of PPARalpha action and its impact on lipid metabolism, inflammation and fibrosis in non-alcoholic fatty liver disease. *J. Hepatol.* **2015**, *62*, 720–733. [CrossRef]

38. Annie-Mathew, A.S.; Prem-Santhosh, S.; Jayasuriya, R.; Ganesh, G.; Ramkumar, K.M.; Sarada, D.V.L. The pivotal role of Nrf2 activators in adipocyte biology. *Pharmacol. Res.* **2021**, *173*, 105853. [CrossRef]

39. Li, S.; Eguchi, N.; Lau, H.; Ichii, H. The Role of the Nrf2 Signaling in Obesity and Insulin Resistance. *Int. J. Mol. Sci.* **2020**, *21*, 6973. [CrossRef]

40. Park, Y.; Sung, J.; Yang, J.; Ham, H.; Kim, Y.; Jeong, H.S.; Lee, J. Inhibitory effect of esculetin on free-fatty-acid-induced lipid accumulation in human HepG2 cells through activation of AMP-activated protein kinase. *Food Sci. Biotechnol.* **2017**, *26*, 263–269. [CrossRef] [PubMed]

41. Choi, R.Y.; Ham, J.R.; Lee, M.K. Esculetin prevents non-alcoholic fatty liver in diabetic mice fed high-fat diet. *Chem. Biol. Interact.* **2016**, *260*, 13–21. [CrossRef] [PubMed]

42. Li, Y.; Song, W.; Ou, X.; Luo, G.; Xie, Y.; Sun, R.; Wang, Y.; Qi, X.; Hu, M.; Liu, Z.; et al. Breast Cancer Resistance Protein and Multidrug Resistance Protein 2 Determine the Disposition of Esculetin-7-O-Glucuronide and 4-Methylesculetin-7-O-Glucuronide. *Drug Metab. Dispos.* **2019**, *47*, 203–214. [CrossRef] [PubMed]

43. Li, L.; Zheng, W.; Wang, C.; Qi, J.; Li, H. Mogroside V Protects against Hepatic Steatosis in Mice on a High-Fat Diet and LO2 Cells Treated with Free Fatty Acids via AMPK Activation. *Evid. Based Complement. Alternat. Med.* **2020**, *2020*, 7826874. [CrossRef] [PubMed]

Review

Overview of Curcumin and Piperine Effects on Glucose Metabolism: The Case of an Insulinoma Patient's Loss of Consciousness

Simona Servida [1,†], **Elena Panzeri** [2,†], **Laura Tomaino** [3,4], **Giovanni Marfia** [5], **Emanuele Garzia** [5], **Giuseppe Ciniglio Appiani** [5], **Gianluca Moroncini** [4], **Vito De Gennaro Colonna** [1,6], **Carlo La Vecchia** [6] and **Luisella Vigna** [1,*]

[1] Obesity and Work Centre, Occupational Medicine Unit, Clinica del Lavoro L. Devoto, Fondazione IRCCS Ca' Granda Ospedale Maggiore Policlinico, 20122 Milan, Italy
[2] Independent Researcher, Nutrigenetics Consultant, London DA14 5JR, UK
[3] Postgraduate School of Emergency Medicine, Università Politecnica delle Marche, 60126 Ancona, Italy
[4] Department of Clinical and Molecular Sciences, Marche Polytechnic University, 60020 Ancona, Italy
[5] Istituto di Medicina Aerospaziale "A. Mosso", Aeronautica Militare Italiana, 20129 Milan, Italy
[6] Department of Clinical Science and Community Health, DISSCO, Università degli Studi di Milano, 20122 Milan, Italy
[*] Correspondence: luisella.vigna@policlinico.mi.it
[†] These authors contributed equally to this work.

Abstract: The hypoglycemic properties of curcumin supplements in therapeutic doses are well-known and may represent a useful tool for the treatment of chronic diseases such as metabolic syndrome, insulin resistance and type 2 diabetes. The poor bioavailability of curcumin can be improved with the concomitant administration of piperine, with no severe adverse effects on glycemia reported so far in the literature. In this article, we further discuss a previously reported case of a helicopter pilot, affected by grade I obesity who, under curcumin and piperine treatment, experienced a transient loss of consciousness (TLOC), during a low-altitude flight. This episode led to a diagnosis of insulinoma, previously asymptomatic. We hypothesized that the combined effects of curcumin and piperine might have caused a severe hypoglycemic episode and subsequent TLOC. Therefore, further studies should be conducted to evaluate the safety of curcumin and piperine supplementation in subjects with impaired glucose metabolism and insulin secretion.

Keywords: hypoglycemia; insulinoma; curcumin; piperine; bioavailability

1. Introduction

Curcumin is a yellow-colored polyphenol found in the dried rhizome of *Curcuma longa*, commonly known as "turmeric", traditionally used in China and Southeast Asia for centuries. The pharmacological properties of curcumin have received growing attention in the last few decades. Currently, it is included, as an active ingredient, in supplements claiming to have antioxidant, anti-inflammatory, antimicrobial, anti-cancer, anti-diabetic and slimming effects [1,2]. Curcumin has been demonstrated to be generally safe [1,3]. Appendix A provides a summary of bioavailability, adverse effects, plasma peak concentration and safety of curcumin and piperine as single agent and in combination in supplements.

Nevertheless, its potential therapeutic applications have been limited by its poor gastrointestinal absorption and low bioavailability, mainly due to its water insolubility and rapid metabolism and excretion [2]. Therefore, novel formulations have been proposed to improve its adsorption and/or reduce its metabolization. Among them, those containing piperine seem to increase the bioavailability, efficacy and half-life of orally administered curcumin [2,4]. The biotransformation and enzymatic degradation operated by the gut microbiota may increase the biological effects of polyphenols, including curcumin, via the formation of metabolites with specific biological proprieties [1,5]. Several studies have

confirmed the hypoglycemic properties of curcumin, as a single agent or in combination with piperine, through different mechanisms of action (MoA) positively affecting glucose and insulin homeostasis [6,7]. Therefore, the possible occurrence of hypoglycemia as a side effect of curcumin supplementation in combination with piperine should be investigated.

In this article, we reconsider a clinical case in which curcumin and piperine supplementation may have acted as a catalyst for incidental diagnosis of insulinoma, after a transient loss of consciousness (TLOC). On this basis, we discuss both the MoA of curcumin in regulating glucose homeostasis and the synergic effects of piperine hypothesizing its potential side effects as a discussed strong hypoglycemic agent [7].

2. Summary of Case Report

As previously described [8], a 50-year-old man who worked as a helicopter rescue pilot presented a TLOC of approximately 1 min and 20 sec while in service. The incident ended with no one injured as he regained consciousness and control of the helicopter. Previously, the pilot had neither shown warning symptoms nor experienced similar episodes. He presented retrograde amnesia. His past medical history was significant for grade I obesity (BMI 30.5) and mild obstructive sleep apnea syndrome (OSAS). In the 4 months before the incident, he had been on a low-calorie diet plus curcumin and piperine supplementation (curcumin 600 mg a day and piperine 8.55 mg a day) for weight loss.

The pilot was temporarily suspended from his job pending examinations. The tests for the cardiological and neurological causes of the TLOC resulted negative. Nevertheless, blood chemistry tests revealed asymptomatic recurrent fasting hypoglycemia and elevated plasmatic levels of Chromogranin A. Fine needle aspiration guided by endoscopic ultrasonography was performed to confirm the diagnosis of pancreatic insulinoma [8]. A careful analysis of the pilot's health status and his specific work needs was carried out. He underwent a pancreaticoduodenectomy followed by organizational interventions at his workplace. The patient was able to resume his job but under the limitation of flying "only with a safety pilot and in aircrafts with dual controls".

Based on such evidence, we hypothesized the possibility of a severe and transient hypoglycemic event in a patient with asymptomatic insulinoma triggered by the continuous use of a commercially available supplement at a daily dose of 600 mg a day of curcumin and 8.55 mg of piperine, for a period of 4 months.

3. Discussion

3.1. Curcumin and Piperine: Structure, Metabolism, Bioavailability and Safety

Curcumin is a hydrophobic polyphenol extracted from the rhizome of *Curcuma longa* L. (turmeric), a species belonging to the *Curcuma* genus (Zingiberaceae family) [1,2]. The main constituent of curcumin extract is 1,7-bis(4-hydroxy-3-methoxyphenyl)-1,6-heptadiene-3,5-dione, a diferuloylmethane also known as curcumin I. There are, however, two other compounds known as curcumin, curcumin II (demethoxycurcumin) and curcumin III (bis-demethoxycurcumin), which differ in the number of methoxy groups on their aromatic ring (Figure 1a–c) and represent, respectively, 10–20% and 3% of the total curcuminoids [9,10]. These three curcuminoid analogs might display different pharmacological activities [11]. Experimental evidence in vitro and in vivo has shown that curcumin and its analogs exert significant anti-inflammatory and antioxidant effects [1,2], improve lipid and glucose metabolism [12], and exhibit additional beneficial biological activities, including antitumoral, neuroprotective, antimicrobial, hepatoprotective and antirheumatic ones [2,10]. Table 1 briefly summarizes the anti-diabetic activities of curcumin and piperine as single agents and in combination.

Table 1. Summary of the anti-diabetic activities of curcumin and piperine as single agents and in combination.

	Curcumin	Piperine	Complex Curcumin + Piperine
In vitro studies	↓ mTORC1 signal in human intestinal epithelium cells [13] ↑ GLUT4 translocation in skeletal muscle cells, adipocytes and hepatocytes [14,15] ↑ GLUT4 expression and ↓ GLUT1 expression in hypoxic adipocytes [17] ↑ Akt phosphorylation [20] ↓ pro-inflammatory cytokines in skeletal muscle cells, adipocytes and hepatocytes cells [21] ↓ gluconeogenesis and glycogenolysis in hepatocytes cells [22] ↓ G6Pase and PECK activity [22] ↓ mRNA expression of 11 PDE isoenzymes (PDE3B, PDE8A, PDE10A) in pancreatic islets, in dose-dependent [23] ↓ DPP IV in Caco2 cells [24] ↑ GLP-1 secretion via Ca^{2+}/calmodulin-dependent Kinase pathway [25] ↑ insulin secretion in pancreatic islets via PDE/cAMP regulation and ↑ recovery of pancreatic islets [23]	↓ TORC1 signal in human intestinal epithelium cells [13] ↑ intracellular Ca^{2+} level with activation of CaMKKβ and consequent increase of GLUT4 translocation in L6 myotubes [16] ↑ anti-diabetic activity by PPAR-gamma and ↑ insulin-sensibility in 3T3-L1 cells. [18,19]	↓ mTORC1 signal in human intestinal epithelium cells more efficiently than CUR alone [13] ↓ TNFα gene expression [13]
In vivo animal and human studies	↓ glucose serum and HbA1c levels [26,27] ↓ hyperlipidemia and hyperglycemia [29] ↓ Inhibition of NLP3 inflammasome activation in genetic diabetes animals [32] ↓ serum glucose and leptin, ↑ adiponectin and ↓insulin resistance in diet-induced diabetes models [35,36] ↓ serum glucose, TG, LDL and HbA1c levels in human studies [26] ↓ insulin secretion and HOMA-IR in pre-diabetic and diabetic individuals [41,42]	↑ Ca^{2+} level with consequent translocation by APMK phosphorylation in Wistar rats [16] ↓ body weight, hepatotoxicity and peroxidation in diabetic animal models induced by streptozotocin [18,30] ↑ improved lipid profile in high-fat diets induced rats [33] ↑ improves insulin signal in HFD-induced hepatic steatosis, ↓plasma adiponectin and glucose levels [33,37] ↓ β-cell-dysfunction in pre-diabetic mice and reduced LPS level [39]	↑ recovery of intestinal permeability and integrity and ↓ oxidative stress in weaned Wuzhishan piglets [28]↓ inflammation index levels and ↓ weight in high-fat-diet-RC-induced mice [31] → total cholesterol, LDL with no effect on TG in a patient with metabolic syndrome [34] ↓ albumin level and improve glycemic profile in patients with NAFLD [38] ↓ FPI, HOMA index, TG, LDL, hepatic transaminases, γ-GT, cortisol, blood pressure, steatosis index and waist circumference in overweight patients [40] ↓ glucose, HbA1c, C-peptide, alanine and aspartase aminotransferase in T2D patients [12]

↑: increase; ↓: reduction.

(**a**) **Curcumin I**

(**b**) **Curcumin II**

(**c**) **Curcumin III**

(**d**) **Piperine**

Figure 1. Chemical structure of curcumin and its two main analogs and piperine: (**a**) curcumin I (1E,6E)1,7-bis(4-hydroxy-3-methoxy-phenyl)-hepta-1,6-diene-3,5-dione; (**b**) curcumin II (1*E*,6*E*)-1-(4-hydroxy-3-methoxyphenyl)-7-(4-hydroxyphenyl)hepta-1,6-diene-3,5-dione; (**c**) curcumin III (Bis(4-hydroxyphenyl)-1,6-heptadiene-3,5-dione; and (**d**) piperine, (2E,4E)-5-(benzol(*d*)[1,3]dioxol-5-yl)-(piperidin-1-y)penta-2,4-dien-1-one.

Piperine is an alkaloid extracted from the fruits and roots of *Piper nigrum* L. (black pepper) and *Piper longum* L. (long pepper) belonging to the Piperaceae family. Piperine (Figure 1d) exists in four isomeric structures: piperine trans-trans, which displays biological activity, isopiperine cis-trans, chavicine cis-cis, and isochavicine trans-cis, which have significant anti-hepatotoxic and antioxidant effects [33,43].

The therapeutic efficacy of curcumin has been questioned because of its very low bioavailability due to poor absorption, limited tissue distribution and rapid intestinal metabolism and clearance [44]. Curcumin undergoes extensive Phase I and Phase II liver biotransformation and is quickly metabolized via glucuronidation and sulfation and then mostly eliminated through feces [45]. Animal and human studies have confirmed its limited pharmacokinetic profile [46]. Administration of single high doses of oral curcumin may cause saturation of the transport mechanism and, therefore, be counterproductive [47].

Curcumin plasma peak concentrations are usually observed at 1 to 2 h following oral administration but tend to become undetectable within 12 h [46]. New formulations have been designed to improve curcumin bioavailability including micelles, nanoparticles, liposomes, nano-emulsions and phospholipid complexes [48]. For instance, curcumin encapsulation in camel β-casein micelle can increase its solubility by 2500-fold [49]. Phytosomal curcumin also appears to be significantly more bioavailable and biologically active [50].

Although pharmacokinetics studies show improved absorption, longer half-life and higher plasma concentration of formulated curcumin, we still lack conclusive evidence regarding the comparative efficacy of different formulations [51]. In fact, the most recent research highlights the need to consider the broad range of curcuminoid metabolites, and not just unconjugated curcumin, when assessing the real bioavailability [52].

The food matrix might also play an important role in curcumin adsorption. The bioavailability of fresh or dried powdered turmeric appears to be superior compared to supplements, which are compounded with curcumin and other chemicals [53].

Recent studies have emphasized the role of intestinal microbiota in curcumin metabolism and biotransformation: it may affect its bioavailability [1,54]. Gut-derived curcumin metabolites have specific biological activities that may enhance those of the native form of this polyphenol. They could explain the incongruencies between the observed pharmacological effect of curcumin and its poor bioavailability [1]. The beneficial activities of curcumin on gut microbiota could be related to improved dysbiosis and intestinal barrier functions, increased microbial biodiversity and reduction in pro-inflammatory mediators [55]. Curcumin can modulate the ratio between beneficial and potentially pathogenic intestinal bacteria by favoring genera such as Bifidobacteria and Lactobacilli and reducing the abundance of families such as *Prevotellaceae*, *Bacteroidaceae*, *Rikenellaceae* and *Coriobacteriaceae* [1,56]. Moreover, curcumin can decrease intestinal permeability, restore barrier integrity (by preventing tight junction protein disruption [57]), increase the expression of ZO-1 and claudins and attenuate the activation of p38 MAPK [58]. Thus, some of the favorable metabolic actions of curcumin in relation to diabetes and obesity could be ascribable to its effects on microbiota [59].

The co-administration of natural inhibitors of UDP-glucuronyl transferase, such as piperine, quercetin and silybin may increase the bioavailability of oral curcumin by interfering with its glucuronidation [2]. In particular, the combination with piperine has been extensively studied and appears to significantly enhance curcumin absorption [44]. As piperine inhibits one of the enzymes responsible for the metabolization of curcumin (UDP-glucuronyl transferase), the association of the two compounds allows an increased bioavailability of curcumin as its clearance is decreased. Shoba et al. (1998) [60] showed that the co-administration of 2 g of curcumin with 20 mg of piperine to healthy individuals provoked a 2000% increase in bioavailability and much higher serum concentrations with no adverse observed effects. Studies on rats confirmed improved intestinal absorption and tissue distribution when curcumin was combined with piperine [61,62]; however, the dosages in animal studies greatly exceed those utilized in human trials.

Similarly to curcumin, the lipophilic character of piperine limits its bioavailability [18]. Piperine reaches the peak serum concentration at approximately 2–4 h after administration and remains detectable in plasma up to 48 h. It presents a secondary peak, probably due to enterohepatic recirculation of its metabolites and analogs, and a limited hepatic metabolism [63,64]. Animal studies [18] have shown that around 50% of orally administered piperine can be detected in the liver, while lower percentages are present in the heart, spleen, lungs and kidneys tissues. According to Ren et al. [63], piperine can also reach and be distributed uniformly in the brain of Caco-2 models.

Piperine is excreted in the urine in the form of numerous metabolites containing a methoxy group instead of the hydroxyl group in position 3 of the ring, and in bile after being converted into oxidized metabolites [18]. Piperine is also subjected to phase I (e.g., O-demethylation, methylation, amide hydroxylation) and phase II metabolic reactions (e.g., glucuronic acid conjugation and sulfation). Therefore, as for curcumin, its bioavailability after oral administration depends on gastrointestinal content and hepatic enzymatic biotransformation [18].

Nanoparticles can overcome the issue related to hydrophobicity and bypass its first and second metabolism. Polymer nanoparticles and liposomes appear to be the most effective in increasing piperine bioavailability [18,65].

In Kondapalli et al. (2022) [66], the administration of *Piper nigrum* extract to healthy rats enhanced the relative abundance of gut beneficial bacteria such as *Lactobacillus* and *Bifidobacterium* while decreasing *Clostridium* species.

The US Food and Drug Administration (FDA) approved curcumin as a compound "generally recognized as safe". Similarly, JECFA (Joint FAO/WHO Expert Committee on Food Additives) and EFSA (European Food Safety Authority) have indicated, as Acceptable Daily Intake (ADI), a value of 0–3 mg/Kg for curcumin [67]. However, the European Union Herbal Monograph of *Curcuma* L. reports that curcumin may cause flatulence and gastric irritation, stimulation of bile secretion and cholangitis. Therefore, curcumin can exhibit a cholecystokinetic effect, possibly enhanced by piperine, with a contemporary risk of hepatotoxicity [68]. A few cases of hepatotoxicity induced by curcumin are reported in the literature [69,70], inducing the Italian Ministry of Health to prohibit health claims and issue a warning on curcumin-containing products [71]. To date, no severe adverse effects on glycemia have been reported.

An ADI for piperine has not been established yet, but clinical studies predict that the use of piperine, alone or in combination with other drugs, is safe at the dose of 5 mg/day with a limit of toxicity of 50 mg/kg/day [33]. Piperine may cause hemorrhagic stomach ulcers and moderate enteritis with histopathological lesions in the gastrointestinal system. Moreover, it can increase serum gonadotropins and reduce intratesticular testosterone levels in albino rats [33]. Considering the ability of piperine to influence the bioavailability of curcumin, it would be advisable to establish an ADI also for formulations containing both molecules [72].

As already mentioned, many studies evaluated the effects of piperine on the bioavailability of curcumin. The combination of the two molecules, particularly if delivered via nano-emulsions, seems to improve the absorption of curcumin [60–62]. A trial was carried out to evaluate the effect of combining piperine on curcumin bioavailability on albino Wistar rats and healthy human adults (curcumin 2 g/kg body weight and piperine 20 mg/kg for rats, and a dose of curcumin 2 g and piperine 20 mg for humans, respectively). The findings of the study showed that the co-administration of piperine enhanced the oral bioavailability of curcumin both in animals and humans, probably due to the piperine's role in inhibiting the metabolism of curcumin [60]. Similar findings regarding the effects on curcumin absorption and metabolism exerted by piperine co-administration were shown by other studies on mice models [61,62]. However, Suresh and Srinivasan's study [61] showed that the administration of both molecules did not appear to increase curcumin bioavailability in rats, as described elsewhere [72]. The supplementation of curcumin plus piperine can recover intestinal permeability and improve the antioxidant capacity in Wazhishan piglets [28]. In general, the efficacy is greater for the co-administration of curcumin plus piperine compared to high doses of curcumin or single curcumin and piperine. A human study [52] has compared curcumin adsorption after single oral administration of a standard turmeric extract, a liquid micellar preparation, a combination of piperine and curcuminoids, a phytosomal formulation and a dried colloidal suspension. The amount of adsorbed curcumin seems to be greater for the colloidal suspension than both the combination with piperine and the phytosome formulation, while no differences have been observed between piperine-curcumin preparation and turmeric dry extract. In an RCT [73], the co-administration of the two molecules resulted in an improvement of oxidative stress and inflammation in hemodialysis patients (HD).

Several mechanisms can explain the ability of piperine to increase the bioavailability of curcumin. One of these could be a non-specific action carried out at the gastric and gut level, which leads to hyperemia in the intestinal district and an increase in HCl secretion, with a subsequent increase of intestinal permeability [74]. Moreover, piperine can improve some enzymatic activities, like that of the γ-glutamyl trans-peptidase, which is involved in the intracellular transport of nutrients within enterocytes and can inhibit the drug-transporters P-glycoprotein and CYP3A4, expressed in both enterocytes and hepatocytes [68]. Another

well-known mechanism is linked to piperine's capacity to reduce curcumin glucuronidation and sulfation through a reduction in the activity of UGTs and SULTs [75].

Thus, we need further studies and more careful monitoring of patients who use supplements with a combination of curcumin and piperine, especially when there is concomitant use of other drugs [68].

3.2. Curcumin: Mechanism of Action on Insulin Secretion/Activity and Glycemic Homeostasis

The biological activities of insulin begin with its binding to specific Insulin Receptors (IRs) located on the plasma membrane of target cells such as those in the liver, adipose tissue, muscles and brain (although many somatic cells express IRs so insulin has pleiotropic effects) [76]. The activation of the IR, provided with tyrosine kinase activity, provokes its autophosphorylation and recruitment of several substrates, with subsequent initiation of mitogenic and metabolic downstream signaling. Most of the metabolic effects are mediated by the Insulin Receptor Substrate (IRS) family proteins, which in turn recruit phosphoinositide-3-kinase (PI3K) and then phosphoinositide-dependent kinase 1 (PDK1) and AKT [77]. Insulin signaling causes translocation and fusion of the glucose transporter GLUT 4 to the plasma membrane, which enables glucose uptake and glycogen storage in target cells (skeletal muscle and adipose tissue cells). Moreover, insulin suppresses hepatic gluconeogenesis and glycogenolysis, promotes lipid storage and suppresses lipolysis in white adipose tissue (WAT) [77]. Several in vitro and in vivo studies conducted in recent years have identified many possible MoA carried out by curcumin in regulating glucose homeostasis and insulin secretion and signaling.

3.2.1. In Vitro Studies

A recent review coming from in vitro studies [4] has confirmed the positive effects of curcumin as a potential antidiabetic agent. This polyphenol was shown to improve pancreatic beta cell function and survival, increase insulin secretion and improve insulin signaling, enhance glucose uptake in adipocytes and skeletal muscle cells, inhibit gluconeogenesis and reduce lipid deposition and inflammation in liver and adipose tissue cells.

In vitro experiments conducted on skeletal muscle cells have demonstrated that curcumin treatment increases GLUT4 translocation [14,15], enhances AKT phosphorylation [20] and reduces pro-inflammatory cytokines [21]. Similar effects have been observed in adipocytes and hepatocytes [4]. However, a few studies have shown that curcumin might reduce insulin uptake and GLUT4 translocation, possibly because it interferes with AKT signaling [78,79]. Similar effects have been observed in hepatic stellate cells affected by hyperleptinemia [80]. Interestingly, Gunnik et al. (2016) [81] observed that curcumin directly inhibits glucose uptake in fibroblasts by binding to GLUT1 transporters, in an immediate, not additive and reversible way. Moreover, Priyanka et al. (2017) [17] found that curcumin treatment ameliorates hypoxic adipocytes by reducing GLUT1 expression and increasing that of GLUT4 at the same time. It has been postulated that the direct inhibition of GLUT1 and GLUT 4 caused by chronic curcumin treatment might lead to an upregulation of GLUT proteins expression as compensating mechanism. As the evidence on glucose transporters is still controversial, more studies are needed to elucidate this MoA [82]. Given the hormetic effects observed in polyphenols, it might be possible that curcumin produces a biphasic cell response based on dosage and physiological or pathological conditions [83].

Hepatocytes treated with curcumin display a reduction in gluconeogenesis and glycogenolysis accompanied by a decrease in hepatic glucose-6-phosphatase (G6Pase) and phosphoenolpyruvate carboxykinase (PEPCK) activity [22]. Rouse et al. (2014) [23] showed that the treatment of pancreatic islets with curcumin and its curcuminoid analogs resulted in increased insulin secretion and islet recovery, suggesting that it affects insulin signaling and PDE/cAMP regulation. Moreover, the above-mentioned researchers demonstrated that curcumin downregulates, in a dose-dependent manner, the mRNA expression of most of the 11 PDE (phosphodiesterase) isoenzymes, including PDE3B, PDE8A and PDE10A [23].

Additionally, curcumin may improve glucose tolerance via the stimulation of glucagon-like peptide-1 (GLP-1). The mechanism, observed in Caco-2 cells, might be mediated by inhibition of Dipeptidyl peptidase-4 (DPP IV) activity, a surface glycoprotein that degrades GLP-1 [24]. Moreover, curcumin may directly and significantly stimulate GLP-1 secretion via activation of the Ca^{2+}/calmodulin-dependent kinase II pathway (independently from cAMP/PKA) [25].

Overall, the evidence from in vitro studies suggests that curcumin exerts its antidiabetic activity via multiple mechanisms that modulate both glucose uptake and insulin signaling.

3.2.2. In Vivo Animal and Human Studies

In vivo studies indicate that curcumin displays remarkable antidiabetic properties by regulating glucose and lipids levels, improving insulin sensitivity and pancreatic beta-cell function, decreasing inflammation and oxidative stress and decreasing lipid peroxidation [84].

In a cohort of adult albino Wistar rats of both sexes with streptozotocin (STZ)-induced diabetes, curcumin treatment has resulted in decreased Glucose-6- phosphatase [85]. Another study on male C57BL/6 mice with STZ-induced diabetes showed that cur-cumin analog, C66, efficiently attenuated diabetic renal injury via inhibition of MAPK-mediated ACE expression and RAS activation [86]. Finally, a trial on curcumin pretreated C57/BL6J mice, which were given multiple low doses of streptozotocin to induce diabetes, showed that curcumin prevented STZ-induced diabetes, as confirmed by normoglycemia, normal glucose clearance and maintained pancreatic GLUT2 levels [87].

The evidence coming from other animal studies (diabetic KK-Ay and db/db mice) showed that curcumin significantly decreases serum glucose and HbA1c levels [26,27], with additional beneficial effects on lipids profile. Noteworthily, the administration of curcumin to db/db mice not only decreased hyperlipidemia and hyperglycemia [29] but also inhibited NLP3 inflammasome activation, showing a significant downregulation of inflammation [32].

In addition, in high-fat diet-induced diabetes models of C57BL/6J mice and albino rats, interventions with curcumin reduced circulating glucose and leptin, with a concomitant increase in adiponectin and overall improvement of insulin resistance [35,36].

It is interesting to notice that many of these research papers showed decreased insulin secretion. The dosages used in animal studies varied considerably, ranging from 0.08 mg/kg to 1500 mg/kg [84], making the efficacy comparison challenging.

Human studies seem to confirm the effects observed in those conducted on animals as curcumin has been shown to reduce serum glucose, triglyceride, LDL and HbA1c levels, as shown by a double-blind randomized clinical trial conducted on 70 type-2 diabetic (T2D) patients randomly assigned to receive curcumin (80 mg/day) or placebo for 3 months [88]. Another randomized, double-blinded, placebo-controlled trial included 240 participants with prediabetes which were assigned to receive curcumin (250 mg/day) or a placebo for 9 months. The findings showed that the intervention group presented significantly higher HOMA-β and lower C-peptide and none of the curcumin-treated participants developed T2D mellitus during the study period [41]. Similarly, another randomized, double-blinded, placebo-controlled trial carried out on 240 adult participants with T2D assigned to receive curcumin (250 mg/day) or a placebo for 6 months, showed that the intervention group presented increased serum adiponectin and decreased leptin, with an overall reduced atherogenic risk, compared to controls [42].

A recent systematic review and meta-analysis [7] have corroborated the positive effects of curcumin supplementation in improving both glycemic status and lipid profile in T2D individuals via a decreased hepatic production of glucose; it improved glucose uptake, suppressed nuclear factor-kappa B pathways and upregulated PPAR-gamma. The effects on insulin secretion are, however, not clear as some studies seem to indicate a promotion of insulin release, which is in contrast with some of the results observed in animals but aligned with those seen in vitro. More human studies are, therefore, needed to elucidate

the MoA of curcumin and its analogs on glucose and insulin homeostasis, particularly to demonstrate the consequences of long-term use.

3.3. Piperine: Mechanism of Action on Insulin Secretion/Activity and Glycemic Homeostasis

Piperine has been demonstrated to exert various therapeutic activities: antibacterial, anticancer, antidiarrheal, antihypertensive, anti-inflammatory, antioxidant, antiparasitic and hepatoprotective [18,33]. Moreover, piperine, like curcumin, seems to have anti-diabetic properties, performed through different mechanisms of action, as confirmed by in vitro and in vivo studies.

3.3.1. In Vitro Studies

Park et al. (2012) [19] showed that piperine performs its anti-diabetic activity by interacting with peroxisome proliferator-activated receptor gamma (PPAR-γ) with consequently improved insulin-sensibility in 3T3-L1 preadipocytes [19]. Moreover, the findings of a study on L6 myotubes showed that piperine increases the intracellular Ca^{2+} level thus allowing the activation, through the vanilloid channel 1 (TRPV1), of Ca^{2+}/calmoduline-dependent protein kinase beta (CaMKKβ) necessary for AMPK phosphorylation, which in turn enables the translocation of GLUT4 to the plasma membrane. Also, the authors observed that oral administration of piperine to Wistar rats at 0.01 and 0.1 mg/kg body weight reduced postprandial hyperglycemia [16]. Another study carried out on HT-29 cells and Caco-2 cells showed that curcumin repressed mTORC1 in HT-29 and undifferentiated Caco-2 cells, while piperine was able to enhance the mTORC1-inhibitory effect of curcumin in the same cells [13].

3.3.2. In Vivo Animal and Human Studies

Studies on animal models confirmed that piperine exhibits an anti-diabetic activity, as demonstrated by a glucose-tolerance test in male Wistar rats with STZ-induced diabetes supplemented with different piperine derivatives [30], and can reduce body weight, lipid peroxidation and hepatotoxicity [18].

In a study on male Sprague Dawley rats with obesity-induced dyslipidemia, piperine supplementation at a dose of 40 mg/kg of body weight has been shown to improve lipid profile, by reducing body weight, total cholesterol, TG, and increasing HDL serum levels [89]. The mechanism of action is unknown, but it could be linked to an MC-4 agonism performed by the alkaloid. Moreover, piperine supplementation at a dose of 50 mg/kg body weight to male C57BL/6N mice with high-fat diet-induced hepatic steatosis, resulted in a significant increase in plasma adiponectin levels, together with reduced insulin, blood glucose and hepatic lipid levels [37].

Furthermore, oral administration of piperine to Wistar rats allows an increase in the Ca^{2+} levels, with consequent activation of CaMMkβ/AMPK and translocation of GLUT4 transporters, as already noted in the vitro study on preadipocyte cells [16]. Piperine has also been demonstrated to protect against β-cell dysfunction in pre-diabetic C57BL/6C mice and reduce their serum levels of LPS [39].

3.4. Curcumin and Piperine Combined: Mechanism of Action on Insulin Secretion/Activity and Glycemic Homeostasis

Several recent studies have demonstrated the synergic activity of curcumin and piperine in regulating glucose homeostasis when administered in combination.

In Vitro and In Vivo Studies

Kaur et al. (2018) [13] carried out a study on human HT-29 and Caco-2 cells where piperine has been shown to inhibit mTORC1 activity more efficiently than curcumin alone. Moreover, curcumin plus piperine resulted in greater inhibition of TNFα gene expression, thus exerting a significant anti-inflammatory activity.

The anti-inflammatory effect expressed by curcumin plus piperine is confirmed by the weight reduction in high-fat-diet mice and by reduced levels of high-fat diet-induced inflammation and reduction in IFN-γ, IL-10, IL-12 p 70, IL1β, IL6. The combination of these two compounds seems to improve metabolic syndrome in animal models, e.g., male C57BL/6 mice with high-fat diet-induced obesity [31].

In 2020, Shi et al. [28] carried out a study on a cohort of weaned piglets to assess the effects of curcumin and piperine performance, intestinal barrier function and antioxidant capacity. The co-administration of the two compounds has been shown to be more effective compared to a single high dose of curcumin, in recovering intestinal permeability and integrity and suppressing oxidative stress in this animal model.

Hoseini et al. review (2023) [34] showed that the co-administration of curcumin and piperine, independently of the dose, in patients suffering from metabolic syndrome, can restore optimal blood lipid values, with a large reduction of total cholesterol and LDL, but no effect on TG levels.

The daily co-administration of 500 mg of curcuminoids with 5 mg of piperine for 12 weeks, in 70 patients with NAFLD [38], was showed to cause a reduced hematocrit, erythrocyte sedimentation rate, serum concentration of alanine aminotransferase, total cholesterol, LDL, iron and hemoglobin, iron-binding capacity and albumin levels. Therefore, curcumin plus piperine can positively influence the lipid, glycemic and enzymatic profiles in patients with NAFLD and its advancement.

A double-blind placebo-controlled trial [40] involving 80 overweight participants with suboptimal fasting plasma glucose, which were randomized to be treated with curcumin 800 mg/day or a placebo for 8 weeks, demonstrated that the supplementation of a phytosomal preparation of curcumin containing phosphatidylserine and piperine for 56 days of treatment, reduced plasma insulin (FPI), HOMA index, TG, LDL, hepatic transaminases, γ-GT, cortisol level, and a reduction of waist circumference, blood pressure and liver steatosis index as well.

In a randomized-controlled trial conducted in T2D adult patients aged 18–65 years [12], the daily co-administration of 500 mg/day of curcuminoids with 5 mg/day of piperine for three months versus placebo caused a reduction of serum glucose, C-peptide and HbA1c, alanine aminotransferase and aspartate aminotransferase level. Therefore, the combination of curcumin and piperine may significantly improve the glycemic profile in T2D patients.

3.5. TLOC and Curcumin plus Piperine Supplementation

Based on the described evidence, we might postulate that the patient under examination, on a four-month treatment with a supplement containing curcumin and piperine, experienced a single and serious episode of hypoglycemia, responsible for the TLOC.

The dose taken by the patient was within the range of concentrations used in human studies to exert a pharmacological effect [85]. Moreover, the supplement in question also contained magnesium salts fatty acids (E 470) as an emulsifier, which might have promoted the formation of lipid micelles that further increased curcumin and piperine bioavailability. Considering the characteristics and pharmacokinetics of curcumin formulated with piperine, it can be assumed that after about 5 h from intake (12:30 PM was the time of meal and supplement intake and 5 PM was the time when the TLOC event was recorded), curcumin could still be sufficiently bioavailable to express its biological activity, including the hypoglycemic effects.

4. Conclusions

The hypoglycemic action of curcumin, mainly attributable to increased glucose uptake by cells, and the augmented secretion of insulin might have exacerbated the hypersecretion of the hormone caused by insulinoma and possibly led to hypoglycemia. We could also hypothesize that the action of curcumin on GLUT1 transporters in the brain might have contributed to a reduction of glucose available in brain tissue.

Considering the growing use of curcumin (also in combination with piperine) for the treatment of various pathologies, it would be preferable that these supplements were prescribed by competent healthcare providers.

Given the above considerations, we suggest that further research be conducted to elucidate the effects of curcumin in patients with impaired glucose metabolism and/or increased insulin secretion.

Appendix A

Table A1. Summary of bioavailability, adverse effects, plasma peak concentrations and safety of curcumin and piperine as single agents and in combination in supplements.

	Curcumin (CUR)	Piperine (PIP)	Complex Curcumin + Piperine (CUR + PIP)
Bioavailability and pharma-cokinetics	Low bioavailability Poor absorption [2] • lipophilic [9] • limited tissue distribution [44] • single high dose causes saturation of the transport mechanism [47] • rapid intestinal metabolism and clearance [44] • extensive Phase I and Phase II liver transformation [45] • excreted in feces as metabolites [45]	Low bioavailability Poor absorption [18] • lipophilic [18] • tissues distribution: liver (50%), heart, spleen, lungs, kidneys, and brain [18,63,64] • subjected to oxidation, hydrogenation, methylation, glucuronidation, demethylation, sulfation and oxidation [18,65]	PIP causes higher adsorption, plasma concentration of CUR [2,4,28,44,51,60–62,72,73] • lipophilic [9,18] • ↑ bioavailability of CUR [2,4,47–49,65,72]
	↑ bioavailability in formulations, including micelles, nanoparticles, nano-emulsion liposomes, phospholipid complexes [48], β-casein-micelles [49], phytosomal formulations [50]	Excreted in urine and bile in form of metabolites [18,65]	↑ PIP reduces CUR glucuronidation and sulfation (red UGTs and SULTs activity) [75]
	↑ bioavailability with fresh or dried powder compared to supplements due to food matrix [53]	↑ bioavailability in the formulation including liposomes, polymeric micelles, nanoparticles, nanofibers and solid-lipid nanoparticles. [18,65]	↑ PIP enhances enzymes for the intracellular transport of nutrients (γ-glutamil transpeptidase) and inhibits drug-transporter (P-glycoprotein and CYP3A4) in enterocytes and hepatocytes [68]
	↑ intestinal microbiota enhances metabolism and biotransformation into derivates with specific biological activities [1,54] Modulation of beneficial bacteria [1,56]	↑ PIP enhances gut beneficial bacteria [66]	↑ PIP increases intestinal permeability [28]

Table A1. *Cont.*

	Curcumin (CUR)	Piperine (PIP)	Complex Curcumin + Piperine (CUR + PIP)
			↑ PIP increases blood supply to the gastrointestinal tract and HCl secretion [74]
			↑ bioavailability nano-emulsion of CUR plus PIP [72]
			no significant differences were observed between the piperine-curcuminoid combination and the standard extract of single curcumin. [52]
Adverse side effect	Flatulence and gastric irritation, stimulation of bile secretion, cholangitis. No effects on glycemia [68].	Hemorrhagic stomach ulceration, mild to moderate enteritis, increased serum gonadotropins and decreased intratesticular testosterone levels. No effects on glycemia [33].	No specific study, but PIP enhanced the risk for hepatotoxicity [68–71]
Plasma peak after oral administration	1–2 h Undetectable within 12 h [46]	2–4 h Undetectable within 48 h [18,63]	No study
Safety: ADI/	0.3 mg/kg/day [67]	5 mg/day (max dose 50 mg/kg/day) [33]	No study

↑: increase; ↓: reduction.

References

1. Scazzocchio, B.; Minghetti, L.; D'Archivio, M. Interaction between gut microbiota and Curcumin: A New Key of Understanding for the Health Effects of Curcumin. *Nutrition* **2020**, *12*, 2499. [CrossRef]
2. Sahebkar, A.; Gandolfo, V.; Bianconi, V.; Mannarino, M.R.; Pirro, M. Effetti della curcumina con possibile impatto sul danno vascolare aterosclerotico. *G. Ital. Dell'aterosclerosi* **2017**, *8*, 90–102.
3. Kocaadam, B.; Sanlier, N. Curcumin, an active component of turmeric (*Curcuma longa*), and its effects on health. *Crit. Rev. Food Sci. Nutr.* **2017**, *57*, 2889–2895. [CrossRef] [PubMed]
4. Den Hartogh, D.J.; Gabriel, A.; Tsiani, E. Antidiabetic Properties of curcumin I: Evidence from In Vitro Studies. *Nutrients* **2020**, *12*, 118. [CrossRef]
5. Peijian, W.; Hui, L.; Hongjun, L.; Wenhong, L. Comparing the Effect of Piperine Ilepcimide on the Pharmacokinetics of curcumin in SD Rats. *Front. Pharmacol.* **2021**, *12*, 725362.
6. Altobelli, E.; Angeletti, P.M.; Marziliano, C.; Mastrodomenico, M.; Giuliani, A.R.; Petrocelli, R. Potential Therapeutic Effects of Curcumin on Glycemic and Lipid Profile in Uncomplicated Type 2 Diabetes-A Meta-Analysis of Randomized Controlled Trial. *Nutrients* **2021**, *13*, 404. [CrossRef]
7. Tian, J.; Feng, B.; Tian, Z. The Effect of Curcumin on Lipid Profile and Glycemic Status of Patients with Type 2 Diabetes Mellitus: A Systematic Review and Meta-Analysis. *Evid. Based Complement. Altern. Med.* **2022**, *2022*, 827874. [CrossRef]
8. Pratò, S.; Didonna, V.; Garletti, F.; Marfia, G.; Barbaresi, A.; Palumbo, F.; Garzia, E.; Ciniglio Appiani, G.; Riboldi, L.; Vigna, L. Loss of consciousness in a helicopter pilot as plausible first sign of insulinoma: A case report. *Med. Lav.* **2022**, *113*, e2022007.
9. Shanmugan, M.K.; Rana, G.; Mathi Kanchi, M.; Arfuso, F.; Cinnathambi, A.; Zayed, M.E.; Alharbi, S.A.; Tan, B.K.H.; Krumar, A.P.; Sethi, G. Multifaced Role of Curcumin in Cancer Prevention and Treatment. *Molecules* **2015**, *20*, 2728–2769. [CrossRef]
10. Sharifi-Rad, J.; Rayess, Y.E.; Rizk, A.A.; Sadaka, C.; Zgheib, R.; Zam, W.; Sestito, S.; Rapposelli, S.; Neffe-Skocińska, K.; Zielińska, D. Turmeric and Its Major Compound Curcumin on Health: Bioactive Effects and Safety Profiles for Food, Pharmaceutical, Biotechnological and Medicinal Applications. *Front. Pharmacol.* **2020**, *11*, 01021. [CrossRef]
11. Cavaleri, F. The 3 Curcuminoid Analogs Comprising the Curcumin Extract Comparably Inhibit Nuclear Factor kappa-light-chain-enhancer Activation. *Prog. Prev. Med.* **2019**, *4*, e0023. [CrossRef]
12. Panahi, Y.; Khalili, N.; Sahebi, E.; Namazi, S.; Simental-Mendía, L.E.; Majeed, M.; Sahebkar, A. Effects of Curcuminoids Plus Piperine on Glycemic, Hepatic and Inflammatory Biomarkers in Patients with Type 2 Diabetes Mellitus: A Randomized Double-Blind Placebo-Controlled Trial. *Drug Res.* **2018**, *68*, 403–409. [CrossRef] [PubMed]
13. Kaur, H.; He, B.; Zhang, C.; Rodriguez, E.; Hage, D.S.; Moreau, R. Piperine potentiates curcumin-mediated repression of mTORC1 signalling in human intestinal epithelial cells: Implication for the inhibition of protein synthesis and TNFα signalling. *J. Nutr. Biochem.* **2018**, *57*, 276–286. [CrossRef]
14. Kang, C.; Kim, E. Synergistic effect of curcumin and insulin on muscle cell glucose metabolism. *Food Chem. Toxicol.* **2010**, *48*, 2366–2373. [CrossRef] [PubMed]

15. Chauhan, P.; Tamrakar, A.K.; Mahajan., S.; Prasad, G.B.K.S. Chitosan encapsulated nanocurcumin induces GLUT-4 translocation and exhibits enhanced anti-hyperglycaemic function. *Life Sci.* **2018**, *213*, 226–235. [CrossRef]

16. Maeda, A.; Shirao, T.; Shirasava, D.; Yoshioka, Y.; Yamashita, Y.; Akagawa, M.; Ashida, H. Piperine Promotes Glucose Uptake through ROS-Dependent Activation of the CAMKK/AMPK Signalling Pathway in Skeletal Muscle. *Mol. Nutr. Food Res.* **2018**, *62*, e1800086. [CrossRef]

17. Priyanka, A.; Shyni, G.L.; Anupama, N.; Raj, P.S.; Anusree, S.S.; Raghu, K.G. Development of insulin resistance through sprouting of inflammatory markers during hypoxia in 3T3-L1 adipocytes and amelioration with curcumin. *Eur. J. Pharmacol.* **2017**, *812*, 73–81. [CrossRef]

18. Quijia, C.R.; Araujo, V.H.; Chorilli, M. Piperine: Chemical, biological and nanotechnological applications. *Acta Pharm.* **2021**, *71*, 185–213. [CrossRef]

19. Park, U.H.; Jeong, H.S.; Jo, E.Y.; Park, T.; Yoon, S.K.; Kim, E.J.; Jeong, J.C.; Um, S.J. Piperine, a component of black pepper, inhibits adipogenesis by antagonizing PPAR-g activity in 3T3-L1 cells. *J. Agric. Food Chem.* **2012**, *60*, 3853–3860. [CrossRef]

20. Deng, Y.T.; Chang, T.W.; Lee, M.S.; Lin, J.K. Suppression of free fatty acid-induced insulin resistance by phytopolyphenols in C2C12 mouse skeletal muscle cells. *J. Agric. Food Chem.* **2012**, *60*, 1059–1066. [CrossRef]

21. Sadeghi, A.; Rostamirad, A.; Seyyedebrahimi, S.; Meshkani, R. Curcumin ameliorates palmitate-induced inflammation in skeletal muscle cells by regulating JNK/NF-kB pathway and ROS production. *Inflammopharmacology* **2018**, *26*, 1265–1272. [CrossRef]

22. Fujiwara, H.; Hosokawa, M.; Zhou, X.; Fujimoto, S.; Fukuda, K.; Toyoda, K.; Nishi, Y.; Fujita, Y.; Yamada, K.; Yamada, Y.; et al. Curcumin inhibits glucose production in isolated mice hepatocytes. *Diabetes Res. Clin. Pract.* **2008**, *80*, 185–191. [CrossRef] [PubMed]

23. Rouse, M.; Younès, A.; Egan, J.M. Resveratrol and curcumin enhance pancreatic β-cell function by inhibiting phosphodiesterase activity. *J. Endocrinol.* **2014**, *223*, 107–117. [CrossRef] [PubMed]

24. Huang, P.K.; Lin, S.R.; Chang, C.H.; Tsai, M.J.; Lee, D.N.; Weng, C.F. Natural phenolic compounds potentiate hypoglycemia via inhibition of Dipeptidyl peptidase IV. *Sci. Rep.* **2019**, *9*, 15585. [CrossRef] [PubMed]

25. Takikawa, M.; Kurimoto, Y.; Tsuda, T. Curcumin stimulates glucagon-like peptide-1 secretion in GLUT cells via Ca^{2+}/calmodulin-dependent kinase II activation. *Biochem. Biophys. Res. Commun.* **2013**, *435*, 165–170. [CrossRef] [PubMed]

26. Nishiyama, T.; Mae, T.; Kishida, H.; Tsukagawa, M.; Mimaki, Y.; Kuroda, M.; Sashida, Y.; Takahashi, K.; Kawada, T.; Nakagawa, K.; et al. Curcuminoids and sesquiterpenoids in turmeric (*Curcuma longa* L.) suppress an increase in blood glucose level in type 2 diabetic KK-Ay mice. *J. Agric. Food Chem.* **2005**, *53*, 959–963. [CrossRef]

27. Seo, K.I.; Choi, M.S.; Jung, U.J.; Kim, H.J.; Yeo, J.; Jeon, S.M.; Lee, M.K. Effect of curcumin supplementation on blood glucose, plasma insulin, and glucose homeostasis related enzyme activities in diabetic db/db mice. *Mol. Nutr. Food Res.* **2008**, *52*, 995–1004. [CrossRef] [PubMed]

28. Shi, L.; Xun, W.; Peng, W.; Hu, H.; Cao, T.; Hou, G. Effect of the Single and Combined Use of Curcumin and Piperine on Growth Performance, Intestinal Barrier Function, and Antioxidant Capacity of Weaned Wuzhishan Piglets Front. *Vet. Sci.* **2020**, *7*, 418. [CrossRef]

29. Soto-Urquieta, M.G.; López-Briones, S.; Pérez-Vázquez, V.; Saavedra-Molina, A.; González-Hernández, G.A.; Ramírez-Emiliano, J. Curcumin restores mitochondrial functions and decreases lipid peroxidation in liver and kidneys of diabetic db/db mice. *Biol. Res.* **2014**, *47*, 74. [CrossRef]

30. Kharbanda, C.; Alam, M.S.; Hamid, H.; Javed, K.; Bano, S.; Ali, Y.; Dhulap, A.; Alam, P.; Pasha, M.A. Novel Piperine Derivatives with Antidiabetic Effect as PPAR-γ Agonists. *Chem. Biol. Drug Des.* **2016**, *88*, 354–362. [CrossRef]

31. Miyazawa, T.; Nakagawa, K.; Kim, S.H.; Thomas, M.J.; Paul, L.; Zingg, J.M.; Dolnikowski, G.G.; Roberts, S.B.; Kiura, F.; Miyazawa, T.; et al. Curcumin and piperine supplementation of obese mice under caloric restriction modulates body fat and interleukin-1β. *Nutr. Metab.* **2018**, *15*, 12. [CrossRef] [PubMed]

32. Lu, M.; Yin, N.; Liu, W.; Cui, X.; Chen, S.; Wang, E. Curcumin Ameliorates Diabetic Nephropathy by Suppressing NLRP3 Inflammasome Signalling. *Biomed. Res. Int.* **2017**, *2017*, 1516985. [CrossRef]

33. Tripathi, A.K.; Ray, A.K.; Mishra, S.K. Molecular and pharmacological aspects of piperine as a potential molecule for disease prevention and management: Evidence from clinical trials. *Beni Suef Univ. J. Basic Appl. Sci.* **2022**, *11*, 16. [CrossRef] [PubMed]

34. Hoseini, H.; Ghavidel, F.; Panhai, G.; Majeed, M.; Sahebcar, A. A systematic review and meta-analysis of randomized controlled trials investigating the effect of the curcumin and piperine combination on lipid profile in patients with metabolic syndrome and related disorders. *Phytother. Res.* **2023**, *37*, 1212–1224. [CrossRef]

35. Shao, W.; Yu, Z.; Chiang, Y.; Yang, Y.; Chai, T.; Foltz, W.; Lu, H.; Fantus, I.G.; Jin, T. Curcumin prevents high fat diet induced insulin resistance and obesity via attenuating lipogenesis in liver and inflammatory pathway in adipocytes. *PLoS ONE* **2012**, *7*, e28784. [CrossRef] [PubMed]

36. Kelany, M.E.; Hakami, T.M.; Omar, A.H. Curcumin improves the metabolic syndrome in high-fructose-diet-fed rats: Role of TNF-α, NF-κB, and oxidative stress. *Can. J. Physiol. Pharmacol.* **2017**, *95*, 140–150. [CrossRef]

37. Choi, S.; Choi, Y.; Choi, Y.; Kim, S.; Jang, J.; Park, T. Piperine reverses high Ft diet-induced hepatic steatosis and insulin resistance in mice. *Food Chem.* **2013**, *141*, 3727–3735. [CrossRef] [PubMed]

38. Panahi, Y.; Valizadegan, G.; Ahamdi, N.; Ganjali, S.; Majeed, M.; Sahebkar, A. Curcuminoids plus piperine improve nonalcoholic fatty liver disease: A clinical trial. *J. Cell. Biochem.* **2019**, *120*, 15989–15996. [CrossRef]

39. Yuan, Y.; Zhou, J.; Hu, R.; Zou, L.; Ji, L.; Jiang, G. Piperine protects against pancreatic β-cell dysfunction by alleviating macrophage inflammation in obese mice. *Life Sci.* **2021**, *274*, 119312. [CrossRef]

40. Cicero, A.F.G.; Sahebkar, A.; Fogacci, F.; Bove, M.; Giovannini, M.; Borghi, C. Effect of phytosomal curcumin on anthropometric parameters, insulin resistance, cortisolemia and non-alcoholic fatty liver disease indices; a double bind, placebo-controlled clinical trial. *Eur. J. Nutr.* **2020**, *59*, 477–483. [CrossRef]

41. Chuengsamarn, S.; Rattanamongkolgul, S.; Luechapudiporn, R.; Phisalaphong, C.; Jirawatnotai, S. Curcumin extract for prevention of type 2 diabetes. *Diabetes Care* **2012**, *35*, 2121–2127. [CrossRef]

42. Chuengsamarn, S.; Rattanamongkolgul, S.; Phonrat, B.; Tungtrongchitr, R.; Jirawatnotai, S. Reduction of atherogenic risk in patients with type 2 diabetes by curcuminoid extract: A randomized controlled trial. *J. Nutr. Biochem.* **2014**, *25*, 144–150. [CrossRef]

43. Embuscado, M.E. Bioactives From Spices and Herbs. In *Encyclopedia of Food Chemistry*; Elsevier: Amsterdam, The Netherlands, 2019; pp. 497–514.

44. Anand, P.; Kunnumakkara, A.B.; Newman, R.A.; Aggarwal, B.B. Bioavailability of curcumin: Problems and promises. *Mol. Pharm.* **2007**, *4*, 807–818. [CrossRef]

45. Sharma, R.A.; Steward, W.P.; Gescher, A.J. Pharmacokinetics and pharmacodynamics of curcumin. *Adv. Exp. Med. Biol.* **2007**, *595*, 453–470. [CrossRef] [PubMed]

46. Dei Cas, M.; Ghidoni, R. Dietary Curcumin: Correlation between Bioavailability and Health Potential. *Nutrients* **2019**, *11*, 2147. [CrossRef]

47. Vareed, S.K.; Kakarala, M.; Ruffin, M.T.; Crowell, J.A.; Normolle, D.P.; Djuric, Z.; Brenner, D.E. Pharmacokinetics of curcumin conjugate metabolites in healthy human subjects. *Cancer Epidemiol. Biomark. Prev.* **2008**, *17*, 1411–1417. [CrossRef] [PubMed]

48. Prasad, S.; Tyagi, A.K.; Aggarwal, B.B. Recent developments in delivery, bioavailability, absorption and metabolism of curcumin: The golden pigment from golden spice. *Cancer Res. Treat.* **2014**, *46*, 2–18. [CrossRef]

49. Hu, B.; Liu, X.; Zhang, C.; Zeng, X. Food macromolecule based nanodelivery systems for enhancing the bioavailability of polyphenols. *J. Food Drug Anal.* **2017**, *25*, 3–15. [CrossRef]

50. Mirzaei, H.; Shakeri, A.; Rashidi, B.; Jalili, A.; Banikazemi, Z.; Sahebkar, A. Phytosomal curcumin: A review of pharmacokinetic, experimental and clinical studies. *Biomed. Pharmacother.* **2017**, *85*, 102–112. [CrossRef] [PubMed]

51. Mimica, B.; Bučević Popović, V.; Banjari, I.; Jeličić Kadić, A.; Puljak, L. Methods Used for Enhancing the Bioavailability of Oral Curcumin in Randomized Controlled Trials: A Meta-Research Study. *Pharmaceuticals* **2022**, *15*, 939. [CrossRef]

52. Fança-Berthon, P.; Tenon, M.; Le Bouter-Banon, S.; Manfré, A.; Maudet, C.; Dion, A. Pharmacokinetics of a Single Dose of Turmeric Curcuminoids Depends on Formulation: Results of a Human Crossover Study. *J. Nutr.* **2021**, *151*, 1802–1816. [CrossRef] [PubMed]

53. Ahmed Nasef, N.; Loveday, S.M.; Golding, M.; Martins, R.N.; Shah, T.M.; Clarke, M.; Coad, J.; Moughan, P.J.; Garg, M.L.; Singh, H. Food matrix and co-presence of turmeric compounds influence bioavailability of curcumin in healthy humans. *Food Funct.* **2019**, *10*, 4584–4592. [CrossRef]

54. Lopresti, A.L. The Problem of Curcumin and Its Bioavailability: Could Its Gastrointestinal Influence Contribute to Its Overall Health-Enhancing Effects? *Adv. Nutr.* **2018**, *9*, 41–50. [CrossRef]

55. Jabczyk, M.; Nowak, J.; Hudzik, B.; Zubelewicz-Szkodzińska, B. Curcumin and Its Potential Impact on Microbiota. *Nutrients* **2021**, *13*, 2004. [CrossRef] [PubMed]

56. Pluta, R.; Januszewski, S.; Ułamek-Kozioł, M. Mutual Two-Way Interactions of Curcumin and Gut Microbiota. *Int. J. Mol. Sci.* **2020**, *21*, 1055. [CrossRef] [PubMed]

57. Wang, J.; Ghosh, S.S.; Ghosh, S. Curcumin improves intestinal barrier function: Modulation of intracellular signalling, and organization of tight junctions. *Am. J. Physiol.* **2017**, *312*, C438–C445. [CrossRef]

58. Ghosh, S.S.; He, H.; Wang, J.; Gehr, T.W.; Ghosh, S. Curcumin-mediated regulation of intestinal barrier function: The mechanism underlying its beneficial effects. *Tissue Barriers* **2018**, *6*, e1425085. [CrossRef] [PubMed]

59. Jin, T.; Song, Z.; Weng, J.; Fantus, I.G. Curcumin and other dietary polyphenols: Potential mechanisms of metabolic actions and therapy for diabetes and obesity. *Am. J. Physiol. -Endocrinol. Metab.* **2018**, *314*, E201–E205. [CrossRef] [PubMed]

60. Shoba, G.; Joi, D.; Joseph, T. Influence of piperine on the pharmacokinetics of curcumin in animals and human volunteers. *Planta Med.* **1998**, *64*, 353–356. [CrossRef]

61. Suresh, M.; Srinivasan, K. Tissue distribution & elimination of capsaicin, piperine & curcumin following oral intake in rats. *Indian J. Med. Res.* **2010**, *131*, 682–691.

62. Sharma, V.; Nehru, B.; Munshi, A. Antioxidant potential of curcumin against oxidative insult induced by pentylenetetrazol in epileptic rats. *Methods Find. Exp. Clin. Pharmacol.* **2010**, *32*, 227–232. [CrossRef]

63. Ren, T.; Wang, Q.; Li, C.; Yang, M.; Zuo, Z. Efficient brain uptake of piperine and its pharmacokinetics characterization after oral administration. *Xenobiotica* **2018**, *48*, 1249–1257. [CrossRef]

64. Itharat, A.; Kanokkangsadal, P.; Khemawoot, P.; Wanichsetakul, P.; Davies, N.M. Pharmacokinetics of piperine after oral administration of Sahastara remedy capsules in healthy volunteers. *Res. Pharm. Sci.* **2020**, *15*, 410–417. [CrossRef]

65. Patel, S.S.; Acharya, A.; Ray, R.S.; Agrawal, R.; Raghuwanshi, R.; Jain, P. Cellular and molecular mechanisms of curcumin in prevention and treatment of disease. *Crit. Rev. Food Sci. Nutr.* **2020**, *60*, 887–939. [CrossRef] [PubMed]

66. Kondapalli, N.B.; Hemalatha, R.; Uppala, S.; Yathapu, S.R.; Mohammed, S.; Venkata Surekha, M.; Rajendran, A.; Bharadwaj, D.K. Ocimum sanctum, Zingiber officinale, and Piper nigrum extracts and their effects on gut microbiota modulations (prebiotic potential), basal inflammatory markers and lipid levels: Oral supplementation study in healthy rats. *Pharm. Biol.* **2022**, *60*, 437–450. [CrossRef] [PubMed]

67. Hewlings, S.J.; Kalman, D.S. Curcumin: A Review of Its Effects on Human Health. *Foods* **2017**, *6*, 92. [CrossRef]
68. Menniti-Ippolito, F.; Ippoliti, I.; Pastorelli, A.A.; Altieri, I.; Scalise, F.; De Santis, B.; Debegnach, F.; Brera, C.; Pacifici, R.; Pichini, S.; et al. Turmeric (*Curcuma longa* L.) food supplements and hepatotoxicity: An integrated evaluation approach. *Ann. Ist. Super Sanita* **2020**, *56*, 462–469. [CrossRef]
69. Bucchini, L. The 2019 curcumin crisis in Italy: What we know so far, and early lessons. *Planta Med.* **2019**, *85*, 1401-0. [CrossRef]
70. Pancholi, V.; Smina, T.P.; Kunnumakkara, A.B.; Maliakel, B.; Krishnakumar, I.M. Safety assessment of a highly bioavailable curcumin-galactomannoside complex (CurQfen) in healthy volunteers, with a special reference to the recent hepatotoxic reports of curcumin supplements: A 90-days prospective study. *Toxicol. Rep.* **2021**, *8*, 1255–1264. [CrossRef]
71. Ministero della Salute, Direzione Generale per l'Igiene e la Sicurezza degli Alimenti e la Nutrizione. Integratori Alimentari Contenenti Estratti e Preparati di Piante di *Curcuma longa e* spp*: Modifica* All'allegato 1 del DM 10 Agosto 2018. Available online: https://www.cna.it/wp-content/uploads/2022/08/01082022-cambio-decreto-curcuma-associazioni-rev-2.pdf (accessed on 2 March 2023).
72. Bundesinstitut fur Risikobewertung. Curcumin in Food Supplements: Acceptable Daily Intake May be Exceeded. BfR Opinion No 040/2021 Issued 14 December 2021. Available online: https://www.bfr.bund.de/cm/349/curcumin-in-food-supplements-acceptable-daily-intake-may-be-exceeded.pdf (accessed on 2 March 2023).
73. Freitas, E.; Silva-Santana, N.C.; Rodrigues, H.C.N.; Pereira Martins, T.F.; Braga, C.C.; Silva, M.A.C.; Carlos da Cunha, L.; de Souza Freitas, A.T.V.; Costa, N.A.; Peixoto, M.D.R.G. Turmeric supplementation with piperine is more effective than turmeric alone in attenuating oxidative stress and inflammation in hemodialysis patients: A randomized, double-blind clinical trial. *Free Radic. Biol. Med.* **2022**, *193 Pt 2*, 648–655. [CrossRef]
74. Racz, Z.R.; Pop, L.C.; Tomoaia, G.; Mounca, A.; Barbu, I.; Sarkozi, M.; Racz, C.P.; Roman, I.; Avram, A.; Tomoaia-Cotisel, M. Strategies for Improving Bioavailability, Bioactivity, and Physical-Chemical Behaviour of Curcumin. *Molecules* **2022**, *27*, 6854. [CrossRef] [PubMed]
75. Balakumar, P.; Alqahtani, T.; Alqahtani, A.; Lakshmiraj, R.S.; Singh, G.; Rupeshkumar, M.; Thangathirupathi, A.; Sundram, K. A Unifying Perspective in Blunting the Limited Oral Bioavailability of Curcumin: A Succinct Look. *Curr. Drug Metab.* **2022**, *23*, 897–904. [CrossRef] [PubMed]
76. Haeusler, R.A.; McGraw, T.E.; Accili, D. Biochemical and cellular properties of insulin receptor signalling. *Nat. Rev. Mol. Cell Biol.* **2018**, *19*, 31–44. [CrossRef]
77. Petersen, M.C.; Shulman, G.I. Mechanisms of Insulin Action and Insulin Resistance. *Physiol. Rev.* **2018**, *98*, 2133–2223. [CrossRef]
78. Green, A.; Kranse, J.; Rumemerger, J.M. Curcumin is a direct inhibitor of glucose transport in adipocytes. *Phytomedicine* **2014**, *21*, 118–122. [CrossRef] [PubMed]
79. Zhan, D.; Zhang, Y.; Ye, M.; Din, Y.; Tang, Z.; Li, M.; Zhan, Y.; Wangh, C. Interference with AKT signalling pathway contributes curcumin-induced adipocyte insulin resistance. *Mol. Cell. Endocrinol.* **2016**, *429*, 1–9. [CrossRef]
80. Tang, Y.; Chen, A. Curcumin prevents leptin raising glucose levels in hepatic stellate cells by blocking translocation of glucose transporter-4 and increasing glucokinase. *Br. J. Pharmacol.* **2010**, *161*, 1137–1149. [CrossRef] [PubMed]
81. Gunnink, L.K.; Alabi, O.D.; Kuiper, B.D.; Gunnink, S.M.; Schuiteman, S.J.; Strohbehn, L.E.; Hamilton, K.E.; Wrobel, K.E.; Louters, L.L. Curcumin directly inhibits the transport activity of GLUT1. *Biochimie* **2016**, *125*, 179–185. [CrossRef]
82. Mohammadi, E.; Behnam, B.; Mohammadinejad, R.; Guest, P.C.; Simental-Mendía, L.E.; Sahebkar, A. Antidiabetic Properties of Curcumin: Insights on New Mechanisms. *Adv. Exp. Med. Biol.* **2021**, *1291*, 151–164. [CrossRef]
83. Moghaddam, N.S.A.; Oskouie, M.N.; Butler, A.E.; Petit, P.X.; Barreto, G.E.; Sahebkar, A. Hormetic effects of curcumin: What is the evidence? *J. Cell. Physiol.* **2019**, *234*, 10060–10071. [CrossRef]
84. Den Hartogh, D.J.; Gabriel, A.; Tsiani, E. Antidiabetic Properties of Curcumin II: Evidence from in Vivo Studies. *Nutrients* **2020**, *12*, 58. [CrossRef] [PubMed]
85. Ali Hussain, H.E. Hypoglycemic, hypolipidemic and antioxidant properties of combination of Curcumin from Curcuma longa, Linn, and partially purified product from Abroma augusta, Linn. in streptozotocin induced diabetes. *Indian J. Clin. Biochem.* **2002**, *17*, 33–43. [CrossRef]
86. Pan, Y.; Huang, Y.; Wang, Z.; Fang, Q.; Sun, Y.; Tong, C.; Peng, K.; Wang, Y.; Miao, L.; Cai, L.; et al. Inhibition of MAPK-mediated ACE expression by compound C66 prevents STZ-induced diabetic nephropathy. *J. Cell. Mol. Med.* **2014**, *18*, 231–241. [CrossRef]
87. Kanitkar, M.; Gokhale, K.; Galande, S.; Bhonde, R.R. Novel role of curcumin in the prevention of cytokine-induced islet death in vitro and diabetogenesis in vivo. *Br. J. Pharmacol.* **2008**, *155*, 702–713. [CrossRef] [PubMed]
88. Rahimi, H.R.; Mohammadpour, A.H.; Dastani, M.; Jaafari, M.R.; Abnous, K.; Ghayour Mobarhan, M.; Kazemi Oskuee, R. The effect of nano-curcumin on HbA1c, fasting blood glucose, and lipid profile in diabetic subjects: A randomized clinical trial. *Avicenna J. Phytomed.* **2016**, *6*, 567–577. [PubMed]
89. Shah, S.S.; Shah, G.B.; Singh, S.D.; Gohil, P.V.; Chauhan, K.; Shah, K.A.; Chorawala, M. Effect of piperine in the regulation of obesity-induced dyslipidemia in high-fat diet rats. *Indian J. Pharmacol.* **2011**, *43*, 296–299. [CrossRef] [PubMed]

Article

Long-Term Ingestion of Sicilian Black Bee Chestnut Honey and/or D-Limonene Counteracts Brain Damage Induced by High Fat-Diet in Obese Mice

Simona Terzo [1], Pasquale Calvi [1,2], Domenico Nuzzo [3], Pasquale Picone [3], Mario Allegra [1], Flavia Mulè [1] and Antonella Amato [1,*]

[1] Dipartimento di Scienze e Tecnologie Biologiche, Chimiche e Farmaceutiche (STEBICEF), Università degli Studi di Palermo, 90128 Palermo, Italy
[2] Dipartimento di Biomedicina, Neuroscienze e Diagnostica Avanzata (Bi.N.D.), Università degli Studi di Palermo, 90127 Palermo, Italy
[3] National Research Council of Italy—CNR, Institute for Biomedical Research and Innovation—IRIB, 90146 Palermo, Italy
*   Correspondence: antonella.amato@unipa.it; Tel.: +39-091-2389-7506

Abstract: Obesity is linked to neurodegeneration, which is mainly caused by inflammation and oxidative stress. We analyzed whether the long-term intake of honey and/or D-limonene, which are known for their antioxidant and anti-inflammatory actions, when ingested separately or in combination, can counteract the neurodegeneration occurring in high fat diet (HFD)-induced obesity. After 10 weeks of HFD, mice were divided into: HFD-, HFD + honey (HFD-H)-, HFD + D-limonene (HFD-L)-, HFD + honey + D-limonene (HFD-H + L)-fed groups, for another 10 weeks. Another group was fed a standard diet (STD). We analyzed the brain neurodegeneration, inflammation, oxidative stress, and gene expression of Alzheimer's disease (AD) markers. The HFD animals showed higher neuronal apoptosis, upregulation of pro-apoptotic genes Fas-L, Bim P27 and downregulation of anti-apoptotic factors BDNF and BCL2; increased gene expression of the pro-inflammatory IL-1β, IL-6 and TNF-α and elevated oxidative stress markers COX-2, iNOS, ROS and nitrite. The honey and D-limonene intake counteracted these alterations; however, they did so in a stronger manner when in combination. Genes involved in amyloid plaque processing (APP and TAU), synaptic function (Ache) and AD-related hyperphosphorylation were higher in HFD brains, and significantly downregulated in HFD-H, HFD-L and HFD-H + L. These results suggest that honey and limonene ingestion counteract obesity-related neurodegeneration and that joint consumption is more efficacious than a single administration.

Keywords: obesity; high-fat diet; neuronal damage; neurodegeneration; honey; D-limonene

1. Introduction

Neurodegenerative diseases (NDs), including Alzheimer's disease (AD), are characterized by the progressive loss of neurons in areas of the brain, leading to cognitive and functional deterioration. NDs represent a serious problem because they affect about 50 million patients worldwide and this number is estimated to reach 115 million in 2050 [1]. Different factors contribute to the onset and progression of neurodegeneration such as aging, genetics, environment [2] and oxidative stress and inflammation [3,4]. Moreover, obesity and diabetes increase the risk of developing dementia and AD. In fact, the neurodegenerative process is exacerbated by obesity or diabetes, leading to the concept of metabolism-dependent neurodegeneration [5]. Indeed, insulin receptor down-regulation has been observed in the brains of patients with AD [6] confirming the theory that AD may be considered as "type 3 diabetes" [7]. Furthermore, studies on animal models pointed out that obesity affects learning and memory [8,9] and long-term ingestion of high-fat diet (HFD) in rodents is responsible for neuronal loss and synaptic plasticity damage [10–13].

NDs are as yet incurable and strongly debilitating for the patients. Nevertheless, current research is pushing towards effective therapies [14,15]. Numerous nutraceuticals and/or functional foods are considered protective and/or therapeutic against the metabolic dysfunctions and the related neurodegeneration [16–20]. For example, foods rich in antioxidants, micronutrients, phytochemicals, essential oils, and probiotics have been found to be helpful in maintaining body weight and reducing the incidence of neurodegenerative diseases [1,20].

In particular, honey might prove useful in the treatment of chronic diseases linked to oxidative stress and inflammation due to its high content in polyphenols [21]. Although the composition of honey is variable depending on various factors such as botanical origin, geographical region and climatic conditions, most of the polyphenols present in honey are flavonoids and phenolic acid derivatives that possess anti-inflammatory and neuroprotective properties [22].

More specifically, our recent investigation demonstrated the ability of honey consumption to prevent HFD-dependent neuronal injury. In particular, a 16-week-intake of Sicilian black bee chestnut honey, which is particularly rich in kaempferol and quercetin [22], prevented peripheral and central insulin resistance and neuroinflammation in mice fed with a hyperlipidic diet [23]. This neuroprotective effect proved to be mainly due to the positive modulation of brain genes involved in insulin signaling, neuroinflammation and apoptosis [23]. However, it remains to be investigated whether the long-term ingestion of honey is able to revert obesity-related metabolic dysfunctions and related neurodegeneration.

Recently, D-limonene (1-methyl-4-(1-methylethenyl) cyclohexane), a monocyclic monoterpene that is the major constituent of citrus essential oils, has also received notable scientific interest due to its ability to mitigate inflammation and oxidative stress and reduce apoptotic cell death [24]. In fact, it possesses antidiabetic, antioxidant, anti-inflammatory, antinociceptive and anticancer properties [25]. In animal models, D-limonene has been reported to alleviate obesity-related metabolic disorders [26,27]. However, although D-limonene has recently been shown in vitro to inhibit acetylcholinesterase [28] and to exert beneficial effects in the *Drosophila* AD model by reducing oxidative stress and neuroinflammation [29], data on neuroprotective actions against neuronal damage caused by HFD are lacking. Moreover, a recent study suggested that the usage of D-limonene together with other drugs, such as aminoguanidine, is more efficient in the prevention of secondary complications in diabetes in comparison to single treatment [30].

Therefore, the present research was undertaken with the purpose of exploring whether honey, administered alone or in combination with D-limonene, can represent a potential dietary supplement that can aid in ameliorating or reverting HFD-caused brain damage. In this view, we investigated the effects of the long-term ingestion of honey and D-limonene, separately or in combination, on brain damage in HFD mice when the pathological conditions were overt.

2. Results

2.1. Body Weight, Glycaemia and Serum Lipids

As shown in Figure 1A, at the end of the experimental protocol, HFD mice were significantly heavier than STD mice. The weight gain of HFD-L and HFD-H + L mice was significantly lower than that of HFD animals. The fasting blood glucose concentration of HFD mice was significantly higher than that of the STD group. HFD-H and HFD-H + L mice had similar fasting blood glucose concentrations to the HFD group. However, the D-limonene supplementation markedly reduced the fasting blood glucose levels induced by HFD (Figure 1B). The lipid profile of mice that were fed with the different diets is represented in Figure 1C. Total cholesterol and triglyceride levels, that were high in the plasma of the HFD mice compared to STD group, did not significantly differ in HFD-H, HFD-L and HFD-H + L mice, suggesting that honey and D-limonene, alone or in combination, did not impact on the lipid metabolism of obese mice.
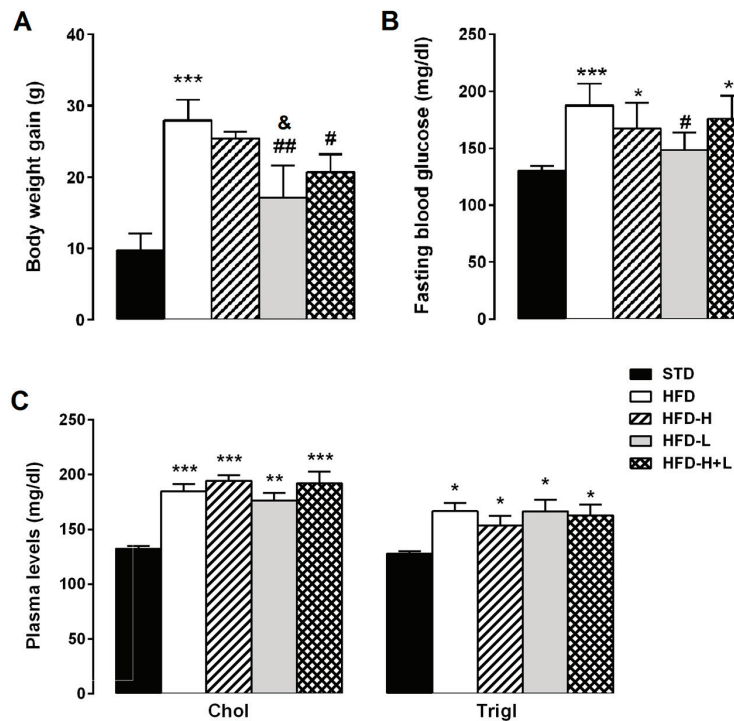
Figure 1. Metabolic parameters. (**A**) body weight gain, (**B**) fasting blood glucose concentrations and (**C**) plasma levels of cholesterol and triglycerides in obese mice. Data are mean values $\pm$ S.E.M. ($n = 8$/group). * $p < 0.05$, ** $p < 0.01$, *** $p < 0.001$ vs. STD mice; [#] $p < 0.05$, [##] $p < 0.01$; [&] $p < 0.05$ vs. HFD-H mice.

2.2. Neurodegeneration: TUNEL Assay

Neurodegeneration has been suggested to be associated with cell apoptosis. To identify whether apoptotic cells were present in the brain tissues of the different groups of mice, we used the TUNEL assay. A higher number of TUNEL-positive cells was observed in the cortex of HFD mice in comparison with STD mice. As shown in Figure 2, neuronal apoptosis resulting from a high-fat diet was significantly decreased in the cortex of HFD-H, HFD-L, and HFD-H + L mice, suggesting that both honey and D-limonene contributed to neuroprotective effects. Interestingly, the diet containing honey and D-limonene together was more efficacious than the single supplement.

2.3. Pro-Apoptosis and Anti-Apoptosis Genes Expression

In this work, the gene expression of the most important regulators of apoptosis. The pro-apoptotic factors *FAS-L*, *P27*, and *BIM* were significantly upregulated in mouse brain tissues from the HFD group compared to the STD group. A high-fat diet supplemented with honey, D-limonene or honey plus D-limonene significantly decreased the gene expression levels of all investigated factors, suggesting a reduced presence of neurons that undergo programmed cell death (Figure 3A,B). On the contrary, the brain gene expression of factors that help neuronal survival, such as BDNF and BCL2, was decreased in the HFD mice compared to the STD group. This down-regulation induced by HFD was counteracted by the simultaneous ingestion of honey or D-limonene. HFD-H + L proved to be the most efficacious diet to increase BCL2 and BDNF expression (Figure 3C,D).
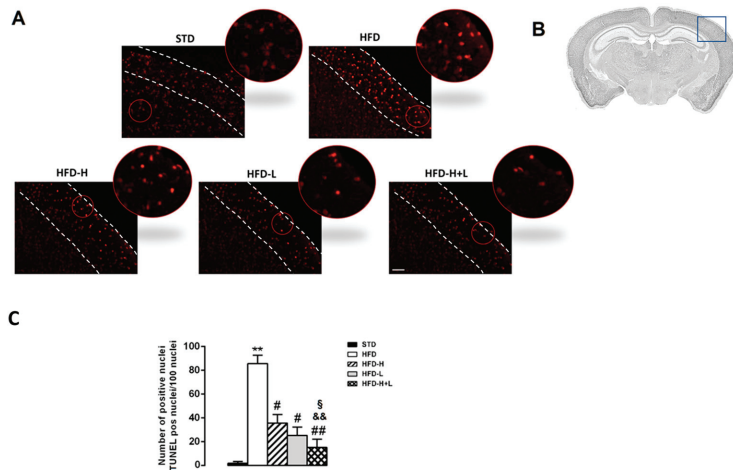
Figure 2. Neurodegeneration. (**A**) TUNEL assay; the outlined area is enlarged in the circle; white dotted lines represent the mouse brain cortex. (**B**) Schematic representation of cerebral cortex of positive areas. (**C**) Number of apoptotic nuclei in cerebral cortex of STD, HFD, HFD-H, HFD-L and HFD-H + L mice. Data are mean values ± S.E.M. (n = 8/group). ** $p < 0.01$ vs. STD mice; # $p < 0.05$, ## $p < 0.01$ vs. HFD mice; && $p < 0.01$ vs. HFD-H mice; § $p < 0.05$ vs. HFD-L mice. Microscope magnification 10×. Scale bar, 200 μm.
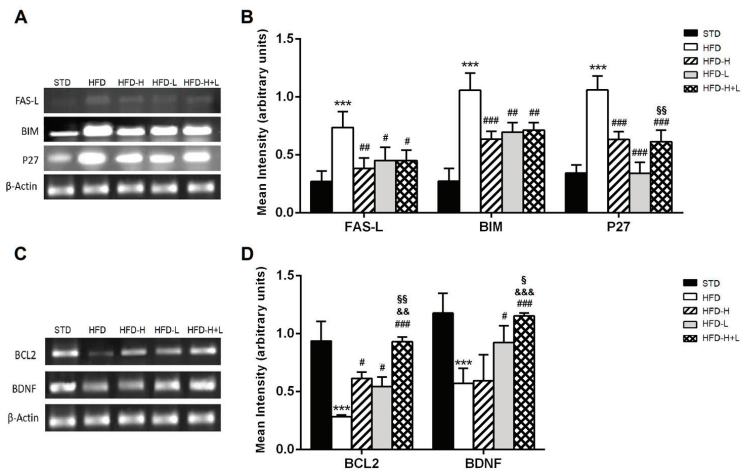
Figure 3. Apoptosis. (**A**) result of the RT-PCR and (**B**) mRNA levels of pro-apoptotic genes: *FAS-L*, *BIM* and *P27* in the mouse brain of different groups; (**C**) Representative image of the RT-PCR results and (**D**) mRNA levels of survival genes: *BCL2* and *BDNF* in the mouse brain of different groups. Data are mean values ± S.E.M. (n = 8/group). *** $p < 0.001$ vs. STD mice; # $p < 0.05$, ## $p < 0.01$, ### $p < 0.001$ vs. HFD mice; && $p < 0.01$, &&& $p < 0.001$ vs. HFD-H mice; § $p < 0.05$, §§ $p < 0.01$ vs. HFD-L mice.

2.4. Brain Pro-Inflammatory Gene and Protein Expression

To determine whether honey and D-limonene, together or separately, reduced neuroinflammation, we examined the brain expression of some pro-inflammatory cytokines and other proteins, which are markers of inflammation. The IL-1β, IL-6 e TNF-α increased expression, found in HFD brains, was reduced by honey or D-limonene ingested separately, and it returned to control levels in the brain of HFD-H + L mice, suggesting that the combined administration of honey and D-limonene was more efficacious than single ad-

ministration (Figure 4A,B). Moreover, the elevated expression of COX-2 and iNOS induced by HFD, was mitigated by honey, D-limonene, and honey plus D-limonene (Figure 5A,B).

Figure 4. Brain inflammation. (**A**) Representative image of the RT-PCR results and (**B**) mRNA levels of IL-1β, TNF-α and IL-6 in the mouse brain of different groups. Data are mean values ± S.E.M. (n = 8/group). * $p < 0.05$, *** $p < 0.001$ vs. STD mice; ### $p < 0.001$ vs. HFD mice, && $p < 0.01$ vs. HFD-H mice; §§ $p < 0.01$ vs. HFD-L mice.
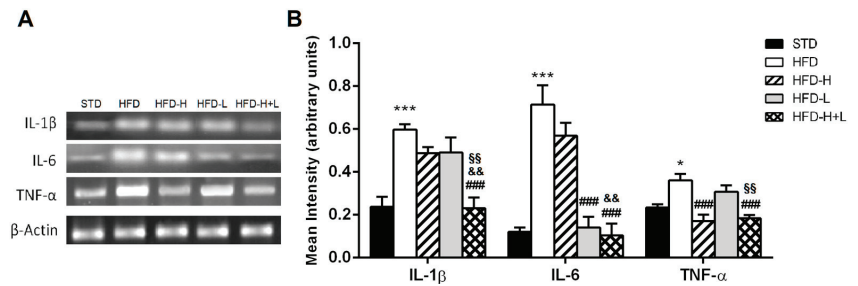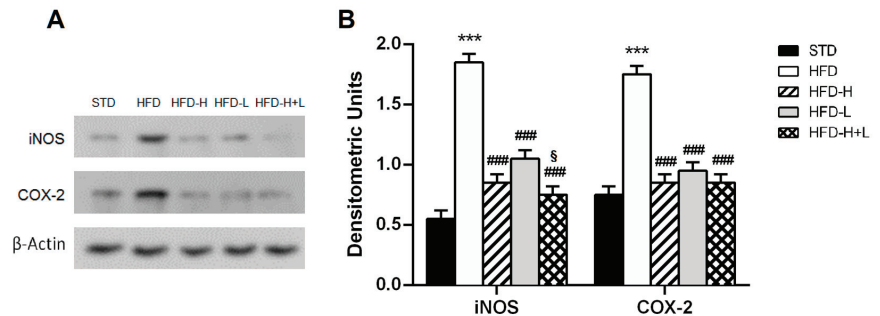

Figure 5. Brain stress. (**A**) protein expression levels of COX-2 and iNOS in the mouse brain of different groups; (**B**) densitometric analysis of iNOS and COX-2 protein levels normalized for β-actin levels. Data are mean values ± S.E.M. (n = 8/group). *** $p < 0.001$ vs. STD mice; ### $p < 0.001$ vs. HFD mice; § $p < 0.05$ vs. HFD-L mice.

2.5. Brain Oxidative Stress

Increasingly, studies have demonstrated that oxidative stress is critical for neuronal injury. Therefore, we determined the effect of the different supplemented diets on ROS generation and nitrite content in the brain of the different groups of animals. After a 20-week HFD administration, ROS generation assessed with H_2DCF-DA was significantly increased in HFD brain compared not only to STD, but also to HFD-H, HFD-L, and HFD-H + L (Figure 6A). Moreover, we found a significant increase in nitrite levels in the brains of HFD obese animals in comparison with STD animals. HFD-H, HFD-L, and HFD-H + L mice showed nitrite values that were significantly lower than those of HFD mice (Figure 6B).

2.6. Expression of Genes Involved in AD

Using a Mouse Alzheimer's Disease RT^2 Profiler PCR Array we analyzed expression changes of genes involved in the onset, development and progression of Alzheimer's disease in the different groups of animals. Among them, there are genes that contribute to amyloid beta-peptide (Aβ) generation, clearance and degradation but also genes related to neuronal toxicity. The list of genes is shown in Table S1. We focused on the gene expression levels that were affected more than two-fold among the analyzed groups. The results showed that in the HFD brains, various genes involved in the processing of Amiloid β Precursor (APP) and TAU (*Aplp1*, *Aplp2*, *App*, *Apba3*, *Apbb2*, *Apoe*, *Ckk5*, *Clu*, *Ctsl*, *Mapt*, *Prkca*, *Prkce* and *Hsd17b10*), in synaptic function (*Ache*), in AD-related iperphosphorylation

(*Gsk3α*, *GCdk5* and *Prkca*), and in inflammation (*MPO* and *Il-1α*) (Table 1) were upregulated in comparison with lean brains. These abnormal expressions were significantly ameliorated in the brain of obese animals fed with honey, D-limonene and honey plus D-limonene with a major improvement in the HFD-H group (Table 1).
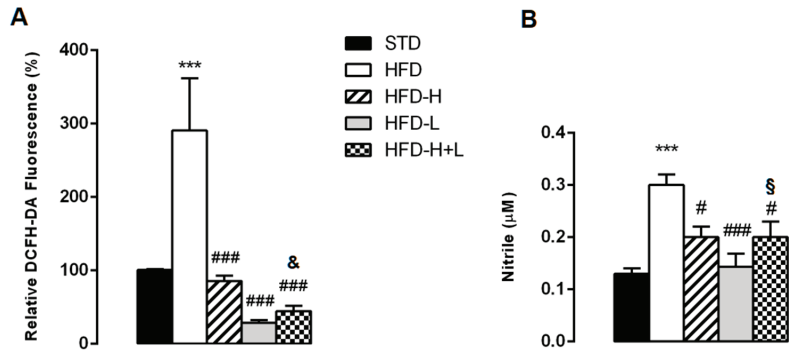

Figure 6. Brain oxidative stress. (**A**) Levels of ROS in the brain of STD, HFD, HFD-H, HFD-L and HFD-H + L mice. (**B**) Nitrite concentration in the brain of STD, HFD, HFD-H, HFD-L and HFD-H + L mice. Data are mean values ± S.E.M. (n = 8/group). *** $p < 0.001$ vs. STD mice; # $p < 0.05$, ### $p < 0.001$ vs. HFD mice; & $p < 0.05$ vs. HFD-H mice; § $p < 0.05$ vs. HFD-L mice.

Table 1. Gene expression profiles involved in AD in HFD/Lean, HFD-H/HFD, HFD-L/HFD and HFD-H + L/HFD, which were significantly downregulated by 2-fold.

Gene Name	Protein	HFD/Lean	HFD-H/HFD	HFD-L/HFD	HFD-H + L/HFD
Ache	Acetylcholinesterase	2.10	−30.84	−12.01	−16.31
Apba3	Amyloid beta (A4) precursor protein-binding, family A, member 3	44.94	−59.17	−30.02	−29.88
Apbb2	Amyloid beta (A4) precursor protein-binding, family B, member 2	2.60	−18.46	−10.71	−17.39
Aplp1	Amyloid beta (A4) precursor-like protein 1	5.17	−8.79	−8.53	−5.00
Aplp2	Amyloid beta (A4) precursor-like protein 2	15.97	−45.55	−15.49	−17.72
Apoe	Apolipoprotein E	5.16	−26.20	−9.36	−9.77
App	Amyloid beta (A4) precursor protein	6.05	−15.85	−9.94	−10.12
Bdnf	Brain derived neurotrophic factor	−17.99	−5.49	−3.44	−2.67
Cdk5	Cyclin-dependent kinase 5	2.92	−36.93	−17.68	−13.99
Clu	Clusterin	26.50	−4.04	−3.76	−2.19
Ctsl	Cathepsin L	5.08	−13.34	−4.65	−4.90
Gsk3a	Glycogen synthase kinase 3 α	7.20	−22.22	−14.11	−15.35
Hsd17b10	Hydroxy steroid deydrogenase10	5.87	−15.93	−9.38	−11.82
Il1a	Interleukin 1 α	4.31	−90.55	−49.60	−98.59
Mapt	Microtubule-associated protein tau	44.58	−23.78	−9.87	−8.28
Mpo	Myeloperoxidase	14.87	−33.10	−14.25	−28.87
Prkca	Protein kinase C, alpha	6.17	−16.16	−15.98	−10.33
Prkce	Protein kinase C, epsilon	5.89	−16.58	−12.56	−16.61
Psen1	Presenilin 1	4.68	−225.85	−152.13	−193.57

3. Discussion

The results of the present study suggest that long-term intake of Sicilian black bee chestnut honey and/or D-limonene, ingested separately or in combination, can protect central neurons against HFD-induced cerebral damage by reducing oxidative stress and neuroinflammation. To our knowledge, our study is the first report on the neuroprotective effects of D-limonene against the damage induced by HFD.

Epidemiological human studies pointed out that a high-calorie diet is associated with worse performance on cognitive tasks [31]. It increases the risk of dementia because high lipid content causes oxidative stress and neuronal dysfunctions [32]. Indeed, high stress oxidative triggers the up-regulation of pro-inflammatory factors leading to neuroinflammation [33]. However, different biological mechanisms including insulin resistance, developmental disturbances, altered membrane functioning, and altered vascularization have been involved in HFD-induced neuronal damage and cognitive decline [5,32].

In our experiments we used mice which, following chronic consumption of HFD, developed obesity accompanied by hyperglycemia, dyslipidaemia, insulin resistance [34–36], activation of amyloidogenic pathways, neuroinflammation and neurodegeneration [10,18,37–39]; consequently, they are suitable for verifying the potential effects of functional food/phytochemicals on neuronal survival. First of all, we analyzed the presence of apoptosis in the cerebral cortex and the gene expression of pro- and anti-apoptotic factors in the brains of the different animal groups. It is well known that apoptosis plays a key role in the pathogenesis of neurodegenerative diseases [40], involving mainly the BCL-2 protein family. This family includes proteins that control the mithocondrion membrane permeability such as Bax, Bim (pro-apoptotic proteins) and BCL-2, Bcl-xL, Bcl-w (anti-apoptotic proteins). Additionally, FAS ligand (FAS-L) has been involved in neuronal death [41] and P-27, an inhibitor of cyclin-dependent kinase, has been reported to promote neuronal apoptosis induced by the neurotoxic $\alpha\beta42$ peptide [42]. According to our previous reports [10,17,18], our results confirmed the presence of neurodegeneration caused by HFD as suggested by the increase of apoptotic neurons in the brain cortex of obese mice in comparison with STD mice. In HFD-H or HFD-L cerebral cortexes, the level of apoptotic neurons was significantly reduced suggesting that the daily ingestion of honey or D-limonene inhibits programmed cellular death. Moreover, honey and D-limonene ingested in combination further decreased the apoptotic neuron number, suggesting a synergistic neuroprotective action. The results from molecular analysis also supported our hypothesis on the neuroprotective effect of honey and D-limonene. In fact, the pro-apoptotic gene up-regulation and the anti-apoptotic gene down-regulation that was found in the HFD brain was attenuated in HFD-H, HFD-L and HFD-H + L animal groups. We also found a down-regulation of BDNF in the HFD brain, which was in accordance with previous studies that reported reductions in levels of BDNF in the hippocampus of obese rodents [11,43] as a consequence of increased oxidative stress [44]. However, honey and D-limonene when separately ingested increased the BDNF gene expression; even more so when ingested in combination, suggesting that an increase of survival factors can also be responsible for the observed beneficial effects.

Neurodegeneration can be triggered by various pro-inflammatory and neurotoxic mediators, such as IL-1β, IL-6, and TNF-α, and neuroinflammation is strictly associated with oxidative stress [45]. Indeed, several studies demonstrated that neuroinflammation is linked to high levels of ROS and high expression of AD biomarkers in the brains of HFD mice [10,46,47]. Because both honey and D-limonene have been reported to possess anti-inflammatory and antioxidant properties, leading to the assumption that they could be used as a supplement in anti-inflammatory therapies [21,48,49] we examined and compared the expression of pro-inflammatory factors, the levels of oxidative stress and nitrite in the brains of the different animal groups. The results suggested that HFD increases the gene expression of inflammatory cytokines (IL-1β, IL-6, TNF-α) and other proteins, markers of inflammation (i-NOS and COX-2) and ROS and nitrite levels in the brain as previously shown [10,18,32,50,51]. Interestingly, long-term ingestion of honey or D-limonene, and even more so, the combined ingestion of honey and D-limonene reduced the inflammatory and

oxidative stress markers suggesting once more a beneficial action against damage induced by HFD in the brain. We can only speculate about the honey compounds responsible for the observed beneficial effects, which generally have been attributed to polyphenols [21]. However, it is noteworthy that we used Sicilian black bee chestnut honey, whose kaempferol and quercetin levels corresponded to 69% of the total content [22]. Quercetin as well as kaempferol can cross the blood–brain barrier [52]. Quercetin has been reported to protect neurons from oxidative stress and inflammation and to have beneficial properties against mechanisms involved in AD in different in vitro and in vivo models [53], and kaempferol can act positively in various models of neurodegenerative diseases [54,55].

Although recent research using a Drosophila AD model suggested that D-limonene has a neuroprotective action against $A\beta_{42}$-induced toxicity associated with its antioxidant and anti-inflammatory properties [29], the effects of D-limonene on AD have not been well-studied yet. Therefore, by using a mouse Alzheimer's disease microarray, we have analyzed and compared the expression of genes involved in amyloid beta-peptide (Aβ) generation and processing and/or genes related to neuronal toxicity in the brains of different mouse groups. The results clearly suggest that long-term HFD feeding promotes the expression of genes associated with AD, including *Ache*, *App*, *Apba3*, *Apbb2*, *Aplp1*, *Aplp2*, *Apoe*, *CdK5*, *Clu*, *Ctls*, *GSK3α*, *Hsd17b10*, *Mapt*, *Psen1*, *Prkca*,*Prkcb* and genes linked to inflammation such as *Mpo and Il1α* [56,57]. However, these deleterious changes in gene expression were counteracted in the brains of HFD-H, HFD-L and HFD-H + L, suggesting that the increased neurotoxicity induced by HFD may be mitigated by long-term ingestion of honey and D-limonene, both separately and in combination. In particular, the down regulation of *App*, *Apba3*, *Apbb2*, *Aplp1*, *Aplp2*, *Apoe* and *Psen1* could suggest that the eventual endogenous APP generation and processing were reduced after the long-term ingestion of honey and D-limonene [58]. Moreover, *Cdk5*, a promoter of neuronal death [59] and *Clu*, encoding clusterin, a protein involved in several processes such as suppression of the complement system, lipid transport, and neuronal cell death and cell-survival mechanisms, whose levels are increased in AD [60], were mitigated by the intake of honey and D-limonene either alone or in combination.

4. Materials and Methods

4.1. Animals and Diets

Male C57BL/6 mice, purchased from Envigo (S.Pietro al Natisone, Udine, Italy) were maintained in the ATeN center animal house according to the European guide lines. The animals (4-weeks old) were housed (2 mice/cage) in a temperature- (23 ± 1 °C) and relative humidity (55% ± 5%)-controlled facility, under a 12-h light–dark cycle, according to the Italian legislative decree n. 26/2014 and were approved by the Ministry of Health (Rome, Italy; Authorization n. 891/2018-PR).

After two weeks of acclimatization, 8 mice were fed a standard diet (STD) (negative control) containing protein 20.0%, fat 10.0%, carbohydrate 70.0%, *w/w*, and water (code 4RF25, Mucedola, Milan, Italy), and 32 mice were fed a HFD, containing protein 20.0%, fat 60.0%, carbohydrate 20.0%, *w/w* (PF4215, Mucedola, Milan, Italy) for 10 weeks to induce obesity. Subsequently, HFD mice were divided randomly into four groups Then, four groups (n = 8/group) were created from the HFD mice: one group received HFD, the second group received HFD supplemented with honey (45 mg per day/mouse) (HFD-H), the third received HFD supplemented with D-limonene (0.5% *w/w*) (HFD-L) and the last one received HFD supplemented with honey and D-limonene in combination at the same doses (HFD-H + L), for another 10 weeks. The doses of D-limonene (Sigma—St. Louis, MO, USA) and honey (Prezzemolo and Vitale Supermarket, Palermo, Italy) were taken from the literature [23,27,61] and added to the HFD cow in a percentage amount that was useful so as not to change the HFD caloric value. Body weight and food intake were monitored every week.

At the end of the experimental protocol (20th week), biochemical analyses were performed on blood collected from the tail vein and then the animals were sacrificed. The

aorta was perfused with a buffer solution of Dulbecco and the right atrium was incised to allow outflow. Brains were rapidly explanted, weighed and coronally cut into two halves. One part was fixed in 4% formalin was utilized for histological investigation; the other half was ice-covered and used for molecular analysis.

4.2. Biochemical Analyses

Glucose concentration was measured using a glucometer (GlucoMen LX meter, Menarini, Florence, Italy) in overnight fasting mice. Plasma total cholesterol and triglyceride concentrations were determined using the ILAB 600 Analyzer (Instrumentation Laboratory, Bedford, MA, USA).

4.3. Apoptosis Investigation

The Tunel assay was used to determine the level of apoptosis (Promega, Madison, WI, USA) in the cerebral cortex sections, following the manufacturer's instructions. The values of the damaged nuclei were counted by two blind investigators and the ratio of apoptotic nuclei in respect of normal nuclei was calculated.

4.4. Reactive Oxygen Species Analysis

To determine the reactive oxygen species (ROS), 5 mg of brain tissue was homogenized with 1 mL of cold PBS1X and 10 µL of protease inhibitors (Amersham Life Science, Munich, Germany). The preparate brain homogenates were incubated with 1 mM dichlorofluorescein diacetate (DCFH-DA) at room temperature in the dark for 15 min, then the fluorescence was measured by fluorimeter (GloMax® Plate Reader, Promega, Milano, Italy) with an excitation filter set at 485 nm and an emission filter set at 530 nm. ROS levels were expressed as a percentage of the fluorescence emitted by STD cerebral samples.

4.5. Determination of Nitric Oxide (NO) Levels

The level of nitric oxide (NO) in the brains was evaluated by using Griess reagent (Thermo Fisher Scientific Inc., Waltham, MA, USA). Briefly, 5 mg of brain tissue was homogenized with 1 mL of PBS1X and centrifuged at 14,000 rpm, for 30 min at 4 °C. 100 µL of supernatant was incubated with equal volumes of Griess reagent (1% sulphanilamide in 5% phosphoric acid and 0.1% N-(1-naphthyl)-ethylenediamine), the absorbance was immediately read at 520 nm in a microplate reader (GloMax® Plate Reader, Promega).

4.6. Molecular Analyses

Whole brain was used to extract RNA by using a RNeasy plus Mini Kit (Qiagen, Valencia, CA, USA). Subsequently, by using High-Capacity cDNA Reverse Transcription Kit (Applied Biosystems, Waltham, MA, USA). cDNA was prepared by 2 ng of total RNA. Then the expression of target genes was performed by using Reverse Transcription Polymerase Chain Reaction (RT-PCR) with the subsequent primers: β-actin *For* 5′-CGGGATCCCCGCCCTAGGCACCAGGGT-3′; *Rev* 5′-GGAATTCGGCTGGGGTGTTGAAGGTCTCAAA-3′; for pro-inflammatory factors: IL-1β *For* 5′-CATGGGATGATGATAACCTGCT-3′; *Rev* 5′-CCCATACTTTAGGAAGACACGATT-3′; IL-6 *For* 5′-CTGGTGACAACCACGGCCTTCCCT-3′; *Rev* 5′-ATGCTTAGGCATAACGCACTAGGT-3′; TNF-α *For* 5′-AGCCCACGTCGTAGCAAACCA-3′; *Rev* 5′-GCAGGGGCTCTTGACGGCAG-3′; for pro-apoptotic factors: FAS-L *For* 5′-CAAGTCCAACTCAAGGTCCATGCC-3′; *Rev* 5′-AGAGAGAGCTCAGATACGTTTGAC-3′; BIM *For* 5′-AACCTTCTGATGTAAGTTCT-3′; *Rev* 5′-GTGATTGCCTTCAGGATTAC-3′; p27 *For* 5′-TGCGAGTGTCTAACGGGAG-3′; *Rev* 5′-GTTTGACGTCTTCTGAGGCC-3′; for anti-apoptosis factors: BCL-2 *For* 5′-ATGTGTGTGGAGAGCGTCAA-3′; *Rev* 5′-AGAGACAGCCAGGAGAAATCA-3′; BDNF *For* 5′-GGCTGACACTTTTGAGCACGTC-3′; *Rev* 5′-CTCCAAAGGCACTTGACTGCTG-3′. The amplification cycles comprised denaturation (45 s at 95 °C), annealing (45 s at 52 °C) and elongation (45 s at 72 °C), for 40 cycles. The amplification products were visualized by ultraviolet light using E-Gel GelCapture (Thermo Fisher Scientific, Monza, Italy) after separation on agarose gel. The quantification

of gene expression was obtained by using E-Gel GelQuant Express Analysis Software (version 1.14.6.0 (Dongle)) (Thermo Fisher Scientific, Monza, Italy). The signal intensity of the products was normalized to its respective β-actin signal intensity.

Protein expression. Brains dissected from the experimental animals were homogenized in ice-cold solubilization buffer (50 mM Tris-HCl pH 7.4, 150 mM NaCl, 1 mM DDT, 1% Triton X-100, 24 mM sodium deoxycholate, 0.01% SDS, 10 mM sodium pyrophosphate, 100 mM sodium fluoride, 10 mM sodium orthovanadate, 1.5 μM aprotinin, 1 mM phenylmethanesulfonylfluoride and 2.1 μM leupeptin) and centrifuged at $12,000 \times g$ at 4 °C for 30 min. Then, the supernatants were used for protein determination, as previously described [62]. Samples containing 50 μg protein were resolved by SDS-PAGE electrophoresis on 12% acrylamide gels and transferred to nitrocellulose membranes. After blocking for 2 h in 5% (w/v) skimmed dry milk, the membranes were incubated in the presence of primary antibodies overnight at 4 °C (Santa Cruz, Milan, Italy, 1:1000 dilution): anti-COX-2 (sc-376861), anti-iNOS (sc-7271). Subsequently, the samples were incubated with the secondary for 90 min. HRP-conjugated antibodies (Dako, Milan, Italy, 1:10,000 dilution) and chemiluminescent bands were detected by a C-Digit Blot Scanner (LI-COR, Lincoln, NE, USA) and densitometric analysis was used to analyze band intensities, by using LI-COR Image Studio 4.0.

4.7. RT^2 Profiler PCR Array

Mouse Alzheimer's disease array (Alzheimer's Disease RT^2 Profiler PCR Array, QIAGEN, Monza, Italy) was used in order to analyze factors in HFD brains that are involved in the onset, development and progression of AD. The 96 genes reported in the plate are listed in the Supplementary data (Table S1).

RNA from whole brains was utilized. A High-Capacity cDNA Reverse Transcription kit (Applied Biosystems, Bedford, MA, USA) was used to synthetize cDNA from 2 ng of RNA. The array was executed by using a StepOne Real-Time instrument (Applied Biosystem) and the results were obtained through the relative quantification method ($2^{-\Delta\Delta CT}$).

We chose to highlight only the genes showing changes in the expression levels that were more than two-fold among the different groups analyzed (HFD vs. Lean; HFD-H vs. HFD; HFD-L vs. HFD; HFD-H + L vs. HFD).

4.8. Statistical Analysis

The results are presented as mean values $\pm$ the standard error of the mean SEM. The number of animals is indicated with the letter 'n'. The comparison between the groups was performed by ANOVA, and then a Bonferroni post hoc test was used. All the analyses were obtained using Prism 6.0, GraphPad software (San Diego, CA, USA). Results with a *p*-value ≤ 0.05 were considered statistically significant.

5. Conclusions

In conclusion, our results confirm that HFD causes detrimental effects on AD-related neuropathological and neuroinflammatory pathways leading to neurodegeneration. However, the long-term ingestion of honey and D-limonene, either separately or in combination, is able to counteract and to ameliorate the cerebral stressing conditions related to HFD-induced metabolic disorders.

Institutional Review Board Statement: The animal study protocol was approved by the Ministry of Health (Rome, Italy; Authorization n. 891/2018-PR).

Informed Consent Statement: Not applicable.

Data Availability Statement: Not applicable.

Acknowledgments: The authors wish to thank Valentina Scatassa for her valuable technical contribution.

Conflicts of Interest: The authors declare no conflict of interest.

References

1. Livingston, G.; Huntley, J.; Sommerlad, A.; Ames, D.; Ballard, C.; Banerjee, S.; Brayne, C.; Burns, A.; Cohen-Mansfield, J.; Cooper, C.; et al. Dementia prevention, intervention, and care: 2020 report of the Lancet Commission. *Lancet* **2020**, *396*, 413–446. [CrossRef] [PubMed]
2. Reitz, C.; Brayne, C.; Mayeux, R. Epidemiology of Alzheimer disease. *Nat. Rev. Neurol.* **2011**, *7*, 137–152. [CrossRef] [PubMed]
3. Singh, A.; Kukreti, R.; Saso, L.; Kukreti, S. Oxidative stress: A key modulator in neurodegenerative diseases. *Molecules* **2019**, *24*, 1583. [CrossRef] [PubMed]
4. Stephenson, J.; Nutma, E.; van der Valk, P.; Amor, S. Inflammation in CNS neurodegenerative diseases. *Immunology* **2018**, *154*, 204–219. [CrossRef]
5. Terzo, S.; Amato, A.; Mulè, F. From obesity to Alzheimer's disease through insulin resistance. *J. Diabetes Complicat.* **2021**, *35*, 108026. [CrossRef]
6. Frazier, H.; Ghoweri, A.; Anderson, K.; Lin, R.; Porter, N.M.; Thibault, O. Broadening the definition of brain insulin resistance in aging and Alzheimer's disease. *Exp. Neurol.* **2019**, *313*, 79–87. [CrossRef]
7. De la Monte, S. Type 3 diabetes is sporadic Alzheimer's disease: Mini-review. *Eur. Neuropsychopharmacol.* **2014**, *24*, 1954–1960. [CrossRef]
8. Farr, S.; Yamada, K.; Butterfield, D.; Abdul, H.M.; Xu, L.; Miller, N.E.; Banks, W.A.; Morley, J.E. Obesity and hypertriglyceridemia produce cognitive impairment. *Endocrinology* **2008**, *149*, 2628–2636. [CrossRef]
9. Valladolid-Acebes, I.; Stucchi, P.; Cano, V.; Fernández-Alfonso, M.; Merino, B.; Gil-Ortega, M.; Fole, A.; Morales, L.; Ruiz-Gayo, M.; Del Olmo, N. High-fat diets impair spatial learning in the radial-arm maze in mice. *Neurobiol. Learn. Mem.* **2011**, *95*, 80–85. [CrossRef]
10. Nuzzo, D.; Picone, P.; Baldassano, S.; Caruana, L.; Messina, E.; Marino Gammazza, A.; Cappello, F.; Mulè, F.; Di Carlo, M. Insulin resistance as common molecular denominator linking obesity to Alzheimer's disease. *Curr. Alzheimer Res.* **2015**, *12*, 723–735. [CrossRef]
11. Stranahan, A.; Norman, E.; Lee, K.; Cutler, R.G.; Telljohann, R.S.; Egan, J.M.; Mattson, M.P. Diet-induced insulin resistance impairs hippocampal synaptic plasticity and cognition in middle-aged rats. *Hippocampus* **2008**, *18*, 1085–1088. [CrossRef]
12. Siino, V.; Amato, A.; Di Salvo, F.; Caldara, G.F.; Filogamo, M.; James, P.; Vasto, S. Impact of diet-induced obesity on the mouse brain phosphoproteome. *J. Nutr. Biochem.* **2018**, *58*, 102–109. [CrossRef]
13. Siino, V.; Jensen, P.; James, P.; Vasto, S.; Amato, A.; Mulè, F.; Accardi, G.; Larsen, M.R. Obesogenic Diets Cause Alterations on Proteins and Theirs Post-Translational Modifications in Mouse Brains. *Nutr. Metab. Insights* **2021**, *14*, 11786388211012405. [CrossRef]
14. Salman, M.; Al-Obaidi, Z.; Kitchen, P.; Loreto, A.; Bill, R.M.; Wade-Martins, R. Advances in Applying Computer-Aided Drug Design for Neurodegenerative Diseases. *Int. J. Mol. Sci.* **2021**, *22*, 4688. [CrossRef]
15. Aldewachi, H.; Al-Zidan, R.; Conner, M.; Salman, M. High-Throughput Screening Platforms in the Discovery of Novel Drugs for Neurodegenerative Diseases. *Bioengineering* **2021**, *8*, 30. [CrossRef]
16. Carvalho, J.; Fernandes, C.; Daleprane, J.; Alves, M.S.; Stien, D.; Dhammika Nanayakkara, N.P. Role of Natural Antioxidants from Functional Foods in Neurodegenerative and Metabolic Disorders. *Oxid. Med. Cell Longev.* **2018**, *18*, 459753. [CrossRef]
17. Nuzzo, D.; Amato, A.; Picone, P.; Terzo, S.; Galizzi, G.; Bonina, F.P.; Mulè, F.; Di Carlo, M. A natural dietary supplement with a combination of nutrients prevents neurodegeneration induced by a high fat diet in mice. *Nutrients* **2018**, *10*, 1130. [CrossRef]
18. Nuzzo, D.; Galizzi, G.; Amato, A.; Terzo, S.; Picone, P.; Cristaldi, L.; Mulè, F.; Di Carlo, M. Regular intake of pistachio mitigates the deleterious effects of a high fat-diet in the brain of obese mice. *Antioxidants* **2020**, *9*, 317. [CrossRef]
19. Storz, M. Is there a lack of support for whole-food, plant-based diets in the medical community? *Perm. J.* **2018**, *23*, 18-068. [CrossRef]
20. González-Castejón, M.; Rodriguez-Casado, A. Dietary phytochemicals and their potential effects on obesity: A review. *Pharm. Res.* **2011**, *64*, 438–455. [CrossRef]
21. Terzo, S.; Mulè, F.; Amato, A. Honey and obesity-related dysfunctions: A summary on health benefits. *J. Nutr. Biochem.* **2020**, *82*, 108401. [CrossRef] [PubMed]
22. Lo Dico, G.A.; Ulrici, A.; Pulvirenti, A.; Camilleri, G.; Macaluso, A. Multivariate statistical analysis of the polyphenols content for the discrimination of honey produced in Sicily (Southern Italy). *J. Food Compos. Anal.* **2019**, *82*, 103225. [CrossRef]

23. Terzo, S.; Calvi, P.; Nuzzo, D.; Picone, P.; Galizzi, G.; Caruana, L.; Di Carlo, M.; Lentini, L.; Puleio, R.; Mulè, F. Preventive impact of long-term ingestion of chestnut honey on glucose disorders and neurodegeneration in obese mice. *Nutrients* **2022**, *14*, 756. [CrossRef] [PubMed]

24. Eddin, L.; Jha, N.; Meeran, M.; Kesari, K.K.; Beiram, R.; Ojha, S. Neuroprotective Potential of Limonene and Limonene Containing Natural Products. *Molecules* **2021**, *26*, 4535. [CrossRef]

25. Vieira, A.; Beserra, F.; Souza, M.; Totti, B.M.; Rozza, A.L. Limonene: Aroma of innovation in health and disease. *Chem. Biol. Interact.* **2018**, *283*, 97–106. [CrossRef]

26. Jesudoss, V.A.S.; Jayachitra, J.; Shenbagam, M.; Nalini, N. Dietary d-limonene alleviates insulin resistance and oxidative stress-induced liver injury in high-fat diet and L-NAME-treated rats. *Eur. J. Nutr.* **2012**, *51*, 57–68. [CrossRef]

27. Jing, L.; Zhang, Y.; Fan, S.; Gu, M.; Guan, Y.; Lu, X.; Huang, C.; Zhou, Z. Preventive and ameliorating effects of citrus D-limonene on dyslipidemia and hyperglycemia in mice with high-fat diet-induced obesity. *Eur. J. Pharm.* **2013**, *715*, 46–55. [CrossRef]

28. Szwajgier, D.; Baranowska-Wójcik, E. Terpenes and phenylpropanoids as acetyl- and butyrylcholinesterase inhibitors: A comparative study. *Curr. Alzheimer Res.* **2019**, *16*, 963–973. [CrossRef]

29. Shin, M.; Liu, Q.; Choi, B.; Shin, C.; Lee, B.; Yuan, C.; Song, Y.J.; Yun, H.S.; Lee, I.S.; Koo, B.S. Neuroprotective Effects of Limonene (+) against Aβ42-Induced Neurotoxicity in a Drosophila Model of Alzheimer's Disease. *Biol. Pharm. Bull.* **2020**, *43*, 409–417. [CrossRef]

30. Joglekar, M.; Bavkar, L.; Sistla, S.; Arvindekar, A. Effective inhibition of protein glycation by combinatorial usage of limonene and aminoguanidine through differential and synergistic mechanisms. *Int. J. Biol. Macromol.* **2017**, *99*, 563–569. [CrossRef]

31. Ortega, R.; Requejo, A.; Andres, P.; López-Sobaler, A.M.; Quintas, M.E.; Redondo, M.R.; Navia, B.; Rivas, T. Dietary intake and cognitive function in a group of elderly people. *Am. J. Clin. Nutr.* **1997**, *66*, 803–809. [CrossRef]

32. Freeman, L.R.; Haley-Zitlin, V.; Rosenberger, D.S.; Granholm, A.C. Damaging effects of a high- fat diet to the brain and cognition: A review of proposed mechanisms. *Nutr. Neurosci.* **2014**, *17*, 241–251. [CrossRef]

33. Yeo, E.; Wong, K.; See, M.; See, M.L.; Wong, K.Y.; Yap, J.K.Y.; Gan, S.Y. Piper sarmentosum Roxb. confers neuroprotection on beta-amyloid (Aβ)-induced microglia-mediated neuroinflammation and attenuates tau hyperphosphorylation in SH-SY5Y cells. *J. Ethnopharmacol.* **2018**, *217*, 187–194. [CrossRef]

34. Collins, S.; Martin, T.L.; Surwit, R.S.; Robidoux, J. Genetic vulnerability to diet-induced obesity in the C57BL/6J mouse: Physiological and molecular characteristics. *Physiol. Behav.* **2004**, *81*, 243–248. [CrossRef]

35. Amato, A.; Caldara, G.; Nuzzo, D.; Baldassano, S.; Picone, P.; Rizzo, M.; Mulè, F.; Di Carlo, M. NAFLD and Atherosclerosis Are Prevented by a Natural Dietary Supplement Containing Curcumin, Silymarin, Guggul, Chlorogenic Acid and Inulin in Mice Fed a High-Fat Diet. *Nutrients* **2017**, *9*, 492. [CrossRef]

36. Baldassano, S.; Rappa, F.; Amato, A.; Cappello, F.; Mulè, F. GLP-2 as Beneficial Factor in the Glucose Homeostasis in Mice Fed a High Fat Diet. *J. Cell. Physiol.* **2015**, *230*, 3029–3036. [CrossRef]

37. Glass, C.; Saijo, K.; Winner, B.; Marchetto, M.C.; Gage, F.H. Mechanisms underlying inflammation in neurodegeneration. *Cell* **2010**, *140*, 918–934. [CrossRef]

38. Petrov, D.; Pedrós, I.; Artiach, G.; Sureda, F.X.; Barroso, E.; Pallàs, M.; Casadesús, G.; Beas-Zarate, C.; Carro, E.; Ferrer, I. High-fat diet-induced deregulation of hippocampal insulin signaling and mitochondrial homeostasis deficiences contribute to Alzheimer disease pathology in rodents. *Biochim. Biophys. Acta* **2015**, *1852*, 1687–1699. [CrossRef]

39. Busquets, O.; Ettcheto, M.; Pallàs, M.; Beas-Zarate, C.; Verdaguer, E.; Auladell, C.; Folch, J.; Camins, A. Long-term exposition to a high fat diet favors the appearance of β-amyloid depositions in the brain of C57BL/6J mice. A potential model of sporadic Alzheimer's disease. *Mech. Ageing Dev.* **2017**, *162*, 38–45. [CrossRef]

40. Ghavami, S.; Shojaei, S.; Yeganeh, B.; Ande, S.R.; Jangamreddy, J.R.; Mehrpour, M.; Christoffersson, J.; Chaabane, W.; Moghadam, A.R.; Kashani, H.H.; et al. Autophagy and apoptosis dysfunction in neurodegenerative disorders. *Prog. Neurobiol.* **2014**, *112*, 24–49. [CrossRef]

41. Planells-Ferrer, L.; Urresti, J.; Coccia, E.; Galenkamp, K.M.; Calleja-Yagüe, I.; López-Soriano, J.; Carriba, P.; Barneda-Zahonero, B.; Segura, M.F.; Comella, J.X. Fas apoptosis inhibitory molecules: More than death-receptor antagonists in the nervous system. *J. Neurochem.* **2016**, *139*, 11–21. [CrossRef] [PubMed]

42. Jaiswal, S.; Sharma, P. Role and regulation of p27 in neuronal apoptosis. *J. Neurochem.* **2017**, *140*, 576–588. [CrossRef] [PubMed]

43. Park, H.R.; Park, M.; Choi, J.; Park, K.Y.; Chung, H.Y.; Lee, J. A high-fat diet impairs neurogenesis: Involvement of lipid peroxidation and brain-derived neurotrophic factor. *Neurosci. Lett.* **2010**, *482*, 235–239. [CrossRef] [PubMed]

44. Wu, A.; Ying, Z.; Gomez-Pinilla, F. The interplay between oxidative stress and brain-derived neurotrophic factor modulates the outcome of a saturated fat diet on synaptic plasticity and cognition. *Eur. J. Neurosci.* **2004**, *19*, 1699–1707. [CrossRef] [PubMed]

45. Kempuraj, D.; Thangavel, R.; Natteru, P.; Selvakumar, G.P.; Saeed, D.; Zahoor, H.; Zaheer, S.; Iyer, S.S.; Zaheer, A. Neuroinflammation induces neurodegeneration. *J. Neurol. Neurosurg. Spine* **2016**, *1*, 1003.

46. Duffy, C.; Hofmeister, J.; Nixon, J.; Butterick, T. High fat diet increases cognitive decline and neuroinflammation in a model of orexin loss. *Neurobiol. Learn. Mem.* **2019**, *157*, 41–47. [CrossRef]

47. Spencer, S.; D'Angelo, H.; Soch, A.; Watkins, L.R.; Maier, S.F.; Barrientos, R.M. High-fat diet and aging interact to produce neuroinflammation and impair hippocampal and amygdala-dependent memory. *Neurobiol. Aging* **2017**, *58*, 88–101. [CrossRef]

48. D'Alessio, P.; Ostan, R.; Bisson, J.; Schulzke, J.D.; Ursini, M.V.; Béné, M.C. Oral administration of d-limonene controls inflammation in rat colitis and displays anti-inflammatory properties as diet supplementation in humans. *Life Sci.* **2013**, *92*, 1151–1156. [CrossRef]

49. Roberto, D.; Micucci, P.; Sebastian, T.; Graciela, F.; Anesini, C. Antioxidant activity of limonene on normal murine lymphocytes: Relation to H2O2 modulation and cell proliferation. *Basic Clin. Pharm. Toxicol.* **2010**, *106*, 38–44. [CrossRef]

50. Nuzzo, D.; Baldassano, S.; Amato, A.; Picone, P.; Galizzi, G.; Caldara, G.F.; Di Carlo, M.; Mulè, F. Glucagon-like peptide-2 reduces the obesity-associated inflammation in the brain. *Neurobiol. Dis.* **2019**, *121*, 296–304. [CrossRef]

51. Nuzzo, D.; Presti, G.; Picone, P.; Galizzi, G.; Gulotta, E.; Giuliano, S.; Mannino, C.; Gambino, V.; Scoglio, S.; Di Carlo, M.; et al. Effects of the aphanizomenon flos-aquae extract (Klamin®) on a neurodegeneration cellular model. *Oxid. Med. Cell Longev.* **2018**, *17*, 9089016. [CrossRef]

52. Shimazu, R.; Anada, M.; Miyaguchi, A.; Nomi, Y.; Matsumoto, H. Evaluation of Blood-Brain Barrier Permeability of Polyphenols, Anthocyanins, and Their Metabolites. *Agric. Food Chem.* **2021**, *69*, 11676–11686. [CrossRef]

53. Khan, H.; Ullah, H.; Aschner, M.; Cheang, W.; Akkol, E. Neuroprotective Effects of Quercetin in Alzheimer's Disease. *Biomolecules* **2019**, *10*, 59. [CrossRef]

54. Siddique, Y.R. Neurodegenerative Diseases and Flavonoids: Special Reference to Kaempferol. *CNS Neurol. Disord. Drug Targets* **2021**, *20*, 327–342. [CrossRef]

55. Beg, T.; Jyoti, S.; Naz, F.; Rahul Ali, F.; Ali, S.K.; Reyad, A.M.; Siddique, Y.H. Protective Effect of Kaempferol on the Transgenic Drosophila Model of Alzheimer's Disease. *CNS Neurol. Disord. Drug Targets* **2018**, *17*, 421–429. [CrossRef]

56. Vinklarova, L.; Schmidt, M.; Benek, O.; Kuca, K.; Gunn-Moore, F.; Musilek, K. Friend or enemy? Review of 17β-HSD10 and its role in human health or disease. *J. Neurochem.* **2020**, *155*, 231–249. [CrossRef]

57. Nikolac Perkovic, M.; Pivac, N. Genetic Markers of Alzheimer's Disease. *Adv. Exp. Med. Biol.* **2019**, *1192*, 27–52. [CrossRef]

58. Serrano-Pozo, A.; Das, S.; Hyman, B.T. APOE and Alzheimer's disease: Advances in genetics, pathophysiology, and therapeutic approaches. *Lancet Neurol.* **2021**, *20*, 68–80. [CrossRef]

59. Liu, S.L.; Wang, C.; Jiang, T.; Tan, L.; Xing, A.; Yu, J.T. The Role of Cdk5 in Alzheimer's Disease. *Mol. Neurobiol.* **2016**, *53*, 4328–4342. [CrossRef]

60. Uddin, M.S.; Kabir, M.T.; Begum, M.M.; Islam, M.S.; Behl, T.; Ashraf, G.M. Exploring the Role of CLU in the Pathogenesis of Alzheimer's Disease. *Neurotox. Res.* **2021**, *39*, 2108–2119. [CrossRef]

61. Nasuti, C.; Gabbianelli, R.; Falcioni, G.; Cantalamessa, F. Antioxidative and gastroprotective activities of anti-inflammatory formulations derived from chestnut honey in rats. *Nutr. Res.* **2006**, *26*, 130–137. [CrossRef]

62. Terzo, S.; Attanzio, A.; Calvi, P.; Mulè, F.; Tesoriere, L.; Allegra, M.; Amato, A. Indicaxanthin from Opuntia ficus-indica Fruit Ameliorates Glucose Dysmetabolism and Counteracts Insulin Resistance in High-Fat, Diet-Fed Mice. *Antioxidants* **2021**, *11*, 80. [CrossRef]

Article

Preliminary Evidence of the Potent and Selective Adenosine A2B Receptor Antagonist PSB-603 in Reducing Obesity and Some of Its Associated Metabolic Disorders in Mice

Magdalena Kotańska [1,*], Anna Dziubina [2], Małgorzata Szafarz [3], Kamil Mika [1], Marek Bednarski [1], Noemi Nicosia [1,4], Ahmed Temirak [5], Christa E. Müller [5] and Katarzyna Kieć-Kononowicz [6]

[1] Department of Pharmacological Screening, Jagiellonian University Medical College, 9 Medyczna Street, PL 30-688 Krakow, Poland
[2] Department of Pharmacodynamics, Jagiellonian University Medical College, 9 Medyczna Street, PL 30-688 Krakow, Poland
[3] Department of Pharmacokinetics and Physical Pharmacy, Jagiellonian University Medical College, Medyczna 9, PL 30-688 Cracow, Poland
[4] Division of Neuroscience, Vita Salute San Raffaele University, 20132 Milan, Italy
[5] PharmaCenter Bonn, Pharmaceutical Institute, Pharmaceutical & Medicinal Chemistry, An der Immenburg 4, D-53121 Bonn, Germany
[6] Chair of Technology and Biotechnology of Drugs, Faculty of Pharmacy, Jagiellonian University Medical College, Medyczna 9, PL 30-688 Cracow, Poland
* Correspondence: magda.dudek@uj.edu.pl; Tel./Fax: +48-12-6205530

Abstract: The adenosine A_{2A} and A_{2B} receptors are promising therapeutic targets in the treatment of obesity and diabetes since the agonists and antagonists of these receptors have the potential to positively affect metabolic disorders. The present study investigated the link between body weight reduction, glucose homeostasis, and anti-inflammatory activity induced by a highly potent and specific adenosine A_{2B} receptor antagonist, compound PSB-603. Mice were fed a high-fat diet for 14 weeks, and after 12 weeks, they were treated for 14 days intraperitoneally with the test compound. The $A_1/A_{2A}/A_{2B}$ receptor antagonist theophylline was used as a reference. Following two weeks of treatment, different biochemical parameters were determined, including total cholesterol, triglycerides, glucose, TNF-α, and IL-6 blood levels, as well as glucose and insulin tolerance. To avoid false positive results, mouse locomotor and spontaneous activities were assessed. Both theophylline and PSB-603 significantly reduced body weight in obese mice. Both compounds had no effects on glucose levels in the obese state; however, PSB-603, contrary to theophylline, significantly reduced triglycerides and total cholesterol blood levels. Thus, our observations showed that selective A_{2B} adenosine receptor blockade has a more favourable effect on the lipid profile than nonselective inhibition.

Keywords: adenosine A_{2B} receptor antagonist; glucose tolerance; metabolic disorder; obesity; PSB-603; Theophylline

1. Introduction

In a large number of obese patients, low to severe inflammation associated with white adipose tissue can be observed. Subsequent activation of the immune system leads to insulin resistance, glucose intolerance, and diabetes. In obesity, white adipose tissue produces inflammatory agents, including tumour necrosis factor-alpha (TNF-α) and interleukin-6 (IL-6), which not only have local effects on the physiology of adipose tissue but additionally induce systemic effects in other organs [1–3]. Increased levels of TNF-α and IL-6, in addition to many other factors, are the cause of insulin resistance. Furthermore, IL-6 increases the production of C-reactive protein (CRP) in the liver and can indirectly promote the appearance of cardiovascular disorders [1]. Inflammation also affects β islet cells and alters insulin secretion [4].

Promising therapeutic targets in the treatment of obesity and diabetes are the adenosine receptor subtypes A_{2A} and A_{2B} [5–8]. The agonists [7] and antagonists [9] of A_{2A} adenosine receptors and the agonists and antagonists of A_{2B} adenosine receptors have the potential to positively affect metabolic disorders [7]. Adenosine A_{2A} receptor agonists can induce the anti-inflammatory action necessary for the survival of β cells and increase insulin secretion [7], reduce food intake [10], and increase thermogenesis and lipolysis [6]. Adenosine A_{2A} receptor antagonists can exert anti-inflammatory effects and reduce IL-6 levels [9]. The activation of the A_{2B} adenosine receptor can reduce the dysfunction of β cells, lead to a reduction in hyperglycaemia and insulin resistance and exert anti-inflammatory effects in various cells including adipocytes [7,11]. Antagonists of the A_{2B} adenosine receptor may cause effects, such as increased insulin release [7,8], reduced insulin resistance, decreased fat accumulation in the liver [7], reduced liver glucose production, improved glucose disposal into skeletal muscles and brown adipose tissue in diabetic mice [12], inhibition of the progression of renal fibrosis derived from diabetes [13], induction of anti-inflammatory effects [7,14], and reduction of IL-6 levels [14,15]. Furthermore, obesity is associated with colon inflammation, leading to an increased A_{2B} receptor expression; as a result, the A_{2B} receptor can mediate motor dysfunctions of the colon frequently seen in obesity [16].

Since A_{2A} and A_{2B} adenosine receptors regulate glucose homeostasis in diabetes and obesity ligands of these receptors may be useful for the prevention and treatment of obesity-associated metabolic disorders.

Theophylline is a standard adenosine receptor antagonist, and it blocks non-selectively all subtypes of this receptor in humans [17,18]. This natural plant alkaloid exhibits micromolar affinities at adenosine receptors [18]. The K_i value of theophylline at the A_{2B} adenosine receptor, depending on the species, equals 9070–74,000 nM; 15,100 nM, and 5630 nM for humans [19,20], rat [20], and mice [21] receptors respectively. Some studies demonstrated a beneficial effect of theophylline on body weight in obese animals [22,23], but its side effects, such as hyperactivity [24], and heart rhythm disturbances [25,26] turned out to be a serious problem. It is thus of interest to examine whether a more selective antagonist of the A_{2B} adenosine receptor would also be effective in reducing body weight, but at the same time be safer than chronically applied theophylline.

The present study investigated the link between glucose homeostasis and anti-inflammatory activity induced by a blockade of the A_{2B} adenosine receptor using a highly potent and selective adenosine A_{2B} receptor antagonist [27,28]. The compound PSB-603 (Figure 1) displays > 17,000-fold selectivity over other adenosine receptors (K_i values are $0.553 > 100,000 > 10,000 > 10,000$ nM for human A_{2B}, A_1, A_{2A}, and A_3 receptors, respectively), and is similarly potent and selective in rats and mice [27,28]. The K_i value of PSB-603 at the A_{2B} adenosine receptor, depending on the species, equals 0.553 nM; 0.355 nM, and 0.265 nM for human-, rat-, or mice receptors, respectively [27]. Thus, PSB-603 acts much stronger at the A_{2B} adenosine receptor than theophylline.
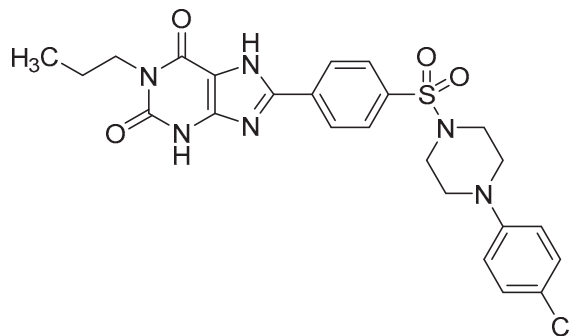

Figure 1. Structure of the potent and selective A_{2B} adenosine receptor antagonist PSB-603.

We have previously studied its effect on the inflammatory process in models of inflammation caused by the administration of zymosan A or carrageenan, and its antioxidant activity in vitro [14]. In this study, we present the results of the effects of PSB-603 on body weight in an obesity model caused by the administration of high-fat feed and sucrose, as well as on the amount of peritoneal fat, cholesterol and triglyceride levels, glucose and insulin tolerance, and spontaneous activity in mice.

2. Results

2.1. Effect of PSB-603 Administration on Body Weight

Mice fed a high-fat diet and a sucrose solution showed greater weight gain during the 12-week period of inducing obesity than control animals. Animals in the control group fed the standard diet weighed approximately 30 g, while mice in the obesity control group fed a high-fat diet weighed approximately 38 g—26.6% more. Animals fed a high-fat diet and treated with PSB-603 (for 14 days) at a dose of 2×5 mg/kg body weight (b.w.)/day showed significantly less weight gain than mice in the obese control group ($F_{(52,494)} = 5.236$, $p < 0.0001$). From the 12th day of compound administration, a statistically significant difference in body weight was observed between these groups (Figure 2A). PSB-603 reversed the effect of the high-fat diet and significantly reduced body weight ($F_{(4,39)} = 14.23$, $p < 0.0001$) (Figure 2B). Theophylline, which served as a positive control, had a much weaker effect. The results are shown in Figure 2A,B.
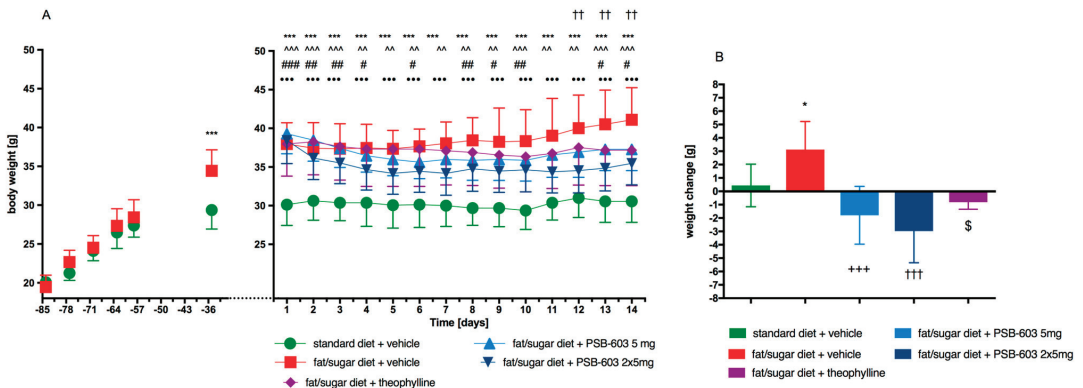

Figure 2. Effect of PSB-603 administration on body weight. (**A**) Body weight throughout the administration. (**B**) Sum of weight changes. Results are expressed as means ± SD, $n = 8$–10. Multiple comparisons were performed by two-way ANOVA, Tukey post hoc, (**A**) or one-way ANOVA Tukey post hoc (**B**). * Significant between control mice fed a standard diet and control mice fed a fat/sugar diet; ˆ Significant between control mice fed a standard diet and mice treated with PSB-603 at a dose of 5 mg/kg b.w./day and fed a fat/sugar diet; # significant between control mice fed a standard diet and mice treated with PSB-603 at a dose of 2×5 mg/kg b.w./day and fed a fat/sugar diet; ● significant between control mice fed a standard diet and mice treated with theophylline at a dose of 2×50 mg/kg b.w./day and fed a fat/sugar diet; + significant between control mice fed a fat/sugar diet and mice treated with PSB-603 at a dose of 5 mg/kg b.w./day and fed a fat/sugar diet; † significant between control mice fed a fat/sugar diet and mice treated with PSB-603 at a dose of 2×5 mg/kg b.w./day and fed a fat/sugar diet; $ significant between control mice fed a fat/sugar diet and mice treated with theophylline at a dose of 2×50 mg/kg b.w./day and fed a fat/sugar diet; *, #, $ $p < 0.05$, ˆˆ, ##, †† $p < 0.01$, ***, ˆˆˆ, +++, †††, ●●●, ### $p < 0.001$.

2.2. Effect of PSB-603 Administration on Peritoneal Fat Pads

The group of animals, which received the tested compound at a dose of 2×5 mg/kg b.w., had a significantly lower amount of fat in the peritoneum compared to obese control mice ($F_{(4,34)} = 16.49$, $p < 0.0001$). In the other two tested groups treated with theophylline

or PSB-603 at a dose of 5 mg/kg b.w./day, no significant decrease in body fat was found compared to the control obese group. The results are shown in Figure 3.
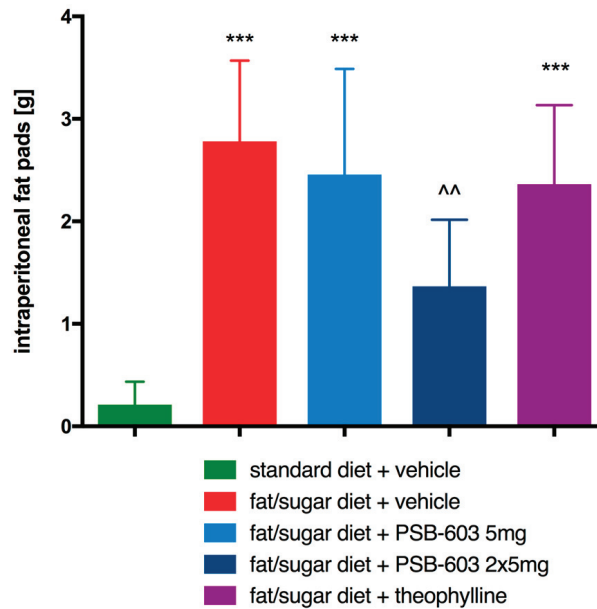
Figure 3. Effect of PSB-603 administration on the mass of adipose pads. Results are expressed as means ± SD, *n* = 7–8. Multiple comparisons were made using Tukey post hoc one-way ANOVA. * Significant against control mice fed standard diet; ^ significant against control mice fed a fat/sugar diet; ^^ *p* < 0.01, *** *p* < 0.001.

2.3. Effect of PSB-603 Administration on Locomotor and Spontaneous Activity of Mice

Locomotor activity was determined in mice after a single intraperitoneal administration of PSB-603 at doses of 10, 5, and 1 mg/kg b.w. Only at a dose of 10 mg/kg b.w. did the antagonist significantly decrease locomotor activity ($F_{(3,30)}$ = 9.743, *p* = 0.0001). The results are shown in Figure 4.

Figure 4. Locomotor activity after a single intraperitoneal administration of PSB-603. Results are expressed as means ± SD, *n* = 8–10. Comparisons were made by one-way ANOVA Bonferroni post hoc, * significant against control mice; ** *p* < 0.01.

Spontaneous activity was determined in obese mice. A single administration of PSB-603 at a dose of 5 mg/kg b.w. and its subchronic (13 days) administration resulted in significant reductions in spontaneous activities compared to the control groups in both phases of the day during the first and/or third h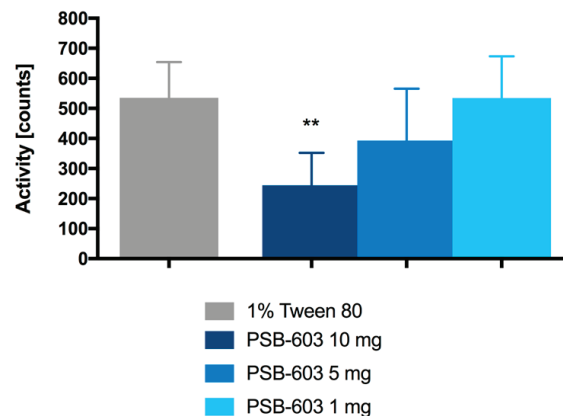ours of observation (the light phase), and in the fifth, seventh, eighth, tenth, or thirteenth hours of observation (the dark phase). The results are shown in Figure 5A,B.
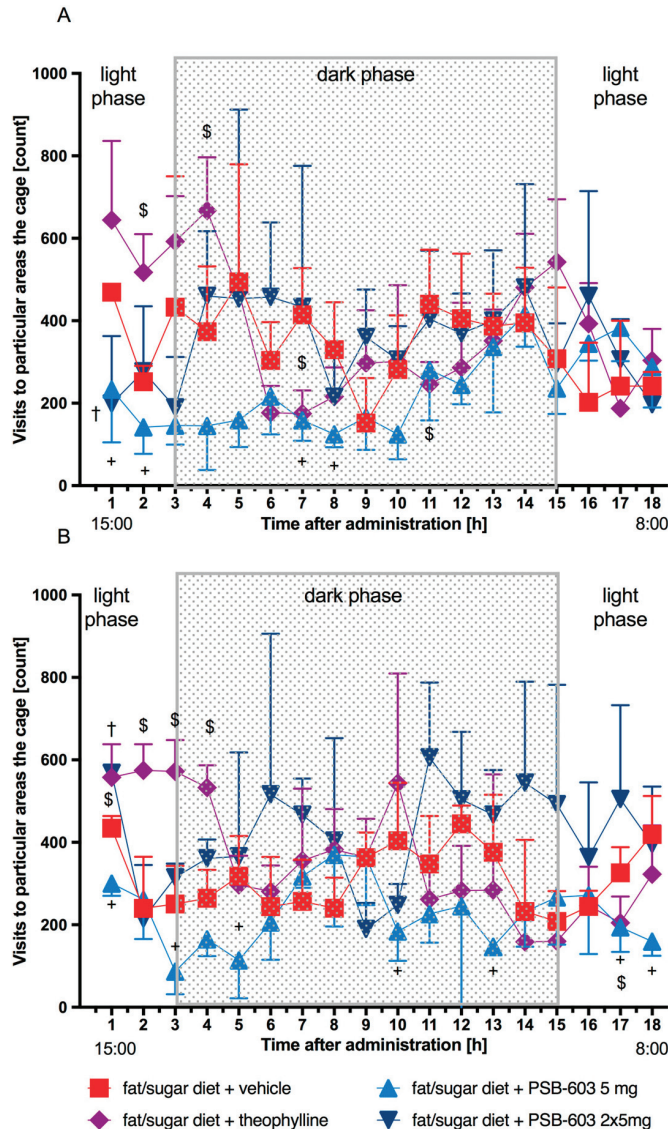
Figure 5. Spontaneous activity measured on the 1st and 13th days of treatment. Results are expressed as means ± SD, *n* = 8. Comparisons were made using the multiple t test; (**A**) after the first dose; (**B**) after 13 days of treatment; + significant between control mice fed a fat/sugar diet and mice treated with PSB-603 at a dose of 5 mg/kg b.w./day and fed a fat/sugar diet; † significant between control mice fed a fat/sugar diet and mice treated with PSB-603 at a dose of 2 × 5 mg/kg b.w./day and fed a fat/sugar diet; $ significant between control mice fed a fat/sugar diet and mice treated with theophylline at a dose of 2 × 50 mg/kg b.w./day and fed a fat/sugar diet; +, †, $ *p* < 0.05.

After administration of PSB-603 at a dose of 2×5 mg/kg b.w. (9.00 am and 1.00 pm) only in the first hour after the second administration mice showed reduced mobility compared to the control group. On the thirteenth day of the experiment, the activity of mice treated with PSB-603 (2×5 mg/kg) was very close to the activity of mice from the control group, which received only solvent (1% Tween 80). Only in the first hour after the second administration was the activity higher (Figure 5A,B).

Theophylline (2×50 mg/kg) significantly increased the activity of mice in the light phase on the first day and after subchronic (13 days) administration. The results are shown in Figure 5A,B.

2.4. Effect of PSB-603 Administration on the Plasma Glucose Levels

There were no significant differences in plasma glucose levels between all groups of obese mice (Figure 6) indicating that neither PSB-603 nor theophylline affected the increased plasma glucose levels in these mice.
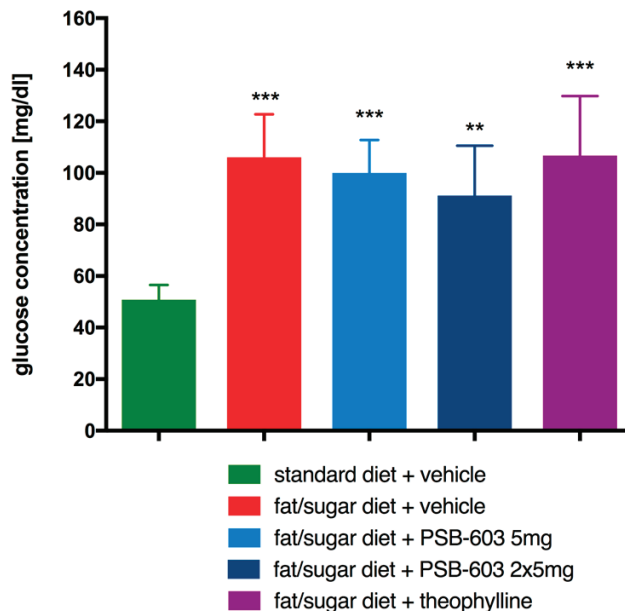
Figure 6. Effect of PSB-603 or theophylline administration on the plasma glucose level. Results are expressed as means $\pm$ SD, $n = 6$–9. Comparisons were performed by one-way ANOVA Tukey post hoc; * significant compared to control mice fed standard diet; ** $p < 0.01$, *** $p < 0.001$.

2.5. Glucose Tolerance and Insulin Sensitivity Tests

Fasting glucose concentrations were measured after 20 h of food deprivation just before the glucose loading test. Blood glucose levels in obese control mice were significantly higher at all time points compared to the blood glucose levels observed in control mice (fed standard feed). On the contrary, blood glucose levels in mice fed a high-fat diet and treated with PSB-603, measured at the same time points, did not differ significantly from the levels determined in control mice fed a standard diet. Furthermore, blood glucose levels at 30 and 60 min after glucose load in all treated groups were significantly lower than glucose levels in obese control mice ($F_{(12,102)} = 6.483$, $p < 0.0001$) (Figure 7A). As shown in Figure 7B, the area under the curve (AUC) decreased after PSB-603 (at a dose of 2×5 mg/kg b.w.) or theophylline treatment compared to the obese control group.
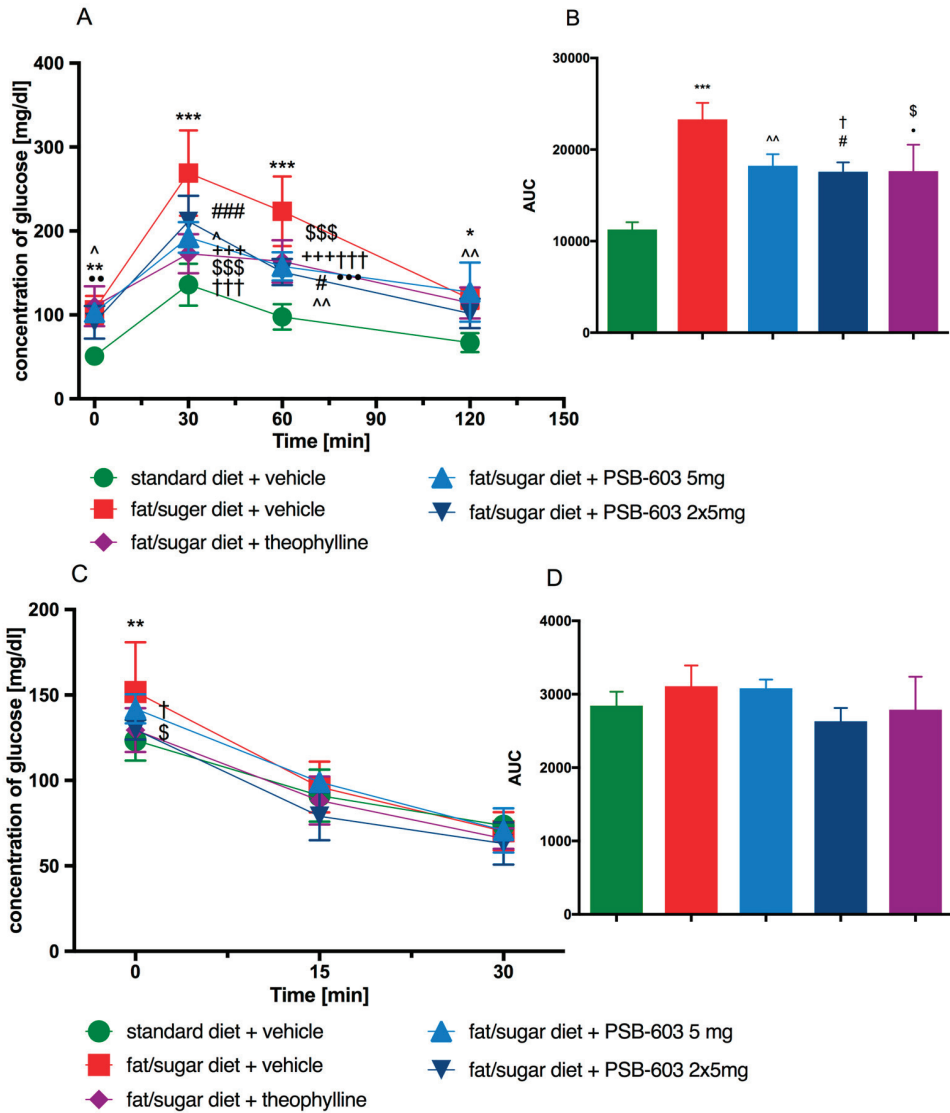
Figure 7. Intraperitoneal glucose tolerance test (IPGTT) (**A**). The area under the IPGTT curve (**B**). Insulin sensitivity test (IST) (**C**). The area under the IST curve (**D**). Results are expressed as means ± SD, $n = 6$–9. Comparisons were made by two-way ANOVA, Bonferroni post hoc; * significant between control mice fed a standard diet and control mice fed a fat/sugar diet; ^ significant between control mice fed a standard diet and mice treated with PSB-603 at a dose of 5 mg/kg b.w./day and fed a fat/sugar diet; # significant between control mice fed a standard diet and mice treated with PSB-603 at a dose of 2 × 5 mg/kg b.w./day and fed a fat/sugar diet; ● significant between control mice fed a standard diet and mice treated with theophylline at a dose of 2 × 50 mg/kg b.w./day and fed a fat/sugar diet; + significant between control mice fed a fat/sugar diet and mice treated with PSB-603 at a dose of 5 mg/kg b.w./day and fed a fat/sugar diet; † significant between control mice fed a fat/sugar diet and mice treated with PSB-603 at a dose of 2 × 5 mg/kg b.w./day and fed a fat/sugar diet; $ significant between control mice fed a fat/sugar diet and mice treated with theophylline at a dose of 2 × 50 mg/kg b.w./day and fed a fat/sugar diet; *, #, ^, $, †, ● $p < 0.05$, **,●●, ^^ $p < 0.01$, ***, +++, †††, ●●●, ###, $$$ $p < 0.001$.

The initial glucose levels before the insulin sensitivity test were significantly lower in the PSB-603 treated group (2×5 mg/kg) compared to the levels in the obese control group (Figure 7C). Similar results were observed for theophylline. In the insulin test, there were no statistically significant differences in the glucose levels between the tested groups, AUC values were also not statistically different (Figure 7D).

2.6. Triglyceride and Total Cholesterol Levels

The level of triglycerides in the blood was higher in obese mice than in mice fed a standard diet. Animals treated for two weeks with PSB-603 at a dose of 2×5 mg/kg b.w./day and fed a high-fat diet had a significantly lower plasma triglyceride level compared to the control group fed a high-fat diet ($F(4,44) = 6.672$, $p = 0.0003$). There was no statistically significant difference between both groups treated with PSB-603 and fed a high-fat diet and the group fed standard feed. The level of triglycerides in the group treated with theophylline was comparable to the level in the obese control group. However, the SD in this group was relatively high. Results are shown in Figure 8A.
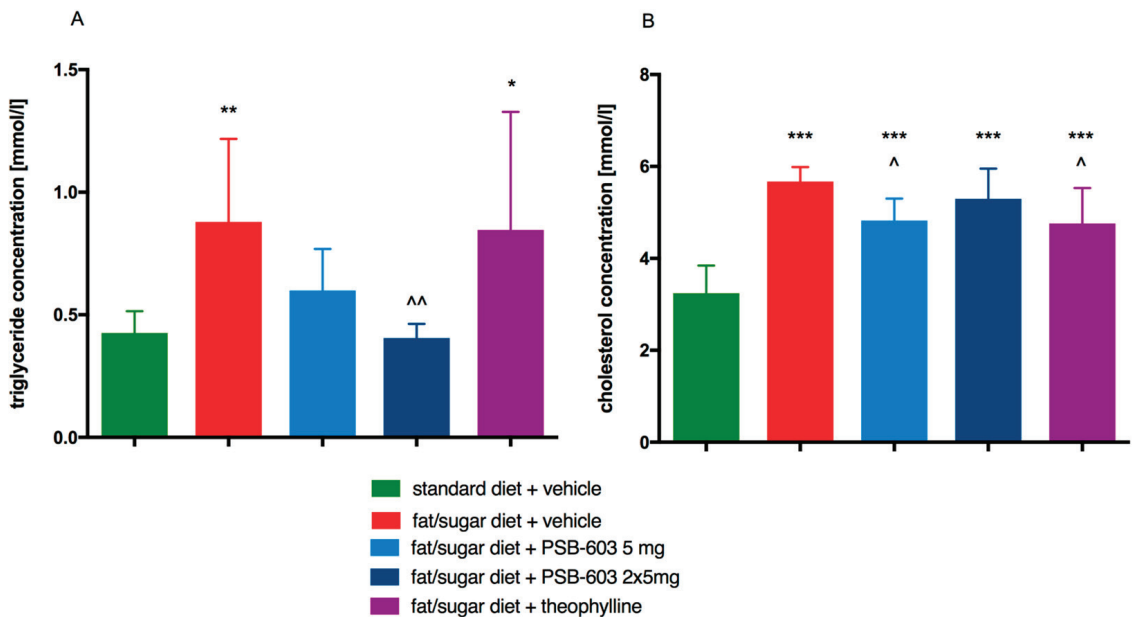
Figure 8. Effect of PSB-603 or theophylline administration on plasma levels of triglycerides (**A**) or total cholesterol (**B**). Results are expressed as means $\pm$ SD, $n = 9$–10. Comparisons were performed by one-way ANOVA Tukey post hoc; * Significant compared to control mice fed a standard diet; ^ Significant compared to control mice fed fat/sugar diet; *, ^ $p < 0.05$, **, ^^ $p < 0.01$, *** $p < 0.001$.

Total cholesterol levels in all obese groups were higher than in the standard-feed control group. There were no significant differences in total plasma cholesterol levels between the obese control group and the PSB-603 treated group at a dose of 2×5 mg/kg b.w./day. In contrast, total cholesterol was significantly lower in the groups treated with PSB-603 at a dose of 5 mg/kg b.w. or with theophylline compared to the control group fed high-fat feed ($F(4,44) = 23.28$, $p < 0.0001$) (Figure 8B).

2.7. TNF-α and IL-6 Levels

In the obese control mice, plasma levels of IL-6 and TNF-α were higher than in the standard-fed control mice. However, the TNF-α level was significantly reduced by PSB-603 administration for 14 days at doses of 5 mg/kg and 2×5 mg/kg b.w./day ($F(4,45) = 4.292$, $p = 0.005$). In the group treated with theophylline, similar changes were

observed (Figure 9A). The level of IL-6 was significantly reduced by PSB-603 administration for 14 days only at the dose of 2×5 mg/kg b.w./day ($F_{(4,38)} = 3.415$, $p = 0.005$) as well as by theophylline (Figure 9B).

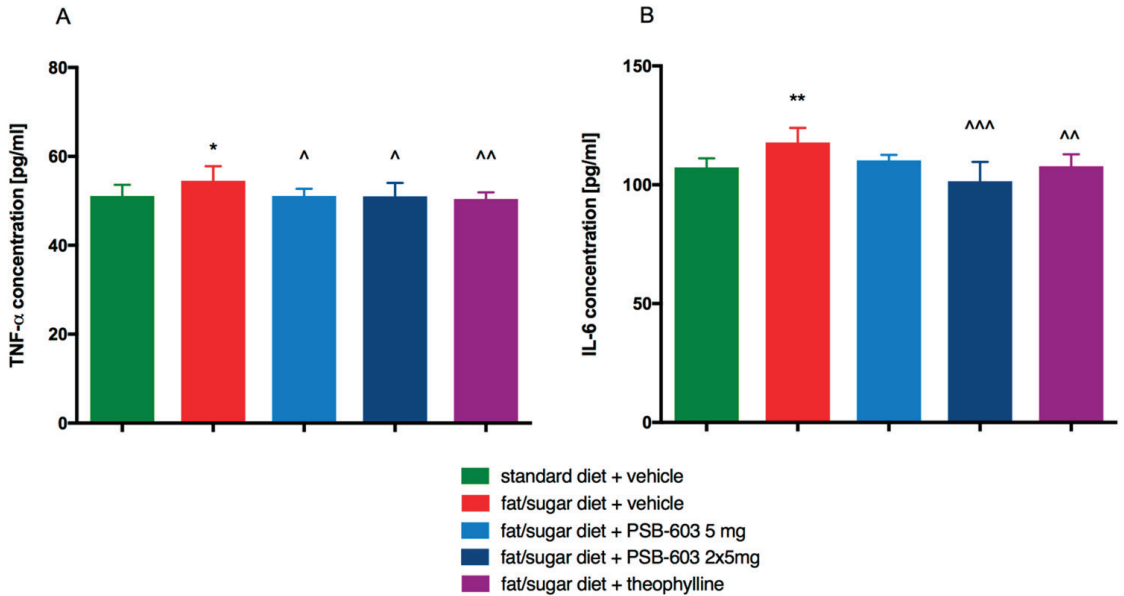**Figure 9.** Effect of PSB-603 administration on (**A**) TNF-α and (**B**) IL-6 levels in plasma. Results are expressed as means ± SD, $n = 8$–10. Comparisons were made by one-way ANOVA Tukey post hoc; * significant compared to control mice fed a standard diet; ^ significant compared to control mice fed a fat/sugar diet; *, ^ $p < 0.05$, **, ^^ $p < 0.01$, ^^^ $p < 0.001$.

3. Discussion

The purpose of this study was to investigate whether a selective A_{2B} adenosine receptor antagonist, PSB-603, can significantly affect body weight and selected biochemical parameters related to obesity as well as inflammatory processes that occur in obese animals. Will chronic administration of PSB-603 lead to weight reduction? Will the potential positive effects be fraught with undesirable side effects, such as increased locomotor activity seen with the non-selective theophylline? An established compound, the selective A_{2B} adenosine receptor antagonist PSB-603, which is similarly potent and selective in humans, mice, and rats [27], was chosen to answer these questions.

The study began with experiments to determine the compound's effect on locomotor activity in CD-1 mice after its single administration at doses of 10, 5, or 1 mg/kg b.w. This was a screening study conducted to select the appropriate dose for chronic experiments. Changes in mobility, such as sedation or excessive stimulation, could alter or falsify the effects of the tested compound on body weight [29,30]. Only at a single dose of 10 mg/kg b.w. PSB-603 significantly reduced the activity of the mice. For this reason, a dose of 5 mg/kg b.w. (for which the anti-inflammatory effect of this compound had previously been demonstrated [9]) and a dose of 2×5 mg/kg b.w. were selected for chronic studies. A study by Pardo et al. showed that even a single administration of theophylline at doses of 5–15 mg/kg b.w. can potentiate locomotor activity [31]. Nevertheless, in our study, the reference compound theophylline was administered at a dose of 2×50 mg/kg b.w. in accordance with the literature data [32]. PSB-603 administered to obese mice at a dose of 2×5 mg/kg b.w. did not have a significant effect on spontaneous activity, which was demonstrated by the chronic mobility monitoring using the telemetry method. The results of the weight reduction are therefore certainly not due to sedation, where animals often eat

less. In contrast, monitoring the activity of obese mice treated with theophylline confirmed its stimulating effect at the tested dose.

In a subsequent study, we evaluated the effects of the potent and selective xanthine-based antagonist PSB-603 [28] and the methylxanthine derivative theophylline, a non-selective adenosine receptor antagonist that blocks all four receptor subtypes (A_1, A_{2A}, A_{2B}, and A_3) in humans, and three subtypes in rodents (A_1, A_{2A}, A_{2B}) [18], on body weight in mice with diet-induced (high-fat/sucrose) obesity. The results obtained by us clearly show that theophylline administered at a dose of 2×50 mg/kg and PSB-603 administered at a dose of 5 mg/kg or 2×5 mg/kg significantly reduced body weight in obese mice. Our results are different from those obtained by Gnad et al., who showed that activation, but not blockade of the A_{2B} receptor, protected against obesity induced by a high-fat diet (HFD) [33]. In turn, Tofovic et al., 2016, showed that combined blockade of A_1 and A_{2B} adenosine receptors significantly increased body weight, but still had beneficial effects on multiple biochemical markers associated with obesity.

Adenosine A_{2B} receptors are located in key tissues related to obesity, i.e., adipocytes or liver and skeletal muscles, where they play an important regulatory role [33,34]. They are also detected in human and animal adipose tissue [34] and their expression is increased in abdominal adipose tissue of mice fed a high-fat diet [35]. Therefore, animals with the missing A_{2B} gene (A_{2B} receptor KO mice) gain more weight than wild type mice, have an increased accumulation of visceral adipose tissue, and developed insulin resistance in an HFD model [36,37]. In vitro studies showed the ability of this receptor to inhibit adipogenesis and lipogenesis [38]. Although A_{2B} receptors are known to be involved in the regulation of body weight, it is still not known whether the reduction of body weight and the decrease in the amount of adipose tissue are due to their stimulation or blockade. The absence of a definitive answer to this question may be due in part to the different models of obesity used by researchers and the use of different time courses of activation or inhibition of the A_{2B} receptor. Genetic deletion of the A_{2B} receptor in adipose tissue of mice fed a high-fat diet is known to result in increased weight gain [37]. However, it is not known whether chronic blockade may lead to its up-regulation, and thus cause a different effect than it seems directly logical (lack of receptors or blockade of receptors—weight gain). Therefore, we suggest that research that explains the potential influences of multiple administrations of selective ligands on changes in the densities of receptors located in individual tissues, which are important in the pathogenesis of obesity, as well as the correlation with the effect on body weight, should be carried out in the future.

Subsequently, our research showed that loss of body weight was accompanied by a reduction in the amount of peritoneal fat. This effect was statistically significant after repeated administration of the selective adenosine A_{2B} receptor antagonist PSB-603. Anti-obesity effects of non-selective methylxanthines blocking A_1/A_{2B} adenosine receptors have been well described [22]. These compounds can effectively reduce body fat and weight gain induced by high-fat diets in rodents [23], stimulate lipolysis, and inhibit adipogenesis through several molecular mechanisms [22,39]. However, in our study, theophylline, as a non-selective antagonist of the A_1/A_{2B} adenosine receptors (as well as the A_{2A} receptor subtype), induced a weaker effect in reducing the amount of adipose tissue compared to the more potent and selective A_{2B} receptor antagonist.

Mice fed a high-fat/sugar diet gained body weight and developed metabolic changes, including disturbances in carbohydrate metabolism and diabetes, as well as hyperlipi-daemia [40]. The A_{2B} receptor subtype appears to play a pivotal role in modulating glucose homeostasis and insulin resistance, thus emerging as a promising target for new drugs aiming at the treatment of metabolic disorders [41]. Adenosine stimulates liver glucose production by activating A_{2B} receptors [8,42,43], and selective A_{2B} receptor antagonists induce hypoglycaemia in diabetic mice [44]. In the present study, mice fed an HFD for 14 weeks developed a marked increase in body weight, followed by a marked alteration of several metabolic indices, such as an increase in blood glucose, cholesterol, and triglyceride levels, and an increase in blood levels of the inflammatory markers TNF-α and IL-6. Taking this

into account, in the next stage, we attempted to assess whether a selective A_{2B} adenosine receptor antagonist could lower elevated glucose levels and prevent the development of glucose tolerance and insulin resistance. Our observations show that PSB-603 and theophylline did not affect basal glucose levels in the obese state. On the contrary, the selective partial A_{2B} receptor agonist BAY60-6583 significantly reduced plasma glucose levels in mice fed the HFD [35]. However, PSB-603 and theophylline improved glucose tolerance, which was clearly observed in the glucose loading test in our study, and in agreement with the observation that BAY60-6583 decreased insulin resistance [35].

The beneficial effects of PSB-603, a selective A_{2B} receptor antagonist, on body weight and metabolic disturbances, may be mediated by its anti-inflammatory activity and the reduction in plasma levels of IL-6 and TNF-α. In current and previous studies, we demonstrated a high anti-inflammatory potential of PSB-603 [14] as well as another adenosine A_{2A}/A_{2B} receptor antagonist (compound KD-64) [9]. In support of our findings, Johnston-Cox et al. showed that expression of the A_{2B} receptor in macrophages plays an important role in controlling insulin sensitivity and glucose tolerance by regulating inflammatory cytokines that affect insulin signalling [45]. Furthermore, they demonstrated that A_{2B} receptor signalling in macrophages plays an important role in the protective effects of the A_{2B} receptor on HFD-induced insulin resistance. The results of Figler et al., suggest that A_{2B} receptor blockade may become an effective way to counteract insulin resistance by altering liver glucose production and reducing the production of IL-6 and other cytokines [46]. Moreover, the authors showed that deletion of the A_{2B} receptor gene and selective blockade of the A_{2B} receptor in mice reduced liver glucose production and increased glucose utilization in skeletal muscles and brown adipose tissue. Other studies showed that the adenosine A_{2B} receptor may modulate whole-body glucose metabolism by regulating insulin receptor substrate-2 (IRS-2) levels. A_{2B} knockout mice had decreased IRS-2 levels, which was associated with impaired insulin signalling in tissues [35].

In our study, chronic feeding of a high fat/sugar diet resulted in higher levels of triglycerides and plasma cholesterol, which is consistent with published results [47,48]. Theophylline, a non-selective antagonist of adenosine receptors, significantly reduced only total cholesterol levels without affecting elevated triglycerides in obese mice. The study by Tovofic et al., showed a beneficial effect of dual A_1/A_{2B} adenosine receptor blockade on lipid homeostasis, resulting in reduced plasma triglycerides and slightly decreased plasma cholesterol levels [49]. PSB-603, on the other hand, significantly reduced triglycerides and total cholesterol levels (only at the lower daily dose). PSB-603 at a dose that has a more beneficial effect on body weight (2×5 mg/kg b.w./day) did not affect the total cholesterol level, which may perhaps be due to an increase in the HDL fraction by this compound, although this issue requires more detailed studies. Thus, we showed that selective A_{2B} receptor blockade has a more favourable effect on the lipid profile than a non-selective blockade. However, the precise role of the adenosine A_{2B} receptor in the regulation of lipid homeostasis is complicated. According to the literature, (i) the A_{2B} receptor is associated with the regulation of liver lipid metabolism, and liver expression of A_{2B} receptors in mice was greatly increased by a high-fat diet [35,50]; (ii) the lack of A_{2B} receptors may have adverse effects on plasma lipids, i.e., it led to the development of liver steatosis with elevated liver and plasma triglyceride and cholesterol levels in HFD-fed mice [50], or it may protect mice from the accumulation of liver triglycerides [51]; (iii) antagonism of the A_{2B} receptor increased the expression of genes required for fatty acid metabolism, while activation of the A_{2B} receptor enhanced lipid accumulation in a cultured mouse hepatocyte cell line [51]. These interesting, often contradictory, results lead to the conclusion that more elaborate studies are needed to elucidate the precise effects of subtype-specific adenosine receptor ligands as well as non-selective compounds, on the lipid profile in specific models of metabolic disorders. The data available in the literature stem from various models that are difficult to compare.

Finally, we want to highlight the possible involvement of more targets, in addition to adenosine receptors, in the activity of individual ligands. Small ligands with a methylxan-

thine structure, such as theophylline, can significantly affect, for example, the activity of phosphodiesterases [52], and this mechanism may contribute to their actions. Therefore, the full spectrum of activities of a tested compound is usually not known, which we consider a significant limitation of our study, as well as of many published studies.

Other limitations of this study need to be highlighted. Since our research is preliminary, there was only a selected number of tests performed to showcase the potential differences between the activities of investigated compounds and selective and non-selective antagonists of adenosine receptors. The promising results open the field for future, more detailed, investigations which allow showing specific changes induced by PSB-603 administration (by histological and molecular characterization of liver morphological and functional changes during treatment, histological and immunohistochemistry analysis performed at the adipose tissue level, etc). Moreover, a comparison of agonist versus antagonist efficacy in the same metabolic disorder model could explain many of the confusing facts about the actions of adenosine A_{2B} receptor agonists and antagonists in metabolic disorders.

In conclusion, the results obtained by us clearly show that theophylline (non-selective adenosine receptor antagonist) and PSB-603 (selective adenosine A_{2B} receptor antagonist) significantly reduced body weight in obese mice. However, theophylline significantly increased the spontaneous activity of mice which could alter the results. Loss of body weight was accompanied by a reduction in the amount of peritoneal fat; however, this effect was statistically significant only after PSB-603 administration. Theophylline and PSB-603 had no effect on glucose levels in the obese state, but PSB-603, contrary to theophylline, significantly reduced triglycerides and total cholesterol blood levels. Thus, our observations show that selective A_{2B} receptor blockade has a more favourable effect on the amount of peritoneal fat and the lipid profile than a non-selective blockade. However, the exact sequence of molecular events in the organism, connecting influence of PSB-603 on adenosine A_{2B} receptor with weight reduction and improvement of metabolic disturbances, remains an open question and requires further studies.

4. Materials and Methods

4.1. Animals

In the study, adult female Albino Swiss mice, CD-1, weighing 18–22 g were used. The animals were kept in environmentally controlled rooms, in standard cages lit with artificial light for 12 h each day. The animals had free access to food and water, except for the time of the acute experiment. The randomly established experimental groups consisted of 8–10 mice. All animal care and experimental procedures were carried out in accordance with the European Union and Polish legislation acts concerning animal experimentation and were approved by the Local Ethics Committee of Jagiellonian University in Cracow, Poland (Permission No: 256/2015, 55/2017).

4.2. Drugs, Chemical Reagents, and Other Materials

Theophylline was purchased from Sigma-Aldrich (Warszawa, Poland). The compound PSB-603 (Figure 1) was synthesised at PharmaCenter Bonn, Pharmaceutical Institute, Bonn, Germany, according to a described procedure [28]. The identity and purity of the final product were assessed by NMR and LC-UV/MS techniques.

For studies, PSB-603 (5 mg/kg b.w. of the mouse or 2 × 5 mg/kg b.w. of the mouse) was suspended in 1% Tween 80 and the volume was adjusted to 10 mL/kg. This dose was chosen because PSB-603 at 5 mg/kg b.w. does not have a sedative effect (locomotor activity study—Section 2.3) and has anti-inflammatory activity [14]. Theophylline was administered intraperitoneally at a dose of 2 × 50 mg/kg b.w. of the mouse [32].

4.3. Experiment Methods

4.3.1. Metabolic Disorders Induced by a High-Fat/Sucrose Diet and Influence of the Tested Compounds on Body Weight and Spontaneous Activity

Mice were fed a high-fat diet consisting of a 40% fat blend (Labofeed B with 40% lard, Morawski Feed Manufacturer, Żurawia, Poland) for 14 weeks, water and a 30% sucrose solution were available ad libitum [53,54]. Control mice were fed a standard diet (Labofeed B, Morawski Feed Manufacturer, Poland) and drank only water. After 12 weeks, mice with diet-induced obesity were randomly divided into four equal groups that had the same mean body weight and were treated intraperitoneally with test compounds at the following doses: PSB-603 5 mg/kg b.w./day; PSB-603 5 mg/kg b.w./two times a day; theophylline 50 mg/kg b.w./two times a day or vehicle—1% Tween 80, 0.35 mL (fat/sugar diet + vehicle = obesity control group) once a day in the morning, between 9:00 and 10:00 am or twice a day at 9:00 am and 2:00 pm for 14 days. Control mice (control without obesity) were kept on a standard diet, with the intraperitoneal administration of vehicle—1% Tween 80, 0.35 mL (standard diet + vehicle = control group). Water and sucrose were measured daily, immediately prior to the morning drug administration. Animals always had free access to food, water, and sucrose.

High-fat feeding composition (932 g of dry mass): protein—193 g, fat (lard)—408 g, fibre—28.1 g, crude ash—43.6 g, calcium—9.43 g, phosphorus—5.99 g, sodium—1.76 g, sugar—76 g, magnesium—1.72 g, potassium—7.62 g, manganese—48.7 mg, iodine—0.216 mg, copper—10.8 mg, iron—125 mg, zinc—61.3 mg, cobalt—0.253 mg, selenium—0.304 mg, vitamin A—15,000 units, vitamin D3—1000 units, vitamin E—95.3 mg, vitamin K3—3.0 mg, vitamin B1—8.06 mg, vitamin B2—6.47 mg, vitamin B12—0.051 mg, folic acid—2.05 mg, nicotinic acid—73.8 mg, pantothenic acid—19.4 mg, choline—1578 mg.

The high-fat diet contained 550 kcal and the standard diet 280 kcal per 100 g.

The spontaneous activity was measured on the first and 13th day of treatment with a special RFID system—TraffiCage (TSE-Systems, Bad Homburg, Germany). Animals were subcutaneously implanted with transmitter identification (RFID), allowing the presence and time spent in different areas of the cage to be counted, and then the data were grouped in a special computer program [55].

4.3.2. Glucose Tolerance Test

The test was performed at the beginning of week 15. After the fourteenth (once daily) or twenty-eighth (twice daily) administration of the test compound, food and sucrose were discontinued for 20 h and then glucose tolerance was tested. Glucose (1 g/kg b.w.) was administered intraperitoneally. Blood samples were taken at time points: 0 (before glucose administration), 30, 60, and 120 min from the tail vein. Glucose levels were measured with a glucometer (ContourTS, Bayer, Leverkusen, Germany, test stripes: ContourTS, Ascensia Diabetes Care Poland Sp. z o.o., Warszawa, Poland, REF:84239666). The area under the curve (AUC) was calculated using the trapezoid rule.

4.3.3. Insulin Sensitivity Test

Insulin tolerance was tested the next day after the glucose tolerance test (after this test, mice had free access to standard food and water). Three hours before the insulin tolerance test, the food was discontinued. Insulin (0.5 IU/kg b.w.) was injected intraperitoneally, blood samples were taken at time points: 0, 15, and 30 min from the tail vein, and glucose levels were measured with a glucometer (ContourTS, Bayer, Leverkusen, Germany, test stripes: ContourTS, Ascensia Diabetes Care Poland Sp. z o.o., Warszawa, Poland, REF:84239666). The AUC was calculated using the trapezoid rule.

4.3.4. Locomotor Activity

Locomotor activity was recorded with an Opto M3 multichannel activity monitor (MultiDevice Software v1.3, Columbus Instruments, Columbus, OH, USA). It was evaluated as the distance travelled by animals when trying to climb [55]. Mice immediately after

intraperitoneal administration of the test compound were placed in parameter counting cages; however, the activity measurement was read 30 min after administration of the test compound for a period of 20 min.

4.3.5. Biochemical Analysis

Blood and fat pads were collected after decapitation and then blood was centrifuged at $600 \times g$ (15 min, 4 °C) to obtain plasma. To determine cholesterol and triglyceride levels in plasma, standard enzymatic spectrophotometric tests (Biomaxima S.A. Lublin, Poland, catalogue number: 1-023-0400 or 1-053-0400) were used. The absorbance was measured at a wavelength of 500 nm.

To determine IL-6 and TNF-α levels LANCE® Ultra Detection Kits (PerkinElmer, Inc., Waltham, MA, USA, catalogue numbers: TRF1505, TRF1504C/TRF1504M) were used. LANCE® Ultra is a homogeneous (no wash) time-resolved fluorescence resonance energy transfer technology.

4.4. Statistical Analysis

Statistical calculations were performed using the GraphPad Prism 6 program (Graph-Pad Software, San Diego, CA, USA). The results are presented as arithmetic means with a standard deviation (means $\pm$ SD). The normality of the data sets was determined using the Shapiro–Wilk test. Statistical significance was calculated using one-way ANOVA, Tukey post hoc test (two control groups), with significance level set at 0.05 (triglyceride, cholesterol, glucose, IL-6, TNF-α levels, amount of fat pads) or one-way ANOVA, Bonferroni post hoc (one control group), with a significance level set at 0.05 (locomotor activity) or two-way ANOVA, Tukey post hoc test with the significance level set at 0.05 (changes in body weight, glucose tolerance test, insulin tolerance test) or the multiple t test, with significance level set at 0.05 (spontaneous activity). Differences were considered statistically significant at: * $p \leq 0.05$, ** $p \leq 0.01$, *** $p \leq 0.001$.

References

1. Bastard, J.-P.; Maachi, M.; Lagathu, C.; Kim, M.J.; Caron, M.; Vidal, H.; Capeau, J.; Feve, B. Recent advances in the relationship between obesity, inflammation, and insulin resistance. *Eur. Cytokine Netw.* **2006**, *17*, 4–12.
2. Van der Heijden, R.A.; Sheedfar, F.; Morrison, M.C.; Hommelberg, P.P.; Kor, D.; Kloosterhuis, N.J.; Gruben, N.; Youssef, S.A.; de Bruin, A.; Hofker, M.H.; et al. High-fat diet induced obesity primes inflammation in adipose tissue prior to liver in C57BL/6j mice. *Aging* **2015**, *7*, 256–268. [CrossRef]

3.   Ye, J. Mechanisms of insulin resistance in obesity. *Front. Med.* **2013**, 7, 14–24. [CrossRef]
4.   Zeyda, M.; Stulnig, T.M. Obesity, inflammation, and insulin resistance—A mini-review. *Gerontology* **2009**, 55, 379–386. [CrossRef]
5.   D'Antongiovanni, V.; Fornai, M.; Pellegrini, C.; Blandizzi, C.; Antonioli, L. Managing obesity and related comorbidities: A potential pharmacological target in the adenosine system? *Front. Pharmacol.* **2021**, 11, 621955. [CrossRef]
6.   Gnad, T.; Scheibler, S.; Von Kügelgen, I.; Scheele, C.; Kilić, A.; Glöde, A.; Hoffmann, L.S.; Reverte-Salisa, L.; Horn, P.; Mutlu, S.; et al. Adenosine activates brown adipose tissue and recruits beige adipocytes via A_{2A} receptors. *Nature* **2014**, 516, 395–399. [CrossRef]
7.   Merighi, S.; Borea, P.A.; Gessi, S. Adenosine receptors and diabetes: Focus on the A_{2B} adenosine receptor subtype. *Pharmacol. Res.* **2015**, 99, 229–236. [CrossRef]
8.   Rüsing, D.; Müller, C.; Verspohl, E. The impact of adenosine and A_{2B} receptors on glucose homoeostasis. *J. Pharm. Pharmacol.* **2006**, 58, 1639–1645. [CrossRef]
9.   Kotańska, M.; Dziubina, A.; Szafarz, M.; Mika, K.; Reguła, K.; Bednarski, M.; Zygmunt, M.; Drabczyńska, A.; Sapa, J.; Kieć-Kononowicz, J. KD-64-A new selective A2A adenosine receptor antagonist has anti-inflammatory activity but contrary to the non-selective antagonist—Caffeine does not reduce diet induced obesity in mice. *PLoS ONE* **2020**, 15, e0229806. [CrossRef]
10.   Micioni Di Bonaventura, M.V.; Cifani, C.; Lambertucci, C.; Volpini, R.; Cristalli, G.; Massi, M. A_{2A} adenosine receptor agonists reduce both high-palatability and low-palatability food intake in female rats. *Behav. Parmacol.* **2012**, 23, 567–574. [CrossRef]
11.   Sanni, O.; Terre'Blanche, G. Therapeutic potentials of agonist and antagonist of adenosine receptors in type 2 diabetes. *Rev. Endocr. Metab. Disord.* **2021**, 22, 1073–1090. [CrossRef]
12.   Wojcik, M.; Zieleniak, A.; Mac-Marcjanek, K.; Wozniak, L.A.; Cypryk, K. The elevated gene expression level of the $A_{(2B)}$ adenosine receptor is associated with hyperglycemia in women with gestational diabetes mellitus. *Diabetes Metab. Res. Rev.* **2014**, 30, 42–53. [CrossRef]
13.   Cárdenas, A.; Toledo, C.; Oyarzún, C.; Sepúlveda, A.; Quezada, C.; Guillén-Gómez, E.; Díaz-Encarnación, M.M.; Pastor-Anglada, M.; San Martín, R. Adenosine $A_{(2B)}$ receptor-mediated VEGF induction promotes diabetic glomerulopathy. *Lab. Invest.* **2013**, 93, 135–144. [CrossRef]
14.   Kotańska, M.; Szafarz, M.; Mika, K.; Dziubina, A.; Bednarski, M.; Müller, C.E.; Sapa, J.; Kieć-Kononowicz, K. PSB 603—A known selective adenosine A_{2B} receptor antagonist—Has anti-inflammatory activity in mice. *Biomed. Pharmacother.* **2021**, 135, 111164. [CrossRef]
15.   Foschetti, D.A.; Braga-Neto, M.B.; Bolick, D.; Moore, J.; Alves, L.A.; Martins, C.S.; Bomfin, L.E.; Santos, A.; Leitão, R.; Brito, G.; et al. Clostridium difficile toxins or infection induce upregulation of adenosine receptors and IL-6 with early pro-inflammatory and late anti-inflammatory pattern. *Braz. J. Med. Biol. Res.* **2020**, 53, e9877. [CrossRef]
16.   Antonioli, L.; Pellegrini, C.; Fornai, M.; Tirotta, E.; Gentile, D.; Benvenuti, L.; Giron, M.C.; Caputi, V.; Marsilio, I.; Orso, G.; et al. Colonic motor dysfunctions in a mouse model of high-fat diet-induced obesity: An involvement of A_{2B} adenosine receptors. *Purinergic Signal.* **2017**, 13, 497–510. [CrossRef]
17.   Kaneko, Y.; Takashima, K.; Suzuki, N.; Yamana, K. Effects of theophylline on chronic inflammatory lung injury induced by LPS exposure in guinea pigs. *Allergol. Int.* **2007**, 56, 445–456. [CrossRef]
18.   Müller, C.E.; Jacobson, K.A. Xanthines as adenosine receptor antagonists. In *Methylxanthines. Handbook of Experimental Pharmacology*; Springer: Berlin/Heidelberg, Germany, 2011; pp. 151–199. [CrossRef]
19.   Bertarelli, D.C.G.; Diekmann, M.; Hayallah, A.M.; Rüsing, D.; Iqbal, J.; Preiss, B.; Verspohl, E.J.; Müller, C.E. Characterization of human and rodent native and recombinant adenosine A2B receptors by radioligand binding studies. *Purinergic Signal.* **2006**, 2, 559–571. [CrossRef]
20.   Kim, S.-A.; Marschall, M.A.; Melman, N.; Kim, H.S.; Müller, C.E.; Linden, J.; Jacobson, K.A. Structure-activity relationships at human and rat A2B adenosine receptors of xanthine derivatives substituted at the 1-, 3-, 7-, and 8-positions. *J. Med. Chem.* **2002**, 45, 2131–2138. [CrossRef]
21.   Auchampach, J.A.; Kreckler, L.M.; Wan, T.C.; Maas, J.E.; van der Hoeven, D.; Gizewski, E.; Narayanan, J.; Maas, G.E. Characterization of the A2B adenosine receptor from mouse, rabbit, and dog. *J. Pharm. Exp. Ther.* **2009**, 329, 2–13. [CrossRef]
22.   Carrageta, D.F.; Dias, T.R.; Alves, M.G.; Oliveira, P.F.; Monteiro, M.P.; Silva, B.M. Anti-obesity potential of natural methylxanthines. *J. Funct. Foods* **2018**, 43, 84–94. [CrossRef]
23.   Inoue, H.; Kobayashi-Hattori, K.; Horiuchi, Y.; Oishi, Y.; Arai, S.; Takita, T. Regulation of the body fat percentage in developmental-stage rats by methylxanthine derivatives in a high-fat diet. *Biosci. Biotechnol. Biochem.* **2006**, 70, 1134–1139. [CrossRef]
24.   Hirose, M.; Yokoyama, H.; Iinuma, K. Theophylline impairs memory/learning in developing mice. *Brain Dev.* **2004**, 26, 448–452. [CrossRef]
25.   Bittar, G.; Friedman, H.S. The arrhythmogenicity of theophylline. A multivariate analysis of clinical determinants. *Chest* **1991**, 99, 1414–1420. [CrossRef]
26.   Skinner, M.H. Adverse reactions and interactions with theophylline. *Drug Saf.* **1990**, 5, 275–285. [CrossRef]
27.   Alnouri, M.W.; Jepards, S.; Casari, A.; Schiedel, A.C.; Hinz, S.; Müller, C.E. Selectivity is species-dependent: Characterization of standard agonists and antagonists at human, rat, and mouse adenosine receptors. *Purinergic Signal.* **2015**, 11, 389–407. [CrossRef]
28.   Borrmann, T.; Hinz, S.; Bertarelli, D.C.; Li, W.; Florin, N.C.; Scheiff, A.B.; Müller, C.E. 1-alkyl-8-(piperazine-1-sulfonyl) phenylxanthines: Development and characterization of adenosine A2B receptor antagonists and a new radioligand with subnanomolar affinity and subtype specificity. *J. Med. Chem.* **2009**, 52, 3994–4006. [CrossRef]

29. Dudek, M.; Knutelska, J.; Bednarski, M.; Nowiński, L.; Zygmunt, M.; Mordyl, B.; Głuch-Lutwin, M.; Kazek, G.; Sapa, J.; Pytka, K. A comparison of the anorectic effect and safety of the alpha2-adrenoceptor ligands guanfacine and yohimbine in rats with diet-induced obesity. *PLoS ONE* **2015**, *10*, e0141327. [CrossRef]

30. Mingote, S.; Pereira, M.; Farrar, A.M.; McLaughlin, P.; Salamone, J.D. Systemic administration of the adenosine A$_{2A}$ agonist CGS 21680 induces sedation at doses that suppress lever pressing and food intake. *Pharmacol. Biochem. Behav.* **2008**, *89*, 345–351. [CrossRef]

31. Pardo, M.; López-Cruz, L.; Valverde, O.; Ledent, C.; Baqi, Y.; Müller, C.E.; Salamone, J.D.; Correa, M. Effect of subtype-selective adenosine receptor antagonists on basal or haloperidol-regulated striatal function: Studies of exploratory locomotion and c-Fos immunoreactivity in outbred and A$_{(2A)}$R KO mice. *Behav. Brain Res.* **2013**, *247*, 217–226. [CrossRef]

32. Tchekalarova, J.; Georgiev, V. Effect of acute versus chronic theophylline administration on acute restraint stress-induced increase of pentylenetetrazol seizure threshold in mice. *Brain Res. Bull.* **2006**, *68*, 464–468. [CrossRef]

33. Gnad, T.; Navarro, G.; Lahesmaa, M.; Reverte-Salisa, L.; Copperi, F.; Cordomi, A.; Naumann, J.; Hochhäuser, A.; Haufs-Brusberg, S.; Wenzel, D.; et al. Adenosine/A$_{2B}$ receptor signaling ameliorates the effects of aging and counteracts obesity. *Cell Metab.* **2020**, *32*, 56–70.e7. [CrossRef]

34. Tozzi, M.; Nowak, I. Purinergic Receptors in Adipose Tissue As Potential Targets in Metabolic Disorders. *Front. Pharmacol.* **2017**, *8*, 878. [CrossRef]

35. Johnston-Cox, H.; Koupenova, M.; Yang, D.; Corkey, B.; Gokce, N.; Farb, M.G.; LeBrasseur, N.; Ravid, K. The A2b adenosine receptor modulates glucose homeostasis and obesity. *PLoS ONE* **2012**, *7*, e40584. [CrossRef]

36. Csóka, B.; Koscsó, B.; Törő, G.; Kókai, E.; Virág, L.; Németh, Z.H.; Pacher, P.; Bai, P.; Hask, O.G. A$_{2B}$ adenosine receptors prevent insulin resistance by inhibiting adipose tissue inflammation via maintaining alternative macrophage activation. *Diabetes* **2014**, *63*, 850–866. [CrossRef]

37. Peleli, M.; Hezel, M.; Zollbrecht, C.; Persson, A.E.; Lundberg, J.O.; Weitzberg, E.; Fredholm, B.B.; Carlström, M. In adenosine A2B knockouts acute treatment with inorganic nitrate improves glucose disposal, oxidative stress, and AMPK signaling in the liver. *Front. Physiol.* **2015**, *6*, 222. [CrossRef]

38. Gharibi, B.; Abraham, A.A.; Ham, J.; Evans, B.A. Contrasting effects of A1 and A$_{2b}$ adenosine receptors on adipogenesis. *Int. J. Obes.* **2012**, *36*, 397–406. [CrossRef]

39. Eisenstein, A.; Ravid, K. G protein-coupled receptors and adipogenesis: A focus on adenosine receptors. *J. Cell. Physiol.* **2014**, *229*, 414–421. [CrossRef]

40. Sumiyoshi, M.; Sakanaka, M.; Kimura, Y. Chronic intake of high-fat and high-sucrose diets differentially affects glucose intolerance in mice. *J. Nutr.* **2006**, *136*, 582–587. [CrossRef]

41. D'Antongiovanni, V.; Benvenuti, L.; Fornai, M.; Pellegrini, C.; Van den Wijngaard, R.; Cerantola, S.; Giron, M.C.; Caputi, V.; Colucci, R.; Haskó, G.; et al. Glial A$_{2B}$ adenosine receptors modulate abnormal tachykininergic responses and prevent enteric inflammation associated with high fat diet-induced obesity. *Cells* **2020**, *9*, 1245. [CrossRef]

42. Buxton, D.B.; Fisher, R.A.; Robertson, S.M.; Olson, M.S. Stimulation of glycogenolysis and vasoconstriction by adenosine and adenosine analogues in the perfused rat liver. *Biochem. J.* **1987**, *248*, 35–41. [CrossRef] [PubMed]

43. Yasuda, N.; Inoue, T.; Horizoe, T.; Nagata, K.; Minami, H.; Kawata, T.; Hoshino, Y.; Harada, H.; Yoshikawa, S.; Asano, O.; et al. Functional characterization of the adenosine receptor contributing to glycogenolysis and gluconeogenesis in rat hepatocytes. *Eur. J. Pharmacol.* **2003**, *459*, 159–166. [CrossRef]

44. Harada, H.; Asano, O.; Hoshino, Y.; Yoshikawa, S.; Matsukura, M.; Kabasawa, Y.; Niijima, J.; Kotake, Y.; Watanabe, N.; Kawata, T.; et al. 2-Alkynyl-8-aryl-9methyladenines as novel adenosine receptor antagonists: Their synthesis and structure-activity relationships toward hepatic glucose production induced via agonism of the A$_{2B}$ receptor. *J. Med. Chem.* **2001**, *44*, 170–179. [CrossRef] [PubMed]

45. Johnston-Cox, H.; Eisenstein, A.S.; Koupenova, M.; Carroll, S.; Ravid, K. The macrophage A$_{2B}$ adenosine receptor regulates tissue insulin sensitivity. *PLoS ONE* **2014**, *9*, e98775. [CrossRef]

46. Figler, R.A.; Wang, G.; Srinivasan, S.; Jung, D.Y.; Zhang, Z.; Pankow, J.S.; Ravid, K.; Fredholm, B.; Hedrick, C.C.; Rich, S.S.; et al. Links between insulin resistance, adenosine A$_{2B}$ receptors, and inflammatory markers in mice and humans. *Diabetes* **2011**, *60*, 669–679. [CrossRef]

47. Mubiru, J.N.; Garcia-Forey, M.; Higgins, P.B.; Hemmat, P.; Cavazos, N.E.; Dick, E.J., Jr.; Owston, M.A.; Bauer, C.A.; Shade, R.E.; Comuzzie, A.G.; et al. A preliminary report on the feeding of cynomolgus monkeys (*Macaca fascicularis*) with a high-sugar high-fat diet for 33 weeks. *J. Med. Primatol.* **2011**, *40*, 335–341. [CrossRef]

48. Wang, K.W.; Xiao, B.Q.; Li, B.H.; Liu, Y.Y.; Wei, Z.Y.; Rao, J.H.; Chen, J.H. Effects of fat-to-sugar ratio in excess dietary energy on lipid abnormalities: A 7-month prospective feeding study in adult cynomolgus monkeys. *Lipids Health Dis.* **2019**, *18*, 1. [CrossRef]

49. Tofovic, S.P.; Salah, E.M.; Smits, G.J.; Whalley, E.T.; Ticho, B.; Deykin, A.; Jackson, E.K. Dual a1/a2b receptor blockade improves cardiac and renal outcomes in a rat model of heart failure with preserved ejection fraction. *J. Pharmacol. Exp. Ther.* **2016**, *356*, 330–340. [CrossRef]

50. Koupenova, M.; Johnston-Cox, H.; Vezeridis, A.; Gavras, H.; Yang, D.; Zannis, V.; Ravid, K. A$_{2b}$ adenosine receptor regulates hyperlipidemia and atherosclerosis. *Circulation* **2012**, *125*, 354–363. [CrossRef]

51. Peng, Z.; Borea, P.A.; Varani, K.; Wilder, T.; Yee, H.; Chiriboga, L.; Blackburn, M.R.; Azzena, G.; Resta, G.; Cronstein, B.N. Adenosine signalling contributes to ethanol-induced fatty liver in mice. *J. Clin. Investig.* **2009**, *119*, 582–594. [CrossRef]

52. Monteiro, J.; Alves, M.G.; Oliveira, P.F.; Silva, B.M. Pharmacological potential of methylxanthines: Retrospective analysis and future expectations. *Crit. Rev. Food Sci. Nutr.* **2019**, *59*, 2597–2625. [CrossRef] [PubMed]

53. Kotańska, M.; Mika, K.; Reguła, K.; Szczepańska, K.; Szafarz, M.; Bednarski, M.; Olejarz-Maciej, A.; Nowak, K.; Latacz, G.; Mogilski, S.; et al. KSK-19-Novel histamine H_3 receptor ligand reduces body weight in diet induced obese mice. *Biochem. Pharmacol.* **2019**, *168*, 193–203. [CrossRef] [PubMed]

54. Kotańska, M.; Kuder, K.J.; Szczepańska, K.; Sapa, J.; Kieć-Kononowicz, K. The histamine H_3 receptor inverse agonist pitolisant reduces body weight in obese mice. *Naunyn-Schmiedebergs Arch. Pharmacol.* **2018**, *391*, 875–881. [CrossRef]

55. Dudek, M.; Kuder, K.; Kołaczkowski, M.; Olczyk, A.; Żmudzka, E.; Rak, A.; Bednarski, M.; Pytka, K.; Sapa, J.; Kieć-Kononowicz, K. H3 histamine receptor antagonist pitolisant reverses some subchronic disturbances induced by olanzapine in mice. *Metab. Brain Dis.* **2016**, *31*, 1023–1029. [CrossRef] [PubMed]

Article

KSK-74: Dual Histamine H$_3$ and Sigma-2 Receptor Ligand with Anti-Obesity Potential

Kamil Mika [1], Małgorzata Szafarz [2], Monika Zadrożna [3], Barbara Nowak [3], Marek Bednarski [1], Katarzyna Szczepańska [4,5], Krzysztof Pociecha [2], Monika Kubacka [1], Noemi Nicosia [1,6,7], Izabela Juda [3], Katarzyna Kieć-Kononowicz [4] and Magdalena Kotańska [1,*]

[1] Department of Pharmacological Screening, Jagiellonian University Medical College, Medyczna 9, 30-688 Cracow, Poland; kamil.mika@doctoral.uj.edu.pl (K.M.); marek.bednarski@uj.edu.pl (M.B.); monika.kubacka@uj.edu.pl (M.K.); noemi.nicosia92@gmail.com (N.N.)

[2] Department of Pharmacokinetics and Physical Pharmacy, Jagiellonian University Medical College, Medyczna 9, 30-688 Cracow, Poland; malgorzata.szafarz@uj.edu.pl (M.S.); k.pociecha@uj.edu.pl (K.P.)

[3] Department of Cytobiology, Jagiellonian University Medical College, Medyczna 9, 30-688 Cracow, Poland; monika.zadrozna@uj.edu.pl (M.Z.); barbara.anna.nowak@uj.edu.pl (B.N.); izabela.juda@student.uj.edu.pl (I.J.)

[4] Technology and Biotechnology of Medical Remedies, Faculty of Pharmacy, Jagiellonian University Medical College, Medyczna 9, 30-688 Cracow, Poland; szczepanskatarzyna@gmail.com (K.S.); katarzyna.kiec-kononowicz@uj.edu.pl (K.K.-K.)

[5] Department of Medicinal Chemistry, Maj Institute of Pharmacology Polish Academy of Sciences, Smętna 12, 31-343 Cracow, Poland

[6] Foundation "Prof. Antonio Imbesi", University of Messina, Piazza Pugliatti 1, 98122 Messina, Italy

[7] Department of Chemical, Biological, Pharmaceutical and Environmental Sciences, University of Messina, Viale Palatucci, 98168 Messina, Italy

* Correspondence: magda.dudek@uj.edu.pl; Tel./Fax: +48-12-6205530

Abstract: Many studies involving compounds that enhance histamine release, such as histamine H$_3$ receptor (H$_3$R) antagonists, have shown efficacy in inhibiting weight gain, but none have passed clinical trials. As part of the search for H$_3$ receptor ligands that have additional properties, the aim of this study is to evaluate the activity in the reduction in weight gain in a rat model of excessive eating, as well as the impact on selected metabolic parameters, and the number and size of adipocytes of two new H$_3$R antagonists, KSK-60 and KSK-74, which also exert a significant affinity at the sigma-2 receptor. Compounds KSK-60 and KSK-74 are homologues and the elongation of the distal part of the molecule resulted in an approximate two-fold reduction in affinity at H$_3$R, but simultaneously an almost two-fold increase in affinity at the sigma-2 receptor. Animals fed palatable feed and receiving KSK-60 or KSK-74 both at 10 mg/kg b.w. gained significantly less weight than animals in the control obese group. Moreover, KSK-74 significantly compensated for metabolic disturbances that accompany obesity, such as an increase in plasma triglyceride, resistin, and leptin levels; improved glucose tolerance; and protected experimental animals against adipocyte hypertrophy. Furthermore, KSK-74 inhibited the development of inflammation in obesity-exposed adipose tissue. The in vivo pharmacological activity of the tested ligands appears to correlate with the affinity at the sigma-2 receptors; however, the explanation of this phenomenon requires further and extended research.

Keywords: histamine H$_3$ receptor ligands; sigma-2 receptor ligands; palatable diet; excessive eating model; obesity

1. Introduction

The World Health Organization (WHO) considers obesity to be one of the most serious public health concerns of the present century. The WHO has estimated that, globally, there are more than 650 million people with obesity (BMI ≥ 30 kg/m^2) and, in 2020, over 39 million children under the age of 5 years were overweight or obese [1]. Further concerns

arise from the strong correlation between obesity or being overweight and the progression of cardiovascular and gastrointestinal diseases and diabetes, along with the increased risk of developing pancreatic, kidney, colorectal, and gallbladder cancer, as well as musculoskeletal disorders and infections [2,3]. Considering its high impact not only on health, but also on the economy and society, over the past few years, the pharmaceutical industry and many research groups have focused on the development of an effective and safe drug to fight this global epidemic. The numerous pharmaceutical anti-obesity treatment options (e.g., dinitrophenol, fenfluramine, fenfluramine-phentermine, sibutramine, and rimonabant) were associated with severe side effects and had to be removed from the market by both the Food and Drug Administration (FDA) and by the European Medicine Agency (EMA). In the treatment of obesity, both of these agencies (EMA and FDA) have only approved the use of Orlistat, Liraglutide, and the combination of Bupropion and Naltrexone [3].

Considering the involvement of the histaminergic system in food intake and body weight regulation through the interaction with histamine receptors in the CNS, many recent studies have focused on the histamine H_3 receptor (H_3R) as a potential target for anti-obesity therapies [4–6]. H_3R is a presynaptic autoreceptor abundantly expressed in the CNS and modestly found peripherally. Its activation leads to a negative feedback modulation of histamine synthesis and inhibition of its release from histaminergic neurons. Furthermore, histamine postsynaptic H_3R has been shown to modulate the release of other neurotransmitters, including dopamine, acetylcholine, serotonin, glutamate, substance P, norepinephrine, and γ-aminobutyric acid [4]. To date, many studies involving compounds that enhance histamine release, such as H_3R antagonists, have shown efficacy in inhibiting weight gain [5–9]. Histamine also increases the lipolysis of white adipose tissue, thus altering peripheral metabolism [10]. This fact may justify the strong interest in the search for new, effective, and safe therapeutic agents to treat obesity among H_3R ligands.

To date, numerous molecules with antagonist/inverse agonist properties have been synthesized from the proposed H_3R pharmacophore structure that contains a basic moiety— mostly a tertiary amine substituted by a linking alkyl group, often incorporating another functionality (frequently polar) [5,11,12]. Early preclinical studies revealed the efficacy of many H_3 receptor antagonists in reducing body weight in rodent models; however, only SCH-497079 and HPP404 were selected to enter phase II clinical trials. Among these, the antagonist SCH-497070 has recently completed the trials. Unfortunately, both molecules were not considered for further development due to the side effects [13]. Furthermore, A-331440, a selective H_3R antagonist, was found to be useful in decreasing body weight. The administration of the highest dose of A-331440 in mice fed a high-fat diet induced weight loss comparable to mice fed a low-fat diet along with lower leptin levels and normalized insulin tolerance. Despite its effectiveness, it was excluded from clinical trials due to genotoxicity [14].

Promising results were obtained from studies on Betahistine, a H_3R antagonist and H_1R agonist (registered for the treatment of vertigo and Meniere's disease). Betahistine induced significant weight loss in an obese animal after olanzapine treatment [15,16]. In addition, in our previous work, we described the effect of the repeated administration of Betahistine on body weight in a rat model of excessive eating. We showed that long-term Betahistine administration slows weight gain and increases high-density lipoprotein (HDL) levels [17]. A clinical study compared the effect of Betahistine with Orlistat® in obese adults [18]. The experiment did not show significant differences between the two molecules in reducing body weight and waist circumference. Apart from Betahistine, Pitolisant is the second approved (in narcolepsy) histamine H_3R antagonist. Kotańska et al. (2018) investigated the effect of the antagonist/inverse agonist, Pitolisant (registered under the name of Wakix®), on body weight and metabolic disturbances in a model of induced obesity in mice. Pitolisant administered intraperitoneally (i.p.) at a dose of 10 mg/kg b.w. for 14 days showed a positive influence on body weight, glucose tolerance, and lipid profile [19].

In our previous publication, we found that KSK19, one of the most active and selective ligands of H_3 receptors, exerted a favorable impact on body weight, after multiple administrations at a dose of 15 mg/kg b.w., in the mice obesity model [20]. Considering its promising anti-obesity properties, our research group chose the KSK19 lead structure as a reference to develop new selective H_3R ligands. Our recent study demonstrated high efficacy in inhibiting weight gain in a model of excessive eating and favorable pharmacokinetic properties for four of the ligands tested: KSK-61 and KSK-63, KSK-59 and KSK-73 [21,22]. Based on our recent work, we included two new histamine H_3R antagonists in our study, KSK-60 and KSK-74 (Figure 1) [12], which are structural analogs of compounds KSK-59 and KSK-73. We used phentermine as the reference compound, which is currently registered in some countries (also in combination with Topiramate) for the treatment of obesity [23]. Our compounds have also been shown to exert a significant affinity at the sigma-2 receptor [24]. Interestingly, looking at the results for the compounds KSK-60 and KSK-74, which are the subject of this study, the elongation of the distal part of the molecules (acetyl vs. propionyl derivatives, Figure 1) resulted in an approximate two-fold reduction in affinity at H_3R, but simultaneously an almost two-fold increase in affinity at the sigma-2 receptor. Therefore, a comparison of the activity in the reduction in weight gain in the model of excessive eating and the impact on selected metabolic parameters, as well as the number and size of adipocytes after the administration of these two compounds, can provide valuable information on the importance of this affinity.
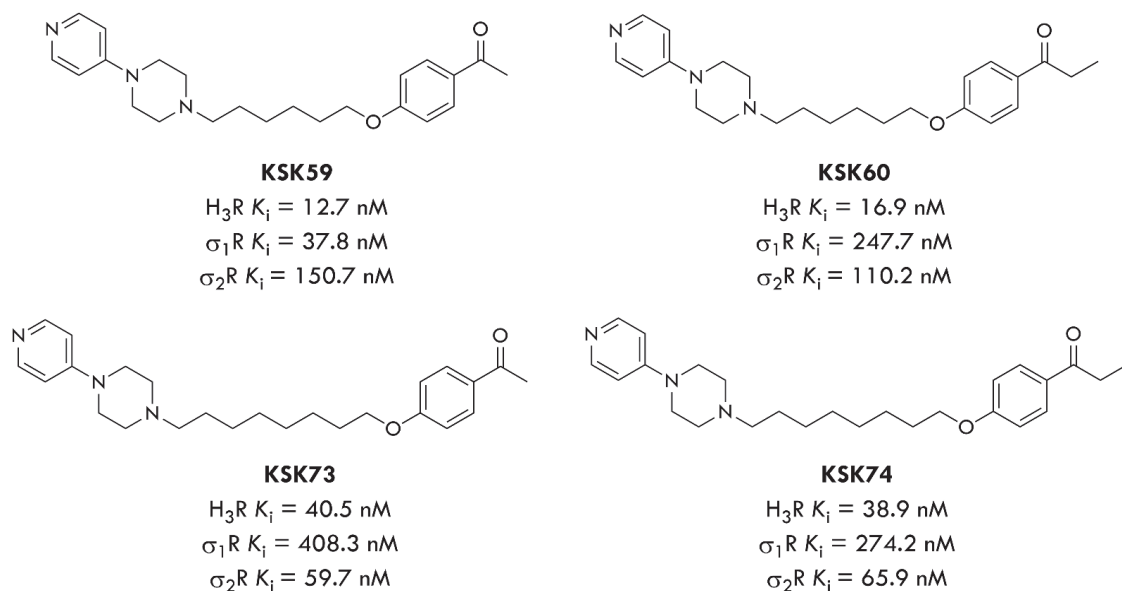

KSK59

$H_3R\ K_i = 12.7$ nM

$\sigma_1R\ K_i = 37.8$ nM

$\sigma_2R\ K_i = 150.7$ nM

KSK60

$H_3R\ K_i = 16.9$ nM

$\sigma_1R\ K_i = 247.7$ nM

$\sigma_2R\ K_i = 110.2$ nM

KSK73

$H_3R\ K_i = 40.5$ nM

$\sigma_1R\ K_i = 408.3$ nM

$\sigma_2R\ K_i = 59.7$ nM

KSK74

$H_3R\ K_i = 38.9$ nM

$\sigma_1R\ K_i = 274.2$ nM

$\sigma_2R\ K_i = 65.9$ nM

Figure 1. Structures of compounds evaluated in our previous work (KSK-59, KSK-73) and in our present work (KSK-60, KSK-74). Affinity values of the ligands tested at the H_3R [12] and the sigma-1 and sigma-2 receptors [24]. Structure and purity confirmation data of compounds KSK-60 and KSK-74 were shown in Supplement File S1.

2. Results

2.1. The Intrinsic Activity at H_3R

The intrinsic activity towards H_3R of all compounds tested was examined using two commercial methods, and the obtained IC_{50} values, despite the slight differences, were comparable. The compound KSK-60 proved to be a more potent antagonist of H_3R, with an IC_{50} value ranging from 0.8 to 1.5 nM, depending on the assay method. The compound KSK-74 was slightly less active in blocking H_3R, and the IC_{50} value for this compound

ranged from 23 to 32 nM depending on the assay method (Table 1, Figure 2). Summing up, both tested compounds showed significant antagonist properties for H_3R, with KSK-60 acting more effectively.

Table 1. The IC_{50} values for the antagonist dose–response with the reference agonist ((R)-alpha-methylhistamine) at a final concentration equivalent to EC_{80} obtained by two methods: LANCE Ultra cAMP and Aequoscreen.

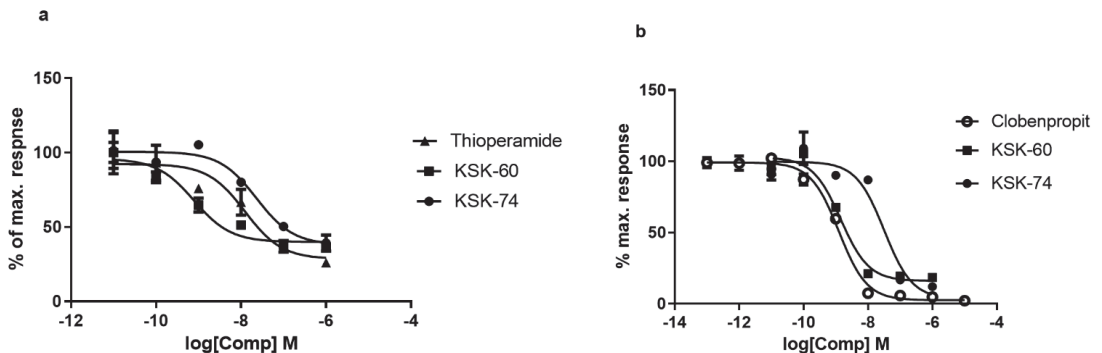| Compound	LANCE Ultra cAMP IC_{50} [nM]	Aequoscreen IC_{50} [nM]
(R)-alpha-methylhistamine	1.05 ± 0.1	10.6 ± 2.2
Clobenpropit	-	1.1 ± 0.3
Thioperamide	14.52 ± 3.2	-
KSK-60	0.78 ± 0.1	1.49 ± 0.2
KSK-74	23.22 ± 3.6	31.9 ± 0.5

Figure 2. The intrinsic activity at the histamine H_3 receptor of the tested compounds presented as concentration-dependence curves. The values (%) obtained by two methods, LANCE cAMP (**a**) and Aequoscreen (**b**), are expressed as a percentage of the action of the full agonist (R)-alpha-methylhistamine at the dose of EC_{80} (100%).

2.2. Effect of KSK-60, KSK-74, or Phentermine on Body Weight and Caloric Intake

A higher weight gain was observed in rats in the palatable diet + vehicle group than in rats in the Standard diet + vehicle group ($p < 0.01$, $p < 0.001$, Figure 3a,b). Animals fed palatable feed and receiving KSK-60 or KSK-74 both at 10 mg/kg b.w. gained significantly less weight than animals in the palatable diet + vehicle group ($p < 0.05$, $p < 0.01$, respectively, Figure 3b). No differences in body weight were observed in the palatable diet + KSK-60 or palatable diet + KSK-74 groups (both 1 mg/kg) compared to the palatable diet + vehicle group. Rats fed palatable feed and treated with phentermine gained less weight than rats receiving palatable diet + vehicle ($p < 0.01$, Figure 3b). In rats fed a palatable diet and treated with compounds KSK-60 or KSK-74 (10 mg/kg), we recorded a significant inhibition of body weight gain around the 10th day of the experiment, and this condition persisted until the 28th day (the end) of the experiment. The results are shown in Figure 3c,d.

KSK-74 or KSK-60 administered i.p. for 28 days at a dose of 10 mg/kg b.w. or phentermine administered at a dose of 7 mg/kg b.w. did not significantly influence the amount of calories consumed by animals in the test groups compared to the control group fed palatable feed (Figure 4). In KSK-74- or phentermine-treated groups, rats ate slightly less calories (lack of significance vs. both control groups). Rats treated with KSK-74 at a dose of 10 mg/kg b.w. consumed significantly less milk in the first and second weeks and significantly less peanuts in the fourth week of treatment vs. control group fed palatable feed (Figure 5).
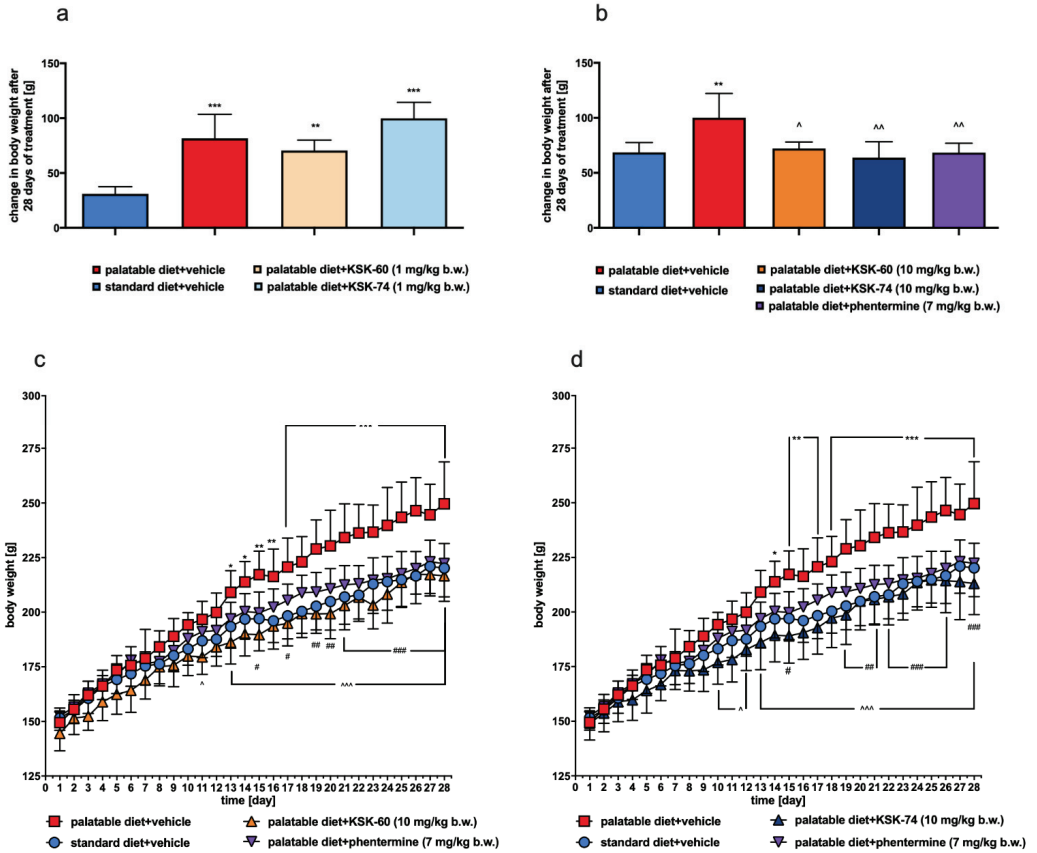
Figure 3. Cumulative changes in body weight (**a**,**b**), body weight during administration of the tested compounds or phentermine, (**c**) KSK-60 (10 mg/kg) and phentermine (7 mg/kg), (**d**) KSK-74 (10 mg/kg) and phentermine (7 mg/kg). Results are expressed as means ± SD, $n = 6$. Multiple comparisons were made using two-way ANOVA, Tukey's post hoc tests. * Significant against standard diet + vehicle group vs. palatable diet + vehicle group; ˆ significant against the tested compound administered group vs. palatable diet + vehicle group; # significant against palatable diet + phentermine group vs. palatable diet + vehicle group; *, ˆ, # $p < 0.05$, **, ˆˆ, ## $p < 0.01$, ***, ˆˆˆ, ### $p < 0.001$.
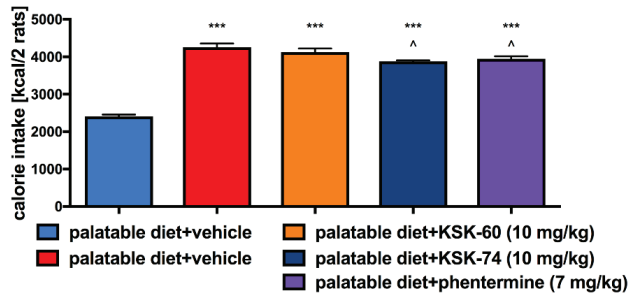

Figure 4. Effect of administration of the tested compounds or phentermine on calorie intake compared to control groups. Results are expressed as means ± SD, $n = 3$. Comparisons were made using the Kruskal–Wallis test followed by the Dunn post hoc test * Significant against control rats fed standard diet; * $p < 0.05$, ** $p < 0.01$.
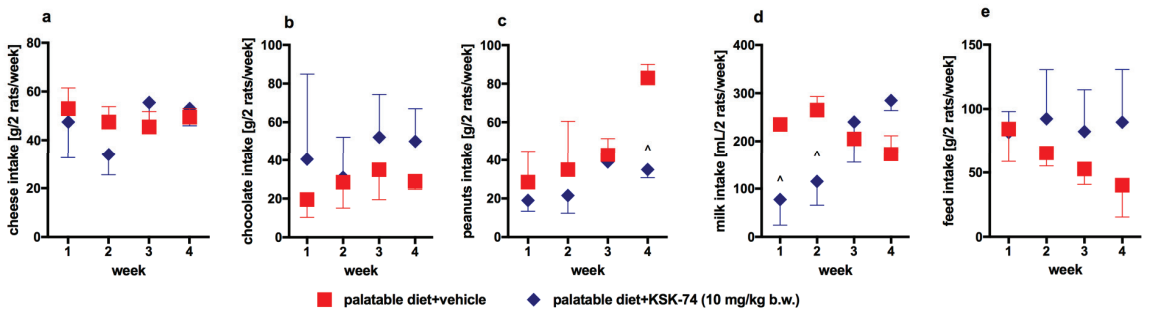
Figure 5. Amount of particular taste products' intake: (**a**) cheese, (**b**) chocolate, (**c**) peanuts, (**d**) milk, (**e**) feed, by rats from group treated with KSK-74 compared to rats from control group fed palatable feed. Results are expressed as means $\pm$ SD, n = 3. Multiple comparisons were made using two-way ANOVA, Bonferroni's post hoc tests. ˆ Significant against the tested compound administered group vs. palatable diet + vehicle group; ˆ $p < 0.05$.

2.3. Effect of KSK-60, KSK-74, or Phentermine on Fat Pads and Plasma Triglyceride Levels

A statistically higher amount of fat pads in the peritoneal cavity was observed in the palatable diet + vehicle group than in the standard diet + vehicle group ($p < 0.05$, Figure 6a). In the palatable diet + KSK-74 (10 mg/kg) group, fewer fat pads were observed than in the palatable diet + vehicle group ($p < 0.001$, Figure 6a). Animals fed palatable feed and receiving KSK-60 at 10 mg/kg or phentermine at 7 mg/kg had fewer peritoneal fat pads compared to animals receiving vehicle and fed palatable feed, since there was no statistically significant difference between the amount of adipose tissue in these groups vs. the control group fed standard feed (Figure 6a). Compared to the standard diet + vehicle group, higher plasma triglyceride levels were observed in rats fed palatable feed and receiving vehicle ($p < 0.01$, Figure 6b). Animals fed palatable feed and receiving KSK-74 at 10 mg/kg or phentermine had lower plasma triglyceride levels than rats from the palatable diet + vehicle group ($p < 0.05$, $p < 0.01$, respectively, Figure 6b). No differences in plasma triglyceride levels were observed between the palatable diet + vehicle group and the palatable diet + KSK-60 group (10 mg/kg) (Figure 6b).

2.4. Effect of KSK-60, KSK-74, or Phentermine on the Numerical Density of Adipocytes

Morphometric analysis of adipose tissue showed a decrease in the number of adipocytes per 0.1 mm^2 of cross-sectional area both in the palatable diet + vehicle and the palatable diet + KSK-60 (10 mg/kg) groups compared to the standard diet + vehicle group (17.69 $\pm$ 1.28 vs. 28.73 $\pm$ 1.54, $p < 0.05$ and 18.02 $\pm$ 1.38 vs. 28.73 $\pm$ 1.54, $p < 0.05$, respectively). The highest number of adipocytes per unit area was observed in the adipose tissue of animals in the palatable diet + KSK-74 (10 mg/kg) group (34.78 $\pm$ 4.78) and was almost two times higher than in the palatable diet + vehicle ($p < 0.05$) and the palatable diet + KSK-60 (10 mg/kg) groups ($p < 0.05$), confirming the protective effect of the KSK-74 compound against adipocyte hypertrophy. The mean number of adipocytes in the adipose tissue of the palatable diet + phentermine (7 mg/kg) group was more similar to the results of the palatable diet + vehicle group than to the results of the non-obese control group, but these differences were not significant in both cases (Figure 7).

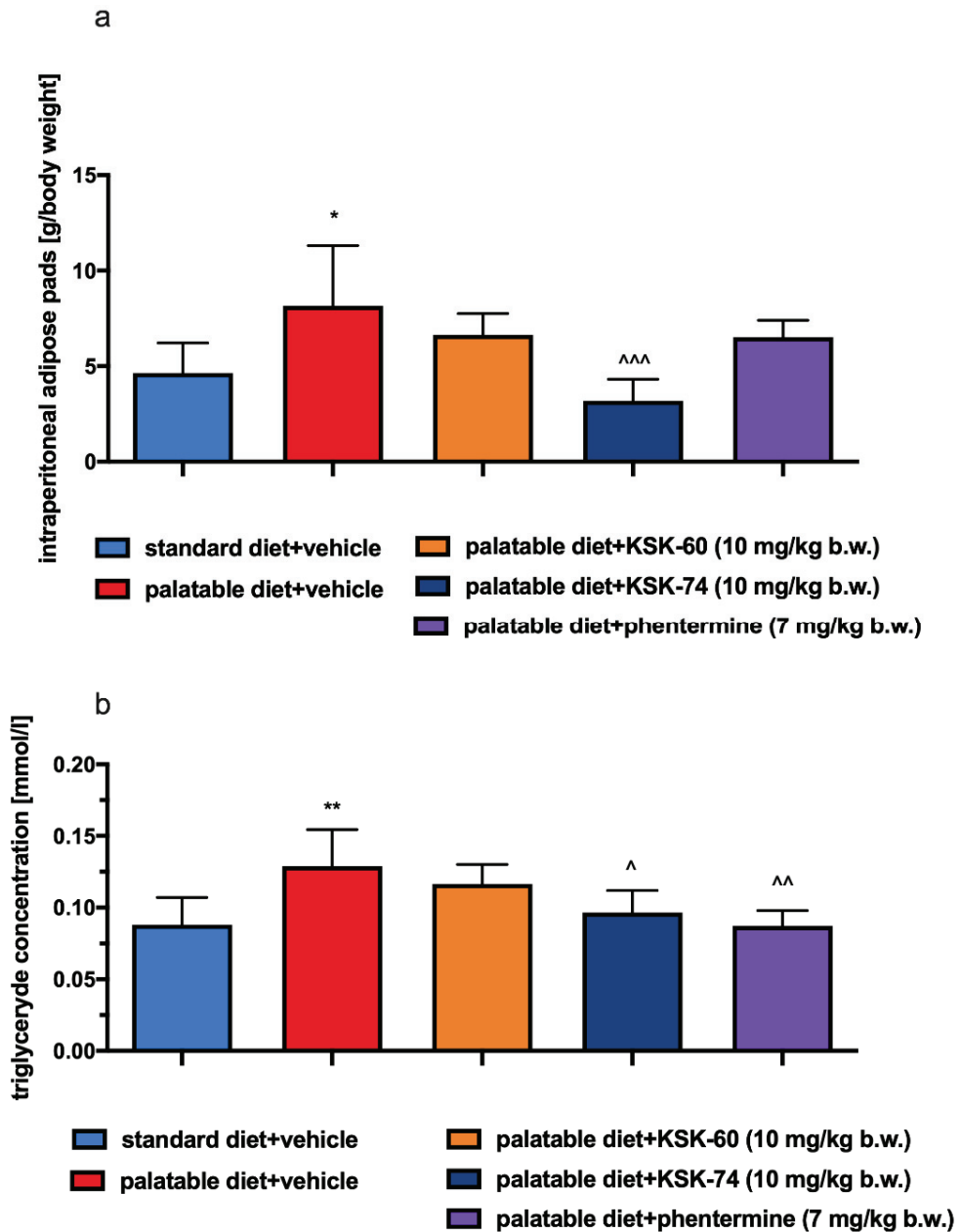**Figure 6.** Mass of adipose pads at the end of the experiment (**a**), effect of the tested compounds or phentermine on the plasma level of triglyceride (**b**). Results are expressed as means $\pm$ SD, $n = 6$. Comparisons were made using one-way ANOVA, Tukey's post hoc tests. * vs. standard diet + vehicle group; ˆ vs. palatable diet + vehicle group; ˆ, * $p < 0.05$, ˆˆ, ** $p < 0.01$, ˆˆˆ $p < 0.001$.
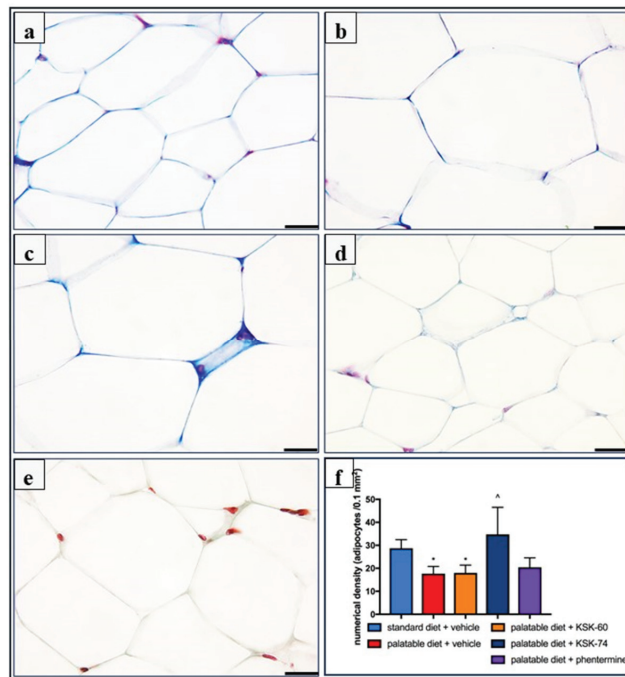
Figure 7. Adipocytes numerical density in Masson's trichrome staining of adipose tissue from the studied groups of rats. Representative microphotographs of tissue sections from the standard diet + vehicle group showing the normal architecture of adipocytes (**a**); palatable diet + vehicle (**b**) and palatable diet + KSK-60 10 mg/kg (**c**) showing a decrease in the number of adipocytes per 0.1 mm^2; palatable diet + KSK-74 10 mg/kg (**d**), which has more adipocytes compared to palatable diet + vehicle; and palatable diet + phentermine 7 mg/kg (**e**). Bar = 20 mm. (**f**) Adipocytes' numerical density expressed as means $\pm$ SD, *n* = 6. Comparisons were made using the Kruskal–Wallis test followed by the Dunn post hoc test; * significant vs. standard diet + vehicle group; ^ significant vs. palatable diet + vehicle group * ^ *p* < 0.05.

2.5. Effect of KSK-60, KSK-74, or Phentermine on the Presence of Pathological Features of Adipose Tissue Inflammation

Histological analysis was performed to identify the pathological features of adipose tissue inflammation. Many inflammatory cells infiltrated the area of adipocytes and the perivascular area, mainly in the adipose tissue of rats from the palatable diet + vehicle and palatable diet + KSK-60 (10 mg/kg) groups. On the other hand, slightly less inflammatory infiltrates, rather in the form of local leukocyte clusters, were observed in tissues of animals from the palatable diet + phentermine (7 mg/kg) and the palatable diet + KSK-74 (10 mg/kg) groups. Masson's trichrome staining of adipose tissue sections revealed a frequent occurrence of trichrome-positive fibrotic streaks in tissue from animals of all groups, except rats from the standard diet + vehicle group. In addition, no leukocyte infiltrates were observed in this group (Figure 8).
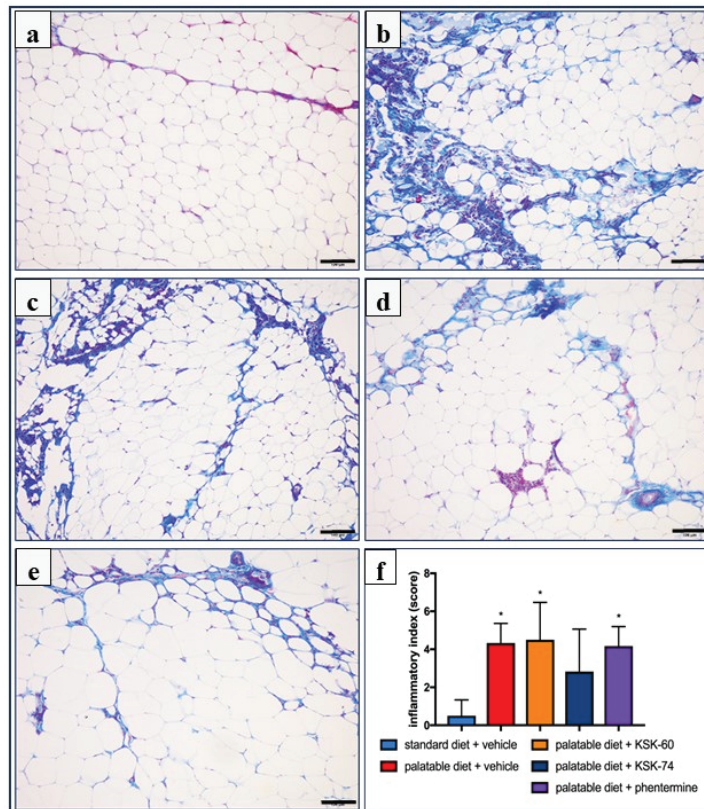
Figure 8. Representative histological pictures of Masson's trichrome-stained adipose tissue sections (bar = 100 mm). (**a**) Standard diet + vehicle group, (**b**) palatable diet + vehicle, (**c**) palatable diet + KSK-60 10 mg/kg, (**d**) palatable diet + KSK-74 10 mg/kg, (**e**) palatable diet + phentermine 7 mg/kg. Many inflammatory cells infiltrating the area of the adipocytes and trichrome-positive fibrotic streaks are visible in the adipose tissue of all studied groups, except the rats in the standard diet + vehicle group. (**f**) Inflammatory index expressed as means ± SD, $n = 6$. Comparisons were made using the Kruskal–Wallis test followed by the Dunn post hoc test; * significant vs. standard diet + vehicle group; * $p < 0.05$.

In the adipose tissue of rats in the palatable diet + phentermine (7 mg/kg) group, our attention was focused on the marked capillary congestion and frequent appearance of crown-like structures formed by mononuclear cells surrounding a presumably dead adipocyte (Figure 9).

All these observations were further confirmed by the histological scoring of inflammation and presented as the inflammatory index. The number of rats in each group, with the appropriate histological grade for the independently assessed components of the inflammatory index is presented in Table 2. The inflammatory index of the adipose tissue of the studied animals was statistically significantly higher in the palatable diet + vehicle (4.33 ± 0.42, $p < 0.05$), palatable diet + KSK-60 (10 mg/kg) (4.5 ± 0.80, $p < 0.05$), and palatable diet + phentermine (7 mg/kg) (4.16 ± 0.48, $p < 0.05$) groups compared to the standard diet + vehicle group (0.5 ± 0.34) (Figure 8f).
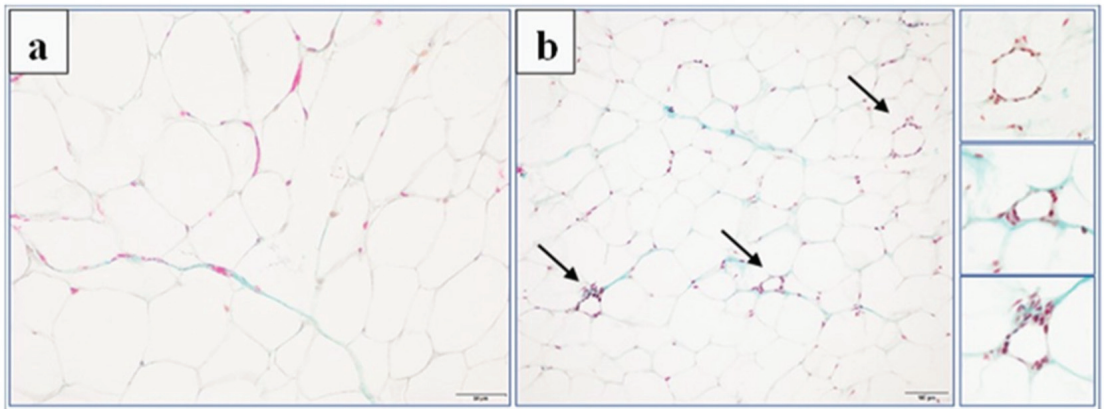
Figure 9. Histological section of adipose tissue from the palatable diet + phentermine 7 mg/kg group stained with Masson's trichrome showing capillary congestion (**a**) and the frequent appearance of crown-like structures (arrow) formed by mononuclear cells surrounding a presumably dead adipocyte (**b**). Bar = 50 mm (**a**) and 100 mm (**b**).

Table 2. Inflammation in adipose tissues. The number of rats in each group, with the appropriate histological grade for the independently assessed components of the inflammatory.

	Inflammatory Cell Infiltration				Perivascular Infiltration			Widening of the Septum		Capillary Congestion	
Grade:	0-Normal	1-Few Cells	2-Local Clusters	3-Extensive Infiltrates	0-Normal	1-Few Cells	2-Ring of Cells	0-Normal	1-Widening	0-Normal	1-Congestion
Standard diet + vehicle	4	2	-	-	6	-	-	5	1	6	-
Palatable diet + vehicle	-	-	5	1	2	2	2	-	6	5	1
Palatable diet + KSK60	-	2	4	-	-	2	4	1	5	2	4
Palatable diet + KSK74	1	3	2	-	2	1	3	3	3	5	1
Palatable diet + phentermine	-	4	2	-	1	4	1	1	5	-	6

2.6. Effects of KSK-60, KSK-74, or Phentermine on IL-6 and MCP-1 Levels in Adipose Tissue

There were no significant changes in IL-6 levels in adipose tissue between the standard diet + vehicle and the palatable diet + vehicle control groups. IL-6 levels were reduced in adipose tissue only in animals fed palatable feed and receiving KSK-74 at 10 mg/kg, compared to the group receiving a palatable diet and vehicle ($p < 0.01$, Figure 10a). Higher levels of MCP-1 were observed in the adipose tissue of rats in the palatable diet + vehicle group compared to the adipose tissue of rats in the standard diet + vehicle group ($p < 0.001$, Figure 10b). The administration of KSK-74 at a dose of 10 mg/kg b.w. decreased the level of MCP-1 in the rat's adipose tissue, compared to the rats that received palatable feed and vehicle ($p < 0.001$, Figure 10b).
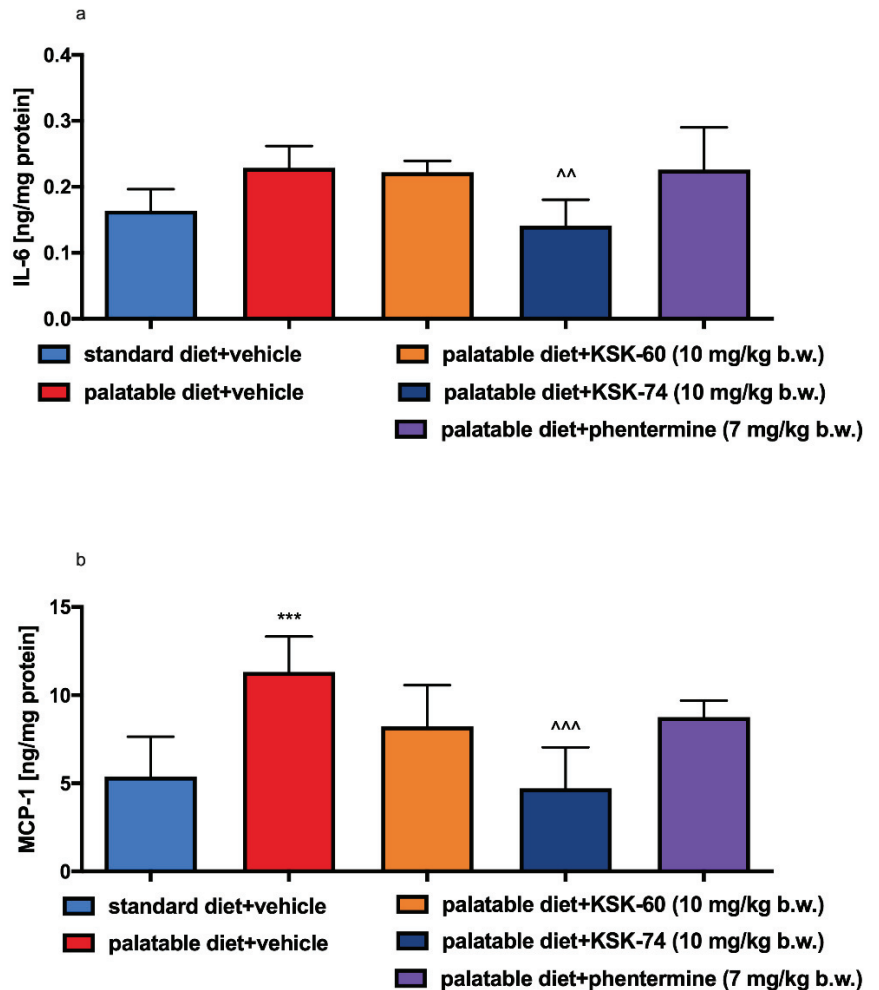
Figure 10. Effect of administration of the tested compounds or phentermine on adipose tissue levels of (**a**) IL-6 and (**b**) MCP-1. Results are expressed as means $\pm$ SD, $n = 6$. Comparisons were made using one-way ANOVA, Tukey's post hoc test; * significant vs. standard diet + vehicle group; ^ significant vs. palatable diet + vehicle group ^^ $p < 0.01$, ***, ^^^ $p < 0.001$.

2.7. Effect of KSK-60, KSK-74, or Phentermine on Leptin and Resistin Levels in Adipose Tissue

There were significant changes in leptin and resistin levels in adipose tissue between rats in control groups that received different diets (standard or palatable) and vehicle ($p < 0.05$, Figure 11a,b). Compared to the palatable diet + vehicle group, reduced levels of leptin and resistin were observed in adipose tissue from animals that received i.p. KSK-74 10 mg/kg ($p < 0.001$, $p < 0.01$, Figure 11a,b). Phentermine did not influence the concentration of leptin or resistin.
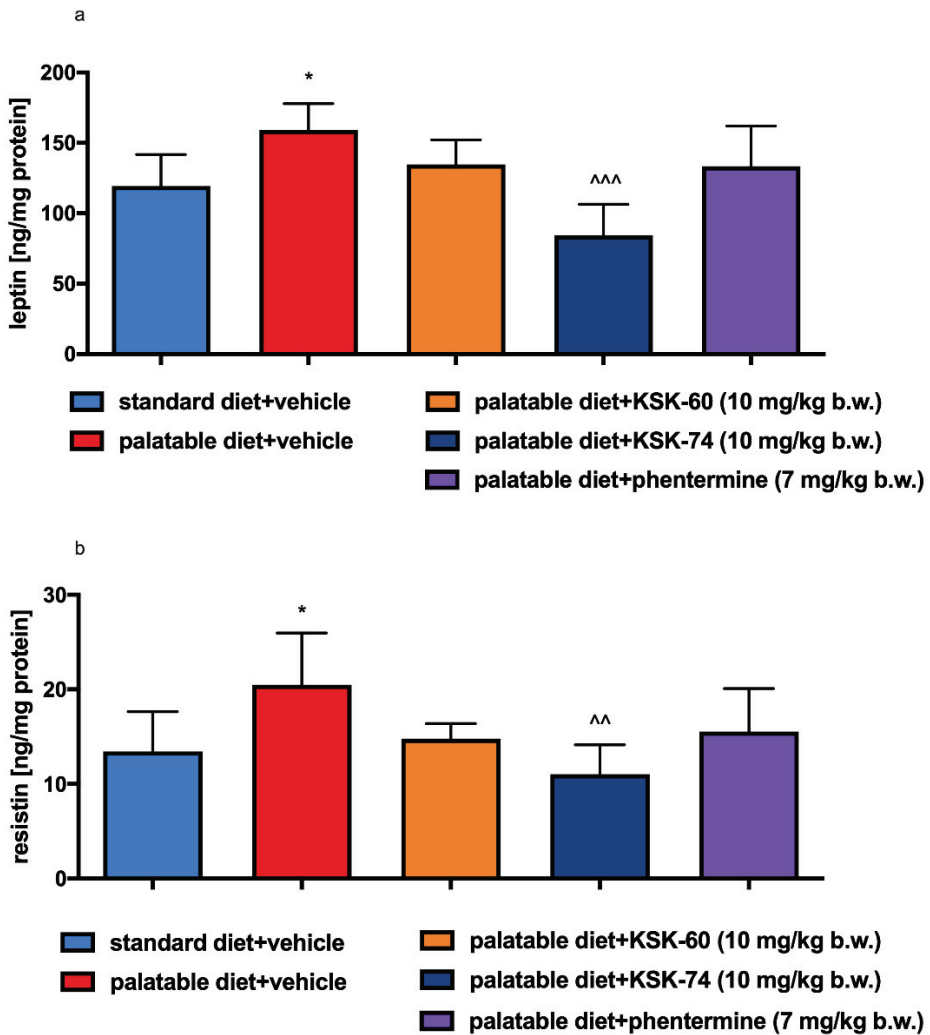
Figure 11. Effect of the tested compounds or phentermine on adipose tissue levels of (**a**) leptin and (**b**) resistin. Results are expressed as means $\pm$ SD, $n = 6$. Comparisons were performed by one-way ANOVA, Tukey's post hoc test; * significant vs. standard diet + vehicle group; ˆ significant vs. palatable diet + vehicle group * $p < 0.05$, ˆˆ $p < 0.01$, ˆˆˆ $p < 0.001$.

2.8. Glucose Tolerance Test

Blood glucose levels at 30 and 60 min after glucose load in rats receiving palatable feed and vehicle were significantly higher, compared to glucose levels determined at the same time points in rats receiving standard feed and vehicle. In the groups treated with KSK-60 or KSK-74 at a dose of 10 mg/kg, glucose levels were significantly lower at 30 or/and 60 min after glucose load than in control animals fed palatable feed (Figure 12). As shown in Figure 12d, AUC decreased significantly after treatment with KSK-60 or KSK-74, compared to the control value observed in rats fed high-calorie feed.
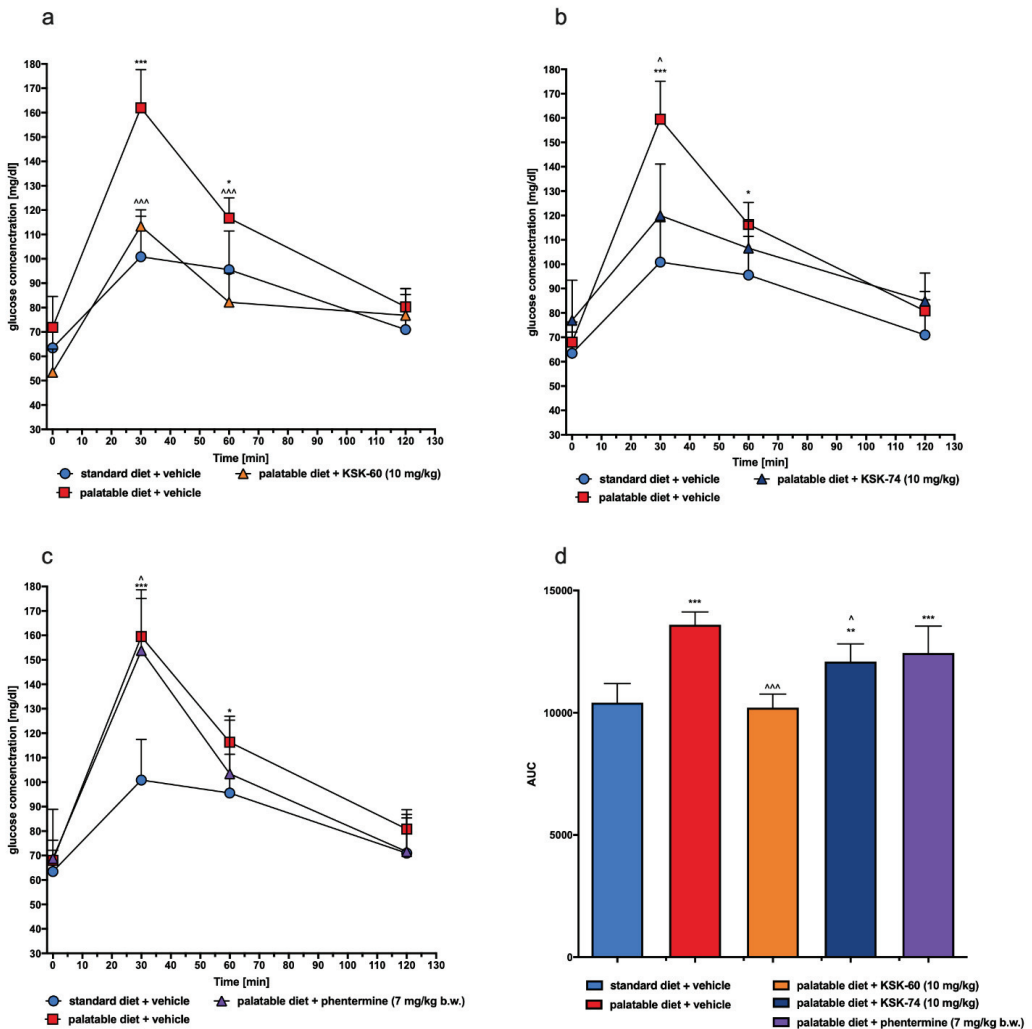
Figure 12. Glucose tolerance test. Results are expressed as means $\pm$ SD, *n* = 6. (**a–c**) Intraperitoneal glucose tolerance test (IPGTT): multiple comparisons were made using two-way ANOVA, Tukey's post hoc tests. (**d**) Area under the IPGTT curve: comparisons were made using one-way ANOVA, Tukey's post hoc test. * Significant vs. standard diet + vehicle group; ˆ significant vs. palatable diet + vehicle group; *, ˆ < 0.05, ** $p < 0.01$, ***, ˆˆˆ $p < 0.001$.

2.9. Effect of KSK-60, KSK-74, or Phentermine on Spontaneous Activity

Spontaneous activity was measured after the 1st (single dose) and 27th (multiple doses) administrations of the tested compounds. The compound KSK-60 after a single administration at a dose of 10 mg/kg b.w. reduced spontaneous activity at the 17th hour of measurement, while, after the repeated administration of this compound, we observed a reduction in spontaneous activity at the 15th hour of measurement. A single injection of phentermine decreased spontaneous activity at the 17th hour of measurement, while, after multiple administrations of this compound, we recorded an increase in spontaneous activity at the 2nd hour of measurement. The single and repeated administrations of compound KSK-74 did not affect spontaneous activity in rats (Figure 13).
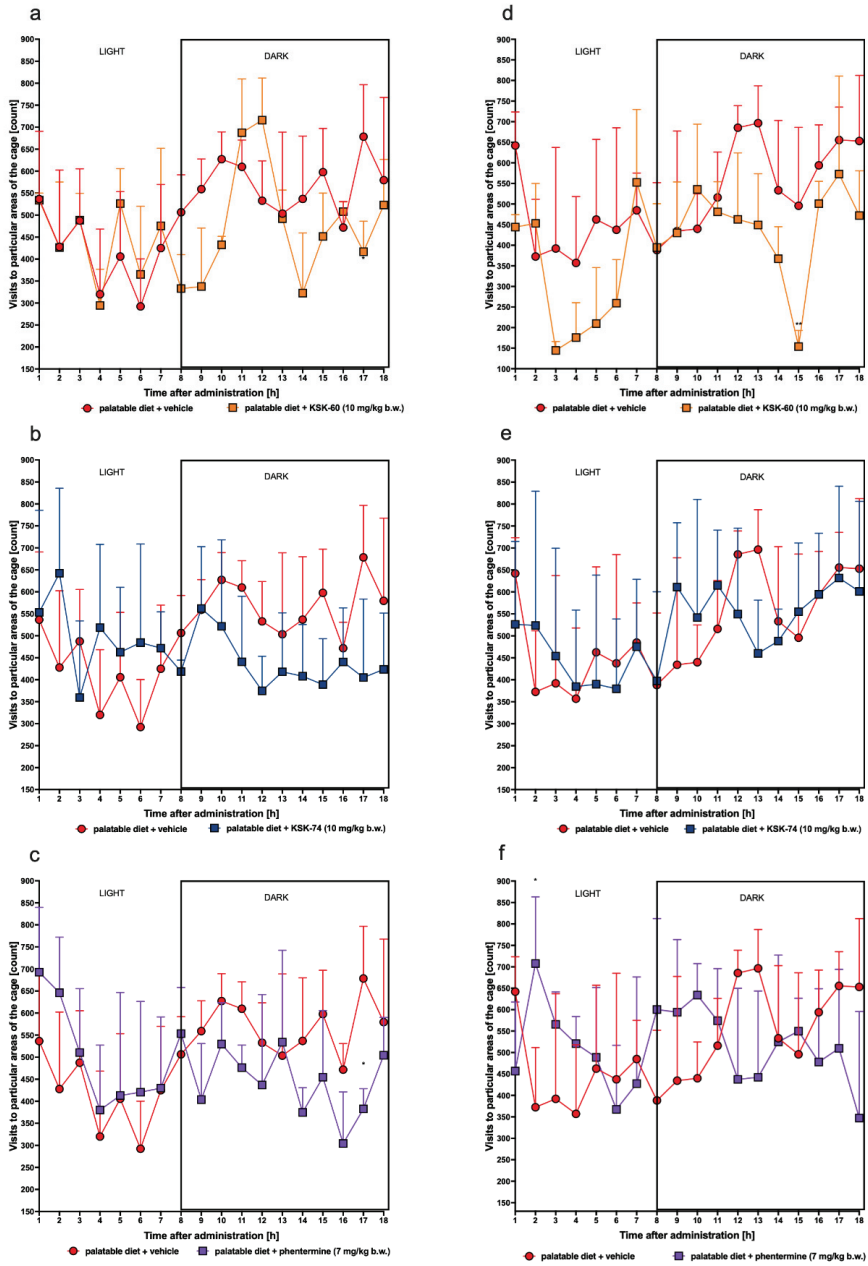
Figure 13. Spontaneous activity after the 1st and 27th administrations of the tested compounds. Results are expressed as means ± SD, *n* = 6. Comparisons were made using Multiple *t*-test; (**a**) palatable diet + vehicle vs. palatable diet + KSK-60 after the 1st administration; (**b**) palatable diet + vehicle vs. palatable diet + KSK-74 after the 1st administration; (**c**) palatable diet + vehicle vs. palatable diet + phentermine after the 1st administration; (**d**) palatable diet + vehicle vs. palatable diet + KSK-60 after the 27th administration; (**e**) palatable diet + vehicle vs. palatable diet + KSK-74 after the 27th administration; (**f**) palatable diet + vehicle vs. palatable diet + phentermine after the 27th administration; * *p* < 0.05, ** *p* < 0.01.

2.10. Effect of KSK-60, KSK-74, or Phentermine Administration on Plasma Corticosterone

There was no significant change in plasma corticosterone levels between different groups of rats. In this experiment, the tested compounds had no effect on the plasma corticosterone levels of rats. Its plasma concentrations ranged between 120–155 pg/mL.

2.11. Pharmacokinetic Analysis

The pharmacokinetic (PK) parameters calculated using non-compartmental analysis based on the concentration-time data after the single i.p. administration of the investigated compounds at a dose of 10 mg/kg b.w. are presented in Table 3. The maximal plasma concentration was attained by both compounds at the first sampling point (5 min after administration), and the values were almost identical (109 vs. 105 μg/L for KSK-60 and KSK-74, respectively). Both compounds also had identical half-lives equal to 2.7 h. However, the compound KSK-74 had much higher clearance due to the larger volume of distribution (272 vs. 513 L/kg for KSK-60 and KSK-74, respectively), indicating that it much easier, compared to the KSK-60, crossed the biological membranes, and distributed throughout the body.

Table 3. Estimated pharmacokinetic parameters (non-compartmental analysis) of the investigated compounds calculated from mean rat plasma concentration values ($n = 3$) after administration of a single i.p. dose of 10 mg/kg.

Parameter	KSK-60	KSK-74
C_{max} [μg/L]	109	105
t_{max} [h]	0.083	0.083
λ_z [h^{-1}]	0.26	0.25
$t_{0.5\lambda z}$ [h]	2.7	2.71
CL_S/F [l/h/kg]	69.98	131.06
AUC_{0-inf} [mg·h/L]	514.40	274.67
V_z/F [l/kg]	272.63	513.14
MRT [h]	3.28	2.45

C_{max}—maximal concentration, t_{max}—time to reach maximal concentration, λz—terminal elimination rate constant, $t_{0.5\lambda z}$—half-life, CLs—clearance, AUC_{0-inf}—area under the concentration–time curve extrapolated to infinity, Vz—volume of distribution, MRT—mean residence time, F—bioavailability.

3. Discussion

In this study, we performed preliminary pharmacological experiments to determine the potential anti-obesity properties of two H_3R ligands, KSK-60 and KSK-74, which are also ligands of sigma receptors. The effect of their chronic administration on body weight, selected metabolic parameters, and spontaneous activity of rats was investigated in the model of excessive eating of preferential feed. We also conducted studies that evaluated the intrinsic activity and selected pharmacokinetic parameters of these compounds. To take a closer look at the action of our selected ligands, we performed histopathological studies showing the numerical density of adipocytes and the pathological features of inflammation in peritoneal adipose tissue.

In our previous work, we published the results for their structural analogues, compounds KSK-59 and KSK-73, which differ only in the distal part of the molecules (acetyl versus propionyl derivatives, Figure 1) [22]. It should be noted that compound KSK-73 prevented weight gain and metabolic disturbances more than compound KSK-59, which is partially consistent with our current results, in which KSK-74 is also more effective than KSK-60. Although both compounds similarly inhibited weight gain in the excessive eating model, for the most part, only compound KSK-74 significantly compensated for metabolic disturbances that accompany obesity.

Comparing the structures of tested compounds, the eight carbon-chain homologues were characterized by higher efficacy in vivo for both acetyl and propionyl derivatives. However, our previous work showed that compounds with the highest affinity for H_3R were not the most active in vivo [20,21]. Therefore, we suspect that the influence on

body weight gain and metabolic activity of these ligands may be additionally related to another non-histaminic mechanism of action. Furthermore, the pharmacokinetic properties of compounds KSK-73 and KSK-74 are more favorable compared to their homologues KSK-59 and KSK-60. In particular, they have a much larger volume of distribution, which could indicate their better ability to freely cross biological membranes and distribute throughout the body [22]. Additionally, according to Lipinski's "Rule of Five" (molecular weight $\leq$ 500; LogP $\leq$ 5; hydrogen-bond donors $\leq$ 5; hydrogen-bond acceptors $\leq$ 10; number of rotatable bonds $\leq$ 10), compounds KSK-60 and KSK-74 are likely to have good absorption and permeability. As for the good CNS penetration, compound KSK-60 meets 4 (molecular weight $\leq$ 400; LogP $\leq$ 5; hydrogen-bond donors $\leq$ 3; hydrogen-bond acceptors $\leq$ 7—calculated by CompuDrug Pallas System, USA) out of 4 criteria, while KSK-74 meets 3 of them (molecular weight is > 400) [25]. Based on the theoretical assumptions, it is likely that both of them are able to cross the blood–brain barrier. However, further studies are necessary to verify this hypothesis. Interestingly, the in vivo pharmacological activity of the tested ligands appears to correlate with the affinity at sigma-2 receptors, and the explanation of this phenomenon requires further extended research. Both the dual affinity at histamine H_3/sigma-2 receptors and the significant in vivo activity of the KSK-73 and KSK-74 ligands give hope for the discovery of unique compounds among a wide variety of histamine H_3R antagonists. Therefore, compounds KSK-73 and KSK-74 have been chosen as new lead structures for the development of H_3/sigma-2 receptors ligands (the affinity ratios are 0.68 and 0.59 for KSK-73 and KSK-74, respectively) with anti-obese activity, and the mechanism of their action would be a subject of further studies.

The excessive eating model used in our study allows us to determine whether the studied compounds affect body weight in animals that have free access to high-calorie foods. It perfectly illustrates the unnecessary high caloric intake by overeating freely available tasty products rich in sugar and fat. It shows that the unlimited availability of tasty foods prompts the body to consume that particular food, even when extra calories are not needed and when such behavior can lead to a significant increase in body weight and the development of metabolic disorders over a short period of time. Animals have access to certain high-calorie foods, such as peanuts, cheese, milk with increased fat content, and chocolate, but also to the standard feed. Most importantly, feeding is not in any way forced [26,27]. Special diet not only induces obesity, but also contributes to metabolic disorders specifically caused by this condition. Therefore, such a model of excessive eating is considered to be an apparent imitation of human models of the obesogenic diet [28].

The effect of H_3 receptor antagonists on food intake has already been described in the literature [20–22,29]. Since treated rats consumed a similar amount of calories to the control rats fed palatable feed, we speculated that, other than a reduction in caloric intake, mechanisms resulting in the lower weight gain in these animals are involved. We obtained similar results earlier when testing other ligands from this group of compounds, namely, not all of them decreased the amount of calories consumed [21,22]. We reported that i.p. administration of H_3R antagonists KSK-60 or KSK-74 effectively and dose-dependently inhibited weight gain, and that this inhibition occurred parallel to the inhibition of fat gain. Interestingly, the animals treated with the tested compounds gained less weight than the animals that received phentermine, a drug used to treat obesity. We also observed that the most active ligands we described to date in the model of excessive eating were characterized by a significant affinity at the sigma-2 receptor [20–22]. We can speculate that the inhibition of weight gain may be related to H_3R and sigma-2 receptors, making them dual ligands. However, more studies are needed to clarify this issue.

The obesity problem is primarily related to an increase in the volume of peritoneal fat. Previous studies have shown that histamine affects body weight not only by inhibiting appetite, but it also regulates visceral fat volume [4]. This fact is probably related to neuronal histamine activity, which can accelerate adipose tissue lipolysis by activating the sympathetic nervous system. The lipolysis process leads to the release of free fatty acids and glycerol,

which can be used as energy substrates for the body and thus contribute to the maintenance of adequate energy homeostasis [30]. One of the main features of obesity is the abnormal metabolism of circulating lipids [31]. The excess calories supplied with food cause unused triglycerides to be stored in adipose tissue. In addition, in our experiment, we observed a significantly lower intraperitoneal fat gain in animals treated with the tested compounds, especially KSK-74, which was closely correlated with the lower body weight gain. Moreover, we noticed that the reduction in plasma triglyceride levels was also correlated with lower fat mass. During the development of obesity, adipose tissue can grow by hypertrophy, which is an increase in the size of adipocytes, or by hyperplasia, which is an increase in the number of adipocytes due to the recruitment of new cells [32]. The volume of adipocytes reflects the balance between lipogenesis and lipolysis, while the number of adipocytes reflects the balance between the proliferation, differentiation, and apoptosis of preadipocytes and the adipocytes [33]. In the early stages of obesity development, when excess calories are supplied to the body, there is an overgrowth of adipocytes that secrete adipokines. In a subsequent step, adipokines stimulate the formation of additional preadipocytes, which differentiate into mature adipocytes that protect the organism against some of the adverse metabolic consequences of obesity [34]. This concept was supported by a Wang et al. in a study conducted on mice fed a high-fat diet. These animals showed signs of visceral hypertrophy within 1 month [35]. We observed a similar phenomenon in our experiment. In animals in the control group fed palatable feed, we recorded significant adipocyte hypertrophy. Interestingly, in the group of animals that received KSK-74, we observed an increase in their numerical density, but not in size, which resembled the condition and shape of adipocytes from adipose tissue from rats fed a standard diet. Therefore, we can speculate that KSK-74 protects against the development of hypertrophy. On the other hand, phentermine did not show any positive effect on the numerical density of adipocytes. Given the current reports that there is a strong association between small adipocytes and increased insulin sensitivity, we can also speculate that the tested ligands for H_3/sigma-2 receptors promote the formation of new adipocytes, protecting against the adverse consequences of obesity, including insulin resistance [36].

Many factors contribute to the formation of obesity, one of which is the hormonal state of the body. Information signals from the body's periphery can be divided into those consisting of short-term signals that are generated during a meal and originate mainly from the gastrointestinal tract, and those that involve long-term signals provided by hormones that determine the body's energy stores [37]. Among the hormones produced by adipose tissue, leptin and resistin deserve special attention. Their levels are closely correlated with the amount of adipose tissue [38,39].

Leptin is otherwise known as the satiety hormone, due to its main functions of regulating food intake and energy balance in the body. An increase in leptin levels sends a signal to the hypothalamus that energy reserves are full, and consumption can be completed; the effect is a reduction in appetite. Furthermore, high levels of leptin also increase energy expenditure (acceleration of metabolism). People who are overweight or obese have higher levels of leptin in plasma and adipose tissue [40]. In obesity, when leptin levels are high, the number of receptors for leptin is gradually reduced and their sensitivity to this hormone decreases. In this situation, the satiety signal that should normally inhibit appetite does not reach the brain [41,42]. In our experiment, in animals fed high-calorie products, we induced a state of elevated leptin levels. Animals treated with KSK-60 or KSK-74 maintained leptin levels at the same level as rats in the control group fed standard feed. Only in animals receiving KSK-74 did we observe lower leptin levels compared to rats in the control group fed palatable feed. This fact allowed us to conclude that the compounds we studied maintained leptin at an adequate level that allowed for the proper functioning of the hunger and satiety centers. These findings also allowed us to confirm that leptin levels were in direct correlation with levels of adipose tissue. Thus, maintaining optimal body fat levels is the best way to ensure physiological leptin levels and control excessive appetite and the development of obesity.

As with leptin, elevated levels of resistin are also observed in the state of excess adipose tissue. Ongoing mild inflammation is observed in overweight or obese individuals. Previous studies have shown that resistin levels correlate significantly with inflammatory markers. It is probably related to the fact that some proinflammatory cytokines, e.g., IL-6 or TNF-α, stimulate the expression of the resistin gene [43,44]. In our study, we noticed a similar relationship. In addition, elevated resistin levels can not only be a biomarker, but also a pathogenic factor for inflammatory diseases.

As mentioned above, a diet rich in high-calorie fatty foods may be the cause of mild chronic inflammation [45,46]. This condition can lead to changes in peripheral signaling associated with the insulin receptor, thereby reducing the sensitivity to insulin-mediated glucose release. These events result in elevated insulin and fasting glucose levels and decreased glucose tolerance, which may indicate that insulin resistance is developing [47]. In the model that we used, we also observed impaired glucose tolerance in the control group that had access to the palatable diet. However, a significant improvement in glucose tolerance was observed in experimental animals treated with the tested compounds. We suspected that this may be due to the fact that the experimental animals did not develop full obesity or to the effect of the tested ligands on H_3R present in pancreatic β cells responsible for insulin secretion and blood glucose regulation [48].

In chronic inflammation, also known as metabolic inflammation, the immune cells responsible for infiltration of proliferating adipose tissue gradually turn into resident adipose tissue macrophages (ATMs). ATMs are classified by the expression of different markers, including pro-inflammatory ones, such as IL-6, MCP-1 TNF-α, CD11c, and iNOS, among others [49]. IL-6 is a pro-inflammatory cytokine responsible for the regulation of inflammation and the defense mechanisms of the body. The level of IL-6 increases significantly in adipose cells in obesity, which is due to the presence of inflammation [50]. In our study, there were no significant differences in IL-6 level in adipose tissue between the control group fed standard and palatable feeds, but there was some upward trend in the level of this mediator in the group fed palatable feed. Perhaps a longer experiment would result in a higher increase in this pro-inflammatory interleukin. Only in animals treated with compound KSK-74 did we observed a decrease in the IL-6 level in adipose tissue. These observations correlate with the results on the severity of inflammation in the tissues tested. One of the first CC chemokines discovered and best described is monocyte chemoattractant protein-1 (MCP-1). Obese people have been shown to have higher levels of this chemokine in adipose tissue than non-obese people [51,52]. In our model, we observed a similar phenomenon of elevated levels of this chemokine in rats from a control group fed palatable feed. Similar to IL-6 levels, compound KSK-74 decreased MCP-1 levels in adipose tissue and therefore nullified the formation of inflammation. To date, many studies indicate that obesity caused by a high-calorie diet leads to the induction of multiple inflammatory pathways [53]. The inflammation that develops is a consequence of the hypertrophy of adipose tissue cells and the damage to cellular structures [54]. Consistent with the reports in the literature mentioned above, we also observed ongoing inflammation among control animals fed palatable food. Of the compounds tested, only compound KSK-74 inhibited the development of inflammation in obesity-exposed adipose tissue and the value of the inflammation index was comparable to the standard control. These results support the current reports that adequate adipogenesis and hyperplasia, or the ability to distribute fat between newly formed adipocytes without the need for significant adipocyte hypertrophy, attenuates inflammation and subsequent insulin resistance [55]. When using phentermine, a drug currently registered for the treatment of obesity, we did not observe significant differences.

Severe, especially chronic, stress can cause significant weight loss. The defense response to stress is the increased secretion of hormones, such as cortisol, in humans. In previous animal studies, the introduction of a stress factor has been shown to cause changes in locomotor activity and increased corticosterone secretion [56,57]. To confirm that our results of decreased weight gain are not related to stress or changes in spontaneous activity,

we determined plasma corticosterone levels in experimental animals and monitored spontaneous activity after initial and chronic administration of the tested ligands. In our study, we did not observe changes in corticosterone levels in both control groups and between animals that received the test compounds. We also did not show any significant effect on spontaneous activity, allowing us to conclude that weight loss was not caused by the stress factor.

LIMITATIONS. The main limitation of this research is that it did not directly indicate that the described actions were really related to the influence on the histamine H$_3$ or sigma receptors. Although we know from the earlier cited studies and from the intrinsic activity studies presented in this manuscript that the tested compounds are ligands for these receptors, further research is needed to confirm the mechanism of their activity. The second limitation was that the number of animals used in this study was small, and the effect on calorie intake requires further research.

4. Materials and Methods

4.1. Drugs, Chemical Reagents, and Other Materials

The tested compounds (KSK-60 and KSK-74) were synthesized at the Department of Technology and Biotechnology of Drugs, Faculty of Pharmacy, Jagiellonian University Medical College, Cracow, Poland. The identity and purity of the final product were assessed by NMR and LC-MS techniques (the minimum purity was greater than 95%). For both pharmacokinetic and pharmacological studies, KSK-60 and KSK-74 (1 or 10 mg/kg) were suspended in 1% Tween 80 and the volume was adjusted to 1 mL/kg. Heparin was delivered from Polfa Warszawa S.A. (Warsaw, Poland), thiopental sodium was obtained from Sandoz GmbH, (Kundl, Austria), and phentermine was obtained from the National Measurement Institute (Pymble, Australia); (R)-alpha-methylhistamine, thioperamide, and clobenpropit were obtained from Merck KGaA (Darmstadt, Germany).

4.2. In Vitro Studies—Intrinsic Activity at the Histamine H$_3$ Receptor

Intrinsic activity studies were performed using two methods, Aequoscreen and LANCE Ultra cAMP assays, according to the manufacturer of the ready-to-use cells with stable expressions of the H$_3$ histamine receptor (Perkin Elmer). In both assays (R)-alpha-methylhistamine dihydrobromide was used as the reference agonist. thioperamide or clobenpropit were used as the reference antagonists in LANCE Ultra cAMP and Aequoscreen assays, respectively.

The Aequoscreen technology uses recombinant cell lines with stable co-expression of apoaequorin and a GPCR as a system to detect activation of the receptor, following the addition of an agonist, via the measurement of light emission. For the measurement, cells (frozen, ready to use) were thawed and resuspended in 10 mL of assay buffer containing 5 μM of coelenterazine h. The cell suspension was then placed in a 10 mL Falcon tube, fixed on a rotating wheel, and incubated overnight at RT° in the dark. Cells were diluted with assay buffer at 5000 cells/20 μL. Agonistic ligands 2 × (50 μL/well), diluted in assay buffer, were prepared in 1/2 area white polystyrene plates, and 50 μL of cell suspension was dispersed on the ligands using the injector. The light emission was recorded for 20 s. Cells were incubated with antagonist for 15 min at RT°. Then, 50 μL of agonist (final concentration equal to 3 × EC80) was injected into the mixture of cells and antagonist and light emission was recorded for 20 s.

The LANCE Ultra cAMP assay as a homogeneous time-resolved fluorescence resonance energy transfer (TR-FRET) immunoassay is designed to measure cAMP produced upon the modulation of adenylyl cyclase activity by GPCRs. The assay is based on the competition between the europium (Eu) chelate-labeled cAMP tracer and sample cAMP for binding sites on cAMP-specific monoclonal antibodies labeled with the ULight dye.

For the measurement, cells (frozen, ready to use) were thawed and resuspended in 4 mL of HBSS 1×. The cell suspension was then placed in a 15 mL Falcon tube and centrifuged for 10 min at 275× *g*. The pellet was resuspended in 1.5 mL of HBSS 1× to de-

termine the cell concentration, and after the next centrifugation the cells were resuspended in stimulation buffer at the appropriate concentration. An antagonist dose–response experiment was performed in 96-well 1/2-area plates using 3000 cells/well, 5 μM forskolin, and 2 nM of reference agonist and antagonist. Cell stimulation was performed for 30 min at RT°, and agonist and antagonists were added simultaneously.

4.3. Animals

Experiments were performed on female Wistar rats with an initial body weight of 140–160 g. The animals were housed in plastic cages (2 rats per cage) at a constant room temperature of 22 ± 2 °C, with a 12:12 h light/dark cycle. Water and food were available ad libitum. The randomly established experimental groups consisted of 6 rats for pharmacological studies and 3 rats for pharmacokinetic studies. All experiments were conducted in accordance with the Guide to the Care and Use of Experimental Animals, and were approved by the Jagiellonian University in Krakow Local Ethics Committee for Experiments on Animals (Permission No: 185/2017, 220/2019 and 223A/2019).

4.4. In Vivo Studies

4.4.1. Effect of KSK-60, KSK-74, and Phentermine on Changes in Body Weight and Calorie Intake in Non-Obese Rats Fed a Palatable Diet (Model of Excessive Eating)

Female rats were randomly divided into several groups ($n = 6$) and studied for 4 weeks. The groups were as follows: standard diet + vehicle, palatable diet + vehicle, palatable diet + KSK-60 (1 mg/kg), palatable diet + KSK-60 (10 mg/kg), palatable diet + KSK-74 (1 mg/kg), palatable diet + KSK-74 (10 mg/kg), palatable diet + phentermine (7 mg/kg).

The studies for the 1 mg/kg b.w. and 10 mg/kg b.w. doses were performed at different times, so the parameters studied were compared to the respective control groups.

Rats fed a palatable diet had access to a diet consisting of milk chocolate with nuts, cheese, salted peanuts, and 7% condensed milk, and simultaneously to a standard feed (Labofeed B, Morawski Manufacturer Feed, Poland) for 4 weeks [11,21,22]. The water was available ad libitum. Animals had access to palatable products, but also to the standard feed. Most importantly, feeding was not in any way forced, as in other models where animals were fed only a high-fat diet, or temporarily deprived of food (binge eating models). In the case of our model, rats decided themselves when, what, and how much to eat. The weight was evaluated daily. Calorie intake was evaluated three times a week. A palatable diet contained 100 g of peanuts—612 kcal; 100 mL of condensed milk—131 kcal; 100 g of milk chocolate—529 kcal; and 100 g of cheese—325 kcal. The standard diet contained 100 g of feed—280 kcal. Standard diet (fats 8%, carbohydrates 67%, proteins 25%) contained 100 g feed—280 kcal.

The palatable control group (palatable diet + vehicle) received vehicle (1% Tween 80 i.p., daily, for 4 weeks), while palatable test groups were injected i.p. with KSK-60 (1 mg or 10 mg/kg i.p, daily, for 4 weeks), KSK-74 (1 mg/kg or 10 mg/kg i.p, daily, for 4 weeks), or phentermine (7 mg/kg i.p., daily, for 4 weeks), respectively.

The dose of phentermine was selected based on the previous research [23].

On the 31st day, 20 min after i.p. administration of heparin (5000 units/rat) and thiopental (70 mg/kg b.w.), animals were sacrificed, and plasma as well as peritoneal fat pads were collected (food was stopped for 6 h prior to organ, tissue, and plasma collection) for further study.

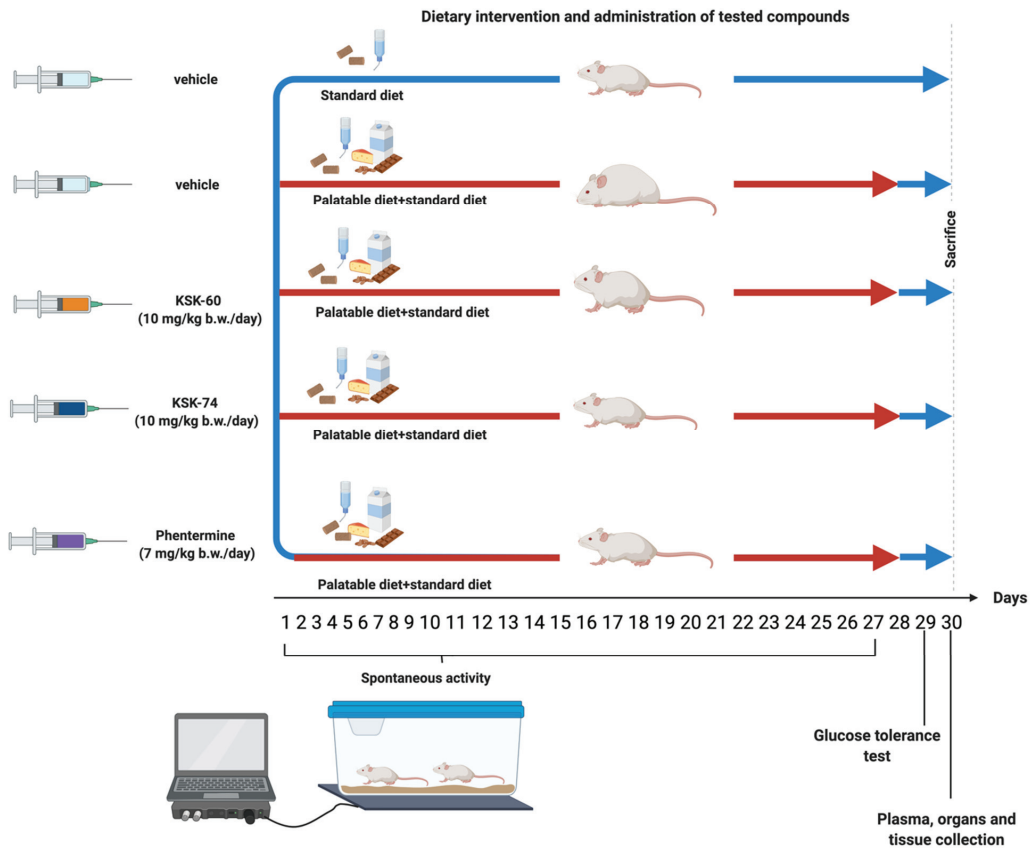Figure 14 shows the experiment scheme.

Figure 14. Experiment scheme.

4.4.2. Glucose Tolerance Test

The test was conducted on the 29th day of the experiment. After twenty-eight administrations of the test compounds, the food was stopped for 20 h and then glucose tolerance was tested. Glucose (1 g/kg b.w.) was administered i.p. [19,20]. Blood samples were obtained from the tail vein at the time points 0 (before glucose administration), 30, 60, and 120 min after administration. Glucose levels were measured with a glucometer (ContourTS, Bayer, Leverkusen, Germany, test stripes: ContourTS, Ascensia Diabetes care Poland Sp. z o. o., Poland, REF:84239666). The area under the curve (AUC) was calculated using the trapezoidal rule.

4.4.3. Effect of KSK-60, KSK-74, and Phentermine on Corticosterone and Triglyceride Levels in Rat's Plasma

Blood was collected from the left carotid artery and then centrifuged at $600 \times g$ (15 min, 4 °C) to obtain plasma.

To determine plasma triglyceride levels, standard enzymatic and spectrophotometric tests (Cat. No 1-053-A150, Biomaxima S.A., Lublin, Poland) were used. The ELISA Kit (Item No. 501320, Cayman Chemical, Ann Arbor, MI, USA) was used to determine corticosterone levels in plasma.

4.4.4. Effect of KSK-60, KSK-74, and Phentermine on Leptin, Resistin, IL-6, and MCP-1 Concentrations in Adipose Tissue

The frozen peritoneal adipose tissue was weighed, and homogenates were prepared by homogenizing 1 g of tissue in 4 mL of 0.1 M phosphate buffer, pH 7.4, using the IKA-ULTRA-TURRAX T8 homogenizer. The adipose tissue homogenates were then used for biochemical assays.

To determine the levels of leptin, resistin, IL-6, and MCP-1 in adipose tissue, the standard ELISA Kit (Cat. No E0561Ra, Cat. No E0211Ra, Cat. No E0135Ra, Cat. No E0193Ra, Bioassay Technology Laboratory, Shanghai, China) was used. To determine the levels of protein, a standard spectrophotometric test (Cat. No 1-008-B210, Biomaxima S.A. Lublin, Poland) was used.

Biochemical Assays Standard Curves are shown in Supplement File S2.

4.4.5. Effect of KSK-60, KSK-74, and Phentermine on Spontaneous Activity in Non-Obese Rats Fed a Palatable Diet

The spontaneous activity of the rats was measured on the 1st and 27th days of the treatment with a special RFID system—TraffiCage (TSE-Systems, Berlin, Germany) [21,22]. The animals were subcutaneously implanted with transmitter identification (RFID), which allowed the presence and time spent in different areas of the cage to be counted, and then the data were grouped in a special computer program.

4.5. Histological Examinations

Adipose tissue samples were prepared for histology using Masson's trichrome stain (Merck) by fixation in 4% formaldehyde, dehydration in graded alcohol, and embedded in paraffin. The tissue samples were then sectioned using a microtome of 5 μm thickness. Six random fields from each section were analyzed in a blinded manner with an Olympus BX41 light microscope (Olympus, Tokyo, Japan) at magnifications of ×20, ×40 and ×100, and digital images were captured with an Olympus UC90 color camera. The quantitation of the number of adipocytes was performed in eight fields/slide with ×100 objective using an image analysis system: CellSensDimension (Olympus, Tokyo, Japan). The numerical density of the adipocytes was obtained by counting the total number of adipocytes per high-power field (31,324 mm^2), and then this number was converted to 0.1 mm^2. According to stereometric rules, adipocytes tangent to the left and top edges of the image field were not counted. A semi-quantitative scale was used to assess the inflammatory response in adipose tissue. The following were evaluated on a subjective scale: inflammatory cell infiltration between adipocytes (0—normal, 1—few cells, 2—local clusters, and 3—extensive infiltrates), perivascular infiltration of immune cells (0—normal, 1—few cells, and 2—ring of inflammatory cells), widening of the septum (0—normal and 1—widening), and capillary congestion (0—normal and 1—congestion). A sum calculated from independently assessed values was calculated for each animal as an index of inflammation.

4.6. Pharmacokinetic Studies

Six rats divided into two experimental groups were used in pharmacokinetic experiments. Three days before the experiment, the rats' jugular vein was cannulated allowing for multiple blood sampling from a single animal. The investigated compounds were administered i.p. at a single dose of 10 mg/kg. Blood samples (approximately 300 μL) were collected in Eppendorf tubes containing heparin at 5, 15, 30, 60, 120, 240, and 360 min after dosing. Plasma was harvested by centrifuging at $5000 \times g$ for 10 min and stored at $-30\,^\circ$C until bioanalysis.

Plasma concentrations of KSK-60 or KSK-74 were measured using the liquid chromatography tandem mass spectrometry (LC-MS/MS) method. The samples (50 μL) were deproteinized in a 1:3 (v/v) ratio with acetonitrile containing an internal standard (IS—pentoxifylline), briefly vortexed, and then centrifuged for 10 min at a speed of $8000 \times g$

(Eppendorf miniSpin centrifuge). The supernatant was transferred to autosampler vials and a sample volume of 10 μL was injected into the LC-MS/MS system.

Chromatographic separation was performed on the analytical column XBridge™ C18 (3 × 50 mm, 5 μm, Waters, Dublin, Ireland) using the Agilent 1100 HPLC system (Agilent Technologies, Waldbronn, Germany). The mobile phase containing 0.1% formic acid in acetonitrile and 0.1% formic acid in water was run at 0.3 mL/min in gradient mode. Mass spectrometric detection was performed on an Applied Biosystems MDS Sciex (Concord, ON, Canada) API 2000 triple quadrupole mass spectrometer. Electrospray ionization (ESI) in the positive ion mode was used for ion production. The tandem mass spectrometer was operated at unit resolution in the selected reaction monitoring mode (SRM), monitoring the transitions of the protonated molecular ions m/z 396 to 107 (CE 80 V) for KSK-60, m/z 424 to 107 (CE 80 V) for KSK-74, and m/z 279 to 181 (CE 55 V) for IS. Data acquisition and processing were performed using the Applied Biosystems Analyst version 1.6 software. The calibration curves were constructed by plotting the ratio of the peak area of the studied compound to IS versus drug concentration, and generated by weighted $(1/x \cdot x)$ linear regression analysis. The validated quantitation ranges were from 1 to 2000 ng/mL. The calculated accuracy and precision were within the ranges proposed by the guidelines for the validation of bioanalytical methods (FDA, EMA). No significant matrix effect was observed and there were no stability-related problems during the routine analysis of the samples.

Pharmacokinetic parameters were calculated by employing a non-compartmental approach using Monolix version 2019R1 (Antony, France: Lixoft SAS, 2019) software. The area under the mean plasma concentration versus time curve extrapolated to infinity (AUC_{0-inf}) was estimated using the log/linear trapezoidal rule. $AUMC_{0-inf}$ was estimated by calculating the total area under the first-moment curve by combining the trapezoid calculation of AUMC0-t and the extrapolated area. The mean residence time (MRT) was calculated from $AUMC_{0-inf}/AUC_{0-inf}$. The terminal rate constant (λz) was calculated by log-linear regression of the drug concentration data in the terminal phase, and the terminal half-life ($t_{1/2}$) was calculated as 0.693/λz. Clearance (CL/F) was estimated from the administered dose divided by AUC_{0-inf}. The apparent volume of distribution during the terminal phase (Vz/F) was calculated from (CL/F)/λz.

4.7. Statistical Analysis

Statistical calculations were performed using the GraphPad Prism 6 program (Graph-Pad Software, San Diego, CA, USA). The results are presented as arithmetic means with a standard deviation (means ± SD). The normality of the data sets was determined using the Shapiro–Wilk test. Statistical significance was calculated using one-way ANOVA, Tukey's post hoc or two-way ANOVA, Tukey's post hoc (body weight) or two-way ANOVA, Bonferroni post hoc (products intake), or Multiple *t*-test (spontaneous activity). Data on the numerical density of adipocytes and the inflammatory index are presented as means ± SD. Comparisons between groups were made using the Kruskal–Wallis test by ranks followed by Dunn post hoc test. Differences were considered statistically significant at * $p \leq 0.05$, ** $p \leq 0.01$, *** $p \leq 0.001$.

5. Conclusions

In summary, the compounds we studied were potent H_3 histamine and sigma-2 receptor ligands with proven efficacy in preventing weight gain in a rat model of excessive eating. The compound KSK-74 significantly compensates for metabolic disturbances that accompany obesity (plasma triglyceride, resistin, and leptin levels), improves glucose tolerance, and protects against adipocyte hypertrophy. Furthermore, KSK-74 inhibits the development of inflammation in obesity-exposed adipose tissue. The in vivo pharmacological activity of the tested ligands appears to correlate with the affinity for the sigma-2 receptors; however, the explanation of this phenomenon requires further and extended research.

References

1. WHO. Obesity and Overweight. Available online: https://www.who.int/news-room/fact-sheets/detail/obesity-and-overweight (accessed on 10 June 2022).
2. Blüher, M. Obesity: Global epidemiology and pathogenesis. *Nat. Rev. Endocrinol.* **2019**, *15*, 288–298. [CrossRef] [PubMed]
3. Dragano, N.R.; Fernø, J.; Diéguez, C.; López, M.; Milbank, E. Recent Updates on Obesity Treatments: Available Drugs and Future Directions. *Neuroscience* **2020**, *437*, 215–239. [CrossRef] [PubMed]
4. Walter, M.; Stark, H. Histamine receptor subtypes: A century of rational drug design. *Front. Biosci.-Sch.* **2012**, *4*, 461–488. [CrossRef]
5. Malmlöf, K.; Zaragoza, F.; Golozoubova, V.; Refsgaard, H.H.F.; Cremers, T.; Raun, K.; Wulff, B.S.; Johansen, P.B.; Westerink, B.; Rimvall, K. Influence of a selective histamine H3 receptor antagonist on hypothalamic neural activity, food intake and body weight. *Int. J. Obes.* **2005**, *29*, 1402–1412. [CrossRef]
6. Malmlöf, K.; Golozoubova, V.; Peschke, B.; Wulff, B.S.; Refsgaard, H.H.; Johansen, P.B.; Cremers, T.; Rimvall, K. Increase of neuronal histamine in obese rats is associated with decreases in body weight and plasma triglycerides. *Obesity* **2006**, *14*, 2154–2162. [CrossRef]
7. Szczepańska, K.; Karcz, T.; Kotańska, M.; Siwek, A.; Kuder, K.J.; Latacz, G.; Mogilski, S.; Hagenow, S.; Lubelska, A.; Sobolewski, M.; et al. Optimization and preclinical evaluation of novel histamine H3 receptor ligands: Acetyl and propionyl phenoxyalkyl piperazine derivatives. *Bioorg. Med. Chem.* **2018**, *26*, 6056–6066. [CrossRef]
8. Hancock, A.A.; Bennani, Y.L.; Bush, E.N.; Esbenshade, T.A.; Faghih, R.; Fox, G.B.; Jacobson, P.; Knourek-Segel, V.; Krueger, K.M.; Nuss, M.E.; et al. Antiobesity effect of A-331440, a novel non-imidazole histamine H3 receptor antagonist. *Eur. J. Pharmacol.* **2004**, *487*, 183–197. [CrossRef]
9. Hancock, A.A.; Brune, M.E. Assessment of pharmacology and potential anti-obesity properties of H 3 receptor antagonists/inverse agonists. *Expert Opin. Investig. Drugs* **2008**, *14*, 223–241. [CrossRef]
10. Masaki, T.; Yoshimatsu, H. The hypothalamic H1 receptor: A novel therapeutic target for disrupting diurnal feeding rhythm and obesity. *Trends Pharmacol. Sci.* **2006**, *27*, 279–284. [CrossRef] [PubMed]
11. Szczepańska, K.; Pockes, S.; Podlewska, S.; Höring, C.; Mika, K.; Latacz, G.; Bednarski, M.; Siwek, A.; Karcz, T.; Nagl, M.; et al. Structural modifications in the distal, regulatory region of histamine H3 receptor antagonists leading to the identification of a potent anti-obesity agent. *Eur. J. Med. Chem.* **2021**, *213*, 113041. [CrossRef] [PubMed]

12. Szczepańska, K.; Karcz, T.; Siwek, A.; Kuder, K.J.; Latacz, G.; Bednarski, M.; Szafarz, M.; Hagenow, S.; Lubelska, A.; Olejarz-Maciej, A.; et al. Structural modifications and in vitro pharmacological evaluation of 4-pyridyl-piperazine derivatives as an active and selective histamine H3 receptor ligands. *Bioorg. Chem.* **2019**, *91*, 103071. [CrossRef] [PubMed]

13. Leurs, R.; Vischer, H.F.; Wijtmans, M.; de Esch, I.J. En route to new lockbuster anti-histamines: Surveying the offspring of the expanding histamine receptor family. *Trends Pharmacol. Sci.* **2011**, *32*, 250–257. [CrossRef] [PubMed]

14. Hancock, A.A.; Diehl, M.S.; Faghih, R.; Bush, E.N.; Krueger, K.M.; Krishna, G.; Miller, T.R.; Wilcox, D.M.; Nguyen, P.; Pratt, J.K.; et al. In vitro optimization of structure activity relationships by analogues of A-331440 combining radioligand receptor binding assays and micronucleus assays of potential antiobesity histamine H3 receptor antagonists. *Basic Clin. Pharmacol. Toxicol.* **2004**, *95*, 144–152. [CrossRef] [PubMed]

15. Szelg, A.; Trocha, M.; Merwid-Ld, A. Betahistine inhibits food intake in rats. *Pol. J. Pharmacol.* **2001**, *53*, 701–707.

16. Deng, C.; Lian, J.; Pai, N.; Huang, X.F. Reducing olanzapine-induced weight gain side effect by using betahistine: A study in the rat model. *J. Psychopharmacol.* **2012**, *26*, 1271–1279. [CrossRef]

17. Mika, K.; Szafarz, M.; Sapa, J.; Kotańska, M. Influence of betahistine repeated administration on a weight gain and selected metabolic parameters in the model of excessive eating in rats. *Biomed. Pharmacother.* **2021**, *141*, 111892. [CrossRef]

18. Rabeea, I.S. The Effect of Betahistine on Body Weight and Waist Circumference in Obese Adults in Comparison with Orlistat. *J. Kerbala Univ.* **2018**, *14*, 143–149.

19. Kotańska, M.; Kuder, K.J.; Szczepańska, K.; Sapa, J.; Kieć-Kononowicz, K. The Histamine H₃ receptor inverse agonist pitolisant reduces body weight in obese mice. *Naunyn Schmiedebergs Arch. Pharmacol.* **2018**, *391*, 875–881. [CrossRef]

20. Kotańska, M.; Mika, K.; Reguła, K.; Szczepańska, K.; Szafarz, M.; Bednarski, M.; Olejarz-Maciej, A.; Nowak, K.; Latacz, G.; Mogilski, S.; et al. KSK19-Novel histamine H3 receptor ligand reduces body weight in diet induced obese mice. *Biochem. Pharmacol.* **2019**, *168*, 193–203. [CrossRef]

21. Mika, K.; Szafarz, M.; Bednarski, M.; Kuder, K.; Szczepańska, K.; Pociecha, K.; Pomierny, B.; Kieć-Kononowicz, K.; Sapa, J.; Kotańska, M.; et al. Metabolic benefits of novel histamine H₃ receptor ligands in the model of excessive eating: The importance of intrinsic activity and pharmacokinetic properties. *Biomed. Pharmacother.* **2021**, *142*, 111952. [CrossRef]

22. Mika, K.; Szafarz, M.; Bednarski, M.; Latacz, G.; Sudoł, S.; Handzlik, J.; Pociecha, K.; Knutelska, J.; Nicosia, N.; Szczepańska, K.; et al. Histamine H3 receptor ligands-KSK-59 and KSK 73-reduce body weight gain in a rat model of excessive eating. *Pharmaceuticals* **2021**, *14*, 1080. [CrossRef] [PubMed]

23. Roth, J.D.; Rowland, N.E. Anorectic efficacy of the fenfluramine/phentermine combination in rats: Additivity or synergy? *Eur. J. Pharmacol.* **1999**, *373*, 127–134. [CrossRef]

24. Szczepańska, K.; Podlewska, S.; Dichiara, M.; Gentile, D.; Patamia, V.; Rosier, N.; Monnich, D.; Contero, M.C.R.; Karcz, T.; Łażewska, D.; et al. Structural and Molecular Insight into Piperazine and Piperidine Derivatives as Histamine H3 and Sigma-1 Receptor Antagonists with Promising Antinociceptive Properties. *ACS Chem. Neurosci.* **2022**, *13*, 1–15. [CrossRef] [PubMed]

25. Pajouhesh, H.; Lenz, G.R. Medicinal chemical properties of successful central nervous system drugs. *NeuroRx* **2005**, *2*, 541–553. [CrossRef] [PubMed]

26. Kotańska, M.; Śniecikowska, J.; Jastrzębska-Więsek, M.; Kolaczkowski, M.; Pytka, K. Metabolic and Cardiovascular Benefits and Risks of EMD386088-A 5-HT6 Receptor Partial Agonist and Dopamine Transporter Inhibitor. *Front. Neurosci.* **2017**, *11*, 50. [CrossRef] [PubMed]

27. Kotańska, M.; Lustyk, K.; Bucki, A.; Marcinkowska, M.; Śniecikowska, J.; Kołaczkowski, M. Idalopirdine, a selective 5-HT6 receptor antagonist, reduces food intake and body weight in a model of excessive eating. *Metab. Brain Dis.* **2018**, *33*, 733–740. [CrossRef] [PubMed]

28. Suleiman, J.; Mohamed, M.; Bakar, A. A systematic review on different models of inducing obesity in animals: Advantages and limitations. *J. Adv. Vet.-Anim. Res.* **2020**, *7*, 103–114. [CrossRef]

29. Passani, M.B.; Blandina, P.; Torrealba, F. The histamine H3 receptor and eating behavior. *J. Pharmacol. Exp. Ther.* **2011**, *336*, 24–29. [CrossRef]

30. Tsuda, K.; Yoshimatsu, H.; Niijima, A.; Chiba, S.; Okeda, T.; Sakata, T. Hypothalmic histamine neurons activate lipolysis in rat adipose tissue. *Exp. Biol. Med.* **2002**, *227*, 208–213. [CrossRef]

31. Klop, B.; Elte, J.W.F.; Cabezas, M.C. Cabezas. Dyslipidemia in Obesity: Mechanisms and Potential Targets. *Nutrients* **2013**, *5*, 1218–1240. [CrossRef]

32. Spalding, K.L.; Arner, E.; Westermark, P.O.; Bernard, S.; Buchholz, B.A.; Bergmann, O.; Blomqvist, L.; Hoffstedt, J.; Näslund, E.; Britton, T.; et al. Dynamics of fat cell turnover in humans. *Nature* **2008**, *453*, 783–787. [CrossRef] [PubMed]

33. Jo, J.; Gavrilova, O.; Pack, S.; Jou, W.; Mullen, S.; Sumner, A.E.; Cushman, S.W.; Periwal, V. Hypertrophy and/or hyperplasia: Dynamics of adipose tissue growth. *PLoS Comput. Biol.* **2009**, *5*, e1000324. [CrossRef] [PubMed]

34. Goossens, G.H.; Blaak, E.E. Adipose tissue dysfunction and impaired metabolic health in human obesity: A matter of oxygen. *Front. Endocrinol.* **2015**, *6*, 55. [CrossRef] [PubMed]

35. Wang, Q.A.; Scherer, P.E. The adipochaser mouse: A model tracking adipogenesis in vivo. *Adipocyte* **2014**, *3*, 146–150. [CrossRef]

36. Roberts, R.; Hodson, L.; Dennis, A.L.; Neville, M.J.; Humphreys, S.M.; Harnden, K.E.; Micklem, K.J.; Frayn, K.N. Markers of de novo lipogenesis in adipose tissue: Associations with small adipocytes and insulin sensitivity in humans. *Diabetologia* **2009**, *52*, 882–890. [CrossRef]

37. Pucci, A.; Batterham, R.L.; Feingold, K.R.; Anawalt, B.; Boyce, A.; Chrousos, G.; Harder, W.W.D.; Dhatariya, K.; Dungan, K.; Hershman, J.M.; et al. Endocrinology of the Gut and the Regulation of Body Weight and Metabolism. In *Endotext*; MDText.com, Inc.: South Dartmouth, MA, USA, 2020.

38. Vendrell, J.; Broch, M.; Vilarrasa, N.; Molina, A.; Gómez, J.M.; Gutiérrez, C.; Simón, I.; Soler, J.; Richart, C. Resistin, adiponectin, ghrelin, leptin, and proinflammatory cytokines: Relationships in obesity. *Obes. Res.* **2004**, *12*, 962–971. [CrossRef]

39. Ronti, T.; Lupattelli, G.; Mannarino, E. The endocrine function of adipose tissue: An update. *Clin. Endocrinol.* **2006**, *64*, 355–365. [CrossRef]

40. Martínez-Sánchez, N. There and Back Again: Leptin Actions in White Adipose Tissue. *Int. J. Mol. Sci.* **2020**, *21*, 6039. [CrossRef]

41. Considine, R.V.; Sinha, M.K.; Heiman, M.L.; Kriauciunas, A.; Stephens, T.W.; Nyce, M.R.; Ohannesian, J.P.; Marco, C.C.; McKee, L.J.; Bauer, T.L.; et al. Serum immunoreactive-leptin concentrations in normal-weight and obese humans. *N. Engl. J. Med.* **1996**, *334*, 292–295. [CrossRef]

42. Zhang, Y.; Scarpace, P.J. The role of leptin in leptin resistance and obesity. *Physiol. Behav.* **2006**, *88*, 249–256. [CrossRef]

43. Holcomb, I.N.; Kabakoff, R.C.; Chan, B.; Baker, T.W.; Gurney, A.; Henzel, W.; Nelson, C.; Lowman, H.B.; Wright, B.D.; Skelton, N.J.; et al. FIZZ1, a novel cysteine-rich secreted protein associated with pulmonary inflammation, defines a new gene family. *EMBO J.* **2000**, *19*, 4046–4055. [CrossRef] [PubMed]

44. Reilly, M.P.; Lehrke, M.; Wolfe, M.L.; Rohatgi, A.; Lazar, M.A.; Rader, D.J. Resistin is an inflammatory marker of atherosclerosis in humans. *Circulation* **2005**, *111*, 932–939. [CrossRef] [PubMed]

45. Yudkin, J.S. Inflammation, obesity, and the metabolic syndrome. *Horm. Metab. Res.* **2007**, *39*, 707–709. [CrossRef] [PubMed]

46. Monteiro, R.; Azevedo, I. Chronic inflammation in obesity and the metabolic syndrome. *Mediat. Inflamm.* **2010**, *2010*, 289645. [CrossRef]

47. Nagy, C.; Einwallner, E. Study of In Vivo Glucose Metabolism in High-fat Diet-fed Mice Using Oral Glucose Tolerance Test (OGTT) and Insulin Tolerance Test (ITT). *J. Vis. Exp.* **2018**, *131*, 56672. [CrossRef]

48. Rosa, A.C.; Nardini, P.; Sgambellone, S.; Gurrieri, M.; Spampinato, S.F.; Dell'Accio, A.; Chazot, P.L.; Obara, I.; Liu, W.L.; Pini, A. CNS-Sparing Histamine H3 Receptor Antagonist as a Candidate to Prevent the Diabetes-Associated Gastrointestinal Symptom. *Biomolecules* **2022**, *12*, 184. [CrossRef]

49. Sindhu, S.; Thomas, R.; Shihab, P.; Sriraman, D.; Behbehani, K.; Ahmad, R. Obesity Is a Positive Modulator or IL-6R and IL-6 Expression in the Subcutaneous Adipose Tissue: Significance for Metabolic Inflammation. *PLoS ONE* **2015**, *10*, e0133494. [CrossRef]

50. Eder, K.; Baffy, N.; Falus, A.; Fulop, A.K. The major inflammatory mediator interleukin-6 and obesity. *Inflamm. Res.* **2009**, *58*, 727–736. [CrossRef]

51. Panee, J. Monocyte Chemoattractant Protein 1 (MCP-1) in obesity and Diabetes. *Cytokine* **2012**, *60*, 1–12. [CrossRef]

52. Sartipy, P.; Loskutoff, D.J. Loskutoff. Monocyte chemoattractant protein 1 in obesity and insulin resistance. *Proc. Natl. Acad. Sci. USA* **2003**, *100*, 7265–7270. [CrossRef]

53. Xu, H.; Barnes, G.T.; Yang, Q.; Tan, G.; Yang, D.; Chou, C.J.; Sole, J.; Nichols, A.; Ross, J.S.; Tartaglia, L.A.; et al. Chronic inflammation in fat plays a crucial role in the development of obesity-related insulin resistance. *J. Clin. Investig.* **2003**, *112*, 1821–1830. [CrossRef]

54. Ellulu, M.S.; Patimah, I.; KhazáAi, H.; Rahmat, A.; Abed, Y. Obesity and inflammation: The linking mechanism and the complications. *Arch. Med. Sci.* **2017**, *13*, 851–863. [CrossRef] [PubMed]

55. Ghaben, A.L.; Scherer, P.E. Adipogenesis and metabolic health. *Nat. Rev. Mol. Cell Biol.* **2019**, *20*, 242–258. [CrossRef] [PubMed]

56. Marin, M.; Cruz, F.C.; Planeta, C.S. Chronic restraint or variable stresses differently affect the behavior, corticosterone secretion and body weight in rats. *Physiol. Behav.* **2007**, *90*, 29–35. [CrossRef]

57. Araujo, A.P.N.; DeLucia, R.; Scavone, C.; Planeta, C.S. Repeated predictable or unpredictable stress: Effects on cocaine-induced locomotion and cyclic AMP-dependent protein kinase activity. *Behav. Brain Res.* **2003**, *139*, 75–81. [CrossRef]

Management of Obesity and Obesity-Related Disorders: From Stem Cells and Epigenetics to Its Treatment

Sara Cruciani [1,2], Alessandro Palmerio Delitala [3], Maria Laura Cossu [4], Carlo Ventura [5] and Margherita Maioli [1,2,6,*]

1   Department of Biomedical Sciences, University of Sassari, 07100 Sassari, Italy
2   Consorzio Interuniversitario "Istituto Nazionale Biostrutture e Biosistemi" (INBB),
    Viale delle Medaglie d'Oro 305, 00136 Roma, Italy
3   Department of Medicine, Surgery and Pharmacy, University of Sassari, 07100 Sassari, Italy
4   General Surgery Unit 2 "Clinica Chirurgica" Medical, Surgical and Experimental Sciences Department,
    University of Sassari, 07100 Sassari, Italy
5   National Laboratory of Molecular Biology and Stem Cell Engineering, Eldor Lab, Istituto Nazionale di
    Biostrutture e Biosistemi (INBB), Via di Corticella 183, 40128 Bologna, Italy
6   Center for Developmental Biology and Reprogramming (CEDEBIOR), Department of Biomedical Sciences,
    University of Sassari, Viale San Pietro 43/B, 07100 Sassari, Italy
*   Correspondence: mmaioli@uniss.it; Tel.: +39-079228277

Abstract: Obesity is a complex worldwide disease, characterized by an abnormal or excessive fat accumulation. The onset of this pathology is generally linked to a complex network of interactions among genetic and environmental factors, aging, lifestyle, and diets. During adipogenesis, several regulatory mechanisms and transcription factors are involved. As fat cells grow, adipose tissue becomes increasingly large and dysfunctional, losing its endocrine function, secreting pro-inflammatory cytokines, and recruiting infiltrating macrophages. This long-term low-grade systemic inflammation results in insulin resistance in peripheral tissues. In this review we describe the main mechanisms involved in adipogenesis, from a physiological condition to obesity. Current therapeutic strategies for the management of obesity and the related metabolic syndrome are also reported.

Keywords: adipose-derived stem cells; epigenetics; adipogenesis; obesity; cellular mechanisms; bariatric surgery; anti-obesity drugs

1. Introduction

Lifestyle changes, such as the consumption of calorie-dense foods and sedentary living, have progressively led to a profound imbalance between calorie intake and consumption [1]. Obesity is a direct consequence of these changes and is closely related to many metabolic disorders, including type 2 diabetes, insulin resistance, hyperglycemia, dyslipidemia, hypertension, and non-metabolic diseases, such as heart disease and many types of cancer [2–4]. The prevalence of childhood/adolescent obesity is increasing worldwide, rising from 4.5 percent in 1990 to 6.7 percent in 2010 [5]. A survey of the obesity epidemic shows that as of 2022 more than 39 million children worldwide are obese [6]. Obesity is strictly dependent on body composition rather than body weight and particularly on the number of adipocytes. Adipose tissue can be classified into different types, white (WAT) and brown (BAT) [7]. The primary function of WAT is energy storage in the form of triglycerides (TG) [8]. On the other hand, BAT dissipates energy to produce heat, suggesting its possible anti-obesity role [9,10]. In addition to brown and white adipocytes, another class of adipocytes, called beige/brown adipocytes, has recently been described [11]. Preadipocytes are converted into mature adipocytes in the final stage of differentiation when they are exposed to certain stimuli [12]. Thus, identifying the molecular mechanisms underlying resident mesenchymal stem cell (MSCs) differentiation could add new insights for the identification of future therapeutic approaches against obesity [13]. Mesenchymal stem cells (MSCs) are a type of adult stem cells known for their high plasticity and ability to

generate mesodermal and non-mesodermal tissues [14]. Cell proliferation and differentiation are two opposing processes. Adipogenesis is regulated by a complex and highly orchestrated gene expression program, which occurs in stages [15]. The first phase involves the commitment of pluripotent stem cells into preadipocytes. Preadipocytes cannot be morphologically distinguished from their precursor cells, but they have also lost the potential to differentiate into other cell types [16]. Therefore, in the second stage, known as terminal differentiation, preadipocytes gradually acquire the features of mature adipocytes and become able to regulate lipid transport and synthesis, insulin sensitivity, and secretion of adipocyte-specific proteins [17]. During these phases, specific adipogenic-related genes are induced, and, at the same time, a series of epigenetic and chromatin modifications also occurs, leading ultimately to the silencing of the stemness-related genes [18,19]. Several natural or synthetic molecules can therefore act directly on these transcription factors, thus representing promising therapeutic agents to modulate uncontrolled adipose tissue hyperproliferation [20,21]. In this review, we focus on the biological features of adipose tissue, analyzing the transcription factors and key proteins involved in stem cell differentiation and the major surgical and pharmacological interventions for the control of obesity and its related metabolic syndrome.

2. Epigenetic Programming of Adipose-Derived Stem Cells (ADSCs)

Adipose-derived stem cells (ADSCs) have emerged in recent years as the most sought-after source of cells for the treatment of obesity, metabolic and degenerative diseases, due to their availability, rapid expansion, and differentiative potential toward several phenotypes [22,23]. ADSCs are mainly found in the so-called stromal vascular fraction (SVF) of adipose tissue, from which they can be easily isolated by mechanical and enzymatic procedures [24,25]. The application of adult stem cells in regenerative medicine enables the repair of many tissues, including vessels, muscles, nerves, cartilage, and skin [26]. Stem cell differentiation requires the precise activation of genes involved in the development of a definite cell type. On the other hand, differentiation itself involves the suppression of specific stemness-related genes, such as octamer-binding transcription factor 4 (Oct-4), sex determining region Y-box 2 (SOX2), and Nanog Homeobox protein (NANOG) [27,28]. The differentiation of preadipocytes into mature adipocytes is regulated by a complex network of transcription factors [29,30]. Any dysregulation in this process causes lipodystrophy, which impairs glucose and lipid homeostasis [31]. While Runt-related transcription factor 2 (RUNX2), the key osteogenic transcription factor, triggers an osteogenic differentiation program in MSCs, adipogenic differentiation is mainly promoted by peroxisome proliferator-activated receptor gamma (PPARγ) and CCAAT/enhancer binding protein alpha (C/EBPα) [32–34]. PPARγ, in particular, is considered the master regulator of adipogenesis [35]. On the other hand, C/EBPα-deficient cells are able to differentiate as adipocytes; however, these C/EBPα-deficient cells are resistant to insulin [36]. In addition to PPARγ, other genes are also involved in adipogenic commitment, such as uncoupling protein 1 (UCP1), which distinguishes BAT from WAT, whose function is thermogenesis in response to cold stress or β-adrenergic stimulus [37]. Insulin-Like Growth Factor-1 (IGF-1), Transforming Growth Factor beta (TGF-β), or cyclic AMP (cAMP) signaling pathways also play key roles in adipocyte differentiation [38]. Moreover, differential gene expression appears to be strongly influenced by epigenetic factors. DNA demethylation and methylation, acetylation or ubiquitylation of histones, as well as various noncoding RNAs, such as microRNAs, are the most studied epigenetic factors involved in modulating cellular organization [29,39]. Epigenetic changes can directly modulate gene promoters, thus facilitating (or preventing) the recruitment of additional chromatin-modifying enzymes or transcriptional regulators that would drive stem cell differentiation [40,41]. Post-translational modifications (PTMs) of histones by histone deacetylases (HDACs) or histone methyltransferases (HMTs) have been reported to be crucial in shaping the process of adipogenesis [42,43]. Reduced expression of Sirt1 and Sirt2, for example, has been associated with increased differentiation capacity of visceral adipose stem cells [44]. In addition,

altered global DNA methylation pattern was observed during metabolic disorders on various genes involved in adipocyte differentiation, lipid metabolism, and inflammation [45,46]. Decreased expression of some epigenetic factors, such as HDAC1, promotes adipogenesis and visceral fat accumulation in human obesity [47,48]. Within this context, it has been demonstrated that exposure of ADSCs to metformin and vitamin D increases the expression of HDAC1 and other epigenetic modulators [49]. Furthermore, several microRNAs (miRNAs) are indeed found to be involved in the inactivation of the adipogenesis process. After treatment with metformin and vitamin D, for example, ADSCs showed upregulated levels of miR-145 and a downregulated expression of miR-148 [49]. miR-145 is downregulated during adipogenesis, while its upregulation inhibits adipogenesis by reducing the activity of PI3K/Akt and MAPK signaling pathways [50]. The expression of miR-148a is also affected by lipid accumulation. When upregulated, miR-148a promotes adipogenic differentiation, while it inhibits preadipocyte differentiation when miR-145 is upregulated and miR-148 is downregulated [51] (Figure 1). These molecules are also able to modulate inflammation and the expression of other key genes involved in adipogenic differentiation, counteracting WAT formation, and inducing a "brown-like" phenotype [52,53]. The use of bioactive molecules and chemical stimuli can then control the de-novo lipogenesis, differentiation, and physiology of adipose tissue, for the in vivo treatment of chronic pathological conditions of difficult resolution.
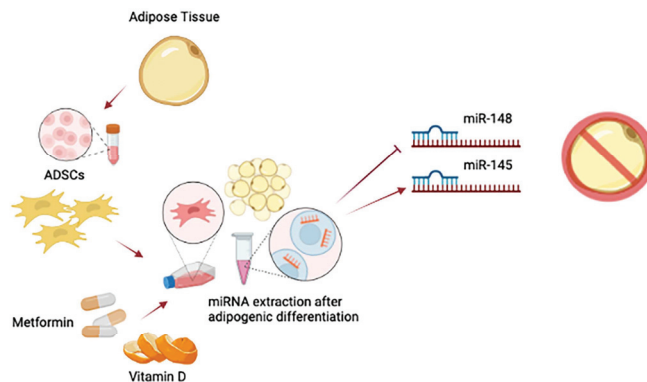

Figure 1. Interaction between molecules and miRNAs. ADSC exposure to metformin and vitamin D modulate miRNAs profile, inducing the upregulation of miR-145 and the simultaneously downregulation of miR-148. The final effect is the inhibition of adipogenesis. Created with BioRender.com accessed on 30 December 2022.

3. Biological Features of Adipose Tissue

Adipose tissue comprises 15–25% of the body weight and it can be classified into subcutaneous and visceral tissue [54]. Adipose tissue represents the main site of energy storage playing an important role as an endocrine organ, and directly modulating systemic lipid, glucose metabolism, and insulin sensitivity [55]. Within adipose tissue, in addition to the adipocytes, the stromal vascular fraction (SVF), containing a type of stem cells called adipose-derived stem cells (ADSCs), can be found [56,57]. These cells are able to differentiate into mature adipocytes following a process called adipogenesis [58]. Within healthy adipose stores, ADSCs have extensive immunomodulatory functions, such as the inhibition of natural killer (NK) cell and T cell proliferation. Moreover, they exert key secretory functions by releasing inflammatory cytokines, as interleukin-6 (IL-6) and tumor necrosis factor-alpha (TNF-α) in response to inflammation [59,60]. Lipid storage is determined by the balance between lipogenesis and lipolysis. The volume of the adipocyte reflects its specific function of storing energy in the form of lipids and, therefore, the ability of the cell to drastically modulate its size in response to changes in energy balance [61]. Adipose tissue expansion is determined by hyperplasia and/or hypertrophy of adipocytes. Hyperplasia

refers to the formation of new adipocytes from preadipocytes at-hormone regulation and mediated by a series of transcription factors [30]. Unlike hyperplasia, hypertrophy is the enlargement of adipocytes by accumulation of lipids, either by uptake from the circulation or through the fatty acid synthesis pathway, known as "de novo lipogenesis" [62]. Generally, adipocyte hypertrophy is mainly associated with insulin resistance, hepatic steatosis, and other markers of metabolic dysfunction [63]. Besides the WAT and BAT, beige/brite adipose tissue shows intermediate characteristics between white and brown fat, with a central nuclei, multilocular lipid droplets, and is rich in mitochondria [64,65]. In addition to being highly insulin-responsive, adipose tissue also secretes several adipokines involved in glucose regulation and metabolic health [66]. These molecules can act as endocrine regulators, influencing different tissues and organs and regulating local signaling in a paracrine or autocrine manner [67,68]. Beige adipocytes are formed by a process named "WAT browning", following stimulation of sympathetic activity during chronic cold exposure or administration of β3-adrenergic receptor agonists or exercise [69]. Several pharmacological and nonpharmacological strategies have consequently been developed to induce WAT browning as a possible mechanism to control weight gain and obesity [70]. In fact, adipose organ dysfunction can lead to age-related metabolic alterations, resulting in increased production of inflammatory peptides and macrophage infiltration, and a decrease in anti-inflammatory activity [71]. The production of pro-inflammatory mediators and the infiltration of immune cells inside the tissue generate a state of chronic inflammation. This inflammatory state that worsens with age is defined as "inflammaging" [72]. With aging, there is an increase in the number of white adipocytes and a decreased activity of brown adipocytes. Aging is also associated with a decrease in the formation of beige adipocytes [73]. During obesity, if compared to WAT, brown and beige adipose tissue are less likely to undergo local inflammation, even though an increased production of pro-inflammatory cytokines, such as TNF-alpha and MCP-1 [74], can be observed. However, the inflammation that is generated can compromise the thermogenic activity in BAT due to impaired insulin sensitivity and reduced glucose absorption [75].

4. Obesity and Obesity-Related Metabolic Syndrome

Obesity is an abnormal or excessive increase in body fat, classified according to the determination of Body Mass Index (BMI) [76]. According to the World Health Organization (WHO), a BMI greater than or equal to 30 kg/m^2 is consistent with obesity, which is divided into different grades according to severity, and a BMI between 25 and 30 kg/m^2 identifies overweight [77]. Excess body fat, especially visceral, is also related to a major risk of numerous chronic diseases including cardiovascular disease, type 2 diabetes, hepatic steatosis, several types of malignancies, and muscular and osteoarticular disorders [78,79]. These diseases are responsible for nearly 3 million deaths per year worldwide. Obesity is the fifth leading cause of death after hypertension, smoking, hyperglycemia, and physical inactivity. A real epidemic of overweight and obese individuals can be detected, especially in undeveloped countries [80,81]. The WHO has predicted a global "obesity epidemic" by 2030, in which 1 in 5 women and 1 in 7 men will be living with obesity. Moreover, this overweight/obesity epidemic and all its complications, have such negative implications on public health, that it can be considered a pandemic disease [82]. Several studies are still underway to better understand the causal factors of obesity. It is a complex hereditary disease whose pathophysiology seems dependent on the interaction between genetics, epigenetics, metagenomics, and environment factors [83,84]. In addition, since the early 1980s, various environmental changes have fostered an "obesogenic environment" with an abundance of high-calorie food, poor-quality food, and, not least, a sedentary lifestyle with reduced physical activity [85]. A long-term imbalance between energy intake and energy expenditure alters the metabolism and functions of WAT. During over-nutrition, lipids are stored within adipocytes [86]. When an enlarged hypertrophic adipocyte reaches maximum capacity, it is no longer able to store excess lipids and becomes fibrotic and inflammatory. Obesity disrupts physiological homeostasis and alters microenvironments

by altering stem cell plasticity and impairing regenerative capacity [87,88]. The decreased plasticity of ADSCs exposed to the obese environment could significantly limit their therapeutic potential and ultimately reduce their therapeutic efficacy [89,90]. Excessive adiposity leads to hyperplasia of adipocytes and the secretion of growth factors, such as insulin-like growth factor-1 (IGF-1), tumor necrosis factor-α (TNF-α), angiotensin II (Ang II), and macrophage colony-stimulating factor (M-CSF) [91,92]. Macrophages and other immune cells produce pro-inflammatory cytokines and reactive oxygen species (ROS) that contribute to the development of a state of chronic low-grade inflammation and insulin resistance [93]. In addition, specific adipokines secreted by adipocytes increase vasomotor endothelial tone and consequently hypertension in obese patients [94]. Obesity can lead to increased synthesis and secretion of low-density lipoprotein (LDL) and very low-density lipoprotein (VLDL), which in turn release triglycerides into extrahepatic tissues. High plasma levels of free fatty acids (FFA) inhibit lipogenesis, preventing proper clearance of serum triacylglycerol levels, leading to hypertriglyceridemia and may result in insulin receptor dysfunction [95,96]. Epigenetic changes are crucial for several key biological processes, including cellular differentiation. Recent evidence suggests that obesity may result from the complex interplay between environmental changes and the epigenome [97–99]. Indeed, many genes are activated or inhibited to regulate energy metabolism. For example, PPARγ promoter methylation is increased in the subcutaneous adipose tissue of obese women [100]. DNMT1-deficient mice exhibit reduced energy expenditure, increased body weight, and susceptibility to diet-induced obesity [101]. HDAC1 deletion has been found to significantly increase the expression of the thermogenic genes UCP1 and Peroxisome proliferator-activated receptor-gamma coactivator (PGC-1α) by increasing acetylation and decreasing methylation of histone H3 lysine 27 (H3K27) [102]. Overexpression of HDAC4 in adipocytes leads to the expansion of beige adipocytes and a reduction in adiposity [103]. Stem cell or brown adipose tissue transplantation, cell lysates, and exosomes have been tested in obese mouse models [104,105]. Overall, ADSCs were found to be effective in treating obesity-associated diabetes and inflammation and protective against cardiovascular disease [106,107]. Therefore, stem cell therapy represents a promising treatment strategy for obesity and obesity-related comorbidities [108].

5. Surgical Management of Obesity

Obesity represents an emerging worldwide disease, with an increased incidence in younger people, that has prompted the development of new and even more effective therapies [109]. Bariatric surgery, also called weight loss surgery, represents one of the approaches for the treatment of severe obesity, with the development of less invasive methods than in the past (Figure 2) [110,111]. Bariatric surgery procedures work by modifying the digestive system, trying to prevent many metabolic obesity-related diseases. The history of obesity surgery is studded with surgical techniques [112]. However, a few main groups can be identified: (1) pure malabsorption (jejunum-ileal bypass or biliointestinal bypass); (2) restrictive (gastroplasties and gastric banding); (3) mixed (bilio-pancreatic diversion and gastric bypass); and (4) alternatives (intragastric balloon and gastric stimulator) [113]. These kinds of procedures are indicated in patients with BMI >40 kg/m^2 or >35 kg/m^2 with complications associated with obesity, and in those who do not improve with medical therapy [114,115]. The gastric sleeve, also called sleeve gastrectomy, is one of the most performed bariatric surgeries [116]. It is a simple procedure that removes a large portion of the stomach, leaving behind a small, tubular portion, like a sleeve. This reduces the intake of food and the secretion of hunger hormones [117]. Gastric bypasses modify the stomach, making it Y-shaped by creating a small pouch in the upper part of the stomach [118]. Food flows through the new smaller stomach and the lower segment of the small intestine, bypassing the rest. The small intestine restriction makes this method more effective than gastric restriction alone [119]. Biliopancreatic diversion with duodenal switch (BPD-DS) is similar to gastric bypass but more extreme [120]. This surgery bypasses most of the small intestine, significantly reducing the hunger hormones produced in the small

intestine and stomach, and greatly limiting the amount of nutrition the small intestine can absorb [121]. Stomach Intestinal Pylorus Sparing Surgery (SIPS) is a modified version of the original duodenal switch [122]. It begins with a sleeve gastrectomy, and divides the first part of the small intestine by closing it back into a loop; in this type of surgery, a smaller part of the small intestine is bypassed, allowing for greater nutrient absorption [123]. These kinds of procedures involve several complications that occur in the short and long term. Early complications include thromboembolism, pulmonary or respiratory failure, hemorrhage, peritonitis, and wound infection [124]. Late complications include gastrointestinal obstruction, marginal ulceration, band malfunction, steatorrhea, diarrhea, micronutrient nutritional deficiencies, and neurological complications [125,126]. This also occurs in general surgery. Excess subcutaneous adipose tissue leads to impaired healing due to low regional perfusion and oxygen tension. Second, the operative time for the obese is quite long and is a significant predictor of postoperative wound infections [127]. The new style of thinking aims to develop less invasive methods in approaching the obese surgical patients [128]. Almost all bariatric surgeons follow a sequence of application of the various techniques available, in which these are ordered according to the criteria of increasing invasiveness but at the same time effectiveness [129,130]. The beginning of this course is represented by the endoscopic placement of an endogastric board (BIB), which is followed in almost all patients by restrictive surgery [131]. This intervention is represented in many cases by adjustable gastric banding (LAGB), which has the advantage of being completely reversible, as it does not involve mutilation of any part of the digestive tract or anastomosis, and of being easily performed laparoscopically [132,133]. Laparoscopic procedures are associated with shorter operative time, less postoperative pain, and earlier recovery, as well as better respiratory function and aesthetic results [134]. The Swedish Obese Subjects (SOS) study showed that weight loss achieved after bariatric surgery significantly improves all obesity-related risk factors such as diabetes, hypercholesterolemia, low lipoprotein levels, hypertension, and hyperuricemia [135,136]. Weight loss after bariatric surgery is also associated with a significant reduction in overall mortality [137].

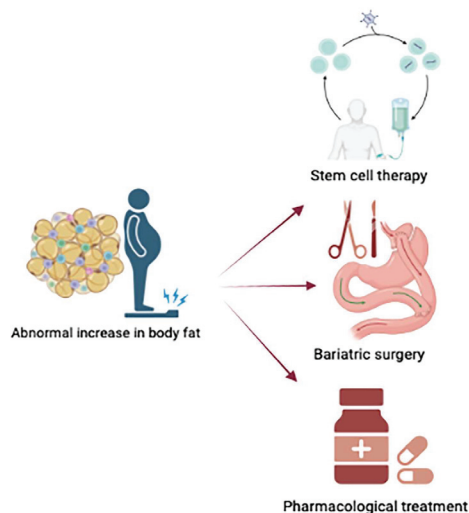**Figure 2.** Some therapeutical approaches for management of obesity. Created with BioRender.com accessed on 30 December 2022.

6. Pharmacological Interventions for Obesity

Pharmacological treatment of obesity became a hot topic in the scientific community (Figure 2), due to the possible wide number of subjects that could potentially benefit, also because behavioral approaches commonly failed and indications for bariatric surgery are becoming narrower [138]. Drugs used to treat obesity can be divided accordingly to their mechanisms of action [139].

6.1. Sympathicomimetic

These compounds are generally used for a short-term treatment of obesity. A weight regain after their discontinuation has been also reported [140]. Among these drugs, two compounds are the most used in the clinical practice: diethylpropion, is an amphetamine derivate and a sympathomimetic stimulant which stimulates the endogenous release of dopamine and norepinephrine causing a suppression of appetite. Further, diethylpropion indirectly elevated leptin level in the brain, thus inhibiting the production of neuropeptide Y [141]. The second compound is phentermine that, likewise to diethylpropion, acts through appetite suppression and by increasing basal energy expenditure. Approved by Food and Drug Administration for short-term use (3 months), a recent trial reported an 8.1 Kg loss after 12 weeks of clinical trial with phentermine, as compared to the placebo [142]. Due to the presence of specific side effects (irritability, mood changes, insomnia, elevation in mean blood pressure and palpitations), its use is discouraged in patients with cardiovascular disease, hyperthyroidism, and anxiety.

6.2. Sympathicomimetic and Anticonvulsivant

Phentermine–topiramate: this combined therapy was approved by FDA in 2012 for the chronic treatment of weight control. The appetite suppressant property of phentermine has been associated with the anti-convulsing drug topiramate which showed weight loss potential. Indeed, it has been hypothesized that topiramate has an appetite suppressant effect by modulating GABA receptor activation [143]. The recommend dose for this combined therapy is 7.5 mg/46 mg every day and was shown to induce a mean weight loss of 9.6 Kg after 108 weeks of treatment. The use of higher dosage (15 mg/92 mg) was associated with a further reduction in body weight [144].

6.3. Pancreatic Lipase Inhibitor

Orlistat was approved both by FDA and European Medicines Agency (EMA) for chronic weight management. Orlistat inhibits pancreas and stomach lipase, thus causing a decrease in fat absorption and a reduction in caloric intake [145]. Common side effects have been reported to be diarrhea, flatulence, and abdominal pains, as well as fat-soluble vitamin deficiencies [146] and scanty cases of liver-injuries [147].

6.4. 5-HT$_{2c}$ Serotonin Agonist

Lorcaserin is a serotonin receptor agonist with high affinity for 5-HT2C receptor, thus limiting the onset of hallucinations and side effects at the cardiac level, respectively caused by the binding of 5-HT$_{2A}$ and 5-HT$_{2B}$ receptors [148]. Despite the possibility of additional side effect (such as headache, nausea, dry mouth, dizziness, and constipation), the use of lorcaserin at 10 mg twice a day was shown to decrease the body weight by at least 5% in 47.5% of the patients, while 22.6% of them had a weight loss $\geq$ 10% after 1 year of follow-up [149].

6.5. Glucagon-like Peptide 1 Agonists

Liraglutide is a glucagon-like peptide 1 (GLP-1) agonist, approved by both FDA and EMA for chronic weight management. GLP-1 is physiologically secreted by the enteroendocrine L-cells of distal ileum and proximal colon after oral meal consumption, but a certain basal rate of secretion has been recently postulated [150]. GLP-1 is an incretin hormone which increases the glucose-dependent insulin secretion but has shown additional

effects: decreases in appetite and food consumption [151], and delays in gastric emptying, thus increasing postprandial feelings of satiety and fullness [152]. The use of Liraglutide was associated with a mean reduction of 8.4 Kg in body weight after 1 year of follow-up and a reduction in cardiovascular risk factors [153]. Gastrointestinal side effects have been reported in some studies [154].

6.6. Opioid Receptor Antagonist/Dopamine and Noradrenaline Reuptake Inhibitor

Naltrexone–bupropion: naltrexone is an opioid antagonist prescribed for the management of alcohol and opioid use disorder. Bupropion is a dopamine and norepinephrine neuronal reuptake inhibitor and was firstly prescribed as an antidepressant. Bupropion also stimulates the α-MSH release, thus inducing appetite regulation. While the exact underlying mechanism is still unknown, it has been suggested that naltrexone and bupropion synergistically act at the melanocortin system [155]. Their combined use is approved by EMA and FDA and has been associated with a mean reduction of 6.1% in body weight [156].

7. Conclusions

Dysfunction of adipocytes and adipose tissue is the main feature of obesity, resulting in an increased risk of insulin resistance, type 2 diabetes, fatty liver disease, hypertension, dyslipidemia, and cardiovascular disorders. In most obese subjects, the compromised physiology of the adipose tissue depends on the hypertrophy of the adipocytes and on the interaction of genetic, epigenetic, and environmental factors. Several surgical procedures, such as biliointestinal bypass or gastric banding, and pharmacological interventions, such as pancreatic lipase inhibitors or Glucagon-Like Peptide 1 agonists, are applied for the management of obesity. Therefore, stem cell therapy and the use of targeted treatment acting on cell differentiation or epigenetic modifications of key target genes, may represent a promising strategy for the management of obesity and obesity-related metabolic syndrome.

References

1. Vicente, A.J.-L.; Beltrán-Carrillo, J.; Megías, Á.; González-Cutre, D. Elements behind sedentary lifestyles and unhealthy eating habits in individuals with severe obesity. *Int. J. Qual. Stud. Health Well-Being* **2022**, *17*, 2056967.
2. Scully, T.; Ettela, A.; LeRoith, D.; Gallagher, E.J. Obesity, Type 2 Diabetes, and Cancer Risk. *Front. Oncol.* **2021**, *10*, 615375. [CrossRef] [PubMed]
3. Jung, U.J.; Choi, M.S. Obesity and its metabolic complications: The role of adipokines and the relationship between obesity, inflammation, insulin resistance, dyslipidemia and nonalcoholic fatty liver disease. *Int. J. Mol. Sci.* **2014**, *15*, 6184–6223. [CrossRef] [PubMed]
4. Hajer, G.R.; Van Haeften, T.W.; Visseren, F.L.J. Adipose tissue dysfunction in obesity, diabetes, and vascular diseases. *Eur. Heart J.* **2008**, *29*, 2959–2971. [CrossRef] [PubMed]
5. De Onis, M.; Blössner, M.; Borghi, E. Global prevalence and trends of overweight and obesity among preschool children. *Am. J. Clin. Nutr.* **2010**, *92*, 1257–1264. [CrossRef]
6. Ling, T.-S.A.K.J.; Chen, S.; Zahry, N.R. Economic burden of childhood overweight and obesity: A systematic review and meta-analysis. *Obes. Rev.* **2022**, *24*, e13535. [CrossRef]
7. Lee, Y.H.; Mottillo, E.P.; Granneman, J.G. Adipose tissue plasticity from WAT to BAT and in between. *Biochim. Biophys. Acta Mol. Basis Dis.* **2014**, *1842*, 358–369. [CrossRef]

8. Welte, M.A.; Gould, A.P. Lipid droplet functions beyond energy storage. *Biochim. Biophys. Acta Mol. Cell Biol. Lipids* **2017**, *1862*, 1260–1272. [CrossRef] [PubMed]

9. Seale, P.; Lazar, M.A. Brown fat in humans: Turning up the heat on obesity. *Diabetes* **2009**, *58*, 1482–1484. [CrossRef]

10. Maliszewska, K.; Kretowski, A. Brown adipose tissue and its role in insulin and glucose homeostasis. *Int. J. Mol. Sci.* **2021**, *22*, 1530. [CrossRef]

11. Pilkington, A.C.; Paz, H.A.; Wankhade, U.D. Beige Adipose Tissue Identification and Marker Specificity—Overview. *Front. Endocrinol.* **2021**, *12*, 599134. [CrossRef]

12. Audano, M.; Pedretti, S.; Caruso, D.; Crestani, M.; De Fabiani, E.; Mitro, N. Regulatory mechanisms of the early phase of white adipocyte differentiation: An overview. *Cell. Mol. Life Sci.* **2022**, *79*, 1–14. [CrossRef]

13. Glenn, J.D. Mesenchymal stem cells: Emerging mechanisms of immunomodulation and therapy. *World, J. Stem Cells* **2014**, *6*, 526–539. [CrossRef] [PubMed]

14. Ullah, I.; Subbarao, R.B.; Rho, G.J. Human mesenchymal stem cells—Current trends and future prospective. *Biosci. Rep.* **2015**, *35*, e00191. [CrossRef] [PubMed]

15. Moseti, D.; Regassa, A.; Kim, W.K. Molecular regulation of adipogenesis and potential anti-adipogenic bioactive molecules. *Int. J. Mol. Sci.* **2016**, *17*, 124. [CrossRef] [PubMed]

16. Cawthorn, W.P.; Scheller, E.L.; MacDougal, O.A. Adipose tissue stem cells meet preadipocyte commitment: Going back to the future. *J. Lipid Res.* **2012**, *53*, 227–246. [CrossRef]

17. Gregoire, F.M.; Smas, C.M.; Sul, H.S. Understanding adipocyte differentiation. *Physiol. Rev.* **1998**, *78*, 783–809. [CrossRef]

18. Nic-Can, G.I.; Rodas-Junco, B.A.; Carrillo-Cocom, L.M.; Zepeda-Pedreguera, A.; Peñaloza-Cuevas, R.; Aguilar-Ayala, F.J.; Rojas-Herrera, R.A. Epigenetic regulation of adipogenic differentiation by histone lysine demethylation. *Int. J. Mol. Sci.* **2019**, *20*, 3918. [CrossRef]

19. Ying, H.; Pan, R.; Chen, Y. Epigenetic Control of Mesenchymal Stromal Cell Fate Decision. In *Post-Translational Modifications in Cell. Functions and Diseases*; InTechOpen: London, UK, 2021. [CrossRef]

20. Szymczak-Pajor, I.; Miazek, K.; Selmi, A.; Balcerczyk, A.; Śliwińska, A. The Action of Vitamin D in Adipose Tissue: Is There the Link between Vitamin D Deficiency and Adipose Tissue-Related Metabolic Disorders? *Int. J. Mol. Sci.* **2022**, *23*, 956. [CrossRef]

21. Santaniello, S.; Cruciani, S.; Basoli, V.; Balzano, F.; Bellu, E.; Garroni, G.; Ginesu, G.C.; Cossu, M.L.; Facchin, F.; Delitala, A.P.; et al. Melatonin and Vitamin D Orchestrate Adipose Derived Stem Cell Fate by Modulating Epigenetic Regulatory. *Genes* **2018**, *15*, 1631–1639. [CrossRef]

22. Fathi, E.; Farahzadi, R. Isolation, culturing, characterization and aging of adipose tissue-derived mesenchymal stem cells: A brief overview. *Braz. Arch. Biol. Technol.* **2016**, *59*. [CrossRef]

23. Schäffler, A.; Büchler, C. Concise Review: Adipose Tissue-Derived Stromal Cells—Basic and Clinical Implications for Novel Cell-Based Therapies. *Stem Cells* **2007**, *25*, 818–827. [CrossRef]

24. Basoli, V.; Santaniello, S.; Cruciani, S.; Ginesu, G.C.; Cossu, M.L.; Delitala, A.P.; Serra, P.A.; Ventura, C.; Maioli, M. Melatonin and vitamin D interfere with the adipogenic fate of adipose-derived stem cells. *Int. J. Mol. Sci.* **2017**, *18*, 981. [CrossRef] [PubMed]

25. Bianchi, F.; Maioli, M.; Leonardi, E.; Olivi, E.; Pasquinelli, G.; Valente, S.; Mendez, A.J.; Ricordi, C.; Raffaini, M.; Tremolada, C.; et al. A new nonenzymatic method and device to obtain a fat tissue derivative highly enriched in pericyte-like elements by mild mechanical forces from human lipoaspirates. *Cell Transplant.* **2013**, *22*, 2063–2077. [CrossRef] [PubMed]

26. Naderi, N.; Combellack, E.J.; Griffin, M.; Sedaghati, T.; Javed, M.; Findlay, M.W.; Wallace, C.G.; Mosahebi, A.; Butler, P.E.; Seifalian, A.M.; et al. The regenerative role of adipose-derived stem cells (ADSC) in plastic and reconstructive surgery. *Int. Wound, J.* **2017**, *14*, 112–124. [CrossRef]

27. Rooj, A.K.; Bronisz, A.; Godlewski, J. The role of octamer binding transcription factors in glioblastoma multiforme. *Biochim. Biophys. Acta Gene Regul. Mech.* **2016**, *18*, 1093–1108. [CrossRef]

28. Kashyap, V.; Rezende, N.C.; Scotland, K.B.; Shaffer, S.M.; Persson, J.L.; Gudas, L.J.; Mongan, A.P. Regulation of Stem cell pluripotency and differentiation involves a mutual regulatory circuit of the Nanog, OCT4, and SOX2 pluripotency transcription factors with polycomb Repressive Complexes and Stem Cell microRNAs. *Stem Cells Dev.* **2009**, *18*, 1093–1108. [CrossRef]

29. Perez-Campo, F.; Riancho, J. Epigenetic Mechanisms Regulating Mesenchymal Stem Cell Differentiation. *Curr. Genom.* **2015**, *16*, 368–383. [CrossRef]

30. Ambele, M.A.; Dhanraj, P.; Giles, R.; Pepper, M.S. Adipogenesis: A complex interplay of multiple molecular determinants and pathways. *Int. J. Mol. Sci.* **2020**, *21*, 4283. [CrossRef]

31. Moreno-Indias, I.; Tinahones, F.J. Impaired adipose tissue expandability and lipogenic capacities as ones of the main causes of metabolic disorders. *J. Diabetes Res.* **2015**, *2015*, 970375. [CrossRef]

32. Chen, Q.; Shou, P.; Zheng, C.; Jiang, M.; Cao, G.; Yang, Q.; Cao, J.; Xie, N.; Velletri, T.; Zhang, X.; et al. Fate decision of mesenchymal stem cells: Adipocytes or osteoblasts? *Cell Death Differ.* **2016**, *23*, 1128–1139. [CrossRef] [PubMed]

33. Meyer, M.B.; Benkusky, N.A.; Sen, B.; Rubin, J.; Pike, J.W. Epigenetic plasticity drives adipogenic and osteogenic differentiation of marrow-derived mesenchymal stem cells. *J. Biol. Chem.* **2016**, *291*, 17829–17847. [CrossRef] [PubMed]

34. Hu, L.; Yin, C.; Zhao, F.; Ali, A.; Ma, J.; Qian, A. Mesenchymal stem cells: Cell fate decision to osteoblast or adipocyte and application in osteoporosis treatment. *Int. J. Mol. Sci.* **2018**, *19*, 360. [CrossRef] [PubMed]

35. Yang, D.; Li, N.; Zhang, G. Spontaneous adipogenic differentiation potential of adipose-derived stem cells decreased with increasing cell passages. *Mol. Med. Rep.* **2018**, *17*, 6109–6115. [CrossRef] [PubMed]

36. Rosen, E.D.; Hsu, C.H.; Wang, X.; Sakai, S.; Freeman, M.W.; Gonzalez, F.J.; Spiegelman, B.M. C/EBPα induces adipogenesis through PPARγ: A unified pathway. *Genes Dev.* **2002**, *16*, 22–26. [CrossRef]

37. Yi, D.; Nguyen, H.P.; Sul, H.S. Epigenetic dynamics of the thermogenic gene program of adipocytes. *Biochem. J.* **2020**, *477*, 1137–1148. [CrossRef]

38. Farmer, S.R. Transcriptional control of adipocyte formation. *Cell Metab.* **2006**, *4*, 263–273. [CrossRef]

39. Zhou, Y.; Kim, J.; Yuan, X.; Braun, T. Epigenetic modifications of stem cells: A paradigm for the control of cardiac progenitor cells. *Circ. Res.* **2011**, *109*, 1067–1081. [CrossRef] [PubMed]

40. Krämer, A.I.; Handschin, C. How epigenetic modifications drive the expression and mediate the action of PGC-1α in the regulation of metabolism. *Int. J. Mol. Sci.* **2019**, *20*, 5449. [CrossRef]

41. Jang, S.; Hwang, J.; Jeong, H.-S. The Role of Histone Acetylation in Mesenchymal Stem Cell Differentiation. *Chonnam Med. J.* **2022**, *58*, 6–12. [CrossRef]

42. Li, H.X.; Xiao, L.; Wang, C.; Gao, J.L.; Zhai, Y.G. Epigenetic regulation of adipocyte differentiation and adipogenesis. *J. Zhejiang Univ. Sci. B* **2010**, *11*, 784–791. [CrossRef] [PubMed]

43. Pant, R.; Firmal, P.; Shah, V.K.; Alam, A.; Chattopadhyay, S. Epigenetic Regulation of Adipogenesis in Development of Metabolic Syndrome. *Front. Cell Dev. Biol.* **2021**, *8*, 619888. [CrossRef] [PubMed]

44. Perrini, S.; Porro, S.; Nigro, P.; Cignarelli, A.; Caccioppoli, C.; Genchi, V.A.; Martines, G.; De Fazio, M.; Capuano, P.; Natalicchio, A.; et al. Reduced SIRT1 and SIRT2 expression promotes adipogenesis of human visceral adipose stem cells and associates with accumulation of visceral fat in human obesity. *Int. J. Obes.* **2020**, *44*, 307–319. [CrossRef]

45. Castellano-Castillo, D.; Moreno-Indias, I.; Sanchez-Alcoholado, L.; Ramos-Molina, B.; Alcaide-Torres, J.; Morcillo, S.; Ocaña-Wilhelmi, L.; Tinahones, F.; Queipo-Ortuño, M.I.; Cardonao, F. Altered adipose tissue DNA methylation status in metabolic syndrome: Relationships between global DNA methylation and specific methylation at adipogenic, lipid metabolism and inflammatory candidate genes and metabolic variables. *J. Clin. Med.* **2019**, *8*, 87. [CrossRef]

46. Mirzaeicheshmeh, E.; Zerrweck, C.; Centeno-Cruz, F.; Baca-Peynado, P.; Martinez-Hernandez, A.; García-Ortiz, H.; Contreras-Cubas, C.; Salas-Martínez, M.G.; Saldaña-Alvarez, Y.; Mendoza-Caamal, E.C.; et al. Alterations of DNA methylation during adipogenesis differentiation of mesenchymal stem cells isolated from adipose tissue of patients with obesity is associated with type 2 diabetes. *Adipocyte* **2021**, *10*, 493–504. [CrossRef]

47. Mayoral, R.; Osborn, O.; McNelis, J.; Johnson, A.M.; Oh, D.Y.; Izquierdo, C.L.; Chung, H.; Li, P.; Traves, P.G.; Bandyopadhyay, G.; et al. Adipocyte SIRT1 knockout promotes PPARγ activity, adipogenesis and insulin sensitivity in chronic-HFD and obesity. *Mol. Metab.* **2015**, *4*, 378–391. [CrossRef]

48. Eung, J.Y.; Chung, J.J.; Sung, S.C.; Kang, H.K.; Jae, B.K. Down-regulation of histone deacetylases stimulates adipocyte differentiation. *J. Biol. Chem.* **2006**, *281*, 6608–6615. [CrossRef]

49. Cruciani, S.; Garroni, G.; Balzano, F.; Pala, R.; Bellu, E.; Cossu, M.L.; Ginesu, G.C.; Ventura, C.; Maioli, M. Tuning adipogenic differentiation in adscs by metformin and vitamin d: Involvement of mirnas. *Int. J. Mol. Sci.* **2020**, *21*, 6181. [CrossRef] [PubMed]

50. Wang, L.L.; Zhang, S.; Mei, G.C.C.; Li, S.; Zhang, W.; Junjvlieke, Z. MiR-145 reduces the activity of PI3K/Akt and MAPK signaling pathways and inhibits adipogenesis in bovine preadipocytes. *Genomics* **2020**, *112*, 2688–2694. [CrossRef]

51. Wang, N.; He, L.; Lin, H.; Tan, L.; Sun, Y.; Zhang, X.; Danser, A.H.J.; Lu, H.S.; He, Y.; Lu, X. MicroRNA-148a regulates low-density lipoprotein metabolism by repressing the (pro)renin receptor. *PLoS ONE* **2020**, *15*, e0225356. [CrossRef]

52. Cruciani, S.; Garroni, G.; Pala, R.; Cossu, M.L.; Ginesu, G.C.; Ventura, C.; Maioli, M. Metformin and vitamin d modulate inflammation and autophagy during adipose-derived stem cell differentiation. *Int. J. Mol. Sci.* **2021**, *22*, 6686. [CrossRef] [PubMed]

53. Cruciani, M.M.S.; Garroni, G.; Pala, R.; Coradduzza, D.; Cossu, M.L.; Ginesu, G.C.; Capobianco, G.; Dessole, S.; Ventura, C. Metformin and vitamin D modulate adipose-derived stem cell differentiation towards the beige phenotype. *Adipocyte* **2022**, *11*, 356–365. [CrossRef] [PubMed]

54. Harvey, I.; Boudreau, A.; Stephens, J.M. Adipose tissue in health and disease: Adipose Tissue in Health and Disease. *Open Biol.* **2020**, *10*, 200291. [CrossRef] [PubMed]

55. Booth, A.; Magnuson, A.; Fouts, J.; Foster, M.T. Adipose tissue: An endocrine organ playing a role in metabolic regulation. *Horm. Mol. Biol. Clin. Investig.* **2016**, *26*, 25–42. [CrossRef] [PubMed]

56. Bora, P.; Majumdar, A.S. Adipose tissue-derived stromal vascular fraction in regenerative medicine: A brief review on biology and translation. *Stem Cell Res. Ther.* **2017**, *8*, 145. [CrossRef]

57. Ramakrishnan, V.M.; Boyd, N.L. The Adipose Stromal Vascular Fraction as a Complex Cellular Source for Tissue Engineering Applications. *Tissue Eng. Part B Rev.* **2018**, *24*, 289–299. [CrossRef]

58. Song, T.; Kuang, S. Adipocyte dedifferentiation in health and diseases. *Clinical Sci.* **2019**, *133*, 2107–2119. [CrossRef]

59. Ceccarelli, S.; Pontecorvi, P.; Anastasiadou, E.; Napoli, C.; Marchese, C. Immunomodulatory Effect of Adipose-Derived Stem Cells: The Cutting Edge of Clinical Application. *Front. Cell Dev. Biol.* **2020**, *8*, 236. [CrossRef]

60. Abbasi, B.; Shamsasenjan, K.; Ahmadi, M.; Beheshti, S.A.; Saleh, M. Mesenchymal stem cells and natural killer cells interaction mechanisms and potential clinical applications. *Stem Cell Res. Ther.* **2022**, *13*, 97. [CrossRef]

61. Rosen, E.D.; Spiegelman, B.M. Adipocytes as regulators of energy balance and glucose homeostasis. *Nature* **2006**, *444*, 847–853. [CrossRef]

62. Hsiao, W.Y.; Guertin, D.A. De Novo Lipogenesis as a Source of Second Messengers in Adipocytes. *Curr. Diabetes Rep.* **2019**, *19*, 138. [CrossRef] [PubMed]
63. Chait, A.; den Hartigh, L.J. Adipose Tissue Distribution, Inflammation and Its Metabolic Consequences, Including Diabetes and Cardiovascular Disease. *Front. Cardiovasc. Med.* **2020**, *7*, 22. [CrossRef] [PubMed]
64. Giralt, M.; Villarroya, F. White, brown, beige/brite: Different adipose cells for different functions? *Endocrinology* **2013**, *154*, 2992–3000. [CrossRef]
65. Rui, L. Brown and beige adipose tissues in health and disease. *Compr. Physiol.* **2017**, *7*, 1281–1306. [CrossRef]
66. Al-Mansoori, L.; Al-Jaber, H.; Prince, M.S.; Elrayess, M.A. Role of Inflammatory Cytokines, Growth Factors and Adipokines in Adipogenesis and Insulin Resistance. *Inflammation* **2022**, *45*, 31–44. [CrossRef]
67. Smith, U.; Kahn, B.B. Adipose tissue regulates insulin sensitivity: Role of adipogenesis, de novo lipogenesis and novel lipids. *J. Intern. Med.* **2016**, *280*, 465–475. [CrossRef] [PubMed]
68. Kahn, D.E.; Bergman, B.C. Keeping It Local in Metabolic Disease: Adipose Tissue Paracrine Signaling and Insulin Resistance. *Diabetes* **2022**, *71*, 599–609. [CrossRef] [PubMed]
69. Lizcano, F.; Arroyave, F. Control of adipose cell browning and its therapeutic potential. *Metabolites* **2020**, *10*, 471. [CrossRef]
70. Cheng, L.; Wang, J.; Dai, H.; Duan, Y.; An, Y.; Shi, L.; Lv, Y.; Li, H.; Wang, C.; Ma, Q.; et al. Brown and beige adipose tissue: A novel therapeutic strategy for obesity and type 2 diabetes mellitus. *Adipocyte* **2021**, *10*, 48–65. [CrossRef]
71. Li, Y.; Yun, K.; Mu, R. A review on the biology and properties of adipose tissue macrophages involved in adipose tissue physiological and pathophysiological processes. *Lipids Health Dis.* **2020**, *19*, 164. [CrossRef]
72. Zoico, E.; Rubele, S.; De Caro, A.; Nori, N.; Mazzali, G.; Fantin, F.; Rossi, A.; Zamboni, M. Brown and beige adipose tissue and aging. *Front. Endocrinol.* **2019**, *10*, 368. [CrossRef] [PubMed]
73. Von Bank, H.; Kirsh, C.; Simcox, J. Aging adipose: Depot location dictates age-associated expansion and dysfunction. *Ageing Res. Rev.* **2021**, *67*, 101259. [CrossRef] [PubMed]
74. Villarroya, F.; Cereijo, R.; Gavaldà-Navarro, A.; Villarroya, J.; Giralt, M. Inflammation of brown/beige adipose tissues in obesity and metabolic disease. *J. Intern. Med.* **2018**, *284*, 492–504. [CrossRef] [PubMed]
75. Omran, F.; Christian, M. Inflammatory Signaling and Brown Fat Activity. *Front. Endocrinol.* **2020**, *11*, 156. [CrossRef] [PubMed]
76. Purnell, J.Q. *Definitions, Classification, and Epidemiology of Obesity*; MDText.com, Inc.: South Dartmouth, MA, USA, 2018.
77. Flegal, K.M.; Graubard, B.I. Estimates of excess deaths associated with body mass index and other anthropometric variables. *Am. J. Clin. Nutr.* **2009**, *89*, 1213–1219. [CrossRef]
78. Gutiérrez-Cuevas, J.; Santos, A.; Armendariz-Borunda, J. Pathophysiological molecular mechanisms of obesity: A link between mafld and nash with cardiovascular diseases. *Int. J. Mol. Sci.* **2021**, *22*, 11629. [CrossRef]
79. Caussy, C.; Aubin, A.; Loomba, R. The Relationship Between Type 2 Diabetes, NAFLD, and Cardiovascular Risk. *Curr. Diabetes Rep.* **2021**, *21*, 15. [CrossRef]
80. Hruby, A.; Hu, F.B. The Epidemiology of Obesity: A Big Picture. *PharmacoEconomics* **2015**, *33*, 673–689. [CrossRef]
81. Ryan, D.; Barquera, S.; Cavalcanti, O.B.; Ralston, J. The Global Pandemic of Overweight and Obesity. In *Handbook of Global Health*; Springer: Cham, Switzerland, 2020. [CrossRef]
82. Lagerros, Y.T.; Rössner, S. Obesity management: What brings success? *Ther. Adv. Gastroenterol.* **2013**, *6*, 77–88. [CrossRef]
83. Pigeyre, M.; Yazdi, F.T.; Kaur, Y.; Meyre, D. Recent progress in genetics, epigenetics and metagenomics unveils the pathophysiology of human obesity. *Clin. Sci.* **2016**, *130*, 943–986. [CrossRef] [PubMed]
84. Ghaben, A.L.; Scherer, P.E. Adipogenesis and metabolic health. *Nat. Rev. Mol. Cell Biol.* **2019**, *20*, 242–258. [CrossRef] [PubMed]
85. Townshend, T.; Lake, A. Obesogenic environments: Current evidence of the built and food environments. *Perspect. Public Health* **2017**, *137*, 38–44. [CrossRef] [PubMed]
86. Longo, M.; Zatterale, F.; Naderi, J.; Parrillo, L.; Formisano, P.; Raciti, G.A.; Beguinot, F.; Miele, C. Adipose tissue dysfunction as determinant of obesity-associated metabolic complications. *Int. J. Mol. Sci.* **2019**, *20*, 2358. [CrossRef] [PubMed]
87. Fuster, J.J.; Ouchi, N.; Gokce, N.; Walsh, K. Obesity-induced changes in adipose tissue microenvironment and their impact on cardiovascular disease. *Circ. Res.* **2016**, *118*, 1786–1807. [CrossRef]
88. Baptista, L.S. Obesity and weight loss could alter the properties of adipose stem cells? *World, J. Stem Cells* **2015**, *7*, 165–173. [CrossRef]
89. Payab, M.; Goodarzi, P.; Foroughi Heravani, N.; Hadavandkhani, M.; Zarei, Z.; Falahzadeh, K.; Larijani, B.; Rahim, F.; Arjmand, B. Stem cell and obesity: Current state and future perspective. In *Advances in Experimental Medicine and Biology*; Springer: Cham, Switzerland, 2018. [CrossRef]
90. Oestreich, A.K.; Collins, K.H.; Harasymowicz, N.S.; Wu, C.L.; Guilak, F. Is Obesity a Disease of Stem Cells? *Cell Stem Cell* **2020**, *27*, 15–18. [CrossRef]
91. Caruso, C.; Balistreri, C.R.; Candore, G. The role of adipose tissue and adipokines in obesity-related inflammatory diseases. *Mediat. Inflamm.* **2010**, *2010*, 802078. [CrossRef]
92. Ahmad, B.; Serpell, C.J.; Fong, I.L.; Wong, E.H. Molecular Mechanisms of Adipogenesis: The Anti-adipogenic Role of AMP-Activated Protein Kinase. *Front. Mol. Biosci.* **2020**, *7*, 76. [CrossRef]
93. Benomar, Y.; Taouis, M. Molecular mechanisms underlying obesity-induced hypothalamic inflammation and insulin resistance: Pivotal role of resistin/tlr4 pathways. *Front. Endocrinol.* **2019**, *10*, 140. [CrossRef]

94. Campia, U.; Tesauro, M.; Cardillo, C. Human obesity and endothelium-dependent responsiveness. *Br. J. Pharmacol.* **2012**, *165*, 561–573. [CrossRef]

95. Klop, B.; Elte, J.W.F.; Cabezas, M.C. Dyslipidemia in Obesity: Mechanisms and Potential Targets. *Nutrients* **2013**, *5*, 1218–1240. [CrossRef] [PubMed]

96. Wang, H.; Peng, D.Q. New insights into the mechanism of low high-density lipoprotein cholesterol in obesity. *Lipids Health Dis.* **2011**, *10*, 176. [CrossRef]

97. Gao, W.; Liu, J.L.; Lu, X.; Yang, Q. Epigenetic regulation of energy metabolism in obesity. *J. Mol. Cell Biol.* **2021**, *13*, 480–499. [CrossRef]

98. Park, Y.J.; Han, S.M.; Huh, J.Y.; Kim, J.B. Emerging roles of epigenetic regulation in obesity and metabolic disease. *J. Biol. Chem.* 2021. [CrossRef] [PubMed]

99. Van Dijk, S.J.; Molloy, P.L.; Varinli, H.; Morrison, J.L.; Muhlhausler, B.S. Members of EpiSCOPE. Epigenetics and human obesity. *Int. J. Obes.* **2015**, *39*, 85–97. [CrossRef] [PubMed]

100. Ma, X.; Kang, S. Functional implications of DNA methylation in adipose biology. *Diabetes* **2019**, *68*, 871–878. [CrossRef]

101. Bruggeman, E.C.; Garretson, J.T.; Wu, R.; Shi, H.; Xue, B. Neuronal Dnmt1 deficiency attenuates diet-Induced obesity in mice. *Endocrinology* **2018**, *159*, 145–162. [CrossRef]

102. Li, F.; Wu, R.; Cui, X.; Zha, L.; Yu, L.; Shi, H.; Xue, B. Histone deacetylase 1 (HDAC1) negatively regulates thermogenic program in brown adipocytes via coordinated regulation of histone H3 lysine 27 (H3K27) deacetylation and methylation. *J. Biol. Chem.* **2016**, *291*, 4523–4536. [CrossRef]

103. Paulo, E.; Wu, D.; Hecker, P.; Zhang, Y.; Wang, B. Adipocyte HDAC4 activation leads to beige adipocyte expansion and reduced adiposity. *J. Endocrinol.* **2018**, *239*, 153–165. [CrossRef]

104. Mikłosz, A.; Nikitiuk, B.E.; Chabowski, A. Using adipose-derived mesenchymal stem cells to fight the metabolic complications of obesity: Where do we stand? *Obes. Rev.* **2022**, *23*, e13413. [CrossRef] [PubMed]

105. Calvo, E.; Keiran, N.; Núñez-Roa, C.; Maymó-Masip, E.; Ejarque, M.; Sabadell-Basallote, J.; Del Mar Rodríguez-Peña, M.; Ceperuelo-Mallafré, V.; Seco, J.; Benaiges, E.; et al. Effects of stem cells from inducible brown adipose tissue on diet-induced obesity in mice. *Sci. Rep.* **2021**, *11*, 13923. [CrossRef] [PubMed]

106. Rochette, L.; Mazini, L.; Malka, G.; Zeller, M.; Cottin, Y.; Vergely, C. The crosstalk of adipose-derived stem cells (Adsc), oxidative stress, and inflammation in protective and adaptive responses. *Int. J. Mol. Sci.* **2020**, *21*, 9262. [CrossRef] [PubMed]

107. Yang, H.; Li, C.; Li, Y.; Tai, R.; Sun, C. Adipose-derived stem cells and obesity: The spear and shield relationship. *Genes Dis.* 2021; *in press*. [CrossRef]

108. Jaber, H.; Issa, K.; Eid, A.; Saleh, F.A. The therapeutic effects of adipose-derived mesenchymal stem cells on obesity and its associated diseases in diet-induced obese mice. *Sci. Rep.* **2021**, *11*, 6291. [CrossRef] [PubMed]

109. Lin, X.; Li, H. Obesity: Epidemiology, Pathophysiology, and Therapeutics. *Front. Endocrinol.* **2021**, *12*, 706978. [CrossRef] [PubMed]

110. Wolfe, B.M.; Kvach, E.; Eckel, R.H. Treatment of Obesity: Weight Loss and Bariatric Surgery. *Circ. Res.* **2016**, *118*, 1844–1855. [CrossRef] [PubMed]

111. Hlinnik, A.A.; Aulas, S.D.; Stebounov, S.S.; Rummo, O.O.; Hermanovich, V.I. Bariatric Surgery for Morbid Obesity. *Nov. Khirurgii* **2021**, *29*, 662–670. [CrossRef]

112. Nguyen, N.T.; Varela, J.E. Bariatric surgery for obesity and metabolic disorders: State of the art. *Nat. Rev. Gastroenterol. Hepatol.* **2017**, *14*, 160–169. [CrossRef]

113. Eisenberg, D.; Duffy, A.J.; Bell, R.L. Update on obesity surgery. *World, J. Gastroenterol.* **2006**, *12*, 3196–3203. [CrossRef]

114. De Luca, M.; Angrisani, L.; Himpens, J.; Busetto, L.; Scopinaro, N.; Weiner, R.; Sartori, A.; Stier, C.; Lakdawala, M.; Bhasker, A.G.; et al. Indications for Surgery for Obesity and Weight-Related Diseases: Position Statements from the International Federation for the Surgery of Obesity and Metabolic Disorders (IFSO). *Obes. Surg.* **2016**, *26*, 1659–1696. [CrossRef]

115. Cummings, D.E.; Rubino, F. Metabolic surgery for the treatment of type 2 diabetes in obese individuals. *Diabetologia* 2018. [CrossRef] [PubMed]

116. Santarpia, L.; Del Piano, C.; Amato, V.; Marra, M.; De Caprio, C.; De Rosa, E.; Contaldo, F.; Pasanisi, F. Impact of laparoscopic sleeve gastrectomy on metabolism and liver structure. *Obes. Facts* **2014**.

117. Bužga, M.; Zavadilová, V.; Holéczy, P.; Švagera, Z.; Švorc, P.; Foltys, A.; Zonča, P. Dietary intake and ghrelin and leptin changes after sleeve gastrectomy. *Wideochir. Inne Tech. Maloinwazyjne* **2014**, *9*, 554–561. [CrossRef]

118. Chen, G.; Zhang, G.; Peng, B.; Cheng, Z.; Du, X. Roux-En-Y Gastric Bypass Versus Sleeve Gastrectomy Plus Procedures for Treatment of Morbid Obesity: Systematic Review and Meta-Analysis. *Obes. Surg.* **2021**, *31*, 3303–3311. [CrossRef] [PubMed]

119. Laurenius, A.M.A.; Wallengren, O.; Alaraj, A.; Forslund, H.B.; Thorell, A.; Wallenius, V. Resolution of diabetes, gastrointestinal symptoms, and self-reported dietary intake after gastric bypass versus sleeve gastrectomy: A randomized study. *Surg. Obes. Relat. Dis.* 2022; *in press*. [CrossRef]

120. Strain, G.W.; Torghabeh, M.H.; Gagner, M.; Ebel, F.; Dakin, G.F.; Abelson, J.S.; Connolly, D.; Pomp, A. The Impact of Biliopancreatic Diversion with Duodenal Switch (BPD/DS) Over 9 Years. *Obes. Surg.* **2017**, *27*, 787–794. [CrossRef] [PubMed]

121. Pereira, S.S.; Guimarães, M.; Almeida, R.; Pereira, A.M.; Lobato, C.B.; Hartmann, B.; Hilsted, L.; Holst, J.J.; Nora, M. Biliopancreatic diversion with duodenal switch (BPD-DS) and single-anastomosis duodeno-ileal bypass with sleeve gastrectomy (SADI-S) result in distinct post-prandial hormone profiles. *Int. J. Obes.* **2019**, *43*, 2518–2527. [CrossRef] [PubMed]

122. Mitzman, B.; Cottam, D.; Goriparthi, R.; Cottam, S.; Zaveri, H.; Surve, A.; Roslin, M.S. Stomach Intestinal Pylorus Sparing (SIPS) Surgery for Morbid Obesity: Retrospective Analyses of Our Preliminary Experience. *Obes. Surg.* **2016**, *26*, 2098–2104. [CrossRef]

123. Neichoy, B.T.; Schniederjan, B.; Cottam, D.R.; Surve, A.K.; Zaveri, H.M.; Cottam, A.; Cottam, S. Stomach intestinal pylorus-sparing surgery for morbid obesity. *J. Soc. Laparoendosc. Surg.* **2018**, *22*, e2017.00063. [CrossRef] [PubMed]

124. Monkhouse, S.J.W.; Morgan, J.D.T.; Norton, S.A. Complication of bariatric surgery: Presentation and emergency management—A review. *Ann. R. Coll. Surg. Engl.* **2009**, *91*, 280–286. [CrossRef]

125. Decker, G.A.; Swain, J.M.; Crowell, M.D.; Scolapio, J.S. Gastrointestinal and nutritional complications after bariatric surgery. *Am. J. Gastroenterol.* **2007**, *102*, 2571–2580. [CrossRef] [PubMed]

126. Collazo-Clavell, M.L.; Shah, M. Common and Rare Complications of Bariatric Surgery. *Endocrinol. Metab. Clin. N. Am.* **2020**, *49*, 329–346. [CrossRef] [PubMed]

127. Tjeertes, E.E.K.M.; Hoeks, S.S.E.; Beks, S.S.B.J.C.; Valentijn, T.T.M.; Hoofwijk, A.A.G.M.; Stolker, R.J.R.J. Obesity—A risk factor for postoperative complications in general surgery? *BMC Anesthesiol.* **2015**, *15*, 112. [CrossRef]

128. Rashti, F.; Gupta, E.; Ebrahimi, S.; Shope, T.R.; Koch, T.R.; Gostout, C.J. Development of minimally invasive techniques for management of medically-complicated obesity. *World J. Gastroenterol.* **2014**, *20*, 13424–13445. [CrossRef] [PubMed]

129. Bhandari, M.; Fobi, M.A.L.; Buchwald, J.N. Bariatric Metabolic Surgery Standardization (BMSS) Working Group. Standardization of Bariatric Metabolic Procedures: World Consensus Meeting Statement. *Obes. Surg.* **2019**, *29*, 309–345. [CrossRef]

130. Al-Mulhim, A.S.; Al-Hussaini, H.A.; Al-Jalal, B.A.; Al-Moagal, R.O.; Al-Najjar, S.A. Obesity Disease and Surgery. *Int. J. Chronic Dis.* **2014**, *2014*, 652341. [CrossRef]

131. Král, J.; Machytka, E.; Horká, V.; Selucká, J.; Doleček, F.; Špičák, J.; Kovářová, V.; Haluzík, M.; Bužga, M. Endoscopic treatment of obesity and nutritional aspects of bariatric endoscopy. *Nutrients* **2021**, *13*, 4268. [CrossRef]

132. Picot, J.; Jones, J.; Colquitt, J.L.; Gospodarevskaya, E.; Loveman, E.; Baxter, L.; Clegg, A.J. The clinical effectiveness and cost-effectiveness of bariatric (weight loss) surgery for obesity: A systematic review and economic evaluation. *Health Technol. Assess.* **2009**, *13*. [CrossRef]

133. Zurawel, R.; Gluck, M.; Piecuch, J.; Nowowiejska-Wiewiora, A.; Niedziela, J.; Wiewiora, M. Effectiveness and Safety of Adjustable Gastric Banding in Morbidly Obese Patients After 5 Years of Follow-up. *Indian, J. Surg.* **2021**, *77*, 853–862. [CrossRef]

134. Mandrioli, M.; Inaba, K.; Piccinini, A.; Biscardi, A.; Sartelli, M.; Agresta, F.; Catena, F.; Cirocchi, R.; Jovine, E.; Tugnoli, G.; et al. Advances in laparoscopy for acute care surgery and trauma. *World J. Gastroenterol.* **2016**, *22*, 668–680. [CrossRef]

135. Torgerson, J.S.; Sjöström, L. The Swedish Obese Subjects (SOS) study—Rationale and results. *Int. J. Obes.* **2001**, *25*, S2–S4. [CrossRef] [PubMed]

136. Scheen, A.J.; Letiexhe, M.; Rorive, M.; De Flines, J.; Luyckx, F.H.; Desaive, C. Bariatric surgery: 10-Year results of Swedish Obese Subjects Study. *Rev. Med.* **2005**, *60*, 121–125.

137. Wiggins, T.; Guidozzi, N.; Welbourn, R.; Ahmed, A.R.; Markar, S.R. Association of bariatric surgery with all-cause mortality and incidence of obesity-related disease at a population level: A systematic review and meta-analysis. *PLoS Med.* **2020**, *17*, e1003206. [CrossRef] [PubMed]

138. Mechanick, J.I.; Apovian, C.; Brethauer, S.; Garvey, W.T.; Joffe, A.M.; Kim, J.; Kushner, R.F.; Lindquist, R.; Pessah-Pollack, R.; Seger, J.; et al. Clinical Practice Guidelines for the Perioperative Nutrition, Metabolic, and Nonsurgical Support of Patients Undergoing Bariatric Procedures—2019 Update: Cosponsored by American Association of Clinical Endocrinologists/American College of Endocrinology. *Endocr. Pract.* **2019**, *25*, 1–75. [CrossRef] [PubMed]

139. Müller, T.D.; Blüher, M.; Tschöp, M.H.; DiMarchi, R.D. Anti-obesity drug discovery: Advances and challenges. *Nat. Rev. Drug Discov.* **2022**, *21*, 201–223. [CrossRef]

140. Apovian, C.M.; Aronne, L.J.; Bessesen, D.H.; McDonnell, M.E.; Murad, M.H.; Pagotto, U.; Ryan, D.H.; Still, C.D.; Endocrine Society. Pharmacological management of obesity: An endocrine society clinical practice guideline. *J. Clin. Endocrinol. Metab.* **2015**, *100*, 342–362. [CrossRef]

141. Bray, G.A. Drug treatment of obesity. *Psychiatr. Clin. N. Am.* **2005**, *28*, 193–217. [CrossRef]

142. Van Dieren, S.; Czernichow, S.; Chalmers, J.; Kengne, A.P.; de Galan, B.E.; Poulter, N.; Woodward, M.; Beulens, J.W.; Grobbee, D.E.; van der Schouw, Y.T.; et al. Weight changes and their predictors amongst 11 140 patients with type 2 diabetes in the ADVANCE trial. *Diabetes Obes. Metab.* **2012**, *14*, 464–469. [CrossRef]

143. Turenius, C.I.; Htut, M.M.; Prodon, D.A.; Ebersole, P.L.; Ngo, P.T.; Lara, R.N.; Wilczynski, J.L.; Stanley, B.G. GABAA receptors in the lateral hypothalamus as mediators of satiety and body weight regulation. *Brain Res.* **2009**, *1262*, 16–24. [CrossRef]

144. Garvey, W.T.; Ryan, D.H.; Look, M.; Gadde, K.M.; Allison, D.B.; Peterson, C.A.; Schwiers, M.; Day, W.W.; Bowden, C.H. Two-year sustained weight loss and metabolic benefits with controlled-release phentermine/topiramate in obese and overweight adults (SEQUEL): A randomized, placebo-controlled, phase 3 extension study. *Am. J. Clin. Nutr.* **2012**, *95*, 297–308. [CrossRef]

145. Drent, M.L.; Popp-Snijders, C.; Adér, H.J.; Jansen, J.B.M.J.; van der Veen, E.A. Lipase Inhibition and Hormonal Status, Body Composition and Gastrointestinal Processing of a Liquid High-Fat Mixed Meal in Moderately Obese Subjects. *Obes. Res.* **1995**, *3*, 573–581. [CrossRef] [PubMed]

146. McDuffie, J.R.; Calis, K.A.; Booth, S.L.; Uwaifo, G.I.; Yanovski, J.A. Effects of orlistat on fat-soluble vitamins in obese adolescents. *Pharmacotherapy* **2002**, *22*, 814–822. [CrossRef] [PubMed]

147. Ioannides-Demos, L.L.; Piccenna, L.; McNeil, J.J. Pharmacotherapies for obesity: Past, current, and future therapies. *J. Obes.* **2011**, *2011*, 179674. [CrossRef] [PubMed]

148. Thomsen, W.J.; Grottick, A.J.; Menzaghi, F.; Reyes-Saldana, H.; Espitia, S.; Yuskin, D.; Whelan, K.; Martin, M.; Morgan, M.; Chen, W.; et al. Lorcaserin, a novel selective human 5-hydroxytryptamine2C agonist: In vitro and in vivo pharmacological characterization. *J. Pharmacol. Exp. Ther.* **2008**, *325*, 577–587. [CrossRef]

149. Smith, S.R.; Weissman, N.J.; Anderson, C.M.; Sanchez, M.; Chuang, E.; Stubbe, S.; Bays, H.; Shanahan, W.R. Behavioral Modification and Lorcaserin for Overweight and Obesity Management (BLOOM) Study Group. Multicenter, Placebo-Controlled Trial of Lorcaserin for Weight Management. *N. Engl. J. Med.* **2010**, *363*, 245–256. [CrossRef]

150. Toft-Nielson, M.; Madsbad, S.; Holst, J.J. The Effect of Glucagon-Like Peptide I (GLP-I) on Glucose Elimination in Healthy Subjects Depends on the Pancreatic Glucoregulatory Hormones. *Diabetes* **1996**, *45*, 552–556. [CrossRef]

151. Flint, A.; Raben, A.; Astrup, A.; Holst, J.J. Glucagon-like peptide 1 promotes satiety and suppresses energy intake in humans. *J. Clin. Investig.* **1998**, *101*, 515–520. [CrossRef]

152. Schirra, J.; Nicolaus, M.; Roggel, R.; Katschinski, M.; Storr, M.; Woerle, H.J.; Göke, B. Endogenous glucagon-like peptide 1 controls endocrine pancreatic secretion and antro-pyloro-duodenal motility in humans. *Gut* **2006**, *55*, 243–251. [CrossRef]

153. Pi-Sunyer, X.; Astrup, A.; Fujioka, K.; Greenway, F.; Halpern, A.; Krempf, M.; Lau, D.C.; le Roux, C.W.; Violante Ortiz, R.; Jensen, C.B.; et al. A Randomized, Controlled Trial of 3.0 mg of Liraglutide in Weight Management. *N. Engl. J. Med.* **2015**, *373*, 11–22. [CrossRef]

154. Pi-Sunyer, X. The medical risks of obesity. *Postgrad. Med.* **2009**, *121*, 21–33. [CrossRef]

155. Pan, A.; Sun, Q.; Czernichow, S.; Kivimaki, M.; Okereke, O.I.; Lucas, M.; Manson, J.E.; Ascherio, A.; Hu, F.B. Bidirectional association between depression and obesity in middle-aged and older women. *Int. J. Obes.* **2012**, *36*, 595–602. [CrossRef] [PubMed]

156. Greenway, F.L.; Fujioka, K.; Plodkowski, R.A.; Mudaliar, S.; Guttadauria, M.; Erickson, J.; Kim, D.D.; Dunayevich, E.; COR-I Study Group. Effect of naltrexone plus bupropion on weight loss in overweight and obese adults (COR-I): A multicentre, randomised, double-blind, placebo-controlled, phase 3 trial. *Lancet* **2010**, *376*, 595–605. [CrossRef] [PubMed]

MDPI

MDPI